SMART TOOLS FOR CARING: NANOTECHNOLOGY MEETS MEDICAL CHALLENGES

EDITED BY: Giada Genchi and Gianni Ciofani

PUBLISHED IN: Frontiers in Bioengineering and Biotechnology

frontiers Research Topics

ISSN 1664-8714
ISBN 978-2-88945-806-6
DOI 10.3389/978-2-88945-806-6

About Frontiers

Frontiers is more than just an open-access publisher of scholarly articles: it is a pioneering approach to the world of academia, radically improving the way scholarly research is managed. The grand vision of Frontiers is a world where all people have an equal opportunity to seek, share and generate knowledge. Frontiers provides immediate and permanent online open access to all its publications, but this alone is not enough to realize our grand goals.

Frontiers Journal Series

The Frontiers Journal Series is a multi-tier and interdisciplinary set of open-access, online journals, promising a paradigm shift from the current review, selection and dissemination processes in academic publishing. All Frontiers journals are driven by researchers for researchers; therefore, they constitute a service to the scholarly community. At the same time, the Frontiers Journal Series operates on a revolutionary invention, the tiered publishing system, initially addressing specific communities of scholars, and gradually climbing up to broader public understanding, thus serving the interests of the lay society, too.

Dedication to Quality

Each Frontiers article is a landmark of the highest quality, thanks to genuinely collaborative interactions between authors and review editors, who include some of the world's best academicians. Research must be certified by peers before entering a stream of knowledge that may eventually reach the public - and shape society; therefore, Frontiers only applies the most rigorous and unbiased reviews.
Frontiers revolutionizes research publishing by freely delivering the most outstanding research, evaluated with no bias from both the academic and social point of view. By applying the most advanced information technologies, Frontiers is catapulting scholarly publishing into a new generation.

What are Frontiers Research Topics?

Frontiers Research Topics are very popular trademarks of the Frontiers Journals Series: they are collections of at least ten articles, all centered on a particular subject. With their unique mix of varied contributions from Original Research to Review Articles, Frontiers Research Topics unify the most influential researchers, the latest key findings and historical advances in a hot research area! Find out more on how to host your own Frontiers Research Topic or contribute to one as an author by contacting the Frontiers Editorial Office: researchtopics@frontiersin.org

SMART TOOLS FOR CARING: NANOTECHNOLOGY MEETS MEDICAL CHALLENGES

Topic Editors:
Giada Genchi, Istituto Italiano di Tecnologia, Italy
Gianni Ciofani, Istituto Italiano di Tecnologia and Politecnico di Torino, Italy

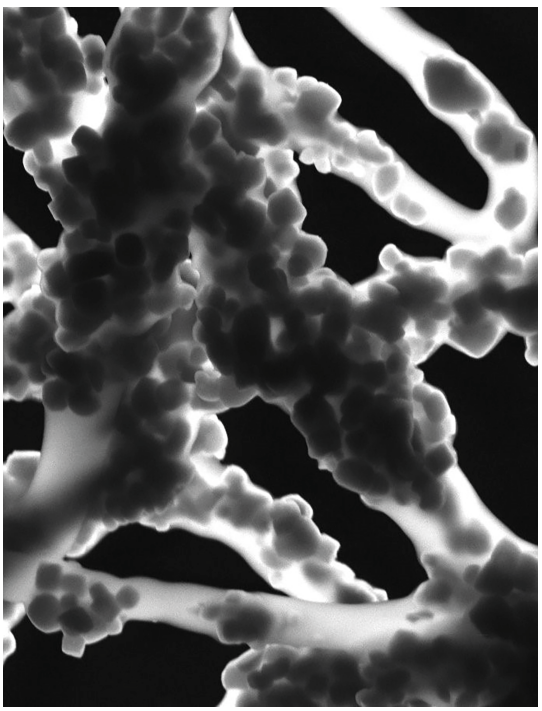

Image by Elisa Mele, Giada Genchi and Gianni Ciofani

Citation: Genchi, G., Ciofani, G., eds. (2019). Smart Tools for Caring: Nanotechnology Meets Medical Challenges. Lausanne: Frontiers Media.
doi: 10.3389/978-2-88945-806-6

Table of Contents

frontiers in Bioengineering and Biotechnology

EDITORIAL
published: 30 January 2019
doi: 10.3389/fbioe.2019.00011

Editorial: Smart Tools for Caring: Nanotechnology Meets Medical Challenges

Giada G. Genchi[1]* *and Gianni Ciofani*[1,2]*

[1] *Smart Bio-Interfaces, Istituto Italiano di Tecnologia, Pontedera, Italy,* [2] *Department of Mechanical and Aerospace Engineering, Politecnico di Torino, Turin, Italy*

Keywords: smart materials, remote stimulation, drug delivery, tissue engineering, clinical translation

Editorial on the Research Topic

Smart Tools for Caring: Nanotechnology Meets Medical Challenges

This Research Topic of Frontiers in Bioengineering and Biotechnology-Nanotechnology stems from the international workshop "Smart tools for caring: Nanotechnology meets medical challenges" held in Pontedera (Italy) on March 2, 2018 with the goal of promoting a multidisciplinary discussion on the most innovative techniques and materials with strong therapeutic potential in human healthcare. The issue presents 14 selected, peer-reviewed contributions (1 Brief Research Report, 7 Mini-Reviews, 1 Opinion, 3 Original Researches, 3 Reviews) from different research fields, ranging from materials science, to biotechnology, physics, and engineering.

In agreement with the scopes of the workshop, this issue reviews general topics of crucial importance in the design of materials for interaction with biological systems, most notably mechanical properties, surface features (including roughness, porosity, and patterning), and their spatiotemporal variation (Cimmino et al.; Palamà et al.). The synthesis and fabrication of innovative materials are presented with focus on the modulation of cell responses in events like cell adhesion, proliferation, and differentiation (Bandiera et al.; Denchai et al.; Şen et al.; Suarato et al.). In this concern, instrumental techniques for characterization of bio-/non bio-interactions (Arai and Ferdinandus; Fujita et al.; Tonda-Turo et al.), light-based methods for remote stimulation of materials and their anatomical targets (Bossio et al.; Polino et al.), and complex approaches for diagnosis and treatment of pathological conditions through genetic manipulations of somatic cells, nanomaterials, and robotic devices (Cervadoro et al.; Robinson et al.; Soto and Chrostowski) are presented.

More in detail, the importance of material properties like stiffness is discussed with relevance to the fabrication of three-dimensional constructs of glioblastoma multiforme, with the final goal of elaborating reliable therapies against this aggressive tumor of the central nervous system (Palamà et al.). Along with stiffness, other biochemical and biophysical signals like ligand exposure and topography of the materials are thoroughly reviewed, and the significance of their time- and space-variant patterns in response to external stimulations (light, temperature, electricity, or even enzymes and cells) is discussed in relation to the elaboration of specific protocols for exposure of cells to dynamic bioinstructive signals (Cimmino et al.).

The importance of the use of polypeptides (for instance collagen, fibroin, and keratin), polysaccharides (like hyaluronic acid, chitosan, and alginate) or even their mixtures of natural origin (such as in mycelia with controlled composition based on the fungal feeding substrate) is stressed as an environmental sustainable strategy for the preparation of biodegradable materials, especially in the context of wound healing (Suarato et al.).

OPEN ACCESS

Edited and reviwed by:
Sandra Camarero-Espinosa, Maastricht University, Netherlands

***Correspondence:**
Giada G. Genchi
giada.genchi@iit.it
Gianni Ciofani
gianni.ciofani@iit.it

Specialty section:
This article was submitted to Nanobiotechnology, a section of the journal Frontiers in Bioengineering and Biotechnology

Received: *07 January 2019*
Accepted: *17 January 2019*
Published: *30 January 2019*

Citation:
Genchi GG and Ciofani G (2019) Editorial: Smart Tools for Caring: Nanotechnology Meets Medical Challenges. Front. Bioeng. Biotechnol. 7:11. doi: 10.3389/fbioe.2019.00011

In this Research Topic, the fabrication of novel materials with controlled architecture is addressed with electrospinning and wet chemistry techniques. Corroborated by computational models that predict and correlate surface properties with biological responses, electrospinning is reviewed as an effective technique for micro- and nanopatterning of materials to impart biologically relevant cues (under the form of fiber orientation, roughness, and density) to tune cell adhesion, proliferation, and differentiation (Denchai et al.). Electrospinning is also used as a technique for the fabrication of hybrid scaffolds with thermoresponsive hydrogels (based on recombinant elastin-like polypeptides) in view of drug loading and release in elastolytic conditions, such as those associated to wound healing (Bandiera et al.). One step synthesis of hexagonal boron nitride nanomaterials (hBNs) from different boron sources and in the absence of catalysts is also described for possible application in cancer treatment. In particular, evidences on hBN stability and degradation under both oxidative and hydrolytic conditions are reported, supporting the use of colemanite as a boron source (Şen et al.).

Microscopy techniques for investigating biological events with intracellular compartment resolution are discussed: basic indications of the choice and application of fluorescent probes are presented with relevance to photothermal and photodynamic therapeutic approaches (Arai and Ferdinandus). Moreover, methods based on probes (genetically encoded fluorophores, chemical fluorescent molecules, and other nanomaterials) are reviewed along with purely optical, probe-less methods (Fujita et al.). Among the techniques for characterization of bio-/non bio-interactions, quartz crystal microbalance is described as a tool for dynamic investigation of chemical, mechanical, and electrical properties of surfaces interacting with cells and of biological response to biomedical devices (Tonda-Turo et al.).

The activation of smart materials on their target sites by non-invasive approaches is here discussed with a focus on phototransduction methods based on photovoltaic devices or photocatalytic nanoparticles. Photovoltaic devices are presented for stimulation of electrogenic cells in the retina and for promotion of non-electrogenic cell proliferation, such as during angiogenesis and wound healing (Polino et al.). Photocatalytic nanoparticles based on poly(3-hexylthiophene) with semiconductive properties are exploited for modulation of calcium influxes in HEK-293 cells through the generation of reactive oxygen species under visible light irradiation, denoting potential for cell behavior tuning with high spatio-temporal resolution (Bossio et al.).

This Research Topic also includes a concise review of innovative materials with theranostic potentiality for modulation of cell response in terms of inflammation control, immune system targeting, and treatment of atherosclerosis (Cervadoro et al.). An innovative approach for genetic reprogramming of somatic cells (astrocytes) into neurons with a non-viral method (based on a fusion protein containing a transcription factor and a protein transduction domain, in association to SMAD, Notch, and histone deacetylase inhibitors) is presented for possible treatment of central nervous system injuries (Robinson et al.). The need of considering emerging clinical translation and potential commercial use of micro- and nanorobotic devices is also thoroughly reviewed: even in this case, the discussion stresses on fine spatiotemporal control of activities such as delivery of drugs, imaging agents or cells, and biopsy collection. The discussion is completed by considerations on experimental methodology reproducibility and standardization requisites, on intellectual property protection, on device fabrication and on the implementation of innovative devices in current therapeutic protocols for the elaboration of concrete translational medicine approaches (Soto and Chrostowski).

To conclude, we hope this Research Topic will represent a useful reference of easy consultation for those readers interested to gather concise information on the state of the art, as well as to understand the necessary directions of multidisciplinary research on innovative materials and related topics of high relevance to human healthcare for the immediate future.

AUTHOR CONTRIBUTIONS

All authors listed have made a substantial, direct and intellectual contribution to the work, and approved it for publication.

ACKNOWLEDGMENTS

This research is partially supported by the *Compagnia di San Paolo* Starting Grant Number 55_AI16GC01.

Conflict of Interest Statement: The authors declare that the research was conducted in the absence of any commercial or financial relationships that could be construed as a potential conflict of interest.

frontiers in Bioengineering and Biotechnology

OPINION
published: 24 September 2018
doi: 10.3389/fbioe.2018.00131

Microenvironmental Rigidity of 3D Scaffolds and Influence on Glioblastoma Cells: A Biomaterial Design Perspective

Ilaria Elena Palamà[1]*, *Stefania D'Amone*[1] and *Barbara Cortese*[2]*

[1] Nanotechnology Institute, CNR-Nanotechnology Institute, Lecce, Italy, [2] Nanotechnology Institute, CNR-Nanotechnology Institute, University La Sapienza, Rome, Italy

Keywords: 3D scaffolds, glioblastoma, stiffness, neurospheres, microenvironment

OPEN ACCESS

Edited by:
Gianni Ciofani,
Politecnico di Torino, Italy

Reviewed by:
Luca Ceseracciu,
Fondazione Istituto Italiano di Technologia, Italy
Giulia Suarato,
Fondazione Istituto Italiano di Technologia, Italy
Piergiorgio Gentile,
Newcastle University, United Kingdom

***Correspondence:**
Ilaria Elena Palamà
ilaria.palama@nanotec.cnr.it
Barbara Cortese
barbara.cortese@nanotec.cnr.it

Specialty section:
This article was submitted to Nanobiotechnology, a section of the journal Frontiers in Bioengineering and Biotechnology

Received: *01 August 2018*
Accepted: *03 September 2018*
Published: *24 September 2018*

Citation:
Palamà IE, D'Amone S and Cortese B (2018) Microenvironmental Rigidity of 3D Scaffolds and Influence on Glioblastoma Cells: A Biomaterial Design Perspective. Front. Bioeng. Biotechnol. 6:131. doi: 10.3389/fbioe.2018.00131

INTRODUCTION

Glioblastoma (GBM), or grade IV glioma, is an extremely aggressive tumor that infiltrates through the brain leaving the patient with a median survival time from 12 to 15 months (Ostrom et al., 2013). Individual aspects of the microenvironment features play a critical role on GBM cell dynamics and treatment resistance (Bellail et al., 2004; Zamecnik, 2005; Calabrese et al., 2007). Because of GBM's aggressive and invasive behavior, inhibition of GBM migration is envisaged as an important therapeutic objective (Bravo-Cordero et al., 2012; Wells et al., 2013). However, current models fail to account for the complex brain microenvironment. The demand of preclinical models that can faithfully mimic the clinical scenario may bridge the discrepancy between preclinical and clinical data and aid to develop treatments that are more effective.

The extracellular matrix (ECM) of the GBM microenvironment is constitutively composed of the polysaccharide hyaluronic acid (HA), and in a distinctive minor degree of tenascin-C, collagen IV and V, fibronectin, and laminin (Giese and Westphal, 1996; Rape et al., 2014). Also, typically with high glioma grade, the HA's cellular receptor CD44 is overexpressed, suggesting that CD44-enriched cells invade more efficiently the brain parenchyma (Bellail et al., 2004). GBM malignancy is furthermore promoted through interactions with the other aforementioned ECM components through different biochemical pathways (Sarkar et al., 2006; Lathia et al., 2012), which trigger an increase of the concentration of the non-cellular components (Bellail et al., 2004; Lathia et al., 2012). This increased density of the tumor ECM consequently increases the mechanical stiffness of the microenvironment (Ananthanarayanan et al., 2011; Wiranowska and Rojiani, 2011; Pathak and Kumar, 2012; Pedron and Harley, 2013; Kim and Kumar, 2014; Umesh et al., 2014; Heffernan et al., 2015).

In our opinion, to gain further insights into tumor invasiveness, heterogeneity and treatment resistance, we have to look more deeply at how cell behavior is influenced by matrix stiffness (a process known as mechanotaxis or durotaxis) (Lo et al., 2000; Cortese et al., 2009; Palamà et al., 2012, 2016).

WHAT IS THE INFLUENCE OF THE 3D SCAFFOLD MECHANICAL PROPERTIES?

Notably, 2D platforms do not adequately mimic the *in vivo* tumor environment. Recent work has focused on 3D scaffolds and matrix influence on cells with different materials and cells, as reported in **Table 1**. However, inconsistencies on how 3D scaffold stiffness affect cell proliferation and influence drug delivery and treatment resistance have been reported in literature

(Wang et al., 2014, 2016; Heffernan et al., 2015; Pedron et al., 2015; Lv et al., 2016; Palamà et al., 2017). In order to tune the mechanical properties of different materials, the most common methods are (1) altering the crosslink density and (2) changing the base polymer concentration which both influence different parameters, such as the ECM architecture, stiffness, pore size, diffusion of soluble factors of the scaffolds, and ligand density. A 3D culture platform that aims to mimic the native GBM microenvironment has also the additional requirement of containing HA. Pure HA lacks mechanical strength and the ability to promote cell adhesion due to its anionic properties (Wang et al., 2012). Moreover, it does not allow control over mechanical stiffness. These downsides have been partly overcome by using synthetic ECM polymers (Lutolf and Hubbell, 2005; Seliktar, 2012). One semi-synthetic material, predominantly used to independently tune the stiffness of the scaffold, is HA-based hydrogel functionalized to favor cell adhesion. For example, Ananthanarayanan studied HA gels of varying stiffness embedded with GBM spheroids and corroborated that their invasive capacity and morphological patterns were similar to what was seen *in vivo* in human brain slices, in opposition to glioma cells cultured in 2D and 3D collagen contexts (Ananthanarayanan et al., 2011). Differences were theorized to be related to the variation of expression of CD44. This was confirmed by Harley and co-workers, who identified CD44 as a key driver of glioma malignancy with cells encapsulated in gelatin and PEG-based hydrogels grafted with a HA hydrogel network (Pedron et al., 2013). Analogous observations were made by Erikson using porous chitosan–hyaluronic acid scaffolds of different stiffness, obtained varying the chitosan content. With a higher polymer content, the pore walls were thicker, with reduced interconnections between pores as well as the pore size (Erickson et al., 2018). Stiffness was shown to influence the morphology of the cell aggregates as well as the expression of

TABLE 1 | A summary of various scaffolds used for glioblastoma responses.

Scaffolds	Stiffness value range	Porosity	Cells	Behavior	References
Chitosan/hyaluronic acid	Tunable between kPa to MPa	77.31 μm with 87.09% porosity; pore diameters between 134 to 179 μm	U-118 MG; GBM6 tumors; U87 MG	Tumor spheroid formation	(Florczyk et al., 2013; Cha et al., 2016; Kievit et al., 2016; Wang et al., 2016; Erickson et al., 2018)
Hyaluronic acid-methacrylate hydrogel	Ranging from 50 Pa to 35 kPa	Mesh sizes ranging from 50 to 150 nm	Human U373-MG and U87-MG; rat C6 glioma	GBM cell morphology and motility are regulated by stiffness. Different GBM invasiveness C6 > U87-MG > U373-MG	(Ananthanarayanan et al., 2011)
Gelatin methacrylate hydrogel	Ranging from 5 to 55 kPa	Micron scale larger	U87-MG	Biophysical regulation of GBM cell activity is not direct or clear	(Pedron and Harley, 2013)
Poly(ethylene-glycol) (PEG)-based hydrogels	Ranging from 1 to 26 kPa	–	U87-MG	Tumor spheroid formation	(Pedron et al., 2013; Wang et al., 2014)
Polyacrylamide hydrogels	Ranging from 0.2 to 50 kPa	–	Patient derived GBM cells (JK2, SJH1, WK1, RN1 and PR1)	Different migratory capacity. No detected association between cell morphology and migratory capacity	(Grundy et al., 2016)
Temperature responsive poly(N-isopropylacrylamide-co-Jeffamine M-1000 acrylamide)	Tunable between 153 and 1,240 Pa	–	Patient-derived GSC cell lines	On soft scaffolds (153–325 Pa), GSCs did not cluster into large neurosphere	(Heffernan et al., 2017)
Chitosan-alginate scaffold coated with hyaluronic acid	–	–	U-87 MG	Tumor spheroid formation	(Kievit et al., 2016)
GBM patient tissue derived ECM	78.09 ± 29.22 Pa	Porous and fibrous structure	Patient-derived GBM cells	GBM cells exhibited heterogeneous morphology and altered the invasion routes in a microenvironment-adaptive manner	(Koh et al., 2018)
Gelatin/alginate/fibrinogen hydrogel	–	–	GSC cell lines	GSC did not maintain their characteristics of cancer stem cells but showed differentiation potential	(Xingliang et al., 2016)
Collagen based hydrogel	Tunable stiffness	Tunable between 30 and 100 μm	U87, U251 and HS683 cell lines; primary glioma cells (OSU-2); patient derived GBM stem cells	Enhancement the malignancy of the glioma cells; spheroid formations	(Rao et al., 2013; Cha et al., 2016; Lv et al., 2016; Jia et al., 2018)

drug resistance, hypoxia, and invasion-related genes (Mih et al., 2011; Zustiak et al., 2016; Erickson et al., 2018).

TYPE OF CELLS USED IN THE *IN VITRO* MODELS

A further critical key parameter is the choice of the cells used (Zustiak et al., 2014). Typically, commercially available human tumor cell lines are used, but they neglect predicting clinical outcomes due to different genetic aberrations. Glioblastoma stem-like cells (GSC) can mimic the tumor of origin being tumor cells with stem cell properties (Saha et al., 2008). However, they require isolating stem cells from each tumor patient and expansion to an adequate number within a clinically acceptable time. Aggregated cultures would recapitulate better the GBM microenvironment, allowing cell–cell contacts and collective migration. Non-adherent cultures lack the cell–matrix interactions present in the tumor stroma, whereas complex spherical cancer models (i.e. non-adherent cancer cell line-derived spheroids, or spheroids derived from primary tumor dissociation) can promote cell–cell interactions. The use of patient-derived cells cultured as neurospheres is a significant advance respect to glioma cell lines (Rao et al., 2013; Cha et al., 2016) however they do not accurately reproduce the original tumor composition due to heterogeneity loss and lack of an adhesive matrix. A solution could be represented by GBM organoids (Hubert et al., 2016), although these require months for generation, thus becoming useless in aid of patient treatment and not necessarily being an improvement to the patient outcomes (Oh et al., 2014), whereas neurosphere cultures can be established within only few weeks.

INFLUENCE OF COMPOUNDING STIMULI ON THE SCAFFOLDS

Diverging results have also been implicated with the matrix metalloprotease (MMP) secretion. For example, an increase of MMP-9 production in hyaluronic acid-based hydrogels with increasing stiffness was reported by Pedron's group while Wang and colleagues described an opposite behavior (Pedron et al., 2013, 2015; Wang et al., 2014). The reason, in our opinion, is related to the difficulty to discriminate the role of stiffness or of the biochemical stimuli on cell invasion. In fact, only a few works report a selected degree of decoupling of the mechanical properties, porosity, and/or biochemical cues. The interference of other compounding stimuli in the design of functional cell culture substrates should be minimized if not isolated. Changes in the ligand density and the pore size of the matrix may obstruct migration of cells and alter solute diffusion (Shu et al., 2002). For example, Cha used a different molecular weight of HA to simply coat the collagen I fibers without modifications and crosslinking (Cha et al., 2016). Using a higher molecular weight and 3D structure of the polymer may have induced different cell responses. Rao reported a high degree of thiolation, which may have altered the bioactivity of the substrate (Rao et al., 2013). Kumar and co-workers managed to decouple the effects by assembling hydrogel networks of collagen I and agarose and increasing the stiffness by increasing the concentration of non-adhesive agarose while keeping collagen I levels constant (Ulrich et al., 2010). However, increasing the concentration of agarose may result in smaller pores that restricted migration on stiffer hydrogels. Moreover, the presence of the agarose interfering with collagen fiber deformation and bundling may have thereby restricted local ability of tumor cells to stiffen their microenvironment (Kilian and Mrksich, 2012; Rape et al., 2015).

In conclusion there is still no existing artificial GBM microenvironment which can replace an *in vivo* model. It is essential to ask if it is worth to increase the complexity of the ECM microenvironment and to define which parameters are at least required to achieve a physiologically relevant model *ex vivo*. We think that tuning matrix stiffness will be pivotal at both a preclinical and clinical level, to move forward this field of investigation of cell behavior during tumorigenesis thereby providing an important tool to target and investigate the more effective therapy at different stages of cancer progression. To unravel the tumor invasiveness and to demonstrate their clinical value, a fully comprehensive analysis approach has to be achieved. This invites further study and highlights the importance of conducting parallel measurements using spheroid cell lines in highly multi-structured conditions as well as comparisons with patient outcomes.

AUTHOR CONTRIBUTIONS

IP, SD, and BC wrote the manuscript. All authors reviewed the manuscript and have given approval to the final version of the manuscript.

FUNDING

FIRS project Tecnopolo di nanotecnologia e fotonica per la medicina di precisione (grant no: CIPE n. 78/2017 B83B17000010001).

ACKNOWLEDGMENTS

This study is supported by the Italian Association for Cancer Research (AIRC) through the grant MFAG n. 16803 and partially by the FIRS project Tecnopolo di nanotecnologia e fotonica per la medicina di precisione.

REFERENCES

Ananthanarayanan, B., Kim, Y., and Kumar, S. (2011). Elucidating the mechanobiology of malignant brain tumors using a brain matrix-mimetic hyaluronic acid hydrogel platform. *Biomaterials* 32, 7913–7923. doi: 10.1016/j.biomaterials.2011.07.005

Bellail, A. C., Hunter, S. B., Brat, D. J., Tan, C., and Van Meir, E. G. (2004). Microregional extracellular matrix heterogeneity in brain

modulates glioma cell invasion. *Int. J. Biochem. Cell Biol.* 36, 1046–1069. doi: 10.1016/j.biocel.2004.01.013

Bravo-Cordero, J. J., Hodgson, L., and Condeelis, J. (2012). Directed cell invasion and migration during metastasis. *Curr. Opin. Cell Biol.* 24, 277–283. doi: 10.1016/j.ceb.2011.12.004

Calabrese, C., Poppleton, H., Kocak, M., Hogg, T. L., Fuller, C., Hamner, B., et al. (2007). A perivascular niche for brain tumor stem cells. *Cancer Cell* 11, 69–82. doi: 10.1016/j.ccr.2006.11.020

Cha, J., Kang, S. G., and Kim, P. (2016). Strategies of mesenchymal invasion of patient-derived brain tumors: microenvironmental adaptation. *Sci. Rep.* 6:24912. doi: 10.1038/srep24912

Cortese, B., Gigli, G., and Riehle, M. (2009). Mechanical gradient cues for guided cell motility and control of cell behavior on uniform substrates. *Adv. Func. Mater.* 19, 2961–2968. doi: 10.1002/adfm.200900918

Erickson, A. E., Lan Levengood, S. K., Sun, J., Chang, F. C., and Zhang, M. (2018). Fabrication and characterization of chitosan-hyaluronic acid scaffolds with varying stiffness for glioblastoma cell culture. *Adv. Healthcare Mater.* 7:e1800295. doi: 10.1002/adhm.201800295

Florczyk, S. J., Wang, K., Jana, S., Wood, D. L., Sytsma, S. K., Sham, J., et al. (2013). Porous chitosan-hyaluronic acid scaffolds as a mimic of glioblastoma microenvironment ECM. *Biomaterials* 34, 10143–10150. doi: 10.1016/j.biomaterials.2013.09.034

Giese, A., and Westphal, M. (1996). Glioma invasion in the central nervous system. *Neurosurgery* 39, 235–250; discussion 250–232.

Grundy, T. J., De Leon, E., Griffin, K. R., Stringer, B. W., Day, B. W., Fabry, B., et al. (2016). Differential response of patient-derived primary glioblastoma cells to environmental stiffness. *Sci. Rep.* 6:23353. doi: 10.1038/srep23353

Heffernan, J. M., McNamara, J. B., Borwege, S., Vernon, B. L., Sanai, N., Mehta, S., et al. (2017). PNIPAAm-co-Jeffamine® (PNJ) scaffolds as *in vitro* models for niche enrichment of glioblastoma stem-like cells. *Biomaterials* 143, 149–158. doi: 10.1016/j.biomaterials.2017.05.007

Heffernan, J. M., Overstreet, D. J., Le, L. D., Vernon, B. L., and Sirianni, R. W. (2015). Bioengineered scaffolds for 3D analysis of glioblastoma proliferation and invasion. *Ann. Biomed. Eng.* 43, 1965–1977. doi: 10.1007/s10439-014-1223-1

Hubert, C. G., Rivera, M., Spangler, L. C., Wu, Q., Mack, S. C., Prager, B. C., et al. (2016). A Three-dimensional organoid culture system derived from human glioblastomas recapitulates the hypoxic gradients and cancer stem cell heterogeneity of tumors found *in vivo*. *Cancer Res.* 76, 2465–2477. doi: 10.1158/0008-5472.CAN-15-2402

Jia, W., Jiang, X., Liu, W., Wang, L., Zhu, B., Zhu, H., et al. (2018). Effects of three-dimensional collagen scaffolds on the expression profiles and biological functions of glioma cells. *Int. J. Oncol.* 52, 1787–1800. doi: 10.3892/ijo.2018.4330

Kievit, F. M., Wang, K., Erickson, A. E., Lan Levengood, S. K., Ellenbogen, R. G., and Zhang, M. (2016). Modeling the tumor microenvironment using chitosan-alginate scaffolds to control the stem-like state of glioblastoma cells. *Biomater. Sci.* 4, 610–613. doi: 10.1039/C5BM00514K

Kilian, K. A., and Mrksich, M. (2012). Directing stem cell fate by controlling the affinity and density of ligand-receptor interactions at the biomaterials interface. *Angewandte Chemie* 51, 4891–4895. doi: 10.1002/anie.201108746

Kim, Y., and Kumar, S. (2014). CD44-mediated adhesion to hyaluronic acid contributes to mechanosensing and invasive motility. *Mol. Cancer Res.* 12, 1416–1429. doi: 10.1158/1541-7786.MCR-13-0629

Koh, I., Cha, J., Park, J., Choi, J., Kang, S. G., and Kim, P. (2018). The mode and dynamics of glioblastoma cell invasion into a decellularized tissue-derived extracellular matrix-based three-dimensional tumor model. *Sci. Rep.* 8:4608. doi: 10.1038/s41598-018-22681-3

Lathia, J. D., Li, M., Hall, P. E., Gallagher, J., Hale, J. S., Wu, Q., et al. (2012). Laminin alpha 2 enables glioblastoma stem cell growth. *Ann. Neurol.* 72, 766–778. doi: 10.1002/ana.23674

Lo, C. M., Wang, H. B., Dembo, M., and Wang, Y. L. (2000). Cell movement is guided by the rigidity of the substrate. *Biophys. J.* 79:8. doi: 10.1016/S0006-3495(00)76279-5

Lutolf, M. P., and Hubbell, J. A. (2005). Synthetic biomaterials as instructive extracellular microenvironments for morphogenesis in tissue engineering. *Nat. Biotechnol.* 23, 47–55. doi: 10.1038/nbt1055

Lv, D., Yu, S. C., Ping, Y. F., Wu, H., Zhao, X., Zhang, H., et al. (2016). A three-dimensional collagen scaffold cell culture system for screening anti-glioma therapeutics. *Oncotarget* 7, 56904–56914. doi: 10.18632/oncotarget.10885

Mih, J. D., Sharif, A. S., Liu, F., Marinkovic, A., Symer, M. M., and Tschumperlin, D. J. (2011). A multiwell platform for studying stiffness-dependent cell biology. *PLoS ONE* 6:e19929. doi: 10.1371/journal.pone.0019929

Oh, Y. T., Cho, H. J., Kim, J., Lee, J. H., Rho, K., Seo, Y. J., et al. (2014). Translational validation of personalized treatment strategy based on genetic characteristics of glioblastoma. *PLoS ONE* 9:e103327. doi: 10.1371/journal.pone.0103327

Ostrom, Q. T., Gittleman, H., Farah, P., Ondracek, A., Chen, Y., Wolinsky, Y., et al. (2013). CBTRUS statistical report: primary brain and central nervous system tumors diagnosed in the United States in 2006-2010. *Neurooncology* 15(Suppl. 2), ii1–ii56. doi: 10.1093/neuonc/not151

Palamà, I. E., Arcadio, V., D'Amone, S., Biasiucci, M., Gigli, G., and Cortese, B. (2017). Therapeutic PCL scaffold for reparation of resected osteosarcoma defect. *Sci. Rep.* 7:12672. doi: 10.1038/s41598-017-12824-3

Palamà, I. E., Coluccia, A. M., Gigli, G., and Riehle, M. (2012). Modulation of alignment and differentiation of skeletal myoblasts by biomimetic materials. *Integr. Biol.* 4, 1299–1309. doi: 10.1039/c2ib20133j

Palamà, I. E., D'Amone, S., and Cortese, B. (2016). *Mechanical Guidance of Cell Migration*. Zagreb: IAPC Publishing.

Pathak, A., and Kumar, S. (2012). Independent regulation of tumor cell migration by matrix stiffness and confinement. *Proc. Natl. Acad. Sci. U.S.A.* 109, 10334–10339. doi: 10.1073/pnas.1118073109

Pedron, S., Becka, E., and Harley, B. A. (2013). Regulation of glioma cell phenotype in 3D matrices by hyaluronic acid. *Biomaterials* 34, 7408–7417. doi: 10.1016/j.biomaterials.2013.06.024

Pedron, S., Becka, E., and Harley, B. A. (2015). Spatially gradated hydrogel platform as a 3D engineered tumor microenvironment. *Adv. Mater.* 27, 1567–1572. doi: 10.1002/adma.201404896

Pedron, S., and Harley, B. A. (2013). Impact of the biophysical features of a 3D gelatin microenvironment on glioblastoma malignancy. *J. Biomed. Mater. Res. A* 101, 3404–3415. doi: 10.1002/jbm.a.34637

Rao, S. S., Dejesus, J., Short, A. R., Otero, J. J., Sarkar, A., and Winter, J. O. (2013). Glioblastoma behaviors in three-dimensional collagen-hyaluronan composite hydrogels. *ACS Appl. Mater. Interfaces* 5, 9276–9284. doi: 10.1021/am402097j

Rape, A., Ananthanarayanan, B., and Kumar, S. (2014). Engineering strategies to mimic the glioblastoma microenvironment. *Adv. Drug Deliv. Rev.* 79–80, 172–183. doi: 10.1016/j.addr.2014.08.012

Rape, A. D., Zibinsky, M., Murthy, N., and Kumar, S. (2015). A synthetic hydrogel for the high-throughput study of cell-ECM interactions. *Nat. Commun.* 6:8129. doi: 10.1038/ncomms9129

Saha, K., Keung, A. J., Irwin, E. F., Li, Y., Little, L., Schaffer, D. V., et al. (2008). Substrate modulus directs neural stem cell behavior. *Biophys. J.* 95, 4426–4438. doi: 10.1529/biophysj.108.132217

Sarkar, S., Nuttall, R. K., Liu, S., Edwards, D. R., and Yong, V. W. (2006). Tenascin-C stimulates glioma cell invasion through matrix metalloproteinase-12. *Cancer Res.* 66, 11771–11780. doi: 10.1158/0008-5472.CAN-05-0470

Seliktar, D. (2012). Designing cell-compatible hydrogels for biomedical applications. *Science* 336, 1124–1128. doi: 10.1126/science.1214804

Shu, X. Z., Liu, Y., Luo, Y., Roberts, M. C., and Prestwich, G. D. (2002). Disulfide cross-linked hyaluronan hydrogels. *Biomacromolecules* 3, 1304–1311. doi: 10.1021/bm025603c

Ulrich, T. A., Jain, A., Tanner, K., MacKay, J. L., and Kumar, S. (2010). Probing cellular mechanobiology in three-dimensional culture with collagen-agarose matrices. *Biomaterials* 31, 1875–1884. doi: 10.1016/j.biomaterials.2009.10.047

Umesh, V., Rape, A. D., Ulrich, T. A., and Kumar, S. (2014). Microenvironmental stiffness enhances glioma cell proliferation by stimulating epidermal growth factor receptor signaling. *PLoS ONE* 9:e101771. doi: 10.1371/journal.pone.0101771

Wang, C., Tong, X., and Yang, F. (2014). Bioengineered 3D brain tumor model to elucidate the effects of matrix stiffness on glioblastoma cell behavior using PEG-based hydrogels. *Mol. Pharm.* 11, 2115–2125. doi: 10.1021/mp500828

Wang, K., Kievit, F. M., Erickson, A. E., Silber, J. R., Ellenbogen, R. G., and Zhang, M. (2016). Culture on 3D chitosan-hyaluronic acid scaffolds enhances stem cell marker expression and drug resistance in human glioblastoma cancer stem cells. *Adv. Healthc. Mater.* 5, 3173–3181. doi: 10.1002/adhm.201600684

Wang, X., He, J., Wang, Y., and Cui, F. Z. (2012). Hyaluronic acid-based scaffold for central neural tissue engineering. *Interface Focus* 2, 278–291. doi: 10.1098/rsfs.2012.0016

Wells, A., Grahovac, J., Wheeler, S., Ma, B., and Lauffenburger, D. (2013). Targeting tumor cell motility as a strategy against invasion and metastasis. *Trends Pharmacol. Sci.* 34, 283–289. doi: 10.1016/j.tips.2013.03.001

Wiranowska, M. R., and Rojiani, M. V. (2011). *Extracellular Matrix Microenvironment in Glioma Progression.* Rijeka: INTECH Open Access Publisher.

Xingliang, D., Cheng, M., Qing, L., and Tao, X. (2016). 3D bioprinted glioma stem cells for brain tumor model and applications of drug susceptibility. *Biofabrication* 8:045005. doi: 10.1088/1758-5090/8/4/045005

Zamecnik, J. (2005). The extracellular space and matrix of gliomas. *Acta Neuropathol.* 110, 435–442. doi: 10.1007/s00401-005-1078-5

Zustiak, S., Nossal, R., and Sackett, D. L. (2014). Multiwell stiffness assay for the study of cell responsiveness to cytotoxic drugs. *Biotechnol. Bioeng.* 111, 396–403. doi: 10.1002/bit.25097

Zustiak, S. P., Dadhwal, S., Medina, C., Steczina, S., Chehreghanianzabi, Y., Ashraf, A., et al. (2016). Three-dimensional matrix stiffness and adhesive ligands affect cancer cell response to toxins. *Biotechnol. Bioeng.* 113, 443–452. doi: 10.1002/bit.25709

Conflict of Interest Statement: The authors declare that the research was conducted in the absence of any commercial or financial relationships that could be construed as a potential conflict of interest.

frontiers in Bioengineering and Biotechnology

REVIEW
published: 04 December 2018
doi: 10.3389/fbioe.2018.00190

Spatio-Temporal Control of Cell Adhesion: Toward Programmable Platforms to Manipulate Cell Functions and Fate

Chiara Cimmino[1,2], *Lucia Rossano*[1,2], *Paolo Antonio Netti*[1,2] *and Maurizio Ventre*[1,2*]

[1] *Department of Chemical, Materials and Industrial Production Engineering, University of Naples Federico II, Naples, Italy,*
[2] *Center for Advanced Biomaterials for Healthcare@CRIB, Fondazione Istituto Italiano di Tecnologia, Naples, Italy*

OPEN ACCESS

Edited by:
Gianni Ciofani,
Politecnico di Torino, Italy

Reviewed by:
Debora Berti,
Università degli Studi di Firenze, Italy
Sandra Camarero-Espinosa,
Maastricht University, Netherlands
Abbas Shafiee,
Queensland University of Technology, Australia

***Correspondence:**
Maurizio Ventre
maventre@unina.it

Specialty section:
This article was submitted to Nanobiotechnology, a section of the journal Frontiers in Bioengineering and Biotechnology

Received: *06 October 2018*
Accepted: *21 November 2018*
Published: *04 December 2018*

Citation:
Cimmino C, Rossano L, Netti PA and Ventre M (2018) Spatio-Temporal Control of Cell Adhesion: Toward Programmable Platforms to Manipulate Cell Functions and Fate. Front. Bioeng. Biotechnol. 6:190. doi: 10.3389/fbioe.2018.00190

Biophysical and biochemical signals of material surfaces potently regulate cell functions and fate. In particular, micro- and nano-scale patterns of adhesion signals can finely elicit and affect a plethora of signaling pathways ultimately affecting gene expression, in a process known as mechanotransduction. Our fundamental understanding of cell-material signals interaction and reaction is based on static culturing platforms, i.e., substrates exhibiting signals whose configuration is time-invariant. However, cells *in-vivo* are exposed to arrays of biophysical and biochemical signals that change in time and space and the way cells integrate these might eventually dictate their behavior. Advancements in fabrication technologies and materials engineering, have recently enabled the development of culturing platforms able to display patterns of biochemical and biophysical signals whose features change in time and space in response to external stimuli and according to selected programmes. These dynamic devices proved to be particularly helpful in shedding light on how cells adapt to a dynamic microenvironment or integrate spatio-temporal variations of signals. In this work, we present the most relevant findings in the context of dynamic platforms for controlling cell functions and fate *in vitro*. We place emphasis on the technological aspects concerning the fabrication of platforms displaying micro- and nano-scale dynamic signals and on the physical-chemical stimuli necessary to actuate the spatio-temporal changes of the signal patterns. In particular, we illustrate strategies to encode material surfaces with dynamic ligands and patterns thereof, topographic relieves and mechanical properties. Additionally, we present the most effective, yet cytocompatible methods to actuate the spatio-temporal changes of the signals. We focus on cell reaction and response to dynamic changes of signal presentation. Finally, potential applications of this new generation of culturing systems for *in vitro* and *in vivo* applications, including regenerative medicine and cell conditioning are presented.

Keywords: dynamic platforms, cell adhesion, switchable signals, ligands, topographic, patterns, substrate stiffness

INTRODUCTION

A major part of our understanding of cell biology is occupied by the effects of soluble signals (drugs, small molecules, peptides, proteins, growth factors) on cell behavior. In fact, several routes have been developed to formulate well-defined media that enabled studying cell response to specific soluble signals systematically (Yao and Asayama, 2017). There are comparatively less studies aimed at investigating the effects of insoluble matricellular signals, in the form of topographic relieves, patterns of biochemical moieties, or mechanical signals, on cell functions. These proved to dramatically affect cell behavior (Ventre et al., 2012). In different biomedical and clinical applications, cells are in close contact with material surfaces that can present one or more signals simultaneously. For instance, prosthetic devices or synthetic scaffolds invariably expose surfaces to the biological environment and the biochemical/biophysical characteristics of the surfaces can have a great impact on the implant performance *in vivo* (Williams and Bhatia, 2014; Rasouli et al., 2018). Therefore, achieving a sound knowledge on the role of material properties on cell functions would provide valuable elements to engineer devices with improved functions. This requires implementing design concepts and fabrication technologies that enable reproducing certain features of the extracellular matrix (ECM) that most effectively affect cell functions and fate. Advancements in materials engineering, functionalization methods and most importantly micro- and nano-fabrication technologies provided researchers with "artificial" alternatives to conventional rigid plates or glass, which more closely mimic the native microenvironment (Leijten and Khademhosseini, 2016). The integration of micro- and nano-engineered platforms with cell cultures not only allowed to elicit specific cellular reactions, thus controlling their functions and fates, but also enabled understanding cell-signal interactions. In fact, micro- and nano-engineered platforms display signals whose spatial arrangement may be targeted to the whole cell, subcellular compartments, cluster of receptors or even individual receptors, thus enabling to achieve a fine-tuning of a broad spectrum of signaling pathways (Dalby et al., 2014; Donnelly et al., 2018). In most of the cases, the signals displayed by materials are static in nature, i.e., once embossed on the culturing platform they cannot be changed in time and space. The native ECM is far from being a static repository of signals, as it constantly changes in time and space in response to or as a part of growth, aging, disease, injuries. For instance, temporal variations of the ECM, including changes in the microarchitecture and stiffness, play an important role in regulating different biological processes *in vivo* including differentiation and morphogenesis, but also the progression of pathologies (Lu et al., 2012; Handorf et al., 2015).

Cell biologists usually relied on reductionist approaches to study cell-signal interactions *in vitro* seeking systems aimed at reducing the complexity of interactions or at eliciting specific cell responses to investigate cell-signal interplay. These systems were instrumental to shape our understanding on the mechanisms underlying cell recognition and reaction to signals, but in most of the cases they are not able to capture specific aspects as multi signal stimulation or dynamic changes. This calls for novel platforms able to more closely mimic the ECM both in terms of signal display and dynamic changes of these signals.

Most of our knowledge on cell-material recognition and response to biochemical/biophysical signals arises from studies performed in two-dimensions (2D). Although most cells live in a three-dimension (3D) context *in vivo*, it is still debated whether adhesion in 3D is identical to a 2D environment or follows different routes (Harunaga and Yamada, 2011; Doyle and Yamada, 2016). This notwithstanding, we prefer to focus our attention on 2D systems as the development of dynamic materials is recent and mostly concerns planar surfaces. Examples of dynamic 3D environments have been already presented which showed enlightening results (Khetan et al., 2013; Das et al., 2016; Brown et al., 2018). However, achieving a precise control on the adhesive processes in 3D at a subcellular level is still challenging. Furthermore, 2D platforms should not be necessarily considered as pure artifacts. Specifically engineered materials proved to be very effective in controlling even complex aspects of cell behavior including stem cell self-renewal, targeted differentiation and morphogenesis (Nikkhah et al., 2012; Ventre et al., 2012; Ventre and Netti, 2016b). These examples have an intrinsic usefulness as the outcomes could be exploited in applications such as drug screening and discovery, cell-based therapies, and tissue engineering.

Increasing the complexity of material substrate to control cell functions and fate *in vitro* with the introduction of dynamically changing signals would better mimic a natural context thus enabling the possibility to guide and stimulate cells with improved effectiveness.

In this review we first illustrate the basic mechanism of cell ECM or material interactions focusing on cell adhesion processes to provide basic guidelines to engineer bioactive platforms to control cell behavior. We also discuss notable examples of cell interaction with "static" platforms to provide insights into cell's reactions and responses to specific signal arrangements, being more details on this aspect reported elsewhere (Bettinger et al., 2009; Ventre et al., 2012; Yao et al., 2013). The central part of the article reviews strategies and technologies to encode dynamic signals on material platforms. In particular, this work focuses on dynamic changes of ligands and their spatial patterns, micro- and submicro-scale topographies and material stiffness. Furthermore, emphasis is given to response of cells to the spatio-temporal changes of signal display. Finally, we will address limits of the current platforms and technologies suggesting possible ways to improve their performances thus creating systems that can affect cell functions in a more thorough and consistent manner.

THE PROCESS OF CELL ADHESION AND CELL RESPONSE TO MATERIAL SIGNALS

Cells interact with the culturing microenvironment, including material surfaces, through an array of receptors that enable perceiving different chemical/physical cues such as roughness, hydrophobicity, ligand density and distribution, stiffness, and charge. The receptors involved in such a process of recognition are located on the cell membrane and they include

immunoglobulin super family of cell adhesion molecules (IgCAMs), cadherins, integrins, selectins, and proteoglycans, as well as non-integrin collagen, laminin, and elastin receptors (Hinek, 1996; Campbell and Humphries, 2011; Humphries et al., 2015; Di Cio and Gautrot, 2016). In particular, the heterodimeric, transmembrane integrin receptors not only are responsible for initiating and maintaining stable adhesion, but take part in the formation of multiprotein signaling hubs that trigger biochemical events that greatly influence cellular behavior (Humphries et al., 2015). While non-specific interactions of cells with materials dominate early adhesion events, stable cell adhesions form when surfaces display ligands to which integrin receptors bind specifically (Cohen et al., 2004; Parsons et al., 2010). Integrins are constituted by α and β subunits. So far, 18 α and 8 β subunits have been identified that can combine to form 24 different receptors with different binding properties (Campbell and Humphries, 2011). Through different combinations of α and β subunits it is possible to determine the affinity of the heterodimer with specific ligands. Several aminoacidic sequences have been recognized to interact with integrins specifically. For example, IKLLI, LGTIPG, LRE, LRGDN, PDGSR, RGD, YIGSR, YKVAV in laminin, DGEA GFOGER and RGD in collagen I and KQAGDV, REDV, RGD, and PHSRN in fibronectin (FN). When sufficiently close to ligands, integrin dimers can acquire an activated form by undergoing to a conformational change that enhances the affinity to ligands and allows the interaction with proteins and signaling molecules from the cytoplasmic side (Calderwood, 2004). After activations, integrins cluster together in discrete locations of the membrane facing the adhesive surface. According to the availability of ligands and stability of the integrin-ligand complex, cluster may mature in focal complexes up to micrometric multiprotein entities named focal adhesions (FAs) (**Figure 1**). Proteins from the cytoplasmic side may stabilize the protein gathering and/or may act as a bridge with the actin cytoskeleton. Integrins, once activated, bind to actin fibers through cytoplasmic proteins such as α–actinin, talin, and vinculin. Cytoskeleton-generated contractile forces promote FA maturation through conformational change of mechanosensitive proteins that modify their functions. For example, vinculin undergoes to a conformational change upon force application, which improves the affinity toward other proteins involved in FA stabilization (Dumbauld et al., 2013). Also, talin possesses cryptic binding sites for vinculin that unfold and become available upon stretching (del Rio et al., 2009). Other examples of mechanosensitive proteins constituting the adhesion plaques are paxillin and p130cas (Janoštiak et al., 2014). Therefore, FAs constitute the gate through which the cytoskeleton interacts with the extracellular environment, allowing the perception of different signals, such as biochemical (ligands density and their spatial distribution) and biophysical (topography and mechanical characteristics), and the reaction to these is accompanied by alterations in FA features, cytoskeleton assembly and cell-generated forces (Geiger et al., 2009).

Moreover, molecules related to FAs are important signaling proteins such as kinases [focal adhesion kinase (FAK), Src] and GTPase (Rho, Rac) that alter their activities when subjected to the mechanical forces exerted by the actomyosin machinery. For example, contractile forces can induce the phosphorylation of additional sites of the Src family kinases substrate p130CAS, which can eventually trigger signal transduction pathways (Sawada et al., 2006). The conversion of mechanical stimuli (either externally applied or cell-generated) into intracellular biochemical events is usually referred to as mechanotransduction (Eyckmans et al., 2011). These mechanical signals are also perceived by the nucleus, as the actin cytoskeleton is connected directly to the nuclear membrane (Isermann and Lammerding, 2013). The nucleus reacts to the forces generated by actin by changing its shape, modifying the assembly of chromatin as well as the accessibility of enzymes and transcription factors, eventually altering gene expression (Li et al., 2011; Gupta et al., 2012; Jain et al., 2013). In this scenario elements affecting cell adhesion (ligand availability and patterning or the transmission of mechanical forces) through biochemical/biophysical signals embossed on material surfaces may enable the activation of intracellular biochemical events ultimately affecting cell behavior in a process that we refer to as the material-cytoskeleton crosstalk (Ventre et al., 2012).

A series of strategies has been developed to control biochemical/biophysical properties of the culturing materials that mostly affect FA formation and growth. The first examples are those concerning functionalization with ligands. Several proteins or peptides involved in cell adhesion process may be linked to the material surfaces by covalent binding or by physical interactions. Arginylglycylaspartic acid (RGD) is among the most studied and used ligand to control cell adhesion (Hersel et al., 2003; VandeVondele et al., 2003). Early studies aimed at identifying the optimal density of the ligands that enable cell adhesion and spreading. In this regard, Massia and Hubbell observed that fibroblasts spreading on glass surfaces required a minimum RGD density of 1.0×10^{-15} mol/cm^2 (corresponding to an interligand spacing of ∼440 nm), while a density of 1.0×10^{-14} mol/cm^2 (interligand spacing of ∼140 nm), was necessary to promote the formation of focal contacts and stress fibers (Massia and Hubbell, 1991). Therefore, precise spatial positioning of adhesive spots may have a profound impact on the process of cell adhesion. Micro- and nano-fabrication techniques have enabled the realization of cell adhesion substrates allowing to modulate the dimension, positioning and spacing of the adhesive zones on a micro- and submicro-scale. For example, block copolymer micelle nanolithography allows to control spacing and density of individual ligands. Through this method, it was proven that adhesion formation occurs in a specific range of interligand densities, i.e., from 58 to 73 nm. Ligand densities surpassing this range cause an excessive adhesion and a decrease of cellular mobility, while lower ligand densities do not allow cell spreading (Arnold et al., 2004). Exerting a tight control on individual FA localization and shape requires achieving a sharp adhesion mismatch on the surface, i.e., zones conducive for FA formation and growth juxtaposed to others not allowing integrin engagement. This prevents FAs to grow and acquire shapes uncontrollably. Surfaces exhibiting micro- or nano-scale relieves in the form of pillars or pits can reproduce such a scenario effectively. In fact, the formation of FAs strongly depends on the geometry of the topography. Proteins and ligands can adsorb

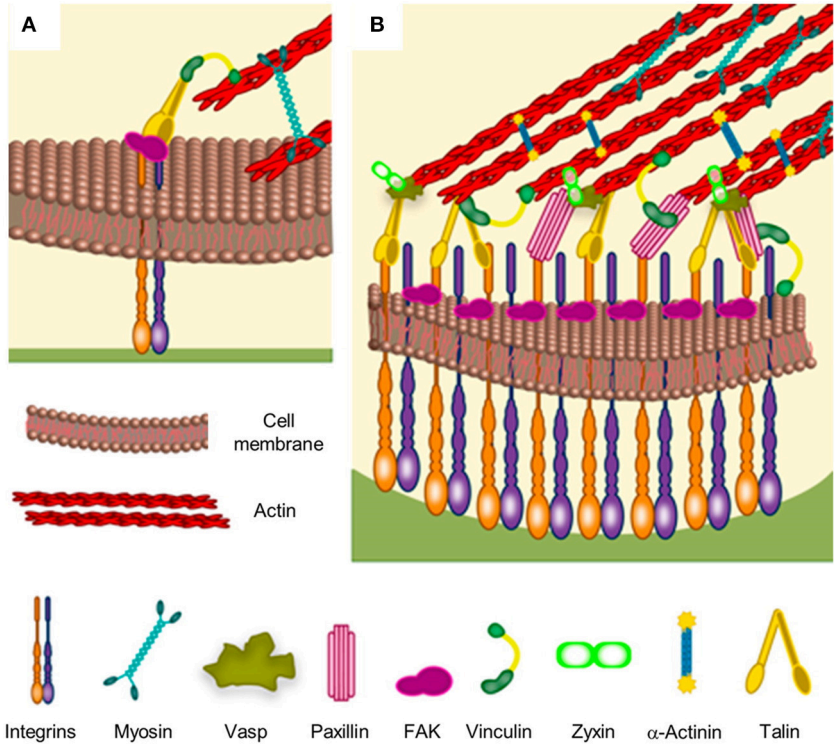

FIGURE 1 | Schematic of focal adhesion formation and maturation. **(A)** Nascent adhesions are thought to form the binding of integrins to extracellular ligands. Additional cytoplasmic components, such as talin, FAK and paxillin are recruited to stabilize the ligand-bound clusters. Myosin-generated forces promote conformational changes of talin, which exposes binding sites for vinculin. Stable clusters can grow further by addition of other integrins and cytoplasmic molecules, thus generating a focal complex and then a focal adhesion. **(B)** The multi-layered structure of a mature focal adhesion comprises proteins with different functions: signaling (integrins, FAK, and paxillin), force transduction (vinculin and talin) and linkers to the cytoskeleton (Vasp, zyxin, and α-actinin). Reprinted with permission from Ventre and Netti (2016b). Copyright 2016 American Chemical Society.

non-uniformly or might not be readily available to cells thus impairing FA dynamics (Lord et al., 2010). There is still a lack of systematic studies that rigorously indicate which combinations of pattern height, spacing and size promote or impair cell adhesion. However, experimental evidences suggest that characteristic dimensions that most effectively interfere with FA dynamics exist, which are suggestive of a possible common mechanism of cellular response to topographies. Examples of insufficient cell adhesion have been reported when cells are seeded on nanoprotrusions with a feature height above 80 nm, as this dimension hampers integrin clustering (Lim et al., 2005b; Biggs et al., 2010). The same situation of insufficient adhesion occurs when cells are grown on pillars whose diameters are <70 nm and the interpillar spacing is >300 nm. FAs formation takes place when integrins are able to bridge the gap between neighboring features or when the distance between these is ∼70 nm (Kim et al., 2005; Lee et al., 2008; Sjöström et al., 2009). Other studies showed that the pitch and size of nanopits are also fundamental parameters in governing cell adhesion. For instance, FAs growth is confined in the interpit area, thus limiting the growth on arrays of nanopits of 100 nm in depth, 120 nm in diameter and 300 nm in spacing arranged in ordered square or hexagonal lattices (Biggs et al., 2007; Dalby et al., 2007).

The geometry of the topographic model, besides influencing the formation of adhesions, strongly affects FAs orientation. In fact, while pillars and pits arrays limit FAs elongation, micro- and nano-gratings guide FAs growth in a specific direction. Directional growth of FAs strongly affects cytoskeleton assembly, as stress fibers are oriented in the same direction of the underlying pattern. In this way the entire cell body assumes an elongated morphology and migrates along the pattern direction. This phenomenon is known as "contact guidance" (Teixeira, 2003; Ventre et al., 2014). This, however, depends on the size and spacing of the topographic features as too wide or too close ridges do not exert an effective confinement on FAs, thus impairing their guiding effect. For example, osteoblasts cultivated on nanogratings with ridge spacing <75 nm allowed integrin clustering over the grooves that caused the cells to respond as on flat substrates (Lamers et al., 2010). Conversely, a change in osteoblast response was observed when lateral spacing exceeded 75 nm. Cells were elongated and coaligned to the pattern direction with ridges and grooves of 80 nm in width or on patterns with 50 nm ridges and 100 nm grooves. Instead, no significant orientation was observed on the pattern with 100 nm ridges and 50 nm grooves (Lamers et al., 2010). In order to visualize the dynamic interplay between

FA formation/maturation and nanogrooved patterns, Natale et al. transfected preosteoblasts with plasmids characterized by fluorescent actin and paxillin (Natale et al., 2014). Actin fibers were observed to bundle and align in directions, not necessarily parallel to the pattern direction. However, fibers oriented in directions other than that of the pattern ended with dashed adhesions that rapidly collapsed under the effect of actin-generated forces. In contrast, the FAs that grew along the direction of the pattern appeared more stable and promoted the formation of actin bundles parallel to the ridges.

The stiffness of the culturing substrate profoundly affects FA morphology and stability (Pelham and Wang, 1997). Usually, cells on rigid materials (plastics, highly crosslinked elastomers, stiff hydrogels) express long and wide FAs connected to well-defined actin bundles. Conversely, cells on compliant substrates (scarcely crosslinked elastomers or soft hydrogels) possess punctuate and highly dynamic FAs and a destabilized cytoskeleton (Ventre and Netti, 2016b). The molecular mechanisms underpinning cell recognition of stiffness are not thoroughly clear as some evidence suggests that different stiffnesses lead to differences in anchoring densities of proteins thus interfering with sensing, whereas other authors report that cells react to changes in stiffness independently from ligand anchoring (Trappmann et al., 2012; Wen et al., 2014). However, the extent of contractility generated on either soft or stiff substrates differently activates mechanotransduction events at FA or nuclear level, ultimately affecting cell functions and fate (Engler et al., 2006; Anderson et al., 2016).

Surface engineering has benefitted from these observations because the material characteristics may be modified in order to influence the dynamic formation and maturation of the FAs hence affecting the activity of the signaling proteins or altering the structure and contractility of the cytoskeleton. Today, concepts as ligand density and patterning, topography and roughness, or material stiffness are regarded as crucial players in affecting various aspects of cell behavior ad are increasingly taken into consideration when designing experiments aimed at capturing certain features of the ECM. However, as the response to soluble drugs or factors depends on their dose and temporal delivery, it is clear that the static presentation of biochemical/biophysical material signals does not fully mimic the dynamic nature of the native microenvironment and might lead to abnormal or non-physiologic reactions. This calls for novel culturing systems conceived to display biochemical/biophysical material signals according to predefined spatio-temporal programmes.

GENERAL CONCEPTS ON DYNAMIC SUBSTRATE ENGINEERING

Synthetic materials with properties that are static in time are often inadequate for mimicking natural cell environments, where temporal changes in chemical and physical properties are important in a wide variety of contexts including development, differentiation, morphogenesis, diseases progression, wound healing, and homeostasis (Frantz et al., 2010; Lu et al., 2011; Bonnans et al., 2014; Kular et al., 2014). To assess the role of the dynamic changes of the biochemical/biophysical microenvironment on cell behavior, the development of platforms enabling a fine control on the spatio-temporal presentation of adhesion sites is key central. Recent developments in materials engineering have led to a variety of approaches in which material properties can be dynamically and reversibly modified in response to user-directed stimuli such as light, temperature, pH, or other external fields (Roy et al., 2010; Stuart et al., 2010). Concerning the fabrication of responsive biomaterials for dynamic signal presentation, different chemical/physical characteristics of the substrate, as well as those of the external stimulus, must fulfill specific requirements. Responsive materials may contain moieties responsible for endowing the materials with the dynamic behavior (Liu and Urban, 2010). These moieties do not have to harm cells whether inactive or activated by an external stimulus. Furthermore, the latter does not have to hamper cell viability by itself or does not have to cause leaching of toxic substances from the material. For instance, temperature or pH responsive materials should perform the intended transformations in a limited range of temperature or pH values (Watanabe and Okada, 1967; Kruse et al., 2017). Similarly, light can only be used at specific wavelengths and intensities (Masuma et al., 2013). Additionally, the choice of employing a particular stimulus may be dictated on whether a uniform or local material actuation is necessary. For instance, temperature and electric fields can be suitable for activating substrates uniformly, whereas laser beam can act locally. This can enable dynamic exposure to signals at a cellular or subcellular level. However, additional devices, such as UV masks or electrodes, can be employed to force the external field to act locally rather than uniformly. Alternatively, the responsive moieties could be spatially patterned thus causing the culturing platforms to be responsive in selected regions only (*vide infra*). Literature is sometimes ambiguous on the term static and dynamic (referred to signal presentation). We here refer to dynamic presentation when signals and more specifically adhesive signals significantly change configuration and or location in a way that cells recognize such a change and modify their behavior accordingly. The extent of change in signal display depends on the specific context that has to be analyzed as changes may occur on different length or time scales (receptor-whole cell level; seconds to weeks).

In what follows we present consolidated strategies along with the recent developments for engineering synthetic substrates displaying signals dynamically. More specifically, we will focus our attention to those signals directly affecting cell adhesion events at different length scales: from FA to whole cell level. We will therefore emphasize the role of dynamic display of biochemical (ligands), topographic and mechanical signals on cell adhesion, spreading, migration, and differentiation.

DYNAMIC DISPLAY OF LIGANDS

Self-assembled monolayers (SAMs) are one among the first and perhaps most used and studied platforms to enable signal

display dynamically. SAMs can be defined as orderly assemblies of molecules formed by the adsorption of an active surfactant on a solid surface (Ulman, 1996). The molecular structure of the individual building blocks that form SAMs can be divided in three parts: a head that binds to a substrate (generally a metal); a central part acting as spacer, whose chemical properties determine the interactions with the surrounding molecules, ultimately defining the packing and stability of the monolayer, which is usually achieved by van der Waals attractive forces between adjacent chains or by the introduction of specific intermolecular interactions; a tail group which can be inert, bioactive or susceptible to functionalization (Ulman, 1996; Srisombat et al., 2011). The composition of SAM-based platforms can be predetermined and the chemical properties can be considered uniform over relatively large areas. Furthermore, SAMs are prone to additional functionalization or patterning after they are formed (Mrksich, 2009). These are fundamental requirements to fabricate artificial platforms to study cell adhesion events or cell response to specific arrangements of ligands in a systematic manner. Examples of SAMs used as cell culture substrates are thiol or silane head groups derivatives on gold or silicon, respectively (Schreiber, 2004; Onclin et al., 2005). Oligo(ethylene glycol) SAMs were used as non-fouling protein surfaces and consequently cell repellent substrates. Alternatively, a number of biomolecules, including DNA, RGD, Laminin-derived Peptide PA22-2, FN, Vascular Endothelial Growth Factor, have been used to bioactivate SAM surfaces on active groups present on the molecules tail (Bamdad, 1998; Liu et al., 2007; Mendes, 2008; Jans et al., 2009; Mrksich, 2009; Afara et al., 2012).

Another method to fabricate cell culturing substrates is polymer casting. Surfaces of cast polymer are compatible with functionalization techniques such as chemical grafting or topographic embossing (Vendra et al., 2011). Phase separation of polymers is a fast and reliable method that enables controlling the morphology and dimensions of micro- and nano- domains in the polymer, which affect surface topography and protein adsorption thus impacting on cell adhesion and eventually cell fate (Lim et al., 2005a; Krishnamoorthy et al., 2006; Frith et al., 2012).

The synthesis of polymer brushes, i.e., thin coatings made of polymer chains covalently attached to a substrate, represents a versatile method to fabricate controlled environments for cell cultures (Chen et al., 2017). Chains can be attached directly to reacting substrates (grafting-to) or might be allowed to polymerize from surface anchored initiators (grafting-from). In both cases, the density of polymers should be sufficiently high to force polymer chains to be in a stretched form, preventing chain collapse in a random coil form. Of the two methods, grafting-from produces high density brushes as preformed polymers in the grafting-to method can be displaced apart owing to steric hindrance (Advincula, 2004). Several parameters related to polymer brush processing including, chain architecture and length, density, functionalization, all proved to significantly affect cell adhesion and behavior (Krishnamoorthy et al., 2014). The development of new synthetic routes allowed to tune these properties, thus leading to the fabrication of culturing platforms with tailored signal display (Chen et al., 2017; Feng and Huang, 2018).

Besides solid substrates, the functionalization of hydrogel surfaces has been successfully used to control local chemical/physical properties of the culturing microenvironment (DeForest and Anseth, 2012; Guvendiren and Burdick, 2013a). Both synthetic and natural hydrogels emerged as versatile and promising system for cell culture since they mimic important aspects of the native ECM such as mechanical properties, viscoelasticity, porosity, along with their ability to sequester proteins and growth factors (Caliari and Burdick, 2016). From a practical standpoint, macromolecules constituting hydrogels can be extensively modified (in pre- or post-processing) thus allowing to tailor the chemical, physical properties of the network in an orthogonal manner and to endow the substrate with complex functions (Kharkar et al., 2013; Ventre and Netti, 2016a). Hydrogels find their natural application field as 3D cell culturing systems. However, they are also useful to study certain cell behaviors in 2D such as mechanosensing and mechanotransduction that require substrate stiffness to be finely tuned (Thiele et al., 2014).

Electrically Controlled Presentation of Ligands

Although SAMs were originally intended as static surfaces, the incorporation of moieties in the polymer chains that induce conformation changes, bond breaking or react with other species under external stimuli, endows SAM-based surfaces with dynamic behavior. In a seminal work by Jiang et al. electrical desorption of SAMs was used to fabricate dynamic surfaces to study bovine capillary endothelial cell migration (Jiang et al., 2003). Micro-printed patters of protein repellent alkanethiols [$HS(CH_2)_{11}(OCH_2OCH_2)_3OH$ and $HS(CH_2)_{17}CH_3$] on gold confined cells in specifically designed rectangles. The application of a cathodic voltage pulse (−1.2 V) caused the alkanethiols to desorb. In the absence of a protein repellent layer, soluble FN in the medium readily adsorbed on the bare gold enabling the cells to move from the initial rectangle onto the newly available adhesive regions (**Figure 2**). Authors from the same research group exploited this strategy to investigate the effect of cell shape on migration and in particular on the initial direction of displacement (Jiang et al., 2005). The authors printed via microcontact printing (μCP) adhesive islets of different shapes (either symmetric circles, rectangles, squares or asymmetric teardrops, wide drops, narrow drops, triangles). By analyzing the Golgi apparatus, centromere and cell centroid positioning the authors noticed that cells had a marked tendency to displace toward the blunt end of the drop-like shapes. The authors suggested that the shape asymmetry was sufficient to bias the direction of motion. The combination of μCP and electrically switchable SAMs, makes this method a robust platform that enables studying cell dynamics without possible complications arising from cell-cell contacts. However, once SAMs desorb, adhesion patterns cannot be restored. An attempt to integrate electric signal switch and reversibility was proposed by Yeo et al. who fabricated hexadecanethiol-based SAMs on gold incorporating O-silyl hydroquinone moiety functionalized with RGD (Yeo et al., 2003). The application of an electric

potential to the substrate causes the oxidation of the O-silyl hydroquinone group yielding the corresponding benzoquinone with the hydrolysis of the silyl ether and the release of the RGD (**Figure 3A**). To prove the validity of the proposed scheme, the authors micropatterned SAMs in the form of 220 μm discs of hexadecanethiol on gold and the remaining regions were filled with a monolayer of RGD electroactive alkanethiolate as described above (**Figure 3B**). The system was coated with FN, which favored homogeneous adhesion of Swiss 3T3 (**Figure 3C**). The application of an electric potential of 550 mV released the RGD, thus promoting cell detachment. Only the cells on the non-electroactive patterned discs remained in place (**Figure 3D**). RGD functionalized cyclopentadiene moiety was then supplemented to the culture medium; this reacted with the benzoquinone tails by means of a Diels-Alder reaction. Microscopic observations revealed cells that invaded the newly formed RGD activated regions (**Figure 3E**). The authors showed an on-off-on pattern of signal display; this, however, required additional steps involving the introduction of specifically synthesized chemicals. A further development of this scheme involved the use of either electroactive RGD tagged quinone ester or the conventional O-silyl hydroquinone (Yeo and Mrksich, 2006). The former releases the RGD under reductive potentials, as opposed to the latter that is sensitive to oxidative potentials (**Figures 4A,B**). To prove selective release of fibroblasts from the substrate the authors micropatterned circular SAMs on gold with either of the two electroactive alkanethiolates all of them displaying RGD. Swiss 3T3 fibroblasts adhered on the micropatterned regions only (**Figure 4C**). Applying either a negative or positive potential caused selective detachment of cells from the electroactive quinone ester or O-silyl hydroquinone moieties, respectively (**Figure 4D–F**). These studies demonstrate the effectiveness of using small voltages to trigger dynamic surfaces. Furthermore, the electric potentials applied are compatible to cell culturing conditions.

A possible drawback of electric desorption of SAMs consists in the impossibility to change the electric potential locally thus achieving a spatial control on the desorption, unless networks of electrodes are assembled together (Yoon and Mofrad, 2011). A possible solution to this issue was proposed by Ng et al. who extended the concept of electrically switching surfaces (Ng et al., 2012). Rather than controlling chemical reactions with electric potentials the authors fabricated charged hexa(ethylene glycol) based SAMs on a silicon electrode. Charged moieties (either sulfonate or ammonium) were conjugated at the distal end of the SAM chains that were juxtaposed to chains terminating with GRGDS adhesive peptide. When the system was subjected to an electric potential of the same polarity as the charged moiety, then polymeric chains projected out masking the neighboring ligands. Conversely, reversing polarity caused the chain to fold back, leaving exposed and accessible the ligands. The authors also created patterns of cationic and anionic regions and were able to revert cell-adhesive/cell-repellent zones dynamically and reversibly.

Photo-Controlled Presentation of Ligands

The use of light as a possible trigger for dynamic surfaces has attracted considerable interests since it in principle allows to directly implement spatial patterns of "switched on-off" signals by controlling the exposure of the irradiating light with (for example) a photomask. This is a substantial advantage as opposed to electrical controlled surfaces for which case embossing adhesive patterns of signals could require the design of complex networks of electrodes or additional manipulations of the substrate with, for instance μCP.

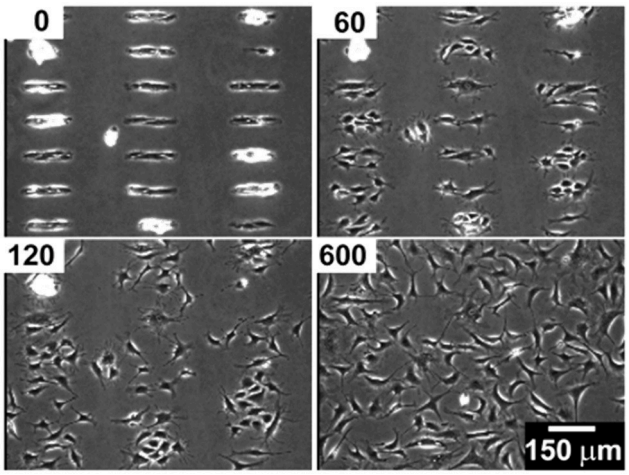

FIGURE 2 | Bovine capillary endothelial cells adhered on a micropatterned gold substrate backfilled with a cell repellent ethylene glycol-terminated SAMs. Application of a −1.2 V voltage pulse (30 s) caused SAMs desorption and subsequent protein adsorption on the bare gold. This enabled cells attachment and migration on previously inert areas. Top left insets indicate the minutes elapsed after the voltage pulse. Reprinted with permission from Jiang et al. (2003). Copyright 2003 American Chemical Society.

Using UV irradiation of a conventional microscope, Nakanishi et al. were able to emboss microscale patterns on alkylsiloxane based SAMs on glass, displaying a photocleavable 2-nitrobenzyl tail group (Nakanishi et al., 2006). Coating the photocleavable SAM with bovine serum albumin (BSA) prevented cell adhesion. Conversely, exposure to a 365 nm UV radiation caused tail cleavage, BSA release and exposure of OH groups. Fibronectin solubilized in the medium adsorbed on the photocleaved regions enabling adhesion. UV exposure can be performed directly, thus activating a wide area or through a photomask. In this case, microscale features could be formed enabling to study cell dynamics at a single or even at a subcellular level. In particular, HEK293 cells on a square array of 6 μm^2 adhesive islets formed FAs on the patterned islets only, whereas they were able to stretch and spread across the non-adhesive areas. These data confirm that photomasking enables achieving sufficient spatial resolution to study cell adhesion at a FA level dynamically (Nakanishi et al., 2006). The same group exploited a similar technique to study cell migration and membrane extension on the dynamic surfaces (Nakanishi et al., 2007). In this case, Pluronic 108 was used as cell repellent backfill. NIH3T3 cells were first seeded on 25 × 25 μm^2 squares and then UV light was directed in order to form either a 25 or 5 μm wide stripe protruding out the edge of the original square. In the case

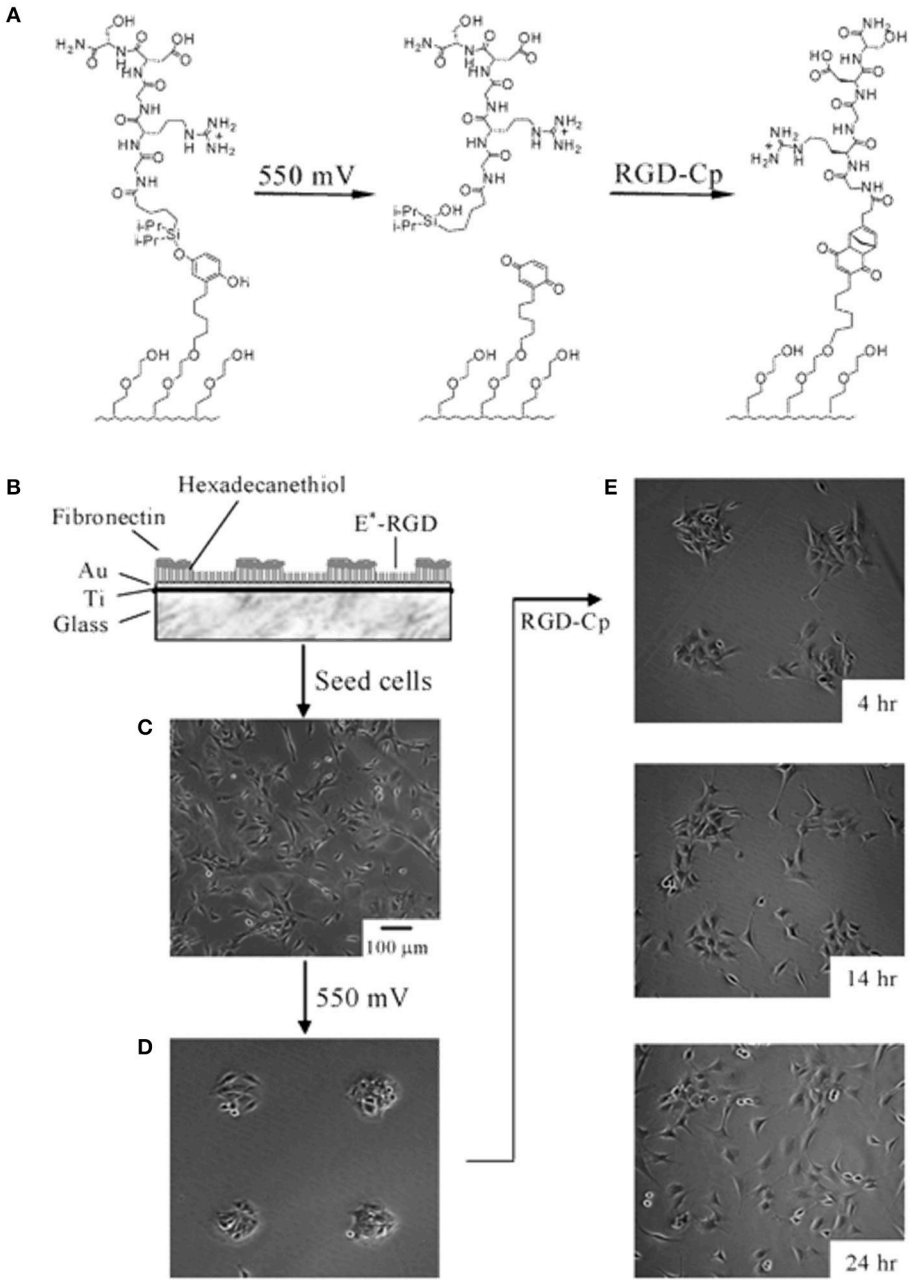

FIGURE 3 | Electrochemical release of ligands. **(A)** A SAM presenting the O-silyl hydroquinone when subjected to a 550 mV voltage oxidizes to benzoquinone, with hydrolysis of the silyl ether and release of the RGD ligand. The resulting benzoquinone may react with soluble cyclopentadiene-tagged RGD via a Diels-Alder reaction, which immobilizes the second ligand. **(B)** Illustration of the dynamic substrate combining the electrochemical release of RGD ligands and of the cells with the (secondary) immobilization of RGD ligands. A SAM was patterned into FN coated circular regions surrounded by RGD tethered with an electroactive linker (E*-RGD). **(C)** Swiss 3T3 fibroblast cells adhered to both FN and E*-RGD over the SAM substrate. **(D)** An electrical potential of 550 mV applied to the gold substrate for 5 min caused RDG and cell release, whereas cells on FN patterns remained attached. **(E)** Supplementation with soluble cyclopentadiene-tagged RGD caused the secondary immobilization of the ligand restoring cell adhesion and migration. Adapted with permission from Yeo et al. (2003). Copyright 2003 American Chemical Society.

of square patterns, cells spread over the entire new bioadhesive area, displaying actin bundles with FA oriented at various angles at their termini. Conversely, NIH3T3 cells displayed long protrusion along the narrow stripe with coaligned FAs and actin bundles. Photoactivated desorption of cell repellent compounds possesses the great advantage of allowing a greater level of spatial control of the adhesive properties of the substrate. Cellular and subcellular resolution can be achieved using conventional apparatuses. However, the methods illustrated so far still rely on the non-specific adsorption of adhesion moieties

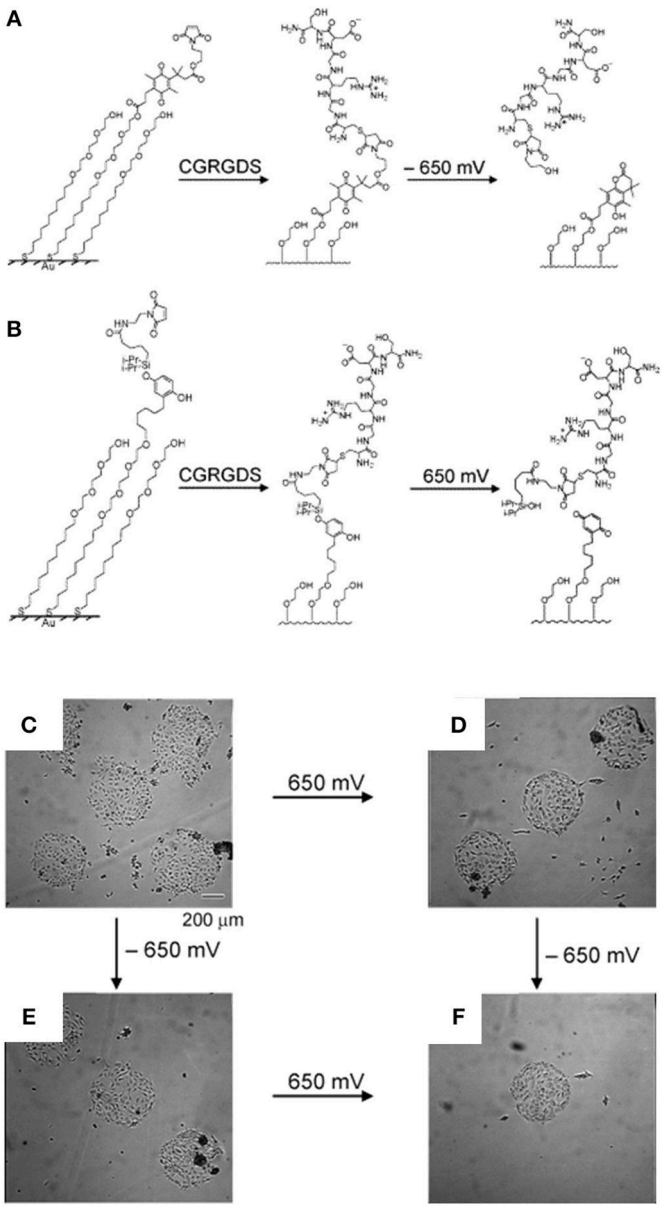

FIGURE 4 | Dynamic substrates for the selective release of ligands in response to applied potentials. **(A)** A SAM presenting a RGD ligand tethered to an electroactive quinone ester. Upon application of the negative voltage causes reduction of the quinone to the corresponding hydroquinone, a cyclization reaction gives a lactone with the release of the RGD ligand. **(B)** A SAM presenting a RGD ligand tethered to an electroactive O-silyl hydroquinone. Application of the positive voltage causes electrochemical oxidation to give a benzoquinone, with the hydrolysis of the silyl ether and the ligands. Effects of the selective electrochemical release of ligands on cell adhesion. **(C)** Swiss 3T3 fibroblasts adhere to circular patterns containing either electroactive O-silyl hydroquinone or quinone ester. **(D)** After application of 650 mV potential, cells detached only from regions presenting the electroactive O-silyl hydroquinone. **(E)** The application of −650 mV potential caused cell release of cells from the regions presenting the electroactive quinone ester only. **(F)** The subsequent application of a potential of −650 mV **(D)** or 650 mV **(E)** results in an additional release of cells. Reprinted (adapted) with permission from Yeo and Mrksich (2006). Copyright 2006 American Chemical Society.

from the medium which could be susceptible to cell-mediated remodeling.

In order to control cell-material adhesion at the molecular level directly and irrespective of influences arising from material properties Petersen et al. exploited a photosensitive ligand caging strategy (Petersen et al., 2008). The authors synthesized a cyclo(-Arg-Gly-Asp-D-Phe-Val) c-(RGDfK), which shows improved affinity for the $\alpha_V\beta_3$ integrins, protected with a photolabile 3-(4,5-dimethoxy-2-nitrophenyl)-2-butyl ester attached on the Asp residue of the ligand. A tetra(ethylene glycol) linker was anchored to a silica surface from the one side, whereas the caged ligand was on the tail side. 3T3 fibroblasts were seeded on the substrate before and after irradiation with UV at 351 nm. The authors found

more than 10-fold increase in adhered cells on substrates exhibiting the ligand in the active form. Furthermore, the authors used photomasks to activate the substrate on selected regions and, as expected, cells adhered on the exposed ligands predominantly. However, a degree of non-specific adhesion was observed on non-irradiated areas especially at longer culturing times.

Light irradiation may also drive conformation changes of sensitive moieties. Displacement caused by the change in molecular conformation can be exploited to alter the chemical-physical properties of material surfaces. Spiropyran or azobenzene are two molecules that were extensively used for this specific purpose (Klajn, 2014; Fedele et al., 2018; Landry et al., 2018). In the context of cell adhesion, Higuchi et al. coated glass plates with a copolymer of nitrobenzospiropyran and methyl methacrylate (Higuchi et al., 2004). This copolymer can be subjected to the reversible transformation from a hydrophobic spiro conformation to a hydrophilic zwitterionic merocyanine isomer by means of irradiation of UV light. The authors first demonstrated the reversibility of the transition (which required at least 24 h in a dark environment) and then proved KUSA-1 cells detachment after a 4-min irradiation with light. Additionally, the authors also reported fibrinogen and platelet detachment. Edahiro et al. synthesized a photoresponsive cell culturing surface composed of poly(N-isopropylacrylamide) with nitrospiropyran as actuating element attached as side chain on the supporting polymer (Edahiro et al., 2005) (**Figure 5**). The authors showed that CHO-K1 cells persisted on the UV irradiated regions of the material, whereas a low temperature washing detached cells. The system proved to be reversible as irradiation with visible light at 400–440 nm released the cells immobilized on the preceding UV exposure. While this system is sufficiently versatile enabling spatial patterns of cell adhesion sites, it requires additional steps of low temperature cell washings to achieve a complete reversibility.

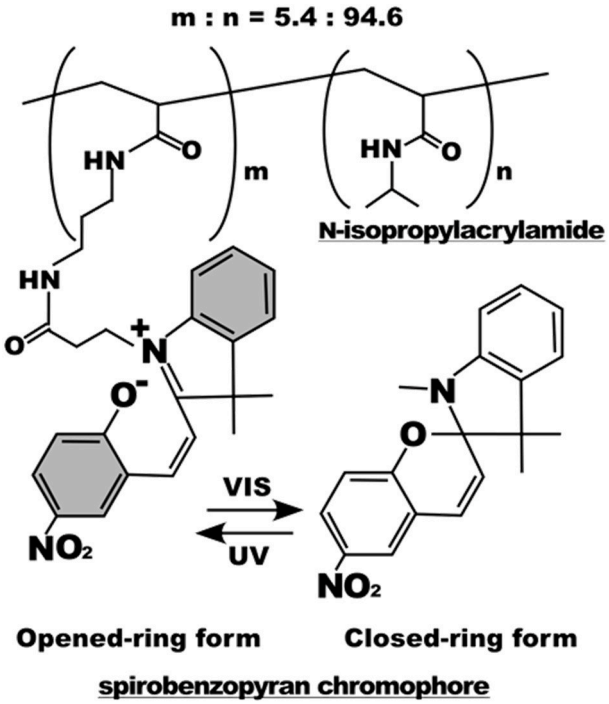

FIGURE 5 | Chemical structure of the poly(N-isopropylacrylamide) with nitrospiropyran chromophore sidechains. Below, photoisomerization scheme of the nitrospiropyran chromophore. Reprinted with permission from Edahiro et al. (2005). Copyright 2005 American Chemical Society.

The light induced *cis-trans* isomerization of azobenzene derivatives has been extensively used into biopolymers to change their structure in a controlled manner (Zhang et al., 2017). Exploiting this peculiar characteristic Auernheimer et al. were able to change distance and orientation of RGD ligands thus affecting cell attachment on poly(methyl methacrylate) (Auernheimer et al., 2005). The authors used 4-[(4-aminophenyl)azo]benzocarbonyl photoswitch as actuating element of spacers with different lengths containing an acrylamide anchor and a cyclic RGD tail (**Figure 6A**). Improved adhesion of MC3T3-E1 preosteoblasts were observed for all the spacers used when the azobenzene was in the *trans* configuration (i.e., after irradiation at 450 nm). Conversely, a general decrease in adhesion was observed when the azobenzene was in the *cis* state, which caused spacer shortening and decreased accessibility to the ligand (**Figure 6B**).

Similar to the approach of Auernheimer et al., Liu et al. designed and fabricated SAMs an Au containing alkanethiols with azobenzene groups and functionalized with GRGDS (Liu et al., 2009). Changing the conformation of the azocompound through light irradiation caused the ligand to be either exposed on the surface (in the *trans* configuration) or hidden in the SAM (in the *cis* configuration). The authors demonstrated that the SAM reversibly enabled/impaired adhesion of NIH3T3 in a time-frame of few hours. Also, in this case, changes in the orientation and conformation occurring at the molecular level are sufficient to alter cell adhesion. Adhering cells could be detached by supplementing the culture medium with soluble GRGDS at pH 8.0. In this condition, the soluble ligand competes with the bound one. After detachment azomolecules could be switched to the *cis* isomer thus hiding the ligand and reducing cell attachment consequently. After irradiating with visible light, azomolecules reverted to the *trans* form, which once again enabled cell adhesion. In this case reversibility is subjected to additional steps therefore this method cannot be considered as fully reversible. RGD ligand burying into a polyelectrolyte multilayer (PEM) was exploited to reversibly modulate NIH3T3 cells adhesion with UV light irradiation (Goulet-Hanssens et al., 2012). Differently from solid substrates, PEMs enable modifying the stiffness according to the processing conditions such as layer numbers and pH.

Changes in azomolecule conformation were also exploited to modulate adhesion on SAMs through a host-guest approach (Gong et al., 2011). Gong et al. synthesized α-cyclodextrins on alkanesilane molecules to form SAMs on SiO_2. This template enabled the formation of inclusion complexes with azobenzene-GRGDS via host-guest recognition. Stable

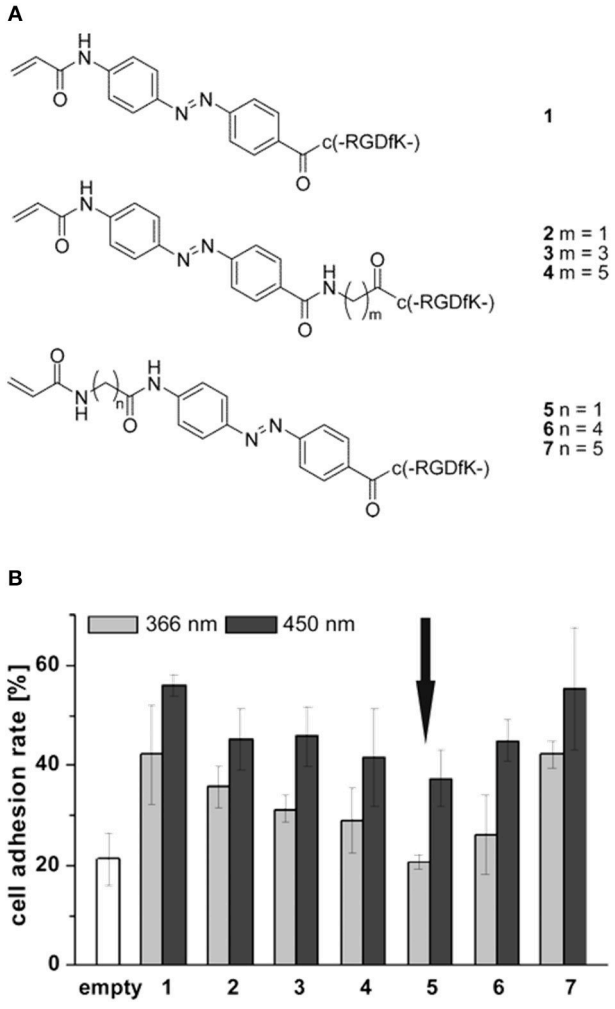

FIGURE 6 | (A) Set of cyclic RGD peptides tethered to a photoswitchable 4-[(4-aminophenyl)azo]benzocarbonyl unit. Spacer length varies according to m or n value and on the isomerization of the switch. **(B)** Effects of spacer length and conformation on MC3T3 adhesion on PMMA. Substrates were irradiated for 3 h at 450 nm (dark gray column) and overnight at 366 nm (light gray column), respectively. Arrow indicates comparable level of cell adhesion with respect to the uncoated material (white column). Adapted with permission from Auernheimer et al. (2005). Copyright 2005 American Chemical Society.

complexes were formed when the azomolecule was in the *trans* configuration allowing ligand display. In this setup HeLa cells effectively adhered and spread on the substrates. However, upon irradiation with UV at 365 nm for 10 min (a condition not harming the cells) caused an extensive cell detachment.

Temperature Controlled Presentation of Ligands

The ability of certain polymers to significantly change conformation and packing with temperature was exploited to modulate polymer-protein interactions and hence cell adhesion to the polymer layer. One of the most effective temperature responsive polymeric systems for cell cultures is the poly(N-isopropylacrylamide) (PNIPAM) showing a lower critical solution temperature (LCST) around 32°C, a temperature that does not alter cell viability significantly. Okano's group pioneered the use of PNIPAM to revert the adhesion of confluent cell layers enabling their detachment from culturing plates (Yamada et al., 1990). This represents a crucial step for harvesting cell layers for cell sheet engineering processes. Briefly, electron beam grafted PNIPAM onto conventional PS dishes allows cell adhesion and proliferation at temperatures above the LCST. In this case, PNIPAM is stabilized by hydrophobic interactions that exclude water from the polymer network (**Figure 7A**). Fibronectin firmly adheres to the hydrophobic network promoting cell adhesion. When cooled below the LCST, interchain H-bonds form allowing network swelling with the inflow of water. This conformational change causes the desorption of FN and subsequent detachment of the cells. The system can be reversibly made hydrophobic by re-heating the network above the LCST (**Figure 7B**). Such an elegant method proved to be effective in detaching large confluent cell sheets without applying mechanical stresses possibly harmful for the cells (Tang and Okano, 2014). This enables the manipulation of macroscopic layers for cell sheet engineering applications (**Figure 7C**). The same group demonstrated a similar mechanism of action by conjugating RGD on temperature responsive P(NIPAM-co-2-carboxyisoprpylacrylamide) (Ebara et al., 2004). Cell adhesion, spreading and proliferation were observed above the LCST. Below this threshold, however, network swelling caused mechanical disruption of RGD-receptor couplings along with shielding RGD sequences from integrin engagement. Generally, changes in temperature cannot be focused in selected part of the samples, therefore local actuation cannot be achieved straightaway. However, conjugating signal patterning and temperature responsive polymers partly solved this issue (Williams et al., 2011).

Enzyme and Mechanical Control of Ligand Presentation

Cells contribute with external stimuli and insults to reconfigure ECM structure dynamically. Common strategies cells pursue to remodel the environment include the secretion of enzymes cleaving ECM proteins and the application of mechanical forces (Janmey and Miller, 2011; Bonnans et al., 2014). Enzymes are characterized by a high selectivity and work in mild, physiologic conditions, making them ideal candidates to trigger the activity of responsive biomaterials. Using the approach of exposing adhesion sites with proteolytic enzymes, Todd et al. exploited the cleaving activity of chymotrypsin to convert a cell repellent polyethylene glycol (PEG)-based polymer film into a bioactive support (Todd et al., 2007). Briefly, a PEG-acrylamide film was spin coated onto an epoxy-functionalized glass. RGD was attached onto the film and capped with a large 9-fluorenylmethoxycarbonylphenylalanine group. The exposure of the film to chymotrypsin caused the enzyme to selectively remove the capping group making the RGD ligand available for

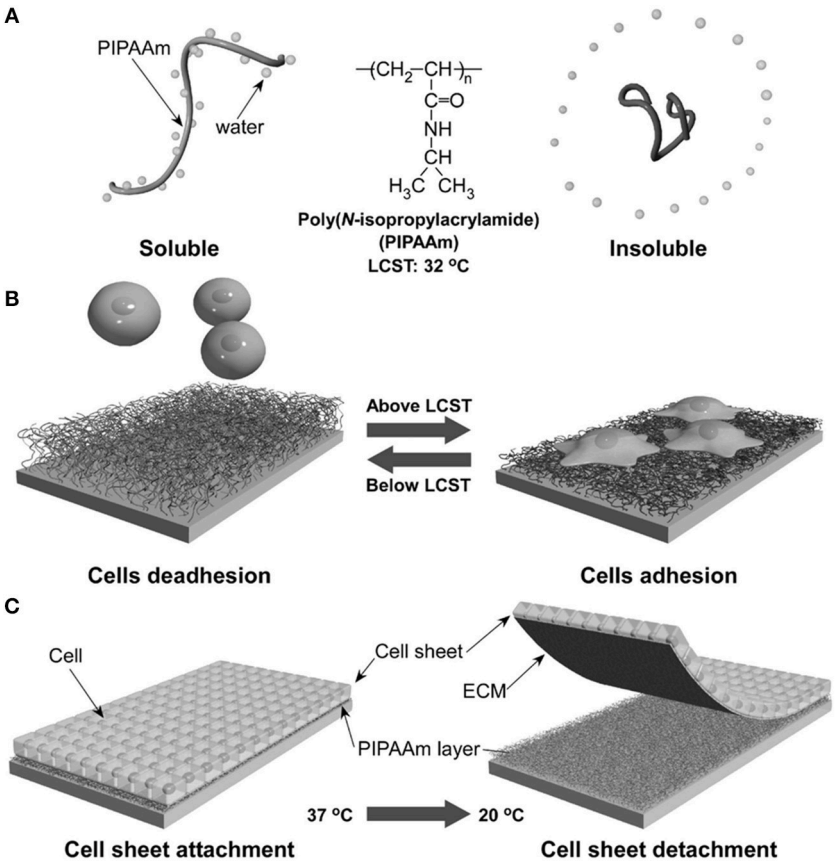

FIGURE 7 | Schematic illustration of the temperature-responsive behavior of PNIPAM. In aqueous solution and above LCST, PNIPAM is stabilized by hydrophobic interactions excluding water **(A)**. This causes FN adsorption and cell adhesion. Conversely cooling below the LCST promotes water inflow and FN release with consequent cell detachment **(B)**. Confluent layers of adhering cells can detach from PNIPAM-grafted substrates when decreasing temperature from 37 to 20°C **(C)**. Reprinted from Tang and Okano (2014).

integrin engagement and cell adhesion. This work demonstrated the feasibility of exploiting the biological activity of molecules to activate dynamic platforms, paving the way toward the development of systems activated on-demand by cell secreted molecules. However, while this system can be conveniently classified as dynamic, it is non-reversible since once unprotected by the enzyme activity the ligands cannot be capped reversibly.

More recently, Roberts et al. exploited enzyme switchable substrates to investigate and manage the delicate adhesion/cytoskeleton balance regulating quiescence or differentiation of human multipotent mesenchymal stromal cells (hMSCs) (Roberts et al., 2016). Glass substrates were functionalized with multifunctional chains constituted by a PEG linker, an RGD peptide, a dialanine cleavable site and either a fluorenylmethyloxycarbonyl blocking group or a PEG adhesion reducing moiety at the distal end. The introduction of elastase cleaves the dialanine site exposing the RGD that allows the transition from a "low" to a "high" adhesion state. hMSCs on platforms in a "low" configuration express β_1 rich FAs and negligible bone morphogenetic protein (BMP) receptor colocalization. Conversely, hMSCs on enzyme activated substrates expressed β_5 rich FAs and increased BMP signaling. Altogether, these data suggest that low (but not null) adhesion prevents metabolome activation for osteogenesis, whereas high adhesion increases BMP signaling through increased levels of intracellular tension. This work demonstrated how delicate the adhesion/tension balance is and subtle perturbations can result in differentiation of stemness maintenance. Only advanced dynamic platforms as the one here described can provide a reliable testing platform to unravel the complex mechanisms underpinning fate decisions.

Several natural biomolecules change their affinity with other molecules or functions when subjected to mechanical stretching (Sawada et al., 2006; del Rio et al., 2009; Singh et al., 2010; Janoštiak et al., 2014). Exploiting such a biomimetic route Bacharouche et al. fabricated an elastomer-based device in polydimethylsiloxane (PDMS) whose adhesion properties changed dynamically and reversibly according to the device deformation (Bacharouche et al., 2013). The authors grafted in sequence PEG chains under elastomer stretching and then RGD was conjugated to chains. In a relaxed state the ligand resulted embedded in the PEG brushes. When the elastomer was

subjected to stretching, RGD became exposed and accessible. Human osteoprogenitor cells firmly adhered to the PDMS in the stretched form and expressed talin rich and well-defined FAs. In the relaxed state cells became round showing a diffuse talin staining all along the cortical region. This suggests that integrin disengagement from the concealing ligands destabilize FAs thus leading to cell detachment. Surface deformation is also responsible for the redistribution of material elements. For example, uniaxial deformation causes material elongation along the stretching direction and a contraction in the orthogonal direction. Following this observation Deng et al. investigated how cells reacted to continuously and reversibly variable interligand spacings (Deng et al., 2017). They transferred a quasi-hexagonal pattern of RGD functionalized gold nanoparticles spaced 35 nm apart (a spacing permissive for adhesion formation) on a highly stretchable poly(N-acryloyl glycinamide) hydrogel. Macroscopic stretching causing a ligand separation above 70 nm impaired the formation of stable adhesions in MC3T3 cells even if the spacing in the orthogonal direction was below 70 nm. Reversing stretching-relaxation forced the REF 72 cells to first acquire a polarized shape and a highly motile behavior and then (after relaxation) to display a spread shape and more stationary behavior. Therefore, not only cells show an extraordinary sensitivity to nanoscale spacing of ligands, but also they finely discriminate spatial variations in the distribution.

Cell-Mediated Remodeling of Ligand

The platforms illustrated so far enable a dynamic display of signals, but do not allow a cell mediated, spatio-temporal redistribution of these. This becomes a critical issue for investigating biologic phenomena such as cell remodeling of ECM or for assessing the role of receptor clustering in signal transduction. To address these issues, platforms based on lipid mono or bilayers proved to be particularly effective. While these may represent the ideal systems to study the dynamics of cell-cell adhesions, various chemical strategies have been developed to functionalize lipidic membranes with matricellular cues (Gooding et al., 2014; Koçer and Jonkheijm, 2018). Molecules incorporated in the layer are endowed with a lateral mobility, whose dynamics is affected by the chemical composition of the layer. Concerning lipid bilayers, those usually employed as culturing substrates are made of 1,2-dicoleoyl-sn-glycero-3-phosphocholine (DOPC) that possess a low gel-fluid transition temperature, indicating a higher lateral molecular diffusion. Conversely, membranes of 1,2-dipalmitoyl-sn-glycero-3-phosphocholine (DPPC) are more thermally stable with less diffusible molecules (Lindblom et al., 2006). Culturing substrates based on bilayers are conveniently formed on hydrophilic surfaces (supported lipid bilayers, SLBs). SLBs provide a good level of spatial control of ligand positioning when physical constraints are introduced on the nanostructured support on which the membranes are formed (Groves, 1997). In this case, nanometric relieves of the substrate locally impair lateral mobility of molecules, thus enabling clustering. Following this approach Yu et al. investigated the early adhesion events and lateral clustering of integrins (Yu et al., 2011). RGD functionalized DOPC membranes were formed on a glass substrate containing 5 $\times$ 100 nm metal wires spaced by 0.5–4 μm gaps. Thanks to lateral diffusion and capture provided by the nano-barriers, the authors observed integrin recruitment and the formation of submicron clusters in which adhesion proteins such as talin, paxillin, and FAK were formed in a contraction-independent manner. This preceded actin filament assembly at cluster sites, for which, myosin contraction produced even longer clusters. Unraveling such a complex dynamics required the versatility and fluidity of SLB as opposed to conventional ligand-immobilized substrates. Along this line, Vafaei et al. have recently compared the biological activity of FN and Collagen type I covalently anchored to DOPC SLBs with that of proteins non-specifically adsorbed onto SiO_2 substrates (Vafaei et al., 2017). The authors found an increased flexibility of the proteins and more efficient cell adhesion and proliferation, providing further evidence that SLBs may represent a more biomimetic microenvironment to study certain biological processes, respect to synthetic platforms not allowing ligand displacement.

SLBs have also been employed to address the role of ligand clustering on stem cell fate decision. Koçer and Jonkhejim correlated hMSCs spreading with receptor clustering and cell differentiation (Koçer and Jonkheijm, 2017). To modulate lateral mobility either DOPC or DPPC membranes functionalized with RGD were used. hMSCs showed higher adhesion, higher level of expression of osteogenic differentiation markers and calcium deposits on DOPC membranes suggesting a positive role of ligand clustering and integrin activation in dictating stem cell fate decisions. Additionally, SLBs proved to be very stable as receptor recruitment and differentiation occurred on very different timescales (minutes vs. days) and yet they allowed cell culture for up to 10 days.

DYNAMIC TOPOGRAPHIES

Static topographic relieves in the form of micro/nano pits, protrusions or channels dramatically affect various aspects of cell behavior including, migration, proliferation and differentiation (Dalby et al., 2014; Ventre and Netti, 2016b). Several technologies have been developed to perform systematic studies of response to topographic signals of a sufficiently large number of cells. Among these, replica molding, nanoimprint lithography, block copolymer micelle nanolithography exhibit a reasonable balance between features fidelity and resolution and large area patterning (Ventre et al., 2018). Extending the studies in a dynamic framework requires the development of stimuli responsive materials, along with manipulating/actuating strategies that must be both effective and cell compatible. The examples of surfaces displaying adhesion signals dynamically all share the common trait that the switches act on a molecular level (capping, conformation changes, desorption). For the successful implementation of dynamic topographies, i.e., relieves changing shape and height, the coordinated motion or matter removal on a submicro- or micro-scale level is necessary. Specific chemical strategies need to be developed for allowing this type of material transformation as well as the triggering stimulus must be effective on a reasonable time scale.

Mechanical Control of Topographic Patterns

An early example of dynamically changing topographic pattern was proposed by Zhu et al. who fabricated a thin silica-like layer on a PDMS elastomer with radiofrequency oxygen plasma (Zhu et al., 2005). The silica layer was rendered protein repellent via chemical vapor deposition of (tridecafluoro-1,1,2,2-tetrahydrooctyl)-1-trichlorosilane and incubation with Pluronic F108. Cyclic stretching of the elastomer caused the thin brittle layer to form parallel arrays of cracks (having width ranging in the 0.1–3 μm interval) on which C2C12 myoblasts adhered and elongated. Cells subjected to cyclic opening-closing of the cracks responded with sequential changes in elongation/retraction. A similar approach was reported by Lam et al. who fabricated patterns of periodic microscale waves by compression-induced buckling of a brittle thin film on the surface of a PDMS elastomeric substrate (Lam et al., 2008). C2C12 cells adhered and retraced the contours of the wavy pattern when the elastomer was compressed, whereas cells displayed a random orientation when the PDMS strain was released. These are elegant examples illustrating the fabrication of dynamic substrates in a simple and cost-effective manner. However, with these strategies it is not possible to achieve a fine control on the features of the topographic patterns. Also, the geometry of the pattern is limited to straight channels and cannot be changed readily.

Guvendiren and Burdick further elaborated this concept by developing a method to spatially control the geometrical features of the strain responsive topographies (Guvendiren and Burdick, 2013b). Exposing to ultraviolet/ozone uniaxially or biaxially stretched PDMS sheets resulting in the formation of a stiffer outer skin. Selective release of the strain produced a wave pattern perpendicular to the strain direction. Release of both directions of strains in the biaxially stretched sheets resulted in a labyrinthine pattern. Also, local masking irradiation enabled site-specific patterning. hMSCs cultivated on the dynamic patterns responded to the switching by altering shape, orientation and nuclear area. Although very effective in the short culturing periods, the effectiveness of the dynamic topographies decreased in time as cell proliferation and cell-cell contacts overruled the topographic guidance.

Light Responsive Topographies

Material degradation induced by light irradiation enables embossing topographic structures with a higher spatial control of the features with respect to the methods described above. Kirschner and Anseth synthesized a photodegradable PEG based hydrogel by coupling nitrobenzyl-based photodegradable acrylate to PEG-bis-amine and PEG macromer (Kirschner and Anseth, 2013). Irradiating the gel with UV light at 365 nm caused photolabile bond breaking and gel erosion. Using photomasks, the authors were able to direct erosion giving rise to topographic patterns whose depth was proportional to the irradiation time. Furthermore, by directing the laser beam of a multiphoton microscope multiple patterns were embossed on the same gel. Dynamic patterning in presence of cells was demonstrated by cultivating hMSCs on the top of a FN coated photolabile hydrogel. Microscale channels were imprinted on the gel which caused the cells to reorient, eventually increasing their aspect ratio. Afterwards, a grating of regular squares was produced by drawing lines orthogonal to the primary pattern. This restored a symmetric condition that induced cells to acquire a round shape. This platform proved to be highly versatile as it enabled writing multiple patterns with different features on the same substrate. Additionally, the patterning procedure along with the hydrogel degradation products does not harm cell. However, once sculpted hydrogel surfaces cannot acquire the initial shape; this may pose severe limitation on the reversibility of the system.

Thanks to their ability to change conformation upon light irradiation, azopolymers have been used in various biological applications (Beharry and Woolley, 2011; Wei et al., 2015; Goulet-Hanssens et al., 2016). One of the first examples of using azopolymers as cell culturing substrates was provided by Baac et al. (2004). Laser holography was used to imprint undulated nanoscale patterns on the commercially available light responsive azopolymer poly[(methylmethacrylate)-co-(Disperse Red 1 acrylate)]. Azopolymeric patterned films proved to be biocompatible enabling the attachment of different cell types. This paved the way to use patterned light to modify surface topography of films dynamically. An early attempt to inscribe a topographic pattern on an azopolymeric cell culturing substrate while preserving cell viability was reported by Barillé et al. (2011). The authors reported pattern inscription via irradiation with a two-laser beam interferometric pattern or through molecular self-organization induced by a single beam. PC12 cells reacted to the flat-grooved transition by elongating and aligning along the pattern direction and extending neurites. Although preserving cell viability, an influence of the liquid medium on the process of pattern inscription was reported. The issue of azopolymer stability in biologic media was addressed by Rocha et al. who noticed material reorganization in aqueous environments that varied according to the polarity and stiffness of the azopolymer (Rocha et al., 2014).

More recently Rianna et al. investigated the feasibility of employing Poly(Disperse Red 1 methacrylate) (pDR1m) as a suitable substrate to emboss topographic patterns reversibly for cell culture experiments (Rianna et al., 2015). Preliminary tests to assess pattern stability under conditions comparable to those experienced during cell culture, were performed. Patterns in the form of microgrooves or microgrids were inscribed on films by using an interference pattern of light. Cells were mostly round when cultivated on flat or grid patterns, whereas they appeared to be highly elongated and aligned along the direction of linear microgrooved patterns (**Figures 8A,B,D**). Circularly polarized light was used to induce pattern erasure on pDR1 films, which caused a sharp decrease in the elongation of cells once cultivated on the erased pattern (**Figures 8C,D**). FA length did not display changes in the writing/erasing cycles, whereas FA orientation was very sensitive to the topography as parallel FAs were observed on the SRG only (**Figure 8E**). Authors from the same group further elaborated this concept by integrating pDR1 patterned with a single photon laser with the aim of developing dynamic substrates to study how spatio-temporal variations of topographic patterns affect the behavior of vital

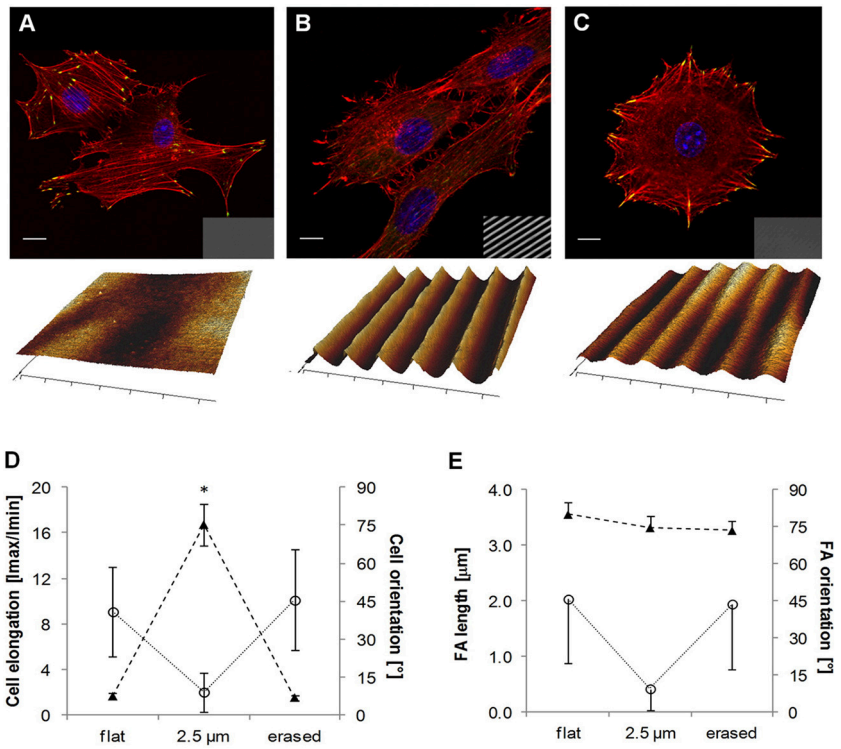

FIGURE 8 | Confocal images of NIH3T3 cells cultivated on **(A)** flat pDR1m substrate, **(B)** SRG linear grating, and **(C)** pattern-erased substrate with circularly polarized light. Insets in the bottom right show images in transmission. Representative AFM scans are reported below each image. **(D)** Plot of cell elongation (solid triangles) and cell orientation (open circles). **(E)** Plot of FA length (solid triangles) and orientation (open circles). The asterisk indicates a significant difference with respect to the flat case. Bars indicate the standard error of the mean in the case of cell elongation and FA length, whereas they represent the standard deviation in the case of cell and FA orientation. Reprinted with permission from Rianna et al. (2015). Copyright 2015 American Chemical Society.

cells in real-time (Rianna et al., 2016). A conventional confocal microscope was used to guide laser beam path to emboss complex patterns on pDR1m thin films with submicrometric resolution. Fibroblasts cells responded to the dynamic patterns by altering their morphology and migration because of cytoskeleton and focal adhesion reorganization. Furthermore, irradiating the substrate with an incoherent and unpolarized light of a mercury lamp enabled the erasure of topographic patterns on cell-populated pDR1m. A further peculiarity of the confocal technique consists in enabling multiple pattern inscriptions on the same platform simultaneously, so that isolated cells can be exposed to different patterns in real-time (**Figures 9A–C**). The possibility to imprint and erase several topographic patterns on azopolymer films with an easy and versatile method may pave the way to an investigation of complex processes involved in cell material-crosstalk (**Figures 9D–G**). Rossano et al. have recently exploited this technique to study NIH3T3 fibroblast response to dynamic circular topographic patterns (Rossano et al., 2018). The authors found that cells reacted to transition from flat to circular topographies quickly and that patterns of circular ridges 2 μm wide and spaced of 10 μm most effectively affected cell shape and local orientation. Since stress fibers and FAs cannot grow in a bent fashion, circular topographies proved very effective in destabilizing cytoskeletal structures and hence in decreasing the mechanical properties of cells.

Koçer et al. integrated microscale topographic cues with dynamic and reversible surface nanoroughness by exploiting the light induced azobenzene isomerization within liquid crystal networks (Koçer et al., 2017). More specifically, the polymer network containing the azobenzene moiety was photocrosslinked in a network whose microstructure was in the cholesteric phase. UV irradiation decreased the order of the phase causing an increase in surface nanoroughness, from 9.0 ± 1.2 to 11.1 ± 1.2 nm. NIH3T3 cells cultivated on the dynamic surfaces dynamically changed the migration behavior from motile to stationary according to the underlying topography.

Temperature Responsive Topographies

Biocompatible shape memory polymers (SMPs) enabled to investigate cell recognition and response to time changing topographies by exploiting consolidated and inexpensive technologies such as casting and hot embossing (Ratna and Karger-Kocsis, 2008; Meier et al., 2015). Generally, SMPs can recover permanent shapes upon stimulation of temporary ones. The latter can be implemented by means of mechanical deformation, whereas the application of an external stimulus, including heat, light, or solvent exposure promotes the recovery of the permanent shape (Mather et al., 2009). SMPs possess the advantage of retaining microscale topographic features, with high fidelity and—if conveniently engineered—SMPs can

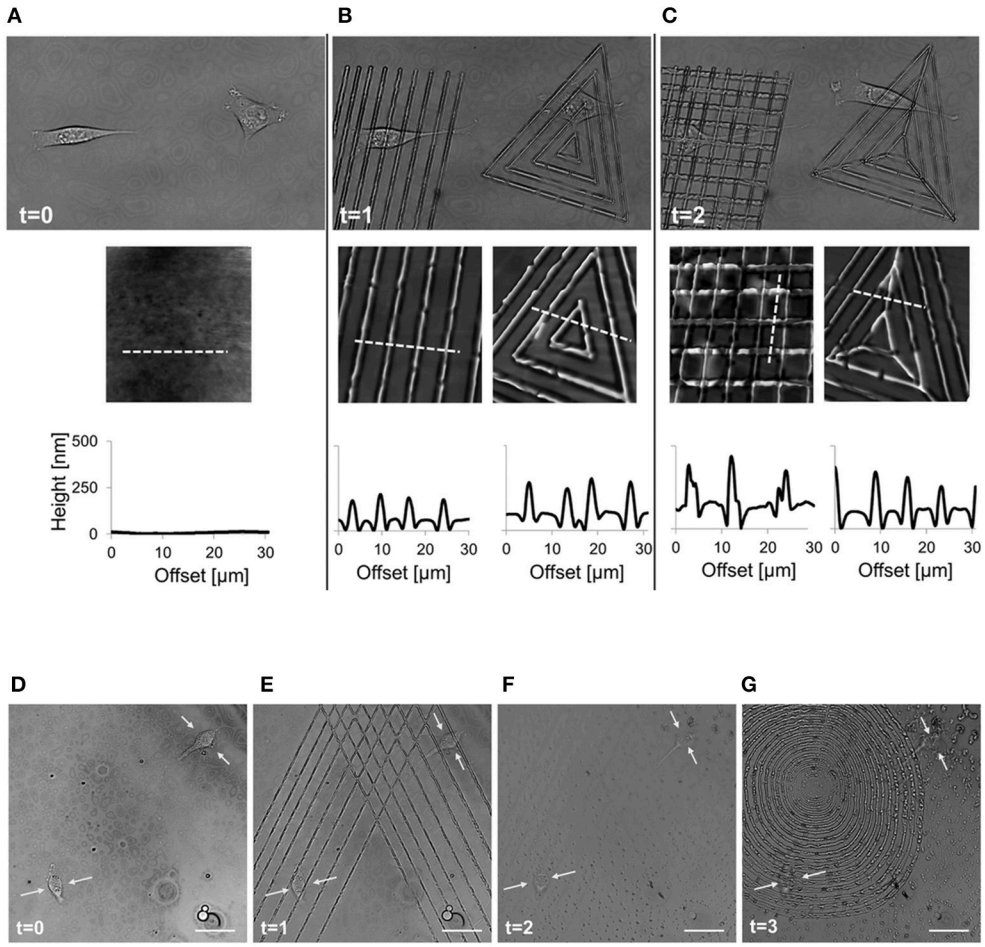

FIGURE 9 | Spatio-temporal control of pattern inscription while preserving NIH3T3 viability. **(A)** Transmission images of two non-interacting cells on flat pDR1m substrate ($t = 0$); **(B)** two different topographic patterns were inscribed on the same location by means of a 514 nm laser, with a 30 s inscription time ($t = 1$); **(C)** after 45 min a second topographic pattern was superimposed to the primary one ($t = 2$). On the bottom of each image, a representative AFM scan and related cross-section profiles are reported. Demonstration of the feasibility of the pattern inscription-erasure process while preserving cell viability. **(D)** Confocal images of two cells non-interacting cells on flat pDR1m substrate; **(E)** Primary pattern inscription with 514 nm laser 30 s inscription time; **(F)** pattern erasure by employing unpolarized and incoherent light for 60 s after removing the medium; **(G)** second pattern inscription with 514 nm laser 30 s inscription time. Images were collected at time zero (before patterning) and later at three different time points. Yellow arrows point to the central portion of the cell body during the entire process. Scale bars are 20 μm. Adapted from Rianna et al. (2016). Copyright Wiley-VCH Verlag GmbH and Co. KGaA. Reproduced with permission.

switch under cytocompatible conditions (Le et al., 2011). One of these materials is polycaprolactone (PCL) that is able to change topography if heated above the transition temperature (T_{trans}) of 40°C (Le et al., 2011; Ebara et al., 2012). In one example, Le et al. crosslinked star shaped PCL liquid prepolymer under UV light in presence of diethoxyacetophenone photoinitiator into specifically designed molds, thus allowing the material to acquire the equilibrium primary topography. Mechanical forces were applied above T_{trans} to impress the transient, secondary topography, and cooled down the T_{trans}. Reduction of the molecular mobility prevented the material to relieve the mechanical stress, thus enabling the secondary topography to remain impressed. Heating above T_{trans} provided sufficient mobility to the polymers to restore the original shape. The authors exploited this to investigate the response of hMSCs to dynamically changing microtopographies. Cells seeded on temporary 3:5 μm grooved pattern elongated and aligned along the pattern direction. However, when the substrate was heated above T_{trans} the primary-planar shape emerged, causing the cell to acquire a stellate morphology. While this method is simple (not requiring expensive device to actuate the transition) and effective, it is not truly reversible as secondary shapes cannot be reacquired. Furthermore, cells on secondary topographies need to be cultivated below the T_{trans} (28°C) which might be an issue for long-term cultures. Beside adhesion and orientation, patterned SMPs were shown to dynamically regulate the structural and contractile properties of cardiomyocytes (Mengsteab et al., 2016). Neonatal rat ventricular myocytes (NRVMs) were cultivated on a PCL-based SMP exhibiting a primary nanogrooved pattern (400 nm wide ridges; 500 nm

grooves; 150 nm depth) and a secondary transient nanogrooved pattern with same dimensions but rotated of 90° with respect to the primary one. This design was aimed at recapitulating the orientation of collagen fibrils in the myocardium. NRVMs on the transient nanopattern exhibited a homogeneous population of elongated FAs, nuclei alignment along the pattern direction and a unidirectional and a homogeneous contractile behavior. The surfacing of the primary pattern determined an increased dispersion of FA orientations and after 48 h cells showed a bimodal distribution of the directions of contraction. These data suggest that nanotopographic patterns do not dictate organization and contractile properties permanently making dynamic topographies a suitable signal to alter the organization of cells on a collective level.

Another class of polymers exhibiting shape memory are the crosslinked polyurethane-based adhesives, commercially available under the name NOA63. Davis et al. processed NOA63-based films displaying dynamic topographies. A flat surface was recovered from a microgrooved pattern by changing the temperature from 30 to 37°C (Davis et al., 2011). Such a temperature preserved cell viability. Mouse embryonic fibroblasts accompanied the transition by remodeling their cytoskeleton and changing their shape accordingly. A drawback of this method relies in the long time-frame required for the topographic switch to occur (∼hours).

DYNAMIC STIFFNESS

Materials whose mechanical properties can be changed dynamically represent unique platforms to investigate complex biological phenomena such as morphogenesis and wound healing. In fact, the mechanical properties of the culturing microenvironment—and more specifically its stiffness—are known to potently regulate cell differentiation (Engler et al., 2006; Ivanovska et al., 2015). However, how changes in ECM mechanics accompany or anticipate physiological or pathological states, are not thoroughly understood and artificial platforms recapitulating the dynamics of stiffness changes *in vitro* would be of great importance for studying the development of physio-pathological states. ECM stiffening is a typical phenomenon accompanying several biologic processes such as *in vivo* organogenesis or the progression of pathologies (Berry et al., 2006; Georges et al., 2007; Krieg et al., 2008). Dynamic changes of substrate stiffness usually rely on degradation or crosslinking of hydrogels that can either proceed spontaneously or can be activated by external triggers such as light.

By exploiting photodegradation, Kloxin et al. aimed at addressing myofibroblastic differentiation in response to microenvironment softening (Kloxin et al., 2010). Fibroblast to myofibroblast differentiation is a crucial step in wound healing. Wounds are highly dynamic environments (in terms of biochemical microenvironment, architecture and mechanical properties) and today the role of biochemical/biophysical signals in governing the dynamics of healing is poorly understood. Dynamic platforms may provide valuable insights into the biology of regenerative/reparative processes. To this aim, valvular interstitial cells were cultivated on a PEG based hydrogel containing photodegradable crosslinkers. The photodegradable hydrogel allowed to change moduli in the physio-pathologic range within minutes after irradiation with UV light. Cells cultivated for 5 days on stiff (32 kPa) hydrogels displayed the characteristic phenotype of activated myofibroblasts, whereas cells cultivated on soft (7 kPa) gels were in quiescent form. However, the stiff to soft transition (3 days on stiff, followed by 2 days on soft) was sufficient to deactivate cells.

Not only the absolute magnitude of the stiffness affects fate decisions, but the way the mechanical stimulus is presented also plays an important role in regulating the differentiation process. Along these lines, Yang et al. used a photodegradable polyethylene glycol di-photodegradable acrylate hydrogel functionalized with RGD to investigate whether stem cells possess a "mechanical memory", i.e., stem cells make fate decisions based on the temporal integration of the perceived dynamic mechanical stimuli (Yang et al., 2014). To this aim, hMSCs were subjected to a mechanical dosing, i.e., they were cultivated on stiff substrates for different time intervals (0, 1, 5, or 10 days) and then the substrate was softened down to 2 kPa. hMSCs supplemented with a small dose of mechanical stimulus (1 day) exhibited transient levels of genes involved in osteogenesis. Conversely, an irreversible activation of the differentiation programme was observed when cells were cultivated for 10 days on stiff hydrogels prior to softening. The authors suggested that stem cells do possess a mechanical memory for which Yes-associated proteins/Transcriptional coactivators with PDZ-binding motif (YAP/TAZ) acts as mechanical rheostats since they persist in the nucleus, hence promoting osteogenesis, if cells are continually exposed to stiff environments.

In the context of addressing the role of dynamic changes of material stiffness on stem cell differentiation, Guvendiren and Burdick developed a methacrylated hyaluronic acid (HA)-based gel whose stiffness can be increased through light-mediated radical polymerization (Guvendiren and Burdick, 2012). hMSCs were cultivated on soft gels for selected time intervals, after which gels were stiffened by light irradiation. Cells quickly reacted to material stiffening by increasing area and the expression of contractile forces. Furthermore, early stiffening (i.e., cells exposed to a stiff environment for a long timeframe) promoted osteogenesis, whereas late stiffening promoted adipogenesis. Besides differentiation, the timing of the materials stiffening proved to be a crucial parameter for activating pathological states in *in vitro* models (Caliari et al., 2016). Using hepatic stellate cells cultivated on a methacrylated HA gel sensitive to blue light irradiation (∼470 nm), Caliari et al. showed that a soft-to-stiff transition occurring after 6 days prompted an accelerated signaling kinetics of both YAP/TAZ and alpha-smooth muscle actin whose time-course was similar to observed *in vivo* activation dynamics. Anticipating the transition at day 1 did not produce the same trend.

These examples suggest that the parameter stiffness has not to be intended as a "state variable" for which the cell response only depends on the initial and final values of the stiffness, being independent from the specific pathway that led to the

change. The systems described above operate on step-wise changes of the stiffness occurring in short-timeframes (minutes-hours). Cells are exposed to continuous changes of the *in vivo* biophysical microenvironment (Montell, 2008; Bonnans et al., 2014). Therefore, it is likely that the kinetics of stiffness variations may also play a role in affecting cell functions and fates. To address this, it is necessary to develop chemical modifications producing crosslinks or bond breakings whose reaction kinetic eventually match the time-variations observed *in vivo*. To verify whether time-dependent stiffening plays a role in establishing an adequate microenvironment for myocardial maturation Young and Engler synthesized a thiolated-hyaluronic acid hydrogel crosslinked with (ethylene glycol)diacrylate whose crosslinking kinetics and hence stiffening dynamics was tuned to match the temporal variations of stiffness observed in developing embryos (Young and Engler, 2011). Precardiac cells cultivated on collagen coated dynamic thiolated-HA gels showed significantly higher expression of mature cardiac markers and improved assembly of contractile fibers with respect to what observed when cells were plated on conventional and static polyacrylamide gels. Even though this experimental model does not allow to change mechanical properties at will, it clearly demonstrates how undifferentiated cells are sensitive to biophysical changes of the microenvironment.

More recently, hydrogels with reversible mechanical properties were fabricated through modular modifications of HA (Rosales et al., 2017). Three different moieties were used: o-nitrobenzyl acrylates (photodegradable), methacrylates (crosslinks with a photoinitiator) and RGD. Hydrogels could be softened and then hardened (or vice versa) through sequential irradiation with specific wavelengths. MSC cultivated on the HA modified gels showed a decrease in the cell area and nuclear localization of YAP/TAZ following *in situ* softening (from 14 to 3.5 kPa), whereas subsequent stiffening (from 3.5 to 28 kPa) increased the cell area and nuclear localization of YAP/TAZ. Authors of the same groups further elaborated the design of the photoresponsive system and successfully produced a supramolecular hydrogel constituted by hyaluronic acid functionalized with the photoresponsive guest-host pair azobenzene and β-cyclodextrin (Rosales et al., 2018). Azobenzene groups in the *trans* configuration form links with cyclodextrins that can be disrupted upon UV irradiation that promotes the *cis* conversion under cytocompatible conditions. Such a design possesses the advantage of decoupling changes in network mechanical properties from changes in chemical composition. This endows the system with well-defined physical/chemical characteristics suitable for studies in mechanobiology.

CONCLUSIONS AND FUTURE PERSPECTIVES

Adhesion mediated signaling regulates various aspects of cell behavior including proliferation, migration, and differentiation. Cell adhesions have a direct impact on cytoskeleton arrangement, cell contractility, and nucleus shape, which altogether affect gene expression and eventually cell functions (Dalby et al., 2014; Murphy et al., 2014; Anderson et al., 2016; Ventre et al., 2018). Therefore, adhesion—cytoskeleton—contractility constitute a tripartite module in which changes in one element invariably induce alterations in the other thus affecting cell behavior. In this context material signals regulating cell adhesion acquire a central role, perhaps as important as chemical supplements or drugs. Culturing substrates, scaffolds or gels proved remarkable effectiveness in finely modulating even complex biological events. Yet, these culturing systems are mostly known for displaying signal in a static manner. Static signal platforms have provided tremendous insights in understanding the optimal configurations of signals to be displayed to elicit a specific response. However, in the way they are conceived static platforms cannot be employed to address other relevant questions. As soluble biochemical signals elicit very different cellular responses according to their dose and on the way they are delivered in time, do biophysical signals behave similarly? How does the variable spatio-temporal presentation of biophysical signals affect cell behavior? Does an optimal spatio-temporal presentation of bound signal to elicit a specific cell response in the most effective manner exist? Answering these questions may not only provide valuable insights for developing more effective and versatile culturing systems but might aid in shedding light on intricate biological processes involved whenever modifications in the microenvironment occur, for example in tissue and organ morphogenesis or in the development or progress of diseases. Dynamic platforms may certainly contribute to address these issues. However, many technical hurdles need to be overcome. First, a fine modulation of adhesion events and exerting a control on the dynamics of specific arrangements of FAs is necessary. Such a spatio-temporal resolution in the actuating elements of dynamic platforms has not been achieved yet. Second, dynamic surfaces have reached a level of performances that enables controlling adhesion processes at a subcellular level in time-scales that are compatible to conventional cell cultures. However, different biological responses may occur on different time scales, i.e., adhesion takes minutes to hours, whereas differentiation occurs in days or weeks. Achieving a proper time control is still an issue. Some triggers are faster than others, but once they are turned "on" or "off" the whole system responds with its own kinetics. Therefore, tuning the dynamics of the signal change to that of a specific biological phenomenon may require a careful design of the molecular switch or the integration of various switches. Third, while 2D surfaces are valuable to understand the behavior of epithelia and endothelia as they more closely mimic the native microenvironment, certain biological events specifically occur in a 3D context. Patterning signals in space with a submicron resolution is technically challenging and requires expensive equipment. Actuating switchable signals in 3D is even more complex. Laser two photon or holographic techniques might be valuable instruments for achieving a spatial control of the chemical/physical properties of the 3D environment with an adequate resolution (Applegate et al., 2015; Tong et al., 2016). Notable examples of dynamic 3D environments able to regulate cell functions and fate decisions have been already reported (Khetan et al., 2013; Das et al., 2016; Brown et al., 2018). However, integrating diverse stimuli in 3D and

achieving a control on individual adhesion points still require further developments. Moreover, activating and deactivating signal exposure in a completely reversible manner is key central. Non-reversible or partially reversible systems might only partly recapitulate the dynamic behavior of the ECM or might not be entirely versatile. Creating complex spatio-temporal patterns of signals requires implementing signal display/conceal in a fast and effective manner. The uncontrolled presence of signal remnants may interfere with the intended signal presentation providing inconsistent results.

Literature data has provided compelling evidence that cell functions and fate are not dictated by a single signal type, but it is rather a complex interplay of multiple signals acting on different length- and time-scales that determines the final cell state (Dalby et al., 2014; Murphy et al., 2014). To actuate different signal acting at different timepoints, specific switches must be engineered. Photoswitches might be particularly suitable for this purpose. In fact, several molecules have been developed, for example the azoderivatives, whose response may fall within a broad range of wavelengths. In principle, by combining different light sensitive switches reacting to different wavelengths it would be possible to fabricate arrays of signals whose display could be controlled in an orthogonal manner, thus increasing the complexity of the system. This, however, requires a sapient positioning of light sensitive elements with non-overlapping absorption spectra.

Furthermore, dynamic platforms are usually engineered and fabricated to display/conceal binding sites. However, dynamic changes of the ECM are not limited to adhesion cues and involve multiple signal changes according to different chronoprogrammes. In fact, the literature on dynamic platform mostly concerns platforms regulating adhesion/detachment and migration. Yet, recent examples demonstrated enormous potentialities of dynamic signal display, particularly in what concerns fate decisions and in the acquisition of specific tissue functions (Young and Engler, 2011; Yang et al., 2014; Roberts et al., 2016). Therefore, beside exploiting soluble signals, engineering complex patterns of bioadhesive signals, the introduction of the parameter "time" acquires a crucial importance in the design of novel and more efficient culturing systems. However, dynamic surfaces, although introducing space, and time variations of biologic properties fall short of capturing more complex features of the native ECM. An intriguing strategy to tackle this issue has been recently proposed by Hay et al. who introduced the concept of bacteria-based materials (Hay et al., 2018). These finely altered the adhesive microenvironment upon external commands, eventually dictating stem cell fate decision. Non-pathogenic bacteria can be engineered as micromachines able to assemble animal proteins or release factors upon external stimulation. Nowadays, biologic genetic circuits can be integrated in bacteria to control the yield and production rate (Bittihn et al., 2018). We expect future research to be focused on integrating different strategies and technologies for the fabrication of multi-functional and dynamic platforms able to recapitulate intricate biochemical, biophysical and cellular processes that are fundamental to promote and guide biologically relevant phenomena. Applications like organoid generation or the development of pathological models would largely benefit from these advancements. Therefore, we expect that the field of dynamic platform engineering can potentially contribute not only to unravel complex biological events such as migration and differentiation, but could impact the medical and pharmaceutical areas thanks to the development of devices for drug screening and discovery and systems for tissue regeneration.

AUTHOR CONTRIBUTIONS

CC, LR, and MV gathered information and data from the literature and drafted the manuscript. MV and PN took the lead in organizing the final version of the manuscript. MV wrote the final version of the manuscript and edited figure panels. All authors provided critical feedback to shape the final version of the manuscript.

REFERENCES

Advincula, R. C. (ed.). (2004). "Polymer Brushes," in *Encyclopedia of Polymer Science and Technology* (Hoboken, NJ: John Wiley and Sons, Inc.), 114–134. doi: 10.1002/0471440264.pst529

Afara, N., Omanovic, S., and Asghari-Khiavi, M. (2012). Functionalization of a gold surface with fibronectin (FN) covalently bound to mixed alkanethiol self-assembled monolayers (SAMs): the influence of SAM composition on its physicochemical properties and FN surface secondary structure. *Thin Solid Films* 522, 381–389. doi: 10.1016/j.tsf.2012.08.025

Anderson, H. J., Sahoo, J. K., Ulijn, R. V., and Dalby, M. J. (2016). Mesenchymal stem cell fate: applying biomaterials for control of stem cell behavior. *Front. Bioeng. Biotechnol.* 4:38. doi: 10.3389/fbioe.2016.00038

Applegate, M. B., Coburn, J., Partlow, B. P., Moreau, J. E., Mondia, J. P., Marelli, B., et al. (2015). Laser-based three-dimensional multiscale micropatterning of biocompatible hydrogels for customized tissue engineering scaffolds. *Proc. Natl. Acad. Sci. U.S.A.* 112, 12052–12057. doi: 10.1073/pnas.1509405112

Arnold, M., Cavalcanti-Adam, E. A., Glass, R., Blümmel, J., Eck, W., Kantlehner, M., et al. (2004). Activation of integrin function by nanopatterned adhesive interfaces. *ChemPhysChem* 5, 383–388. doi: 10.1002/cphc.200301014

Auernheimer, J., Dahmen, C., Hersel, U., Bausch, A., and Kessler, H. (2005). Photoswitched cell adhesion on surfaces with RGD peptides. *J. Am. Chem. Soc.* 127, 16107–16110. doi: 10.1021/ja053648q

Baac, H., Lee, J.-H., Seo, J.-M., Park, T. H., Chung, H., Lee, S.-D., et al. (2004). Submicron-scale topographical control of cell growth using holographic surface relief grating. *Mater. Sci. Eng. C* 24, 209–212. doi: 10.1016/j.msec.2003.09.009

Bacharouche, J., Badique, F., Fahs, A., Spanedda, M. V., Geissler, A., Malval, J.-P., et al. (2013). Biomimetic cryptic site surfaces for reversible chemo- and cyto-mechanoresponsive substrates. *ACS Nano* 7, 3457–3465. doi: 10.1021/nn400356p

Bamdad, C. (1998). A DNA self-assembled monolayer for the specific attachment of unmodified double- or single-stranded DNA. *Biophys. J.* 75, 1997–2003. doi: 10.1016/S0006-3495(98)77641-6

Barillé, R., Janik, R., Kucharski, S., Eyer, J., and Letournel, F. (2011). Photo-responsive polymer with erasable and reconfigurable micro- and nano-patterns: an *in vitro* study for neuron guidance. *Colloids Surf. B Biointerfaces* 88, 63–71. doi: 10.1016/j.colsurfb.2011.06.005

Beharry, A. A., and Woolley, G. A. (2011). Azobenzene photoswitches for biomolecules. *Chem. Soc. Rev.* 40, 4422–4437. doi: 10.1039/c1cs15023e

Berry, M. F., Engler, A. J., Woo, Y. J., Pirolli, T. J., Bish, L. T., Jayasankar, V., et al. (2006). Mesenchymal stem cell injection after myocardial infarction improves myocardial compliance. *Am. J. Physiol. Heart Circ. Physiol.* 290, H2196–H2203. doi: 10.1152/ajpheart.01017.2005

Bettinger, C. J., Langer, R., and Borenstein, J. T. (2009). Engineering substrate topography at the micro- and nanoscale to control cell function. *Angew. Chem. Int. Ed.* 48, 5406–5415. doi: 10.1002/anie.200805179

Biggs, M. J. P., Richards, R. G., and Dalby, M. J. (2010). Nanotopographical modification: a regulator of cellular function through focal adhesions. *Nanomed. Nanotechnol. Biol. Med.* 6, 619–633. doi: 10.1016/j.nano.2010.01.009

Biggs, M. J. P., Richards, R. G., Gadegaard, N., Wilkinson, C. D. W., and Dalby, M. J. (2007). Regulation of implant surface cell adhesion: characterization and quantification of S-phase primary osteoblast adhesions on biomimetic nanoscale substrates. *J. Orthop. Res.* 25, 273–282. doi: 10.1002/jor.20319

Bittihn, P., Din, M. O., Tsimring, L. S., and Hasty, J. (2018). Rational engineering of synthetic microbial systems: from single cells to consortia. *Curr. Opin. Microbiol.* 45, 92–99. doi: 10.1016/j.mib.2018.02.009

Bonnans, C., Chou, J., and Werb, Z. (2014). Remodelling the extracellular matrix in development and disease. *Nat. Rev. Mol. Cell Biol.* 15, 786–801. doi: 10.1038/nrm3904

Brown, T. E., Carberry, B. J., Worrell, B. T., Dudaryeva, O. Y., McBride, M. K., Bowman, C. N., et al. (2018). Photopolymerized dynamic hydrogels with tunable viscoelastic properties through thioester exchange. *Biomaterials* 178, 496–503. doi: 10.1016/j.biomaterials.2018.03.060

Calderwood, D. A. (2004). Integrin activation. *J. Cell Sci.* 117, 657–666. doi: 10.1242/jcs.01014

Caliari, S. R., and Burdick, J. A. (2016). A practical guide to hydrogels for cell culture. *Nat. Methods* 13, 405–414. doi: 10.1038/nmeth.3839

Caliari, S. R., Perepelyuk, M., Cosgrove, B. D., Tsai, S. J., Lee, G. Y., Mauck, R. L., et al. (2016). Stiffening hydrogels for investigating the dynamics of hepatic stellate cell mechanotransduction during myofibroblast activation. *Sci. Rep.* 6:21387. doi: 10.1038/srep21387

Campbell, I. D., and Humphries, M. J. (2011). Integrin structure, activation, and interactions. *Cold Spring Harb. Perspect. Biol.* 3:a004994. doi: 10.1101/cshperspect.a004994

Chen, W.-L., Cordero, R., Tran, H., and Ober, C. K. (2017). 50th anniversary perspective: polymer brushes: novel surfaces for future materials. *Macromolecules* 50, 4089–4113. doi: 10.1021/acs.macromol.7b00450

Cohen, M., Joester, D., Geiger, B., and Addadi, L. (2004). Spatial and temporal sequence of events in cell adhesion: from molecular recognition to focal adhesion assembly. *Chembiochem* 5, 1393–1399. doi: 10.1002/cbic.200400162

Dalby, M. J., Biggs, M. J. P., Gadegaard, N., Kalna, G., Wilkinson, C. D. W., and Curtis, A. S. G. (2007). Nanotopographical stimulation of mechanotransduction and changes in interphase centromere positioning. *J. Cell. Biochem.* 100, 326–338. doi: 10.1002/jcb.21058

Dalby, M. J., Gadegaard, N., and Oreffo, R. O. C. (2014). Harnessing nanotopography and integrin–matrix interactions to influence stem cell fate. *Nat. Mater.* 13, 558–569. doi: 10.1038/nmat3980

Das, R. K., Gocheva, V., Hammink, R., Zouani, O. F., and Rowan, A. E. (2016). Stress-stiffening-mediated stem-cell commitment switch in soft responsive hydrogels. *Nat. Mater.* 15, 318–325. doi: 10.1038/nmat4483

Davis, K. A., Burke, K. A., Mather, P. T., and Henderson, J. H. (2011). Dynamic cell behavior on shape memory polymer substrates. *Biomaterials* 32, 2285–2293. doi: 10.1016/j.biomaterials.2010.12.006

DeForest, C. A., and Anseth, K. S. (2012). Advances in bioactive hydrogels to probe and direct cell fate. *Annu. Rev. Chem. Biomol. Eng.* 3, 421–444. doi: 10.1146/annurev-chembioeng-062011-080945

del Rio, A., Perez-Jimenez, R., Liu, R., Roca-Cusachs, P., Fernandez, J. M., and Sheetz, M. P. (2009). Stretching single talin rod molecules activates vinculin binding. *Science* 323, 638–641. doi: 10.1126/science.1162912

Deng, J., Zhao, C., Spatz, J. P., and Wei, Q. (2017). Nanopatterned adhesive, stretchable hydrogel to control ligand spacing and regulate cell spreading and migration. *ACS Nano* 11, 8282–8291. doi: 10.1021/acsnano.7b03449

Di Cio, S., and Gautrot, J. E. (2016). Cell sensing of physical properties at the nanoscale: mechanisms and control of cell adhesion and phenotype. *Acta Biomater.* 30, 26–48. doi: 10.1016/j.actbio.2015.11.027

Donnelly, H., Salmeron-Sanchez, M., and Dalby, M. J. (2018). Designing stem cell niches for differentiation and self-renewal. *J. R. Soc. Interface* 15:20180388. doi: 10.1098/rsif.2018.0388

Doyle, A. D., and Yamada, K. M. (2016). Mechanosensing via cell-matrix adhesions in 3D microenvironments. *Exp. Cell Res.* 343, 60–66. doi: 10.1016/j.yexcr.2015.10.033

Dumbauld, D. W., Lee, T. T., Singh, A., Scrimgeour, J., Gersbach, C. A., Zamir, E. A., et al. (2013). How vinculin regulates force transmission. *Proc. Natl. Acad. Sci. U.S.A.* 110, 9788–9793. doi: 10.1073/pnas.1216209110

Ebara, M., Uto, K., Idota, N., Hoffman, J. M., and Aoyagi, T. (2012). Shape-memory surface with dynamically tunable nano-geometry activated by body heat. *Adv. Mater. Weinheim* 24, 273–278. doi: 10.1002/adma.201102181

Ebara, M., Yamato, M., Aoyagi, T., Kikuchi, A., Sakai, K., and Okano, T. (2004). Temperature-responsive cell culture surfaces enable "On–Off" affinity control between cell integrins and RGDS ligands. *Biomacromolecules* 5, 505–510. doi: 10.1021/bm0343601

Edahiro, J., Sumaru, K., Tada, Y., Ohi, K., Takagi, T., Kameda, M., et al. (2005). *In situ* control of cell adhesion using photoresponsive culture surface. *Biomacromolecules* 6, 970–974. doi: 10.1021/bm0493382

Engler, A. J., Sen, S., Sweeney, H. L., and Discher, D. E. (2006). Matrix elasticity directs stem cell lineage specification. *Cell* 126, 677–689. doi: 10.1016/j.cell.2006.06.044

Eyckmans, J., Boudou, T., Yu, X., and Chen, C. S. (2011). A Hitchhiker's guide to mechanobiology. *Dev. Cell* 21, 35–47. doi: 10.1016/j.devcel.2011.06.015

Fedele, C., Netti, P. A., and Cavalli, S. (2018). Azobenzene-based polymers: emerging applications as cell culture platforms. *Biomater. Sci.* 6, 990–995. doi: 10.1039/C8BM00019K

Feng, C., and Huang, X. (2018). Polymer brushes: efficient synthesis and applications. *Acc. Chem. Res.* 51, 2314–2323. doi: 10.1021/acs.accounts.8b00307

Frantz, C., Stewart, K. M., and Weaver, V. M. (2010). The extracellular matrix at a glance. *J. Cell Sci.* 123, 4195–4200. doi: 10.1242/jcs.023820

Frith, J. E., Mills, R. J., and Cooper-White, J. J. (2012). Lateral spacing of adhesion peptides influences human mesenchymal stem cell behaviour. *J. Cell Sci.* 125, 317–327. doi: 10.1242/jcs.087916

Geiger, B., Spatz, J. P., and Bershadsky, A. D. (2009). Environmental sensing through focal adhesions. *Nat. Rev. Mol. Cell Biol.* 10, 21–33. doi: 10.1038/nrm2593

Georges, P. C., Hui, J.-J., Gombos, Z., McCormick, M. E., Wang, A. Y., Uemura, M., et al. (2007). Increased stiffness of the rat liver precedes matrix deposition: implications for fibrosis. *Am. J. Physiol. Gastrointest. Liver Physiol.* 293, G1147–G1154. doi: 10.1152/ajpgi.00032.2007

Gong, Y.-H., Li, C., Yang, J., Wang, H.-Y., Zhuo, R.-X., and Zhang, X.-Z. (2011). Photoresponsive "Smart Template" via host–guest interaction for reversible cell adhesion. *Macromolecules* 44, 7499–7502. doi: 10.1021/ma201676w

Gooding, J. J., Parker, S. G., Lu, Y., and Gaus, K. (2014). Molecularly engineered surfaces for cell biology: from static to dynamic surfaces. *Langmuir* 30, 3290–3302. doi: 10.1021/la4037919

Goulet-Hanssens, A., Lai Wing Sun, K., Kennedy, T. E., and Barrett, C. J. (2012). Photoreversible surfaces to regulate cell adhesion. *Biomacromolecules* 13, 2958–2963. doi: 10.1021/bm301037k

Goulet-Hanssens, A., Magdesian, M. H., Lopez-Ayon, G. M., Grutter, P., and Barrett, C. J. (2016). Reversing adhesion with light: a general method for functionalized bead release from cells. *Biomater. Sci.* 4, 1193–1196. doi: 10.1039/C6BM00168H

Groves, J. T. (1997). Micropatterning fluid lipid bilayers on solid supports. *Science* 275, 651–653. doi: 10.1126/science.275.5300.651

Gupta, S., Marcel, N., Sarin, A., and Shivashankar, G. V. (2012). Role of actin dependent nuclear deformation in regulating early gene expression. *PLoS ONE* 7:e53031. doi: 10.1371/journal.pone.0053031

Guvendiren, M., and Burdick, J. A. (2012). Stiffening hydrogels to probe short- and long-term cellular responses to dynamic mechanics. *Nat. Commun.* 3:792. doi: 10.1038/ncomms1792

Guvendiren, M., and Burdick, J. A. (2013a). Engineering synthetic hydrogel microenvironments to instruct stem cells. *Curr. Opin. Biotechnol.* 24, 841–846. doi: 10.1016/j.copbio.2013.03.009

Guvendiren, M., and Burdick, J. A. (2013b). Stem cell response to spatially and temporally displayed and reversible surface topography. *Adv. Healthc. Mater.* 2, 155–164. doi: 10.1002/adhm.201200105

Handorf, A. M., Zhou, Y., Halanski, M. A., and Li, W.-J. (2015). Tissue stiffness dictates development, homeostasis, and disease progression. *Organogenesis* 11, 1–15. doi: 10.1080/15476278.2015.1019687

Harunaga, J. S., and Yamada, K. M. (2011). Cell-matrix adhesions in 3D. *Matrix Biol.* 30, 363–368. doi: 10.1016/j.matbio.2011.06.001

Hay, J. J., Rodrigo-Navarro, A., Petaroudi, M., Bryksin, A. V., García, A. J., Barker, T. H., et al. (2018). Bacteria-based materials for stem cell engineering. *Adv. Mater.* 30:1804310. doi: 10.1002/adma.201804310

Hersel, U., Dahmen, C., and Kessler, H. (2003). RGD modified polymers: biomaterials for stimulated cell adhesion and beyond. *Biomaterials* 24, 4385–4415. doi: 10.1016/S0142-9612(03)00343-0

Higuchi, A., Hamamura, A., Shindo, Y., Kitamura, H., Yoon, B. O., Mori, T., et al. (2004). Photon-modulated changes of cell attachments on Poly(spiropyran-*co* -methyl methacrylate) membranes. *Biomacromolecules* 5, 1770–1774. doi: 10.1021/bm049737x

Hinek, A. (1996). Biological roles of the non-integrin elastin/laminin receptor. *Biol. Chem.* 377, 471–480.

Humphries, J. D., Paul, N. R., Humphries, M. J., and Morgan, M. R. (2015). Emerging properties of adhesion complexes: what are they and what do they do? *Trends Cell Biol.* 25, 388–397. doi: 10.1016/j.tcb.2015.02.008

Isermann, P., and Lammerding, J. (2013). Nuclear mechanics and mechanotransduction in health and disease. *Curr. Biol.* 23, R1113–R1121. doi: 10.1016/j.cub.2013.11.009

Ivanovska, I. L., Shin, J.-W., Swift, J., and Discher, D. E. (2015). Stem cell mechanobiology: diverse lessons from bone marrow. *Trends Cell Biol.* 25, 523–532. doi: 10.1016/j.tcb.2015.04.003

Jain, N., Iyer, K. V., Kumar, A., and Shivashankar, G. V. (2013). Cell geometric constraints induce modular gene-expression patterns via redistribution of HDAC3 regulated by actomyosin contractility. *Proc. Natl. Acad. Sci.U.S.A.* 110, 11349–11354. doi: 10.1073/pnas.1300801110

Janmey, P. A., and Miller, R. T. (2011). Mechanisms of mechanical signaling in development and disease. *J. Cell Sci.* 124, 9–18. doi: 10.1242/jcs.071001

Janoštiak, R., Pataki, A. C., Brábek, J., and Rösel, D. (2014). Mechanosensors in integrin signaling: the emerging role of p130Cas. *Eur. J. Cell Biol.* 93, 445–454. doi: 10.1016/j.ejcb.2014.07.002

Jans, K., Van Meerbergen, B., Reekmans, G., Bonroy, K., Annaert, W., Maes, G., et al. (2009). Chemical and biological characterization of Thiol SAMs for neuronal cell attachment. *Langmuir* 25, 4564–4570. doi: 10.1021/la802217r

Jiang, X., Bruzewicz, D. A., Wong, A. P., Piel, M., and Whitesides, G. M. (2005). Directing cell migration with asymmetric micropatterns. *Proc. Natl. Acad. Sci. U.S.A.* 102, 975–978. doi: 10.1073/pnas.0408954102

Jiang, X., Ferrigno, R., Mrksich, M., and Whitesides, G. M. (2003). Electrochemical desorption of self-assembled monolayers noninvasively releases patterned cells from geometrical confinements. *J. Am. Chem. Soc.* 125, 2366–2367. doi: 10.1021/ja029485c

Kharkar, P. M., Kiick, K. L., and Kloxin, A. M. (2013). Designing degradable hydrogels for orthogonal control of cell microenvironments. *Chem. Soc. Rev.* 42, 7335–7372. doi: 10.1039/C3CS60040H

Khetan, S., Guvendiren, M., Legant, W. R., Cohen, D. M., Chen, C. S., and Burdick, J. A. (2013). Degradation-mediated cellular traction directs stem cell fate in covalently crosslinked three-dimensional hydrogels. *Nat. Mater.* 12, 458–465. doi: 10.1038/nmat3586

Kim, D.-H., Kim, P., Suh, K., Kyu Choi, S., Ho Lee, S., and Kim, B. (2005). Modulation of adhesion and growth of cardiac myocytes by surface nanotopography. *Conf. Proc. Annu. Int. Conf. IEEE Eng. Med. Biol. Soc. IEEE Eng. Med. Biol. Soc. Annu. Conf.* 4, 4091–4094. doi: 10.1109/IEMBS.2005.1615362

Kirschner, C. M., and Anseth, K. S. (2013). *In situ* control of cell substrate microtopographies using photolabile hydrogels. *Small* 9, 578–584. doi: 10.1002/smll.201201841

Klajn, R. (2014). Spiropyran-based dynamic materials. *Chem. Soc. Rev.* 43, 148–184. doi: 10.1039/C3CS60181A

Kloxin, A. M., Benton, J. A., and Anseth, K. S. (2010). *In situ* elasticity modulation with dynamic substrates to direct cell phenotype. *Biomaterials* 31, 1–8. doi: 10.1016/j.biomaterials.2009.09.025

Koçer, G., and Jonkheijm, P. (2017). Guiding hMSC adhesion and differentiation on supported lipid bilayers. *Adv. Healthc. Mater.* 6:1600862. doi: 10.1002/adhm.201600862

Koçer, G., and Jonkheijm, P. (2018). About chemical strategies to fabricate cell-instructive biointerfaces with static and dynamic complexity. *Adv. Healthc. Mater.* 7:1701192. doi: 10.1002/adhm.201701192

Koçer, G., ter Schiphorst, J., Hendrikx, M., Kassa, H. G., Leclère, P., Schenning, A. P. H. J., et al. (2017). Light-responsive hierarchically structured liquid crystal polymer networks for harnessing cell adhesion and migration. *Adv. Mater.* 29:1606407. doi: 10.1002/adma.201606407

Krieg, M., Arboleda-Estudillo, Y., Puech, P.-H., Käfer, J., Graner, F., Müller, D. J., et al. (2008). Tensile forces govern germ-layer organization in zebrafish. *Nat. Cell Biol.* 10, 429–436. doi: 10.1038/ncb1705

Krishnamoorthy, M., Hakobyan, S., Ramstedt, M., and Gautrot, J. E. (2014). Surface-initiated polymer brushes in the biomedical field: applications in membrane science, biosensing, cell culture, regenerative medicine and antibacterial coatings. *Chem. Rev.* 114, 10976–11026. doi: 10.1021/cr500252u

Krishnamoorthy, S., Hinderling, C., and Heinzelmann, H. (2006). Nanoscale patterning with block copolymers. *Mater. Today* 9, 40–47. doi: 10.1016/S1369-7021(06)71621-2

Kruse, C. R., Singh, M., Targosinski, S., Sinha, I., Sørensen, J. A., Eriksson, E., et al. (2017). The effect of pH on cell viability, cell migration, cell proliferation, wound closure, and wound reepithelialization: *in vitro* and *in vivo* study: Effect of pH on wound healing. *Wound Repair Regen.* 25, 260–269. doi: 10.1111/wrr.12526

Kular, J. K., Basu, S., and Sharma, R. I. (2014). The extracellular matrix: structure, composition, age-related differences, tools for analysis and applications for tissue engineering. *J. Tissue Eng.* 5, 1–17. doi: 10.1177/2041731414557112

Lam, M. T., Clem, W. C., and Takayama, S. (2008). Reversible on-demand cell alignment using reconfigurable microtopography. *Biomaterials* 29, 1705–1712. doi: 10.1016/j.biomaterials.2007.12.010

Lamers, E., van Horssen, R., te Riet, J., van Delft, F. C., Luttge, R., Walboomers, X. F., et al. (2010). The influence of nanoscale topographical cues on initial osteoblast morphology and migration. *Eur. Cell. Mater.* 20, 329–343. doi: 10.22203/eCM.v020a27

Landry, M. J., Rollet, F.-G., Kennedy, T. E., and Barrett, C. J. (2018). Layers and multilayers of self-assembled polymers: tunable engineered extracellular matrix coatings for neural cell growth. *Langmuir* 34, 8709–8730. doi: 10.1021/acs.langmuir.7b04108

Le, D. M., Kulangara, K., Adler, A. F., Leong, K. W., and Ashby, V. S. (2011). Dynamic topographical control of mesenchymal stem cells by culture on responsive Poly(ϵ-caprolactone) surfaces. *Adv. Mater.* 23, 3278–3283. doi: 10.1002/adma.201100821

Lee, J., Kang, B. S., Hicks, B., Chancellor, T. F. Jr., Chu, B. H.,Wang, H.-T., et al. (2008). The control of cell adhesion and viability by zinc oxide nanorods. *Biomaterials* 29, 3743–3749. doi: 10.1016/j.biomaterials.2008.05.029

Leijten, J., and Khademhosseini, A. (2016). From nano to macro: multiscale materials for improved stem cell culturing and analysis. *Cell Stem Cell* 18, 20–24. doi: 10.1016/j.stem.2015.12.013

Li, Y., Chu, J. S., Kurpinski, K., Li, X., Bautista, D. M., Yang, L., et al. (2011). Biophysical regulation of histone acetylation in mesenchymal stem cells. *Biophys. J.* 100, 1902–1909. doi: 10.1016/j.bpj.2011.03.008

Lim, J. Y., Hansen, J. C., Siedlecki, C. A., Hengstebeck, R. W., Cheng, J., Winograd, N., et al. (2005a). Osteoblast adhesion on Poly(L-lactic Acid)/Polystyrene demixed thin film blends: effect of nanotopography, surface chemistry, and wettability. *Biomacromolecules* 6, 3319–3327. doi: 10.1021/bm0503423

Lim, J. Y., Hansen, J. C., Siedlecki, C. A., Runt, J., and Donahue, H. J. (2005b). Human foetal osteoblastic cell response to polymer-demixed nanotopographic interfaces. *J. R. Soc. Interface* 2, 97–108. doi: 10.1098/rsif.2004.0019

Lindblom, G., Orädd, G., and Filippov, A. (2006). Lipid lateral diffusion in bilayers with phosphatidylcholine, sphingomyelin and cholesterol. *Chem. Phys. Lipids* 141, 179–184. doi: 10.1016/j.chemphyslip.2006.02.011

Liu, D., Xie, Y., Shao, H., and Jiang, X. (2009). Using Azobenzene-embedded self-assembled monolayers to photochemically control cell adhesion reversibly. *Angew. Chem. Int. Ed.* 48, 4406–4408. doi: 10.1002/anie.200901130

Liu, F., and Urban, M. W. (2010). Recent advances and challenges in designing stimuli-responsive polymers. *Prog. Polym. Sci.* 35, 3–23. doi: 10.1016/j.progpolymsci.2009.10.002

Liu, L., Ratner, B. D., Sage, E. H., and Jiang, S. (2007). Endothelial cell migration on surface-density gradients of Fibronectin, VEGF, or both proteins. *Langmuir* 23, 11168–11173. doi: 10.1021/la701435x

Lord, M. S., Foss, M., and Besenbacher, F. (2010). Influence of nanoscale surface topography on protein adsorption and cellular response. *Nano Today* 5, 66–78. doi: 10.1016/j.nantod.2010.01.001

Lu, P., Takai, K., Weaver, V. M., and Werb, Z. (2011). Extracellular matrix degradation and remodeling in development and disease. *Cold Spring Harb. Perspect. Biol.* 3, a005058–a005058. doi: 10.1101/cshperspect.a005058

Lu, P., Weaver, V. M., and Werb, Z. (2012). The extracellular matrix: a dynamic niche in cancer progression. *J. Cell Biol.* 196, 395–406. doi: 10.1083/jcb.201102147

Massia, S. P., and Hubbell, J. A. (1991). An RGD spacing of 440 nm is sufficient for integrin alpha V beta 3- mediated fibroblast spreading and 140 nm for focal contact and stress fiber formation. *J. Cell Biol.* 114, 1089–1100. doi: 10.1083/jcb.114.5.1089

Masuma, R., Kashima, S., Kurasaki, M., and Okuno, T. (2013). Effects of UV wavelength on cell damages caused by UV irradiation in PC12 cells. *J. Photochem. Photobiol. B* 125, 202–208. doi: 10.1016/j.jphotobiol.2013.06.003

Mather, P. T., Luo, X., and Rousseau, I. A. (2009). Shape memory polymer research. *Annu. Rev. Mater. Res.* 39, 445–471. doi: 10.1146/annurev-matsci-082908-145419

Meier, T., Bur, J., Reinhard, M., Schneider, M., Kolew, A., Worgull, M., et al. (2015). Programmable and self-demolding microstructured molds fabricated from shape-memory polymers. *J. Micromech. Microeng.* 25:065017. doi: 10.1088/0960-1317/25/6/065017

Mendes, P. M. (2008). Stimuli-responsive surfaces for bio-applications. *Chem. Soc. Rev.* 37, 2512–2529. doi: 10.1039/b714635n

Mengsteab, P. Y., Uto, K., Smith, A. S. T., Frankel, S., Fisher, E., Nawas, Z., et al. (2016). Spatiotemporal control of cardiac anisotropy using dynamic nanotopographic cues. *Biomaterials* 86, 1–10. doi: 10.1016/j.biomaterials.2016.01.062

Montell, D. J. (2008). Morphogenetic cell movements: diversity from modular mechanical properties. *Science* 322, 1502–1505. doi: 10.1126/science.1164073

Mrksich, M. (2009). Using self-assembled monolayers to model the extracellular matrix. *Acta Biomater.* 5, 832–841. doi: 10.1016/j.actbio.2009.01.016

Murphy, W. L., McDevitt, T. C., and Engler, A. J. (2014). Materials as stem cell regulators. *Nat. Mater.* 13, 547–557. doi: 10.1038/nmat3937

Nakanishi, J., Kikuchi, Y., Inoue, S., Yamaguchi, K., Takarada, T., and Maeda, M. (2007). Spatiotemporal control of migration of single cells on a photoactivatable cell microarray. *J. Am. Chem. Soc.* 129, 6694–6695. doi: 10.1021/ja070294p

Nakanishi, J., Kikuchi, Y., Takarada, T., Nakayama, H., Yamaguchi, K., and Maeda, M. (2006). Spatiotemporal control of cell adhesion on a self-assembled monolayer having a photocleavable protecting group. *Anal. Chim. Acta* 578, 100–104. doi: 10.1016/j.aca.2006.04.059

Natale, C. F., Ventre, M., and Netti, P. A. (2014). Tuning the material-cytoskeleton crosstalk via nanoconfinement of focal adhesions. *Biomaterials* 35, 2743–2751. doi: 10.1016/j.biomaterials.2013.12.023

Ng, C. C. A., Magenau, A., Ngalim, S. H., Ciampi, S., Chockalingham, M., Harper, J. B., et al. (2012). Using an electrical potential to reversibly switch surfaces between two states for dynamically controlling cell adhesion. *Angew. Chem. Int. Ed.* 51, 7706–7710. doi: 10.1002/anie.201202118

Nikkhah, M., Edalat, F., Manoucheri, S., and Khademhosseini, A. (2012). Engineering microscale topographies to control the cell–substrate interface. *Biomaterials* 33, 5230–5246. doi: 10.1016/j.biomaterials.2012.03.079

Onclin, S., Ravoo, B. J., and Reinhoudt, D. N. (2005). Engineering silicon oxide surfaces using self-assembled monolayers. *Angew. Chem. Int. Ed.* 44, 6282–6304. doi: 10.1002/anie.200500633

Parsons, J. T., Horwitz, A. R., and Schwartz, M. A. (2010). Cell adhesion: integrating cytoskeletal dynamics and cellular tension. *Nat. Rev. Mol. Cell Biol.* 11, 633–643. doi: 10.1038/nrm2957

Pelham, R. J., and Wang, Y. -,l. (1997). Cell locomotion and focal adhesions are regulated by substrate flexibility. *Proc. Natl. Acad. Sci. U.S.A.* 94, 13661–13665. doi: 10.1073/pnas.94.25.13661

Petersen, S., Alonso, J. M., Specht, A., Duodu, P., Goeldner, M., and del Campo, A. (2008). Phototriggering of cell adhesion by Caged cyclic RGD peptides. *Angew. Chem. Int. Ed.* 47, 3192–3195. doi: 10.1002/anie.200704857

Rasouli, R., Barhoum, A., and Uludag, H. (2018). A review of nanostructured surfaces and materials for dental implants: surface coating, patterning and functionalization for improved performance. *Biomater. Sci.* 6, 1312–1338. doi: 10.1039/C8BM00021B

Ratna, D., and Karger-Kocsis, J. (2008). Recent advances in shape memory polymers and composites: a review. *J. Mater. Sci.* 43, 254–269. doi: 10.1007/s10853-007-2176-7

Rianna, C., Calabuig, A., Ventre, M., Cavalli, S., Pagliarulo, V., Grilli, S., et al. (2015). Reversible holographic patterns on azopolymers for guiding cell adhesion and orientation. *ACS Appl. Mater. Interfaces* 7, 16984–16991. doi: 10.1021/acsami.5b02080

Rianna, C., Rossano, L., Kollarigowda, R. H., Formiggini, F., Cavalli, S., Ventre, M., et al. (2016). Spatio-temporal control of dynamic topographic patterns on azopolymers for cell culture applications. *Adv. Funct. Mater.* 26, 7572–7580. doi: 10.1002/adfm.201602577

Roberts, J. N., Sahoo, J. K., McNamara, L. E., Burgess, K. V., Yang, J., Alakpa, E. V., et al. (2016). Dynamic surfaces for the study of mesenchymal stem cell growth through adhesion regulation. *ACS Nano* 10, 6667–6679. doi: 10.1021/acsnano.6b01765

Rocha, L., Păiuș, C.-M., Luca-Raicu, A., Resmerita, E., Rusu, A., Moleavin, I.-A., et al. (2014). Azobenzene based polymers as photoactive supports and micellar structures for applications in biology. *J. Photochem. Photobiol. Chem.* 291, 16–25. doi: 10.1016/j.jphotochem.2014.06.018

Rosales, A. M., Rodell, C. B., Chen, M. H., Morrow, M. G., Anseth, K. S., and Burdick, J. A. (2018). Reversible control of network properties in azobenzene-containing hyaluronic acid-based hydrogels. *Bioconjug. Chem.* 29, 905–913. doi: 10.1021/acs.bioconjchem.7b00802

Rosales, A. M., Vega, S. L., DelRio, F. W., Burdick, J. A., and Anseth, K. S. (2017). Hydrogels with reversible mechanics to probe dynamic cell microenvironments. *Angew. Chem. Int. Ed.* 56, 12132–12136. doi: 10.1002/anie.201705684

Rossano, L., Cimmino, C., Cavalli, S., Ventre, M., and Netti, P. A. (2018). Regulating fibroblast shape and mechanics through photoresponsive surfaces with concentric circular topographic patterns. *Adv. Mater. Interfaces* 5:1800890. doi: 10.1002/admi.201800890

Roy, D., Cambre, J. N., and Sumerlin, B. S. (2010). Future perspectives and recent advances in stimuli-responsive materials. *Prog. Polym. Sci.* 35, 278–301. doi: 10.1016/j.progpolymsci.2009.10.008

Sawada, Y., Tamada, M., Dubin-Thaler, B. J., Cherniavskaya, O., Sakai, R., Tanaka, S., et al. (2006). Force sensing by mechanical extension of the src family kinase substrate p130Cas. *Cell* 127, 1015–1026. doi: 10.1016/j.cell.2006.09.044

Schreiber, F. (2004). Self-assembled monolayers: from simple model systems to biofunctionalized interfaces. *J. Phys. Condens. Matter* 16, R881–R900. doi: 10.1088/0953-8984/16/28/R01

Singh, P., Carraher, C., and Schwarzbauer, J. E. (2010). Assembly of Fibronectin Extracellular Matrix. *Annu. Rev. Cell Dev. Biol.* 26, 397–419. doi: 10.1146/annurev-cellbio-100109-104020

Sjöström, T., Dalby, M. J., Hart, A., Tare, R., Oreffo, R. O. C., and Su, B. (2009). Fabrication of pillar-like titania nanostructures on titanium and their interactions with human skeletal stem cells. *Acta Biomater.* 5, 1433–1441. doi: 10.1016/j.actbio.2009.01.007

Srisombat, L., Jamison, A. C., and Lee, T. R. (2011). Stability: a key issue for self-assembled monolayers on gold as thin-film coatings and nanoparticle protectants. *Colloids Surf. Physicochem. Eng. Asp.* 390, 1–19. doi: 10.1016/j.colsurfa.2011.09.020

Stuart, M. A. C., Huck, W. T. S., Genzer, J., Müller, M., Ober, C., Stamm, M., et al. (2010). Emerging applications of stimuli-responsive polymer materials. *Nat. Mater.* 9, 101–113. doi: 10.1038/nmat2614

Tang, Z., and Okano, T. (2014). Recent development of temperature-responsive surfaces and their application for cell sheet engineering. *Regen. Biomater.* 1, 91–102. doi: 10.1093/rb/rbu011

Teixeira, A. I. (2003). Epithelial contact guidance on well-defined micro- and nanostructured substrates. *J. Cell Sci.* 116, 1881–1892. doi: 10.1242/jcs.00383

Thiele, J., Ma, Y., Bruekers, S. M. C., Ma, S., and Huck, W. T. S. (2014). 25th anniversary article: designer hydrogels for cell cultures: a materials selection guide. *Adv. Mater.* 26, 125–148. doi: 10.1002/adma.201302958

Todd, S. J., Farrar, D., Gough, J. E., and Ulijn, R. V. (2007). Enzyme-triggered cell attachment to hydrogel surfaces. *Soft Matter* 3, 547–550. doi: 10.1039/b618256a

Tong, M. H., Huang, N., Zhang, W., Zhou, Z. L., Ngan, A. H. W., Du, Y., et al. (2016). Multiphoton photochemical crosslinking-based fabrication of protein micropatterns with controllable mechanical properties for single cell traction force measurements. *Sci. Rep.* 6:20063. doi: 10.1038/srep20063

Trappmann, B., Gautrot, J. E., Connelly, J. T., Strange, D. G. T., Li, Y., Oyen, M. L., et al. (2012). Extracellular-matrix tethering regulates stem-cell fate. *Nat. Mater.* 11, 642–649. doi: 10.1038/nmat3339

Ulman, A. (1996). Formation and structure of self-assembled monolayers. *Chem. Rev.* 96, 1533–1554. doi: 10.1021/cr9502357

Vafaei, S., Tabaei, S. R., and Cho, N.-J. (2017). Optimizing the performance of supported lipid bilayers as cell culture platforms based on extracellular matrix functionalization. *ACS Omega* 2, 2395–2404. doi: 10.1021/acsomega.7b00158

VandeVondele, S., Vörös, J., and Hubbell, J. A. (2003). RGD-grafted poly-l-lysine-graft-(polyethylene glycol) copolymers block non-specific protein adsorption while promoting cell adhesion. *Biotechnol. Bioeng.* 82, 784–790. doi: 10.1002/bit.10625

Vendra, V. K., Wu, L., and Krishnan, S. (2011). "Polymer thin films for biomedical applications," in *Nanotechnologies for the Life Sciences*, ed C. S. S. R. Kumar (Weinheim: Wiley-VCH Verlag GmbH and Co. KGaA), 1–54. doi: 10.1002/9783527610419.ntls0179

Ventre, M., Causa, F., and Netti, P. A. (2012). Determinants of cell-material crosstalk at the interface: towards engineering of cell instructive materials. *J. R. Soc. Interface* 9, 2017–2032. doi: 10.1098/rsif.2012.0308

Ventre, M., Coppola, V., Iannone, M., Netti, P. A., Tekko, I., Larrañeta, E., et al. (2018). "Nanotechnologies for tissue engineering and regeneration," in *Nanotechnologies in Preventive and Regenerative Medicine,* eds. V. Uskoković, D. P. Uskoković (Amsterdam: Elsevier), 93–206. doi: 10.1016/B978-0-323-48063-5.00002-2

Ventre, M., Natale, C. F., Rianna, C., and Netti, P. A. (2014). Topographic cell instructive patterns to control cell adhesion, polarization and migration. *J. R. Soc. Interface* 11, 1–11. doi: 10.1098/rsif.2014.0687

Ventre, M., and Netti, P. (2016a). Controlling cell functions and fate with surfaces and hydrogels: the role of material features in cell adhesion and signal transduction. *Gels* 2:12. doi: 10.3390/gels2010012

Ventre, M., and Netti, P. A. (2016b). Engineering cell instructive materials to control cell fate and functions through material cues and surface patterning. *ACS Appl. Mater. Interfaces* 8, 14896–14908. doi: 10.1021/acsami.5b08658

Watanabe, I., and Okada, S. (1967). Effects of temperature on growth rate of cultured mammalian cells (L5178Y). *J. Cell Biol.* 32, 309–323.

Wei, Y., Tang, Q., Gong, C., and Lam, M. H.-W. (2015). Review of the recent progress in photoresponsive molecularly imprinted polymers containing azobenzene chromophores. *Anal. Chim. Acta* 900, 10–20. doi: 10.1016/j.aca.2015.10.022

Wen, J. H., Vincent, L. G., Fuhrmann, A., Choi, Y. S., Hribar, K. C., Taylor-Weiner, H., et al. (2014). Interplay of matrix stiffness and protein tethering in stem cell differentiation. *Nat. Mater.* 13, 979–987. doi: 10.1038/nmat4051

Williams, C., Xie, A. W., Yamato, M., Okano, T., and Wong, J. Y. (2011). Stacking of aligned cell sheets for layer-by-layer control of complex tissue structure. *Biomaterials* 32, 5625–5632. doi: 10.1016/j.biomaterials.2011.04.050

Williams, M. L., and Bhatia, S. K. (2014). Engineering the extracellular matrix for clinical applications: endoderm, mesoderm, and ectoderm. *Biotechnol. J.* 9, 337–347. doi: 10.1002/biot.201300120

Yamada, N., Okano, T., Sakai, H., Karikusa, F., Sawasaki, Y., and Sakurai, Y. (1990). Thermo-responsive polymeric surfaces; control of attachment and detachment of cultured cells. *Makromol. Chem. Rapid Commun.* 11, 571–576. doi: 10.1002/marc.1990.030111109

Yang, C., Tibbitt, M. W., Basta, L., and Anseth, K. S. (2014). Mechanical memory and dosing influence stem cell fate. *Nat. Mater.* 13, 645–652. doi: 10.1038/nmat3889

Yao, T., and Asayama, Y. (2017). Animal-cell culture media: history, characteristics, and current issues. *Reprod. Med. Biol.* 16, 99–117. doi: 10.1002/rmb2.12024

Yao, X., Peng, R., and Ding, J. (2013). Cell-material interactions revealed via material techniques of surface patterning. *Adv. Mater.* 25, 5257–5286. doi: 10.1002/adma.201301762

Yeo, W.-S., and Mrksich, M. (2006). Electroactive self-assembled monolayers that permit orthogonal control over the adhesion of cells to patterned substrates[†]. *Langmuir* 22, 10816–10820. doi: 10.1021/la061212y

Yeo, W.-S., Yousaf, M. N., and Mrksich, M. (2003). Dynamic interfaces between cells and surfaces: electroactive substrates that sequentially release and attach cells. *J. Am. Chem. Soc.* 125, 14994–14995. doi: 10.1021/ja038265b

Yoon, S.-H., and Mofrad, M. R. K. (2011). Cell adhesion and detachment on gold surfaces modified with a thiol-functionalized RGD peptide. *Biomaterials* 32, 7286–7296. doi: 10.1016/j.biomaterials.2011.05.077

Young, J. L., and Engler, A. J. (2011). Hydrogels with time-dependent material properties enhance cardiomyocyte differentiation *in vitro*. *Biomaterials* 32, 1002–1009. doi: 10.1016/j.biomaterials.2010.10.020

Yu, C. H., Law, J. B. K., Suryana, M., Low, H. Y., and Sheetz, M. P. (2011). Early integrin binding to Arg-Gly-Asp peptide activates actin polymerization and contractile movement that stimulates outward translocation. *Proc. Natl. Acad. Sci. U.S.A.* 108, 20585–20590. doi: 10.1073/pnas.1109485108

Zhang, J., Ma, W., He, X.-P., and Tian, H. (2017). Taking orders from light: photo-switchable working/inactive smart surfaces for protein and cell adhesion. *ACS Appl. Mater. Interfaces* 9, 8498–8507. doi: 10.1021/acsami.6b15599

Zhu, X., Mills, K. L., Peters, P. R., Bahng, J. H., Liu, E. H., Shim, J., et al. (2005). Fabrication of reconfigurable protein matrices by cracking. *Nat. Mater.* 4, 403–406. doi: 10.1038/nmat1365

Conflict of Interest Statement: The authors declare that the research was conducted in the absence of any commercial or financial relationships that could be construed as a potential conflict of interest.

frontiers in Bioengineering and Biotechnology

BRIEF RESEARCH REPORT
published: 12 September 2018
doi: 10.3389/fbioe.2018.00127

Composite of Elastin-Based Matrix and Electrospun Poly(L-Lactic Acid) Fibers: A Potential Smart Drug Delivery System

Antonella Bandiera[1]*, *Sabina Passamonti*[1], *Luisa Stella Dolci*[2†] and *Maria Letizia Focarete*[2,3]

[1] Department of Life Sciences, University of Trieste, Trieste, Italy, [2] Department of Chemistry "G. Ciamician" and National Consortium of Materials Science and Technology (INSTM, Bologna RU), Alma Mater Studiorum - Università di Bologna, Bologna, Italy, [3] Health Sciences and Technologies–Interdepartmental Center for Industrial Research, Alma Mater Studiorum - Università di Bologna, Bologna, Italy

OPEN ACCESS

Edited by:
Gianni Ciofani,
Politecnico di Torino, Italy

Reviewed by:
Elisa Mele,
Loughborough University,
United Kingdom
Marc Antoni Fernández Yagüe,
National University of Ireland, Ireland

***Correspondence:**
Antonella Bandiera
abandiera@units.it

†Present Address:
Luisa Stella Dolci,
Department of Pharmacy and Biotechnology, Alma Mater Studiorum - Università di Bologna, Bologna, Italy

Specialty section:
This article was submitted to Nanobiotechnology, a section of the journal Frontiers in Bioengineering and Biotechnology

Received: 12 July 2018
Accepted: 24 August 2018
Published: 12 September 2018

Citation:
Bandiera A, Passamonti S, Dolci LS and Focarete ML (2018) Composite of Elastin-Based Matrix and Electrospun Poly(L-Lactic Acid) Fibers: A Potential Smart Drug Delivery System. Front. Bioeng. Biotechnol. 6:127. doi: 10.3389/fbioe.2018.00127

Stimuli-responsive hydrogel matrices are inspiring manifold applications in controlled delivery of bioactive compounds. Elastin-derived polypeptides form hydrogel matrices that may release bioactive moieties as a function of local increase of active elastases, as it would occur in several processes like inflammation. In view of the development of a patch for healing wounds, recombinant elastin-based polypeptides were combined with a proteolysis-resistant scaffold, made of electrospun poly-L-lactic acid (PLLA) fibers. The results of this study demonstrated the compatibility of these two components. An efficient procedure to obtain a composite material retaining the main features of each component was established. The release of the elastin moiety was monitored by means of a simple protocol. Our data showed that electrospun PLLA can form a composite with fusion proteins bound to elastin-derived polypeptides. Therefore, our approach allows designing a therapeutic agent delivery platform to realize devices capable of responding and interacting with biological systems at the molecular level.

Keywords: elastin, electrospun matrix, composite, smart release, drug delivery

INTRODUCTION

The biomaterial field has enormously evolved in the last decades. Many different materials have been developed and are available to realize devices that can be used for a wide variety of applications. With the advent of bioengineering and regenerative medicine, the field of biomaterials entered the phase of developing devices capable of actively interacting with the biological system, rather than passively integrating within it (Hench and Polak, 2002). However, despite the huge work done in this field, there is a constant demand for innovative solutions in order to address many still unmet biomedical needs (Holzapfel et al., 2013).

Among the many composite biomaterials that have been developed and tested for medical applications, the combination of electrospun fibers and hydrogels recently attracted the attention of researchers. Due to their individual features, combining the advantages of both components results in a product with superior properties, that has a high potential for expanding the range of applications of the final construct (reviewed in Bosworth et al., 2013; Xu et al., 2016).

The advantages achieved by the combination of electrospun fibers and hydrogels have been demonstrated in the field of controlled drug delivery, where controlled release could be obtained by exploiting the release characteristics of the two components (Han et al., 2013; Bruggeman et al., 2017). In the field of tissue engineering, combining the biomimetic properties, hydrophilicity, and softness of hydrogels with the mechanical strength of electrospun sheets, allows to mimic the structure of tissue extracellular matrix (Gualandi et al., 2016). Other fields of application of electrospun fibers/hydrogels composites are those of biotechnology and biosensors (Xu et al., 2016).

Electrospun fibrous mats, made of natural or synthetic polymers, exhibit high porosity, high surface area to volume ratio, and good mechanical properties. Moreover, these properties can be easily tailored by changing the fiber diameter through proper control of the electrospinning process. For these reasons, electrospun mats represent a valuable platform for drug delivery and tissue engineering and regeneration (Chen et al., 2018).

Elastin-like polypeptides are an emerging class of biotechnologically derived biopolymers that are inspired to the tissue structural protein elastin (MacEwan and Chilkoti, 2010; Girotti et al., 2011). In our lab, starting from design, cloning and expression of synthetic genes, a family of recombinant proteins named Human Elastin-like Polypeptides (HELPs) was produced (Bandiera, 2010). This versatile platform can be readily customized by the fusion of bioactive domains of interest, thus embedding the new functionality in the final construct. A method for the preparation of hydrogel matrix based on these HELPs was set up (Bandiera, 2011) and the specific stimuli-induced release was demonstrated (Bandiera et al., 2014).

To the best of our knowledge, there are only few examples of elastin-like based composites that have been developed till now (reviewed in Kakinoki et al., 2014; Yeo et al., 2015). Here, we describe an approach to obtain a new composite material based on deposition of elastin-like based on electrospun poly-L-lactic acid (PLLA-HELP).

MATERIALS AND METHODS

HELP Biopolymers

HELP and mHELP, the latter being a construct of HELP obtained by fusing at the C-terminal region a functional domain (unpublished data) were produced exploiting their inverse phase transition properties as already detailed (Bandiera, 2010). The purified products were checked by SDS-PAGE and lyophilized.

Electrospun PLLA Scaffold Fabrication

Poly(L-lactic acid) (PLLA) (Lacea H.100-E) (Mw = 8.4 10^4g mol^{-1}, PDI = 1.7) was supplied by Mitsui Fine Chemicals. Dichloromethane (DCM) and dimethylformamide (DMF), were purchased by Sigma–Aldrich and were used without any further purification. PLLA was dissolved in a mixed solvent, DCM:DMF = 65:35 v/v, at a concentration of 13% w/v. The polymeric solution was electrospun by means of an electrospinning apparatus (Spinbow srl, Italy) by applying the following processing conditions: applied voltage = 18 kV, feed rate = 0.015 ml min^{-1}, needle-to-collector distance = 15 cm. The electrospun mat was produced at RT and at relative humidity of 40–50% and was kept under vacuum over P_2O_5 at RT overnight in order to remove residual solvents.

Water Contact Angle (WCA) Measurements

Static WCA measurements were performed at RT under ambient conditions by using an optical contact angle and surface tension meter KSV's CAM 100 (KSV, Espoo, Finland). Milli-Q water was used for measurements. The water drop profile images were collected in a time range of 0–60 s, every 1 s. Sixty seconds was selected as the upper time limit since it was verified that, after that period, the WCAs reached a constant value. Optical contact angle and pendant drop surface tension software was used for image processing. Results (WCA at 60 s) were averaged on at least five measurements obtained at different areas of the sample.

HELP Deposition and Cross-Linking on PLLA

Five percent (w/v) of water solution of HELP and the other proteins tested were prepared and 5 μl of each sample were spotted on small sheets of PLLA mat. Water was evaporated at RT and the dried samples were stored (controls) or washed with excess water, respectively. Washed samples were dried as well. For cross-linking, 2 μl of microbial transglutaminase (60 mg/ml, N-Zyme Biotec GmbH, Darmstadt, Germany) were added to 30 μl of 5% (w/v) HELP or its fusion in 10 mM Tris/HCl pH 8 (Sigma-Aldrich, #T1503). Spots of 5 μl were deposited on PLLA mat and the reaction was carried on for 1 h at RT or at 5°C overnight in a wet chamber to avoid drying. After cross-linking the samples were washed overnight as described above and stored dry.

Evaluation of Protein Retention on PLLA

Samples of PLLA with adsorbed or cross-linked HELP were stained for 10 min in 0.5 mg/mL Amidoblack (Serva, #12310), 50% Ethanol and then rinsed twice with water for 10 min. Each spot was cut off and soaked in 200 μl of 50 mM Tris/HCl pH 7.5, 1 mM $CaCl_2$, in the absence or in presence of 0.5 μg elastase (Sigma-Aldrich, #E7885). Samples were incubated overnight at 37°C. Supernatants were read at 620 nm by a microplate reader (Synergy H1, Bio Tek).

Scanning Electron Microscopy (SEM) Analysis

After cross-linking samples were rinsed with excess water. They were frozen at −20°C and lyophilized. Slices were cut, mounted onto stubs using a double-sided adhesive and sputter coated

with gold. Analysis was performed using a Leica Stereoscan 430i Scanning Electron Microscope.

RESULTS

Our strategy to prepare a PLLA-HELP composite is schematized in **Figure 1A**.

The approach used in this study is the physical combination of two materials, through deposition of HELP-based protein onto the surface of PLLA mat. Blending of HELP protein and PLLA solution before electrospinning was not possible since the organic solvents required for electrospinning PLLA were not compatible with the protein. Moreover, only a small amount of the protein would have been available at the surface of the fibers. The first step of composite fabrication consisted in the evaluation of the compatibility of these two materials, since WCA measurement demonstrated that electrospun PLLA is a hydrophobic material (WCA $= 120° \pm 3°$), whereas the HELP protein is soluble in aqueous solution. Both HELP and one of its fusion products were dissolved in water and dropped on a PLLA sheet, avoiding the physical contact with any surface beneath it. A solution of Bovine Serum Albumin (BSA) at the same concentration was tested as reference. Interestingly, as shown in **Figure 1B**, PLLA samples in contact with HELP-based protein solutions immediately became wet and the drop spread over the sheet, whereas when a drop of BSA was deposited onto the PLLA sheet, no wetting was observed. After water evaporation, the sample deposited on PLLA was no longer observable. To assess the presence of HELP protein on PLLA, we stained the samples with Amidoblack. After de-staining, the protein became evident (**Figure 1C**, top left).

In parallel, a replica sample was prepared and submitted to an overnight wash before the staining procedure. As shown in **Figure 1C** (top right), almost no stain was detectable after the overnight wash. On the contrary, when the transglutaminase enzyme was added to the HELP protein to determine its cross-linking (Bandiera, 2011), no difference could be detected between the unwashed (**Figure 1C**, bottom left) and the overnight washed replica (**Figure 1C**, bottom right). This indicated that the enzymatic cross-linking stabilized the HELP protein on the PLLA sheet.

We set up a method to estimate the stability of HELP deposited on PLLA, by exploiting the susceptibility of HELP to protease-dependent elastolysis (Corich et al., 2017). **Figure 1C** shows that after the wash, cross-linked HELP-PLLA samples retained up to 96% of the HELP protein after the wash step, whereas <20% of it remained in the non-cross-linked samples. This suggested that cross-linking caused the formation of a stable HELP-PLLA composite.

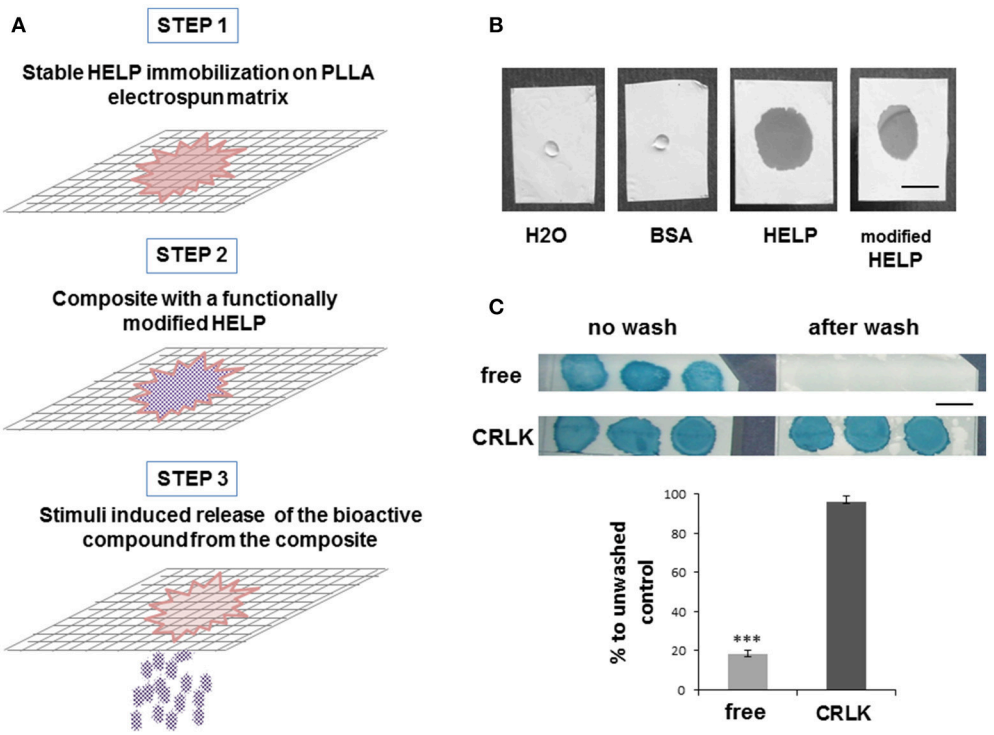

FIGURE 1 | HELP-PLLA composite design. **(A)** Schematic description of the experimental approach; **(B)** Representative images of different protein aqueous solutions 0.5 min after deposition on PLLA matrix. Bar is 5 mm; **(C)** Stabilization effect of the HELP cross-linking process (CRLK) compared to simple deposition of the protein (free) on PLLA matrix: representative images of unwashed and washed samples, Amidoblack staining. Bar is 5 mm. Evaluation of sample stability after washing is reported in the histogram. Each value represented the mean ± SD, $n = 3$. Differences between free and cross-linked samples after extensive washing were assessed by one-way ANOVA, $^{***}p < 0.001$ compared to unwashed samples.

Since this work was undertaken with the aim of realizing smart devices endowed with environmentally-controlled functionality, it was of great interest to assess if fusion-modified HELP could be stabilized in the PLLA matrix as well. For this reason, mHELP, a fusion-modified HELP that we recently obtained by cloning a functional binding domain to the HELP backbone (unpublished results), was employed. The same procedure used for HELP-PLLA composite was applied to mHELP-PLLA samples and the analyses were performed giving results similar to those shown in **Figure 1C** (not shown).

To obtain further information on the morphology of the stabilized mHELP-PLLA samples, SEM analysis was performed. **Figure 2A** shows SEM analysis of PLLA electrospun fibers. Cross-linking the composite, even after extensive overnight washing, changed the morphology of PLLA, which appeared as coated by a continuous, amorphous layer, filling the pores among the fibers (**Figure 2C**). In the absence of cross-linking, tiny deposits of protein were observed on PLLA only after a quick wash (**Figure 2B**).

These results indicate that both HELP macromolecule and its fusion modifications could be employed for preparation of new composites endowed with functional activity. Analysis of activity retention is currently ongoing.

DISCUSSION

HELP matrix has been shown to possess stimuli-responsive properties, undergoing selective degradation in the presence of elastolytic activity. Exploiting this feature represents an attractive option to realize smart systems that can be employed for therapeutic delivery, tissue engineering, and biosensing (Corich et al., 2017).

In this view, we explored the possibility of integrating the HELP hydrogel matrix with an electrospun PLLA support and our approach is schematized in **Figure 1A**. Besides being endowed with adequate mechanical tensile strength, electrospun PLLA has a high degree of biocompatibility and has been extensively employed in the fabrication of bioresorbable scaffolds for tissue engineering applications (Chen et al., 2018). Electrospun PLLA is known to be hydrophobic. To increase its hydrophilicity and wettability, surface modifications with functional groups are needed. These enable conjugation or chemical interactions with hydrogels (Dolci et al., 2014; Gualandi et al., 2016). In our approach, the first step of composite fabrication consisted in the evaluation of the compatibility and in the exploration of the conditions for a stable integration of the HELP-based hydrogel in the PLLA electrospun mat. Interestingly, we found that no treatment was needed to enhance PLLA wettability for HELP deposition. The presence of the protein in solution allowed the instantaneous PLLA fiber permeation by the solution (**Figure 1B**). The finding that physical adsorption of HELP-based proteins onto PLLA mat increased the wetting properties of electrospun PLLA surface is in agreement with previous studies on substrates modified with other elastin-based molecules (Jordan et al., 2007; Srokowski and Woodhouse, 2013) and it is likely related to the relatively high hydropathy index of the HELP protein (Bandiera et al., 2010). Notably, the cross-linking process was the key step to stabilize the HELP moiety on the PLLA mat (**Figure 1C**).

Keeping in mind that the HELP macromolecule can be tailored by addition of a bioactive domain, in principle, these conditions could be extended to any HELP derivative, obtained by C-terminal domain fusion. Thus, the resulting composite will be endowed with a new, specific functionality. Indeed, in this work we demonstrated that similar result could be obtained

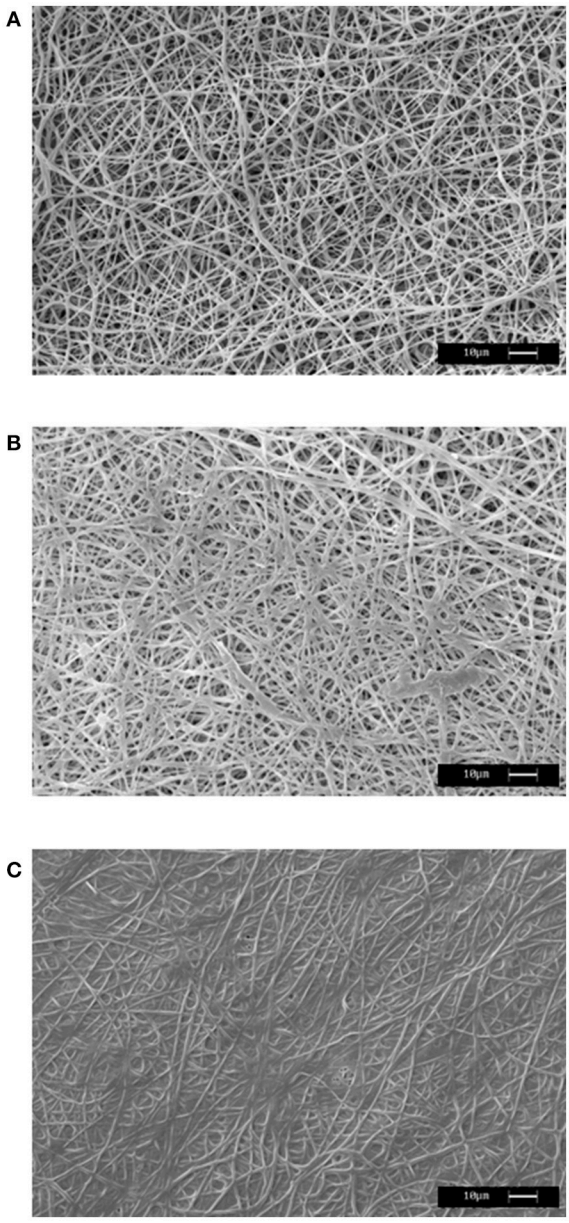

FIGURE 2 | Representative SEM images of PLLA mat **(A)**, mHELP deposited on the PLLA matrix in the absence of cross-linking **(B)** and mHELP undergone cross-linking after deposition on PLLA matrix **(C)**. Bar is 10 μm.

using both a HELP protein and mHELP, a fusion-modified HELP, in which the fusion domain represents about one-fifth of the whole macromolecule. SEM analysis was used to achieve the structural evidence of the integration of both materials in a new composite obtained after the cross-linking process (**Figure 2C**).

This achievement represents the second step of our strategy, i.e., the realization of a composite with a tailored HELP fusion, endowed with a specific functionality (**Figure 1A**).

A third step can be foreseen, consisting in the stimuli-induced release of the active domain. Future work will be dedicated to fully characterize the new material that opens the way for the realization of stimuli-responsive biomedical devices for the delivery of therapeutic and bioactive substances and for regenerative medicine, as well as for the development of biosensors.

CONCLUSION

In this work we explored the opportunity to realize a composite material made of HELP-based hydrogels and PLLA electrospun fibers. The results clearly show that the fabrication of a composite is feasible and that the features of the two materials can be successfully integrated. This strategy is useful to combine the individual performances of the two constituents and future study will clarify the properties of the new hybrid material. The stimuli-responsive nature of the HELP moiety has been already proven and described (Bandiera et al., 2014; Corich et al., 2017) and it represents an advantage that can be conferred to any new material derived from it. Moreover, HELP-based proteins represent a platform that is readily customizable by molecular fusion of exogenous domains, to confer specific functionality to the final product.

We believe that this strategy will contribute to bypass shortcoming and to improve the performance of the single components, opening the way to the realization of devices potentially able to release bioactive compounds upon specific stimuli.

AUTHOR CONTRIBUTIONS

All the authors conceived and planned the experiments. AB and LD carried out the experimental work. All authors discussed the results and contributed to the final manuscript, reading, and approving the submitted version.

ACKNOWLEDGMENTS

The authors gratefully thanks Dr. Francesca Vita for performing SEM analysis. Dr. Lucia Corich is also acknowledged. This work was supported by Beneficentia Stiftung (BEN 2014/125), Vaduz, Lichtenstein to AB, Crossborder Cooperation programme Italy-Slovenia 2007-2013 (Trans2Care project) to SP and by a Regione Emilia Romagna grant (POR-FESR 2014–2020) to MF.

REFERENCES

Bandiera, A. (2010). Assembly and optimization of expression of synthetic genes derived from the human elastin repeated motif. *Prep. Biochem. Biotechnol.* 40, 198–212. doi: 10.1080/10826068.2010.488541

Bandiera, A. (2011). Transglutaminase-catalyzed preparation of human elastin-like polypeptide-based three-dimensional matrices for cell encapsulation. *Enzyme Microb. Tech.* 49, 347–352. doi: 10.1016/j.enzmictec.2011.06.012

Bandiera, A., Markulin, A., Corich, L., Vita, F., and Borelli, V. (2014). Stimuli-induced release of compounds from elastin biomimetic matrix. *Biomacromolecules* 15, 416–422. doi: 10.1021/bm401677n

Bandiera, A., Sist, P., and Urbani, R. (2010). Comparison of thermal behavior of two recombinantly expressed human elastin-like polypeptides for cell culture applications. *Biomacromolecules* 11, 3256–3265. doi: 10.1021/bm100644m

Bosworth, L. A., Turner, L. A., and Cartmell, S. H. (2013). State of the art composites comprising electrospun fibres coupled with hydrogels: a review. *Nanomedicine* 9, 322–335. doi: 10.1016/j.nano.2012.10.008

Bruggeman, K. F., Wang, Y., Maclean, F. L., Parish, C. L., Williams, R. J., and Nisbet, D. R. (2017). Temporally controlled growth factor delivery from a self-assembling peptide hydrogel and electrospun nanofibre composite scaffold. *Nanoscale* 9, 13661–13669. doi: 10.1039/c7nr05004f

Chen, S., Li, R., Li, X., and Xie, J. (2018). Electrospinning: An enabling nanotechnology platform for drug delivery and regenerative medicine. *Adv. Drug Deliv. Rev*. doi: 10.1016/j.addr.2018.05.001. [Epub ahead of print].

Corich, L., Busetti, M., Petix, V., Passamonti, S., and Bandiera, A. (2017). Evaluation of a biomimetic 3D substrate based on the Human Elastin-like Polypeptides (HELPs) model system for elastolytic activity detection. *J. Biotechnol.* 255, 57–65. doi: 10.1016/j.jbiotec.2017.06.006

Dolci, L. S., Quiroga, S. D., Gherardi, M., Laurita, R., Liguori, A., Sanibondi, P., et al. (2014). Carboxyl surface functionalization of poly(L-lactic acid) electrospun nanofibers through atmospheric non-thermal plasma affects fibroblast morphology. *Plasma Process. Polym.* 11, 203–213. doi: 10.1002/ppap.201300104

Girotti, A., Fernández-Colino, A., López, I. M., Rodríguez-Cabello, J. C., and Arias, F. J. (2011). Elastin-like recombinamers: biosynthetic strategies and biotechnological applications. *Biotechnol. J.* 6, 1174–1186. doi: 10.1002/biot.201100116

Gualandi, C., Bloise, N., Mauro, N., Ferruti, P., Manfredi, A., Sampaolesi, M., et al. (2016). Poly-l-lactic acid nanofiber-polyamidoamine hydrogel composites: preparation, properties, and preliminary evaluation as scaffolds for human pluripotent stem cell culturing. *Macromol. Biosci.* 16, 1533–1544. doi: 10.1002/mabi.201600061

Han, N., Bradley, P. A., Johnson, J., Parikh, K. S., Hissong, A., Calhoun, M. A., et al. (2013). Effects of hydrophobicity and mat thickness on release from hydrogel-electrospun fiber mat composites. *J. Biomater. Sci. Polym. Ed.* 24, 2018–2030. doi: 10.1080/09205063.2013.822246

Hench, L. L., and Polak, J. M. (2002). Third-generation biomedical materials. *Science* 295, 1014–1017. doi: 10.1126/science.1067404

Holzapfel, B. M., Reichert, J. C., Schantz, J. T., Gbureck, U., Rackwitz, L., Nöth, U., et al. (2013). How smart do biomaterials need to be? A translational science and clinical point of view. *Adv. Drug Deliv. Rev.* 65, 581–603. doi: 10.1016/j.addr.2012.07.009

Jordan, S. W., Haller, C. A., Sallach, R. E., Apkarian, R. P., Hanson, S. R., and Chaikof, E. L. (2007). The effect of a recombinant elastin-mimetic coating of an ePTFE prosthesis on acute thrombogenicity in a baboon arteriovenous shunt. *Biomaterials* 28, 1191–1197. doi: 10.1016/j.biomaterials.2006.09.048

Kakinoki, S., Nakayama, M., Moritan, T., and Yamaoka, T. (2014). Three-layer microfibrous peripheral nerve guide conduit composed of elastin-laminin mimetic artificial protein and poly(L-lactic acid). *Front. Chem*. 2:52. doi: 10.3389/fchem.2014.00052

MacEwan, S. R., and Chilkoti, A. (2010). Elastin-like polypeptides: biomedical applications of tunable biopolymers. *Biopolymers* 94, 60–77. doi: 10.1002/bip.21327

Srokowski, E. M., and Woodhouse, K. A. (2013). Surface and adsorption characteristics of three elastin-like polypeptide coatings with varying sequence lengths. *J. Mater. Sci. Mater. Med.* 24, 71–84. doi: 10.1007/s10856-012-4772-6

Xu, S., Deng, L., Zhang, J., Yin, L., and Dong, A. (2016). Composites of electrospun-fibers and hydrogels: a potential solution to current challenges in biological and biomedical field. *J. Biomed. Mater. Res. B Appl. Biomater.* 104, 640–656. doi: 10.1002/jbm.b.33420

Yeo, G. C., Aghaei-Ghareh-Bolagh, B., Brackenreg, E. P., Hiob, M. A., Lee, P., and Weiss, A. S. (2015). Fabricated Elastin. *Adv. Healthc. Mater.* 4, 2530–2556. doi: 10.1002/adhm.201400781

Conflict of Interest Statement: The authors declare that the research was conducted in the absence of any commercial or financial relationships that could be construed as a potential conflict of interest.

frontiers in Bioengineering and Biotechnology

MINI REVIEW
published: 24 October 2018
doi: 10.3389/fbioe.2018.00155

Cellular Response to Surface Morphology: Electrospinning and Computational Modeling

Anna Denchai[1], *Daniele Tartarini*[2] *and Elisa Mele*[1]*

[1] Department of Materials, Loughborough University, Loughborough, United Kingdom, [2] Department of Civil Engineering, University of Sheffield, Sheffield, United Kingdom

Surface properties of biomaterials, such as chemistry and morphology, have a major role in modulating cellular behavior and therefore impact on the development of high-performance devices for biomedical applications, such as scaffolds for tissue engineering and systems for drug delivery. Opportunely-designed micro- and nanostructures provides a unique way of controlling cell-biomaterial interaction. This mini-review discusses the current research on the use of electrospinning (extrusion of polymer nanofibers upon the application of an electric field) as effective technique to fabricate patterns of micro- and nano-scale resolution, and the corresponding biological studies. The focus is on the effect of morphological cues, including fiber alignment, porosity and surface roughness of electrospun mats, to direct cell migration and to influence cell adhesion, differentiation and proliferation. Experimental studies are combined with computational models that predict and correlate the surface composition of a biomaterial with the response of cells in contact with it. The use of predictive models can facilitate the rational design of new bio-interfaces.

Keywords: bio-interfaces, surface topography, electrospinning, micro-patterning, mathematical modeling

OPEN ACCESS

Edited by:
Gianni Ciofani,
Politecnico di Torino, Italy

Reviewed by:
Elia Ranzato,
Università degli Studi del Piemonte Orientale, Italy
Simona Martinotti,
Università degli Studi del Piemonte Orientale, Italy

***Correspondence:**
Elisa Mele
e.mele2@lboro.ac.uk

Specialty section:
This article was submitted to Nanobiotechnology, a section of the journal Frontiers in Bioengineering and Biotechnology

Received: *29 August 2018*
Accepted: *08 October 2018*
Published: *24 October 2018*

Citation:
Denchai A, Tartarini D and Mele E (2018) Cellular Response to Surface Morphology: Electrospinning and Computational Modeling. Front. Bioeng. Biotechnol. 6:155. doi: 10.3389/fbioe.2018.00155

INTRODUCTION

The natural regeneration process of human tissues is strongly regulated by the interaction of cells with the extracellular matrix (ECM) (Lutolf and Hubbell, 2005; Liu and Wang, 2014). ECM is a dynamic and complex fibrous network of proteins and polysaccharides, such as collagen, elastin, fibronectin, laminin, proteoglycans and glycosaminoglycans. Cells interact with ECM by transmembrane receptors, known as integrins, that ligate with specific motifs of ECM proteins, for example arginine, glycine and arginylglycylaspartic acid (RGD) peptides (Anderson et al., 2016; Dalby et al., 2018). Cells continuously remodel the ECM environment, which, in turn, influences cell behavior and fate (differentiation, proliferation and migration) by biochemical, physical and mechanical signals (Geiger et al., 2001), and provides structural support to cells. Recent studies have investigated the effects of ECM physical properties, particularly porosity, topography and hierarchical 3D architecture, on cellular functions, and extrapolated rules to design structures for effective tissue regeneration (Li et al., 2017; Marino et al., 2017; Lin et al., 2018).

One of the technologies that is widely used to produce ECM-mimicking structures and particularly to replicate the fibrillar architecture of ECM is electrospinning (Khorshidi et al., 2016). The electrospinning technique allows the production of networks of fibers with a diameter in the range of few nm to few μm via the application of electrical forces to polymer solutions or

melts (Bhardwaj and Kundu, 2010; Mele, 2016; Zhang et al., 2016). Structural modifications of electrospun nanofibres, such as altering topographical characteristics and inducing porosity, can be achieved by controlling and varying the process parameters (polymer concentration, applied voltage, evaporation rate of the solvent used). Similarly, changes to the final makeup of the fibrous network, such as alignment and patterning of fibers, can be obtained by modifications of the electrospinning apparatus or post-processing.

This mini review analyses a selection of recent works on the use of solution electrospinning to create nanofibres with engineered surface topography (random, aligned and patterned fibers) for controlling adhesion, differentiation, and migration of different cells lines. The mini review is divided in two main sections: the first one will focus on experimental studies on electrospun fibers that provide physical cues for cell growth and differentiation; the second section will discuss computational models to predict cell behavior on micropatterns. Although mathematical models that simulate cell behavior on electrospun fibers are not currently available, the computational approaches here discussed can be adapted, in the future, to electrospun scaffolds and used to elucidate the underlying mechanisms responsible for cell-fiber interaction.

EFFECTS OF FIBER TOPOGRAPHY AND MICRO-PATTERNING ON CELLULAR RESPONSE

Multiple studies have demonstrated that the morphology and roughness of fibers produced by electrospinning influence cell adhesion, proliferation, and orientation (Sill and von Recum, 2008; Xie et al., 2008; Bergmeister et al., 2013; Cirillo et al., 2014; Zhu et al., 2015; Sun et al., 2018). All factors that are imperative for successful tissue regeneration (Agarwal et al., 2008). Cells can sense topographical structures on a surface by filipodia that are actin-rich protrusions (0.1–0.3 μm in diameter) of the cell membrane and are involved in cell contact guidance (Mattila and Lappalainen, 2008; Dalby et al., 2014). If nanoscale aligned features are present onto a surface, filopodia tend to orient along the direction of the features and determine cytoskeleton orientation. Focal adhesions at the cell membrane mediate the initial cell-biomaterial interaction, with integrin ligands in direct contact with the substrate and connected to the actin micro-filaments of the cell cytoskeleton by a 40-nm stratum, which includes focal adhesion kinase (FAK), paxillin, talin, and vinculin (Kanchanawong et al., 2010).

This section of the review will discuss how electrospun mats with controlled porosity and surface morphology have been used to influence the behavior of mesenchymal stem cells (MSCs) (Jiang et al., 2015; Yin et al., 2015; Baudequin et al., 2017; Lin et al., 2017; Liu et al., 2017; Nedjari et al., 2017; Su et al., 2017; Zhang et al., 2017; Ghosh et al., 2018; Jin et al., 2018; Rahman et al., 2018; Sankar et al., 2018) and human umbilical vein endothelial cells (HUVECs) (Fioretta et al., 2014; Xu et al., 2015; Shin et al., 2017; Taskin et al., 2017; Yan et al., 2017; Ahmed et al., 2018). The literature on other cell lines, such as on myoblasts (Mele et al., 2015; Jun et al., 2016; Park et al., 2016; Tallawi et al., 2016; Abarzúa-Illanes et al., 2017; Yang et al., 2017) and neuron-like cells (Binan et al., 2014; Xie et al., 2014; Malkoc et al., 2015; Xue et al., 2017; Hajiali et al., 2018; Xia and Xia, 2018), will not be analyzed in detail here but a summary of it is reported in **Table 1**.

Mesenchymal Stem Cells

MSCs are multipotent stem cells that are primarily isolated from bone marrow, but they can also be found in adipose tissue, dental pulp, placenta, umbilical cord and other vascularized tissues throughout the body (Lv et al., 2014; Tartarini and Mele, 2015). MSCs are of great interest in regenerative medicine, because of their therapeutic effects, such as: ability to differentiate into various cell types and therefore promote regeneration of a wide range of tissues (bone, cartilage, muscle, marrow, tendon, ligament, nervous tissue, and skin); secretion of bioactive molecules for tissue repair; migration to inflamed tissues and modulation of local inflammation; immunomodulatory functions (Sharma et al., 2014).

In a recent research, Zhang et al. have studied how the topography and fibrillar organization of electrospun poly (ε-caprolactone) (PCL) fibers influences the recruitment of MSCs *in vivo* and *ex vivo* (Zhang et al., 2017). PCL mats (randomly distributed fibers) were implanted into the subcutaneous tissue of rats and the results were compared with solid PCL films (not electrospun). It was observed that, during the initial post-implantation period (1 day), a great number of macrophages with M1 phenotype (pro-inflammatory) were recruited to the PCL fibers, differently from solid PCL. This was attributed to the high surface area of the fibers and the porosity of the electrospun mats that promoted protein adsorption from the surrounding tissue, such as complement C3a (a chemo-attractant responsible to activate and recruit immune cells), fibronectin and vitronectin. After 4 and 7 days of implantation, the PCL fibers attracted host MSCs and modulated macrophages polarization with an increased number of cells exhibiting M2 (pro-healing) phenotype. While the number of M2 cells continuously increased over the entire period of implantation for PCL fibers, this was not the case for solid PCL where a large population of M1 cells was retained. Migration of MSCs was also observed in *ex vivo* experiments conducted with the implanted PCL samples. It was found that the macrophages at the implanted PCL mats secreted high levels of SDF-1, a chemokine that mediates MSCs recruitment by interacting with CXC chemokine receptors on the MSCs membrane. The study concluded that the physical organization of the PCL electrospun network induced the phenotype M1-to-M2 transition of macrophages that attracted MSCs at the implantation site by releasing SDF-1. This cascade of events was beneficial to stimulate tissue repair. PCL electrospun fibers have been used also to stimulate the production of pro-angiogenic and anti-inflammatory paracrine factors in rat adipose-derived MSCs (Ad-MSCs) (Su et al., 2017) and in skin excisional wound-healing model in rats (**Table 2**). Ad-MSCs were seeded on three types of electrospun PCL fibers, random (REF), aligned (AEF) and with a mesh pattern (MEF). It was observed that scaffolds with oriented fibers (AEF and MEF) promoted the expression of PGE2

TABLE 1 | Summary of the recent literature on the use of electrospun fibers to control morphology, alignment and differentiation of diverse cell lines.

Cells	Material	Fiber characteristics	Main outcomes	References
Human MSCs	Poly (ε-caprolactone)	Randomly distributed fibers; Diameter: ~ 630 nm; Surface roughness: ~ 2 μm.	Recruitment of MSCs *in vivo* and *ex vivo*; Recruitment of macrophages *in vivo*; Phenotype transition of adhered macrophages from pro-inflammatory (M1) to pro-healing (M2).	Zhang et al., 2017
Human MSCs	Poly (ε-caprolactone); Poly (ε-caprolactone)-gelatine	Randomly distributed and aligned fibers; Diameter: 600–780 nm; Porosity: 78–86%.	Cardiomyogenesis; Cytoskeletal arrangement; Changes in the cellular and nuclear morphology.	Ghosh et al., 2018
Human MSCs	Poly (L-lactic acid)	Randomly distributed and aligned fibers coated with poly (3,4-ethylenedioxythiophene; Diameter: ~ 950 nm.	Synergic effect of fiber alignment and electrical stimulation; Promotion of cellular activity and proliferation.	Jin et al., 2018
Human adipose-derived MSCs	Poly (L-lactide ε-caprolactone) and fibrinogen	Random and aligned fibers; Diameter: 200–500 nm; Patterning of electrospun mats using honeycomb shaped collector produced by photolithography; Honeycomb: 160 μm internal diameter, walls of 20 μm width and 60 μm height.	Homotypic interaction of MSCs on honeycomb scaffolds; Osteogenic differentiation of MSCs on honeycomb scaffolds.	Nedjari et al., 2017
Human adipose-derived MSCs	SU-8 photoresist	Randomly oriented fibers; Diameter: 550 nm; Patterning of electrospun mats by photolithography; Pattern dimensions: 20 μm ridges, 20 μm grooves, 5 μm pattern height.	Orientation and alignment of cells resembling the *in vivo* anisotropic multilamellar architecture of bone; Osteodifferentiation of MSCs.	Sankar et al., 2018
Human bone marrow MSCs	Poly (ε-caprolactone)	Random-aligned-random structure; Diameter: 240–450 nm.	Regional induction of MSCs toward tenogenesis and osteogenesis; Collagen deposition.	Lin et al., 2017
Human dental pulp MSCs	Polystyrene	Randomly distributed fibers; Diameter: 300–500 nm; Surface roughness: 0.8 μm.	Increased the expression of bone morphogenetic proteins and Wnt ligands; Odontoblast differentiation of MSCs; Dentin regeneration.	Rahman et al., 2018
Mouse MSCs (C3H10T1/2)	Poly (L-lactic acid)	Random and aligned fibers; Diameter: 740–1070 nm.	Up-regulation of tendon-specific markers for MSCs on aligned fibers; Tendon-like tissue regeneration *in vivo* for aligned fibers; Bone formation *in vivo* for random fibers.	Yin et al., 2015
Mouse MSCs (C3H10T1/2)	Polylactic acid and polycaprolactone	Random and aligned coaxial fibers; Diameter: ~ 2 μm; Porosity: 82–84%.	Expression of tendon-related markers; Tenogenic differentiation of mouse MSCs.	Baudequin et al., 2017
Rat bone marrow MSCs	Poly (ε-caprolactone) and poly (ethylene glycol); Chitosan	Random and aligned fibers; Diameter: 200–600 nm; 3D multi-layered scaffolds: layers of fibers within a porous chitosan matrix.	Ligamentogenesis and partially decreased osteogenesis for MSCs for aligned nanofibers embedded scaffolds *in vitro*; Regeneration of periodontal ligament *in vivo* for aligned nanofibers embedded scaffolds; High expression levels of periostin and formation of tooth-supporting mineralised tissue in the regenerated periodontium for aligned scaffolds.	Jiang et al., 2015
Rat bone marrow MSCs	Poly (ε-caprolactone)	Random and aligned fibers; Diameter: 820–1000 nm; Application of mechanical tension-stress after cell seeding.	Osteogenic differentiation of MSCs onto aligned fibers; Expression of osteogenic genes on aligned fibers; enhanced expression of osteogenic genes after mechanical stimulation.	Liu et al., 2017
Rat adipose-derived MSCs	Poly (ε-caprolactone)	Random and aligned fibers; Diameter: 1 μm; Patterning of electrospun mats using copper mesh with grid length of 830 μm as collector.	Upregulated levels of anti-inflammatory and pro-angiogenic cytokines *in vitro* for MSCs on patterned mats; Therapeutic effects of the fibers in a skin excisional healing model *in vivo*.	Su et al., 2017
HUVECs	Poly (D,L-lactide) and polycaprolactone	Random and aligned fibers; Diameter: 500–700 nm; Patterning of electrospun mats using a wire spring with interval distances of 300, 800, and 1500 μm as collector.	Modification of cytoskeleton morphology; Cell alignment and polarization on aligned fibers; Expression of angiogenesis-related genes.	Xu et al., 2015

(Continued)

TABLE 1 | Continued

Cells	Material	Fiber characteristics	Main outcomes	References.
HUVECs	Polycaprolactone and polyethyleneoxide	Nanostructured, random fibers. Diameter: 4–20 μm.	Enhanced cells' proliferation; Stimulation of adhesion complex formation on nanotextured fibers.	Taskin et al., 2017
HUVECs	Poly (L-lactide)	Random and aligned fibers; Patterning of electrospun mats by femtosecond laser ablation; Pattern dimensions: grooves distance of 20.9 and 81.3 μm; grooves width of 9.4 and 7.6 μm; grooves depth of 12.5 and 13.9 μm.	Changes in morphology and orientation of cells on micropatterned scaffolds; Reduction of monocytes adhesion on the micropatterned mats; Anti-inflammatory response.	Shin et al., 2017
HUVECs	Poly (L-lactic acid)	Random fibers; Diameter: 540 nm; Patterning of electrospun mats by hot embossing; Pattern dimensions: 50, 100, and 200 μm wide grooves.	Cells alignment along the direction of the grooves; Expression of endothelial biomarkers by cells cultured on micropatterned scaffolds.	Yan et al., 2017
HUVECs	Poly (lactic-co-glycolic acid)	Aligned fibers; Diameter: 0.5–10 μm.	Cell alignment and polarization on fibers with intermediate diameter; Stimulation of a migratory phenotype.	Ahmed et al., 2018
C2C12 myoblasts and neonatal rat cardiomyocytes	Poly (glycerol sebacate) and poly (caprolactone)	Random fibers; Diameter: 1.2 μm; Patterning of electrospun mats using a microstructured collector; Parallel grooves of 10 μm diameter and interspatial distances of 200 and 7 μm; Square-shaped structures of 100 μm size and 50 μm distance. Surface roughness: 0.4–1.3 μm.	Cells alignment along parallel grooves topography.	Tallawi et al., 2016
C2C12 myoblasts	Poly (caprolactone)	Random and aligned fibers; Diameter: 0.8-2.5 μm. Distance between aligned fibers: 2.2 and 13.8 μm.	Uniaxial orientation and elongation of cells on aligned fibers; Myogenic differentiation and elongation of myotubes along the aligned fibers.	Park et al., 2016
C2C12 myoblasts	Poly (L-lactic acid)	Random fibers; Diameter: 720 nm; Patterning of electrospun mats using a femtosecond laser ablation; Parallel grooves of 5 μm width and spacing of 10, 25, and 80 μm.	Cells alignment along the micro-grooves; Regulation of cellular adhesive morphology, proliferation, and distribution of focal adhesion proteins.	Jun et al., 2016
C2C12 myoblasts	Poly (ε-caprolactone) and poly (lactic-co-glycolic acid)	Random and aligned fibers; Diameter: 0.4–3.2 μm;	Increased alignment and aspect ratio of myotubes on aligned fibers.	Abarzúa-Illanes et al., 2017
Neuron-like PC12 cells	Poly (caprolactone) and gelatin; Collagen; Polystyrene	Random fibers; Diameter: 440 nm; Patterning of electrospun mats using polystyrene 5 μm wide grooves and 18 μm diameter wells by thermal fusion.	Increased extension of neurites within the grooves; High neurite length per differentiated cell for the micropatterned substrates.	Malkoc et al., 2015
Neural stem cells	Polyphenylene sulfone	Random and aligned fibers; Diameter: 735 nm.	Enhanced neuronal differentiation on the fibrous scaffolds; Growth and activity of primary neural cells on nanofibres; Parallel axon growth on aligned nanofibers.	Hajiali et al., 2018

(Prostaglandin E2, a potent inflammatory mediator), iNOS (inducible Nitric Oxide Synthase), VEGF (vascular endothelial growth factor) and HGF (hepatocyte growth factor), compared to REF scaffolds. In order to elucidate the molecular signaling mechanism responsible for the paracrine secretion of Ad-MSCs, the cells were treated with an inhibitor of NF-kB (a transcription factor that induces the expression of pro-inflammatory genes) and this significantly reversed the paracrine response of MSCs to the electrospun scaffolds. The authors therefore speculated that, in the presence of the scaffolds, MSCs behaved as if they were exposed to an external inflammatory stimulus. Similar results have been recently reported for MSCs cultured on electrospun fibers of PCL/polytetrahydrofuran (PTHF) urethane (P fibers) and PCL-PTHF urethane/collagen I (PC fibers) (Jiang et al., 2018). In this case, down-regulation of genes that contribute to inflammation and suppression of the NF-kB pathway signaling pathway were achieved by changing the mechanical properties of the fibers. PC fibers with a Young's modulus of 4.3 MPa were able to suppress inflammation, differently from P fibers (Young's modulus of 6.8 MPa).

Another study has investigated how electrospun PCL scaffolds with a novel random-aligned-random structure can be used to mimic bone-ligament connections and native ligaments (Lin et al., 2017). The authors designed a fiber collecting device for the fabrication of electrospun scaffolds with a controlled spatial distribution of random and aligned fibers.

TABLE 2 | Summary of main results reported in selected recent papers on electrospun scaffolds used *in vivo* experiments.

Scaffolds	*In vivo* outcomes	References
Mono-component (MC) and bi-component (BC) conduits made of random PCL and PCL/gelatin fibers, respectively, implanted in rat sciatic nerve defects.	Formation of numerous myelinated axons and vasculature in the MC conduit group; fibrous tissue and inflammatory cells with no evidence of myelinated axons for BC conduits, due to gelatin degradation or mechanical collapse. Superior functional recovery recorded for MC conduits over BC conduits after 18 weeks of implantation. Recover of tibialis anterior and gastrocnemius muscle weights after 18 weeks for MC conduit group; muscle atrophy for BC conduit group.	Cirillo et al., 2014
Random and aligned PCL-PEG fibers within a chitosan matrix implanted in a surgically created defect in maxillary first molar of rats.	Rat bone marrow mesenchymal stem cells (rBMSCs) with spindle shape and oriented actin filaments on scaffolds consisting of aligned fibers; while rBMSCs with polygonal or dentritic shape of scaffolds with random fibers. Increased ligamentogenesis and partially decreased osteogenesis for rBMSCs for scaffolds with aligned fibers. Increased stability and maturation of the periodontal ligament matrix, and increased regenerated bone volume and density for scaffolds with aligned fibers.	Jiang et al., 2015
Vascular grafts with oriented PCL microfibers coated with electrospun random PCL nanofibres and implanted in rat abdominal aorta.	Enhanced growth of vascular smooth muscle cells (VSMCs) after 2 and 4 weeks of implantation. Regeneration of arteries with notable VSMCSs vaso-activity after 12 weeks of implantation, and synthesis of elastin and collagen type I/II with phenotypic and structural similarities to the native arteries. Complete endothelialisation after 4 weeks with endothelial cells (ECs) having a morphology similar to the native endothelium. Regeneration of healthy and functional neaoarteries where VSMCs and ECs response to the endothelial-specific activator acetylcholine, hence showing vasodilation.	Zhu et al., 2015
Random PCL fibers implanted into the subcutaneous tissues of rats.	Macrophage recruitment, elongation and increased the expression of Arginase-1 or IL-4. Macrophage phenotype transition from M1 (pro-inflammatory) to M2 (pro-healing). High adsorption of proteins, particularly the chemotactic factor Complement C3a, vitronectin and fibronectin. Macrophages' secretion of high levels of SDF-1, a chemokine that mediates MSCs recruitment by interacting with CXC chemokine receptors on the MSCs membrane.	Zhang et al., 2017
Conditioned-medium (CM) from Ad-MSCs cultured on oriented (AEF and MEF) PCL fibers. CM applied to a skin wound-healing model.	High wound closure rate for animals treated with the MSC-MEF CM. Collagen deposition in a fine reticular pattern for group of MSC-MEF CM. High density of macrophages and M2 macrophages for MSC-MEF CM.	Su et al., 2017
PCL-PTHF urethane (P fibers) and PCL-PTHF urethane/collagen I (PC fibers) implanted in defects on the surface of the patellar groove of rat femurs.	After 4 weeks of implantation, newly formed tissues for both P and PC groups with minor inflammatory cells after 4 weeks. Fibrous tissue with a loose and detached for P group; fibrocartilage-like tissue and integration with the surrounding tissue for PC group. After 8 weeks of implantation, hyaline cartilage with round cells in the lacuna for both P and PC groups. More uniform and compact tissue for PC group. Stronger positive immunohistochemical staining of collagen II for PC group after 4 weeks.	Jiang et al., 2018
Random and aligned PCL/Collagen I fibers used to treat full-thickness wounds in diabetic rats.	Remarkable increase of the expression of Arginase I and NOS2 for oriented fibers and consequent stimulation of macrophages transition from M1 to M2. Detection of new blood vessels at the wound site for scaffolds with oriented fibers. Infiltration of fibroblasts and macrophages and collagen deposition in the wound sites for all nanofiber groups.	Sun et al., 2018

(Continued)

TABLE 2 | Continued

Scaffolds	*In vivo* outcomes	References
Random and aligned PLLA fibers implanted in rats for Achilles tendon repair.	After implantation, for scaffolds with aligned fibers, tendon-like tissue formation, continuous collagen fibers, expression of tendon-specific markers, such as scleraxis, tenomodulin, and Msx-2 (role in preventing tendons from mineralizing). After implantation, for scaffolds with random fibers, substantial chondrogenesis and tissue ossification, high levels of chondro-lineage specific genes, such as collagen type II, Sox9, and aggrecan.	Yin et al., 2015
Polyurethane (PU) grafts with low (void fraction of 53%) and high (void fraction of 80%) porosity, implanted into the infrarenal aorta of rats.	Growth of vimentin-positive fibroblasts, actin-positive myofibroblasts and desmin-positive myocytes at the adventitial interface of the grafts in the early phase after implantation. Growth of myofibroblasts and myocytes within the whole graft wall of the coarse-mesh grafts, 6 months after implantation; while limited cell growth for fine-mesh grafts. Superior cell migration and long-term survival of cells for grafts with high porosity than for grafts with low porosity.	Bergmeister et al., 2013

The regions of the scaffold with random fibers were then mineralized with Ca-P. *In vitro* tests on human bone marrow MSCs (hBMSCs) revealed that fiber anisotropy modified cells' morphology: polygonal, round-shaped cells without alignment were detected in the random, mineralized regions of the scaffold; while elongated spindle-shaped cells aligned along the fiber direction were visible in the aligned region. Moreover, the aligned fibers significantly up-regulated tendon-specific and tendon-related markers (Tnmd, Mkx) and therefore guided tenogenic phenotypes of hBMSCs; while, the regions with random, mineralized fibers determined the expression of bone-specific markers (Runx-2, Ocn, Opn) and consequently hBMSCs osteogenic phenotypes. Although the authors have not elucidated the underlying cell signaling mechanisms, this work demonstrates that electrospun scaffolds with engineered fiber anisotropy are advantageous to achieve region-specific distribution of tendon- and bone-related genes and find potential application in ligament repair and regeneration of bone-ligament connections.

The possibility to mediate the expression of signaling biomolecules by electrospun fibers and hence guide MSCs differentiation has been demonstrated also by Rahman and co-workers (Rahman et al., 2018). They investigated the odontoblastic differentiation of human dental pulp MSCs (DP-MSCs) on polystyrene (PS) random fibers. The cells cultured on PS mats strongly increased the expression of bone morphogenetic proteins (BMPs) and Wnt ligands that are essential in tooth development: Wnt3a transcript expression was more than 50 folds higher after 4 days of culturing on PS fibers than on standard petri dishes. The levels of odontoblast/osteoblast markers, such as dentin sialophosphoprotein (DSPP), osteocalcin, and bone sialoprotein, were also higher for DP-MSCs cultured on electrospun fibers. The results of this study indicate that nanofibres mimicking the *in vivo* microenvironment are crucial to stimulate the differentiation of DP-MSCs into odontoblasts (specialized cells responsible for dentin formation) by mediating the production of signaling molecules including Wnt3a, and to promote dentinogenesis. Osteogenesis of MSCs has been reported also on random Poly-L-lactic acid (PLLA) fibers, due to cytoskeletal rearrangements and tensions, which in turn influence intracellular mechanotransductive pathways (Yin et al., 2015). In fact, when the cells were treated with Rho kinase (ROCK) inhibitor Y-27632 (inhibitor of myosin-generated cytoskeletal tension), loss of lineage commitment was detected, and cells' morphology was not affected by the fibers topography.

The works here summarized and the others conducted on the interaction of MSCs with electrospun substrates (**Tables 1**, **2**) demonstrate that networks of polymer fibers (random, aligned and hierarchical) are effective in providing topographical and physical cues to guide differentiation of stem cells. These observations have led to the development of bioinspired scaffolds with potential future implications in diverse clinical areas, including the regeneration and repair of bone, tendon, ligament, dentin, and skin.

Human Umbilical Vein Endothelial Cells

Vascular endothelial cells are of fundamental importance for the entire circulatory system, because they are involved in fluid filtration, homeostasis and prevention of thrombosis (Rajendran et al., 2013). Endothelial cells and particularly HUVECs, which are isolated from human umbilical cord veins, are widely used to study cardiovascular diseases and develop biomedical devices for vascular tissue engineering (Lei et al., 2016). One important aspect to consider when designing scaffolds for endothelial cells is the role played by surface topography, at micro- and nano-scale, on cell adhesion, proliferation and migration, to create a physiological environment that stimulates the formation of a functional endothelium.

A recent work of Ahmed and co-workers has reported on the influence of the diameter of electrospun fibers on HUVECs migration (Ahmed et al., 2018). Aligned poly(lactic-co-glycolic acid) (PLGA) fibers with five different diameters (0.5, 1, 2, 4, and 10 μm) were analyzed. The greater cell displacement in a scratch wound assay was measured for HUVECs seeded on fibers with intermediate diameter (1 and 2 μm) with peak migration velocity of 24 μm/h after 12 h of cell culture. HUVECs were able also to move on scaffolds with 0.5 μm size fibers

but at lower migration rates. On these scaffolds cell alignment and polarization, and higher levels of FAK expression were detected. FAK is a non-receptor tyrosine kinase that regulates cell shape, adhesion and motility. The fiber diameter influenced the focal adhesion of HUVECs but not their metabolism or the formation of cell-matrix anchorage points. At 12 h, a significant increase in phosphorylated FAK (pFAK, associated with actin regulation and adhesion dynamics) was detected, which is linked to the peak migration velocity. On the contrary, limited cell motility was observed for scaffolds with 4 and 10 μm fibers. Investigations of the spatial distribution of pFAK revealed that pFAK was localized in the HUVECs cytosol for 0.5, 1.0, and 2.0 μm fibers, and at the cell periphery for 4 and 10 μm fibers (non-uniform distribution). This promoted uniaxial cell morphology and stimulated the migratory process to occur preferentially along the fiber longitudinal direction for scaffolds with intermediate fiber diameter. A similar conclusion has been drawn by other researchers working on HUVECs cultured on micropatterned scaffolds with spatially heterogeneous alignment of poly(D,L-lactide) (PDLLA)/PCL electrospun fibers of 0.5–1 μm size (Xu et al., 2015). Fibrous scaffolds with patterns of random and well-aligned PDLLA/PCL fibers were prepared using a wire spring as template collector. It was observed that the micropatterned scaffolds induced the proliferation of HUVECs and modifications to their cytoskeleton morphology (**Figure 1**). The lowest values of mean cell body shape index (a parameter indicating the degree of cell polarization) were measured for cells cultured on patterned scaffolds having the longest distance (1,500 μm) between regions with random and aligned fibers, indicating the highest degree of cell polarization and alignment. Furthermore, those scaffolds stimulated the cells to express high levels of angiogenesis-related genes and therefore they have potential applications in vascular tissue engineering. The combination of electrospinning and micro-pattering techniques has proven to be effective for creating hierarchical bio-interfaces that direct the arrangement of endothelial cells and their biological functions (Shin et al., 2017; Yan et al., 2017).

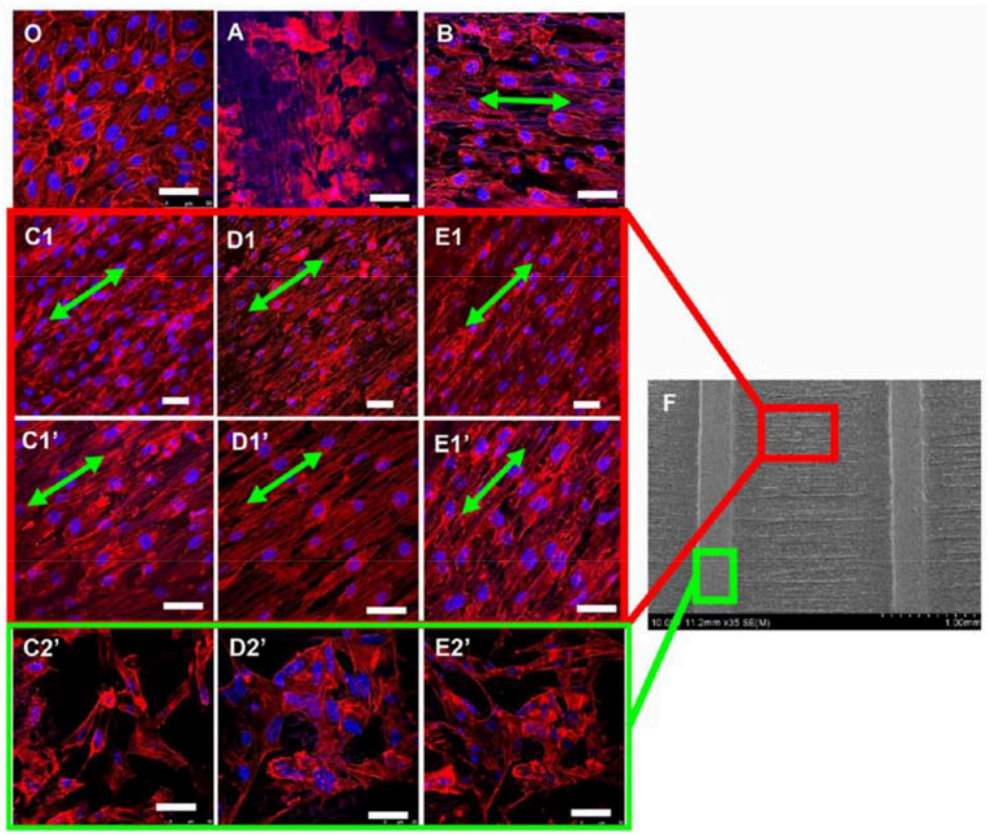

FIGURE 1 | Confocal images of HUVECs (actin filaments in red and nuclei in blue) cultured for 7 days on **(O)** standard petri dish (typical cobblestone-like structure) and electrospun scaffolds with different patterns: **(A)** nonwoven (cells with flat, round shape morphology); **(B)** single directionally aligned pattern (cell alignment along fibers direction, green arrows); **(C1–E1)** anisotropic aligned patterns with interval distances of 300, 800, and 1500 μm, respectively; **(C1′-E1′)** anisotropic aligned patterns with interval distances of 300, 800, and 1500 μm (high magnification images), respectively (spindle shape along the long fiber axes for cells between the embossments) **(C2′- E2′)** anisotropic aligned patterns with interval distances of 300, 800, and 1500 μm, respectively (polygonal shape with random stretching for cells on the embossments). **(F)** SEM image of anisotropic aligned pattern. Scale bar = 50 μm. Reprinted with permission from Xu et al. (2015). Copyright 2018 of the American Chemical Society.

COMPUTATIONAL MODELS

The literature that has been discussed so far in this review provides experimental evidences that the surface topography of biomaterials influences cellular behavior, including cells' alignment, elongation, migration, phenotype transitions and differentiation. *In vitro* and *in vivo* studies are incredibly beneficial to collect data and results on how artificially created micro- and nano-features perform in realistic applications (**Tables 1**, **2**). The underlying mechanisms of cell-material interactions are only partially understood and further investigations are required to define the best scaffold design for promoting the regeneration of a target tissue (Kennedy et al., 2017; Paim et al., 2018). However, time and cost requirements for *in vitro* and *in vivo* tests pose limitations on the use of and reliance on experimental studies alone, together with ethical issues when animal models are concerned. Computational modeling has the significant advantage of facilitating research by conducting thousands of simulated trials with a wide range of variations and for a plethora of complex biological systems (Geris et al., 2018).

Albert and Schwarz have developed mathematical models to predict the dynamics of cell shape and forces on micropatterned substrates (Albert and Schwarz, 2014, 2016a,b). Their models are based on the cellular Potts model (CPM) that allows to simulate the behavior of single or interacting cells by describing them as internally structureless but spatially extended objects on a regular lattice (Voss-Böhme, 2012; Tartarini and Mele, 2015). The number of lattice sites belonging to a single cell defines the area occupied by the cell. By changing the lattice resolution and the indices of the lattice sites, cells with arbitrary shape and shape evolutions can be represented. Initially, the authors compared simulations with experimental data on single cell attached on crossbow, Y and H patterns (Albert and Schwarz, 2014). The model well described how the cell contour adapted to the pattern's geometry and reconstructed the traction forces in agreement with experiments. The forces were higher at the extremities of the patterns (adhesive edges of the contour) and increased with the curvature of the contour depending on the availability of receptors for focal adhesion. The CPM-based model was then used to predict the collective behavior of cells on micropatterns, including cell division, cell-cell contacts and migration (Albert and Schwarz, 2014). The model predicted, for example, that for a cell dividing on a L shaped pattern, the two daughter cells were most likely to be located on the two arms of the L, as confirmed by experimental results. In order to identify the optimal adhesive patterns to control cell functions, CPM was combined with genetic algorithms (GAs) (Albert and Schwarz, 2016c) (**Figure 2**), which are computational techniques inspired by natural evolution for the heuristic search of problem solutions (McCall, 2005). The migration of cells on rachet micropatterns in a linear arrangement was analyzed and the algorithm predicted that a triangular shape was ideal to guide cell migration in the direction of the tip of the triangle, as also demonstrated experimentally. Differently from what expected though, the most effective pattern to achieve unidirectional migration of cells consisted of asymmetric triangles that were rotated and connected to one another to form a pattern with an almost straight horizontal edge. The computational model developed is a useful tool to predict cell interactions with structured scaffolds and it can be adapted to simulate diverse cellular processes.

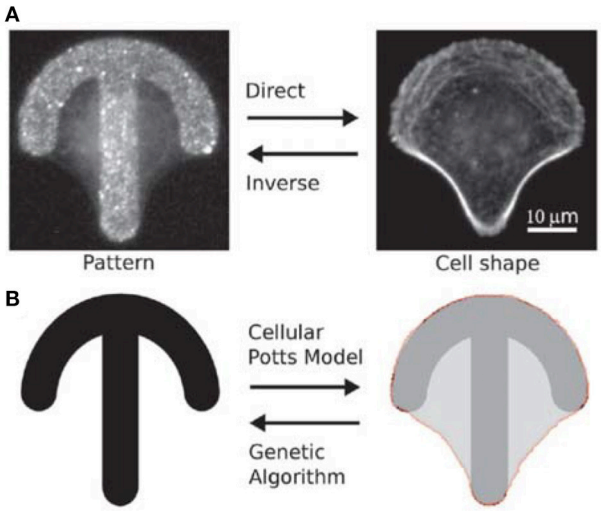

FIGURE 2 | (A) Fluorescence images of a HeLa cell stained for actin on a crossbow microstructure coated with fibronectin. Given a micro-pattern, cell shape can be observed with optical microscopy (direct problem). Give a cell shape, it is not always straightforward to experimentally identify the original pattern (inverse problem). **(B)** CPM can be used to predict cell shape on a microstructure, and genetic algorithms can help to define pattern geometry. Reproduced with permission from Albert and Schwarz (2016c). Copyright 2016 of the Royal Society of Chemistry.

With a distinct lack of literature on computational/numerical modeling that predicts how cells interact with electrospun nanofibrous structures (role of roughness and topography), there is a clear gap in the field which has great potential if correctly pursued. This will open even more possibilities to design and create novel fibrous scaffolds with engineered surface structures (Ziebert and Aranson, 2016). For example, computer aided characterization of complex biointerfacial interactions of specific polymer fibers could be created. Computational algorithms and numerical solutions could be formulated to generate a method of predicting the most suitable surface topography of electrospun mats for specific cells and to prompt tissue regeneration processes. In the development of computational models that describe how cell behavior is affected by the surface properties of electrospun scaffolds, geometrical parameters to be considered include fibers diameter, fibers organization and degree of alignment, porosity of the mat, presence of nanostructures or nanopores on single fiber surface, overall roughness of the electrospun mat. All these aspects have been evaluated experimentally, as discussed in the previous section of this mini review.

CONCLUSIONS

Electrospun nanofibers have become vital structures for a plethora of different applications, with the field of biomedical

TABLE 3 | Clinical trials of electrospun scaffolds.

Study	Status	Condition/disease	Aim	Number of participants	Scaffold	Results
Experimental study of the vascular prosthesis manufactured by electrospinning (NCT02255188)	Completed	Arterial occlusive disease	Determination of the safety of electrospun vascular grafts for the development of thrombosis.	120	PCL grafts; PCL/gelatin grafts; PLGA/PCL/gelatin grafts; Nylon 6 grafts.	Not currently available
EktoTherix™ regenerative tissue scaffold for repair of surgical excision wounds (NCT02409628)	Completed	Non-melanoma skin cancer; Basal cell carcinoma; Squamous cell carcinoma	Assessment of the safety and performance of EktoTherix™ Tissue Repair Scaffold for the treatment of full-thickness, dermatologic wounds due to the surgical removal of non-melanoma skin cancers.	12	EktoTherix™ Tissue Repair Scaffold:	Not currently available
Clinical trial for the treatment of diabetic foot ulcers using a nitric oxide releasing patch: PATHON	Completed	Diabetic foot	Evaluation of the effectiveness and safety of nitric oxide releasing wound dressings for the treatment of diabetic foot ulcers.	100	Multilayer polymeric transdermal patch with a continuous release of nitric oxide (polyurethane-based fibers).	Not currently available
Controlled nitric oxide releasing patch vs. meglumine antimoniate in the treatment of cutaneous Leishmaniasis	Terminated	Cutaneous Leishmaniasis	Evaluation of the effectiveness of a nitric oxide topical donor for the treatment of cutaneous leishmaniasis.	178	Multilayer polymeric transdermal patch with a continuous release of nitric oxide (polyurethane-based fibers).	Not currently available

The data are obtained from ClinicalTrials.gov, a resource provided by the U.S. National Library of Medicine (Accessed on September 2018).

engineering being, arguably, one of the most important. Thanks to the versatility of electrospinning, nanofibrous scaffolds can be tailored and modified to improve their biocompatibility for applications such as tissue engineering, drug delivery and wound dressings. For example, electrospun mats have been used in clinical studies for the treatment of arterial occlusive disease, skin cancer and diabetic foot (**Table 3**). As discussed in this review, fiber alignment, micropatterning, and controlled porosity of nanofibrous mats have all been found to have significant effect on cellular behavior, inducing cell attachment, migration and differentiation. Extensive research has been conducted on exploring morphological cues provided by 2D electrospun mats, and only recently fibrous 3D scaffolds have been proposed to closely mimic the ECM structure (Cai et al., 2013; Lee et al., 2014; Cho et al., 2016; Hwang et al., 2018; Unnithan et al., 2018). The studies conducted so far have demonstrated that a fine tuning of the 3D porosity of the electrospun scaffolds is crucial to promote cell infiltration. Future research in the field should combine experimental studies with numerical and computational modeling for the design and fabrication of novel micro- and nanostructured 3D scaffolds. Computer aided simulations could not only be used to predict cell interaction with specific topography but be formulated in a manner which then advises on the most suitable functional group (or biological molecule) that ought to be immobilized on the surface or embedded within the scaffold. This would require taking in consideration a complex combination of parameters that include the chemical composition of the scaffold (exposed chemical groups, wetting properties, and biodegradation), micro- and nano-porosity, organization of the fibrous network (random or aligned fibers) and mechanical properties of the scaffold.

AUTHOR CONTRIBUTIONS

AD and EM contributed to the conception and design of the study. AD and EM wrote the first draft of the manuscript. DT wrote sections of the manuscript. All authors contributed to manuscript revision, read and approved the submitted version.

REFERENCES

Abarzúa-Illanes, P. N., Padilla, C., Ramos, A., Isaacs, M., Ramos-Grez, J., Olguín, H. C., et al. (2017). Improving myoblast differentiation on electrospun poly(ε-caprolactone) scaffolds. *J. Biomed. Mater. Res. A.* 105, 2241–2251. doi: 10.1002/jbm.a.36091

Agarwal, S., Wendorff, J., and Greiner, A. (2008). Use of electrospinning technique for biomedical applications. *Polymer* 49, 5603–5621. doi: 10.1016/j.polymer.2008.09.014

Ahmed, M., Ramos, T., Wieringa, P., Blitterswijk, C. V., Boer, J., and Moroni, L. (2018). Geometric constraints of endothelial cell migration on electrospun fibres. *Sci. Rep.* 8:6386. doi: 10.1038/s41598-018-24667-7

Albert, P. J., and Schwarz, U. S. (2014). Dynamics of cell shape and forces on micropatterned substrates predicted by a cellular Potts model. *Biophys. J.* 106, 2340–2352. doi: 10.1016/j.bpj.2014.04.036

Albert, P. J., and Schwarz, U. S. (2016a) Modeling cell shape and dynamics on micropatterns. *Cell Adh. Migrat.* 10, 516–528. doi: 10.1080/19336918.2016.1148864

Albert, P. J., and Schwarz, U. S. (2016b) Dynamics of cell ensembles on adhesive micropatterns: bridging the gap between single cell spreading and collective cell migration. *PLoS Comput. Biol.* 12:e1004863. doi: 10.1371/journal.pcbi.1004863

Albert, P. J., and Schwarz, U. S. (2016c) Optimizing micropattern geometries for cell shape and migration with genetic algorithms. *Integr. Biol.* 11, 741–750. doi: 10.1039/c6ib00061d

Anderson, H. J., Sahoo, J. K., Ulijn, R. V., and Dalby, M. J. (2016). Mesenchymal stem cell fate: applying biomaterials for control of stem cell behaviour. *Front. Bioeng. Biotechnol.* 4:38. doi: 10.3389/fbioe.2016.00038

Baudequin, T., Gaut, L., Mueller, M., Huepkes, A., Glasmacher, B., Duprez, D., et al. (2017). The osteogenic and tenogenic differentiation potential of C3H10T1/2 (mesenchymal stem cell model) cultured on PCL/PLA electrospun scaffolds in the absence of specific differentiation medium. *Materials* 10:E1387. doi: 10.3390/ma10121387

Bergmeister, H., Schreiber, C., Grasl, C., Walter, I., Plasenzotti, R., Stoiber, M., et al. (2013). Healing characteristics of electrospun polyurethane grafts with various porosities. *Acta Biomater.* 9, 6032–6040. doi: 10.1016/j.actbio.2012.12.009

Bhardwaj, N., and Kundu, S. C. (2010). Electrospinning: a fascinating fiber fabrication technique. *Biotechnol. Adv.* 28, 325–347. doi: 10.1016/j.biotechadv.2010.01.004

Binan, L., Tendey, C., De Crescenzo, G., El Ayoubi, R., Ajji, A., and Jolicoeur, M. (2014). Differentiation of neuronal stem cells into motor neurons using electrospun poly-L-lactic acid/gelatin scaffold. *Biomater* 35, 664–674. doi: 10.1016/j.biomaterials.2013.09.097

Cai, S., Xu, H., Jiang, Q., and Yang, Y. (2013). Novel 3D electrospun scaffolds with fibers oriented randomly and evenly in three dimensions to closely mimic the unique architectures of extracellular matrices in soft tissues: fabrication and mechanism study. *Langmuir* 29, 2311–2318. doi: 10.1021/la304414j

Cho, M., Kim, S. H., Jin, G., Park, K. I., and Jang, J. H. (2016). Salt-induced electrospun patterned bundled fibers for spatially regulating cellular responses. *ACS Appl. Mater. Interfaces* 8, 13320–13331. doi: 10.1021/acsami.6b03848

Cirillo, V., Clements, B. A., Guarino, V., Bushman, J., Kohn, J., and Ambrosio, L. (2014). A comparison of the performance of mono- and bi-component electrospun conduits in a rat sciatic model. *Biomaterials* 35, 8970–8982. doi: 10.1016/j.biomaterials.2014.07.010

Dalby, M. J., Gadegaard, N., and Oreffo, R. O. C. (2014). Harnessing nanotopography and integrin–matrix interactions to influence stem cell fate. *Nat. Mater.* 13, 558–569. doi: 10.1038/nmat3980

Dalby, M. J., García, A. J., and Salmeron-Sanchez, M. (2018). Receptor control in mesenchymal stem cell engineering. *Nat. Rev. Mater.* 3:17091. doi: 10.1038/natrevmats.2017.91

Fioretta, E. S., Simonet, M., Smits, A. I., Baaijens, F. P., and Bouten, C. V. (2014). Differential response of endothelial and endothelial colony forming cells on electrospun scaffolds with distinct microfiber diameters. *Biomacromolecules* 15, 821–829. doi: 10.1021/bm4016418

Geiger, B., Bershadsky, A., Pankov, R., and Yamada, K. M. (2001). Transmembrane extracellular matrix-cytoskeleton crosstalk. *Nat. Rev. Molec. Cell Biol.* 2, 793–805. doi: 10.1038/35099066

Geris, L., Lambrechts, T., Carlier, A., and Papantoniou, I. (2018). The future is digital: in silico tissue engineering. *Curr. Opinion Biomed. Eng.* 6, 92–98. doi: 10.1016/j.cobme.2018.04.001

Ghosh, L. D., Jain, A., Sundaresan, N. R., and Chatterjee, K. (2018). Elucidating molecular events underlying topography mediated cardiomyogenesis of stem cells on 3D nanofibrous scaffolds. *Mater. Sci. Eng. C* 88, 104–114. doi: 10.1016/j.msec.2018.03.012

Hajiali, H., Contestabile, A., Mele, E., and Athanassiou, A. (2018). Influence of topography of nanofibrous scaffolds on functionality of engineered neural tissue. *J. Mater. Chem. B* 6, 930–939. doi: 10.1039/C7TB02969A

Hwang, T. I., Maharjan, B., Tiwari, A. P., Lee, S., Joshi, M. K., Park, C. H., et al. (2018). Facile fabrication of spongy nanofibrous scaffold for tissue engineering applications. *Mater. Lett.* 219, 119–122. doi: 10.1016/j.matlet.2018.02.040

Jiang, T., Kai, D., Liu, S., Huang, X., Heng, S., Zhao, J., et al. (2018). Mechanically cartilage-mimicking poly(PCL-PTHF urethane)/collagen nanofibers induce chondrogenesis by blocking NF-kappa B signalling pathway. *Biomaterials* 178, 281–292. doi: 10.1016/j.biomaterials.2018.06.023

Jiang, W., Li, L., Zhang, D., Huang, S., Jing, Z., Wu, Y., et al. (2015). Incorporation of aligned PCL-PEG nanofibers into porous chitosan scaffolds improved the orientation of collagen fibers in regenerated periodontium. *Acta Biomater.* 25, 240–252. doi: 10.1016/j.actbio.2015.07.023

Jin, L., Hu, B., Li, Z., Li, J., Gao, Y., Wang, Z., et al. (2018). Synergistic effects of electrical stimulation and aligned nanofibrous microenvironment on growth behavior of mesenchymal stem cells. *ACS Appl. Mater. Interfaces* 10, 18543–18550. doi: 10.1021/acsami.8b04136

Jun, I., Chung, Y. W., Heo, Y. H., Han, H. S., Park, J., Jeong, H., et al. (2016). Creating hierarchical topographies on fibrous platforms using femtosecond laser ablation for directing myoblasts behaviour. *ACS Appl. Mater. Interfaces* 8, 3407–3417. doi: 10.1021/acsami.5b11418

Kanchanawong, P., Shtengel, G., Pasapera, A. M., Ramko, E. B., Davidson, M. W., Hess, H. F., et al. (2010). Nanoscale architecture of integrin-based cell adhesions. *Nature* 468, 580–584. doi: 10.1038/nature09621

Kennedy, K. M., Bhaw-Luximon, A., and Jhurry, D. (2017). Cell-matrix mechanical interaction in electrospun polymeric scaffolds for tissue engineering: implications for scaffold design and performance. *Acta Biomater.* 50, 41–55. doi: 10.1016/j.actbio.2016.12.034

Khorshidi, S., Solouk, A., Mirzadeh, H., Mazinani, S., Lagaron, J. M., Sharifi, S., et al. (2016). A review of key challenges of electrospun scaffolds for tissue engineering applications. *J. Tissue Eng. Regen. Med.* 10, 715–738. doi: 10.1002/term.1978

Lee, S., Cho, S., Kim, M., Jin, G., Jeong, U., and Jang, J. H. (2014). Highly moldable electrospun clay-like fluffy nanofibers for three-dimensional scaffolds. *ACS Appl. Mater. Interfaces* 6, 1082–1091. doi: 10.1021/am404627r

Lei, J., Peng, S., Samuel, S. B., Zhang, S., Wu, Y., Wang, P., et al. (2016). A simple and biosafe method for isolation of human umbilical vein endothelial cells. *Anal. Biochem.* 508, 15–18. doi: 10.1016/j.ab.2016.06.018

Li, Y., Xiao, Y., and Liu, C. (2017). The horizon of materiobiology: a perspective on material-guided cell behaviours and tissue engineering. *Chem. Rev.* 117, 4376–4421. doi: 10.1021/acs.chemrev.6b00654

Lin, J., Zhou, W., Han, S., Bunpetch, V., Zhao, K., Liu, C., et al. (2018). Cell-material interactions in tendon tissue engineering. *Acta Biomater.* 70, 1–11. doi: 10.1016/j.actbio.2018.01.012

Lin, Z., Zhao, X., Chen, S., and Du, C. (2017). Osteogenic and tenogenic induction of hBMSCs by an integrated nanofibrous scaffold with chemical and structural mimicry of the bone-ligament connection. *J. Mater. Chem. B* 5, 1015–1027. doi: 10.1039/C6TB02156E

Liu, X., and Wang, S. (2014). Three-dimensional nano-biointerface as a new platform for guiding cell fate. *Chem. Soc. Rev.* 43, 2385–2401. doi: 10.1039/C3CS60419E

Liu, Y., Yang, G., Ji, H., Xiang, T., Luo, E., and Zhou, S. (2017). Synergetic effect of topological cue and periodic mechanical tension-stress on osteogenic differentiation of rat bone mesenchymal stem cells. *Colloids Surf. B Biointerfaces* 154, 1–9. doi: 10.1016/j.colsurfb.2017.02.035

Lutolf, M. P., and Hubbell, J. A. (2005). Synthetic biomaterials as instructive extracellular microenvironments for morphogenesis in tissue engineering. *Nat. Biotech.* 23, 47–55. doi: 10.1038/nbt1055

Lv, F. J., Tuan, R. S., Cheung, K. M., and Leung, V. Y. (2014). Concise review: the surface markers and identity of human mesenchymal stem cells. *Stem Cells* 32, 1408–1419. doi: 10.1002/stem.1681

Malkoc, V., Gallego-Perez, D., Nelson, T., Lannutti, J. J., and Hansford, D. J. (2015). Controlled neuronal cell patterning and guided neurite growth on micropatterned nanofiber platforms. *J. Micromech. Microeng.* 25:125001. doi: 10.1088/0960-1317/25/12/125001

Marino, A., Genchi, G. G., Sinibaldi, E., and Ciofani, G. (2017). Piezoelectric effects of materials on bio-interfaces. *ACS Appl. Mater. Interfaces* 9, 17663–17680. doi: 10.1021/acsami.7b04323

Mattila, P. K., and Lappalainen, P. (2008). Filopodia: molecular architecture and cellular functions. *Nat. Rev. Mol. Cell Biol.* 9, 446–454. doi: 10.1038/nrm2406

McCall, J. (2005). Genetic algorithms for modelling and optimisation. *J. Computat. Appl. Mathemat.* 184, 205–222. doi: 10.1016/j.cam.2004.07.034

Mele, E. (2016). Electrospinning of natural polymers for advanced wound care: towards responsive and adaptive dressings. *J. Mater. Chem. B* 4, 4801–4812. doi: 10.1039/C6TB00804F

Mele, E., Heredia-Guerrero, J. A., Bayer, I. S., Ciofani, G., Genchi, G. G., Ceseracciu, L., et al. (2015). Zwitterionic nanofibers of super-glue for transparent and biocompatible multi-purpose coatings. *Sci. Rep*. 5:14019. doi: 10.1038/srep14019

Nedjari, S., Awaja, F., and Altankov, G. (2017). Three dimensional honeycomb patterned fibrinogen based nanofibers induce substantial osteogenic response of mesenchymal stem cells. *Sci Rep*. 7:15947. doi: 10.1038/s41598-017-15956-8

Paim, Á., Tessaro, I. C., Cardozo, N. S. M., and Pranke, P. (2018). Mesenchymal stem cell cultivation in electrospun scaffolds: mechanistic modeling for tissue engineering. *J. Biol. Phys*. 44, 245–271. doi: 10.1007/s10867-018-9482-y

Park, S. H., Kim, M. S., Lee, B., Park, J. H., Lee, H. J., Lee, N. K., et al. (2016). Creation of a hybrid scaffold with dual configuration of aligned and random electrospun fibers. *ACS Appl. Mater. Interfaces* 8, 2826–2832. doi: 10.1021/acsami.5b11529

Rahman, S. U., Oh, J. H., Cho, Y. D., Chung, S. H., Lee, G., Baek, J. H., et al. (2018). Fibrous topography-potentiated canonical Wnt signaling directs the odontoblastic differentiation of dental pulp-derived stem cells. *ACS Appl. Mater. Interfaces* 10, 17526–17541. doi: 10.1021/acsami.7b19782

Rajendran, P., Rengarajan, T., Thangavel, J., Nishigaki, Y., Sakthisekaran, D., Sethi, G., et al. (2013). The vascular endothelium and human diseases. *Int. J. Biol. Sci*. 9, 1057–1069. doi: 10.7150/ijbs.7502

Sankar, S., Kakunuri, M., D., Eswaramoorthy, S., Sharma, C. S., and Rath, S. N. (2018). Effect of patterned electrospun hierarchical structures on alignment and differentiation of mesenchymal stem cells: biomimicking bone. *J. Tissue Eng. Regen. Med*. 12, e2073–e2084. doi: 10.1002/term.2640

Sharma, R. R., Pollock, K., Hubel, A., and McKenna, D. (2014). Mesenchymal stem or stromal cells: a review of clinical applications and manufacturing practices. *Transfusion* 54, 1418–1437. doi: 10.1111/trf.12421

Shin, Y. M., Shin, H. J., Heo, Y., Jun, I., Chung, Y. W., Kim, K., et al. (2017). Engineering an aligned endothelial monolayer on a topologically modified nanofibrous platform with a micropatterned structure produced by femtosecond laser ablation. *J. Mater. Chem. B* 5, 318–328. doi: 10.1039/C6TB02258H

Sill, T., and von Recum, H. A. (2008). Electrospinning: applications in drug delivery and tissue engineering. *Biomater* 29, 1989–2006. doi: 10.1016/j.biomaterials.2008.01.011

Su, N., Gao, P. L., Wang, K., Wang, J. Y., Zhong, Y., and Luo, Y. (2017). Fibrous scaffolds potentiate the paracrine function of mesenchymal stem cells: a new dimension in cell-material interaction. *Biomater* 141, 74–85. doi: 10.1016/j.biomaterials.2017.06.028

Sun, L., Gao, W., Fu, X., Shi, M., Xie, W., Zhang, W., et al. (2018). Enhanced wound healing in diabetic rats by nanofibrous scaffolds mimicking the basket weave pattern of collagen fibrils in native skin. *Biomater. Sci*. 6, 340–349. doi: 10.1039/C7BM00545H

Tallawi, M., Dippold, D., Rai, R., D'Atri, D., Roether, J. A., Schubert, D. W., et al. (2016). Novel PGS/PCL electrospun fiber mats with patterned topographical features for cardiac patch applications. *Mater. Sci. Eng. C Mater. Biol. Appl*. 69, 569–576. doi: 10.1016/j.msec.2016.06.083

Tartarini, D., and Mele, E. (2015). Adult stem cell therapies for wound healing: biomaterials and computational models. *Front. Bioeng. Biotechnol*. 3:206. doi: 10.3389/fbioe.2015.00206

Taskin, M. B., Xia, D., Besenbacher, F., Dong, M., and Chen, M. (2017). Nanotopography featured polycaprolactone/polyethyleneoxide microfibers modulate endothelial cell response. *Nanoscale* 9, 9218–9229. doi: 10.1039/C7NR03326E

Unnithan, A. R., Sasikala, A. R. K., Thomas, S. S., Nejad, A. G., Cha, Y. S., Park, C. H., et al. (2018). Strategic design and fabrication of biomimetic 3d scaffolds: unique architectures of extracellular matrices for enhanced adipogenesis and soft tissue reconstruction. *Sci Rep*. 8:5696. doi: 10.1038/s41598-018-23966-3

Voss-Böhme, A. (2012). Multi-scale modeling in morphogenesis: a critical analysis of the cellular Potts model. *PLoS ONE* 7:e42852. doi: 10.1371/journal.pone.0042852

Xia, H., and Xia, Y. (2018). An *in vitro* study of non-aligned or aligned electrospun poly(methyl methacrylate) nanofibers as primary rat astrocytes-loading scaffold. *Mater. Sci. Eng*. 91, 228–235. doi: 10.1016/j.msec.2018.05.050

Xie, J., Li, X., and Xia, Y. (2008). Putting electrospun nanofibers to work for biomedical research. *Macromol. Rapid Comm*. 29, 1775–1792. doi: 10.1002/marc.200800381

Xie, J., Liu, W., MacEwan, M. R., Bridgman, P. C., and Xia, Y. (2014). Neurite outgrowth on electrospun nanofibers with uniaxial alignment: the effects of fiber density, surface coating, and supporting substrate. *ACS Nano*. 8, 1878–1885. doi: 10.1021/nn406363j

Xu, H., Li, H., Ke, Q., and Chang, J. (2015). An anisotropically and heterogeneously aligned patterned electrospun scaffold with tailored mechanical property and improved bioactivity for vascular tissue engineering. *ACS Appl. Mater. Interfaces* 7, 8706–8718. doi: 10.1021/acsami.5b00996

Xue, J., Yang, J., O'Connor, D. M., Zhu, C., Huo, D., Boulis, N. M., et al. (2017). Differentiation of bone marrow stem cells into schwann cells for the promotion of neurite outgrowth on electrospun fibers. *ACS Appl. Mater. Interfaces* 9, 12299–12310. doi: 10.1021/acsami.7b00882

Yan, S., Zhang, X., Zhang, L., Liu, H., Wang, X., and Li, Q. (2017). Polymer scaffolds for vascular tissue engineering fabricated by combined electrospinning and hot embossing. *Biomed. Mater*. 13:015003. doi: 10.1088/1748-605X/aa8a81

Yang, G. H., Jeon, H., and Kim, G. (2017). Alternately plasma-roughened nanosurface of a hybrid scaffold for aligning myoblasts. *Biofabrication* 9:025035. doi: 10.1088/1758-5090/aa77ba

Yin, Z., Chen, X., Song, H. X., Hu, J. J., Tang, Q. M., Zhu, T., et al. (2015). Electrospun scaffolds for multiple tissues regeneration *in vivo* through topography dependent induction of lineage specific differentiation. *Biomaterials* 44, 173–185. doi: 10.1016/j.biomaterials.2014.12.027

Zhang, L.-H., Duan, X.-P., Yan, X., Yu, M., Ning, X., Zhao, Y., et al. (2016). Recent advances in melt electrospinning. *RSC Adv*. 6, 53400–53414. doi: 10.1039/C6RA09558E

Zhang, Q., Hwang, J. W., Oh, J. H., Park, C. H., Chung, S. H., Lee, Y. S., et al. (2017). Effects of the fibrous topography-mediated macrophage phenotype transition on the recruitment of mesenchymal stem cells: an *in vivo* study. *Biomater* 149, 77–87. doi: 10.1016/j.biomaterials.2017.10.007

Zhu, M., Wang, Z., Zhang, J., Wang, L., Yang, X., Chen, J., et al. (2015). Circumferentially aligned fibers guided functional neoartery regeneration *in vivo*. *Biomater* 61, 85–94. doi: 10.1016/j.biomaterials.2015.05.024

Ziebert, F., and Aranson, I. S. (2016). Computational approaches to substrate-based cell motility. *Comput. Mater*. 2:16019. doi: 10.1038/npjcompumats.2016.19

Conflict of Interest Statement: The authors declare that the research was conducted in the absence of any commercial or financial relationships that could be construed as a potential conflict of interest.

frontiers in Bioengineering and Biotechnology

MINI REVIEW
published: 02 October 2018
doi: 10.3389/fbioe.2018.00137

Borrowing From Nature: Biopolymers and Biocomposites as Smart Wound Care Materials

Giulia Suarato [1,2], Rosalia Bertorelli [2] and Athanassia Athanassiou [1]**

[1] *Smart Materials, Istituto Italiano di Tecnologia, Genoa, Italy,* [2] *In vivo Pharmacology Facility, Istituto Italiano di Tecnologia, Genoa, Italy*

Wound repair is a complex and tightly regulated physiological process, involving the activation of various cell types throughout each subsequent step (homeostasis, inflammation, proliferation, and tissue remodeling). Any impairment within the correct sequence of the healing events could lead to chronic wounds, with potential effects on the patience quality of life, and consequent fallouts on the wound care management. Nature itself can be of inspiration for the development of fully biodegradable materials, presenting enhanced bioactive potentialities, and sustainability. Naturally-derived biopolymers are nowadays considered *smart materials*. They provide a versatile and tunable platform to design the appropriate extracellular matrix able to support tissue regeneration, while contrasting the onset of adverse events. In the past decades, fabrication of bioactive materials based on natural polymers, either of protein derivation or polysaccharide-based, has been extensively exploited to tackle wound-healing related problematics. However, in today's World the exclusive use of such materials is becoming an urgent challenge, to meet the demand of environmentally sustainable technologies to support our future needs, including applications in the fields of healthcare and wound management. In the following, we will briefly introduce the main physico-chemical and biological properties of some protein-based biopolymers and some naturally-derived polysaccharides. Moreover, we will present some of the recent technological processing and green fabrication approaches of novel composite materials based on these biopolymers, with particular attention on their applications in the skin tissue repair field. Lastly, we will highlight promising future perspectives for the development of a new generation of environmentally-friendly, naturally-derived, smart wound dressings.

Keywords: wound healing, biomimetic, alginate, chitosan, hyaluronic acid, silk fibroin, keratin, antibacterial

OPEN ACCESS

Edited by:
Gianni Ciofani, Politecnico di Torino, Italy

Reviewed by:
Gozde Ozaydin Ince, Sabanci University, Turkey
Satoshi Arai, Waseda University, Japan
Filippo Rossi, Politecnico di Milano, Italy

****Correspondence:***
Giulia Suarato
giulia.suarato@iit.it
Athanassia Athanassiou
athanassia.athanassiou@iit.it

Specialty section:
This article was submitted to Nanobiotechnology, a section of the journal Frontiers in Bioengineering and Biotechnology

Received: *27 July 2018*
Accepted: *13 September 2018*
Published: *02 October 2018*

Citation:
Suarato G, Bertorelli R and Athanassiou A (2018) Borrowing From Nature: Biopolymers and Biocomposites as Smart Wound Care Materials. Front. Bioeng. Biotechnol. 6:137. doi: 10.3389/fbioe.2018.00137

INTRODUCTION

Skin is our major external defense system, in charge of protecting our inner body structures from microorganisms' attacks, and the adverse effects of the external environment. Adult skin is composed of three layers: *epidermis* or *stratum corneum*, mainly consisting of keratinocytes; *dermis*, the connective tissue rich in collagen; and *hypodermis* or *subcutaneous layer*, composed of fat tissue, which provides thermal isolation and mechanical protection to the body (Gurtner et al., 2008).

Wounds are breaks or defects within the skin, which may form due to physicochemical or thermal damage. Acute wounds define injured tissues that need a healing period over 8–12 weeks, (e.g., burns, chemical injuries, cuts). In contrast, chronic wounds are a fallout of diseases, such as venous or arterial vascular insufficiency, pressure necrosis, cancer, and diabetes (Sen et al., 2009; Moura et al., 2013). They require longer healing time (weeks-months to years) and often fail to reach a normal healthy state, persisting in a pathological condition of inflammation (Guo and Dipietro, 2010). Therefore, delayed or impaired wound healing poses a significant socio-economic burden on patients and health care systems worldwide, in terms of treatment costs and waste production (Sen et al., 2009).

Insight into the intricate biochemical events activated during skin repair is crucial to design appropriate wound dressings (Weller and Sussman, 2006; Gurtner et al., 2008; Pereira et al., 2013). The healing process can be divided into the following, overlapping stages: homeostasis, inflammation, proliferation, and remodeling (Martin, 1997; Gurtner et al., 2008; Bielefeld et al., 2013; Das and Baker, 2016). *Homeostasis* is the immediate response of the body to an injury, in order to stop blood loss at the wound site, by means of fibrin cloths as temporary barriers (Sinno and Prakash, 2013). *Inflammation* (form 24 h to 4–6 days) is mediated by neutrophils and macrophages (Broughton et al., 2006), that sweep the wound bed from foreign particles and tissue debris. Cytokines and enzymes are released to stimulate fibroblasts and myofibroblasts (Das and Baker, 2016), while the wound exudate provides the essential moisture for the recovery. In the *proliferation* phase epithelialization occurs and newly formed granulation tissue begins to fill the wound area, producing new extracellular matrix (ECM). Finally, during the *remodeling* phase, collagen-based cross-linking is responsible for a tight 3D network formation, increasing the tensile strength of the new tissue (Sinno and Prakash, 2013).

Given the multiple mechanisms involved in the skin wound healing and the interplay of several external factors, the choice of suitable dressing materials is compelling. Specifically, for biodegradable natural materials, their degradation needs to follow the dynamics of the wound repair, guaranteeing the physiological healing evolution, and releasing active principles when needed. At last but not least, proper consideration should be put onto the environmental sustainability of these biomaterials, in terms of green chemistry fabrication approaches, and complete biodegradation without harmful by-products. While numerous reviews on traditional wound dressing biomaterials have been extensively published (Sell et al., 2010; Mogoşanu and Grumezescu, 2014; Norouzi et al., 2015; Mele, 2016), in this mini-review we will focus our attention on the most recent naturally-derived, active systems, pursuing the quest for an environmentally sustainable wound management.

MIMICKING NATURE AS A THERAPEUTIC STRATEGY

Successful wound management relies on understanding the healing process combined with a know-how on the properties of the various dressing materials available. Principal purpose of any wound treatment is to maximize the treatment efficiency (Weller and Sussman, 2006). Currently, standard care procedures consist of swabbing the infection, cleaning the wound bed from tissue debris, and applying the dressing (Dreifke et al., 2015). In case of extended skin lesions, the use of split-thickness skin autografts or allografts might be required, carrying safety issues related to disease transmission and immune rejection.

An ideal dressing should remove excessive exudate to avoid tissue maceration and promote autolytic debridement, while keeping moisture, adequate oxygen and water vapor permeability within the wound. It should be adhesive and flexible, to favor mechanical compliance to the patient body and ease the application/removal. Deliverable bioactive compounds, such as antibiotics, essential oils, and natural antioxidants, stimulate the dressing interaction with the wound microenvironment and further enhance the therapeutic action via antimicrobial, antifungal, and antiseptic activities (Pereira et al., 2013). A number of fabrication techniques, such as film-casting, electrospinning, self-assembly, freeze-drying, emulsions, microsphere injection, have been employed to produce wound dressings, either based on synthetic macromolecules or on materials of natural origin (Sell et al., 2007, 2010; Wei and Ma, 2008; Huang and Fu, 2010; Zhong et al., 2010; Rieger et al., 2013; Mogoşanu and Grumezescu, 2014; Norouzi et al., 2015; Liakos et al., 2016; Mele, 2016).

Recently, natural biopolymers have largely attracted the scientific community interest. On top of their notable biocompatibility and biodegradability, natural occurring proteins and polysaccharides allow to achieve the highest level of biomimicry, recapitulating the native ECM biological and physico-chemical features. Further architectural resemblance can be obtained with an appropriate processing (e.g., nanofibers, sponge-like hydrogels; Huang and Fu, 2010; Mogoşanu and Grumezescu, 2014; Liakos et al., 2015; Mele, 2016). Despite their batch-to-batch variations in terms of mechanical properties and their rather limited shelf-life, naturally-derived biopolymers confer ECM support (collagen, gelatin, hyaluronic acid), present cell-recognition domains and biomolecule binding sites (RGD and LDV sequences in silk fibroin and keratin), and may possess inherent antibacterial and anti-inflammatory properties (chitosan, alginate). Moreover, in the past decades, clinical understanding advancements have directed significant exploitation of natural materials in clinical trials (Vyas and Vasconez, 2014; Dhivya et al., 2015). By looking into our natural surroundings and by re-using some of the discarded natural resources, several functional biomaterials can be easily identified and implemented for promising wound healing applications, with a reduced impact on the environment (**Figure 1**).

PROTEIN-BASED BIOPOLYMERS

Collagen and Gelatin

Collagen is the most abundant animal protein, which provides mechanical strength to tissues and stimulates cell-adhesion and proliferation (Neel et al., 2013; An et al., 2016). Twenty-nine different types of collagen have been identified, displaying a triple-helical tertiary structure of polypeptide sequences (**Figure 2a**), but only a few are used in the production of

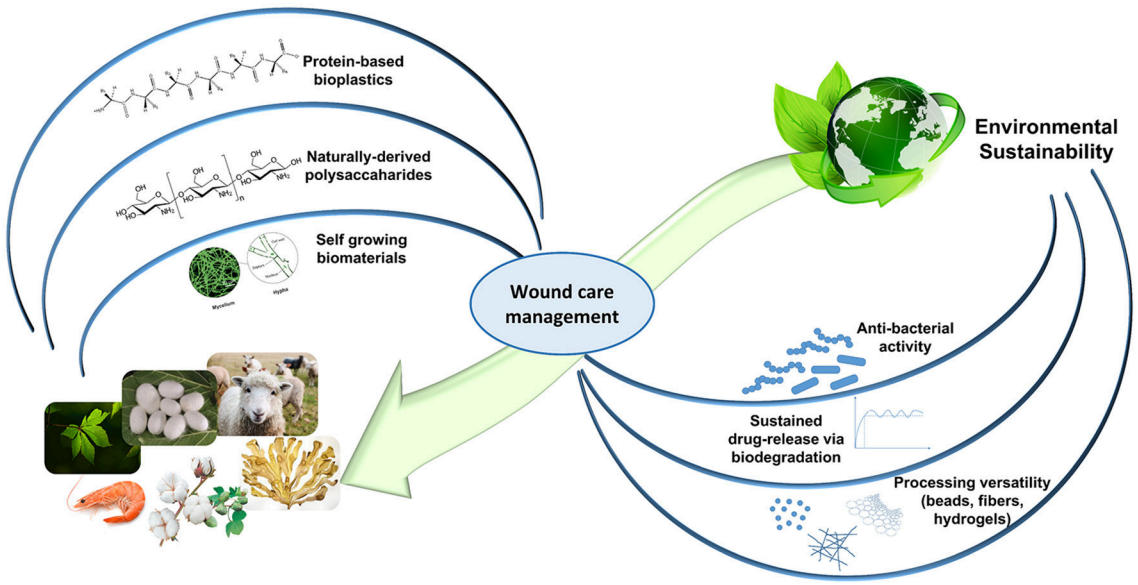

FIGURE 1 | The circularity concept of Nature-mimicking for an environmentally-friendly wound healthcare. Self-growing biomaterials panel is adapted from Haneef et al. (2017). This material is licensed under the Creative Commons Attribution 4.0 International Public License (https://creativecommons.org/licenses/by/4.0/legalcode).

collagen-based biomaterials. As animal-derived proteins may be responsible for allergic reactions and pathogen transmissions (Koide, 2007), an alternative is constituted by collagen from heterologous expression in mammalian, insect and yeast cells (Olsen et al., 2003), or produced by *Escherichia coli* (Pinkas et al., 2011). High biocompatibility and biodegradability by endogenous collagenases make collagen ideal for biomedical applications (Parenteau-Bareil et al., 2010; Chattopadhyay and Raines, 2014). During wound healing, fibroblasts produce collagen molecules that aggregate to form fibrils with diameter in the range of 10–500 nm. This fibrous network facilitates cell migration to the wounded site, actively supporting tissue repair (Baum and Arpey, 2005).

Thanks to a facile chemical functionalization of the protein structure, various dressing architectures have been exploited. Collagen-based wound dressings, either in forms of hydrogels, electrospun fibers, or nanocrystal-containing scaffolds, have been applied to cover burn wounds, treat ulcers (Ghica et al., 2017; Guo et al., 2017; Bhowmick et al., 2018; Yoon et al., 2018), reduce tissue contraction and scarring, and increase epithelialization rate (Powell et al., 2008). Collagen sponges and fibrous membranes were found particularly promising, due to their wet-strength that allows suturing to soft tissues and provides a template for new tissue growth. Composites with other natural materials, such as dextran, chitosan, hyaluronic acid, and alginate (Karri et al., 2016; Ghica et al., 2017; Wei et al., 2018) or constructs based on collagen and synthetic biopolymers, such as poly-α-hydroxyl esters (Hall Barrientos et al., 2017; Albright et al., 2018; Bhowmick et al., 2018) have been extensively exploited. Moreover, acetylated, succinylated, methylated, or biotinylathed collagen have been used to immobilize therapeutic enzymes or growth factors and to control drug delivery (Lima et al., 2015; Mele, 2016; Qu et al., 2018; Zhu et al., 2018). Albright and coworkers (Albright et al., 2018) proposed a multi-structured nanofibrous dressing, composed of poly-ε-caprolactone/collagen electrospun matrix, loaded with transforming growth factor TGF-β1 and modified with polypeptide-based nanocarriers incorporating tannic acid and gentamicin. The multifunctional platform showed anti-bacterial and anti-inflammatory properties, while retaining a favorable topography for cell proliferation, thus accelerating healing and wound closure. A similar construct was proposed by Karri et al. (2016), where a composite scaffold of collagen and alginate was impregnated with curcumin-loaded chitosan nanoparticles to obtain an all-natural wound dressing.

A collagen-derivative with promising biomedical values is gelatin. Gelatin is obtained by an incomplete denaturalization of collagen extracted from connective tissues, skin, and boiling bones (Jaipan et al., 2017). It has been employed to fabricate strong hydrogel-like membranes (Thanusha et al., 2018), microspheres (Thyagarajan et al., 2017), sponges, and electrospun mats (Chen et al., 2016), for dermal tissue applications and to treat severe burn wounds. Various combinations of gelatin and modified chitosan have been proposed (Han et al., 2014; Agarwal et al., 2016), as well as blends with poly-vinyl alcohol based via enzymatic crosslinking, to support fibroblast culture and proliferation (Hago and Li, 2013).

Despite their rather extensive usage as biomaterials for scaffold design, collagen and gelatin remain sustainable materials with highly engineering potential yet unexplored (Hall Barrientos et al., 2017; Golser et al., 2018).

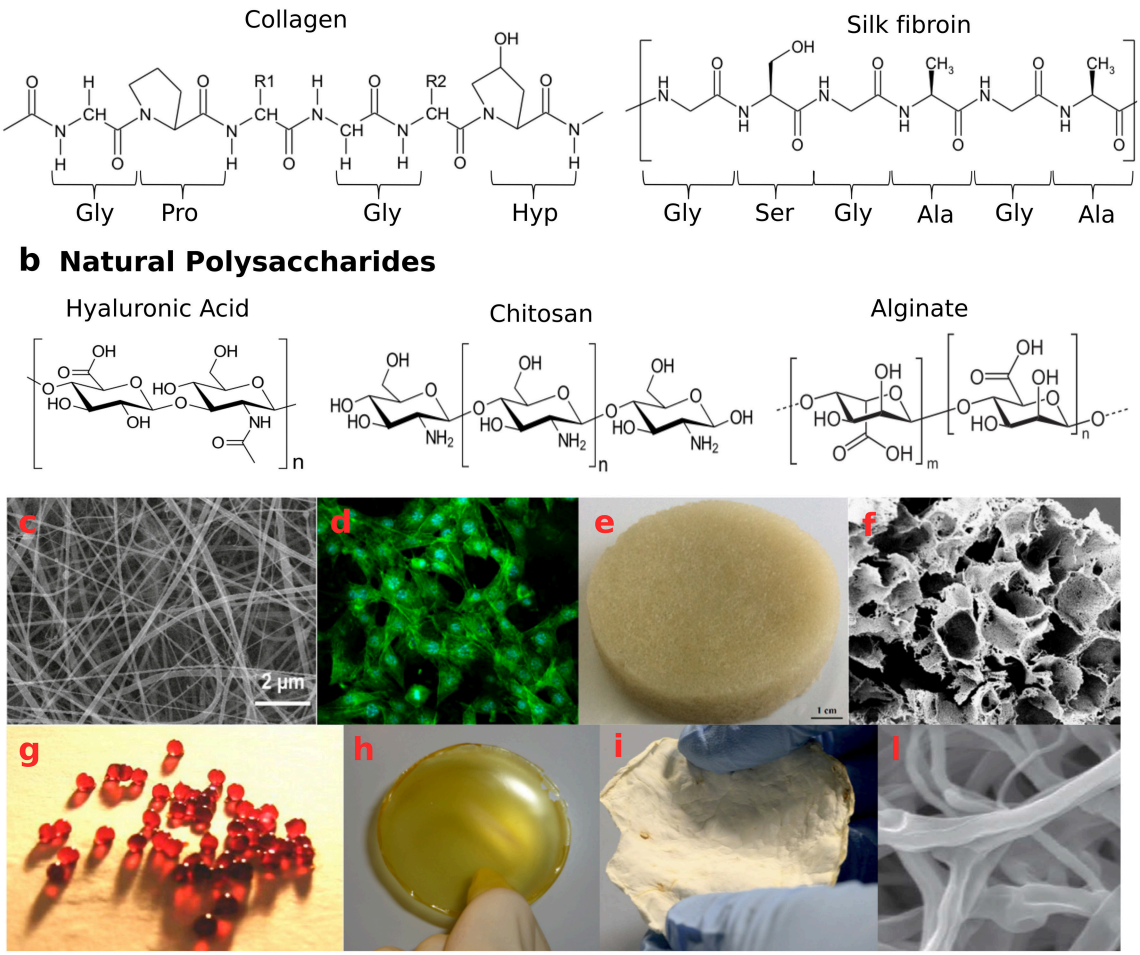

FIGURE 2 | Naturally-derived biopolymer-based structures with potential application as wound healing systems. **(a)** examples of protein-based biopolymers primary structures—aminoacidic sequence of collagen type I molecules and aminoacidic sequence of silk fibroin molecules: Gly, glycine; Ala, alanine; Pro, proline; Ser, serine; Hyp, hydroxyproline; **(b)** natural polysaccharide structures—hyaluronic acid, chitosan, and alginate; **(c,d)** Biocompatible silk/parsley electrospun fibers (average diameter 50 nm) able to grow NIH3T3 fibroblast cells adapted with permission from Guzman-Puyol et al. (2016) Copyright©2016 American Chemical Society; **(e,f)** wool keratin sponges, reprinted from Patrucco et al. (2016) Copyright©2016 with permission from Elsevier; **(g)** calcium cross-linked alginate beads and **(h)** film incorporating antiseptic PVPI complex, reprinted from Liakos et al. (2013) Copyright©2013 with permission from Elsevier; **(i,l)** mycelia material from *P. ostreatus* after 20 days of growth on potato-dextrose broth and cellulose, presenting a 3D network of hyphae. Panels **(i,l)** are adapted from Haneef et al. (2017). This material is licensed under the Creative Commons Attribution 4.0 International Public License (https://creativecommons.org/licenses/by/4.0/legalcode).

Silk Fibroin

Silks are proteins produced in the epithelial cells of specialized glands of various arthropods, such as spiders and silkworms. The secreted silk fibers present a highly repetitive sequence, consisting mainly of glycine (43%), alanine (30%), and serine (12%)—$[GAGSGA]_n$ motifs, arranged in β-sheets regions embedded in an amorphous matrix (Chutipakdeevong et al., 2013; Reimers et al., 2015), which confer high toughness and elasticity (**Figure 2a**). Regarding more specifically silk from the cocoons of *Bombyx mori* silkworms, two kinds of proteins are its major components: the fibroin and the sericin. The fibroins are composed of three types of protein fibers: 350 kDa-heavy chain, 30 kDa-glycoprotein, and 25 kDa-light chain, the latter conferring hydrophilicity, water uptake ability and cell adhesion properties. Light and heavy chains are connected by disulfide bonds, while the glue protein sericin coats the silk fibers. Thanks to high mechanical resistance, enzymatic-driven biodegradability and favorable cell attachment, silk fibroins have been successfully exploited for skin tissue engineering and wound healing applications.

Bombyx mori silkworm-derived fibroins are obtained from cocoon and separated from sericin by degumming in alkaline boiling water and following solubilization in hot LiBr solution (Reimers et al., 2015). Regenerated silk water soluble form, silk I, can be converted into insoluble silk II, by modifying the α-helical chain arrangements into β-sheets via alcohol treatment

or water vapor annealing (WVA; Min et al., 2006; Wharram et al., 2010; Hu et al., 2011). In fact, by controlling the protein secondary structure, fibroin scaffolds' biodegradation can be properly tuned, in order to modulate the release of bioactive molecules (Hofmann et al., 2006), such as antibiotics (Pritchard et al., 2013; Chouhan et al., 2017), growth factors (Schneider et al., 2009; Chouhan et al., 2017; Pignatelli et al., 2018), and anti-oxidant compounds (Fan et al., 2012; Sheng et al., 2013; Lin et al., 2016). In their study, Pignatelli and coworkers (Pignatelli et al., 2018) encapsulated human platelet lysate into electrospun silk-PEO patches, to prolong the growth factor shelf life and ease its handling during wound management. By changing the crystallinity degree of the fibrous matrices via WVA from 21 to 35 or 44%, the 24-h drug release drastically decreased from 100 to 80 and 46%, respectively.

Proteins' versatile nature allows for a plethora of processing techniques, with the consequent fabrication of multiple scaffold morphologies, such as films (Srivastava et al., 2015), foams and sponges (Roh et al., 2006), gels, and fibrous matrices. In the last decade, electrospun fibroin has been extensively proposed for the design of anti-bacterial, anti-inflammatory and anti-oxidant patches (Lin et al., 2016; Selvaraj and Fathima, 2017; Yang et al., 2017). To ease a water-based electrospinning process, silk has been processed either in combination with natural polymers, such as cellulose (Guzman-Puyol et al., 2016; **Figures 2c,d**), gelatin (Shan et al., 2015), sericin (Hang et al., 2012), chitosan (Cai et al., 2010), alginate (Roh et al., 2006), elastin (Zhu et al., 2016), and hyaluronic acid (Yan et al., 2013), or mixed with synthetic materials, such as polyethylene oxide (Schneider et al., 2009; Wharram et al., 2010; Chutipakdeevong et al., 2013), polyvinyl alcohol (PVA; Chouhan et al., 2017), and poly-hydroxy esters (Lian et al., 2014; Shahverdi et al., 2014; Suganya et al., 2014; Shanmugam and Sundaramoorthy, 2015). Silk/PVA mats loaded with Ciprofloxacin and epidermal growth factors (Chouhan et al., 2017) enhanced human dermal fibroblasts and keratinocytes proliferation *in vitro*, and favored re-epithelization, mature collagen deposition and complete wound closure at 14 days in a *in vivo* wound healing rabbit model. In a different work, Ju and coworkers (Ju et al., 2016) investigated the intrinsic anti-inflammatory effects of a porous fibroin/PEO electrospun nanomatrix in a mice burn-model, observing downregulation of pro-inflammatory cytokines IL-1α and IL-6.

Keratin

Keratins (Ker) are the most abundant group of insoluble and filament-forming proteins produced in epithelial cells of mammals, birds, reptiles, and humans. As structural components of wool, nails, horn, feathers, and hair, they exploit mechanical support and protective functions against the environment (Reichl, 2009; Wang et al., 2016). Keratins present a complex intermediate filament (IF)-matrix hierarchical structure and are categorized according to the polypeptide chain secondary assembly. α-Ker (40–68 kDa) comprise α-helices arranged in coiled-coil heterodimers to form 7-nm IF, while β-Ker (10–22 kDa) consist of packed β-sheets disposed in 3-nm IF. The high-sulfur containing matrix (γ-Ker, below 10 kDa), rich in cysteine, tyrosine, glycine and phenylalanine residues, present a globular assembly (Dowling et al., 1986; Fraser et al., 1986; Steinert and Marekov, 1993; Rouse and Van Dyke, 2010; Wang et al., 2016). The secondary structure of keratinous materials largely affects their mechanical resistance, solubility, and hydration sensitivity (Wang et al., 2016). Tons of Ker-containing biomasses are produced every year, from meat and poultry market, wool industry and hair salons, leading to continuous accumulation of wastes in the ecosystem. The challenges associated with this waste disposal have been considered by the European Parliament and Council regulation EC 1774/2002 (Sharma and Gupta, 2016). Due to the presence of strong disulfide and H-bonds, keratin extraction from biomasses involves rather complicated methods, such as microbial and enzymatic hydrolysis, mechanical treatments, or chemical protocols with alkali, reducing agents or ionic liquids (Yamauchi et al., 2003; Ozaki et al., 2014; Sharma and Gupta, 2016; Shavandi et al., 2017).

However, thanks to its biocompatibility, biodegradability, and hemostatic properties, keratin constitutes a potential green secondary raw material for wound healing, tissue repair, drug delivery, and cosmetics applications (Sharma and Gupta, 2016; Arslan et al., 2017; Shavandi et al., 2017). Since its earliest documented use in medicinal applications (China, sixteenth century; Rouse and Van Dyke, 2010), in the past decades several Ker-based biomaterials have been proposed, given the ability of this biopolymer to self-assembly into 3D networks favorable for cell infiltration, and its intrinsic bioactivity for the presence of cell binding motifs (such as EDS, LDV, and RGD; Rouse and Van Dyke, 2010). Keratin extracted from chicken feathers, wool and human hair have been processed in films (Yamauchi et al., 2003; Fujii and Ide, 2004; Tonin et al., 2007; Reichl, 2009; Cui et al., 2013), sponge-like and hydrogel-like scaffolds for tissue engineering and wound healing (**Figures 2e,f**; Tachibana et al., 2002; Verma et al., 2008; Hill et al., 2010; Saul et al., 2011; Richter et al., 2012; Wang et al., 2012; Xu et al., 2013; Patrucco et al., 2016; Singaravelu et al., 2016). Electrospun fibers have also been obtained in combination with PEO (Aluigi et al., 2007, 2008; Fan et al., 2016; Ma et al., 2017), PVA (Choi et al., 2015; He et al., 2017; Wang et al., 2017), fibroin (Zoccola et al., 2008; Yen et al., 2016), poly-caprolactone (Boakye et al., 2015; Edwards et al., 2015; Li et al., 2016; Zhu et al., 2017), poly(3-hydroxybutyrate-co-3-hydroxyvalerate) (Yuan et al., 2015), chitosan (Singaravelu et al., 2016), and gelatin (Yao et al., 2017).

NATURALLY-DERIVED POLYSACCHARIDES

Hyaluronic Acid

Hyaluronic acid (HA) is a non-immunogenic polysaccharide consisting of glucuronic acid and N-acetyl-D-glucosamine units (**Figure 2b**). This glycosaminoglycan is one of the main components of the connective tissue in mammals (Mele, 2016). Due to its hygroscopic nature, HA has been used to prepare hydrogel-like constructs, to support keratinocyte migration and angiogenesis, and promote a scar-free wound healing (Mogoşanu and Grumezescu, 2014; Dreifke et al., 2015). The molecular

weight (MW) plays a key role in the process (Tolg et al., 2014): low MWHA degradation products were found to be pro-inflammatory (Campo et al., 2010; Dreifke et al., 2015), while high MWHA appeared to inhibit nutrient supply. Interestingly, medium MWHA (100–300 kDa) showed enhanced wound closure capability through up-regulation of adhesion molecules (Ghazi et al., 2012). Moreover, the hydrophilicity of the HA chains allows the 3D network swelling and the consequent gradual release of encapsulated active compounds, making this biomaterial suitable as drug delivery platform (Maeda et al., 2014). HA-based electrospun fibers, either pure or in combination with other biomacromolecules (Xu et al., 2009; Hsu et al., 2010; Uppal et al., 2011; Dogan et al., 2016), have been proposed for tunable degradation and sustained release *in vitro* and *in vivo*.

Chitosan

Chitosan (CS), a deacetylated chitin-derivative found in the exoskeletons and shells of crustaceans, is a linear polysaccharide consisting of β(1-4)-D-glucosamine and N-acetyl-D-glucosamine groups randomly distributed (**Figure 2b**). Owing to its intrinsic antifungal, antibacterial, hemostatic, and muco-adhesive properties, chitosan has been widely exploited in the biomedical field for wound and burn treatments (Dash et al., 2011; Croisier and Jérôme, 2013; Norouzi et al., 2015; Zhao et al., 2015). Several dressing architectures have been proposed: CS-*Aloe vera* membranes (Wani et al., 2010), thyme oil-CS films (Altiok et al., 2010), CS-gelatin sponges (He et al., 2007), CS-silk hydrogels (Silva et al., 2012), CS-cellulose films (Niyas Ahamed and Sastry, 2011; Romano et al., 2015a), cinnamon oil-CS/polyethylene oxide nanofibers (Rieger and Schiffman, 2014), and CS/poly(3-hydroxybutyrate-*co*-3-hydroxyvalerate) scaffolds (Veleirinho et al., 2012). In addition, water-soluble derivatives, such as carboxymethyl-CS and methacrylate glycol CS have been synthetized and investigated for wound healing applications (Romano et al., 2015b).

Alginate

Alginate (Alg) is a linear co-polymer of β-D-Mannuronic acid and α-L-Glucuronic acid (**Figure 2b**). This polysaccharide is mostly abundant in *Brown Algae* or produced by some bacteria (Khan and Ahmad, 2013). It is highly hydrophilic, biocompatible, and able to absorb wound exudate, maintaining a moist microenvironment (Chiu et al., 2008). The combination of alginate with antimicrobial and enzymatic components can promote elimination of necrotic tissues and microbial bodies, while the polysaccharide base can stimulate reparative wound processes (Patel et al., 2007). Alginate dressings are also useful as delivery platforms, in order to provide a controlled release of therapeutic substances to exuding wounds (e.g., pain-relieving, antibacterial, and anti-inflammatory agents; Maver et al., 2015; Szekalska et al., 2016; Setti et al., 2018). Biodegradable Na-Alg/PVPI (povidone iodine complex) films and Ca-Alg/PVPI beads have displayed antimicrobial and antifungal activities (Liakos et al., 2013; **Figures 2g,h**). Moreover, Na-Alg/PVPI films have shown to reduce the inflammatory response and accelerate the wound healing providing a controlled release of PVPI (Summa et al., 2018). To treat UV-induced skin burns, instead, electrospun nanofibers loaded with lavender essential oil have been used: the composite mats exhibited antibacterial and anti-inflammatory properties, being able to reduce the production of pro-inflammatory cytokines both *in vitro* and *in vivo* (Hajiali et al., 2016).

SELF-GROWING MYCELIUM-BASED BIOMATERIALS

Mycelium, the fungi vegetative part, comprises a network of filamentous hyphae, which penetrate the substrate. Hyphae are tubular structures of micrometric diameter, composed of aligned and elongated cells, separated by walls, called septa (**Figures 2i,l**). A continuous cell wall protects the hyphae and confers mechanical strength and shape to the mycelium (Haneef et al., 2017; Jones et al., 2017). Being constituted of chitin, chitosan, glucans, mannoproteins, and glycoproteins (Synytsya and Novák, 2013), the cell wall is a biopolymer composite that prevents the hyphae from collapsing during their sprouting and movement (Cairney, 2005).

Peculiarity of these living, self-growing composites is the possibility to tune the physico-chemical properties during their growth phase, reducing sophisticated processing and by-product formation, while allowing for ready-to-use systems. Throughout its dynamic growth, the mycelium "senses" the substrate and responds to the surrounding, depending on edaphic conditions, substrate pH and composition, or the presence of other living organisms (Krull et al., 2013). A polarized extension of the cell wall occurs at the apical region of the hyphae, as the mycelium secretes a variety of enzymes, hydrolyzes the substrate and absorbs the solubilized nutrients. By properly exploiting different feeding substrates for hyphae digestion, the resulting properties of the interwoven fibrous mycelium material can be efficiently tailored. Type and amount of absorbed nutrients may affect mycelia growth rate, extension and biological activity (Frimpong-Manso et al., 2011; Da Silva et al., 2012; Larsen, 2015; Anderson and Cairney, 2018). Similarly, culture conditions and feeding substrate highly influence the final chemical composition (Krull et al., 2013; Haneef et al., 2017), either stimulating plasticizer biosynthesis (lipids and small glycoproteins) or promoting rigid macromolecule production (chitin, β-D-glucans; Synytsya and Novák, 2013). In this regard, mycelia can be considered as 3D smart, micro-reactors, able to bio-convert various agro-residues into enzymes, polysaccharides, and bioactive metabolites (Vassilev et al., 1995; Krull et al., 2013; Vamanu, 2014; Yan et al., 2014; Salati et al., 2017), with potential bio-pharmaceutical and neutraceutical relevance.

In the past, mycelia-derived scaffolds have been exploited (Su et al., 1999, 2005; Hung et al., 2001). Su et al. (1997) developed a filament-structured membrane from the residue of *Ganoderma tsugae*, called *Sacchachitin*, composed of β-1,3-glucan (60%), and N-acetylglucosamine (40%), to be used as skin substitute. The new biomaterial demonstrated wound healing potential *in vivo*, by promoting fibroblast proliferation and migration. In a

following study (Su et al., 2005), the *Sacchachitin* membranes appeared to boost keratinocytes proliferation and prevent metalloproteinase-related ECM degradation, contributing to accelerate the healing process of a chronic wound *in vivo* model. Furthermore, a micronized *Sacchachitin* nanogel has been investigated to treat superficial chemical corneal burns *in vivo* (Chen et al., 2012), while the anti-oxidant and immuno-modulating effects of extracts from mycelia of some medicinal fungi have been investigated for skin aging (Kim et al., 2014), dermatitis (Hwang et al., 2012), and UV-protection (Nanbu et al., 2011; Bae et al., 2012), suggesting a promising mycelia biological value yet unexplored.

CONCLUSIONS - A QUEST FOR AN ENVIRONMENTALLY SUSTAINABLE WOUND MANAGEMENT

Environmental sustainability has nowadays become an imperative issue to front, in an effort to balance both the industrial productivity and the planet ability to generate resources, with the neutralization of wastes and the mitigation of polluting processes. Material and energy consumption related to the healthcare industry, ranging from complex material manufacturing processes, to drug packaging, to high-volume medical wastes, might heavily contribute to increase the overall pollution, with an unsought negative impact on the human health (Jameton and Pierce, 2001). Nature itself can be of inspiration to develop cost-competitive, low-energy consumption and fully biodegradable materials, presenting greater environmental sustainability. The increasing interest of the scientific community in the use of either protein-based or polysaccharide-derived dressings is striking, and it reflects the growing perspective of giving back what we borrowed from Nature. In this regard, self-growing mycelia, which are biocomposites constituted of both proteins and polysaccharides, can represent a smart strategy to fabricate healthcare products of the future, as economically and environmentally valid alternatives to synthetic materials. In conclusion, naturally derived biopolymers provide a versatile, multifunctional, and tunable platform to design appropriate extracellular environments, able to actively contrast the onset of infections and inflammations, while promoting tissue regeneration, and scar remodeling.

AUTHOR CONTRIBUTIONS

GS and RB conceived and wrote the main manuscript text. AA edited and reviewed the whole manuscript.

REFERENCES

Agarwal, T., Narayan, R., Maji, S., Behera, S., Kulanthaivel, S., Maiti, T. K., et al. (2016). Gelatin/Carboxymethyl chitosan based scaffolds for dermal tissue engineering applications. *Int. J. Biol. Macromol.* 93, 1499–1506. doi: 10.1016/j.ijbiomac.2016.04.028

Albright, V., Xu, M., Palanisamy, A., Cheng, J., Stack, M., Zhang, B., et al. (2018). Micelle-coated, hierarchically structured nanofibers with dual-release capability for accelerated wound healing and infection control. *Adv. Healthc. Mater.* 7:e1800132. doi: 10.1002/adhm.201800132

Altiok, D., Altiok, E., and Tihminlioglu, F. (2010). Physical, antibacterial and antioxidant properties of chitosan films incorporated with thyme oil for potential wound healing applications. *J. Mater. Sci. Mater. Med.* 21, 2227–2236. doi: 10.1007/s10856-010-4065-x

Aluigi, A., Varesano, A., Montarsolo, A., Vineis, C., Ferrero, F., Mazzuchetti, G., et al. (2007). Electrospinning of keratin/poly(ethylene oxide) blend nanofibers. *J. Appl. Polym. Sci.* 104, 863–870. doi: 10.1002/app.25623

Aluigi, A., Vineis, C., Varesano, A., Mazzuchetti, G., Ferrero, F., and Tonin, C. (2008). Structure and properties of keratin/PEO blend nanofibres. *Eur. Polym. J.* 44, 2465–2475. doi: 10.1016/j.eurpolymj.2008.06.004

An, B., Lin, Y. S., and Brodsky, B. (2016). Collagen interactions : drug design and delivery. *Adv. Drug Deliv. Rev.* 97, 69–84. doi: 10.1016/j.addr.2015.11.013

Anderson, I. C., and Cairney, J. W. (2018). Ectomycorrhizal fungi: exploring the mycelial frontier. *FEMS Microbiol. Rev.* 31, 388–406. doi: 10.1111/j.1574-6976.2007.00073.x

Arslan, Y. E.,Sezgin Arslan, T., Derkus, B., Emregul, E., and Emregul, K. C. (2017). Fabrication of human hair keratin/jellyfish collagen/eggshell-derived hydroxyapatite osteoinductive biocomposite scaffolds for bone tissue engineering : from waste to regenerative medicine products. *Colloids Surf. B Biointerf.* 154, 160–170. doi: 10.1016/j.colsurfb.2017.03.034

Bae, J. T., Ko, H. J., Kim, G. B., Pyo, H. B., and Lee, G. S. (2012). Protective effects of fermented citrus unshiu peel extract against ultraviolet-a-induced photoageing in human dermal fibrobolasts. *Phytother. Res.* 26, 1851–1856. doi: 10.1002/ptr.4670

Baum, C. L., and Arpey, C. J. (2005). Normal cutaneous wound healing: clinical correlation with cellular and molecular events. *Dermatol. Surg.* 31, 674–686. doi: 10.1097/00042728-200506000-00011

Bhowmick, S., Thanusha, A. V., Kumar, A., Scharnweber, D., Rother, S., and Koul, V. (2018). Nanofibrous artificial skin substitute composed of mPEG–PCL grafted gelatin/hyaluronan/chondroitin sulfate/sericin for 2nd degree burn care: *in vitro* and *in vivo* study. *RSC Adv.* 8, 16420–16432. doi: 10.1039/C8RA01489B

Bielefeld, K. A., Amini-Nik, S., and Alman, B. A. (2013). Cutaneous wound healing: recruiting developmental pathways for regeneration. *Cell. Mol. Life Sci.* 70, 2059–2081. doi: 10.1007/s00018-012-1152-9

Boakye, M. A. D., Rijal, N. P., Adhikari, U., and Bhattarai, N. (2015). Fabrication and characterization of electrospun PCL-MgO-Keratin-based composite nanofibers for biomedical applications. *Materials* 8, 4080–4095. doi: 10.3390/ma8074080

Broughton, G., Janis, J. E., and Attinger, C. E. (2006). Wound healing: an overview. *Plast. Reconstr. Surg.* 117(Suppl. 7), 1e-S—32e-S. doi: 10.1097/01.prs.0000222562.60260.f9

Cai, Z. X., Mo, X. M., Zhang, K. H., Fan, L. P., Yin, A. L., He, C. L., et al. (2010). Fabrication of chitosan/silk fibroin composite nanofibers for Wound-dressing applications. *Int. J. Mol. Sci.* 11, 3529–3539. doi: 10.3390/ijms11093529

Cairney, J. W. (2005). Basidiomycete mycelia in forest soils: dimensions, dynamics and roles in nutrient distribution. *Mycol. Res.* 109, 7–20. doi: 10.1017/S0953756204001753

Campo, G. M., Avenoso, A., Campo, S., Ascola, A. D., Nastasi, G., and Calatroni, A. (2010). Biochimie molecular size hyaluronan differently modulates toll-like receptor-4 in LPS-induced inflammation in mouse chondrocytes. *Biochimie* 92, 204–215. doi: 10.1016/j.biochi.2009.10.006

Chattopadhyay, S., and Raines, R. T. (2014). Collagen-based biomaterials for wound healing. *Biopolymers* 101,821–833. doi: 10.1002/bip.22486

Chen, J., Liu, Z., Chen, M., Zhang, H., and Li, X. (2016). Electrospun gelatin fibers with a multiple release of antibiotics accelerate dermal regeneration in infected deep burns. *Macromol. Biosci.* 16, 1368–1380. doi: 10.1002/mabi.201600108

Chen, R. N., Lee, L. W., Chen, L. C., Ho, H. O., Lui, S. C., Sheu, M. T., et al. (2012). Wound-healing effect of micronized sacchachitin (mSC) nanogel

on corneal epithelium. *Int. J. Nanomed.* 7, 4697–4706. doi: 10.2147/IJN.S34530

Chiu, C. T., Lee, J. S., Chu, C. S., Chang, Y. P., and Wang, Y. J. (2008). Development of two alginate-based wound dressings. *J. Mater. Sci. Mater. Med.* 19, 2503–2513. doi: 10.1007/s10856-008-3389-2

Choi, J., Panthi, G., Liu, Y., Kim, J., Chae, S., Lee, C., et al. (2015). Keratin/poly (vinyl alcohol) blended nanofibers with high optical transmittance. *Polymer* 58, 146–152. doi: 10.1016/j.polymer.2014.12.052

Chouhan, D., Chakraborty, B., Nandi, S. K., and Mandal, B. B. (2017). Role of non-mulberry silk fibroin in deposition and regulation of extracellular matrix towards accelerated wound healing. *Acta Biomater.* 48, 157–174. doi: 10.1016/j.actbio.2016.10.019

Chutipakdeevong, J., Ruktanonchai, U. R., and Supaphol, P. (2013). Process optimization of electrospun silk fibroin fiber mat for accelerated wound healing. *J. Appl. Polym. Sci.* 3634–3644. doi: 10.1002/app.39611

Croisier, F., and Jérôme, C. (2013). Chitosan-based biomaterials for tissue engineering. *Eur. Polym. J.* 49, 780–792. doi: 10.1016/j.eurpolymj.2012.12.009

Cui, L., Gong, J., Fan, X., Wang, P., Wang, Q., and Qui, Y. (2013). Transglutaminase-modified wool keratin film and its potential application in tissue engineering. *Eng. Life Sci.* 13, 149–155. doi: 10.1002/elsc.201100206

Da Silva, M. C. S., Naozuka, J., Maria, J., Luz, R., de Assunção, L. S., Oliveira, P. V., et al. (2012). Enrichment of *Pleurotus ostreatus* mushrooms with selenium in coffee husks. *Food Chem.* 131, 558–563. doi: 10.1016/j.foodchem.2011.09.023

Das, S., and Baker, A. B. (2016). Biomaterials and nanotherapeutics for enhancing skin wound healing. *Front. Bioeng. Biotechnol.* 4:82. doi: 10.3389/fbioe.2016.00082

Dash, M., Chiellini, F., Ottenbrite, R. M., and Chiellini, E. (2011). Chitosan - A versatile semi-synthetic polymer in biomedical applications. *Prog. Polymer Sci.* 36, 981–1014. doi: 10.1016/j.progpolymsci.2011.02.001

Dhivya, S., Padma, V. V., and Santhini, E. (2015). Wound dressings – a review. *BioMedicine* 5, 24–28. doi: 10.7603/s40681-015-0022-9

Dogan, G., Başal, G., Bayraktar, O., Özyildiz, F., Uzel, A., and Erdogan, I. (2016). Bioactive sheath/core nanofibers containing olive leaf extract. *Microsc. Res. Tech.* 79, 38–49. doi: 10.1002/jemt.22603

Dowling, L. S., Crewther, W. G., and Parry, D. A. D. (1986). Secondary structure of component 8c-1 of a-keratin. *Biochem. J.* 236, 705–712. doi: 10.1042/bj2360705

Dreifke, M. B., Jayasuriya, A. A., and Jayasuriya, A. C. (2015). Current wound healing procedures and potential care. *Mater. Sci. Eng. C.* 48, 651–662. doi: 10.1016/j.msec.2014.12.068

Edwards, A., Jarvis, D., Hopkins, T., Pixley, S., and Bhattarai, N. (2015). Poly(e-caprolactone)/keratin-based composite nanofibers for biomedical applications. *J. Biomed. Mater. Res.Part B Appl. Biomater.* 103B, 21–30. doi: 10.1002/jbm.b.33172

Fan, J., Lei, T., Li, J., Zhai, P., Wang, Y., Cao, F., et al. (2016). High protein content keratin/poly (ethylene oxide) nanofibers crosslinked in oxygen atmosphere and its cell culture. *JMADE* 104, 60–67. doi: 10.1016/j.matdes.2016.05.022

Fan, L., Wang, H., Zhang, K., Cai, Z., and He, C. (2012). Vitamin C-reinforcing silk fibroin nanofibrous matrices for skin care application. *RSC Adv.* 2, 4110–4119. doi: 10.1039/c2ra20302b

Fraser, R. D. B., Macrae, T. P., and Parry, D. A. D. (1986). Intermediate filaments in a-keratins. *Proc. Natl. Acad. Sci. U.S.A.* 83, 1179–1183.

Frimpong-Manso, J., Obodai, M., Dzomeku, M., and Apertorgbor, M. M. (2011). Influence of rice husk on biological efficiency and nutrient content of *Pleurotus ostreatus* (Jacq. ex. Fr.) Kummer. *Int. Food Res. J.* 18, 249–254.

Fujii, T., and Ide, Y. (2004). Preparation of translucent and flexible human hair protein films and their properties. *Biol. Pharm. Bull.* 27, 1433–1436. doi: 10.1248/bpb.27.1433

Ghazi, K., Deng-Pichon, U., Warnet, J. M., and Rat, P. (2012). Hyaluronan fragments improve wound healing on *in vitro* cutaneous model through P2X7 purinoreceptor basal activation: role of molecular weight. *PLoS ONE* 7:e48351. doi: 10.1371/journal.pone.0048351

Ghica, M. V., Albu Kaya, M. G., Dinu-Pîrvu, C. E., Lupuleasa, D., Udeanu, D. I. (2017). Development, optimization and *in vitro*/*in vivo* characterization of collagen-dextran spongious wound dressings loaded with flufenamic acid. *Molecules* 22:E1552. doi: 10.3390/molecules22091552

Golser, A. V., Ro, M., Bo, H. G., and Scheibel, T. (2018). Engineered collagen: a redox switchable framework for tunable assembly and fabrication of biocompatible surfaces. *ACS Biomater. Sci. Eng.* 4, 2106–2114. doi: 10.1021/acsbiomaterials.7b00583

Guo, R., Lan, Y., Xue, W., Cheng, B., Zhang, Y., and Wang, C. (2017). Collagen-cellulose nanocrystal scaffolds containing curcumin-loaded microspheres on infected full-thickness burns repair. *J. Tissue Eng. Regen. Med.* 11, 3544–3555. doi: 10.1002/term.2272

Guo, S., and Dipietro, L. A. (2010). Factors affecting wound healing. *J. Dent. Res.* 89, 219–229. doi: 10.1177/0022034509359125

Gurtner, G. C., Werner, S., Barrandon, Y., and Longaker, M. (2008). Wound repair and regeneration. *Nature* 453, 314–321. doi: 10.1159/000339613

Guzman-Puyol, S., Heredia-Guerrero, J. A., Ceseracciu, L., Hajiali, H., Canale, C., Scarpellini, A., et al. (2016). Low-cost and effective fabrication of biocompatible nanofibers from silk and cellulose-rich materials. *ACS Biomater. Sci. Eng.* 2, 526–534. doi: 10.1021/acsbiomaterials.5b00500

Hago, E., and Li, X. (2013). Interprenetating polymer network hydrogels based on gelatin and PVA by biocompatible approaches: synthesis and characterization. *Adv. Mater. Sci. Eng.* 2013:328763. doi: 10.1155/2013/328763

Hajiali, H., Summa, M., Russo, D., Armirotti, A., Brunetti, V., Bertorelli, R., et al. (2016). Alginate–lavender nanofibers with antibacterial and anti-inflammatory activity to effectively promote burn healing. *J. Mater. Chem. B.* 4, 1686–1695. doi: 10.1039/C5TB02174J

Hall Barrientos, I. J., Paladino, E., Szab,ó, P., Brozio, S., Hall, P. J., Oseghale, C. I., et al. (2017). Electrospun collagen-based nanofibres : a sustainable material for improved antibiotic utilisation in tissue engineering applications. *Int. J. Pharm.* 531, 67–79. doi: 10.1016/j.ijpharm.2017.08.071

Han, F., Dong, Y., Su, Z., Yin, R., Song, A., and Li, S. (2014). Preparation, characteristics and assessment of a novel gelatin – chitosan sponge scaffold as skin tissue engineering material. *Int. J. Pharm.* 476, 124–133. doi: 10.1016/j.ijpharm.2014.09.036

Haneef, M., Ceseracciu, L., Canale, C., Bayer, I. S., Heredia-Guerrero, J. A., and Athanassiou, A. (2017). Advanced materials from fungal mycelium: fabrication and tuning of physical properties. *Sci. Rep.* 7:41292. doi: 10.1038/srep41292

Hang, Y., Zhang, Y., Jin, Y., Shao, H., and Hu, X. (2012). Preparation of regenerated silk fibroin/silk sericin fibers by coaxial electrospinning. *Int. J. Biol. Macromol.* 51, 980– 986. doi: 10.1016/j.ijbiomac.2012.08.010

He, L. Z., Liu, Y., and Yang, D. (2007). Preparation and performance of chitosan–gelatin sponge-like wound-healing dressing. *J. Clin. Rehabil. Tissue Eng. Res.* 11, 5252–5256.

He, M., Zhang, B., Dou, Y., Yin, G., and Chen, X. (2017). Feather keratin / poly (vinyl alcohol) composite. *RSC Adv.* 7, 9854–9861. doi: 10.1039/C6RA25009B

Hill, P., Brantley, H., and Van Dyke, M. (2010). Some properties of keratin biomaterials: kerateines. *Biomaterials* 31, 585–593. doi: 10.1016/j.biomaterials.2009.09.076

Hofmann, S., Foo, C. T., Rossetti, F., Textor, M., Vunjak-Novakovic, G., Kaplan, D. L. et al. (2006). Silk fibroin as an organic polymer for controlled drug delivery. *J. Control. Release* 111, 219–227. doi: 10.1016/j.jconrel.2005.12.009

Hsu, F. Y., Hung, Y. S., Liou, H. M., and Shen, C. H. (2010). Electrospun hyaluronate-collagen nanofibrous matrix and the effects of varying the concentration of hyaluronate on the characteristics of foreskin fibroblast cells. *Acta Biomater.* 6, 2140–2147 doi: 10.1016/j.actbio.2009.12.023

Hu, X., Shmelev, K., Sun, L., Gil, E. S., Park, S. H., Cebe, P., et al. (2011). Regulation of silk material structure by temperature-controlled water vapor annealing. *Biomacromolecules* 12, 1686–1696. doi: 10.1021/bm200062a

Huang, S., and Fu, X. (2010). Naturally derived materials-based cell and drug delivery systems in skin regeneration. *J. Control. Release* 142, 149–159. doi: 10.1016/j.jconrel.2009.10.018

Hung, W. S., Fang, C. L., Su, C. H., Lai, W. F., Chang, Y. C., and Tsai, Y. H. (2001). Cytotoxicity and immunogenicity of SACCHACHITIN and its mechanism of action on skin wound healing. *J. Biomed. Mater. Res.* 56, 93–100. doi: 10.1002/1097-4636(200107)56:1<93::AID-JBM1072>3.0.CO;2-B

Hwang, J. S., Kwon, H. K., Kim, J. E., Rho, J., and Im, S. H. (2012). Immunomodulatory effect of water soluble extract separated from mycelium of Phellinus linteus on experimental atopic dermatitis Immunomodulatory effect of water soluble extract separated from mycelium of Phellinus linteus on experimental atopic dermatitis. *BMC Complement. Altern. Med.* 12:159. doi: 10.1186/1472-6882-12-159

Jaipan, P., Nguyen, A., and Narayan, R. J. (2017). Gelatin-based hydrogels for biomedical applications. *MRS Commun.* 7, 416–426. doi: 10.1557/mrc.2017.92

Jameton, A., and Pierce, J. (2001). Environment and health: 8. Sustainable health care and emerging ethical responsibilities. *CMAJ* 164, 365–369.

Jones, M. P., Jones, M., Huynh, T., Dekiwadia, C., Daver, F., and John, S. (2017). Mycelium composites : a review of engineering characteristics and growth kinetics. *J. Bionanosci.* 11, 241–257. doi: 10.1166/jbns.2017.1440

Ju, H. W., Lee, O. J., Lee, J. M., Moon, B. M., Park, H. J., Park, Y. R., et al. (2016). Wound healing effect of electrospun silk fibroin nanomatrix in burn-model. *Int. J. Biol. Macromol.* 85, 29–39. doi: 10.1016/j.ijbiomac.2015.12.055

Karri, V. V. S., Kuppusamy, G., Talluri, S. V., Mannemala, S. S., Kollipara, R., Wadhwani, A. D., et al. (2016). International journal of biological macromolecules curcumin loaded chitosan nanoparticles impregnated into collagen-alginate scaffolds for diabetic wound healing. *Int. J. Biol. Macromol.* 93, 1519–1529. doi: 10.1016/j.ijbiomac.2016.05.038

Khan, F., and Ahmad, S. R. (2013). Polysaccharides and their derivatives for versatile tissue engineering application. *Macromol. Biosci.* 13, 395–421. doi: 10.1002/mabi.201200409

Kim, S. Y., Go, K. C., Song, Y. S., Jeong, Y. S., Kim, E. J., and Kim, B. J. (2014). Extract of the mycelium of T. matsutake inhibits elastase activity and TPA-induced MMP-1 expression in human fibroblasts. *Int. J. Mol. Med.* 34, 1613–1621. doi: 10.3892/ijmm.2014.1969

Koide, T. (2007). Designed triple-helical peptides as tools for collagen biochemistry and matrix engineering. *Phil. Trans. R. Soc. B* 362, 1281–1291. doi: 10.1098/rstb.2007.2115

Krull, R., Wucherpfennig, T., Eslahpazir, M. E., Walisko, R., Melzer, G., Hempel, D. C., et al. (2013). Characterization and control of fungal morphology for improved production performance in biotechnology. *J. Biotechnol.* 163, 112–123. doi: 10.1016/j.jbiotec.2012.06.024

Larsen, J. (2015). Biotic interactions in the rhizosphere in relation to plant and soil nutrient dynamics. *J. Soil Sci. Plant Nutr.* 15, 449–463. doi: 10.4067/S0718-95162015005000039

Li, Y., Wang, Y., Ye, J., Yuan, J., and Xiao, Y. (2016). Fabrication of poly (ε-caprolactone)/keratin nano fibrous mats as a potential scaffold for vascular tissue engineering. *Mater. Sci. Eng. C.* 68, 177–183. doi: 10.1016/j.msec.2016.05.117

Liakos, I., Rizzello, L., Bayer, I. S., Pompa, P. P., Cingolani, R., and Athanassiou, A. (2013). Controlled antiseptic release by alginate polymer films and beads. *Carbohydr. Polym.* 92, 176– 183. doi: 10.1016/j.carbpol.2012.09.034

Liakos, I., Rizzello, L., Hajiali, H., Brunetti, V., Carzino, R., and Pompa, P. P. (2015). Fibrous wound dressings encapsulating essential oils as natural antimicrobial agents. *J. Mater. Chem. B Mater. Biol. Med.* 3, 1583–1589. doi: 10.1039/C4TB01974A

Liakos, I. L., D'autilia, F., Garzoni, A., Bonferoni, C., Scarpellini, A., Brunetti, V., et al. (2016). All natural cellulose acetate—Lemongrass essential oil antimicrobial nanocapsules. *Int. J. Pharm.* 510, 508–515. doi: 10.1016/j.ijpharm.2016.01.060

Lian, Y., Zhan, J. C., Zhang, K. H., and Mo, X. M. (2014). Fabrication and characterization of curcumin-loaded silk fibroin/P(LLA-CL) nanofibrous scaffold. *Front. Mater. Sci.* 8, 354–362. doi: 10.1007/s11706-014-0270-8

Lima, A. C., Mano, J. F., Concheiro, A., and Alvarez-lorenzo, C. (2015). Fast and mild strategy, using superhydrophobic surfaces, to produce collagen / platelet lysate gel beads for skin regeneration. *Stem Cell Rev. Rep.* 11, 161–179. doi: 10.1007/s12015-014-9548-6

Lin, S., Chen, M., Jiang, H., Fan, L., Sun, B., Yu, F., et al. (2016). Colloids and surfaces B : biointerfaces green electrospun grape seed extract-loaded silk fibroin nanofibrous mats with excellent cytocompatibility and antioxidant effect. *Colloids Surf. B Biointerf.* 139, 156–163. doi: 10.1016/j.colsurfb.2015.12.001

Ma, H., Shen, J., Cao, J., Wang, D., Yue, B., Mao, Z., et al. (2017). Fabrication of wool keratin/polyethylene oxide nano-membrane from wool fabric waste. *J. Clean. Prod.* 161, 357–361. doi: 10.1016/j.jclepro.2017.05.121

Maeda, N., Miao, J., Simmons, T. J., Dordick, J. S., and Linhardt, R. J. (2014). Composite polysaccharide fibers prepared by electrospinning and coating. *Carbohydr. Polym.* 102, 950– 955. doi: 10.1016/j.carbpol.2013.10.038

Martin, P. (1997). Wound healing — aiming for perfect skin regeneration. *Science* 276, 75–81. doi: 10.1126/science.276.5309.75

Maver, T., Hribernik, S., Mohan, T., Smrke, D. M., Maver, U., and Stana-Kleinschek, K. (2015). Functional wound dressing materials with highly tunable drug release properties. *RSC Adv.* 5, 77873–77884. doi: 10.1039/C5RA11972C

Mele, E. (2016). Electrospinning of natural polymers for advanced wound care: towards responsive and adaptive dressings. *J. Mater. Chem. B* 4, 4801–4812. doi: 10.1039/C6TB00804F

Min, B. M., Jeong, L., Lee, K. Y., and Park, W. H. (2006). Regenerated silk fibroin nanofibers: water vapor-induced structural changes and their effects on the behavior of normal human cells. *Macromol. Biosci.* 6, 285–292. doi: 10.1002/mabi.200500246

Mogoşanu, G. D., and Grumezescu, A. M. (2014). Natural and synthetic polymers for wounds and burns dressing. *Int. J. Pharm.* 463, 127– 136. doi: 10.1016/j.ijpharm.2013.12.015

Moura, L. I., Dias, A. M., Carvalho, E., and De Sousa, H. C. (2013). Recent advances on the development of wound dressings for diabetic foot ulcer treatment: a review. *Acta Biomater.* 9, 7093–7114. doi: 10.1016/j.actbio.2013.03.033

Nanbu, T., Matsuta, T., Sakagami, H., Shimada, J., Maki, J., and Makino, T. (2011). Anti-UV activity of Lentinus edodes mycelia extract (LEM). *In vivo* 25, 733–740.

Neel, E. A. A., Bozec, L., Knowles, J. C., Syed, O., Mudera, V., Day, R., et al. (2013). Collagen — emerging collagen based therapies hit the patient. *Adv. Drug Deliv. Rev.* 65, 429–456. doi: 10.1016/j.addr.2012.08.010

Niyas Ahamed, M. I., and Sastry, T. P. (2011). Wound dressing application of chitosan basedbioactive compounds. *Int. J. Pharm. Life Sci.* 2, 991–996.

Norouzi, M., Boroujeni, S. M., Omidvarkordshouli, N., and Soleimani, M. (2015). Advances in skin regeneration: application of electrospun scaffolds. *Adv. Healthc. Mater.* 4, 1114–1133. doi: 10.1002/adhm.201500001

Olsen, D., Yang, C., Bodo, M., Chang, R., Leigh, S., Baez, J., et al. (2003). Recombinant collagen and gelatin for drug delivery. *Adv. Drug Deliv. Rev.* 55, 1547–1567. doi: 10.1016/j.addr.2003.08.008

Ozaki, Y., Takagi, Y., Mori, H., and Hara, M. (2014). Porous hydrogel of wool keratin prepared by a novel method : an extraction with guanidine / 2-mercaptoethanol solution followed by a dialysis. *Mater. Sci. Eng. C.* 42, 146–154. doi: 10.1016/j.msec.2014.05.018

Parenteau-Bareil, R., Gauvin, R., and Berthod, F. (2010). Collagen-based biomaterials for tissue engineering applications. *Materials* 3, 1863–1887. doi: 10.3390/ma3031863

Patel, G., Patel, G., Patel, R., Patel, J., Bharadia, P., and Patel, M. (2007). Sodium alginate: physiological activity, usage & potential applications. *Drug Deliv. Technol.* 7, 28–37.

Patrucco, A., Cristofaro, F., Simionati, M., Zoccola, M., Bruni, G., Fassina, L., et al. (2016). Wool fibril sponges with perspective biomedical applications. *Mater. Sci. Eng. C.,* 61, 42–50. doi: 10.1016/j.msec.2015.11.073

Pereira, R. F., Barrias, C. C., Granja, P. L., and Bartolo, P. J. (2013). Advanced biofabrication strategies for skin regeneration and repair. *Nanomedicine* 8, 603–621. doi: 10.2217/nnm.13.50

Pignatelli, C., Perotto, G., Nardini, M., Cancedda, R., Mastrogiacomo, M., and Athanassiou, A. (2018). Electrospun silk fibroin fibers for storage and controlled release of human platelet lysate. *Acta Biomater.* 73, 365–376. doi: 10.1016/j.actbio.2018.04.025

Pinkas, D. M., Ding, S., Raines, R. T., and Barron, A. E. (2011). Tunable, post-translational hydroxylation of collagen domains in *Escherichia coli*. *ACS Chem. Biol.* 6, 320–324. doi: 10.1021/cb100298r

Powell, H. M., Supp, D. M., and Boyce, S. T. (2008). Influence of electrospun collagen on wound contraction of engineered skin substitutes. *Biomaterials* 29, 834–843. doi: 10.1016/j.biomaterials.2007.10.036

Pritchard, E. M., Valentin, T., Panilaitis, B., Omenetto, F., and Kaplan, D. L. (2013). Antibiotic-releasing silk biomaterials for infection prevention and treatment. *Adv. Funct. Mater.* 23, 854–861. doi: 10.1002/adfm.201201636

Qu, Y., Cao, C., Wu, Q., Huang, A., Song, Y., Li, H. (2018). The dual delivery of KGF and bFGF by collagen membrane to promote skin wound healing. *J. Tissue Eng. Regen. Med.* 12, 1508–1518. doi: 10.1002/term.2691

Reichl, S. (2009). Biomaterials films based on human hair keratin as substrates for cell culture and tissue engineering. *Biomaterials* 30, 6854–6866. doi: 10.1016/j.biomaterials.2009.08.051

Reimers, K., Liebsch, C., Radtke, C., Kuhbier, J. W., and Vogt, P. M. (2015). Silks as scaffolds for skin reconstruction. *Biotechnol. Bioeng.* 112, 2201–2205. doi: 10.1002/bit.25654

Richter, J. R., De Guzman, R. C., Greengauz-Roberts, O. K., and Van Dyke, M. (2012). Structure-property relationships of meta-kerateine biomaterials derived from human hair. *Acta Biomater.* 8, 274–281. doi: 10.1016/j.actbio.2011.08.020

Rieger, K. A., Birch, N. P., and Schiffman, J. D. (2013). Designing electrospun nanofiber mats to promote wound healing – a review. *J. Mater. Chem., B.* 1, 4531–4541. doi: 10.1039/c3tb20795a

Rieger, K. A., and Schiffman, J. D. (2014). Electrospinning an essential oil : cinnamaldehyde enhances the antimicrobial efficacy of chitosan / poly (ethylene oxide) nanofibers. *Carbohydr. Polym.* 113, 561–568. doi: 10.1016/j.carbpol.2014.06.075

Roh, D. H., Kang, S. Y., Kim, J. Y., Kwon, Y. B.,Young Kweon, H., Lee, K. G., et al. (2006). Wound healing effect of silk fibroin/alginate-blended sponge in full thickness skin defect of rat. *J. Mater. Sci. Mater. Med.* 17, 547–552. doi: 0.1007/s10856-006-8938-y

Romano, I., Ayadi, F., Rizzello, L., Summa, M., Bertorelli, R., Pompa, P. P., et al. (2015a). Controlled antiseptic/eosin release from chitosan-based hydrogel modified fibrous substrates. *Carbohydr. Polym.* 92, 176– 183. doi: 10.1016/j.carbpol.2015.05.057

Romano, I., Mele, E., Heredia-Guerrero, J. A., Ceseracciu, L., Hajiali, H., Goldoni, L., et al. (2015b). Photo-polymerisable electrospun fibres of N-methacrylate glycol chitosan for biomedical applications. *RSC Adv.* 5, 24723–24728. doi: 10.1039/C5RA02301G

Rouse, J. G., and Van Dyke, M. E. (2010). A review of keratin-based biomaterials for biomedical applications. *Materials* 3, 999–1014. doi: 10.3390/ma3020999

Salati, S., Imporzano, G. D., Menin, B., Veronesi, D., Scaglia, B., Abbruscato, P., et al. (2017). Bioresource technology mixotrophic cultivation of chlorella for local protein production using. *Bioresour. Technol.* 230, 82–89. doi: 10.1016/j.biortech.2017.01.030

Saul, J. M., Ellenburg, M. D., de Guzman, R. C., and Van Dyke M (2011). Keratin hydrogels support the sustained release of bioactive ciprofloxacin. *Biomed Mater Res Part A* 98A, 544–553. doi: 10.1002/jbm.a.33147

Schneider, A., Wang, X. Y., Kaplan, D. L., Garlick, J. A., and Egles, C. (2009). Biofunctionalized electrospun silk mats as a topical bioactive dressing for accelerated wound healing. *Acta Biomater.* 5, 2570–2578. doi: 10.1016/j.actbio.2008.12.013

Sell, S., Barnes, C., Smith, M., McClure, M., Madurantakam, P., Grant, J., et al. (2007). Extracellular matrix regenerated: tissue engineering via electrospun biomimetic nanofibers. *Polym. Int.* 56, 1349–1360. doi: 10.1002/pi.2344

Sell, S. A., Wolfe, P. S., Garg, K., McCool, J. M., Rodriguez, I. A., and Bowlin, G. L. (2010). The use of natural polymers in tissue engineering: a focus on electrospun extracellular matrix analogues. *Polymers* 2, 522–553. doi: 10.3390/polym2040522

Selvaraj, S., and Fathima, N. N. (2017). Fenugreek incorporated silk fibroin nanofibers - A potential antioxidant scaffold for enhanced wound healing. *ACS Appl. Mater. Interf.* 9, 5916–5926. doi: 10.1021/acsami.6b16306

Sen, C. K., Gordillo, G. M., Roy, S., Kirsner, R., Lambert, L., Hunt, T. K., et al. (2009). Human skin wounds: a major and snowballing threat to public health and the economy. *Wound Repair Regen.* 17, 763–771. doi: 10.1111/j.1524-475X.2009.00543.x

Setti, C., Suarato, G., Perotto, G., Athanassiou, A., and Bayer, I. S. (2018). Investigation of *in vitro* hydrophilic and hydrophobic dual drug release from polymeric films produced by sodium alginate-MaterBi® drying emulsions. *Eur. J. Pharm. Biopharm.* 130, 71–82. doi: 10.1016/j.ejpb.2018.06.019

Shahverdi, S., Hajimiri, M., Amin, M., Akbar, A., and Dinarvand, R. (2014). Fabrication and structure analysis of poly (lactide-co-glycolic acid)/ silk fibroin hybrid scaffold for wound dressing applications. *Int. J. Pharm.* 473, 345–355. doi: 10.1016/j.ijpharm.2014.07.021

Shan, Y. H., Peng, L. H., Liu, X., Chen, X., Xiong, J., and Gao, J. Q. (2015). Silk fibroin / gelatin electrospun nanofibrous dressing functionalized with astragaloside IV induces healing and anti-scar effects on burn wound. *Int. J. Pharm.* 479, 291–301. doi: 10.1016/j.ijpharm.2014.12.067

Shanmugam, K., and Sundaramoorthy, S. (2015). Development and characterization of an electrospun mat from Eri silk fibroin and PLA blends. *RSC Adv.* 5, 31352–31364. doi: 10.1039/C4RA15268A

Sharma, S., and Gupta, A. (2016). Sustainable management of keratin waste biomass: applications and future perspectives. *Braz. Arch. Biol. Technol. Int. J.* 59:e16150684. doi: 10.1590/1678-4324-2016150684

Shavandi, A., Silva, T. H., Bekhit, A. A., and Bekhit, A. E. A.(2017). Keratin: dissolution, extraction and biomedical application. *Biomater. Sci.* 5, 1699–1735. doi: 10.1039/C7BM00411G

Sheng, X., Fan, L., He, C., Zhang, K., and Mo, X. (2013). Vitamin E-loaded silk fibroin nanofibrous mats fabricated by green process for skin care application. *Int. J. Biol. Macromol.* 56, 49–56. doi: 10.1016/j.ijbiomac.2013.01.029

Silva, S. S., Santos, T. C., Cerqueira, M. T., Marques, A. P., Reys, L. L., Silva, T. H., et al. (2012). The use of ionic liquids in the processing of chitosan/silk hydrogels for biomedical applications. *Green Chem.* 14, 1463–1470. doi: 10.1039/c2gc16535j

Singaravelu, S., Ramanathan, G., Muthukumar, T., Raja, M. D., Nagiah, N., Thyagarajan, S., et al. (2016). Durable keratin-based bilayered electrospun mats for wound closure. *J. Mater. Chem. B* 3982, 3982–3997. doi: 10.1039/C6TB00720A

Sinno, H., and Prakash, S. (2013). Complements and the wound healing cascade : an updated review. *Plastic Surg. Int.* 2013:146764. doi: 10.1155/2013/146764

Srivastava, C. M., Purwar, R., Kannaujia, R., and Sharma, D. (2015). Flexible silk fibroin films for wound dressing. *Fibers Polym.* 5, 1020–1030. doi: 10.1007/s12221-015-1020-y

Steinert, P. M., and Marekov, L. N. (1993). Keratin intermediate filament structure. *J. Mol. Biol.* 230, 436–452. doi: 10.1006/jmbi.1993.1161

Su, C. H., Liu, S. H., Yu, S. Y., Hsieh, Y. L., Ho, H. O., Hu, C. H., et al. (2005). Development of fungal mycelia as a skin substitute: characterization of keratinocyte proliferation and matrix metalloproteinase expression during improvement in the wound-healing process. *J. Biomed. Mater. Res.Part A* 72, 220–227. doi: 10.1002/jbm.a.30235

Su, C. H., Sun, C. S., Juan, S. W., Ho, H. O., Hu, C. H., and Sheu, M. T. (1999). Development of fungal mycelia as skin substitutes: effects on wound healing and fibroblast. *Biomaterials* 20, 61–68. doi: 10.1016/S0142-9612(98)00139-2

Su, C. H., Sun, C. S., Juan, S. W., Hu, C. H., Ke, W. T., and Sheu, M. T. (1997). Fungal mycelia as the source of chitin and polysaccharides and their applications as skin substitutes. *Biomaterials* 18, 1169–1174. doi: 10.1016/S0142-9612(97)00048-3

Suganya, S., Venugopal, J., Ramakrishna, S., Lakshmi, B. S., and Dev, V. R. (2014). Naturally derived biofunctional nanofibrous scaffold for skin tissue regeneration. *Int. J. Biol. Macromol.* 68, 135–143. doi: 10.1016/j.ijbiomac.2014.04.031

Summa, M., Russo, D., Penna, I., Margaroli, N., Bayer, I. S., Bandiera, T., et al. (2018). A biocompatible sodium alginate/povidone iodine film enhances wound healing. *Eur. J. Pharm. Biopharm.* 122, 17–24. doi: 10.1016/j.ejpb.2017.10.004

Synytsya, A., and Novák, M. (2013). Structural diversity of fungal glucans. *Carbohydr. Polym.* 92, 792–809. doi: 10.1016/j.carbpol.2012.09.077

Szekalska, M., Puciłowska, A., Szymanska, E., Ciosek, P., and Winnicka, K. (2016). Alginate: current use and future perspectives in pharmaceutical and biomedical applications. *Int. J. Polym. Sci.* 2016:7697031. doi: 10.1155/2016/7697031

Tachibana, A., Furuta, Y., Takeshima, H., Tanabe, T., and Yamauchi, K. (2002). Fabrication of wool keratin sponge scaffolds for long-term cell cultivation. *J. Biotechnol.* 93, 165–170. doi: 10.1016/S0168-1656(01)00395-9

Thanusha, A. V., Dinda, A. K., and Koul, V. (2018). Evaluation of nano hydrogel composite based on gelatin/HA/CS suffused with Asiatic acid/ZnO and CuO nanoparticles for second degree burns. *Mater. Sci. Eng. C* 89, 378–386. doi: 10.1016/j.msec.2018.03.034

Thyagarajan, S. L., Ramanathan, G., Singaravelu, S., Kandhasamy, S., Perumal, P. T., and Sivagnanam, U. T. (2017). Characterization and evaluation of siderophore-loaded gelatin microspheres : a potent tool for wound-dressing material. *Polym. Bull.* 74, 2349–2363. doi: 10.1007/s00289-016-1840-y

Tolg, C., Telmer, P., and Turley, E. (2014). Specific sizes of hyaluronan oligosaccharides stimulate fibroblast migration and excisional wound repair. *PLoS ONE* 9:e88479. doi: 10.1371/journal.pone.0088479

Tonin, C., Aluigi, A., Vineis, C., Varesano, A., Montarsolo, A., and Ferrero, F. (2007). Thermal and structural characterization of Poly(ethylene-oxide)/Keratin blend films. *J. Therm. Anal. Calorim.* 89, 601–608. doi: 10.1007/s10973-006-7557-7

Uppal, R., Ramaswamy, G. N., Arnold, C., Goodband, R., and Wang, Y. (2011). Hyaluronic acid nanofiber wound dressing-production, characterization, and *in vivo* behavior. *J. Biomed. Mater. Res.Part B Appl. Biomater.* 97B, 20–29. doi: 10.1002/jbm.b.31776

Vamanu, E. (2014). Antioxidant properties of mushroom mycelia obtained by batch cultivation and tocopherol content affected by extraction procedures. *Biomed Res. Int*. 2014:974804. doi: 10.1155/2014/974804

Vassilev, N., Baca, M., Vassileva, M., Franco, I., and Azcon, R. (1995). Rock phosphate solubilization by *Aspergillus niger* grown on sugar-beet waste medium. *Appl. Microbiol. Biotechnol.* 44, 546–549. doi: 10.1007/BF00169958

Veleirinho, B., Coelho, D. S., Dias, P. F., Maraschin, M., Ribeiro-do-valle, R. M., and Lopes-da-silva, J. A. (2012). Nanofibrous pol7(3-hydroxybutyrate-co-3-hydroxyvalerate)/chitosan scaffolds for skin regeneration. *Int. J. Biol. Macromol.* 51, 343–350. doi: 10.1016/j.ijbiomac.2012.05.023

Verma, V., Verma, P., Ray, P., and Ray, A. R. (2008). Preparation of scaffolds from human hair proteins for tissue-engineering applications. *Biomed. Mater.* 3:025007. doi: 10.1088/1748-6041/3/2/025007

Vyas, K. S., and Vasconez, H. C. (2014). Wound healing: biologics, skin substitutes, biomembranes and scaffolds. *Healthcare* 2, 356–400. doi: 10.3390/healthcare2030356

Wang, B., Yang, W., McKittrick, J., and Meyers, M. A. (2016). Keratin: structure, mechanical properties, occurrence in biological organisms, and efforts at bioinspiration. *Prog. Mater. Sci.* 76, 229–318. doi: 10.1016/j.pmatsci.2015.06.001

Wang, J., Hao, S., Luo, T., Zhou, T., Yang, X., and Wang, B. (2017). Keratose / poly (vinyl alcohol) blended nanofibers : fabrication and biocompatibility assessment. *Mater. Sci. Eng C* 72, 212–219. doi: 10.1016/j.msec.2016.11.071

Wang, S., Taraballi, F., Tan, L. P., and Ng, K. W. (2012). Human keratin hydrogels support fibroblast attachment and proliferation *in vitro*. *Cell Tissue Res.* 347, 795–802. doi: 10.1007/s00441-011-1295-2

Wani, M. Y., Hasan, N., and Malik, M. A. (2010). Chitosan and Aloe vera: two gifts of nature. *J. Dispers. Sci. Technol.* 31, 799–811. doi: 10.1080/01932690903333606

Wei, G., and Ma, P. X. (2008). Nanostructured biomaterials for regeneration. *Adv. Funct. Mater.* 18, 3568–3582. doi: 10.1002/adfm.200800662

Wei, Y., Chang, Y. H., Liu, C. J., and Chung, R. J. (2018). Integrated Oxidized-Hyaluronic Acid/Collagen Hydrogel with β-TCP using Proanthocyanidins as a crosslinker for drug delivery. *Pharmaceutics* 10:E37. doi: 10.3390/pharmaceutics10020037

Weller, C., and Sussman, G. (2006). Wound dressings update. *J. Pharm. Prac. Res.* 36, 318–324. doi: 10.1002/j.2055-2335.2006.tb00640.x

Wharram, S. E., Zhang, X., Kaplan, D. L., and McCarthy, S. P. (2010). Electrospun silk material systems for wound healing. *Macromol. Biosci.* 10, 246–257. doi: 10.1002/mabi.200900274

Xu, S., Li, J., He, A., Liu, W., Jiang, X., Zheng, J., et al. (2009). Chemical crosslinking and biophysical properties of electrospun hyaluronic acid based ultra-thin fibrous membranes. *Polymer* 50, 3762–3769. doi: 10.1016/j.polymer.2009.06.009

Xu, S., Sang, L., Zhang, Y., Wang, X., and Li, X. (2013). Biological evaluation of human hair keratin scaffolds for skin wound repair and regeneration. *Mater. Sci. Eng C* 33, 648–655. doi: 10.1016/j.msec.2012.10.011

Yamauchi, K., Hojo, H., Yamamoto, Y., and Tanabe, T. (2003). Enhanced cell adhesion on RGDS-carrying keratin film. *Mater. Sci. Eng. C* 23, 467–472. doi: 10.1016/S0928-4931(02)00280-1

Yan, J., Wang, W., and Wu, J. (2014). Recent advances in *Cordyceps sinensis* polysaccharides : mycelial fermentation, isolation, structure, and bioactivities : a review. *J. Funct. Foods* 6, 33–47. doi: 10.1016/j.jff.2013.11.024

Yan, S., Zhang, Q., Wang, J., Liu, Y., Lu, S., Li, M., et al. (2013). Silk fibroin/chondroitin sulfate/hyaluronic acid ternary scaffolds for dermal tissue reconstruction. *Acta Biomater.* 9, 6771–6782. doi: 10.1016/j.actbio.2013.02.016

Yang, X., Fan, L., Ma, L., Wang, Y., Lin, S., Yu, F., et al. (2017). Green electrospun Manuka honey/silk fibroin fibrous matrices as potential wound dressing. *Mater. Design* 119, 76–84. doi: 10.1016/j.matdes.2017.01.023

Yao, C. H., Lee, C. Y., Huang, C. H., Chen, Y. S., and Chen, K. Y. (2017). Novel bilayer wound dressing based on electrospun gelatin/keratin nanofibrous mats for skin wound repair. *Mater. Sci. Eng. C* 79, 533–540. doi: 10.1016/j.msec.2017.05.076

Yen, K.-C., Chen, C.-Y., Huang, J.-Y., Kuo, W.-T., and Lin, F.-H. (2016). Fabrication of keratin/fibroin membranes by electrospinning for vascular tissue engineering. *J. Mater. Chem. B* 4, 237–244. doi: 10.1039/C5TB01921D

Yoon, D., Yoon, D., Cha, H., and Lee, J. (2018). Enhancement of wound healing efficiency mediated by artificial dermis functionalized with EGF or NRG1 Enhancement of wound healing efficiency mediated by artificial dermis functionalized with EGF or NRG1. *Biomed. Mater.* 13:045007. doi: 10.1088/1748-605X/aaac37

Yuan, J., Geng, J., Xing, Z., Shim, K. J., Han, I., and Kim, J. C. (2015). Novel wound dressing based on nanofibrous PHBV – keratin mats. *J. Tissue Eng. Regen. Med.* 9, 1027–1035. doi: 10.1002/term.1653

Zhao, W., Liu, W., Li, J., Lin, X., and Wang, Y. (2015). Preparation of animal polysaccharides nanofibers by electrospinning and their potential biomedical applications. *J. Biomed. Mater. Res.Part A* 103A, 807–818. doi: 10.1002/jbm.a.35187

Zhong, S. P., Zhang, Y. Z., and Lim, C. T. (2010). Tissue scaffolds for skin wound healing and dermal reconstruction. *Wiley Interdiscip. Rev. Nanomed. Nanobiotechnol.* 2, 510–525. doi: 10.1002/wnan.100

Zhu, C., Lei, H., Fan, D., and Duan, Z. (2018). Novel enzymatic crosslinked hydrogels that mimic extracellular matrix for skin wound healing. *J. Mater. Sci.* 53, 5909–5928. doi: 10.1007/s10853-017-1956-y

Zhu, H., Li, R., Wu, X., Chen, K., and Che, J. (2017). Controllable fabrication and characterization of hydrophilic PCL/wool keratin nanonets by electronetting. *Eur. Polym. J.* 86, 154–161. doi: 10.1016/j.eurpolymj.2016.11.023

Zhu, J., Huang, W., Zhang, Q., Ling, S., Chen, Y., and Kaplan, D. L. (2016). Aqueous-based coaxial electrospinning of genetically engineered silk elastin core-shell nanofibers. *Materials* 9:E221. doi: 10.3390/ma9040221

Zoccola, M., Aluigi, A., Vineis, C., Tonin, C., Ferrero, F., and Piacentino, M. G. (2008). Study on cast membranes and electrospun nanofibers made from keratin/fibroin blends. *Biomacromolecules* 9, 2819–2825. doi: 10.1021/bm800579a

Conflict of Interest Statement: The authors declare that the research was conducted in the absence of any commercial or financial relationships that could be construed as a potential conflict of interest.

frontiers in Bioengineering and Biotechnology

ORIGINAL RESEARCH
published: 21 June 2018
doi: 10.3389/fbioe.2018.00083

One-Step Synthesis of Hexagonal Boron Nitrides, Their Crystallinity and Biodegradation

*Özlem Şen†, Melis Emanet† and Mustafa Çulha**

Department of Genetics and Bioengineering, Faculty of Engineering, Yeditepe University, Istanbul, Turkey

Hexagonal boron nitrides (hBNs) have recently been investigated for several novel applications due to their unique properties such as biocompatibility, superhydrophobicity, electrical insulation, and thermal and chemical stability. In addition, their biodegradation products have recently reported to have therapeutic effect on certain cancer types. hBNs are easily synthesized from boron and nitrogen precursors at moderately low temperatures. However, crystallinity and yield vary depending on the type of precursor, reaction temperature, and duration. In this study, a simple one-step hBNs synthesis method is reported without a catalyst, which might be an undesired contaminant for biomedical applications. The influence of boron precursors (boric acid, colemanite, or boron trioxide) on hBNs crystallinity, stability, and biodegradation in suspensions containing oxidative and hydrolytic degradation agents is investigated with the aim of their possible application in biomedicine. We found that the choice of boron precursor is a critically important parameter controlling the hBNs crystallinity and dependently influencing the biodegradation rate.

Keywords: hexagonal boron nitride, synthesis, biodegradation, boric acid, boron trioxide, colemanite

OPEN ACCESS

Edited by:
Gianni Ciofani,
Politecnico di Torino, Italy

Reviewed by:
Attilio Marino,
Fondazione Istituto Italiano di Technologia, Italy
Kaan Kececi,
Istanbul Medeniyet University, Turkey
Yuriy Bogdanovich Stetsyshyn,
Lviv Polytechnic, Ukraine

***Correspondence:**
Mustafa Çulha
mculha@yeditepe.edu.tr

† These authors have contributed equally to this work.

Specialty section:
This article was submitted to Nanobiotechnology, a section of the journal Frontiers in Bioengineering and Biotechnology

Received: *29 April 2018*
Accepted: *01 June 2018*
Published: *21 June 2018*

Citation:
Şen Ö, Emanet M and Çulha M (2018) One-Step Synthesis of Hexagonal Boron Nitrides, Their Crystallinity and Biodegradation. Front. Bioeng. Biotechnol. 6:83. doi: 10.3389/fbioe.2018.00083

INTRODUCTION

In recent years, boron nitride (BN) based nanomaterials have grasped attention of researchers for their possible use in medical applications due to their biocompatibility (Chen et al., 2009; Salvetti et al., 2015; Li et al., 2017), chemical and mechanical stability (Lahiri et al., 2011; Liu et al., 2016). Since they are composed of boron and nitrogen, they can be excellent needed as boron and nitrogen source in biosystems. Recently, it was demonstrated that BNs can be used as a boron source to promote wound healing and treat prostate cancer, and their degree of crystallinity is an important factor due to its influence on biodegradation (Dousset et al., 2002; Li et al., 2017).

Although hexagonal boron nitrides (hBNs) were discovered in 1842, their first stable form was obtained about a century later. The BNs do not naturally occur, thus they must be synthetically synthesized from boron and nitrogen precursors to prepare structures analog to their counterpart, graphene (Arenal and Lopez-Bezanilla, 2015). In hBNs, boron and nitrogen atoms are covalently bound in a hexagonal structure and their layers are stacked on top of each other. Similar to graphene, the two-dimensional (2D) BN layers interact with each other through van der Waals forces (Du Frane et al., 2016), and constitute hBN films (Shi et al., 2010) or spherical nanostructures (Bhimanapati et al., 2014), Given their excellent physical and chemical properties, hBNs are considered as promising nanomaterials in many technological applications (Han, 2010).

The use of hBNs in a range of applications was reported in the literature including their exploitation as 2D dielectric thin films and deep UV emitters at around 215 nm (Kubota et al., 2007; Song et al., 2010). It was also reported that composite of hBNs with polyether ether ketone showed improved mechanical and thermo mechanical properties, since hBNs possess high elastic modulus, excellent lubrication properties, and good thermal conductivity (Liu et al., 2016). In last few years, the hBNs are also gaining attention as a promising nanomaterial in medical and biomedical applications due to their high biocompatibility (Sukhorukova et al., 2015). Their use as a tablet lubricant in pharmacy and additive in cosmetics are also encouraging points for their consideration in the biomedical field (Turkoglu et al., 2005; Shi et al., 2010; Liu et al., 2016). In our recent study, their cytotoxicity was assessed, and conjugation with doxorubicin and folate has been proposed to enable their potential in cancer therapy (Emanet et al., 2017).

There are several hBNs synthesis methods reported in the literature by using a variety of boron and nitrogen precursors under different experimental conditions (Singhal et al., 2008). The synthesis methods influence reaction yield, number of layers, shape, and size of hBNs (Li et al., 2011). In one study, boric acid and urea were mixed and heated under ammonia atmosphere to produce hBNs (Chakrabartty and Kumar, 1995). In another, it was reported that hBN films were synthesized using diborane and ammonia as gas precursors, and the number of hBN layers can be controlled at various temperatures, gas pressure and flow rates (Ismach et al., 2012). Moreover, spherical BNs were synthesized using trimethoxyborane [$B(OMe)_3$] under ammonia gas flow via chemical vapor deposition (CVD) method (Tang et al., 2008). It was found that the spherical morphology of the BNs strongly depends on the elimination yield of Me_2O groups from the BN structures during the intermediate phase of the synthesis (Tang et al., 2008). In addition, hollow BN spheres were synthesized using $B(OMe)_3$ and Ar instead of ammonia in the second stage of the synthesis that is the key point to form hollow structures. Furthermore, an increase in post-treatment temperature decreases the wall thickness of the hBNs while increasing the crystallinity of the structures (Li et al., 2017).

The studies reporting the inhibitory effect of boron containing compounds on cancer cell proliferation including prostate and breast cancer by reducing the release of stored Ca^{2+} ions into the cytosol of cells suggests that boron compounds can be promising agents for cancer treatment (Henderson et al., 2009). However, the frequent administration of boron compounds due to their short half-life for systemic administration limits their use because it requires continues administrations. Since boron-based nanomaterials such as hBNs can behave as a controlled boron release source (Li et al., 2017). Their use can open up new venues in cancer treatment. Therefore, it is important to synthesize hBNs as pure as possible with desired crystallinity, which might also be an important factor for further chemical modification with targeting ligands. These mentioned points could also be important factors for their dissolution/degradation in biological medium for a successful therapeutic approach (Barranco and Eckhert, 2004, 2006; Scorei et al., 2008; Emanet et al., 2015; Li et al., 2017).

In this study, from three different boron compounds, boric acid, colemanite, and boron trioxide were used to synthesize hBNs under ammonia gas atmosphere with CVD technique. The synthesized hBNs were characterized with imaging and spectroscopic techniques. The colloidal stability of the hBNs was investigated by monitoring zeta potential and time dependent size distribution with dynamic light scattering (DLS) technique. Thermogravimetric analysis (TGA) was carried out to observe the resistance against heat decomposition. Finally, the biodegradation behavior of the hBNs in oxidative and hydrolytic degradation conditions was assessed by TGA, ICP-MS, and Raman spectroscopy.

MATERIALS AND METHODS

hBNs Synthesis

Boric acid, colemanite, and boron trioxide, as boron and ammonia as nitrogen source were used. The synthesis was performed based on a method previously reported by our group (Emanet et al., 2017). First, 2 g of boric acid or colemanite or boron trioxide were suspended in 3 mL of 13.38 M ammonia solution. This mixture was transferred onto a silicon carbide boat and dried on a hot plate adjusted to 100°C for approximately 20 min. Then, this silicon carbide boat was placed in a Protherm Furnace PTF 14/50/450 and heated until 1,300°C with a heating rate of 10°C/min under ammonia gas flow for 2 h. Following the heating, the silicon carbide boat was removed from furnace at around 550°C and hBNs were scratched from the surface of the silicon carbide boat with the help of spatula and stored under room conditions.

SEM and TEM Imaging

The morphology and size of the synthesized hBNs were characterized using SEM and TEM. SEM (Helios Nano-Lab 600i FIB/SEM, FEI) imaging was carried out on samples previously gold-sputtered for 25 s at 60 nA, obtaining a 3-nm thick conductive layer over the hBNs. TEM images were acquired with a JEOL-2100 HRTEM microscopy system at 200 kV (equipped with LaB6 filament and an Oxford Instruments 6498 EDS system).

TABLE 1 | Composition of LMS.

Composition of lysosome mimicking solution	Concentration
Calcium chloride dehydrate	197.0 mM
Sodium chloride	113.8 mM
Potassium hydrogen phthalate	0.0 mM
Glycine	6.0 mM
Sodium phosphate dibasic anhydrous	1.0 mM
Sodium sulfate (anhydrous)	0.5 mM
Alkylbenzyldimethylammonium chloride	50.0 ppm

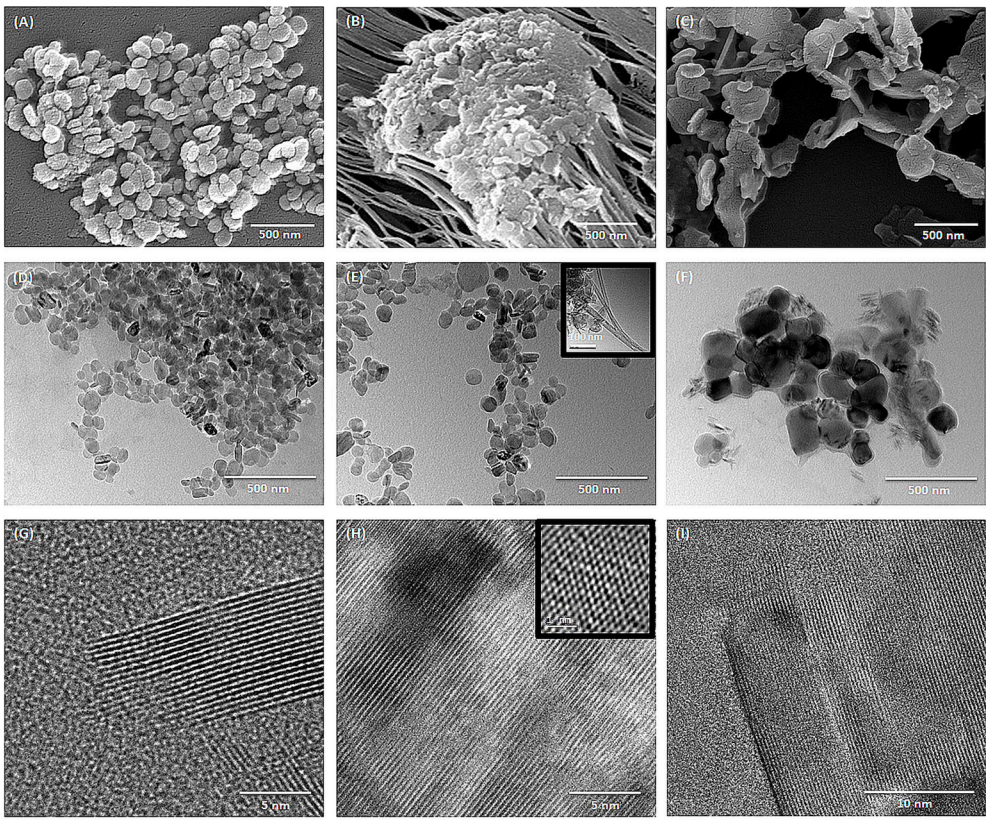

FIGURE 1 | SEM images of **(A)** hBNs_boric acid, **(B)** hBNs_colemanite, and **(C)** hBNs_boron trioxide. TEM images of **(D,G)** hBNs_boric acid, **(E,H)** hBNs_colemanite, and **(F,I)** hBNs_boron trioxide.

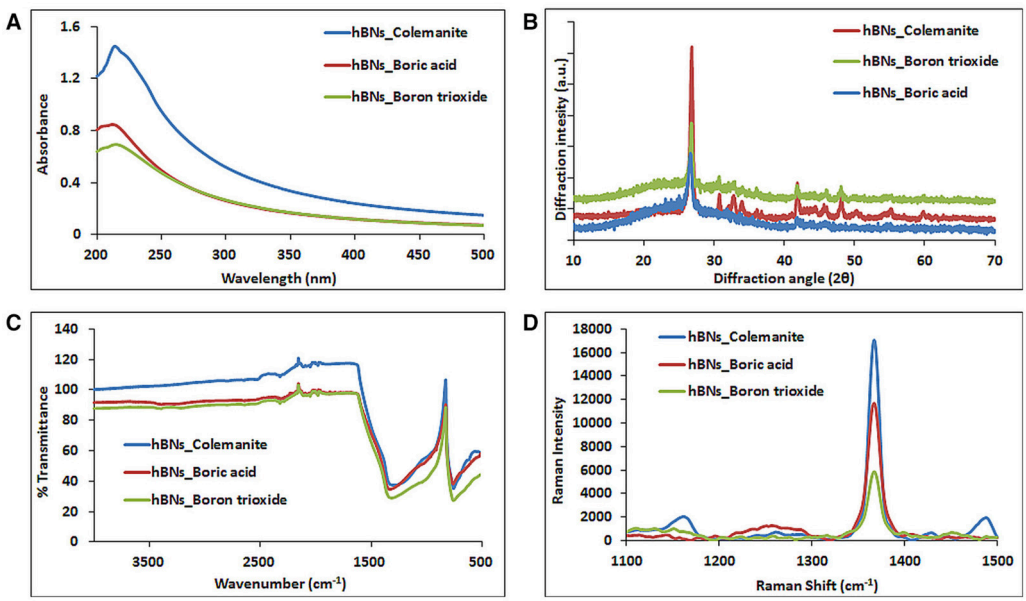

FIGURE 2 | Characterization of hBNs obtained from various precursors. **(A)** UV-Vis, **(B)** XRD, **(C)** FT-IR, and **(D)** Raman spectroscopy.

UV-Vis, XRD, FT-IR, and Raman Spectroscopy

The hBNs were dispersed in double distilled water (ddH_2O) by sonication for 2 min at before the analysis (Bandelin Sonopuls HD 3100). A Perkin Elmer Lambda 25 UV-Vis spectrometer was used to obtain absorption spectra. IR spectra were acquired with a Thermo NICOLET IS50 Spectrometer. XRD analysis was performed using a Shimadzu XRD-6000 with a ICDD PDF 4 software. The scanning area was in continuous mode with a scanning range of 2.000–69.980° and a scanning speed of 2.0000°/min. The sampling pitch was set to 0.0200°, and the preset time was set to 0.60 s. Raman spectra of the hBNs were recorded using a Renishaw In Via Reflex Raman Microscopy system (Renishaw Plc., New Mills, Wotton-under-Edge, UK) equipped with a 514 nm Argon ion laser. A minimum of 16 spectra was acquired from a 16-μm^2 hBNs sample area. All measurements were performed at least three times.

Thermogravimetric Analysis (TGA)

TGA analyses were performed using a Mettler Toledo TGA/SDTA 851 instrument. The samples were analyzed under 20-mL/min N_2 gas flow. The temperature was increased up to 700°C and was set at 10°C/min.

Dynamic Light Scattering (DLS) and Zeta Potential Measurements

The colloidal stability analysis of the hBNs was carried out by monitoring the size distribution and the Z-potential using a Malvern Zetasizer Nano ZS. The hBNs were sonicated for optimal dispersion in ddH_2O at for 2 min. The concentration of the hBNs was fixed as 1 mg/mL. Then, the sonicated samples were analyzed using DLS at different times (0 and 60 min) to assess their time-dependent colloidal stability. Furthermore, zeta potential measurements were performed and all experiments were repeated at least three times.

Biodegradation Studies

Biodegradation of hBNs was performed under two different conditions: in lysosome mimicking solution (LMS) for oxidative degradation, and in phosphate-buffered saline (PBS) for hydrolytic degradation. To observe the oxidative degradation of hBNs in lysosome mimicking condition, a LMS was prepared according to **Table 1** (Russier et al., 2011). The pH of the solution was brought to 4.5. Then, 25 mg of hBNs were dispersed in 25 mL of LMS, which contains physiological concentration of hydrogen peroxide (H_2O_2, 1 mM). Then, they were sonicated for 1 h. To maintain the physiological oxidizing environment of lysosomes, 1 mM of H_2O_2 was weekly added. For hydrolytic degradation of hBNs in PBS, 25 mg hBNs were dispersed in 25 mL PBS and sonicated for 1 h. After the sonication, all samples for oxidative and hydrolytic degradation were placed in dark and incubated at 37°C while shaking at 180 rpm up to 30 days. In both cases, 1 mL sample was taken from the LMS or PBS suspensions at 0, 1, 3, 7, 14, and 30 days of the incubation, and stored at 4°C in the dark until characterization.

TABLE 2 | Zeta potential of synthesized hBNs.

Samples	hBNs_boric acid	hBNs_colemanite	hBNs_boron trioxide
Zeta potential (mV)	−20.72 ± 0.11	−18.07 ± 0.07	−18.96 ± 0.08

Characterization of Degradation Products

After the degradation process in the LMS and PBS suspensions, samples taken from the suspensions were used for TGA analysis. An unprocessed hBNs suspension was used as a control for comparison. The suspensions were centrifuged at 10,000 rpm for 10 min, the supernatants were removed, and the pellets including hBNs were dried under vacuum. The TGA analysis was carried out using the pellets.

The degradation products were evaluated with ICP-MS to determine boron content. First, 1 mL of the samples was centrifuged at 10,000 rpm for 10 min at 4°C to remove non-degraded hBNs from solution as a pellet. Then, 0.5 mL of the supernatant containing degradation products was mixed with 4.5 mL of 1% nitric acid solution. Thereafter, the samples were filtered with a 0.22 μm Millipore filter to further remove any non-degraded hBNs from the samples, which were evaluated with an X Series 2 ICP-MS (Thermo Scientific) instrument equipped with a CETAC asx-520 autosampler. In the ICP-MS system, the plasma power, the plasma gas, the nebulizer gas flow rate, the clutch duration, and the wash duration were set to 1,350 W, Ar, 0.95, 35, and 35 s, respectively. VHG Labs Z frequency 1007-100 multi-element standard stock solution (1 mg/mL) containing Al, B, Cu, Ag, As, Cd, Fe, Ni, Sr, Zn, Ca was used for calibration. The standards were prepared at the concentrations of 0.1, 1.0, 10.0, and 100.0 μg/mL in 5% nitric acid using this stock solution. The calibration curves were created for each metal and the experiments were performed at least three times.

The characterization of hBNs after the degradation process was further analyzed by Raman spectroscopy. Five microliters of LMS and PBS suspensions containing hBNs were placed on a CaF_2 slide and allowed to dry. A minimum of 16 spectra was recorded from a dried droplet area by choosing arbitrary points. All experiments were performed at least three times and their average values were calculated.

RESULTS AND DISCUSSION

Morphological Characterization of hBNs

The size and morphology of hBNs can vary depending on synthesis conditions and the type of boron precursor. **Figure 1** shows the SEM and TEM images of the hBNs synthesized from three different boron precursors. As seen, the hBNs synthesized from each precursor have platelet-like morphology with varying sizes. The hBNs synthesized from boric acid (hBNs_boric acid) show a more uniform structure with lateral size dimension between 50 and 70 nm as seen in **Figure 1A** while the lateral size dimensions of the hBNs synthesized from colemanite (hBNs_colemanite) are between 50 and 80 nm. The hBNs_colemanite also include boron nitride nanotubes (BNNTs) in the product mixture (**Figure 1B**). This can be explained with

the presence of metal oxides such as CaO, B_2O_3, Fe_2O_3, Al_2O_3, MgO, and Na_2O in colemanite acting as catalysts (Gür, 2007). Transition metals and their oxides play an important role in synthesis of BNNTs as catalysts to roll the hBN layers into tube shape (Pakdel et al., 2012). The hBNs synthesized from boron trioxide (hBNs_boron trioxide) show non-uniform lateral sizes in the range of 200–300 nm indicating a poor regularity as seen in **Figure 1C**. **Figures 1D–F** show TEM images of the synthesized hBNs. As seen in **Figure 1D**, the hBNs_boric acid present uniform platelet-like structures while both hBNs and incomplete BNNTs are visible in the hBNs_colemanite sample reported in **Figure 1E** (inset image) similar to the case observed in SEM images. **Figure 1F** shows that the hBNs_boron trioxide have varying sizes confirming their structures as observed from their SEM images. **Figures 1G–I** show the parallel straight-line like crystalline features of the synthesized hBNs indicating the high quality of the samples. The honeycomb lattice structure of atomic boron and nitrogen was observed using HRTEM as shown in **Figure 1H** as inset image.

Spectroscopic Characterization of hBNs

The hBNs were characterized with UV-Vis, XRD, FT-IR, and Raman spectroscopy. **Figure 2A** shows comparison of UV-Vis spectra of hBNs synthesized from all three precursors. A characteristic maximum absorption band at around 210 nm is observed on the spectra. The highest absorption and background intensity are observed with the hBNs_colemanite probably due to the presence of BNNTs and other impurities in the final product (Behura et al., 2015).

Figure 2B shows the XRD pattern of the synthesized hBNs. The peaks originating from hBNs were observed at 2θ angles of 26.8° and 41.8° indicating successful synthesis for all hBNs derived from three different precursors. The synthesized hBNs show high crystallinity exhibiting narrow peak width around 26.8° and 41.8°. However, hBNs_colemanite show the highest crystallinity with respect to the hBNs_boric acid and hBNs_boron trioxide characterized with the increased peak intensities. Furthermore, hBNs_colemanite have varying peaks around 30–40° attributed to characteristic peaks of colemanite (Bayca et al., 2014).

The FT-IR spectra show that the hBNs have broad peaks at around 1,364 and 820 cm^{-1} that is attributed to the B–N vibrations as shown in **Figure 2C**. Moreover, a weak band at around 3,400 cm^{-1} attributed to O–H stretching in hBNs_boric acid and hBNs_boron trioxide, which is an important indicator for the degradation tendency of samples (Tang et al., 2008).

Figure 2D shows the Raman spectra of the hBNs with a sharp peak at around 1,364 cm^{-1} originating from B–N vibrations. The spectroscopic evaluation of the hBNs obtained from the boric acid, colemanite, and boron trioxide shows the unique characteristic spectral features for hBN structure.

Colloidal Stability of hBNs

Zeta potential of nanomaterials can be used as an indicator for their colloidal stability in aqueous environment. It is a fact that neutral and low density of charged molecular structures or nanomaterials cannot resist to attractive forces and form aggregates while highly charged particles repel each other and show better stability (Zhang et al., 2008). The zeta potentials of the synthesized hBNs in this study were measured and shown in **Table 2**. As seen, the zeta potential values are -20.72 ± 0.11 for the hBNs_boric acid, -18.02 ± 0.07 for the hBNs_colemanite, and -18.96 ± 0.08 for the hBNs_boron trioxide. These values indicate that the stability of colloidal suspensions of hBNs in aqueous environment is quite good.

In addition, their hydrodynamic stabilities were investigated by measuring their particle size distributions at different time-points from 0 to 60 min with DLS (**Figure 3**). The samples were sonicated for 2 min for an optimal dispersion. The size

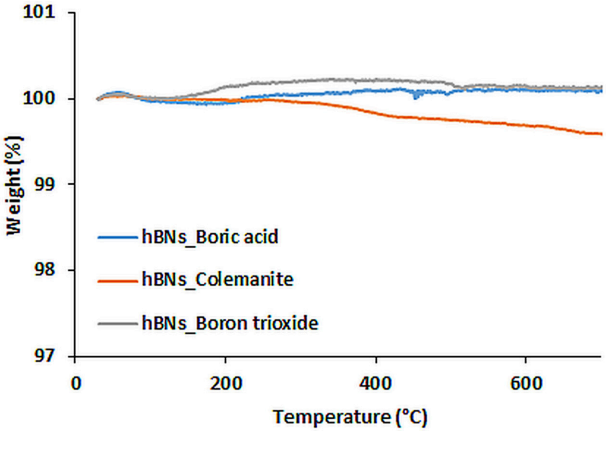

FIGURE 4 | TGA curves of hBNs synthesized from different precursors.

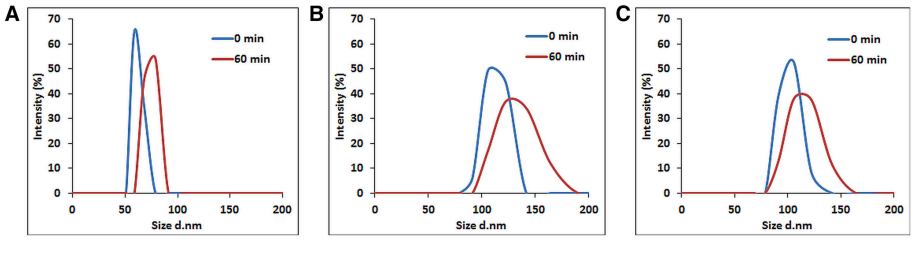

FIGURE 3 | Size distribution of **(A)** hBNs_boric acid, **(B)** hBNs_colemanite, and **(C)** hBNs_boron trioxide.

distribution of the hBNs_boric acid was found between 50 and 91 nm as shown in **Figure 3A**, and the maximum hydrodynamic size increased to 78 from 58 nm after 60 min. The size distribution of the hBNs_colemanite was found to be between 78 and 190 nm as shown in **Figure 3B**, and their maximum size was also approximately increased to 141 from 122 nm. The size distribution of hBNs_boron trioxide was between 78 and 164 nm as shown in **Figure 3C**, and their maximum size approximately increased to 122 from 105 nm after 60 min.

The results indicate that the hBNs_boric acid are more efficiently dispersed in aqueous environment considering their smaller average size as compared to the hBNs_colemanite and hBNs_boron trioxide. Furthermore, it has been observed that the size distribution of hBNs_boric acid is narrower as compared to the hBNs_colemanite and hBNs_boron trioxide indicating higher uniformity of hBNs_boric acid. Besides, the low differences in size distribution of each sample at 0 and 60 min show their high colloidal stability confirming the Z-potential results.

Thermal Stability of hBNs

TGA analysis was performed to investigate thermal stability of the hBNs within the temperatures range of 30–700°C. **Figure 4** shows TGA analysis of the synthesized hBNs. As seen, hBNs synthesized from all precursors have high thermal stability since no significant weight loss was observed with heating up to 700°C. A slight different result is observed for the hBNs_colemanite. This may be due to presence of metal oxides originating from colemanite. Since the hBNs_colemanite may include incomplete BNNTs in the sample, the high thermal stability of BNNTs also contributes to the thermal stability of the mixture (Ferreira et al., 2015; Kalay et al., 2015, 2016).

Biodegradation of hBNs

Biodegradability of nanomaterials is an important issue to be investigated before their use in medicine (Naahidi et al., 2013). In addition to the therapeutic effect, biodegradable nanomaterials have an additional advantage since they can be eliminated from the body through their degradation (Kalashnikova et al., 2015).

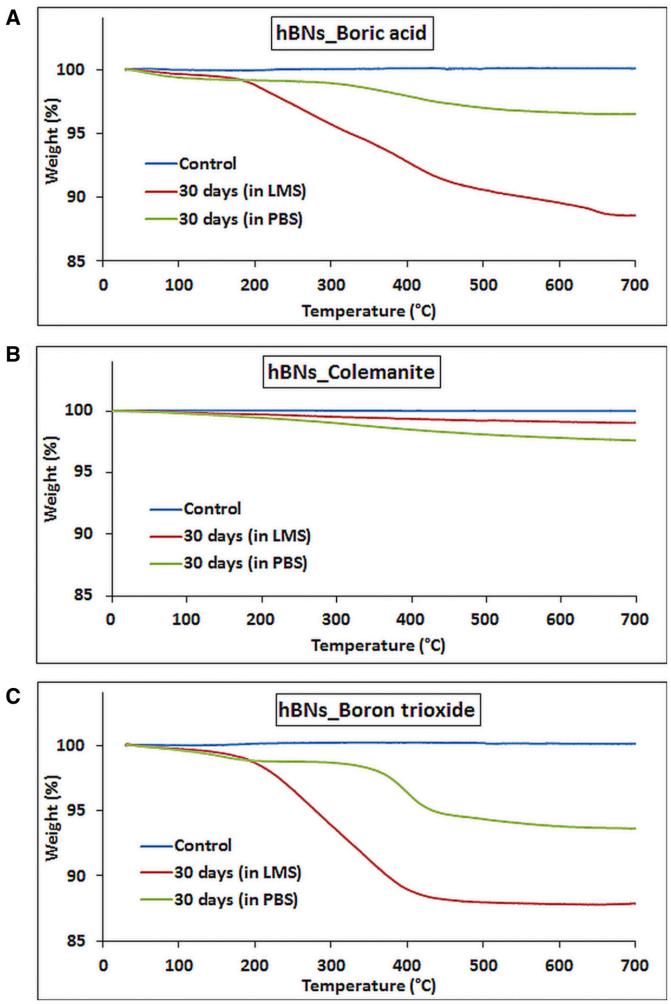

FIGURE 5 | TGA curves of hBNs before and after biodegradation treatment. **(A)** hBNs_boric acid, **(B)** hBNs_colemanite, and **(C)** hBNs_boron trioxide.

Furthermore, boron compounds such as boric acid can be used in some cancer types as therapeutic agents as mentioned earlier (Barranco and Eckhert, 2004; Scorei et al., 2008). However, frequent administration is needed because of short half-life circulation and low bioavailability of boron compounds. Thus, slow release of boron derivatives is important for therapeutic applications particularly in a cancer treatment (Li et al., 2017). Boron exists as boric acid at the physiological pH and it is considered having the therapeutic effect (Barranco and Eckhert, 2006).

The biodegradation of the hBNs under oxidative and hydrolytic conditions was examined for 30 days. After 30 days, hBNs in LMS or PBS suspensions were centrifuged to remove the supernatants. Then, TGA analysis was performed on the remaining pellets. **Figure 5** shows the result of the experiments. The control hBNs_boric acid was found thermally stable during the temperature gradient. The approximate weight loss of hBNs_boric acid incubated in LMS was 12% while it was only 3% for hBNs_boric acid incubated in PBS. The mass loss of the hBNs_colemanite incubated in LMS was around 1% while it was 2% incubated in PBS indicating that hBNs_colemanite were chemically stable in LMS and PBS suspensions after a 30-day incubation as seen in **Figure 5B**. Furthermore, **Figure 5C** shows that approximately 12% weight of hBNs_boron trioxide incubated in LMS was lost while the mass loss of the hBNs incubated in PBS was found to be around 6%. The data show that hBNs_colemanite are more resistant to both oxidative and hydrolytic degradation processes compared to the hBNs synthesized from other two precursors. This might be again due to the presence of incomplete BNNTs along with the hBNs. In addition, the hBNs_boric acid and hBNs_boron trioxide were more resistant in hydrolytic degradation compared to the oxidative degradation. It is hypothesized that adding hydrogen peroxide into the test suspensions could damage the B-N bonds and these defects leads to the degradation of the hBNs. Furthermore, as seen in **Figure 2C** in FT-IR results, a weak band at around 3,400 cm^{-1}, which is attributed to O–H stretching,

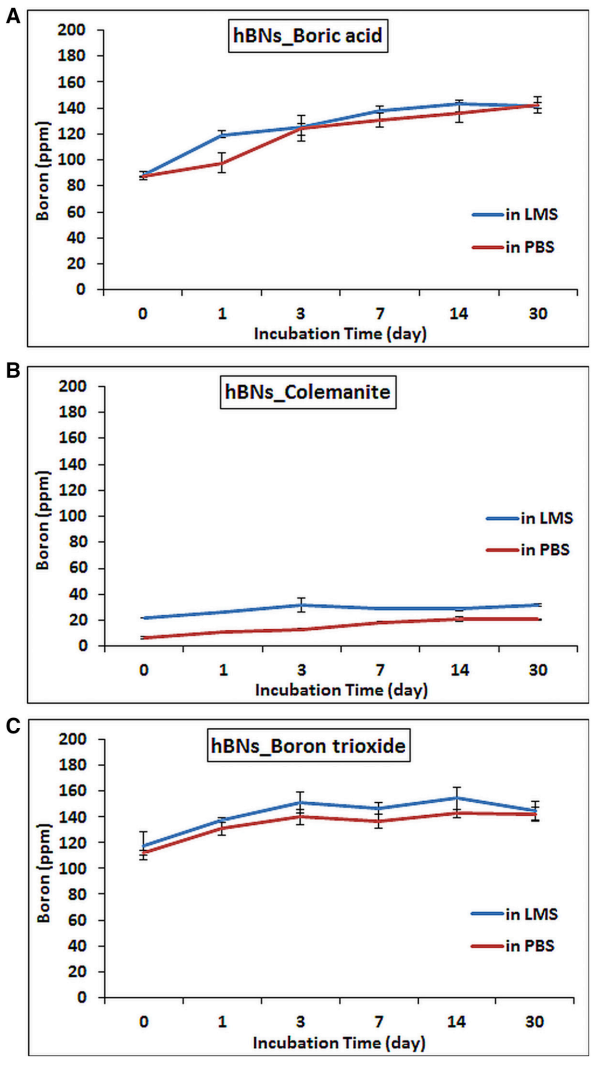

FIGURE 6 | ICP-MS results of hBNs in LMS and PBS suspensions at increasing time points during biodegradation process. **(A)** hBNs_boric acid, **(B)** hBNs_colemanite, and **(C)** hBNs_boron trioxide.

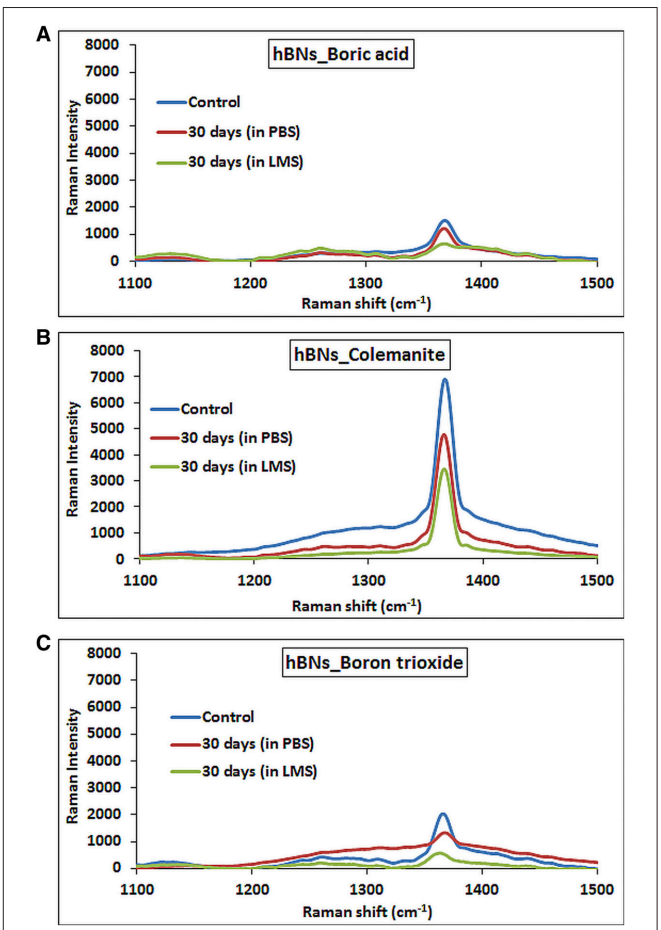

FIGURE 7 | Raman spectra of hBNs before and after biodegradation process. **(A)** hBNs_boric acid, **(B)** hBNs_colemanite, and **(C)** hBNs_boron trioxide.

could make the hBNs_boric acid and hBNs_boron trioxide more prone to oxidative degradation (Tang et al., 2008). The mass loss of the hBNs demonstrates that the degradation of the hBNs depends on their precursors and dependently crystallinity in both oxidative and hydrolytic degradation environments. Please note that after the centrifugation, it is possible that all hBNs are not precipitated as a pellet. However, the same experimental conditions were applied for all types of hBNs, we think that the trend in the data should be the same.

The amount of the released boron from hBNs in the LMS and PBS suspensions along with their degradation is investigated using ICP-MS. It was found that as the incubation time increased, the boron content in their suspensions increased. After 30 days, the amount of released boron from hBNs_boric acid increased to 142.0 ± 6.4 ppm from 88.1 ± 3.0 ppm in LMS and PBS suspensions of hBNs_boric acid (**Figure 6A**). The boron concentration was found to be lower in both LMS and PBS suspensions of hBNs_colemanite as seen in **Figure 6B**, because of higher crystallinity of hBNs_colemanite. As mentioned earlier, crystallinity of the hBNs affects the boron release from the hBNs (Li et al., 2017). The amount of released boron from hBNs_colemanite increased to approximately 20.7 ± 0.4 ppm from 6.2 ± 0.9 ppm in PBS solution while the amount of released boron increased to approximately 31.4 ± 0.9 ppm from 22.0 ± 0.1 ppm in LMS. Thus, a decreased amount of boron release (approximately 7-fold) was found for hBNs_colemanite in PBS due to its crystallinity. After 30 days, the boron content in both suspensions of the hBNs_boron trioxide was found similar to the case of hBNs_boric acid as shown in **Figure 6C**. The amount of released boron from hBNs_boron trioxide increased to approximately 142.1 ± 5.4 ppm from 112.5 ± 1.8 ppm in PBS solution while the amount of released boron increased to approximately 144.5 ± 7.3 ppm from 117.2 ± 10.8 ppm in LMS.

A further demonstration of hBNs degradation process was provided with Raman spectroscopy analysis. **Figure 7A** shows the Raman spectra of hBNs_boric acid before and after degradation process. The decrease of peak intensity at around 1,360 cm^{-1} suggests the degradation of the hBNs after 30-day incubation in LMS. For hBNs_colemanite, a sharp peak at around 1,360 cm^{-1} decreases as seen in **Figure 7B** resulting from the degradation of the hBN structures. The wide and decreased peak at around 1,360 cm^{-1} for hBNs_boron trioxide indicates the degradation of the hBNs after 30 days (**Figure 7C**). A decrease in the peak intensity at around 1,360 cm^{-1} demonstrates the biodegradation of the hBNs. These results are also in good agreement with TGA and ICP-MS results.

CONCLUSION

In this study, hBNs were synthesized from three different precursors; boric acid, colemanite, and boron trioxide, and their crystallinity, size, shape, and biodegradation behavior were investigated. The morphological and spectroscopic characterization results indicate that the hBNs_boric acid show high crystallinity, uniform, and unique platelet-like structures. In the sample prepared from hBNs_colemanite, incomplete BNNTs were observed along with the highest crystalline hBNs. The formation of BNNTs is attributed to the presence of metal oxides behaving as catalysts. The hBNs_boron trioxide have also high crystallinity despite irregular lateral size dimensions. It is found that the size of the hBNs varies and their colloidal suspension is quite stable. The biodegradation studies show that hBNs_colemanite are more resistant to both oxidative and hydrolytic degradation (approximately 7-fold) due to their high crystallinity while hBNs_boric acid and hBNs_boron trioxide are more prone to both oxidative and hydrolytic degradation. The degradation study indicate a slow boron release possible in the form of borate, which can be an important finding in the treatment of certain cancer types (Barranco and Eckhert, 2006). The hBNs are suggested as possible therapeutic agents for use in some cancer types such as prostate due to boron content. In addition, using hBNs as a boron source might be a significant improvement for wound healing applications due their slow degradation. Over all, the type of precursors affects the synthesized product crystallinity, structural uniformity, and their biodegradation behavior. Thus, an appropriate boron precursor should be chosen based on the target application.

AUTHOR CONTRIBUTIONS

ÖS and ME carried out the experimental work and the analysis of the data. All authors contributed to manuscript revision, read and approved the submitted version.

FUNDING

The authors acknowledge the financial support from Yeditepe University.

ACKNOWLEDGMENTS

The authors also acknowledge the help of Seda Keleştemur with ICP-MS experiment.

REFERENCES

Arenal, R., and Lopez-Bezanilla, A. (2015). Boron nitride materials: an overview from 0D to 3D (nano) structures. *Wiley Interdisciplin. Rev. Comput. Mol. Sci.* 5, 299–309. doi: 10.1002/wcms.1219

Barranco, W. T., and Eckhert, C. D. (2004). Boric acid inhibits human prostate cancer cell proliferation. *Cancer Lett.* 216, 21–29. doi: 10.1016/j.canlet.2004.06.001

Barranco, W. T., and Eckhert, C. D. (2006). Cellular changes in boric acid-treated DU-145 prostate cancer cells. *Br. J. Cancer* 94, 884–890. doi: 10.1038/sj.bjc.6603009

Bayca, S. U., Kocan, F., and Abali, Y. (2014). Dissolution of colemanite process waste in oxalic acid solutions. *Environ. Prog. Sustain. Energy* 33, 1111–1116. doi: 10.1002/ep.11889

Behura, S., Nguyen, P., Che, S., Debbarma, R., and Berry, V. (2015). Large-area, transfer-free, oxide-assisted synthesis of hexagonal boron nitride films and their

heterostructures with MoS2 and WS2. *J. Am. Chem. Soc.* 137, 13060–13065. doi: 10.1021/jacs.5b07739

Bhimanapati, G. R., Kozuch, D., and Robinson, J. A. (2014). Large-scale synthesis and functionalization of hexagonal boron nitride nanosheets. *Nanoscale* 6, 11671–11675. doi: 10.1039/c4nr01816h

Chakrabartty, S., and Kumar, S. (1995). Preparation of hexagonal boron nitride from boric acid and characterization of the materials. *Trans. Ind. Ceram. Soc.* 54, 48–51. doi: 10.1080/0371750X.1995.10804678

Chen, X., Wu, P., Rousseas, M., Okawa, D., Gartner, Z., Zettl, A., et al. (2009). Boron nitride nanotubes are noncytotoxic and can be functionalized for interaction with proteins and cells. *J. Am. Chem. Soc.* 131, 890–891. doi: 10.1021/ja807334b

Dousset, B., Benderdour, M., Hess, K., Mayap-Nzietchueng, R., Belleville, F., and Duprez, A. (2002). "Effects of boron in wound healing," in *Trace Elements in Man and Animals*, Vol. 10, eds A. M. Roussel, R. A. Anderson and A. E. Favrier (Boston, MA: Springer), 1061–1065. doi: 10.1007/0-306-47466-2_325

Du Frane, W., Cervantes, O., Ellsworth, G., and Kuntz, J. (2016). Consolidation of cubic and hexagonal boron nitride composites. *Diam. Relat. Mater.* 62, 30–41. doi: 10.1016/j.diamond.2015.12.003

Emanet, M., Sen, Ö., Çobandede, Z., and Çulha, M. (2015). Interaction of carbohydrate modified boron nitride nanotubes with living cells. *Colloids Surf. B Biointerfaces* 134, 440–446. doi: 10.1016/j.colsurfb.2015.07.036

Emanet, M., Sen, Ö., and Çulha, M. (2017). Evaluation of boron nitride nanotubes and hexagonal boron nitrides as nanocarriers for cancer drugs. *Nanomedicine (Lond).* 12, 797–810. doi: 10.2217/nnm-2016-0322

Ferreira, T. H., Marino, A., Rocca, A., Liakos, I., Nitti, S., Athanassiou, A., et al. (2015). Folate-grafted boron nitride nanotubes: possible exploitation in cancer therapy. *Int. J. Pharm.* 481, 56–63. doi: 10.1016/j.ijpharm.2015.01.048

Gür, A. (2007). Dissolution mechanism of colemanite in sulphuric acid solutions. *Kor. J. Chem. Eng.* 24, 588–591. doi: 10.1007/s11814-007-0007-9

Han, W.-Q. (2010). Anisotropic hexagonal boron nitride nanomaterials: synthesis and applications. *Nanotechnol. Life Sci.* doi: 10.1002/9783527610419.ntls0161

Henderson, K., Stella, S. L., Kobylewski, S., and Eckhert, C. D. (2009). Receptor activated Ca^{2+} release is inhibited by boric acid in prostate cancer cells. *PLoS ONE* 4:e6009. doi: 10.1371/journal.pone.0006009

Ismach, A., Chou, H., Ferrer, D. A., Wu, Y., McDonnell, S., Floresca, H. C., et al. (2012). Toward the controlled synthesis of hexagonal boron nitride films. *ACS Nano* 6, 6378–6385. doi: 10.1021/nn301940k

Kalashnikova, I., Das, S., and Seal, S. (2015). Nanomaterials for wound healing: scope and advancement. *Nanomedicine (Lond).* 10, 2593–2612. doi: 10.2217/nnm.15.82

Kalay, S., Stetsyshyn, Y., Lobaz, V., Harhay, K., Ohar, H., and çulha, M. (2016). Water-dispersed thermo-responsive boron nitride nanotubes: synthesis and properties. *Nanotechnology* 27:035703. doi: 10.1088/0957-4484/27/3/035703

Kalay, S., Yilmaz, Z., Sen, O., Emanet, M., Kazanc, E., and Çulha, M. (2015). Synthesis of boron nitride nanotubes and their applications. *Beilstein J. Nanotechnol.* 6, 84–102. doi: 10.3762/bjnano.6.9

Kubota, Y., Watanabe, K., Tsuda, O., and Taniguchi, T. (2007). Deep ultraviolet light-emitting hexagonal boron nitride synthesized at atmospheric pressure. *Science* 317, 932–934. doi: 10.1126/science.1144216

Lahiri, D., Singh, V., Benaduce, A. P., Seal, S., Kos, L., and Agarwal, A. (2011). Boron nitride nanotube reinforced hydroxyapatite composite: mechanical and tribological performance and *in-vitro* biocompatibility to osteoblasts. *J. Mech. Behav. Biomed. Mater.* 4, 44–56. doi: 10.1016/j.jmbbm.2010.09.005

Li, L. H., Chen, Y., Behan, G., Zhang, H., Petravic, M., and Glushenkov, A. M. (2011). Large-scale mechanical peeling of boron nitride nanosheets by low-energy ball milling. *J. Mater. Chem.* 21, 11862–11866. doi: 10.1039/C1JM11192B

Li, X., Wang, X., Zhang, J., Hanagata, N., Wang, X., Weng, Q., et al. (2017). Hollow boron nitride nanospheres as boron reservoir for prostate cancer treatment. *Nat. Commun.* 8:13936. doi: 10.1038/ncomms13936

Liu, L., Xiao, L., Li, M., Zhang, X., Chang, Y., Shang, L., et al. (2016). Effect of hexagonal boron nitride on high-performance polyether ether ketone composites. *Colloid Polym. Sci.* 294, 127–133. doi: 10.1007/s00396-015-3733-2

Naahidi, S., Jafari, M., Edalat, F., Raymond, K., Khademhosseini, A., and Chen, P. (2013). Biocompatibility of engineered nanoparticles for drug delivery. *J. Control. Release* 166, 182–194. doi: 10.1016/j.jconrel.2012.12.013

Pakdel, A., Zhi, C., Bando, Y., Nakayama, T., and Golberg, D. (2012). A comprehensive analysis of the CVD growth of boron nitride nanotubes. *Nanotechnology* 23, 215601. doi: 10.1088/0957-4484/23/21/215601

Russier, J., Ménard-Moyon, C., Venturelli, E., Gravel, E., Marcolongo, G., Meneghetti, M., et al. (2011). Oxidative biodegradation of single- and multi-walled carbon nanotubes. *Nanoscale* 3, 893–896. doi: 10.1039/c0nr00779j

Salvetti, A., Rossi, L., Iacopetti, P., Li, X., Nitti, S., Pellegrino, T., et al. (2015). *In vivo* biocompatibility of boron nitride nanotubes: effects on stem cell biology and tissue regeneration in planarians. *Nanomedicine (Lond).* 10, 1911–1922. doi: 10.2217/nnm.15.46

Scorei, R., Ciubar, R., Ciofrangeanu, C. M., Mitran, V., Cimpean, A., and Iordachescu, D. (2008). Comparative effects of boric acid and calcium fructoborate on breast cancer cells. *Biol. Trace Elem. Res.* 122, 197–205. doi: 10.1007/s12011-007-8081-8

Shi, Y., Hamsen, C., Jia, X., Kim, K. K., Reina, A., Hofmann, M., et al. (2010). Synthesis of few-layer hexagonal boron nitride thin film by chemical vapor deposition. *Nano Lett.* 10, 4134–4139. doi: 10.1021/nl10 23707

Singhal, S., Srivastava, A., Singh, B., and Gupta, A. K. (2008). Synthesis and characterization of boron nitride nanotubes using a simple chemical method. *Indian J. Eng. Mater. Sci.* 15, 419–424.

Song, L., Ci, L., Lu, H., Sorokin, P. B., Jin, C., Ni, J., et al. (2010). Large scale growth and characterization of atomic hexagonal boron nitride layers. *Nano Lett.* 10, 3209–3215. doi: 10.1021/nl1022139

Sukhorukova, I. V., Zhitnyak, I. Y., Kovalskii, A. M., Matveev, A. T., Lebedev, O. I., Li, X., et al. (2015). Boron nitride nanoparticles with a petal-like surface as anticancer drug-delivery systems. *ACS Appl. Mater. Interfaces* 7, 17217–17225. doi: 10.1021/acsami.5b04101

Tang, C., Bando, Y., Huang, Y., Zhi, C., and Golberg, D. (2008). Synthetic routes and formation mechanisms of spherical boron nitride nanoparticles. *Adv. Funct. Mater.* 18, 3653–3661. doi: 10.1002/adfm.2008 00493

Turkoglu, M., Sahin, I., and San, T. (2005). Evaluation of hexagonal boron nitride as a new tablet lubricant. *Pharm. Dev. Technol.* 10, 381–388. doi: 10.1081/pdt-65684

Zhang, Y., Chen, Y., Westerhoff, P., Hristovski, K., and Crittenden, J. C. (2008). Stability of commercial metal oxide nanoparticles in water. *Water Res.* 42, 2204–2212. doi: 10.1016/j.watres.2007.11.036

Conflict of Interest Statement: The authors declare that the research was conducted in the absence of any commercial or financial relationships that could be construed as a potential conflict of interest.

frontiers in Bioengineering and Biotechnology

MINI REVIEW
published: 23 January 2019
doi: 10.3389/fbioe.2019.00005

The ABC Guide to Fluorescent Toolsets for the Development of Future Biomaterials

Ferdinandus[1] *and Satoshi Arai*[2,3]*

[1] *Waseda Bioscience Research Institute in Singapore, Singapore, Singapore,* [2] *Research Institute for Science and Engineering, Waseda University, Tokyo, Japan,* [3] *PRIME-AMED, Tokyo, Japan*

In recent decades, diversified approaches using nanoparticles or nano-structured scaffolds have been applied to drug delivery and tissue engineering. Thanks to recent interdisciplinary studies, the materials developed have been intensively evaluated at animal level. Despite these efforts, less attention has been paid to what is really going on at the subcellular level during the interaction between a nanomaterial and a cell. As the proposed concept becomes more complex, the need for investigation of the dynamics of these materials at the cellular level becomes more prominent. For a deeper understanding of cellular events, fluorescent imaging techniques have been a powerful means whereby spatiotemporal information related to cellular events can be visualized as detectable fluorescent signals. To date, several excellent review papers have summarized the use of fluorescent imaging toolsets in cellular biology. However, applying these toolsets becomes a laborious process for those who are not familiar with imaging studies to engage with owing to the skills gap between them and cell biologists. This review aims to highlight the valuable essentials of fluorescent imaging as a tool for the development of effective biomaterials by introducing some cases including photothermal and photodynamic therapies. This distilled information will be a convenient short-cut for those who are keen to fabricate next generation biomaterials.

Keywords: fluorescent probes, bioimaging, chemical indicators, fluorescent proteins, single-cell studies

OPEN ACCESS

Edited by:
Giada Graziana Genchi, Fondazione Istituto Italiano di Technologia, Italy

Reviewed by:
Stefan G. Stanciu, Politehnica University of Bucharest, Romania
Stefano Luin, Scuola Normale Superiore di Pisa, Italy
Robert E. Campbell, University of Alberta, Canada

***Correspondence:**
Satoshi Arai
satoshiarai@aoni.waseda.jp

Specialty section:
This article was submitted to Nanobiotechnology, a section of the journal Frontiers in Bioengineering and Biotechnology

Received: *15 October 2018*
Accepted: *07 January 2019*
Published: *23 January 2019*

Citation:
Ferdinandus and Arai S (2019) The ABC Guide to Fluorescent Toolsets for the Development of Future Biomaterials. Front. Bioeng. Biotechnol. 7:5. doi: 10.3389/fbioe.2019.00005

HOW DO NANOMATERIALS AFFECT CELLULAR ACTIVITIES?

Recent advances in the development of biomaterials have yielded various types of nanomaterials for medical imaging, drug delivery, and regenerative medicine. The words nanomaterials and nanomedicine increasingly appear in these studies (Wagner et al., 2006). A nanometer-sized object is compatible with the scale of a single cell. For instance, drug-containing nanoparticles or nanorods are able to be taken up into a micron-sized cell efficiently, reach subcellular compartments, and lead to the alteration of cellular activities (Peer et al., 2007). To further benefit therapeutic efficiency, the surface of the nanomaterials can be modified to target the cells of interests (Chauhan and Jain, 2013; Yhee et al., 2014). Apart from nano-sized objects, two or three dimensional bulk-sized materials have also emerged, where their thickness is in the order of nanometers and/or their surface possesses a sophisticated nanostructure (Fujie, 2016). These nanomaterials effectively interact with biomacromolecules located at the cellular surface at a nanoscale interface (Luo et al., 2013). As potential applications, the modification of medical devices decorated with functional surfaces can prevent undesirable side effects, such as immune responses, when they are

introduced into the body (Franz et al., 2011). Also, customized culture dishes with nanostructured surfaces enable the induction of cellular differentiation and the morphological control of multicellular components (Discher et al., 2005; Marino et al., 2015b).

When developing ideas for biomedical applications, one starts with the design of a nanomaterial that can alter cellular functions at the subcellular level. After a proof of concept is demonstrated in simple cellular studies, one may go further and carry out studies in animal models. In recent years, material scientists carried out animal studies themselves due to the growth in interdisciplinary studies between medicine and material science. However, despite these efforts, the evaluation of whether the designed material is really able to function as expected has been overlooked. In particular, little is known about the spatiotemporal information in real time regarding the behavior of the nanomaterials in cells.

Thanks to advances in molecular and chemical biology, various toolsets are easily accessible to light up cellular events using fluorescence imaging. As the first step, it is necessary to choose an adequate microscope (epi-microscope, confocal microscope, etc.) and then make a decision on the appropriate fluorescent indicators (probes or sensors). Although the development of indicators has progressed tremendously in chemistry and biology, the strategy adopted in both fields is likely to be common, which means that these indicators are capable of reporting changes in intracellular events as fluorescent signals. In general, the indicators are classified into small chemical or genetically encoded indicators. This review will skip over detailed descriptions as these have already been reviewed in depth (Giepmans et al., 2010; Kang et al., 2011; Newman et al., 2011; Specht et al., 2017). In brief, genetically encoded indicators can specifically target organelles or events and exhibit long-term (for example, days) stability under microscopic observation (Greenwald et al., 2018). On the other hand, chemical indicators are easy to handle and thus accessible for anyone without the need for expertise in cell biology (**Figure 1**). Owing to recent developments, there is a risk to oversimplify the difference between the two types of indicators. For instance, the modified Baculovirus allows a safe and easy-handling protocol for genetically encoded indicators for researchers without any molecular biology skills. Such technology could contribute to solve the gap between the two indicators in future.

This review paper stresses the significance of the interaction between nanomaterials and biospecimens at the submicron scale. It therefore focuses on the tools for observing the dynamics of cellular events in real-time rather than simple immune staining. We will also skip any references to commercially available kits or indicators.

TOOLSETS TO VISUALIZE INTRACELLULAR EVENTS IN REAL-TIME

(i) How to See Changes in Cell State

Nano-sized carriers invade cells and then release drugs; so what happens to the cells and how do we visualize it? In the case of anticancer drug-loaded carriers, a cell viability assay (**live/dead assay kit**) could be the primary option. Of further interest would be the pathway through which cell death is executed, either apoptosis or necrosis. Necrosis involves the collapse of the outer cellular membrane, which can be evaluated with **propidium iodide (PI)**. During apoptosis, phosphatidylserine appears on the outer leaflet of the lipid bilayer, which can be identified with **fluorescent labeled Annexin V**. Looking at apoptosis more closely, indicators for mitochondrial membrane potentials (**JC1**) and Caspase activities (**Caspase-3/7 Green**) would be helpful.

To date, most drug delivery systems are designed to cause cell death in diseased cells and in such cases a simple live/dead test is frequently done. If the drug does not lead to complete cell death, it is possible to overlook the chance that nanomaterials could be affecting other cellular functions such as the cell cycle and proliferation. In fact, it was reported that even old-fashioned hyperthermia therapy perturbed the cell cycle (Dewey, 2009). In such cases, a genetically encoded indicator, Fluorescent Ubiquitination-based Cell Cycle Indicator (**Fucci**), could be used to distinguish S, G2, and M phases (Sakaue-Sawano et al., 2008).

In addition to the cell cycle, the change in energy metabolism resulting from nanomaterials is worth considering, though rarely discussed. A proliferating cell, such as a cancer cell, adopts a unique way to produce ATP as an energy source via strong glycolytic pathways, which is known as the Warburg effect (Heiden et al., 2009). Cancer cells therefore depend primarily on external glucose to survive while differentiated, non-cancerous cells rely on oxidative phospholyration (Oxphos) in mitochondria. ATP measurements are commonly performed using the well-known luciferin-luciferase assay (Manfredi et al., 2002). However, this method loses the spatiotemporal information of intracellular ATP dynamics. In order to visualize ATP fluctuations in real-time inside the cell, several fluorescent indicators have been developed, starting with genetically encoded indicators (**ATeam** and **Perceval/PercevalHR**), followed by the advent of small molecule indicators (Kurishita et al., 2012; Tantama et al., 2013; Tsuyama et al., 2013; Yaginuma et al., 2014). More recently, a team including an author of this review published a paper on the success of red, green, blue (RGB) color fluorescent indicators (**MaLions**) (Arai et al., 2018). This handy colorful toolset allows the observation of ATP dynamics at different organelles in the same cell simultaneously.

Other tools for visualizing energy metabolism include genetically encoded indicators sensing glucose (Ye and Schultz, 2003) and lactate (San Martín et al., 2013). These provide direct evidence for changes in metabolic pathways.

(ii) How to image Signaling molecules

In recent years, pioneering groups have attempted to generate stimulation devices that allow remote control of physiological functions in brains and muscles (Stanley et al., 2012; Marino et al., 2015a). The targeted functions are frequently associated with intracellular Ca^{2+} flux by external stimulation, which can be visualized using commercially available chemical indicators such as Fluo 4 and Fluo 8. Surprisingly, even a couple of decades after the advent of its prototype, Fluo 4 is still commonly used as a gold

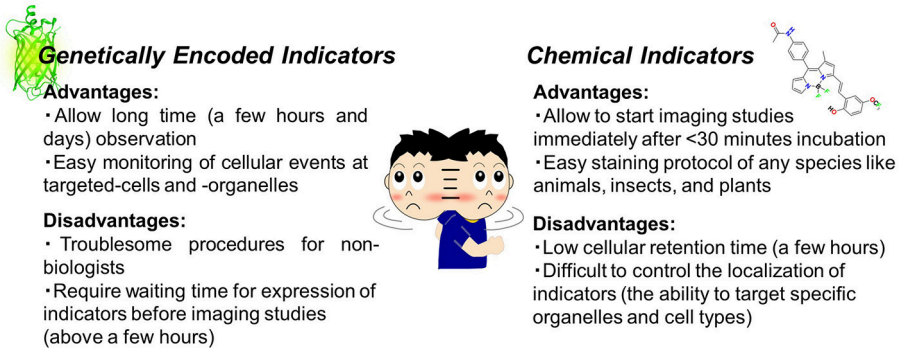

FIGURE 1 | Chemical indicators vs. genetically encoded indicators (PDB ID: 3DPW).

standard (Russell, 2011). Although there is no doubt regarding the viability of such indicators, their major drawback is their short cellular retention time. Due to the multiple carboxyl groups of the indicators in the anionic charged state, these chemical indicators are likely to be pumped out from cells via the anion transporter (Takei et al., 2013). On the other hand, genetically encoded Ca^{2+} indicators such as **GCaMP** enable long-term observations (Nakai et al., 2001). Moreover, the expanded color set of genetically encoded indicators prevails over chemical ones as color palettes, such as the R-, G-, B-**Geco** series, have already been established (Zhao et al., 2011). For more quantitative analysis, one should consider using the fluorescence resonance energy transfer (FRET)-based **Cameleon** series (Miyawaki et al., 1997). Considering its potential applications, the genetically encoded glutamate indicator, **iGluSnFr**, could be useful to visualize synaptic communications (Marvin et al., 2013). Also, as the other second messenger in addition to Ca^{2+}, indicators to detect cAMP, such as the **Flamindo** series, are effective (Odaka et al., 2014; Harada et al., 2017).

Reactive oxygen species (ROS) play a critical role in several cascades. A commercially available indicator, 2′,7′-dichlorodihydrofluorescein diacetate (**H2DCFDA**), is capable of capturing any kind of ROS non-specifically. For advanced studies, more specific indicators are available for distinguishing between several ROS species (hydroxyl radical; **OxiOrange**^{TM}, HClO; **HySOx**, H_2O_2; **HYDROP**, ONOO radical; **NiSPY-3**, Molecule Oxygen; **LOX-1**). Although limited to H_2O_2, genetically encoded indicators (**Hyper** series) are also applicable for monitoring ROS dynamics at target organelles (Bilan et al., 2013).

(iii) How to see invisible physicochemical elements

Many biomedical applications, such as therapeutic devices and nanomaterials, are associated with external physical stresses, such as force, magnetic fields, and temperature. For example, how does a single cell experience the temperature change produced by heat therapeutic devices? **ER thermo yellow** (or **ERthermAC**) and **Mito thermo yellow** are available to monitor temperature changes at the ER (endoplasmic reticulum) and mitochondria, respectively; these were developed by teams including an author of this review (Arai et al., 2014, 2015). As genetically encoded indicators, **gTEMP** and **tsGFPs**, which can target organelles, were developed (Kiyonaka et al., 2013; Nakano et al., 2017) and allow thermometry at the target organelles.

In addition to temperature as an obvious physical parameter for biomedical applications, there are several other elements to be examined in the biophysics field. For instance, several indicators were reported to visualize invisible factors, such as viscosity (Battisti et al., 2013; Liu et al., 2014), molecular crowding (Boersma et al., 2015), polarity (Sunahara et al., 2007; Abbandonato et al., 2018), and tension (Grashoff et al., 2010). Although the importance of these factors for biomaterials development still remains vague, these options should be kept in mind.

One may also have the interests in measuring the change of intracellular pH as a common physicochemical parameter. To monitor the pH, small chemical indicators (**SNARF** series) and genetic ones (**pHluorin** series) are available, some of which can be applied for two photon, ratiometric, and fluorescence life time imaging (Miesenböck et al., 1998; Bizzarri et al., 2009; Shen et al., 2014).

(iv) How to avoid the misinterpretation due to Artifacts

It is fascinating that a wide range of indicators are available for detecting various elements, however, one should take great care regarding pH fluctuations. Most indicators, regardless of whether they are genetically encoded or are chemical, follow the mechanism that the fluorescence intensity is altered as the change in the concentration of targeted analyte. Yet, the fluorescence of many indicators is also sensitive to pH changes owing to their pH-sensitive components, such as phenol and carboxylic groups. Though the cytoplasmic pH is maintained around 7.4 (different organelles being slightly different), the metabolic stress may cause an acidic change (Matsuyama et al., 2000). When the experimental conditions result in exposure to severe pH changes, this can be accounted for using pH indicators. This is vitally important to clarify whether the fluorescence change originates from the pH fluctuation or from the change in the concentration of targeted analyte (Berg et al., 2009). For example, one may correct the pH fluctuation using an additional pH indicator as

reported (Berg et al., 2009). In another unique approach, Sato et al. published a success of simultaneous imaging of chloride ion and pH, where the pH correction was done using the indicator capable of detecting pH and chloride ion simultaneously (Sulis Sato et al., 2017). In addition to pH fluctuation, the fluorescence signal can also be affected by focus drift, different concentration of indicators, photobleaching, photoactivation, and several other variables. To avoid misinterpretation of the results, the detection limits of the indicators should be accounted for and the predicted artifacts considered.

"MUST HAVE", NOT "NICE TO HAVE"!

Although it is quite obvious that imaging technology is a powerful tool for the development of biomaterials, most researchers consider it as supplementary, that is, "nice to have," but not "must have." We would like to stress the importance of imaging studies as the concept of the materials gets more advanced. In this section, we present a few examples of the effective use of indicators.

(i) What happens inside a cell during "photothermal therapy"?

Thermal therapy to kill tumors by means of elevated temperature is a popular therapeutic approach as medical treatment for cancers, in which one of key things is the mechanism to heat up cells and tissues. Among several thermal therapeutic ways, photothermal therapy (PTT) has been the most appealing means which enables local treatment with minimal invasiveness. This method requires photothermal materials which absorb near infrared (NIR) light and convert the energy into heat. To date, innumerable materials such as inorganic materials, organic dyes, and semicondutive polymers, have been fabricated in order to achieve more efficient photothermal therapeutic effect (Zhang et al., 2013, 2015). However, these materials also possess the risks of generating ROS, aside from producing heat. In some cases, ROS is harmful for normal tissues and cells, thus making the development of a pure photothermal material challenging. Recently, Jung et al. successfully generated novel photothermal materials using the organic dyes, cryptocyanines, which are ineffective ROS generators and also specifically target the mitochondria (Jung et al., 2017). It is easy to imagine that a strategy to target a critical organelle would benefit therapeutic efficiency. The team clarified the mechanism using a fluorescent ROS indicator targeting mitochondria (**MitoSOX**); the heat generated from the dye by photoirradiation perturbed the electron transport chain, resulting in a change in endogenous ROS dynamics at the mitochondria, leading to cell death. In other words, the change in ROS dynamics is not triggered by ROS derived from the materials.

As the other point in PTT, we need to pay attentions to how a single cell senses a rise in intracellular temperature caused by external heating. For example, when a temperature change was brought about in the multicellular spheroidal HeLa cells by external heating, a mitochondrial targeting temperature indicator, **Mito thermo yellow**, showed that each cell in the spheroidal aggregates experienced a different temperature change depending on its position (Arai et al., 2015) (**Figure 2A**). The maximum temperature difference between cells turned out to be around a couple of degrees even within the same bunch of cells. This result implies that maximal therapeutic efficiency cannot be achieved if heating is not homogeneous at the single cell level. This thermometry was also applied to evaluate the stimulation of skeletal muscles by heat (Marino et al., 2017). Attilio et al. demonstrated that once a gold nanoparticle, as a heat generator, was taken into the skeletal muscles, its contraction could be induced by heat with the irradiation of a NIR laser. A small fluorescent temperature indicator, ER thermo yellow, assisted in monitoring the intracellular temperature change while the muscle was contracting. For a more advanced example, Zhu et al. reported an intelligent nanocomposite that comprises a photothermal material and a fluorescent thermometer together (Zhu et al., 2016) which allows more accurate thermometry at the heat spot owing to the zero distance between the heater and the thermometer (**Figure 2B**).

(ii) What happens inside a cell during "photodynamic therapy"?

Much like photothermal therapy (PTT), photodynamic therapy (PDT) has a long history. However, there are scarce reports where cellular events were observed during the photodynamic therapy. For example, Kuimova et al. reported a unique porphyrin-dimer that possesses dual functionalities as an intracellular viscosity indicator as well as a photosensitizer to generate singlet oxygen species acting as cytotoxic agents (Kuimova et al., 2009) (**Figure 2C**). After photoirradiation, the generated singlet oxygen led to cell death while also causing a change in viscosity, which was visualized using their ratiometric viscosity indicator. Interestingly, it turned out that the increase in intracellular viscosity was not homogeneous and decreased the diffusivity of intracellular species. They suggested that the increase in the viscosity resulting from the photosensitizer altered the formation of singlet oxygen species and also their decay. The viscosity at subcellular compartmentalized spaces could be an important factor as it may also alter the transport efficiency of drugs.

Very recently, Wang et al. proposed a new type of therapeutic mechanism where the free radical generator is coupled with the NIR light (**Figure 2D**) (Wang et al., 2018). Unlike common previous approaches, their designed material does not generate ROS from intracellular oxygens but instead produces free radical species from the thermal initiator (V057: 2,2′-Azobis [N-(2-carboxyethyl)-2-methylpro-pionamidine] hydrate). More specifically, the gold nanocage (AuNc) which acts as an efficient photothermal material was decorated with V057 and a fluorescent dye (Cy5.5). Once the temperature is elevated on the surface of AuNc by NIR irradiation, the free radical is produced due to the cleavage of the thermal initiator, V057. Simultaneously, the free radical generation could be monitored with the fluorescence intensity change of Cy5.5 since the fluorescence is recovered from quenched state involved in the free radical production. Importantly, the material is also designed

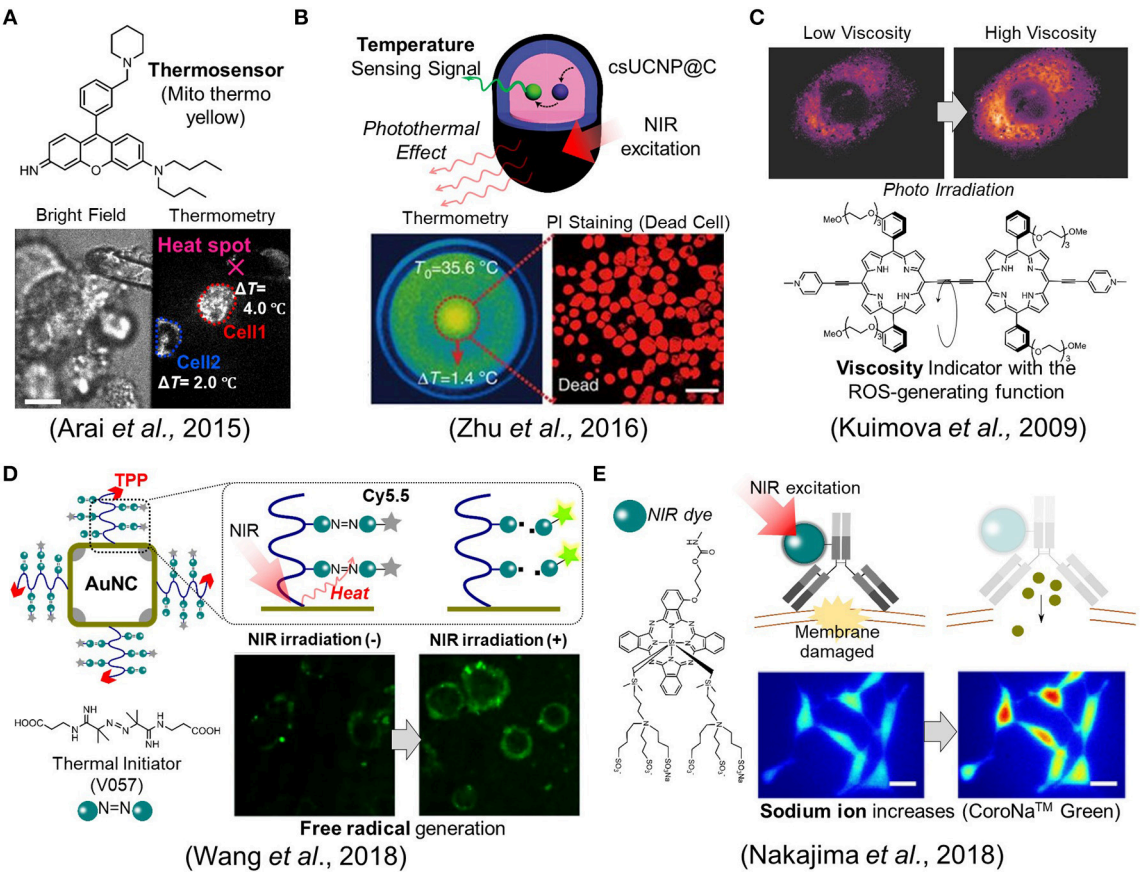

FIGURE 2 | Fluorescence imaging studies in biomaterials development. **(A)** A mitochondrial targeting temperature indicator (Mito thermo yellow) detected the different temperature increment of each cell within a bunch of HeLa cells. Scale bar, 10 μm. **(B)** The nanocomposite, csUCNP@C, which comprises a photothermal heater and a thermometer, allows the induction of cell death while concurrently measures the temperature. Scale bar, 50 μm. **(C)** The porphyrin-dimer functions as a photosensitizer and an intracellular viscosity indicator. **(D)** The gold nanocage (AuNC) which acts as an efficient photothermal material was decorated with the thermal initiator (V057) and a fluorescent dye (Cy5.5). The free radical species was generated following the cleavage of V057 by photothermal effect. The free radical generation could be monitored with the fluorescence intensity change of Cy5.5. **(E)** The ion indicator, CoroNa^{TM} Green, detected the sodium ion influx during photoimmunotherapy. Scale bar, 20 μm. Reproduced with permission from **(A)** (Arai et al., 2015); copyright Royal Society of Chemistry, **(B)** (Zhu et al., 2016); copyright Nature Publishing Group, **(C)** (Kuimova et al., 2009); copyright Nature Publishing Group, **(D)** (Wang et al., 2018); copyright American Chemical Society, and **(E)** (Nakajima et al., 2018); copyright John Wiley & Sons.

to target to mitochondria in order to maximize the therapeutic efficiency. Thus, the total system allows the induction of the cell death with concurrent monitoring of the free radical generation in the targeted mitochondria. It was also noted that this system works in both normoxic and hypoxic conditions because of the oxygen-independent principle.

(iii) Tackles for "unknown mechanism" and future perspective

Though not quite often, we sometime face complicated situations where a material works well in animals but its mechanism remains vague. In such cases, imaging technology can provide vital clues by visualizing the dynamics at a cellular level. Mitsunaga et al. pioneers in photoimmunotherapy, developed a near-infrared dye-labeled antibody that binds specifically to cancer cells and then effectively induces cell death via NIR illumination (Mitsunaga et al., 2011). The system is also able to work efficiently in animal level, although the mechanism still remains unclear at cellular level. Crucially, it is unlikely to result in ROS or heat production. Recently, Nakajima et al. investigated the mechanism regarding this photoimmunotherapy and then verified that the plasma membrane was damaged for a short time by observing the sodium ion influx using a fluorescent indicator (Nakajima et al., 2018). This minute damage on the membrane resulted in the increase (**Figure 2E**) of its permeability, cell swelling, and cell death. In this case, though it is not still perfectly understood, the imaging technique provided a hint to elucidate the unknown mechanism.

The importance of the physical stimulus will evolve following the development of biomaterials. This is because attempts to manipulate cellular functions using physical stresses is one of the biggest topics in biophysics, known as mechanobiology, providing fresh insights for material science. Pioneers in this field are dedicated to revealing how cells sense mechanical stress and

what the molecular players are (Uhler and Shivashankar, 2017). Concurrently, leading biologists have also produced various tools to help unveil the sensing mechanism at a molecular level; these tools will be of benefit to material scientists as well in the development of novel biomaterials. Ideally, the development of indicators, that are applicable for two-photon and NIR imaging, should be also significant to achieve the subcellular resolution for *in vivo* imaging using animals (Hong et al., 2017). We positively believe the promising future of imaging studies which will claim their place as a "must have" approach in biomaterials development.

AUTHOR CONTRIBUTIONS

F and SA conceived and revised the manuscript.

FUNDING

This work was partially supported by Japan Agency for Medical Research and Development (AMED) PRIME (JP18gm5810001), a Grant-in-Aid for Scientific Research on Innovative Areas Chemistry for Multimolecular Crowding Biosystems (18H04566) and a Grand-in-Aid for Young Scientists (A) (16H06044).

REFERENCES

Abbandonato, G., Polli, D., Viola, D., Cerullo, G., Storti, B., Cardarelli, F., et al. (2018). Simultaneous detection of local polarizability and viscosity by a single fluorescent probe in cells. *Biophys. J.* 114, 2212–2220. doi: 10.1016/j.bpj.2018.02.032

Arai, S., Kriszt, R., Harada, K., Looi, L. S., Matsuda, S., Wongso, D., et al. (2018). RGB-color intensiometric indicators to visualize spatiotemporal dynamics of ATP in single cells. *Angew. Chem. Int. Ed.* 57, 10873–10878. doi: 10.1002/anie.201804304

Arai, S., Lee, S.-C., Zhai, D., Suzuki, M., and Chang, Y.-T. (2014). A molecular fluorescent probe for targeted visualization of temperature at the endoplasmic reticulum. *Sci. Rep.* 4:6701. doi: 10.1038/srep06701

Arai, S., Suzuki, M., Park, S.-J., Yoo, J. S., Wang, L., Kang, N.-Y., et al. (2015). Mitochondria-targeted fluorescent thermometer monitors intracellular temperature gradient. *Chem. Commun.* 51, 8044–8047. doi: 10.1039/C5CC01088H

Battisti, A., Panettieri, S., Abbandonato, G., Jacchetti, E., Cardarelli, F., Signore, G., et al. (2013). Imaging intracellular viscosity by a new molecular rotor suitable for phasor analysis of fluorescence lifetime optical nanosensing in cells. *Anal. Bioanal. Chem.* 405, 6223–6233. doi: 10.1007/s00216-013-7084-x

Berg, J., Hung, Y. P., and Yellen, G. (2009). A genetically encoded fluorescent reporter of ATP:ADP ratio. *Nat. Methods* 6, 161–166. doi: 10.1038/NMETH.1288

Bilan, D. S., Pase, L., Joosen, L., Gorokhovatsky, A. Y., Ermakova, Y. G., Gadella, T. W. J., et al. (2013). HyPer-3: a genetically encoded H_2O_2 probe with improved performance for ratiometric and fluorescence lifetime imaging. *ACS Chem. Biol.* 8, 535–542. doi: 10.1021/cb300625g

Bizzarri, R., Serresi, M., Luin, S., and Beltram, F. (2009). Green fluorescent protein based pH indicators for *in vivo* use: a review. *Anal. Bioanal. Chem.* 393, 1107–1122. doi: 10.1007/s00216-008-2515-9

Boersma, A. J., Zuhorn, I. S., and Poolman, B. (2015). A sensor for quantification of macromolecular crowding in living cells. *Nat. Methods* 12, 227–229. doi: 10.1038/nmeth.3257

Chauhan, V. P., and Jain, R. K. (2013). Strategies for advancing cancer nanomedicine. *Nat. Mater.* 12, 958–962. doi: 10.1038/nmat3792

Dewey, W. C. (2009). Arrhenius relationships from the molecule and cell to the clinic. *Int. J. Hyperthermia* 25, 3–20. doi: 10.1080/02656730902747919

Discher, D. E., Janmey, P., and Wang, Y.-L. (2005). Tissue cells feel and respond to the stiffness of their substrate. *Science* 310, 1139–1143. doi: 10.1126/science.1116995

Franz, S., Rammelt, S., Scharnweber, D., and Simon, J. C. (2011). Immune responses to implants - A review of the implications for the design of immunomodulatory biomaterials. *Biomaterials* 32, 6692–6709. doi: 10.1016/j.biomaterials.2011.05.078

Fujie, T. (2016). Development of free-standing polymer nanosheets for advanced medical and health-care applications. *Polym. J.* 48, 773–780. doi: 10.1038/pj.2016.38

Giepmans, B. N. G., Adams, S. R., Ellisman, M. H., and Tsien, R. Y. (2010). The fluorescent toolbox for assessing. *Science* 217, 217–225. doi: 10.1126/science.1124618

Grashoff, C., Hoffman, B. D., Brenner, M. D., Zhou, R., Parsons, M., Yang, M. T., et al. (2010). Measuring mechanical tension across vinculin reveals regulation of focal adhesion dynamics. *Nature* 466, 263–266. doi: 10.1038/nature09198

Greenwald, E. C., Mehta, S., and Zhang, J. (2018). Genetically encoded fluorescent biosensors illuminate the spatiotemporal regulation of signaling networks. *Chem. Rev.* 118, 11707–11794. doi: 10.1021/acs.chemrev.8b00333

Harada, K., Ito, M., Wang, X., Tanaka, M., Wongso, D., Konno, A., et al. (2017). Red fluorescent protein-based cAMP indicator applicable to optogenetics and *in vivo* imaging. *Sci. Rep.* 7:7351. doi: 10.1038/s41598-017-07820-6

Heiden, M. G., Vander, C. L. C., Thompson, C. B., and Mammalian (2009). Understanding the warburg effect: the metabolic requirements of cell proliferation. *Science* 324, 1029–1034. doi: 10.1126/science.1160809

Hong, G., Antaris, A. L., and Dai, H. (2017). Near-infrared fluorophores for biomedical imaging. *Nat. Biomed. Eng.* 1:0010. doi: 10.1038/s41551-016-0010

Jung, H. S., Lee, J.-H., Kim, K., Koo, S., Verwilst, P., Sessler, J. L., et al. (2017). A mitochondria-targeted cryptocyanine-based photothermogenic photosensitizer. *J. Am. Chem. Soc.* 139, 9972–9978. doi: 10.1021/jacs.7b04263

Kang, N.-Y., Ha, H.-H., Yun, S.-W., Yu, Y. H., and Chang, Y.-T. (2011). Diversity-driven chemical probe development for biomolecules: beyond hypothesis-driven approach. *Chem. Soc. Rev.* 40, 3613–3626. doi: 10.1039/c0cs00172d

Kiyonaka, S., Kajimoto, T., Sakaguchi, R., Shinmi, D., Omatsu-Kanbe, M., Matsuura, H., et al. (2013). Genetically encoded fluorescent thermosensors visualize subcellular thermoregulation in living cells. *Nat. Methods* 10, 1232–1238. doi: 10.1038/nmeth.2690

Kuimova, M. K., Botchway, S. W., Parker, A. W., Balaz, M., Collins, H. A., Anderson, H. L., et al. (2009). Imaging intracellular viscosity of a single cell during photoinduced cell death. *Nat. Chem.* 1, 69–73. doi: 10.1038/nchem.120

Kurishita, Y., Kohira, T., Ojida, A., and Hamachi, I. (2012). Organelle-localizable fluorescent chemosensors for site-specific multicolor imaging of nucleoside polyphosphate dynamics in living cells. *J. Am. Chem. Soc.* 134, 18779–18789. doi: 10.1021/ja308754g

Liu, T., Liu, X., Spring, D. R., Qian, X., Cui, J., and Xu, Z. (2014). Quantitatively mapping cellular viscosity with detailed organelle information via a designed PET fluorescent probe. *Sci. Rep.* 4:5418. doi: 10.1038/srep05418

Luo, T., Mohan, K., Iglesias, P. A., and Robinson, D. N. (2013). Molecular mechanisms of cellular mechanosensing. *Nat. Mater.* 12, 1064–1071. doi: 10.1038/nmat3772

Manfredi, G., Yang, L., Gajewski, C. D., and Mattiazzi, M. (2002). Measurements of ATP in mammalian cells. *Methods* 26, 317–326. doi: 10.1016/S1046-2023(02)00037-3

Marino, A., Arai, S., Hou, Y., Degl'Innocenti, A., Cappello, V., Mazzolai, B., et al. (2017). Gold nanoshell-mediated remote myotube activation. *ACS Nano* 11, 2494–2505. doi: 10.1021/acsnano.6b08202

Marino, A., Arai, S., Hou, Y., Sinibaldi, E., Pellegrino, M., Chang, Y.-T., et al. (2015a). Piezoelectric nanoparticle-assisted wireless neuronal stimulation. *ACS Nano* 9, 7678–7689. doi: 10.1021/acsnano.5b03162

Marino, A., Filippeschi, C., Mattoli, V., Mazzolai, B., and Ciofani, G. (2015b). Biomimicry at the nanoscale: current research and perspectives of two-photon polymerization. *Nanoscale* 7, 2841–2850. doi: 10.1039/c4nr06500j

Marvin, J. S., Borghuis, B. G., Tian, L., Cichon, J., Harnett, M. T., Akerboom, J., et al. (2013). An optimized fluorescent probe for visualizing glutamate neurotransmission. *Nat. Methods* 10, 162–170. doi: 10.1038/nmeth.2333

Matsuyama, S., Llopis, J., and Deveraux, Q. (2000). Changes in intramitochondrial and cytosolic pH: early events that modulate caspase activation during apoptosis. *Nat. Cell Biol.* 2, 318–325. doi: 10.1038/35014006

Miesenböck, G., De Angelis, D. A., and Rothman, J. E. (1998). Visualizing secretion and synaptic transmission with pH-sensitive green fluorescent proteins. *Nature* 394, 192–195. doi: 10.1038/28190

Mitsunaga, M., Ogawa, M., Kosaka, N., Rosenblum, L. T., Choyke, P. L., and Kobayashi, H. (2011). Cancer cell–selective *in vivo* near infrared photoimmunotherapy targeting specific membrane molecules. *Nat. Med.* 17, 1685–1691. doi: 10.1038/nm.2554

Miyawaki, A., Llopis, J., Heim, R., McCaffery, J. M., Adams, J. A., Ikurak, M., et al. (1997). Fluorescent indicators for Ca^{2+} based on green fluorescent proteins and calmodulin. *Nature* 388, 882–887. doi: 10.1038/42264

Nakai, J., Ohkura, M., and Imoto, K. (2001). A high signal-to-noise Ca^{2+} probe composed of a single green fluorescent protein. *Nat. Biotechnol.* 3, 137–141. doi: 10.1038/84397

Nakajima, K., Takakura, H., Shimizu, Y., and Ogawa, M. (2018). Changes in plasma membrane damage inducing cell death after treatment with near-infrared photoimmunotherapy. *Cancer Sci.* 109, 2889–2896. doi: 10.1111/cas.13713

Nakano, M., Arai, Y., Kotera, I., Okabe, K., Kamei, Y., and Nagai, T. (2017). Genetically encoded ratiometric fluorescent thermometer with wide range and rapid response. *PLoS ONE* 12:e0172344. doi: 10.1371/journal.pone.0172344

Newman, R. H., Fosbrink, M. D., and Zhang, J. (2011). Genetically encodable fluorescent biosensors for tracking signaling dynamics in living cells. *Chem. Rev.* 111, 3614–3666. doi: 10.1021/cr100002u

Odaka, H., Arai, S., Inoue, T., and Kitaguchi, T. (2014). Genetically-encoded yellow fluorescent cAMP indicator with an expanded dynamic range for dual-color imaging. *PLoS ONE* 9:e100252. doi: 10.1371/journal.pone.0100252

Peer, D., Karp, J. M., Hong, S., Farokhzad, O. C., Margalit, R., and Langer, R. (2007). Nanocarriers as an emerging platform for cancer therapy. *Nat. Nanotechnol.* 2, 751–760. doi: 10.1038/nnano.2007.387

Russell, J. T. (2011). Imaging calcium signals *in vivo*: a powerful tool in physiology and pharmacology. *Br. J. Pharmacol.* 163, 1605–1625. doi: 10.1111/j.1476-5381.2010.00988.x

Sakaue-Sawano, A., Kurokawa, H., Morimura, T., Hanyu, A., Hama, H., Osawa, H., et al. (2008). Visualizing spatiotemporal dynamics of multicellular cell-cycle progression. *Cell* 132, 487–498. doi: 10.1016/j.cell.2007.12.033

San Martín, A., Ceballo, S., Ruminot, I., Lerchundi, R., Frommer, W. B., and Barros, L. F. (2013). A genetically encoded FRET lactate sensor and its use to detect the warburg effect in single cancer cells. *PLoS ONE* 8:e57712. doi: 10.1371/journal.pone.0057712

Shen, Y., Rosendale, M., Campbell, R. E., and Perrais, D. (2014). pHuji, a pH-sensitive red fluorescent protein for imaging of exo- and endocytosis. *J. Cell Biol.* 207, 419–432. doi: 10.1083/jcb.201404107

Specht, E. A., Braselmann, E., and Palmer, A. E. (2017). A critical and comparative review of fluorescent tools for live-cell imaging. *Annu. Rev. Physiol.* 79, 93–117. doi: 10.1146/annurev-physiol-022516-034055

Stanley, S. A., Gagner, J. E., Damanpour, S., Yoshida, M., Dordick, J. S., and Friedman, J. M. (2012). Radio-wave heating of iron oxide nanoparticles can regulate plasma glucose in mice. *Science* 336, 604–608. doi: 10.1126/science.1216753

Sulis Sato, S., Artoni, P., Landi, S., Cozzolino, O., Parra, R., Pracucci, E., et al. (2017). Simultaneous two-photon imaging of intracellular chloride concentration and pH in mouse pyramidal neurons *in vivo*. *Proc. Natl. Acad. Sci. U.S.A.* 114, E8770–E8779. doi: 10.1073/pnas.1702861114

Sunahara, H., Urano, Y., Kojima, H., and Nagano, T. (2007). Design and synthesis of a library of BODIPY-based environmental polarity sensors utilizing photoinduced electron-transfer-controlled fluorescence ON/OFF switching. *J. Am. Chem. Soc.* 129, 5597–5604. doi: 10.1021/ja068551y

Takei, Y., Murata, A., Yamagishi, K., Arai, S., Nakamura, H., Inoue, T., et al. (2013). Intracellular click reaction with a fluorescent chemical Ca^{2+} indicator to prolong its cytosolic retention. *Chem. Commun.* 49, 7313–7315. doi: 10.1039/c3cc42489h

Tantama, M., Martínez-François, J. R., Mongeon, R., and Yellen, G. (2013). Imaging energy status in live cells with a fluorescent biosensor of the intracellular ATP-to-ADP ratio. *Nat. Commun.* 4:2550. doi: 10.1038/ncomms3550

Tsuyama, T., Kishikawa, J.-I., Han, Y.-W., Harada, Y., Tsubouchi, A., Noji, H., et al. (2013). *in vivo* fluorescent adenosine 5'-triphosphate (ATP) imaging of *Drosophila melanogaster* and *Caenorhabditis elegans* by using a genetically encoded fluorescent ATP biosensor optimized for low temperatures. *Anal. Chem.* 85, 7889–7896. doi: 10.1021/ac4015325

Uhler, C., and Shivashankar, G. V. (2017). Regulation of genome organization and gene expression by nuclear mechanotransduction. *Nat. Rev. Mol. Cell Biol.* 18, 717–727. doi: 10.1038/nrm.2017.101

Wagner, V., Dullaart, A., Bock, A.-K., and Zweck, A. (2006). The emerging nanomedicine landscape. *Nat. Biotechnol.* 24, 1211–1217. doi: 10.1038/nbt1006-1211

Wang, X. Q., Peng, M., Li, C. X., Zhang, Y., Zhang, M., Tang, Y., et al. (2018). Real-time imaging of free radicals for mitochondria-targeting hypoxic tumor therapy. *Nano Lett.* 18, 6804–6811. doi: 10.1021/acs.nanolett.8b02670

Yaginuma, H., Kawai, S., Tabata, K. V., Tomiyama, K., Kakizuka, A., Komatsuzaki, T., et al. (2014). Diversity in ATP concentrations in a single bacterial cell population revealed by quantitative single-cell imaging. *Sci. Rep.* 4:6522. doi: 10.1038/srep06522

Ye, K., and Schultz, J. S. (2003). Genetic engineering of an allosterically based glucose indicator protein for continuous glucose monitoring by fluorescence resonance energy transfer. *Anal. Chem.* 75, 3451–3459. doi: 10.1021/ac034022q

Yhee, J. Y., Lee, S., and Kim, K. (2014). Advances in targeting strategies for nanoparticles in cancer imaging and therapy. *Nanoscale* 6, 13383–13390. doi: 10.1039/c4nr04334k

Zhang, Y., Ang, C. Y., and Zhao, Y. (2015). Polymeric nanocarriers incorporating near-infrared absorbing agents for potent photothermal therapy of cancer. *Polym. J.* 48, 1–15. doi: 10.1038/pj.2015.117

Zhang, Z., Wang, J., and Chen, C. (2013). Near-infrared light-mediated nanoplatforms for cancer thermo-chemotherapy and optical imaging. *Adv. Mater.* 25, 3869–3880. doi: 10.1002/adma.201301890

Zhao, Y., Araki, S., Wu, J., Teramoto, T., Chang, Y.-F., Nakano, M., et al. (2011). An expanded palette of genetically encoded Ca^{2+} indicators. *Science* 333, 1888–1891. doi: 10.1126/science.1208592

Zhu, X., Feng, W., Chang, J., Tan, Y., Chen, M., Zou, X., et al. (2016). Temperature-feedback upconversion nanocomposite for accurate photothermal therapy at facile temperature. *Nat. Commun.* 7:10437. doi: 10.1038/ncomms10437

Conflict of Interest Statement: The authors declare that the research was conducted in the absence of any commercial or financial relationships that could be construed as a potential conflict of interest.

frontiers in Bioengineering and Biotechnology

MINI REVIEW
published: 04 January 2019
doi: 10.3389/fbioe.2018.00204

Bright Dots and Smart Optical Microscopy to Probe Intracellular Events in Single Cells

Hideaki Fujita[1], *Chongxia Zhong*[2], *Satoshi Arai*[3,4] *and Madoka Suzuki*[2,5]*

[1] WASEDA Bioscience Research Institute in Singapore, Singapore, Singapore, [2] Institute for Protein Research, Osaka University, Osaka, Japan, [3] Research Institute for Science and Engineering, Waseda University, Tokyo, Japan, [4] PRIME-AMED, Tokyo, Japan, [5] PRESTO, Japan Science and Technology Agency, Saitama, Japan

Probing intracellular events is a key step in developing new biomedical methodologies. Optical microscopy has been one of the best options to observe biological samples at single cell and sub-cellular resolutions. Morphological changes are readily detectable in brightfield images. When stained with fluorescent molecules, distributions of intracellular organelles, and biological molecules are made visible using fluorescence microscopes. In addition to these morphological views of cells, optical microscopy can reveal the chemical and physical status of defined intracellular spaces. This review begins with a brief overview of genetically encoded fluorescent probes and small fluorescent chemical dyes. Although these are the most common approaches, probing is also made possible by using tiny materials that are incorporated into cells. When these tiny materials emit enough photons, it is possible to draw conclusions about the environment in which the tiny material resides. Recent advances in these tiny but sufficiently bright fluorescent materials are nextly reviewed to show their applications in tracking target molecules and in temperature imaging of intracellular spots. The last section of this review addresses purely optical methods for reading intracellular status without staining with probes. These non-labeling methods are especially essential when biospecimens are thereafter required for *in vivo* uses, such as in regenerative medicine.

Keywords: fluorescent protein, nanoparticle, infrared, nanodiamond, quantum dot, Raman, temperature

OPEN ACCESS

Edited by:
Gianni Ciofani,
Politecnico di Torino, Italy

Reviewed by:
Tzu-Ming Liu,
University of Macau, China
Satya Ranjan Sarker,
Jahangirnagar University, Bangladesh
Takayuki Uchihashi,
Nagoya University, Japan

***Correspondence:**
Madoka Suzuki
suzu_mado@protein.osaka-u.ac.jp

Specialty section:
This article was submitted to Nanobiotechnology, a section of the journal Frontiers in Bioengineering and Biotechnology

Received: *11 October 2018*
Accepted: *12 December 2018*
Published: *04 January 2019*

Citation:
Fujita H, Zhong C, Arai S and Suzuki M (2019) Bright Dots and Smart Optical Microscopy to Probe Intracellular Events in Single Cells. Front. Bioeng. Biotechnol. 6:204. doi: 10.3389/fbioe.2018.00204

INTRODUCTION

Since Robert Hooke observed a cork and named a compartment he found within it a "cell" using a simple microscope composed of two lenses in the 17th century, microscopic observation has become one of the most essential techniques in cell biology. Most animal cells are almost transparent and various techniques were developed to image these transparent cells. The simplest method is to label the cells with colored probes. Haematoxylin-Eosin staining was introduced back in the 19th century and it is still commonly used in histological labs for diagnostics. Now, there are many probes with various functions and characteristics (**Figure 1**), which are briefly summarized in section Genetically encoded probes vs. chemical dyes to highlight the variety. These fluorescent probes were not designed to work on single molecules. The signal is captured as an average value of many molecules. When many molecules are concentrated in a small space, a bright fluorescent nanoprobe can be obtained. When optical microscopy is optimized for nanoprobes, location tracking as well as environment probing are made possible using a single particle.

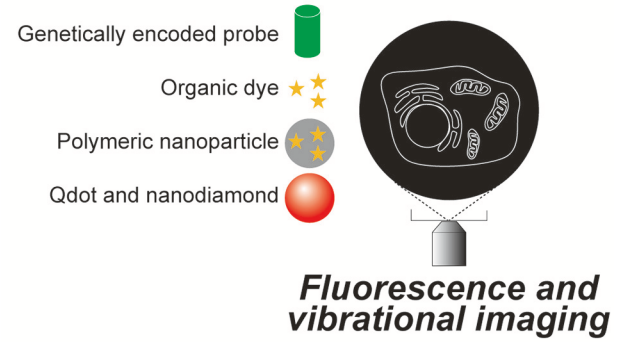

FIGURE 1 | Fluorescent probes and optical microscopy techniques introduced in this review.

Section Bright nano-dots as single probes for tracking of this review focuses on nanoprobes that are designed to be imaged one by one with a purpose to monitor intracellular parameters such as the location of biomolecules and spatial and temporal changes in temperature. Other methods do not involve staining. Differential interference contrast microscopy and phase contrast microscopy both utilize the phase shift between the illuminating light and the light which passes through the specimen and in so doing can visualize transparent cells without labeling. These are not discussed in this review as there is much less information on the cellular states that can be determined using these techniques when compared to the other methods we will discuss. Imaging utilizing the vibrational information of a molecule is discussed in section Imaging technologies without labeling of this review (**Figure 2**).

GENETICALLY ENCODED PROBES VS. CHEMICAL DYES

Fluorescent sensors are defined as those in which the signal, such as fluorescence intensity, wavelength, or lifetime, is altered in response to a change in the environment. They are called fluorescent probes, indicators, and sensors (hereafter referred to as "fluorescent probes") (Zhang et al., 2002). The probes can be broadly categorized into two groups: genetically encoded probes and small chemical dyes. Which probe to choose depends on what intracellular events need monitoring and the duration of the observation.

Genetically Encoded Fluorescent Probes

From the standpoint of long-term observation in fluorescence microscopy, genetically encoded probes are preferred. If we are keen to make observations for a few hours or days using small molecule indicators, we need to employ the strategy where the dyes are anchored to the target places or proteins covalently, which is still challenging (Wakayama et al., 2017). Also, to specifically observe an evenet of interest, genetically encoded probes once again prevail over small chemical dyes due to the working mechanism that they employ. The ability of natural proteins to bind to a specific target is adaptable in genetically encoded probes, while small chemical indicators use synthetic modules for sensing which are usually less specific to the target molecule than natural counterparts. Thus, genetically encoded probes exhibit better specificity to a target, especially against small molecules such as Ca^{2+}, cAMP, ATP, and glucose (DiPilato et al., 2004; Imamura et al., 2009; Zhao et al., 2011; Hofig et al., 2018).

Regarding the delivery of probes into cells, genetically encoded probes require transfection using reagents, or physical delivery. To evaluate the probes for more than several days, preparation of a stable cell line into which the genetic code of the probe is integrated into the genome is necessary. Also, if transfection is difficult, such as in the case of primary cultured cells, viral infection is unavoidable. Another feature worth highlighting is that the location of the probes can be controlled at an organelle level. For example, a target sequence, such as for the nucleus (nuclear localization signal), mitochondria (subunit VIII of cytochrome c oxidase), or cellular membrane (growth-associated protein 43, neuromodulin), is conjugated to the N or C terminus of the probe, which then selectively localizes the probe to the target organelle (De Giorgi et al., 1999; Arai et al., 2018). Lastly, once the plasmid for a probe is purchased or given as a gift from the developer, it is always possible to amplify the plasmid at little cost.

Organic Dyes

One may feel that genetically encoded probes are the perfect choice. However, there is one critical issue–ease of handling. Genetically encoded probes require around 1–3 days for expression in cells after delivery of the gene. On the other hand, small chemical indicators are easy to apply for staining, usually taking around 30 min to take effect before imaging can begin (Zhu et al., 2016). For those who rarely perform molecular biology protocols, transfection might be difficult to apply to their biospecimens or it may be that the use of viruses for infection is not allowed in their laboratory. In some cases, biological samples cannot withstand the 1 day incubation time needed for gene expression. In these instances small chemical dyes are the only remaining option. Across the field of research, imaging is often required for a variety of cell and tissue types, as well as different animal species, beyond that of commonly used cell lines (Vendrell et al., 2012). Gene delivery frequently proves to be a challenge under these conditions. Small chemical dyes can therefore prove to be helpful and even be considered the first choice for imaging. One can find in the literature positive examples of labeling using small near-infrared dyes in biomedical research at tissue and animal levels (Hong et al., 2017). The purpose of the experiment and the type of specimen should always be the primary factors in determining which probes to use, regardless of whether they are small chemical dyes, or genetically encoded probes.

These fluorescent probes were designed to take an average of many molecules to measure a given parameter. Thus, spatial resolution is limited by optical microscopy. Are there means to

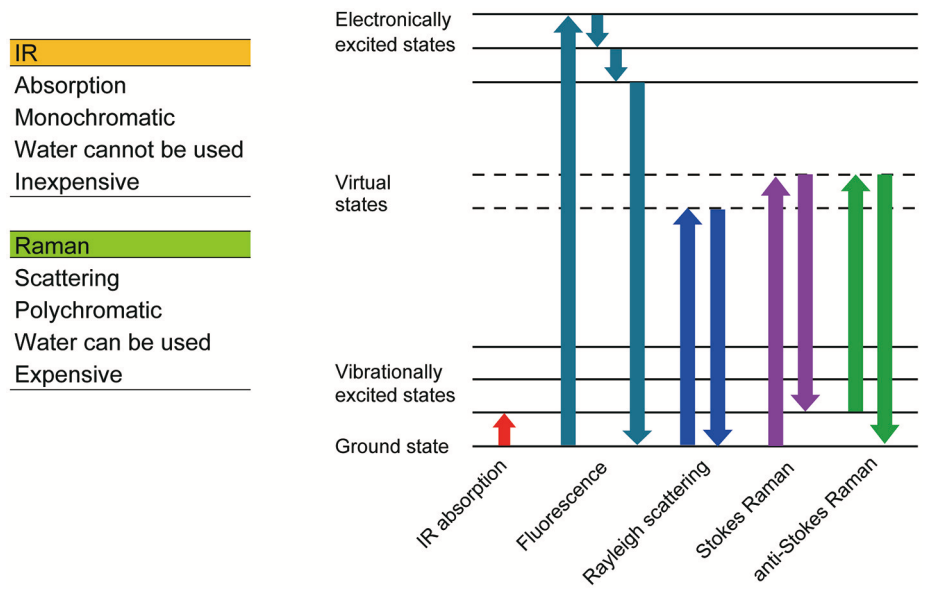

FIGURE 2 | Comparison between Raman and IR spectrometry.

improve accuracy in location while probing parameters using optical microscopy?

BRIGHT NANO-DOTS AS SINGLE PROBES FOR TRACKING

The accumulation of fluorescent molecules creates a fluorescent nanoparticle. Quantum dots (Qdots) and nanodiamonds are also nanoparticles that emit photons upon excitation by light. These nanoparticles can be so bright that each dot is tracked in single camera frames repeatedly at 30 Hz or faster. When the nanoparticle is designed as a sensor, it is possible to probe the position of the nanoparticle as well as garner information about its local environment. If said probing is repeated frame by frame, time courses of the measured parameters can be obtained instantly. Among the large variety of applications of nanoparticles for probing, temperature sensing is one of the most advanced for biological usage. As the temperature is a fundamental parameter that can influence chemical and physical processes in any biological systems, the mechanism how living organism senses the temperature and how it releases heat in its body has been one of the major research topics in biology, and in animal, and plant physiologies. Recent advances in optical probes has brought our interest from the macroscopic (such as the temperature of the animal body or of the cell culture medium) to microscopic scale as small as a single cell. However, local event of heat release is still unclarified in live cells. Excellent reviews on fluorescent thermometers in general can be found in the literature (Brites et al., 2012; Wang et al., 2013). Lists detailing the advantages and disadvantages of materials and methods, operating principles, accuracy, and resolution of sensing have been described in reviews (Brites et al., 2012; Wang et al., 2013; Suzuki et al., 2016; Arai and Suzuki, 2018), as well as debates on single-cell thermometry (Baffou et al., 2014, 2015; Kiyonaka et al., 2015; Suzuki et al., 2015). Instead of repeating these details, this section introduces fluorescent nanoparticles that have been applied for probing purposes, including temperature sensing, with single particle analyses in physiological situations. Their functional ranges cover the temperature from ∼25°C to ∼42°C. Although the accuracy of determining the temperature depends on the optical setup that reads out signals from the probe, 0.5°C or better values are frequently reported. The nanoparticles can be further "functionalized" to target biological molecules and organelles.

Fluorescent Polymeric Nanoparticles for Probing Temperature Changes

We have developed fluorescent polymeric nanoparticles that are able to probe temperature changes in single cells (Oyama et al., 2012; Takei et al., 2014). Each nanoparticle contains temperature-sensitive fluorophores such as Eu-thenolytrifluoroacetonate (EuTTA) or Eu-tris(dinaphthoylmethane)-bis-trioctylphosphine oxide) (EuDT), of which emission intensities inversely correlate with temperature changes. In some cases, less temperature-sensitive fluorophores were also embedded in the same polymeric matrix to form a nanoparticle, whose surface is further covered by a hydrophilic polymer outer layer (Takei et al., 2014; Arai et al., 2015; Ferdinandus et al., 2016). Measurement of the temperature can be achieved by determining the reduction of emission intensity of EuTTA or EuDT, or by the ratio of the intensity of EuTTA or EuDT to that of the less temperature-sensitive fluorophores which act as internal references. The nanoparticle thermosensor assures strong emission intensity since it can pack multiple fluorophores into one particle. Furthermore, it is capable

of measuring temperature without being affected by various intracellular factors, such as pH, viscosity, ionic strength, etc.

Quantum Dots

Qdots are fluorescent semiconductor nanocrystals which possess distinct optical and electrical properties. These properties render Qdots as a promising alternative to organic dyes in biological applications from cell biology to *in vitro* diagnostics. Qdots have broad excitation spectra and narrow emission spectra, which are composition- and size-dependent. Furthermore, the strong photoluminescence and high photostability of Qdots enable them to play an important role in single particle tracking (Michalet et al., 2005; Ichimura et al., 2014b; Pisanic et al., 2014). Applications in intracellular temperature measurement have also been reported using the shift of emission spectra caused by temperature changes (Yang et al., 2011; Tanimoto et al., 2016).

Functionalization is essential for Qdots to be applied to biological investigations. Being mostly synthesized in organic solvents, Qdots are too hydrophobic to be dissolved in aqueous buffers. Ligand exchange with hydrophilic compounds or encapsulation within amphiphilic coatings are therefore necessary to achieve solubility in water. Surface modification of Qdots provides an interface for conjugating to target molecules (cf. section Targeting).

Blinking and cytotoxicity are two major weak points of Qdots, which limit their biological and therapeutic applications. Blinking, also called intermittent fluorescence, is the phenomenon of a single Qdot particle exhibiting light and dark periods under continuous laser illumination (Ko et al., 2011). Blinking interferes with the tracing process in single-particle tracking studies. Both cadminium-containing and cadminium-free Qdots were found to induce the elevation of intracellular reactive oxygen species levels and increase cell apoptosis, which contributes to a decrease in cell viability (Derfus et al., 2004). Qdots in high concentrations also affect embryo development (Dubertret et al., 2002).

Fluorescent Nanodiamonds

One of the newly emerging fluorescent probes is nanodiamonds containing nitrogen vacancy centers (NVCs) (Chang et al., 2018). An NVC is composed of a substitutional nitrogen adjacent to a defect in the lattice. The NVC excited by green light emits light in the range of red. Thus, the nanodiamonds containing NVCs are called fluorescent nanodiamonds. When NVCs are embedded within the nanodiamond they show an outstanding robustness to changes in environmental parameters (Sekiguchi et al., 2018). Similar to Qdots, fluorescent nanodiamonds are extremely photostable. In contrast to Qdots, no blinking is observed. Modification of the surface is also relatively easy (Sotoma et al., 2018); e.g., Tsai et al. successfully used this advantage to attach gold nanorods as tiny heat sources onto the surface of nanodiamonds to probe the local temperature at the heated dot (Tsai et al., 2017). Biocompatibility has been shown to be good. Bearing these advantages in mind, fluorescent nanodiamonds can be considered close to the ideal fluorescent probe.

There remain at least two issues regarding the use of fluorescent nanodiamonds as probes. Firstly, the NVC can be exposed at the surface of the nanodiamond, thus eradicating its robustness to the surrounding environment. Greater care should therefore be taken as the diameter of the nanodiamond gets smaller. Secondly, measurement can require long periods of time when extreme accuracy is required or when the amount of NVCs in the nanodiamond is reduced. For example, it is possible to measure the temperature using the negatively charged NVC, NV^-. All optical methods detect changes of the emission peak by changing temperature (Plakhotnik et al., 2014). The temperature-dependent status of NV^- can also be detected by the downward peaks in emission intensity when the microwave is swept, known as optically detected magnetic resonance, or ODMR (Kucsko et al., 2013). Collecting enough photons or sweeping the microwave is required to draw spectra to determine the peaks. Efforts to shorten the sweeping process continue (Tzeng et al., 2015).

Targeting

It is a challenging task to target nanoparticles to specific cells, organelles, or molecules within a living cell. Yet several attempts have been successful in biological uses. In *in vivo* conditions, a probe was prepared based on Qdots by immobilizing a ligand with a high affinity for hexahistidine (Arai et al., 2012). By using this Qdot probe, single molecule-tracking of his-tagged myosin V was achieved. Fujita et al. discovered the major sequestration mechanism for glucose transporter 4 in fully differentiated single 3T3L1 adipocytes (Fujita et al., 2010). Gonda et al. conjugated anti-protease-activated receptor1, a tumor cell membrane protein, with Qdots to uncover changes in membrane fluidity and morphology during tumor metastasis in living mice (Gonda et al., 2010). The extreme photostability of Qdots was one of the major reasons that these studies were made possible. More recently, single nanodiamonds surface functionalized with poly-dopamine followed by thiol terminated poly (ethylene glycol) were successfully targeted to single DNAs using the avidin-biotin system to track their locations (Jung et al., 2018).

There are other types of nanoparticles that are constructed step-by-step directly within living cells at the desired target regions. The first step is to prepare cells expressing single chain avidin (ScAVD) at the target region. The second and the third are to incubate the cells with dibenzocyclooctyne-biotin followed by azide-functionalized organic dyes to perform a copper-free click reaction to construct a ScAVD-biotin-functional dye conjugated nanoprobe (Hou et al., 2016a,b). These nanoprobes have increased brightness and photostability as well as improved localization specificity when compared to single fluorescent dyes.

IMAGING TECHNOLOGIES WITHOUT LABELING

Although labeling is a powerful technique to visualize the structure of the cell, it is not always preferred. Even when using a bio-safe dye, the detection of cancerous tissue using a labeling method during a surgical operation can significantly prolong the

surgery, which increases the chances of complications. Labeling is also not preferred when producing cells for regenerative medicine. In this section, we introduce imaging techniques that don't require labeling. Raman microscopy and fluorescent lifetime imaging microscopy (FLIM) using auto-florescence are discussed (**Figure 2**).

Raman Imaging Spectroscopy

When light enters a molecule, three types of scatters are generated, Reyleigh scattering, Stokes Raman scattering, and anti-Stokes Raman scattering. Reyleigh scattering has the same energy as incident light, whereas Stokes and anti-Stokes Raman scattering have less and more energy than incident light, respectively. The shift in wavelength (Raman shift) relates to the chemical bonds within the molecule, thus the molecule can be identified using the Raman spectrum. Raman spectroscopy is a non-labeling and non-destructive analysis method, which can obtain information relating to the chemical bonds of a molecule.

Raman imaging spectroscopy usually uses visible light for illumination so the optical resolution is generally higher than Infrared (IR) imaging spectroscopy. Other than standard Spontaneous Raman spectroscopy, there are several other modes of Raman imaging techniques, including Coherent anti-Stokes Raman spectroscopy (CARS), Surface-enhanced Raman spectroscopy (SERS), and Stimulated Raman spectroscopy (SRS). The various types of Raman spectroscopy are reviewed in Krafft and Popp (Krafft and Popp, 2015).

Raman spectra can be used to identify the state of the cell, thus, clinical diagnosis is possible at a tissue level. Raman spectroscopy has been used diagnostically for cancer (Austin et al., 2016; Santos et al., 2017), atherosclerosis (MacRitchie et al., 2018) and liver steatosis (Pacia et al., 2018). Raman imaging of living cells was difficult because the Raman signal is far weaker than fluorescence; strong illumination with a visible laser and a long exposure is therefore needed, which significantly damages the cell. However, recent advances in detectors, spectroscopes, and optical filters have enabled Raman imaging of living cells (Hamada et al., 2008). Now, cell state can be monitored using Raman spectroscopy at a single cell level (Ichimura et al., 2014a, 2015, 2016).

Fluorescent Lifetime Imaging (FLIM)

FLIM is one of the most important technologies in optical microscopy, especially in live cell imaging, as fluorescence lifetime is independent of fluorophore concentration and focus drift. FLIM has been frequently used in Förester resonance energy transfer (FRET) based on fluorescent sensors that comprise two fluorescent proteins as a donor and an acceptor. The lifetime of the fluorescent protein is altered during energy transfer, thus a FRET sensor can be applied for FLIM. As such, small chemical sensors are also possible for FLIM, which are sensitive to the surrounding environment in the fluorescence lifetime domain. For successful examples, intracellular conditions such as levels of Ca^{2+} (Zheng et al., 2018), K^+ (Paredes et al., 2013), Na^+ (Roder and Hille, 2014), and Cl^- (Chao et al., 1989), as well as pH (Schmitt et al., 2014), and temperature (Itoh et al., 2016) can be monitored using FLIM. FLIM can also be performed in non-label imaging as there are naturally occurring endogenous fluorescent biomolecules, such as reduced nicotinamide adenine dinucleotide (phosphate) [NAD(P)H] and flavines present in the cell. Using FLIM, NADH, and NADPH can be distinguished and the relative ratio can be calculated, which is not possible using fluorescence intensity as their spectra are identical (Blacker et al., 2014).

FLIM using auto fluorescence, which is non-labeling, is especially useful in diagnostic purposes. Detection of macrophages in an atherosclerotic model (Marcu et al., 2005), glioma in brain tissue (Yong et al., 2006), retinal pigment epithelium (Miura, 2018), and basal cell carcinoma in skin (Galletly et al., 2008) are made possible using FLIM. Two-photon FLIM is preferred for tissue diagnostics purposes as it reduces photo-damage to the cells and reaches deeper within the tissue. Two-photon excitation is now used to distinguish between papillary and reticular dermis (Shirshin et al., 2017), in the diagnostics of inflamed human skin (Huck et al., 2016), and in melanoma detection (Seidenari et al., 2013). Second Harmonic Generation (SHG) and two-photon FLIM can be combined to increase the information obtained and used in diagnosis as the same laser source can be used (Provenzano et al., 2009; Ranjit et al., 2016).

Other Non-label Imaging Technologies

There are other modes of non-label imaging technologies such as SHG and infrared (IR) spectroscopy. The information obtained by IR spectroscopy complements that obtained by Raman spectroscopy as when the IR signal from a particular chemical bond is strong, the signal obtained from Raman spectroscopy is weak, and vice versa. A number of products capable of obtaining Raman, FLIM, or IR are released every year, which will further advance this field.

SUMMARY

Nanotechnology provides tools to control, create, or cure biospecimens. The effect should be evaluated in a quantitative manner to gauge the efficacy of the methods or the quality of the results. Optical microscopy can provide essential information on how and why samples have reacted at sub-cellular resolution. Observation of morphological changes of cells (e.g., axon-like elongation for neuronal cells, multi-nucleus, and contractile structures in muscular cells, or lipid droplets in adipocytes) is one of the first steps to be performed. Probing intracellular reactions provides additional and much more detailed insights. In this article, we reviewed optical methods to probe intracellular events at sub-cellular resolutions in living cells using optical microscopes. Some methods use fluorescent nanoprobes, several of which are designed to change their properties in fluorescence in response to changes in the chemical and physical conditions surrounding the probe. Other methods do not require these tiny probes, but are performed in purely optical manner. Considering the ease of availability, optical microscopy should continue to be a standard method. With the wide variety in probes as well as in equipment, methods are available to meet a range of specific

needs. Optimal choices will always be dependent on the sample being studied.

AUTHOR CONTRIBUTIONS

HF, SA, and MS conceived the story. All the authors co-wrote and critically revised the manuscript.

ACKNOWLEDGMENTS

This work was supported by JSPS KAKENHI Grant Numbers JP15K05251 (to MS), by the Japan Science and Technology Agency Grant Number JPMJPR15F5 (to MS), by the Human Frontier Science Program RGP0047/2018 (to MS), and by Kurita Water and Environment Foundation 17D002 (to MS).

REFERENCES

Arai, S., Ferdinandus, Takeoka, S., Ishiwata, S., and Suzuki, M. (2015). Micro-thermography in millimeter-scale animals by using orally-dosed fluorescent nanoparticle thermosensors. *Analyst* 140, 7534–7539. doi: 10.1039/c5an01287b

Arai, S., Hirosawa, S., Oguchi, Y., Suzuki, M., Murata, A., Ishiwata, S., et al. (2012). Mass spectrometric screening of ligands with lower off-rate from a clicked-based pooled library. *ACS Combi. Sci*. 14, 451–455. doi: 10.1021/co300028n

Arai, S., Kriszt, R., Harada, K., Looi, L. S., Matsuda, S., Wongso, D., et al. (2018). RGB-color intensiometric indicators to visualize spatiotemporal dynamics of ATP in single cells. *Angew. Chem. Int. Ed*. 57, 10873–10878. doi: 10.1002/anie.201804304

Arai, S., and Suzuki, M. (2018). "Nano-sized optical thermometers," in *Smart Nanoparticles for Biomedicine*, ed. G. Ciofani (Amsterdam: Elsevier), 199–217. doi: 10.1016/B978-0-12-814156-4.00014-8

Austin, L. A., Osseiran, S., and Evans, C. L. (2016). Raman technologies in cancer diagnostics. *Analyst* 141, 476–503. doi: 10.1039/C5AN01786F

Baffou, G., Rigneault, H., Marguet, D., and Jullien, L. (2014). A critique of methods for temperature imaging in single cells. *Nat. Methods* 11, 899–901. doi: 10.1038/nmeth.3073

Baffou, G., Rigneault, H., Marguet, D., and Jullien, L. (2015). Reply to: "Validating subcellular thermal changes revealed by fluorescent thermosensors" and "The 10(5) gap issue between calculation and measurement in single-cell thermometry." *Nat. Methods* 12, 803. doi: 10.1038/nmeth.3552

Blacker, T. S., Mann, Z. F., Gale, J. E., Ziegler, M., Bain, A. J., Szabadkai, G., et al. (2014). Separating NADH and NADPH fluorescence in live cells and tissues using FLIM. *Nat. Commun.* 5:3936. doi: 10.1038/ncomms4936

Brites, C. D., Lima, P. P., Silva, N. J.I, Millán, A., Amaral, V. S., Palacio, F., and Carlos, L. D. (2012). Thermometry at the nanoscale. *Nanoscale* 4, 4799–4829. doi: 10.1039/c2nr30663h

Chang, H.-C., Hsiao, W. W.-W., and Su, M.-C. (2018). *Fluorescent Nanodiamonds*. Chichester: John Wiley & Sons. doi: 10.1002/9781119477099

Chao, A. C., Dix, J. A., Sellers, M. C., and Verkman, A. S. (1989). Fluorescence measurement of chloride transport in monolayer cultured cells. Mechanisms of chloride transport in fibroblasts. *Biophys. J.* 56, 1071–1081. doi: 10.1016/S0006-3495(89)82755-9

De Giorgi, F., Ahmed, Z., Bastianutto, C., Brini, M., Jouaville, L. S., Marsault, R., et al. (1999). Targeting GFP to organelles. *Methods Cell Biol*. 58, 75–85. doi: 10.1016/S0091-679X(08)61949-4

Derfus, A.M., Chan, W.C.W., and Bhatia, S.N., (2004). Probing the cytotoxicity of semiconductor quantum dots. *Nano Lett*. 4, 11–18. doi: 10.1021/nl0347334

DiPilato, L. M., Cheng, X., and Zhang, J. (2004). Fluorescent indicators of cAMP and Epac activation reveal differential dynamics of cAMP signaling within discrete subcellular compartments. *Proc. Natl. Acad. Sci. U.S.A*. 101, 16513–16518. doi: 10.1073/pnas.0405973101

Dubertret, B., Skourides, P., Norris, D. J., Noireaux, V., Brivanlou, A. H., and Libchaber, A. (2002). *In vivo* imaging of quantum dots encapsulated in phospholipid micelles. *Science* 298, 1759–1762. doi: 10.1126/science.1077194

Ferdinandus, Arai, S., Takeoka, S., Ishiwata, S., Suzuki, M., and Sato, H. (2016). Facilely fabricated luminescent nanoparticle thermosensor for real-time microthermography in living animals. *ACS Sens.* 1, 1222–1227. doi: 10.1021/acssensors.6b00320

Fujita, H., Hatakeyama, H., Watanabe, T. M., Sato, M., Higuchi, H., and Kanzaki, M. (2010). Identification of three distinct functional sites of insulin-mediated GLUT4 trafficking in adipocytes using quantitative single molecule imaging. *Mol. Biol. Cell*. 21, 2721–2731. doi: 10.1091/mbc.e10-01-0029

Galletly, N. P., McGinty, J., Dunsby, C., Teixeira, F., Requejo-Isidro, J., Munro, I., et al. (2008). Fluorescence lifetime imaging distinguishes basal cell carcinoma from surrounding uninvolved skin. *Br. J. Dermatol.* 159, 152–161. doi: 10.1111/j.1365-2133.2008.08577.x

Gonda, K., Watanabe, T.M., Ohuchi, N., and Higuchi, H. (2010). *In vivo* nano-imaging of membrane dynamics in metastatic tumor cells using quantum dots. *J. Biol. Chem*. 285, 2750–2757. doi: 10.1074/jbc.M109.075374

Hamada, K., Fujita, K., Smith, N. I., Kobayashi, M., Inouye, Y., and Kawata, S. (2008). Raman microscopy for dynamic molecular imaging of living cells. *J. Biomed. Opt*. 13:044027. doi: 10.1117/1.2952192

Hofig, H., Otten, J., Steffen, V., Pohl, M., Boersma, A. J., and Fitter, J. (2018). Genetically encoded forster resonance energy transfer-based biosensors studied on the single-molecule level. *ACS Sens*. 3, 1462–1470. doi: 10.1021/acssensors.8b00143

Hong, G., Antaris, A.L., and Dai, H. (2017). Near-infrared fluorophores for biomedical imaging. *Nat. Biomed. Eng*. 1:0010. doi: 10.1038/s41551-016-0010

Hou, Y., Arai, S., Kitaguchi, T., and Suzuki, M. (2016a). Intracellular bottom-up generation of targeted nanosensors for single-molecule imaging. *Nanoscale* 8, 3218–3225. doi: 10.1039/C5NR08012F

Hou, Y., Arai, S., Takei, Y., Murata, A., Takeoka, S., and Suzuki, M. (2016b). Focal calcium monitoring with targeted nanosensors at the cytosolic side of endoplasmic reticulum. *Sci. Technol. Adv. Mater*. 17, 293–299. doi: 10.1080/14686996.2016.1190258

Huck, V., Gorzelanny, C., Thomas, K., Getova, V., Niemeyer, V., Zens, K., et al. (2016). From morphology to biochemical state - intravital multiphoton fluorescence lifetime imaging of inflamed human skin. *Sci. Rep*. 6:22789. doi: 10.1038/srep22789

Ichimura, T., Chiu, L. D., Fujita, K., Kawata, S., Watanabe, T. M., Yanagida, T., et al. (2014a). Visualizing cell state transition using Raman spectroscopy. *PLoS ONE* 9:e84478. doi: 10.1371/journal.pone.0084478

Ichimura, T., Chiu, L. D., Fujita, K., Machiyama, H., Kawata, S., Watanabe, T. M., et al. (2015). Visualizing the appearance and disappearance of the attractor of differentiation using Raman spectral imaging. *Sci. Rep*. 5:11358. doi: 10.1038/srep11358

Ichimura, T., Chiu, L. D., Fujita, K., Machiyama, H., Yamaguchi, T., Watanabe, T. M., et al. (2016). Non-label immune cell state prediction using Raman spectroscopy. *Sci. Rep*. 6:37562. doi: 10.1038/srep37562

Ichimura, T., Jin, T., Fujita, H., Higuchi, H., and Watanabe, T.M. (2014b). Nano-scale measurement of bio molecules by optical microscopy and semiconductor nanoparticles. *Front. Physiol*. 5:273. doi: 10.3389/fphys.2014.00273

Imamura, H., Nhat, K. P., Togawa, H., Saito, K., Iino, R., Kato-Yamada, Y., et al. (2009). Visualization of ATP levels inside single living cells with fluorescence resonance energy transfer-based genetically encoded indicators. *Proc. Natl. Acad. Sci. U.S.A*. 106, 15651–15656. doi: 10.1073/pnas.0904764106

Itoh, H., Arai, S., Sudhaharan, T., Lee, S. C., Chang, Y. T., Ishiwata, S., et al. (2016). Direct organelle thermometry with fluorescence lifetime imaging microscopy in single myotubes. *Chem. Commun (Camb).* 52, 4458–4461. doi: 10.1039/C5CC09943A

Jung, H.-S., Cho, K.-J., Seol, Y., Takagi, Y., Dittmore, A., Roche, P.A., et al. (2018). Polydopamine encapsulation of fluorescent nanodiamonds for biomedical applications. *Adv. Funct. Mater*. 28:1801252. doi: 10.1002/adfm.201801252

Kiyonaka, S., Sakaguchi, R., Hamachi, I., Morii, T., Yoshizaki, T., and Mori, Y. (2015). Validating subcellular thermal changes revealed by fluorescent thermosensors. *Nat. Methods* 12, 801–802. doi: 10.1038/nmeth.3548

Ko, H-C., Yuan, C-T., and Tang, J. (2011). Probing and controlling fluorescence blinking of single semiconductor nanoparticles. *Nano Rev*. 2:5895. doi: 10.3402/nano.v2i0.5895

Krafft, C., and Popp, J. (2015). The many facets of Raman spectroscopy for biomedical analysis. *Anal. Bioanal. Chem*. 407, 699–717. doi: 10.1007/s00216-014-8311-9

Kucsko, G., Maurer, P.C., Yao, N.Y., Kubo, M., Noh, H.J., Lo, P.K., et al. (2013). Nanometre-scale thermometry in a living cell. *Nature* 500, 54–58. doi: 10.1038/nature12373

MacRitchie, N., Grassia, G., Noonan, J., Garside, P., Graham, D., and Maffia, P. (2018). Molecular imaging of atherosclerosis: spotlight on raman spectroscopy and surface-enhanced raman scattering. *Heart* 104, 460–467. doi: 10.1136/heartjnl-2017-311447

Marcu, L., Fang, Q., Jo, J. A., Papaioannou, T., Dorafshar, A., Reil, T., et al. (2005). *In vivo* detection of macrophages in a rabbit atherosclerotic model by time-resolved laser-induced fluorescence spectroscopy. *Atherosclerosis* 181, 295–303. doi: 10.1016/j.atherosclerosis.2005.02.010

Michalet, X., Pinaud, F.F., Bentolila, L.A., Tsay, J.M., Doose, S., Li, J.J., et al. (2005). Quantum dots for live cells, *in vivo* imaging, and diagnostics. *Science* 307, 538–544. doi: 10.1126/science.1104274

Miura, Y. (2018). Two-photon microscopy (TPM) and fluorescence lifetime imaging microscopy (FLIM) of retinal pigment epithelium (RPE) of mice *in vivo*. *Methods Mol. Biol.* 1753, 73–88. doi: 10.1007/978-1-4939-7720-8_5

Oyama, K., Takabayashi, M., Takei, Y., Arai, S., Takeoka, S, Ishiwata, S., (2012). Walking nanothermometers: spatiotemporal temperature measurement of transported acidic organelles in single living cells. *Lab Chip* 12, 1591–1593. doi: 10.1039/c2lc00014h

Pacia, M. Z., Czamara, K., Zebala, M., Kus, E., Chlopicki, S., and Kaczor, A. (2018). Rapid diagnostics of liver steatosis by Raman spectroscopy via fiber optic probe: a pilot study. *Analyst* 143, 4723–4731. doi: 10.1039/C8AN00289D

Paredes, J. M., Giron, M. D., Ruedas-Rama, M. J., Orte, A., Crovetto, L., Talavera, E. M., et al. (2013). Real-time phosphate sensing in living cells using fluorescence lifetime imaging microscopy (FLIM). *J. Phys. Chem. B* 117, 8143–8149. doi: 10.1021/jp405041c

Pisanic, T. R., Zhang, Y., and Wang, T. H. (2014). Quantum dots in diagnostics and detection: principles and paradigms. *Analyst* 139, 2968–2981. doi: 10.1039/C4AN00294F

Plakhotnik, T., Doherty, M.W., Cole, J.H., Chapman, R., and Manson, N.B. (2014). All-optical thermometry and thermal properties of the optically detected spin resonances of the NV^- center in nanodiamond. *Nano Lett*. 14, 4989–4996. doi: 10.1021/nl501841d

Provenzano, P. P., Eliceiri, K. W., and Keely, P. J. (2009). Multiphoton microscopy and fluorescence lifetime imaging microscopy (FLIM) to monitor metastasis and the tumor microenvironment. *Clin. Exp. Metastasis* 26, 357–370. doi: 10.1007/s10585-008-9204-0

Ranjit, S., Dobrinskikh, E., Montford, J., Dvornikov, A., Lehman, A., Orlicky, D. J., et al. (2016). Label-free fluorescence lifetime and second harmonic generation imaging microscopy improves quantification of experimental renal fibrosis. *Kidney Int*. 90, 1123–1128. doi: 10.1016/j.kint.2016.06.030

Roder, P., and Hille, C. (2014). ANG-2 for quantitative Na(+) determination in living cells by time-resolved fluorescence microscopy. *Photochem. Photobiol. Sci.* 13, 1699–1710. doi: 10.1039/C4PP00061G

Santos, I. P., Barroso, E. M., Bakker Schut, T. C., Caspers, P. J., van Lanschot, C. G. F., Choi, D. H., et al. (2017). Raman spectroscopy for cancer detection and cancer surgery guidance: translation to the clinics. *Analyst* 142, 3025–3047. doi: 10.1039/C7AN00957G

Schmitt, F. J., Thaa, B., Junghans, C., Vitali, M., Veit, M., and Friedrich, T. (2014). eGFP-pHsens as a highly sensitive fluorophore for cellular pH determination by fluorescence lifetime imaging microscopy (FLIM). *Biochim. Biophys. Acta* 1837, 1581–1593. doi: 10.1016/j.bbabio.2014.04.003

Seidenari, S., Arginelli, F., Dunsby, C., French, P. M., König, K., Magnoni, C., et al. (2013). Multiphoton laser tomography and fluorescence lifetime imaging of melanoma: morphologic features and quantitative data for sensitive and specific non-invasive diagnostics. *PLoS One* 8:e70682. doi: 10.1371/journal.pone.0070682

Sekiguchi, T., Sotoma, S., and Harada, Y. (2018). Fluorescent nanodiamonds as a robust temperature sensor inside a single cell. *Biophys. Physicobiol*. 15, 229–234. doi: 10.2142/biophysico.15.0_229

Shirshin, E. A., Gurfinkel, Y. I., Priezzhev, A. V., Fadeev, V. V., Lademann, J., and Darvin, M. E. (2017). Two-photon autofluorescence lifetime imaging of human skin papillary dermis *in vivo*: assessment of blood capillaries and structural proteins localization. *Sci. Rep*. 7:1171. doi: 10.1038/s41598-017-01238-w

Sotoma, S., Hsieh, F.-J., and Chang, H.-C. (2018). Biohybrid fluorescent nanodiamonds as dual-contrast markers for light and electron microscopies. *J. Chin. Chem. Soc*. 65, 1136–1146. doi: 10.1002/jccs.201800157

Suzuki, M., Arai, S., Oyama, K., and Ishiwata, S. (2016). "Nanothermometers: luminescent nanothermometers for biological applications," in *CRC Concise Encyclopedia of Nanotechnology*, eds. B. I. Kharisov, O. V. Kharissova, and U. O. Mendez (Boca Raton, FL: CRC Press), 851–859.

Suzuki, M., Zeeb, V., Arai, S., Oyama, K., and Ishiwata, S. (2015). The 10(5) gap issue between calculation and measurement in single-cell thermometry. *Nat. Methods* 12, 802–803. doi: 10.1038/nmeth.3551

Takei, Y., Arai, S., Murata, A., Takabayashi, M., Oyama, K., Ishiwata, S., et al. (2014). A nanoparticle-based ratiometric and self-calibrated fluorescent thermometer for single living cells. *ACS Nano* 8, 198–206. doi: 10.1021/nn405456e

Tanimoto, R., Hiraiwa, T., Nakai, Y., Shindo, Y., Oka, K., Hiroi, N., et al. (2016). Detection of temperature difference in neuronal cells. *Sci. Rep*. 6:22071. doi: 10.1038/srep22071

Tsai, P. C., Epperla, C. P., Huang, J. S., Chen, O. Y., Wu, C. C., and Chang, H. C. (2017). Measuring nanoscale thermostability of cell membranes with single gold-diamond nanohybrids. *Angew. Chem. Int. Ed*. 56, 3025–3030. doi: 10.1002/anie.201700357

Tzeng, Y. K., Tsai, P. C., Liu, H. Y., Chen, O.Y., Hsu, H., Yee, F. G., et al. (2015). Time-resolved luminescence nanothermometry with nitrogen-vacancy centers in nanodiamonds. *Nano Lett*. 15, 3945–3952. doi: 10.1021/acs.nanolett.5b00836

Vendrell, M., Zhai, D., Er, J. C., and Chang, Y. T. (2012). Combinatorial strategies in fluorescent probe development. *Chem. Rev*. 112, 4391–4420. doi: 10.1021/cr200355j

Wakayama, S, Kiyonaka, S., Arai, I., Kakegawa, W., Matsuda, S., Ibata, K., et al. (2017). Chemical labelling for visualizing native AMPA receptors in live neurons. *Nat. Commun*. 8:14850. doi: 10.1038/ncomms14850

Wang, X. D., Wolfbeis, O.S., and Meier, R.J. (2013). Luminescent probes and sensors for temperature. *Chem. Soc. Rev*. 42, 7834–7869. doi: 10.1039/c3cs60102a

Yang, J. M., Yang, H., and Lin, L. (2011). Quantum dot nano thermometers reveal heterogeneous local thermogenesis in living cells. *ACS Nano* 5, 5067–5071. doi: 10.1021/nn201142f

Yong, W. H., Butte, P. V., Pikul, B. K., Jo, J. A., Fang, Q., Papaioannou, T., et al. (2006). Distinction of brain tissue, low grade and high grade glioma with time-resolved fluorescence spectroscopy. *Front. Biosci.* 11, 1255-1263. doi: 10.2741/1878

Zhang, J., Campbell, R. E., Ting, A. Y., and Tsien, R. Y. (2002). Creating new fluorescent probes for cell biology. *Nat. Rev. Mol. Cell Biol*. 3, 906–918. doi: 10.1038/nrm976

Zhao, Y., Araki, S., Wu, J., Teramoto, T., Chang, Y. F., Nakano, M., et al. (2011). An expanded palette of genetically encoded Ca(2)(+) indicators. *Science* 333, 1888–1891. doi: 10.1126/science.1208592

Zheng, K., Jensen, T. P., and Rusakov, D. A. (2018). Monitoring intracellular nanomolar calcium using fluorescence lifetime imaging. *Nat. Protoc*. 13, 581–597. doi: 10.1038/nprot.2017.154

Zhu, H., Fan, J., Du, J., and Peng, X. (2016). Fluorescent probes for sensing and imaging within specific cellular organelles. *Acc. Chem. Res*. 49, 2115–2126. doi: 10.1021/acs.accounts.6b00292

Conflict of Interest Statement: The authors declare that the research was conducted in the absence of any commercial or financial relationships that could be construed as a potential conflict of interest.

frontiers in Bioengineering and Biotechnology

MINI REVIEW
published: 30 October 2018
doi: 10.3389/fbioe.2018.00158

Quartz Crystal Microbalance With Dissipation Monitoring: A Powerful Method to Predict the *in vivo* Behavior of Bioengineered Surfaces

Chiara Tonda-Turo [1,2], Irene Carmagnola [1,2] and Gianluca Ciardelli [1,2,3]*

[1] Department of Mechanical and Aerospace Engineering, Politecnico di Torino, Turin, Italy, [2] POLITO BIOMedLAB, Politecnico di Torino, Turin, Italy, [3] Department for Materials and Devices of the National Research Council, Institute for the Chemical and Physical Processes (CNR-IPCF UOS), Pisa, Italy

The Quartz Crystal Microbalance with dissipation monitoring (QCM-D) is a tool to measure mass and viscosity in processes occurring at or near surfaces, or within thin films. QCM-D is able to detect extremely small chemical, mechanical, and electrical changes taking place on the sensor surface and to convert them into electrical signals which can be investigated to study dynamic process. Surface nanotopography and chemical composition are of pivotal importance in biomedical applications since interactions of medical devices with the physiological environment are mediated by surface features. This review is intended to provide readers with an up-to-date summary of QCM-D applications in the study of cell behavior and to discuss the future trends for the use of QCM-D as a high-throughput method to study cell/surface interactions overcoming the current challenges in the design of biomedical devices.

Keywords: quartz crystal microbalance with dissipation monitoring (QCM-D), cell adhesion, cell death, cell cytoskeleton, bioengineered surface characterization

OPEN ACCESS

Edited by:
Giada Graziana Genchi, Fondazione Istituto Italiano di Technologia, Italy

Reviewed by:
Giuseppe Maruccio, University of Salento, Italy
Cristina Satriano, Università degli Studi di Catania, Italy
Hamit Yurtseven, Middle East Technical University, Turkey

****Correspondence:***
Chiara Tonda-Turo
chiara.tondaturo@polito.it

Specialty section:
This article was submitted to Nanobiotechnology, a section of the journal Frontiers in Bioengineering and Biotechnology

Received: *29 August 2018*
Accepted: *10 October 2018*
Published: *30 October 2018*

Citation:
Tonda-Turo C, Carmagnola I and Ciardelli G (2018) Quartz Crystal Microbalance With Dissipation Monitoring: A Powerful Method to Predict the in vivo Behavior of Bioengineered Surfaces. Front. Bioeng. Biotechnol. 6:158. doi: 10.3389/fbioe.2018.00158

INTRODUCTION

Quartz crystal microbalance with dissipation monitoring (QCM-D) is an easy, highly versatile as well as highly sensitive method to study processes occurring at the surfaces or within thin films. QCM was introduced in 1960s to monitor layer formation in vacuum and air thanks to the high mass sensitivity of the 5 MHz quartz system (0.057 Hz cm^2 ng^{-1}) which was superior compared with other available technologies (Janshoff et al., 2000). Then, it gained interest in biomedical application since 1980s when novel QCM systems able to work in liquid media was introduced (Marx, 2003). However, the QCM has achieved resounding success since 1995 when a new system able to measure changes in damping properties of adsorbed layers (QCM-D) were developed, patented and commercialized by Q-Sense (Rodahl et al., 1995; Rodahl, 1996).

To date, QCM-D can be applied to monitor processes in real-time by measuring changes in frequency and energy dissipation of the system composed by the surface or thin film of interest adsorbed on a piezoelectric quartz sensor. Quartz sensors are applied in the QCM-D devices as a mechanical oscillation of characteristic frequency can be produced on the crystal by applying an alternated electric field. When a change on the mass occurred at the surface interface or within the thin film, a frequency shift from the fundamental resonant frequency of the crystal (Δf) is

measured making the QCM-D a quantitatively and ultrasensitive technology to measure mass changes. In addition to Δf, QCM-D simultaneously monitors the viscoelastic properties of the overlayer or thin film adsorbed to the quartz sensors by recording changes in the energy dissipation factor (D) (**Figure 1A**). When the generator is switched off the crystal oscillation amplitude decays exponentially and the energy dissipation factor can be measured by recording the amplitude of the oscillation as a function of time (Rodahl et al., 1995). Higher are the dissipative properties of the overlayer faster is the decay time resulting in substantial energy dissipation factor shift (ΔD) from rigid state.

In the case of rigid layer ($\Delta D = 0$), when the change in mass occurs in air or in vacuum, the frequency shift (Δf) is proportional to mass change and it can be quantified applying the Sauerbrey equation (Sauerbrey, 1959). However, biological processes take place in liquid environment where the Sauerbery equation is no more valid and the equation described by Kanazawa and Gordon has to be used to relate Δf to mass changes (Kanazawa and Gordon, 1985). For not rigid layers where the damping of the layer is significant ($\Delta D > 0$), the Voight model is applied to analyze collected data and equations developed by Voinova et al. (1998) provide information on the mass and viscoelastic properties of the viscous layer. Latest QCM-D devices allow for simultaneously recording of Δf and ΔD for multiple harmonics (up to the 13th overtone) which permit to better extract the adsorbed overlayer characteristics (such as density, storage, and loss moduli; Hovgaard et al., 2007). An historical perspective describing the QCM-D working principles and its applications to study complex systems was recently published by Chen et al. (2016).

In the past 15 years, QCM-D has been increasingly used as a tool to characterize the biological interactions of engineered surfaces. To date, QCM-D crystals have been mainly applied to monitor the binding efficacy of probing surface of biosensors (Chen et al., 2010; Xu et al., 2011; Ertekin et al., 2016) as well as to verify the biofunctionalization of nanoengineered surfaces through self-assembled monolayers (SAMs; Minsky et al., 2016) or layer-by-layer (LbL) technologies (Chen et al., 2010). In addition, proteins adsorption competitive studies on biomedical device surfaces have been performed thanks to the possibility to measure at the same time the mass and the viscoelastic properties of absorbed biomolecules, which can be related to protein conformation. Protein adsorption kinetics on polyHEMA (Teichroeb et al., 2008), stainless steel (Chandrasekaran et al., 2013), and titanium oxide (Pegueroles et al., 2012) were analyzed to study interaction between biomedical devices and biological fluids after implantation. Furthermore, QCM-D has been used to assess the antifouling properties of surfaces such those composed of branched polymers (Luan et al., 2017). Besides composition and nanoscale chemistry, different surface morphologies were investigated to relate nanostructures to protein adsorption kinetics (Hovgaard et al., 2008; Chandrasekaran et al., 2013).

Phenomena occurring at the interface within surfaces and biological fluids are fundamental to address specific cell response on biomedical surfaces. QCM-D allows to study these phenomena in real-time without requiring labeling processes which could interfere with the system, thus preventing any loss of information (Nowacki et al., 2014). Furthermore, QCM-D experimental setup is equipped with a temperature-controlled system able to mimic the physiological conditions within the equipment chamber. In the last 5 years a growing interest on QCM-D related to cell behavior studies has been observed as this technique appears to be particularly well-suited for real-time acquisition of cell responses and to monitor cytoskeleton changes after internal or external stimuli. Recently, novel crystal chamber set-ups have been commercialized to permit a multiple characterization of the processes occurring on the crystal surface. Among others, the open window chamber, which combined traditional QCM-D measurements with light microscopy, and the ellipsometric modulus are applied to monitor cell-surface interactions as they allow to follow in real-time changes in cell morphology (Marcus et al., 2012; Tymchenko et al., 2012) and in overlayer thickness (van der Meulen et al., 2014), respectively.

The purpose of this article is to provide a summary of the present state of the art of QCM-D as a tool to monitor cell behavior on surfaces. Then, the future trends in the use of QCM-D as a tool to study phenomena occurring at surface/cell interface, which are pivotal for innovation in the biomedical field, are envisioned.

QCM-D AS A TOOL TO MONITOR CELL ADHESION

QCM-D sensors was applied in the study of cell-surface interactions as the piezoelectric mass sensing combined with the monitoring of dissipation changes was related to different colonization stages of cells on surfaces (as attachment, adhesion, and spreading; Saitakis and Gizeli, 2012; Tymchenko et al., 2012). When a cell is interacting with the sensor surface a shift in the Δf can be detected, however the majority of the information on cell state is provided by the energy dissipation factor (ΔD), index of the fact that the signal is mainly attributable to the viscoelastic behavior of the cell part adhering on the crystal. This is mainly ascribed to the size of cells, which overcome the sensitive limit of the instrument. Indeed, the QCM-D penetration signal is $\sim$0.25 μm in water, allowing the detection of only a fraction of the adhered cell size and consequently effects on frequency shift are mainly associated to adhesion contact points located on the cell membranes (Saitakis and Gizeli, 2012). The contact of the cells with the substrate induces a small decrease of Δf which is not proportional to the real mass adsorbed while in contrast ΔD strongly increases having higher shift when adhesion involved a small fraction of the cell membranes (low spreading and limited numbers of focal contact points). During the cell spreading no significant changes are detected in frequency shift compared to adhesion, whereas dissipation slightly decrease due to the rearrangement of cytoskeleton and a subsequent cell stiffening (Tymchenko et al., 2012) responsible for the decrease in damping events (**Figure 2**). The information collected from the temporal

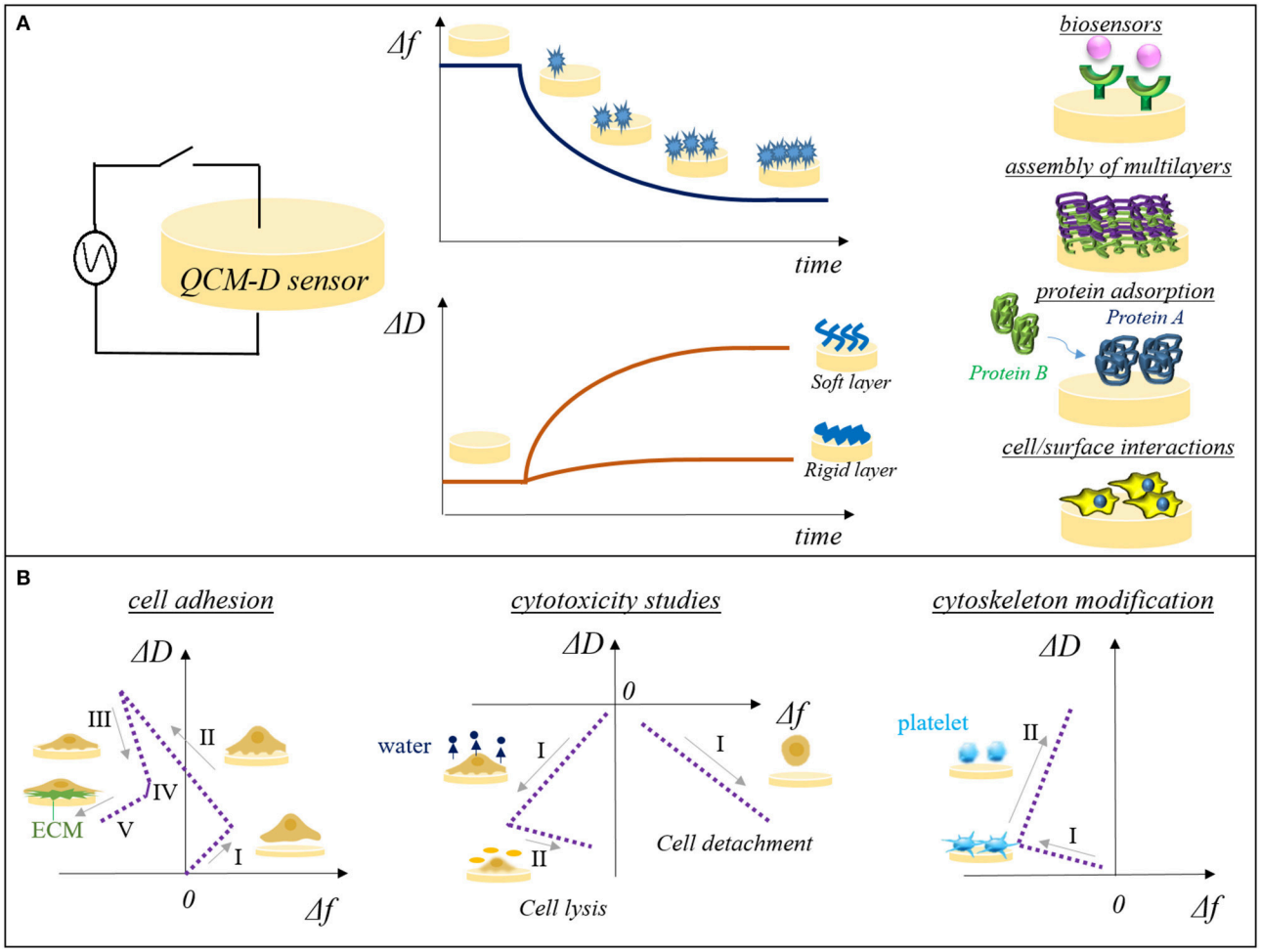

FIGURE 1 | (A) Schematic representation of QCM-D plots reporting frequency factor (Δf) and dissipation energy factor (ΔD) vs. time. QCM-D system is mainly applied in the study of binding efficacy of probing surface of biosensors, assembly of multilayers, competitive protein adsorption studies, and recently for cell/surface interactions. **(B)** Representative ΔD-Δf plot signatures for cell adhesion on sensor surfaces (I-initial adhesion, II-formation of attachment points, III-cell spreading, IV-steady state of spread cells, V-production of ECM), cytotoxicity studies (left side: I-water release from cytoskeleton, II-cell lysis; right side: I-cell detachment) and cytoskeleton modification such as platelets activation (I-initial interactions among surface sensor and platelets, II-platelets spreading and pseudopodia formation).

plot of Δf and ΔD can be combined in a ΔD-Δf plot. In this contest, ΔD-Δf plot (frequency shift plotted vs. energy dissipation shift) provides greater insight into changes in the structural conformation of cells and it is used to monitor the different stages of the cell adhesion: from initial cell/surface interactions (initial adhesion, formation of attachment points) to the following changes in the cytoskeleton conformation characteristics of cell spreading. Westas et al. (2015) monitored the interaction of human gingival fibroblasts on osteoinductive surfaces functionalized with hydroxyapatite nanoparticles when a complete coverage of the sensor surface was achieved. Five consecutive stages were identified by analyzing the recorded QCM-D signals: (i) initial adhesion when cells were close to the surface and started making few attachment points [Δf increased as cells behaving like a coupled oscillator (Granéli et al., 2004) and ΔD slightly increased], (ii) the number of adhered cells increased as well as the attachment points (Δf decreased as the number of attachment point increased and a more homogenous layer is formed at the sensor interface causing ΔD increase), (iii) cell spreading occurred (ΔD rapidly decreased due to the formation of mature focal adhesion complex and Δf decrease as the number of mature focal adhesion complex was lower than the initial adhesion points formed at the second stage), (iv) steady state of spread cells (Δf and ΔD decreased slowly), and (v) production of extracellular matrix (ECM) from adhered cells (Δf decreased due to new mass on the crystal; **Figure 1B**).

The real-time monitoring of cells behavior on surfaces was recently exploited in the optimization of implantable surfaces in order to design *ad-hoc* substrates having chemical-physical features able to enhance cell adhesion. As the electric charge of the surface material is crucial for the integration in the

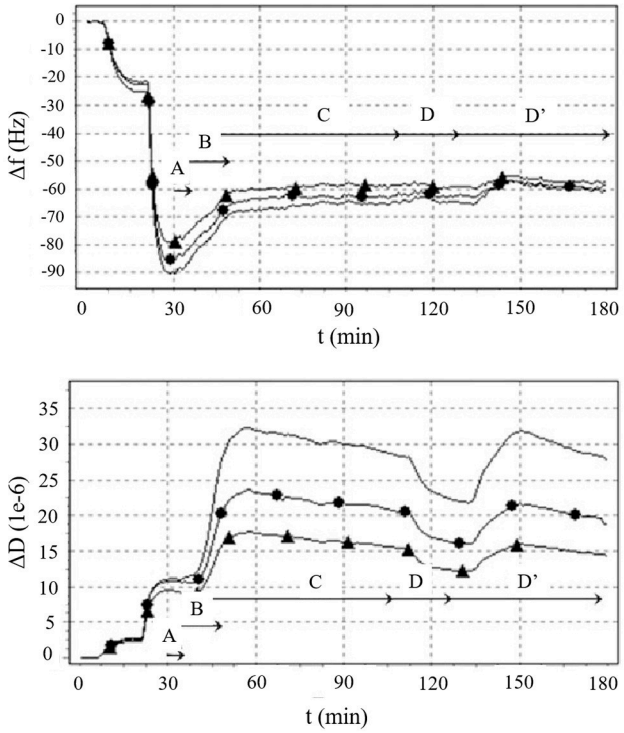

FIGURE 2 | The Δf and ΔD signals (3rd-line, 5th-circle, and 7th-triangle overtones) over time of NIH3T3 fibroblasts cultured on a collagen I functionalized sensor. Five events were identified: (A) cell seeding, (B) cell adhesion, (C) cell spreading, (D) cytoskeleton rearrangement after addition of the cytoskeleton-perturbing agent cytochalasin D (2 μg/ml) and (D′) cell recovery after cytochalasin D removal. Reproduced with permission from Tymchenko et al. (2012). The different phases of cell/surface interaction were confirmed by real-time monitoring of cell morphology and distribution through polarized light microscopy.

biological environment, Kao et al. (2017) employed the potential of QCM-D equipment to follow the NIH3T3 mouse embryonic fibroblast adhesion on surface with different ζ-potentials. Higher ζ-potential surfaces allowed the direct interaction between cells and surface resulting in a high adhesion and cell spreading while the electrostatic repulsions among surface and cells occurring in presence of lower ζ-potentials required the formation of an ECM-like layer prior to cell adhesion and spreading. Kushiro et al. (2016) used the same approach to monitor the cell adhesion process on various SAM surfaces. Interestingly, QCM-D signals allowed to distinguish from different material-cell interactions that were not detected by morphological analysis using confocal microscopy. These findings confirmed the strength of QCM-D setup in the detection of cell changes at the micro and nanoscale, which cannot be measured through conventional methods. Furthermore, Chronaki et al. (2016) employed QCM-D to analyze the difference between the adhesion pattern of normal thyroid and anaplastic thyroid cancer cells demonstrating that starting from dissipation over frequency curves it is possible to accurately discriminate cancer cell from healthy ones, envisioning the use of QCM-D as a promising diagnostic tool.

In addition to cell, bacteria-surface interactions were monitored using QCM-D device (Reipa et al., 2006; Olsson et al., 2010, 2011). Bacteria adhesion is a highly studied topic as adhesion of bacteria on biomedical device surfaces results in biofilm formation, which is one of the more frequent cause of implant failure. QCM-D was applied in the attempt to monitor the antibacterial efficacy of two well-known aminoglycosides, kanamycin A, and neomycin B (Joshi et al., 2015). The modeling of frequency and dissipation energy shifts allowed to get detailed knowledge on mechanism of action of different aminoglycosides in bacteria membrane disruption.

QCM-D AS A TOOL TO MONITOR CYTOTOXICITY AND CELL VIABILITY

Cells are highly sensitive to perturbations in the surrounding environment and changes interfering with the cell activities can lead to cell death. The monitoring of cell behavior when cells are in contact with bioengineered surfaces, biomaterials, or drugs is fundamental to identify cytotoxic or non-cytotoxic effects. Traditional methodologies to study cytotoxicity and cell viability are based on microscopy and flow cytometry which are unable to monitor cell health *in situ* and in real-time. Hence, the ability of QCM-D signals to detect cytoskeletal changes can be exploited to assess the cell health in response to external perturbations. Fatisson et al. (2011a) investigated the cellular response during exposure to two different cytomorphic agents (Triton-X 100 and lipopolysaccharide—LPS) on bovine aortic endothelial cells (BAECs) adhering on QCM-D sensor. QCM-D sensors were pre-incubated with BAECs, then coated sensors were mounted into the device chamber and the chemicals were injected in the chamber flowing on the cells attached to the sensor. Both changes in frequency and in energy dissipation were recorded to model cytoskeleton changes in real time. ΔD-Δf plots revealed two different cell death mechanisms induced by the two cytomorphic agents. High concentrations of Triton-X 100 led to cell lysis, as confirmed by the ΔD-Δf plot. In this plot, a first phase of Δf and ΔD drop was detected suggesting mass adsorption and more rigid layer formation (probably ascribed to Triton-X 100 micelles adsorption and water release from cytoskeleton), followed by the effective cell lysis which induced a Δf increase and a slow ΔD drop (**Figure 1B**). On the other hand, LPS exposure resulted in a single slope of the ΔD-Δf plot with a steady increase of Δf and decrease of ΔD. LPS induced a progressive detachment of the BEACs from the QCM-D sensor (from spread cells to round cells) which resulted in mass loss and reduction of damping. Kandel et al. (2014) assessed the viability of human umbilical vein endothelial cells (HUVECs) on different fibronectin-coated QCM-D sensors monitoring the cytoskeleton changes in presence or absence of an actin depolymerizing agent.

Further evidences of the ability of QCM-D to sense cell death were described by Nowacki et al. (2014) which investigated QCM-D signal changes when human breast

cancer cells (MCF-7) adhering on quartz crystal surfaces were treated with staurosporine (STS), a protein kinase inhibitor known to induce cell apoptosis. ΔD-Δf plot displayed a simultaneous increase of Δf and a decrease of ΔD, which is typical of apoptosis-mediated cell death.

These findings pave the way for the use of QCM-D not only in the study of cell cytotoxicity but also as a tool to investigate the efficacy of drugs in fighting cancer or other diseases where selective cell death is targeted. The high sensitivity of QCM-D and its ability to continuously monitor the events occurring on the quartz sensors allow to distinguish between the various cell death subtypes and pathways which are fundamental aspects for drug efficacy evaluation (Kepp et al., 2011). Pioneering work of Zhang et al. tracked changes in frequency and energy dissipation of MCF-7 cells treated with resveratrol reporting the use of QCM-D as a cancer drug screening technology for the first time (Zhang et al., 2015a).

QCM-D AS A TOOL TO MONITOR IMPORTANT PHENOMENA IN CELLS

The opportunity to detect in real time the rearrangement of cell cytoskeleton through QCM-D technology is of pivotal importance in the monitoring of cell biological phenomena such as cell migration and cell differentiation. Data collected by the microgravimetric analyses using the QCM-D system could give information on biological mechanisms which are still difficult to predict. In this context platelets conformational modifications and cytoskeleton changes are involved in the platelet activation process, which is the major player in the formation of blood clotting on biomaterial surfaces. QCM-D was employed to evaluate how composition of bioengineered surfaces affected the platelet activation, which is crucial in the design of blood-contacting devices, as no activation is foreseen to avoid thrombogenic effects. Platelets activation was observed on fibronectin-coated sensors as fibronectin is a highly thrombogenic protein. As discussed above, Δf alone does not give sufficient information and the analysis ΔD-Δf plot is the more appropriate method to observe changes in cell shape. ΔD-Δf plot revealed two phases in platelet activation process, a first phase corresponding to initial interactions among surface sensor and cells with a decrease of Δf and a slight increase of ΔD followed by a second phase characterized by an increase of ΔD ascribed to the platelet spreading and pseudopodia formation (**Figure 1B**). The higher is the slope of the second phases, the lower is the thrombogenicity of the surface as a low anchorage of the platelets on the surfaces resulted in a less rigid layer (Fatisson et al., 2008). Assays on thrombogenicity of high-density polyethylene (HDPE) and polycarbonate (PC) were performed evaluating the effect of surface chemical composition, roughness, and wettability, on platelet activation highlighting that the hemocompatibility effect of these polymers was mainly due to their hydrophobic nature (Fatisson et al., 2011b).

QCM-D system was also applied by Zhang et al. (2015b) to study the difference between healthy erythrocytes (RBCs) and RBCs derived from type 2 diabetic patients, as vascular thrombosis is the most frequent complication in diabetic patients. ΔD-Δf plot revealed that RBCs from diabetic individuals are stiffer and less prone to cytoskeleton rearrangements than healthy cells. Furthermore, RBCs were co-cultured for 30 min on a QCM-D sensor previously coated with HUVECs. QCM-D signals revealed that pathological RBCs adhered to HUVECs while no adhesion was observed for healthy RBCs.

Among other potential applications, QCM-D was exploited to give novel insights in the study of cancer cell motility which has been recognized as an essential value to quantify the metastatic potential of cancer cells (Friedl and Gilmour, 2009). Tarantola et al. (2010) proposed a QCM-based sensor to determine the motility of four breast cancer lines with different invasiveness by correlating frequency fluctuations recorded by QCM system to collective motility. High fluctuations were associated to collective mobility, which is typical of tumor progression phase. The higher was the fluctuation the more invasive was the cell population as confirmed by the traditionally used Boyden chamber method. This new approach allows measuring the invasiveness of tumor in colonizing adjacent connective tissues helping to identify the degree of tumor malignancy and to define the more appropriate treatment.

CONCLUSION AND FUTURE PERSPECTIVES

The collected literature highlighted the role of QCM-D technology as a new and non-conventional facility to monitor cells in real time using a label-free methodology. Several phenomena can be detected from initial cell binding, focal adhesion formation, cell spreading, and complex changes in cytoskeleton. The attachment and growth of cells is the key step to achieve device biointegration and many efforts are addressed to the design of bioengineered surface able to enhance cell growth. *In vitro* and *in vivo* tests currently applied lack the ability to follow the initial phase of cell/surface interactions which can be monitored modeling QCM-D signals. Complex phenomena occurring during cell/external environment interactions can be distinguished and analyzed by combining temporal frequency and energy dissipation shifts in ΔD-Δf plots.

To date, QCM-D is rarely applied in materials and surfaces characterization, however, the data collected from this measuring system are unique and could drive to a better understanding of biological phenomena which is fundamental to engineer devices with enhanced biological performances. In addition, taking advantage of the high sensitivity of QCM-D instruments in detecting tiny changes in cell conformation, it is possible to analyse the cytoskeleton changes induced by different drugs on pathological and healthy cells. Consequently, the more

appropriate pharmacological treatment can be defined helping in developing methodologies for advanced and/or personalized therapies as well as screening tools. Furthermore, recent upgrades of the QCM-D device allow to match the recorded Δf and ΔD signals with morphology and optical properties of studied platforms by connecting the sensor chamber with additional apparatus such as microscope and ellipsometer.

In conclusion, the recent literature clearly indicates that QCM-D is already a promising methodology to study cell behavior since it provides data which are pivotal to achieve a complete understanding of many biological phenomena consequently helping in tackling the current challenges in the biomedical field.

AUTHOR CONTRIBUTIONS

CT-T revised the current literature on QCM-D and wrote the main text. IC summarized the state of the art focused on application of QCM-D in cytoskeleton changes analysis. GC revised the manuscript discussing the future trends of QCM-D applications.

REFERENCES

Chandrasekaran, N., Dimartino, S., and Fee, C. J. (2013). Study of the adsorption of proteins on stainless steel surfaces using QCM-D. *Chem. Eng. Res. Design.* 91, 1674–1683. doi: 10.1016/j.cherd.2013.07.017

Chen, Q., Tang, W., Wang, D., Wu, X., Li, N., and Liu, F. (2010). Amplified QCM-D biosensor for protein based on Aptamer-functionalized gold nanoparticles. *Biosens. Bioelectron.* 26, 575–579. doi: 10.1016/j.bios.2010.07.034

Chen, Q., Xu, S., Liu, Q., Masliyah, J., and Xu, Z. (2016). QCM-D study of nanoparticle interactions. *Adv. Colloid Interface Sci.* 233, 94–114. doi: 10.1016/j.cis.2015.10.004

Chronaki, D., Stratiotis, D. I., Tsortos, A., Anastasiadou, E., and Gizeli, E. (2016). Screening between normal and cancer human thyroid cells through comparative adhesion studies using the quartz crystal microbalance. *Sens. Bio-Sensing Res.* 11, 99–106. doi: 10.1016/j.sbsr.2016.10.001

Ertekin, Ö., Öztürk, S., and Öztürk, Z. Z. (2016). Label free QCM immunobiosensor for AFB1 detection using monoclonal IgA antibody as recognition element. *Sensors* 16:E1274. doi: 10.3390/s16081274

Fatisson, J., Azari, F., and Tufenkji, N. (2011a). Real-time QCM-D monitoring of cellular responses to different cytomorphic agents. *Biosens. Bioelectron.* 26, 3207–3212. . doi: 10.1016/j.bios.2010.12.027

Fatisson, J., Mansouri, S., Yacoub, D., Merhi, Y., and Tabrizian, M. (2011b). Determination of surface-induced platelet activation by applying timedependency dissipation factor versus frequency using quartz crystal microbalance with dissipation. *J. R. Soc. Interface* 8, 988–997. doi: 10.1098/rsif.2010.0617

Fatisson, J., Merhi, Y., and Tabrizian, M. (2008). Quantifying blood platelet morphological changes by dissipation factor monitoring in multilayer shells. *Langmuir* 24, 3294–3299 doi: 10.1021/la7023204

Friedl, P., and Gilmour, D. (2009). Collective cell migration in morphogenesis, regeneration and cancer. *Nat. Rev. Mol. Cell Biol.* 10, 445–457. doi: 10.1038/nrm2720

Granéli, A., Edvardsson, M., and Höök, F. (2004). DNA-based formation of a supported, three-dimensional lipid vesicle matrix probed by QCM-D and SPR. *ChemPhysChem* 5, 729–733. doi: 10.1002/cphc.200301061

Hovgaard, M. B., Dong, M., Otzen, D. E., and Besenbacher, F. (2007). Quartz crystal microbalance studies of multilayer glucagon fibrillation at the solid-liquid interface. *Biophys. J.* 93, 2162–2169. doi: 10.1529/biophysj.107.109686

Hovgaard, M. B., Rechendorff, K., Chevallier, J., Foss, M., and Besenbacher, F. (2008). Fibronectin adsorption on tantalum: the influence of nanoroughness. *J. Phys. Chem. B* 112, 8241–8249. doi: 10.1021/jp801103n

Janshoff, A., Galla, H. J., and Steinem, C. (2000). Piezoelectric mass-sensing devices as biosensors - an alternative to optical biosensors? *Ang. Chem. Int.* 39, 4004–4032. doi: 10.1002/1521-3773(20001117)39:22<4004::AID-ANIE4004>3.0.CO;2-2

Joshi, T., Voo, Z. X., Graham, B., Spiccia, L., and Martin, L. L. (2015). Real-time examination of aminoglycoside activity towards bacterial mimetic membranes using quartz crystal microbalance with dissipation monitoring (QCM-D). *Biochim. Biophys. Acta* 1848, 385–391. doi: 10.1016/j.bbamem.2014.10.019

Kanazawa, K. K., and Gordon, J. G. (1985). Frequency of a quartz microbalance in contact with liquid. *Anal. Chem.* 57, 1770–1771. doi: 10.1021/ac00285a062

Kandel, J., Lee, H. S., Sobolewski, P., Tomczyk, N., Composto, R. J., and Eckmann, D. M. (2014). Chemically grafted fibronectin for use in QCM-D cell studies. *Biosens. Bioelectron.* 58, 249–257. doi: 10.1016/j.bios.2014.02.053

Kao, W. L., Chang, H. Y., Lin, K. Y., Lee, Y. W., and Shyue, J. J. (2017). Effect of surface potential on the adhesion behavior of NIH3T3 cells revealed by quartz crystal microbalance with dissipation monitoring (QCM-D). *J. Phys. Chem. C* 121, 533–541. doi: 10.1021/acs.jpcc.6b11217

Kepp, O., Galluzzi, L., Lipinski, M., Yuan, J., and Kroemer, G. (2011). Cell death assays for drug discovery. *Nat. Rev. Drug Discov.* 10, 221–237. doi: 10.1038/nrd3373

Kushiro, K., Lee, C. H., and Takai, M. (2016). Simultaneous characterization of protein-material and cell-protein interactions using dynamic QCM-D analysis on SAM surfaces. *Biomater Sci.* 4, 989–997. doi: 10.1039/C5BM00613A

Luan, Y., Li, D., Wei, T., Wang, M., Tang, Z., Brash, J. L., et al. (2017). "Hearing Loss" in QCM measurement of protein adsorption to protein resistant polymer brush layers. *Anal. Chem.* 89, 4184–4191. doi: 10.1021/acs.analchem.7b00198

Marcus, I. M., Herzberg, M., Walker, S. L., and Freger, V. (2012). *Pseudomonas aeruginosa* attachment on QCM-D sensors: the role of cell and surface hydrophobicities. *Langmuir* 28, 6396–6402. doi: 10.1021/la300333c

Marx, K. A. (2003). Quartz crystal microbalance: a useful tool for studying thin polymer films and complex biomolecular systems at the solution-surface interface. *Biomacromolecules* 4, 1099–1120. doi: 10.1021/bm020116i

Minsky, B. B., Antoni, C. H., and Boehm, H. (2016). Controlled immobilization strategies to probe short hyaluronan-protein interactions. *Sci. Rep.* 6:21608. doi: 10.1038/srep21608

Nowacki, L., Follet, J., Vayssade, M., Vigneron, P., Rotellini, L., Cambay, F., et al. (2014). Real-time QCM-D monitoring of cancer cell death early events in a dynamic context. *Biosens. Bioelectron.* 64, 469–476. doi: 10.1016/j.bios.2014.09.065

Olsson, A. L. J., van der Mei, H. C., Busscher, H. J., and Sharma, P. K. (2011). Acoustic sensing of the bacterium-substratum interface using QCM-D and the influence of extracellular polymeric substances. *J. Colloid Interface Sci.* 357, 135–138 doi: 10.1016/j.jcis.2011.01.035

Olsson, A. L. van der Mei, J. H. C., Busscher, H. J., and Sharma, P. K. (2010). Novel analysis of bacterium–substratum bond maturation measured using a quartz crystal microbalance. *Langmuir* 26, 11113–11117. doi: 10.1021/la100896a

Pegueroles, M., Tonda-Turo, C., Planell, J. A., Gil, F. J., and Aparicio, C. (2012). Adsorption of fibronectin, fibrinogen, and albumin on TiO2: time-resolved kinetics, structural changes, and competition study. *Biointerphases* 7:48. doi: 10.1007/s13758-012-0048-4

Reipa, V., Almeida, J., and Cole, K. D. (2006). Long-term monitoring of biofilm growth and disinfection using a quartz crystal microbalance and reflectance measurements. *J. Microbiol. Methods* 66, 449–459. doi: 10.1016/j.mimet.2006.01.016

Rodahl, M. (1996). QCM-D patent No. WO96/35103. WO1996035103A1.pdf.

Rodahl, M., Höök, F., Krozer, A., Brzezinski, P., and Kasemo, B. (1995). Quartz crystal microbalance setup for frequency and Q-factor measurements in gaseous and liquid environments. *Rev. Sci. Instr.* 66:3924. doi: 10.1063/1.1145396

Saitakis, M., and Gizeli, E. (2012). Acoustic sensors as a biophysical tool for probing cell attachment and cell/surface interactions. *Cell. Mol. Life Sci.* 69, 357–371 doi: 10.1007/s00018-011-0854-8

Sauerbrey, G. (1959). Verwendung von schwingquarzen zur wäigung diinner schichten und zur mikrowäigung. *Z. Phys.* 155, 206–222. doi: 10.1007/BF01337937

Tarantola, M. A.-,Marel, K., Sunnick, E., Adam, H., Wegener, J., and Janshoff, A. (2010). Dynamics of human cancer cell lines monitored by electrical and acoustic fluctuation analysis. *Integr. Biol.* 2, 139–150. doi: 10.1039/b920815a

Teichroeb, J. H., Forrest, J. A., Jones, L. W., Chan, J., and Dalton, K. (2008). Quartz crystal microbalance study of protein adsorption kinetics on poly(2-hydroxyethyl methacrylate). *J. Colloid Interface Sci.* 325, 157–164. doi: 10.1016/j.jcis.2008.05.052

Tymchenko, N., Nileba, E., Voinova, M. V., Gold, J., Kasemo, B., and Svedhem, S. (2012). Reversible changes in cell morphology due to cytoskeletal rearrangements measured in real-time by QCM-D. *Biointerphases* 7:43. doi: 10.1007/s13758-012-0043-9

van der Meulen, S. A., Dubacheva, G. V., Dogterom, M., Richter, R. P., and Leunissen, M. E. (2014). Quartz crystal microbalance with dissipation monitoring and spectroscopic ellipsometry measurements of the phospholipid bilayer anchoring stability and kinetics of hydrophobically modified DNA oligonucleotides. *Langmuir* 30, 6525–6533. doi: 10.1021/la500940a

Voinova, M. V., Rodahl, M., Jonson, M., and Kasemo, B. (1998). Viscoelastic acoustic response of layered polymer films at fluid-solid interfaces: continuum mechanics approach. *Phys. Script.* 59:5.

Westas, E., Svanborg, L. M., Wallin, P., Bauer, B., Ericson, M. B., Wennerberg, A., et al. (2015). Using QCM-D to study the adhesion of human gingival fibroblasts on implant surfaces. *J. Biomed. Mater. Res. A* 103, 3139–3147 doi: 10.1002/jbm.a.35458

Xu, J.ia, Liu, K. W., Matthews, K. S., and Biswal, S. L. (2011). Monitoring DNA binding to *Escherichia coli* lactose repressor using quartz crystal microbalance with dissipation. *Langmuir* 27, 4900–4905. doi: 10.1021/la200056h

Zhang, S., Bai, H., Pi, J., Yang, P., and Cai, J. (2015a). Label-free quartz crystal microbalance with dissipation monitoring of resveratrol effect on mechanical changes and folate receptor expression levels of living MCF-7 cells: a model for screening of drugs. *Anal. Chem.* 87, 4797–4805. doi: 10.1021/acs.analchem.5b00083

Zhang, S., Bai, H., and Yang, P. (2015b). Real-time monitoring of mechanical changes during dynamic adhesion of erythrocytes to endothelial cells by QCM-D. *Chem. Commun.* 51, 11449–11451. doi: 10.1039/C5CC03264D

Conflict of Interest Statement: The authors declare that the research was conducted in the absence of any commercial or financial relationships that could be construed as a potential conflict of interest.

frontiers in Bioengineering and Biotechnology

ORIGINAL RESEARCH
published: 23 August 2018
doi: 10.3389/fbioe.2018.00114

Photocatalytic Activity of Polymer Nanoparticles Modulates Intracellular Calcium Dynamics and Reactive Oxygen Species in HEK-293 Cells

*Caterina Bossio[1], Ilaria Abdel Aziz[1,2], Gabriele Tullii[1,2], Elena Zucchetti[1,2], Doriana Debellis[3], Mattia Zangoli[4], Francesca Di Maria[4], Guglielmo Lanzani[1,2] and Maria Rosa Antognazza[1]**

[1] Center for Nano Science and Technology@PoliMi, Istituto Italiano di Tecnologia, Milan, Italy, [2] Dipartimento di Fisica, Politecnico di Milano, Milan, Italy, [3] Electron Microscopy Facility, Istituto Italiano di Tecnologia, Genova, Italy, [4] Institute for Organic Synthesis and Photoreactivity, CNR-ISOF, Bologna, Italy

OPEN ACCESS

Edited by:
Gianni Ciofani, Politecnico di Torino, Italy

Reviewed by:
Varpu Seija Marjomäki, University of Jyväskylä, Finland
Valeria Piazza, Centro de Investigaciones en Optica, Mexico
Grazia Tamma, Università degli studi di Bari Aldo Moro, Italy

***Correspondence:**
Maria Rosa Antognazza
Mariarosa.antognazza@iit.it

Specialty section:
This article was submitted to Nanobiotechnology, a section of the journal Frontiers in Bioengineering and Biotechnology

Received: *18 May 2018*
Accepted: *20 July 2018*
Published: *23 August 2018*

Citation:
Bossio C, Abdel Aziz I, Tullii G, Zucchetti E, Debellis D, Zangoli M, Di Maria F, Lanzani G and Antognazza MR (2018) Photocatalytic Activity of Polymer Nanoparticles Modulates Intracellular Calcium Dynamics and Reactive Oxygen Species in HEK-293 Cells. Front. Bioeng. Biotechnol. 6:114. doi: 10.3389/fbioe.2018.00114

Optical modulation of living cells activity by light-absorbing exogenous materials is gaining increasing interest, due to the possibility both to achieve high spatial and temporal resolution with a minimally invasive and reversible technique and to avoid the need of viral transfection with light-sensitive proteins. In this context, conjugated polymers represent ideal candidates for photo-transduction, due to their excellent optoelectronic and biocompatibility properties. In this work, we demonstrate that organic polymer nanoparticles, based on poly(3-hexylthiophene) conjugated polymer, establish a functional interaction with an *in vitro* cell model (Human Embryonic Kidney cells, HEK-293). They display photocatalytic activity in aqueous environment and, once internalized within the cell cytosol, efficiently generate reactive oxygen species (ROS) upon visible light excitation, without affecting cell viability. Interestingly, light-activated ROS generation deterministically triggers modulation of intracellular calcium ion flux, successfully controlled at the single cell level. In perspective, the capability of polymer NPs to produce ROS and to modulate Ca^{2+} dynamics by illumination on-demand, at non-toxic levels, may open the path to the study of biological processes with a gene-less approach and unprecedented spatio-temporal resolution, as well as to the development of new biotechnology tools for cell optical modulation.

Keywords: conjugated polymer, bio-organic electronics, cell optical stimulation, Ca^{2+} imaging, reactive oxygen species, light, organic semiconductor, photomodulation

INTRODUCTION

By and large, cells are essentially transparent and do not directly respond to light. Visible light is, however, a vital drive for animal behavior and species development. Accordingly, natural evolution resulted in the appearance of photoreceptors cells containing light-sensitive opsin proteins that provide a broad range of photo-induced functions (Morshedian and Fain, 2017). Photoreceptors detect light and trigger a phototransduction chain that ends in a biochemical signaling. Since long

ago, scientists have explored possibilities to artificially induce light sensitivity in living tissues, in order to control physiological functions by photons. This does not simply mean copying nature in order to restore lost photo-functions in damaged organs, but it opens up a wealth of new applications in research, diagnostics and therapy. Light-induced cell control has indeed a number of advantages with respect to more traditional electrical stimulation, such as space and time resolution, reduced invasiveness and selectivity. Optogenetics is one major approach (Deisseroth, 2011). Unfortunately, in spite of the important record of experimental results, it requires the viral transfer of the sample (cell or organ) with exogenous DNA, which raises important safety constraints for application in human subjects and is still considered to be a critical limitation.

For this reason, there is a number of attempts to induce light sensitivity by a gene-less approach. The direct heating of water with a near IR laser radiation (Shapiro et al., 2012), the use of organic and inorganic devices such as photocapacitors and photodetectors (Goda and Colicos, 2006; Farah et al., 2013; Antognazza et al., 2015; Martino et al., 2015; Feyen et al., 2016; Maya-Vetencourt et al., 2017), and the introduction of conducting or semiconducting nanoparticles (Colombo et al., 2016) are among reported strategies. The latter approach is quite interesting, because it allows an easy sensitization of the target tissue and, in principle, it can select specific sites within cell sub-compartments. Nano-scaled inorganic semiconductors, such as quantum dots, are widely studied for the peculiar optical properties induced by the reduced dimensionality. Indeed, they have a huge potential for biological applications, being their dimensions close to the size of biomolecules as proteins and nucleic acids. Although there are many studies on surface functionalization being carried out, the cytotoxicity of QDs still remains an issue, halting their possible biomedical applications (Medintz et al., 2005). Despite this, they offer a strongly selective and sensitive tool for biosensing (Howes et al., 2014) and fluorescence imaging (Bruni et al., 2017). The plasmonic resonance of metallic nanoparticles has been also successfully exploited to gain efficient photo-thermal processes upon NIR radiation (Yang et al., 2017), but in this case high photo-excitation densities are usually required.

Here, we focus our attention on organic semiconducting nanoparticles (NPs), based on poly(3-hexylthiophene) (P3HT). *In vitro* use of conjugated polymer NPs has been widely reported in the literature (Tuncel and Demir, 2010; Feng et al., 2013). However, the exploitation of excellent NPs biocompatibility properties has been mainly limited, so far, to imaging and drug delivery applications (Feng et al., 2010). Conversely, their possible use as functional, light-sensitive actuators was not intensively investigated (Zangoli et al., 2017). Only very recently, we demonstrated an optical modulation effect of P3HT NPs on animal model of *Hydra vulgaris*. P3HT NPs act on the animal both at a macroscopic level, by inducing a behavioral change, and from a molecular point of view, by causing enhanced expression of opsin proteins (Tortiglione et al., 2017).

The goal of the present work is to explore the photoinduced coupling mechanism between P3HT NPs and living cells. Interestingly, we demonstrate that upon illumination polymer NPs both increase the intracellular production of reactive oxygen species (ROS) and modulate Ca^{2+} dynamics. ROS, such as the superoxide anion O_2^- and the hydrogen peroxide H_2O_2, are widely involved in both physiological and pathophysiological processes (Halliwell, 2015). ROS overproduction is highly detrimental since it induces non-specific damage of proteins, lipids, and DNA (Finkel and Holbrook, 2000), causing oxidative stress (Fu et al., 2014) and leading in some cases to irreversible cell damage and apoptosis (Martindale and Holbrook, 2002). Conversely, endogenously produced ROS are essential to life (Trachootham et al., 2009), being involved in different biological functions: among others, signal transduction (Kamata and Hirata, 1999), neurotransmission (Newsholme et al., 2010), blood pressure modulation (Lee and Griendling, 2008), immune system control (Glassman, 2011), and metabolism regulation (Dröge, 2002). These versatile functions of ROS are finely modulated by their amount, duration and localization, and are currently the object of intensive investigation. Alteration in physiological ROS production leads to important pathological conditions, including autoimmune, cardiovascular, and neurodegenerative diseases, so that several ROS-responsive drug delivery systems are under investigation (Saravanakumar et al., 2017). Overall, controlled release of ROS can have highly beneficial therapeutic effects (Bergamini et al., 2004). However, suitable, fully biocompatible, precise, externally modulated and minimally invasive tools are almost completely missing at the moment. Optical modulation represents an interesting route to achieve it (Wang et al., 2012; Waiskopf et al., 2016).

Not invasive ways to modulate calcium ions flow are attracting considerable attention as well, given their key role in cell metabolism and inter-cell communication processes. Several attempts have been reported to modulate Ca^{2+} by external mediators, for instance by using magnetic NPs (Huang et al., 2010; Stanley et al., 2012; Bar-Shir et al., 2014; Lee et al., 2014; Chen et al., 2015; Wheeler et al., 2016), metallic NPs (Nakatsuji et al., 2015), organic molecules and polymers (Stein et al., 2013; Lyu et al., 2016; Takano et al., 2016) and other carbon-based materials (Miyako et al., 2014; Chechetka et al., 2016).

Interestingly, there is a close interplay between ROS and Ca^{2+} dynamics (Chakraborti et al., 1999; Brookes et al., 2004; Görlach et al., 2015), whose intensive investigation may benefit from the availability of not-invasive, locally confined and reversible tools.

Here, we show that photoexcitation of P3HT NPs internalized within Human Embryonic Kidney (HEK-293) cells leads to an increase of ROS level, associated to a variation of the intracellular Ca^{2+} dynamics. In perspective, this work may pave the way to the development of new tools for local, optical modulation of the cell physiological activity.

MATERIALS AND METHODS

Cell Cultures

HEK-293 cells were grown in Dulbecco's modified Eagles' medium (D-MEM, Sigma Aldrich) with 10% fetal bovine serum (FBS, Sigma Aldrich), supplemented with 2 mM glutamine (Sigma Aldrich), 100 U/ml streptomycin (Sigma Aldrich) and

100 U/ml penicillin (Sigma Aldrich). Cells were kept in T-75 culture flasks and maintained in incubator at 37°C in a humidified atmosphere with 5% CO_2. After reaching 80–90% of confluence, cells were detached by incubation with 0.5% trypsin-0.2% EDTA (Sigma Aldrich) for 5 min and plated for experiments. To promote cell adhesion, a layer of 2 mg/ml fibronectin (from bovine plasma, Sigma Aldrich) in phosphate buffer saline (PBS, Sigma Aldrich) was deposited on the surface of the glass coverslips and incubated for 30 min. After rinsing the fibronectin with PBS, cells were plated in their culture medium and eventually treated with polymer NPs.

Preparation and Characterization of P3HT NPs Dispersions

Sterile P3HT and Polystyrene (PS) NPs were prepared by the re-precipitation method working under a laminar flow hood. P3HT (regio-regular, Sigma Aldrich) was dissolved in tetrahydrofuran (THF, Sigma Aldrich) and the resulting polymer solution was added drop-wise to sterilized water under magnetic stirring. The resulting colloidal dispersion was put in a dialysis sack and subjected to dialysis against 2 l sterilized water overnight to remove the residual organic solvent. Afterwards, the water colloidal suspension was centrifuged at different rates for 10 min, from 2,000 to 8,000 rpm, separating every time the supernatant from the precipitate, to obtain a wide range of samples with different particle dimensions (from 100 to 600 nm) and different optical density (OD). The NPs used in this work have an average hydrodynamic radius of 237 ± 82 nm, a polydispersity index of 0.12. The ODs of the dispersion administered to the cell cultures are 0.05, 0.2, 0.4. NPs are dissolved in a volume of 1 ml of culture medium 24 h before measurements. Dynamic Light Scattering (DLS) measurements were performed with a Nanobrook Omni Particle Size Analyzer, with a wavelength of 659 nm in back-scattering mode. Particles were dispersed in distilled water or cell culturing medium during analysis. Measurements were taken at 25°C. Zeta potential evaluation was performed using Smoluchowski equation. The optical absorption spectra were acquired by using Perkin Elmer Lambda 1050 UV/Vis/NIR Spectrophotometer and, for NPs upload estimation, TECAN Spark 10M Plate reader. The photoemission spectra were recorded by using HORIBA Jobin Yvon NanoLogTM spectrofluorimeter.

Scanning Electron Microscopy (SEM)

Cells treated with P3HT NPs and grown on an indium-tin oxide (ITO) covered coverslip were fixed with Glutaraldehyde (Sigma Aldrich) 2.5% for 20 min. Then cells were dehydrated with incubation in solutions at increasing concentration of ethanol (Sigma Aldrich). Images were acquired with the Scanning Electron Microscope MIRA3 TESCAN.

Transmission Electron Microscopy (TEM)

HEK293 cells were incubated with P3HT NPs for 24 h and were processed following a published protocol (Marotta et al., 2013). Briefly the cells after incubation were fixed for 1 h in 1.2% glutaraldehyde in 0.1 M sodium cacodylate buffer (Sigma Aldrich, pH 7.4), post fixed in 1% osmium tetroxide (Sigma Aldrich) in the same buffer and en bloc stained with 1% uranyl acetate aqueous solution. The cells were then dehydrated in a graded ethanol series and embedded in epoxy resin (Epon 812, TAAB). Semi-thin and thin sections of the embedded cell monolayer were cut with an ultramicrotome (UC6, Leica) equipped with a diamond knife (Diatome). Projection images were acquired using a JEOL JEM 1011 transmission electron microscope operating at at 100 kV of acceleration voltage and recorded with a 2 Mp charge-coupled device (CCD) camera (Gatan Orius SC100).

Immunocytochemical Studies

Cells treated with P3HT NPs grown on fibronectin-coated glass coverslips were washed twice with PBS and fixed for 20 min at RT in 4% paraformaldehyde (Sigma Aldrich) and 4% sucrose (Sigma Aldrich) in 0.12 M sodium phosphate buffer, pH 7.4. Labeling with phalloidin and fluorescein Isothiocyanate (Sigma Aldrich) was applied in GDB buffer (30 mM phosphate buffer, pH 7.4, containing 0.2% gelatin, 0.5% Triton X-100 and 0.8 M NaCl (Sigma Aldrich) for 2 h at RT.

Viability Assay

In order to preliminarily evaluate the NPs cytotoxicity, the MTT [3-(4,5-dimethylthiazol-2-yl)-2,5-diphenyltetrazolium bromide] (Sigma Aldrich) assay was performed on HEK-293 cells. Cells were seeded in 12 wells plates at a density of 2×10^4 cells/well, together with the NPs. Cell proliferation was evaluated after 24, 48, 72, and 96 h incubation. For each time point, the growing medium was replaced with RPMI without phenol red (Sigma Aldrich) containing 0.5 mg/ml of MTT. The samples were incubated again for 3 h at 37°C in dark. Formazan salt produced by cells through reduction of MTT was then solubilized with 200 μl of ethanol and the absorbance was read at 560 and 690 nm. The proliferation cell rate was calculated as the difference in absorbance at 560 and 690 nm. Photocytoxicity of NPs- treated cells subjected to optical excitation has been evaluated by Fluorescein Diacetate (FDA, Sigma Aldrich) assay. FDA is a non-fluorescent molecule, which is hydrolyzed to fluorescent fluorescein in viable cells only. Different cohorts of HEK-293 cells (treated/untreated with P3HT NPs, subjected/not subjected to photoexcitation) were incubated for 5 min with FDA 5 μM. After careful wash outs of the excess FDA from the extracellular medium and repeated rinses with physiological saline solution, representative images were acquired (excitation/emission wavelengths, 490/520 nm, integration time 100 ms) using an inverted fluorescence microscope (Nikon Eclipse Ti; 20× objective), equipped with an Analog-WDM Camera (Cool Snap Myo, Photometrics). Photocytotoxicity tests have been carried out in different experimental conditions, namely: (i) at different NPs doses, corresponding to OD values in the range 0–0.5, at 2 DIV/24 h after illumination. The photoexcitation protocol used in FDA assay is the same employed in ROS detection experiments (see below); (ii) at fixed NP dose, corresponding to OD = 0.2, at different time points after the photoexcitation protocol, up to 4 DIV/72 h after illumination. Specific care was taken in order to image, at different time points, exactly the same sample area previously subjected to optical excitation. All

experiments were carried out in relevant control samples as well (untreated and/or not illuminated cell cultures).

Chronoamperometry Measurements

Photocurrent measurement was carried out by using a potentiostat/galvanostat (Autolab, PGSTAT 302N). The electrochemical cell was in three-electrode configuration and was divided into two compartments, connected by a saline bridge. One compartment contained the reference and the counter electrodes, a saturated KCl Ag/AgCl and Pt wire respectively, immersed in the pure electrolyte (phosphate buffer 10 mM, pH 7). The second compartment contained the Indium-Tin-Oxide (XynYan Technology, 15 nm thickness, sheet resistance 15 ohm/sq) working electrode and the P3HT NPs dissolved in the same electrolyte solution. Chronoamperometry measurements were performed at the electrochemical equilibrium, by applying a potential equal to the open circuit potential (OCP), and by changing the applied voltage in the range (OCP - 300 mV) $\leq$ V $\leq$ OCP vs. Ag/AgCl. A continuous light source (Thorlabs LED M470L3-C5, 470 nm central emission wavelength) was used for the photoexcitation, with a power density of 2.7 mW/mm^2. The photocurrent data at fixed wavelengths were obtained by exciting the NPs dispersion with six CW LED light sources in the visible spectrum. Peak emission wavelengths and corresponding power densities are: $\lambda_1 = 470$ nm, $P_{D1} = 3.45$ mW/mm^2; $\lambda_2 = 505$ nm, $P_{D2} = 1.69$ mW/mm^2, $\lambda_3 = 530$ nm, $P_{D3} = 1.36$ mW/mm^2, $\lambda_4 = 617$ nm, $P_{D4} = 2.02$ mW/mm^2, $\lambda_5 = 627$ nm, $P_{D5} = 2.01$ mW/mm^2, $\lambda_6 = 655$ nm, $P_{D6} = 2.21$ mW/mm^2).

Reactive Oxygen Species (ROS) Detection

Dichlorofluorescein diacetate (H_2DCF–DA, Sigma Aldrich), 2-[6-(4′-amino)-phenoxy-3H-xanthen-3-on-9-yl] benzoic acid (APF, Sigma Aldrich) and 2-[6-(4′-Hydroxy)-phenoxy-3H-xanthen-3-on-9-yl] benzoic acid (HPF, Sigma Aldrich) were employed for intracellular detection of Reactive Oxygen Species (ROS). Sterile P3HT and PS NPs were administered to the cells at the plating step, by diluting them in the extracellular medium up to the desired concentration, corresponding to OD = 0.05, 0.2, 0.4. At 1DIV HEK-293 cells already showed uniform coverage of the substrate (about 40% confluence) and NPs were efficiently internalized within the cell cytosol. Excess, non-internalized NPs were removed by subsequent, repeated rinses of the extracellular medium. NPs treated cells and control, untreated cells were photo-excited by illuminating each sample for 2 min with a LED system (Lumencor Spectra X light engine, $\lambda = 540$ nm, $P_D = 95$ mW/mm^2). Subsequently, cells were incubated with the ROS probes for different times according to the employed probe ($t_{H2DCF-DA} = 30$ min, $t_{APF} = t_{HPF} = 40$ min). After careful wash-out of the excess probe from the extracellular medium, the fluorescence of the probes was recorded (excitation/emission wavelengths, 490/520 nm; integration time, 70 ms for H_2DCF–DA and 500 ms for HPF e APF) with an inverted microscope (Nikon Eclipse Ti), equipped with an Analog-WDM Camera (Cool Snap Myo, Photometrics). The same protocol was employed for control, untreated cells. Variation of fluorescence intensity was evaluated over Regions of Interest covering single cells areas, and reported values represents the average over multiple cells. See figure captions and SI for additional details about statistical analysis. Image processing was carried out with ImageJ and subsequently analyzed with Origin 8.0.

Intracellular Ca^{2+} Measurements

HEK-293 cultures were loaded for 30 min at 37°C with 1 μM Fluo-4 (Life Technologies) in extracellular solution (5 mM HEPES; 135 mM NaCl, 5,4 mM KCl, 1 mM $MgCl_2$, 1,8 mM $CaCl_2$, 10 mM glucose, all purchased from Sigma Aldrich; pH 7.4) and Ca^{2+} free extracellular solution (10 mM HEPES; 150 mM NaCl, 3 mM $MgCl_2$, 5 mM EGTA, all purchased from Sigma Aldrich; pH 7.4). Then, cells were washed for 10 min with pre-warmed extracellular solution before recordings. Cells treated with P3HT and PS NPs, as well as untreated samples, were illuminated for 3 min (emission peak wavelength, 485 nm; photoexcitation density, 2.1 mW/mm^2 and 14.6 mW/mm^2, spot size 0.9 mm^2) by using a LED source light (Lumencor Spectra X light engine). Videos were collected with an inverted microscope Nikon Eclipse Ti equipped with an Analog-WDM Camera (Cool Snap Myo, Photometrics). Variation of fluorescence intensity was evaluated over Regions of Interest covering single cells areas, and reported values represents the average over multiple cells. See Figure captions and SI for additional details about statistical analysis. Image processing was carried out with ImageJ and subsequently analyzed with Origin 8.0. ROS inhibition was obtained by administration of N–Acetyl–Cysteine (NAC, Sigma Aldrich), dissolved in extracellular solution (with and without Ca^{2+}) at a final concentration of 10 μM.

Statistical Analysis

See SI section.

RESULTS

Optical and Microscopy Characterization of Polymer P3HT Nanoparticles (P3HT NPs)

Polymer NPs, entirely constituted by poly(3-hexylthiophene), have been synthesized by the re-precipitation method in sterile conditions, as previously described (Zucchetti et al., 2016). P3HT NPs have an average hydrodynamic diameter of 237 ± 82 nm and a polydispersity index of 0.12, as measured by dynamic light scattering (**Figure S1A**). They also show excellent colloidal stability, being characterized by a zeta-potential value of −35 ± 8 mV. Recent literature has firmly established the importance of studying in detail the interaction between polymer-coated NPs and proteins, which largely affects cellular uptake and cytotoxicity (Hühn et al., 2013). Here, colloidal stability within the cell culturing medium (D-MEM, without the pH indicator phenol red) was evaluated over time, by carrying out both DLS measurements (i.e., by assessing modifications of the hydrodynamic diameter, **Figure S1B**), UV-Vis absorption and photoluminescence spectroscopy (**Figures S1C,D**). Three different NPs dispersions have been considered, corresponding to optical density values of 0.2, 0.4, and 0.5. In all cases, NPs dispersions do not show significant aggregation effects within the cell culturing medium, up to 48 h. The optical absorption and emission spectra of P3HT NPs aqueous dispersion are

reported in **Figures 1A,B**, respectively (inset, P3HT chemical structure). It has been recently demonstrated that the optical properties of P3HT NPs are well preserved within the cell cytosol environment (Zucchetti et al., 2016). Preliminary studies of P3HT NPs toxicity both in Human Embryonic Kidney (HEK-293) cells (Zucchetti et al., 2016) and in *Hydra Vulgaris* animal models (Tortiglione et al., 2017) have been previously carried out in dark condition, and no clear adverse effects were reported. In this work, P3HT NPs were administered to the HEK-293 cell culturing medium at the cell plating step, and their cytotoxicity was preliminarily evaluated by measuring cellular proliferation through the MTT method. The assay relies on the capability of living cells to metabolize/reduce a water-soluble tetrazolium salt (3-(4′,5′-dimethylthiazol-2′-yl)-2,5-diphenyl-2H-tetrazolium hydrobromide, MTT) into a water-insoluble formazan product, which has a characteristic purple color. The optical absorption of formazan is thus considered a clear indicator of cell viability and capability to proliferate, being proportional to the number of living cells. **Figure S2** shows the formazan optical absorption recorded in NPs -treated and -untreated cells at four different time points, 1, 2, 3, and 4 days after incubation (DIV). The presence of NPs

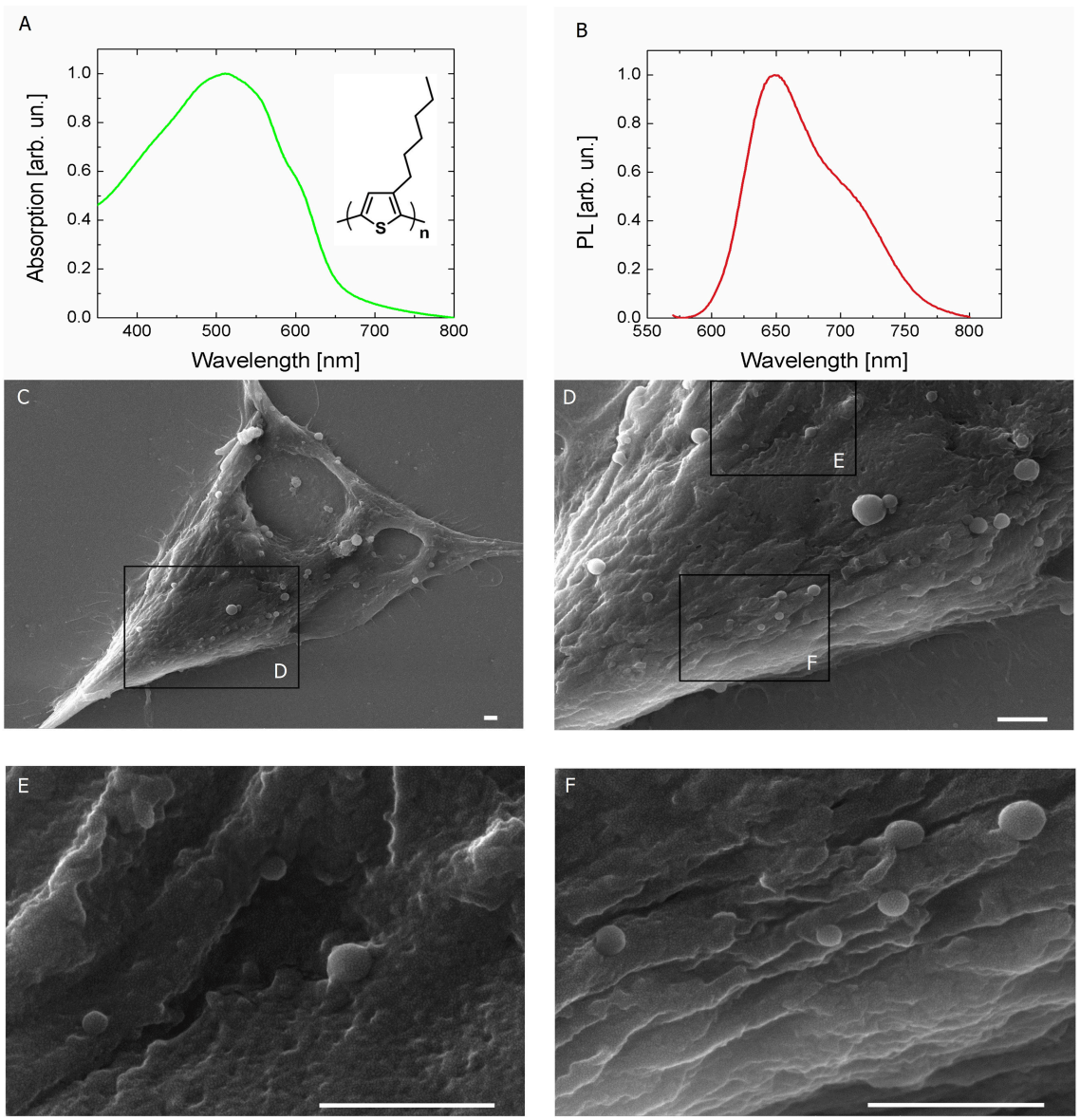

FIGURE 1 | Light sensitive P3HT NPs and HEK-293 living cells. **(A,B)** Optical absorption and fluorescence (PL) spectra of P3HT NPs in aqueous dispersion. P3HT chemical structure is also shown in the inset. **(C–F)** Top view scanning electron microscopy (SEM) images of HEK-293 cells treated with P3HT NPs, at increasing magnification. Scale bar, 1 μm.

leads in general to a reduced cell proliferation with respect to untreated samples; the absorption percentage variation between treated and untreated cell cultures is about 45% at DIV 1. This difference, however, shows a partial recovery over time, and amounts at 20%, from DIV 2 onwards, up to DIV 4. Scanning electron microscopy (SEM) images (**Figures 1C–F**) document the very well defined spherical geometry and the good surface smoothness of NPs. The limited presence of aggregates is a further index of the high stability properties within the cellular environment of P3HT NPs, despite the absence of any surfactant agent during the fabrication protocol. P3HT NPs can be easily visualized by fluorescence imaging, thanks to their intrinsic photoluminescence peaking in the red spectral region (**Figure 1B**). Effective P3HT NPs internalization within HEK-293 cell cytosol was previously assessed by confocal laser scanning microscopy (Zucchetti et al., 2016). Here, P3HT NPs cellular uptake was quantitatively estimated by using two different methods, based on fluorescence imaging (**Figure S3**) and variation of the optical absorption spectrum of the NPs dispersion before and after 24 h administration to the cell cultures (**Figure S4**). In both cases, three initial concentrations of P3HT NPs dispersions were considered, corresponding to optical density values of 0.05, 0.2, and 0.4. In the latter two cases, effective NPs upload is detected, in the order of few hundreds of NPs /cell, in agreement with previously reported CLSM data. Conversely, for the lowest considered concentration of the dispersion, a considerably lower fraction of NPs undergoes efficient internalization within the cell cytosol (see details in the SI section). Finally, for control experiments, we used light-insensitive polystyrene NPs (PS NPs). These NPs have dimensions and zeta-potential values (hydrodynamic diameter, 225 ± 72 nm; zeta-potential, −41.8 ± 1.1 mV) similar to P3HT NPs, but do not have remarkable optoelectronic properties: they have negligible absorption in the blue-green spectral range, do not generate electric charges upon optical excitation and are electrically insulating materials, thus representing a good model for control, optically and electrically inert NPs. Detailed characterization of PS NPs properties and colloidal stability within the cell culturing medium over time are reported in the SI section (**Figure S5**). Transmission electron microscopy (TEM) analysis corroborates SEM and fluorescence imaging showing the presence of endosome-like compartments inside the cell cytoplasm. These compartments are filled with electron-dense nanoparticles compatible in shape and size with the P3HT NPs (**Figure S11**).

P3HT NPs Photo-Electrochemical Characterization

The photo-electrochemical activity of P3HT polymer thin films in an aqueous saline environment has been reported in a number of recent works (Lanzarini et al., 2012; Bellani et al., 2015; Giron et al., 2016; Tullii et al., 2017). The observed photocurrent generation has been attributed to photo-electrochemical reactions, leading to oxygen and, less efficiently, to hydrogen reduction. In the present case, P3HT NPs are dispersed in a phosphate buffer solution (10 mM, pH 7, optical density of 2). Their capability to photo-generate charges has been initially assessed. We carried out chrono-amperometry and spectral responsivity measurements on the NPs dispersion in a three electrode configuration, employing a planar ITO slab, a saturated KCl Ag/AgCl and a Pt wire as the working (WE), the reference (RE) and the counter electrode (CE), respectively (**Figure 2A**). Visible light is incident from the glass substrate of the ITO slab. In order to avoid electrode contamination by P3HT NPs, the WE, immersed in the dispersion, was separated from the RE and CE compartment by a saline bridge. Prior to chrono-amperometry measurements, the open circuit potential (OCP) value was estimated, being about 150 mV. Photocurrent has been measured at different excitation wavelengths by using six LED light sources (**Figure 2B**, red diamond symbols). The spectral dependence shows a symbatic behavior, closely resembling the optical absorption spectrum of the P3HT thin film (red dashed line). This indicates that the recorded current is undoubtedly due to charge photogeneration by polymer NPs and allows to exclude spurious reduction/oxidation effects. Chronoamperometry measurements have been then carried out, by applying fixed bias V in the range (OCP-300 mV) $\leq V \leq$ OCP, with steps of 100 mV amplitude (**Figure 2C**). Upon light excitation (470 nm peak excitation wavelength, 3 min stimuli duration, 2.7 mW/mm^2 photoexcitation density), a photocurrent signal is recorded, with increasing amplitude at increasingly negative bias. The external quantum efficiency, defined as the ratio between the number of electrons flowing in the external circuit and the number of incident photons per unit time at a fixed wavelength (470 nm in our case), is very low, in the order of 10^{-6}, four orders of magnitude lower than the value obtained in hybrid solid/liquid devices based on bulk heterojunction polymer thin films, namely P3HT doped with the fullerene derivative electron acceptor phenyl-C61-butyric acid methyl ester (Lanzarini et al., 2012; Bellani et al., 2015). Still, these results unequivocally demonstrate that P3HT NPs can photo-generate free charges, which interact with the surrounding electrolyte and sustain photo-electrochemical reactions. Photocurrent dynamics recorded by using P3HT polymer samples prepared in different ways (namely, P3HT thin films spin-coated from solution onto the ITO WE, P3HT NPs thin films casted from dispersion and ITO WE previously subjected to P3HT NPs exposure) all show negative photocurrent signal, like in the case of NPs dispersion (**Figure S6**), thus indicating similar interfacial charge transfer mechanisms at the ITO electrode. In particular, in accordance with the observed photocurrent sign, photogenerated holes (carried by the ionized NPs or NP^+) are efficiently transferred to the WE, while electrons react with species present in solution. In analogy with results obtained with polymer thin films (Tullii et al., 2017), we believe that the predominant photo-electrochemical reaction at NPs surface is reversible oxygen reduction, which leads to the creation of reactive oxygen species, such as O_2^-. This is fully confirmed by photocurrent measurements with P3HT NPs dispersion in de-oxygenated condition, and after partial re-oxygenation (**Figure 2D**).

The energetic alignment of HOMO and LUMO levels of P3HT polymer (∼5 and ∼3.5 eV, respectively) with respect to the ITO work function (∼4.5 eV for oxygen-plasma treated substrates,

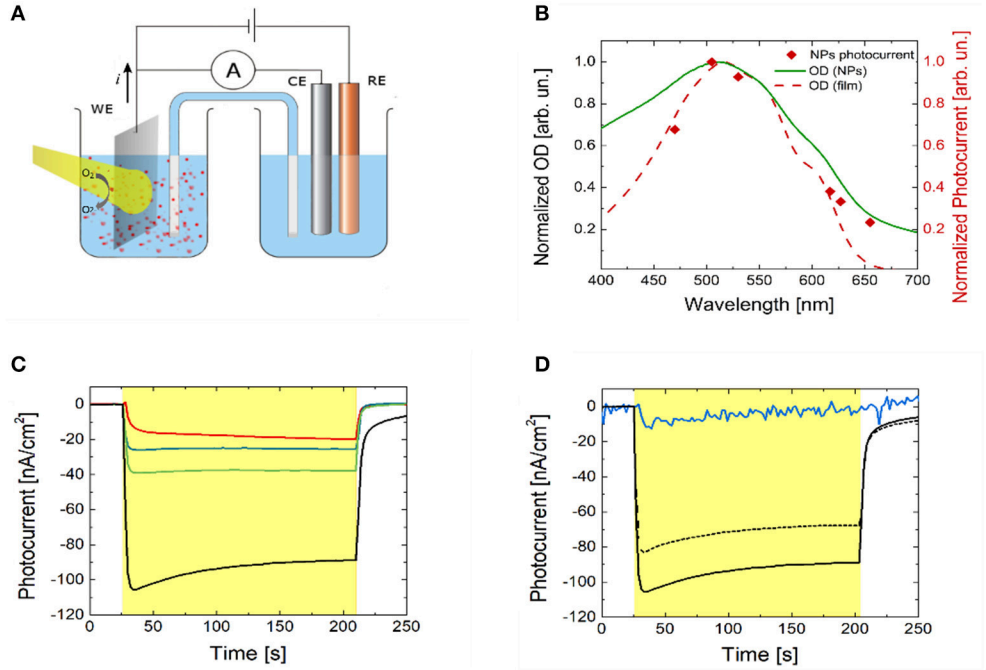

FIGURE 2 | P3HT NPs photo-electrochemical characterization. **(A)** Experimental set-up used for photocurrent action spectrum and chronoamperometry experiments. A planar ITO slab, a saturated KCl Ag/AgCl, and a Pt wire are used as the back contact, the reference (RE) and the counter electrode (CE), respectively. Phosphate Buffer Saline solution at 10 mM molar concentration and pH = 7.0 has been used as the electrolyte. Light is incident from the glass side of the ITO slab. **(B)** Normalized absorption spectra of P3HT thin solid film (red dashed line) and of NPs dispersion (green solid line) are compared with the P3HT NPs photocurrent action spectrum (red diamonds). The latter was obtained by plotting the steady value of the photocurrent obtained by exciting the NPs dispersion with six narrow-band light sources covering the visible range (emission peak wavelengths at 470, 505, 530, 617, 627, 655 nm). **(C)** Photocurrent dynamics recorded in P3HT NPs dispersion (light source emission peak wavelength, 470 nm). The red line represents the photocurrent at the OCP value. The blue, green and black lines show the photocurrent signals recorded upon externally applied bias OCP–100 mV, OCP–200 mV, and OCP–300 mV, respectively. The yellow shaded area represents the temporal window corresponding to optical excitation. **(D)** Photocurrent dynamics with and without molecular oxygen in solution at V = OCP–300 mV. The black solid line represents the photocurrent recorded in ambient conditions (i.e., in equilibrium with the atmosphere). Upon removal of oxygen from the electrolyte and in sealed, nitrogen atmosphere the photocurrent signal is almost completely suppressed (blue solid line). Upon partial re-oxygenation of the electrolyte solution and recovery to the atmospheric equilibrium condition, photocurrent signal is almost completely restored to the initial value (black dashed line). The yellow shaded area represents the temporal window corresponding to optical excitation.

well aligned with the polymer HOMO level) and to the 1-electron oxygen reduction reaction $O_2/O_2^{\cdot-}$ (– 0.33 V vs. SHE at pH 7, corresponding to ∼4.1 V in the absolute scale, well aligned with the P3HT LUMO level) are in agreement with this picture. P3HT NPs work function has been experimentally evaluated by Kelvin Probe measurements, obtaining values slightly lower than P3HT polymer thin films [4.5 vs. 4.8 eV, respectively, in line with recent literature (Di Maria et al., 2017)], which may further facilitate the occurrence of oxygen reduction reactions.

Production of Reactive Oxygen Species (ROS)

Photocurrent measurements demonstrate the occurrence of photo-electrochemical reactions, possibly involving reactive oxygen species (ROS) as intermediates and/or final products.

We experimentally compared the modulation of ROS production within the cell cytosol, in NPs treated and control samples, either in dark or subjected to photoexcitation. To this goal, we use intracellular ROS fluorescent probes, namely 2,7-dichlorodihydrofluorescein diacetate (H_2DCF-DA), 2-[6-(4′-amino)-phenoxy-3H-xanthen-3-on-9-yl] benzoic acid (APF) and 2-[6-(4′-Hydroxy)-phenoxy-3H-xanthen-3-on-9-yl] benzoic acid (HPF). H_2DCF-DA has been widely employed for the detection of ROS in several cell models, due to its capability to rapidly diffuse through the cellular membrane (Wang and Joseph, 1999). Cellular esterase first hydrolyzes the non-fluorescent H_2DCF-DA to H_2DCF, which is then oxidized by ROS and originates the fluorescent compound 2,7-dichlorofluorescein (DCF). Three different samples cohorts have been taken into account: non treated cells, cells treated with P3HT NPs, and cells treated with electrochemically inert, light-insensitive PS NPs. For each experimental group, two different conditions have been considered, cells subjected to illumination (2 min, 95 mW/mm^2 photoexcitation density) prior to ROS detection analysis, and cells kept into dark conditions. We found that cells treated with NPs and subjected to illumination protocol show a statistically significant increase in ROS production, as compared to control untreated cells, and/or to treated cells in dark condition (**Figure 3A**). Since H_2DCF-DA is sensitive to a large variety of different ROS,

including H_2O_2, $HO^{\cdot}$, $ROO^{\cdot}$, we also used APF and HPF, which exhibit strong fluorescence enhancement upon O-dearylation, as induced by reactive species. APF and HPF provide complementary information with respect to H_2DCF-DA because they are sensitive to $HO^{\cdot}$, $ONOO^{-}$, and HOCl, but not to H_2O_2 (Gomes et al., 2005). In addition, they show much higher resistance to auto-photo-oxidation, being more suitable for the comparative evaluation of the effects of visible light illumination. APF and HPF data, shown in **Figures 3B,C** respectively, confirm that significant production of ROS occurs only in the case of cells treated with polymer NPs and previously subjected to the illumination protocol. **Figures 3D–F** show representative images of the fluorescence enhancement obtained in HEK-293 cells treated with P3HT NPs and illuminated for 2 min prior to ROS detection tests with H_2DCF-DA (**Figure 3D**), APF (**Figure 3E**), and HPF (**Figure 3F**).

Modulation of Intracellular Ca^{2+} Dynamics

Recent literature highlighted the mutual crosstalk between ROS and Ca^{2+} dynamics. It has been reported that the cell redox state can efficiently modulate the activity of a variety of Ca^{2+} channels, and, on the other hand, Ca^{2+} signaling actively contributes to control the production of ROS[47].

To determine if the observed ROS enhancement leads to specific modulation of calcium dynamics, we monitored the intracellular Ca^{2+} ion concentration by using Fluo-4 as a calcium indicator. We employed two different light photoexcitation densities, namely 2.1 and 14.6 mW/mm^2.

Taking advantage of the partial spectral overlap between the light absorption of the polymer NPs and the excitation spectrum of the Fluo-4 calcium indicator, we used the same illumination protocol both to optically excite the P3HT NPs and to monitor Ca^{2+} dynamics at the same time. In all considered cases continuous illumination for 3 min has been employed, coherently with protocols used in photoelectrochemical measurements and ROS detection analysis.

While optical stimulation at low excitation density (2.1 mW/mm^2) did not lead to significant differences among considered experimental conditions (**Figures S7A,D,G**), higher intensity (14.6 mW/mm^2) optical excitation of P3HT NPs - treated cells led to significant activation of Ca^{2+} dynamics (**Figure 4**). **Figure 4A** shows 3 representative Ca^{2+} transient dynamics for each considered case; the whole ensemble of registered curves ($n \geq 100$) is reported in **Figures S7B,E,H**. Ca^{2+} peak amplitude shows a relative increase of about 60% both with respect to untreated cells and to cells treated with PS NPs. No significant changes in Ca^{2+} dynamics were detected in positive

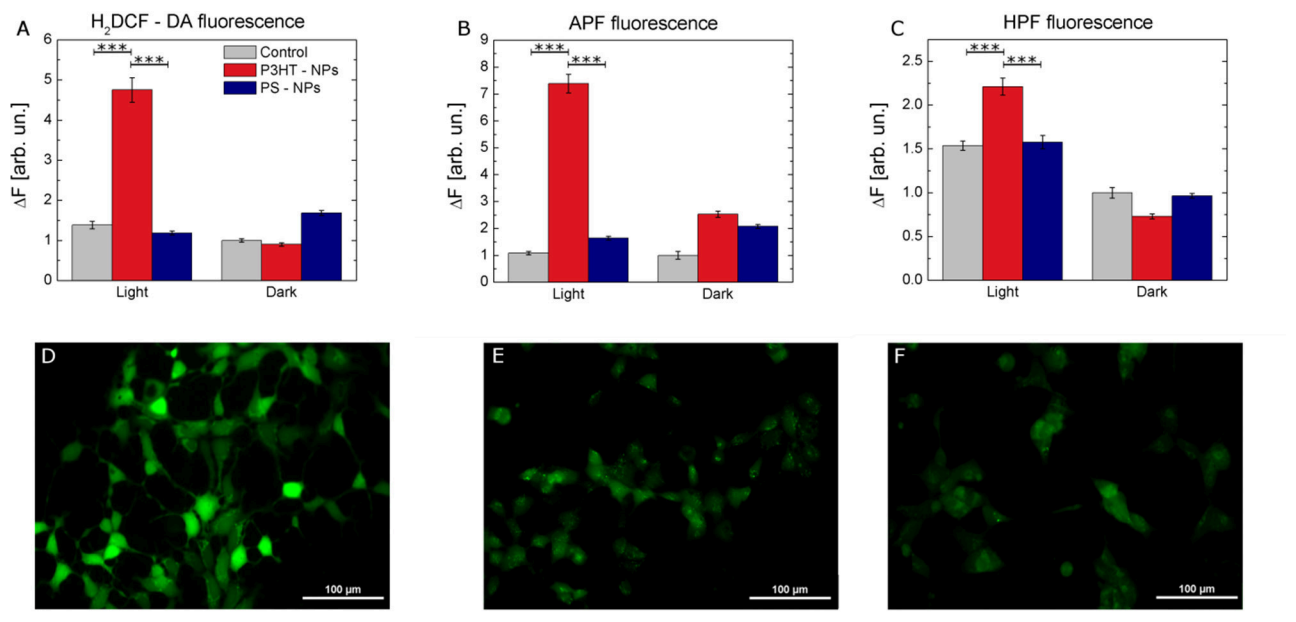

FIGURE 3 | Intracellular ROS production by P3HT NPs optical excitation. **(A–C)** Fluorescence variation intensity measured in control (gray), P3HT NPs–treated (red), and PS NPs treated (blue) cells, due to ROS sensitive intracellular probes (H_2DCF-DA, **A**, APF, **B**, and HPF, **C**). Data are represented as mean ± SE values, over statistical samples of $n = 34$ (control light), $n = 81$ (control dark), $n = 49$ (P3HT NPs light), $n = 102$ (P3HT NPs dark), $n = 109$ (PS NPs light), $n = 105$ (PS NPs dark) for H_2DCF-DA; $n = 57$ (control light), $n = 26$ (control dark), $n = 90$ (P3HT NPs light), $n = 63$ (P3HT NPs dark), $n = 70$ (PS NPs light), $n = 69$ (PS NPs dark) for APF; $n = 110$ (control light), $n = 118$ (control dark), $n = 137$ (P3HT NPs light), $n = 120$ (P3HT NPs dark), $n = 147$ (PS NPs light), $n = 120$ (PS NPs dark) for HPF, where n represents the number of cells over three different experiments for each condition. Statistical significance has been evaluated by one-way ANOVA analysis followed by *post-hoc* Tukey test. *P*-values of the test are assigned as follows: *** for $p < 0.001$. Statistically non-significant results are not marked in the figures. All details of statistical analysis are reported in the SI section. **(D-F)** Representative images of ROS-induced fluorescence response of H_2DCF-DA **(D)**, APF **(E)**, HPF **(F)** in P3HT NPs treated cells. Fluorescence images have been acquired after carrying out the protocol for NPs excitation, as described in detail in the Methods section. Scale bar, 100 μm.

and negative control experiments, i.e., in illuminated, untreated cells and illuminated cells treated with inert, light-insensitive PS NPs (**Figure 4B**). Representative fluorescence images at different time points are reported in Figures S12A–H, to give a direct reply of the reported curves.

The Ca^{2+} sources involved in the stimulation, e.g., intracellular stores and/or extracellular environment, were investigated in Ca^{2+}-free conditions, and in the presence of 5 mM of the Ca^{2+} chelator ethylene glycol tetraacetic acid, EGTA. **Figure 4D** shows 3 representative curves for each case. The whole data set is reported in **Figures S8A,D,G** at lower intensity photoexcitation and **Figures S8B,E,H** at a higher intensity photoexcitation. Representative fluorescence images at different time points are reported in **Figures S12I–R**, to give a direct reply of the reported curves. **Figure 4E** shows that the relative increase of fluorescence intensity exhibited by P3HT NPs-treated cells in absence of extracellular Ca^{2+} is not significantly different from the one obtained in standard conditions ($\Delta F = 1.92$ and $\Delta F = 1.85$, respectively). This indicates that Ca^{2+} influx through the plasma membrane does not play a significant role and that the main origin of activation is in intracellular Ca^{2+} stores.

Based on results reported so far, we conjecture that light-evoked production of ROS in the cell cytosol acts as the main source of the observed intracellular Ca^{2+} increase. In order to verify this hypothesis, after cell cultures illumination, we supplemented cell cultures with a well-known ROS inhibitor, N-Acetyl-L-cysteine (NAC), and thereafter we carried out Ca^{2+} fluorescence imaging experiments, reported in **Figures 4C,F** (complete data sets are shown in panels **C,F,I** of **Figures S7, S8**). Interestingly, Ca^{2+} dynamics were significantly silenced, in the presence of extracellular Ca^{2+} as well as in Ca^{2+} free extracellular solution.

Dependence of ROS Production and Ca^{2+} Modulation on P3HT NPs Concentration

We investigated the effect of different polymer NPs dispersion concentrations on ROS production and modulation of Ca^{2+} dynamics (**Figure 5**). We compared three concentrations of NPs, corresponding to optical densities of 0.05, 0.2, and 0.4. **Figures 5A–C** show the effect of different NPs doses on ROS production, as evaluated by using H_2DCF-DA, HPF, and APF probes, respectively. In all the considered cases, the increased number of internalized P3HT NPs does not influence, *per se,* the production of ROS, which is not statistically different from the values recorded in untreated, control samples (dark condition, gray histograms). Conversely, upon visible light excitation, NPs concentration strongly affects ROS evolution (light condition, red histograms). We notice that the lowest NP concentration, corresponding to an initial optical density

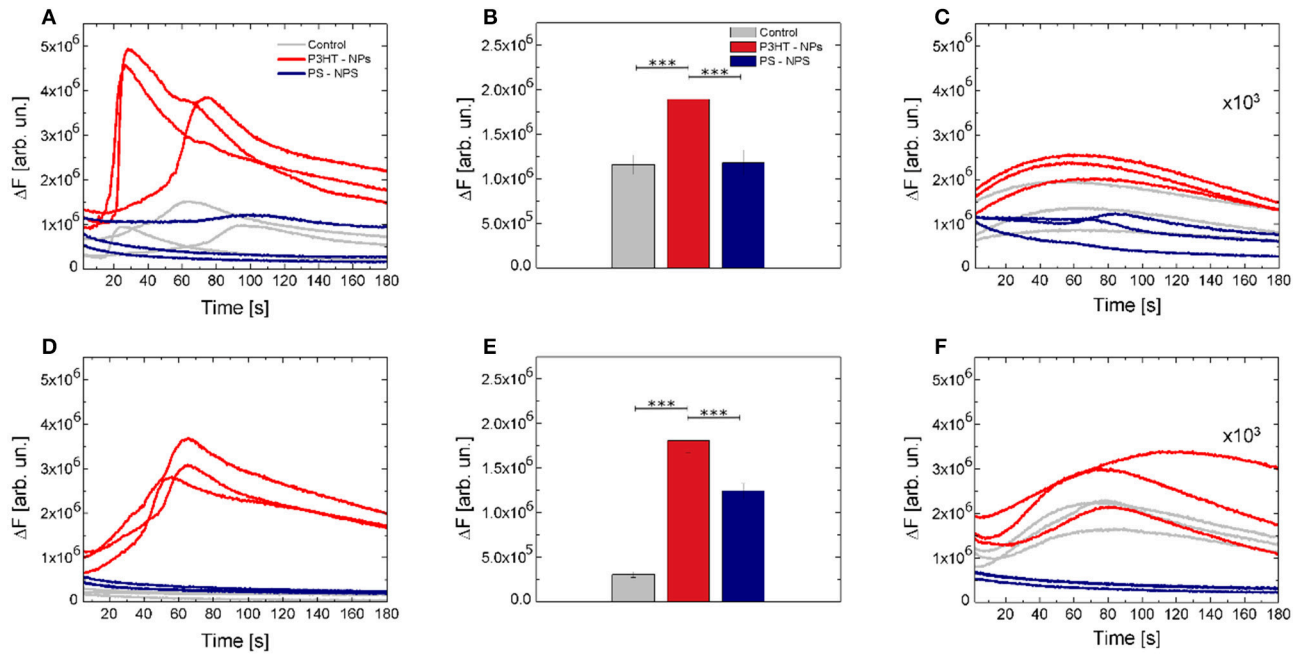

FIGURE 4 | Optical modulation of intracellular Ca^{2+} dynamics. **(A)** Representative Ca^{2+} dynamics recorded in control (gray solid lines), P3HT NPs treated cells (red solid lines) and PS NPs treated cells (blue solid lines). **(B)** Fluorescence relative increase of the Fluo-4 calcium indicator. Data are shown as mean ± SE, over statistical sample sets of $n = 71$, $n = 68$, $n = 55$ cells (for control, P3HT NPs and PS-NPs samples, three experiments for each condition, respectively). Statistical analysis has been carried out by one-way ANOVA, followed by *post-hoc* Tukey test. *P*-values of the test are assigned as follows: *** for $p < 0.001$. Statistically non-significant results are not marked in the figure. See SI section for all details of statistical analysis. **(C)** Effect of the specific ROS inhibitor (NAC) on Ca^{2+} dynamics. Data have been multiplied by a 10^3 factor, to make them visible over the same y-axis scale used in **(A)**. **(D–F)** Representative Ca^{2+} dynamics, Fluo-4 fluorescence relative increase and effect of NAC ROS inhibitor, in absence of extracellular Ca^{2+} ions. In panel **E**, data are shown as mean ± SE, over statistical sample sets of $n = 29$, $n = 60$, $n = 37$ cells (for control, P3HT NPs and PS-NPs samples, respectively).

of the dispersion of 0.05, does not lead to a substantial increase of ROS production, thus representing a lower limit for obtaining sizable physiological effects. Conversely, as expected, an increasingly higher number of NPs leads to enhanced photogeneration of charges, thus determining an overall, sizable increase of ROS production. It is worth noting how the enhancement of ROS in dependence on NPs concentration is more pronounced in the case of the H_2DCF-DA probe, being the latter sensitive to several species. Conversely, the response of APF and HPF probes presents a smoother

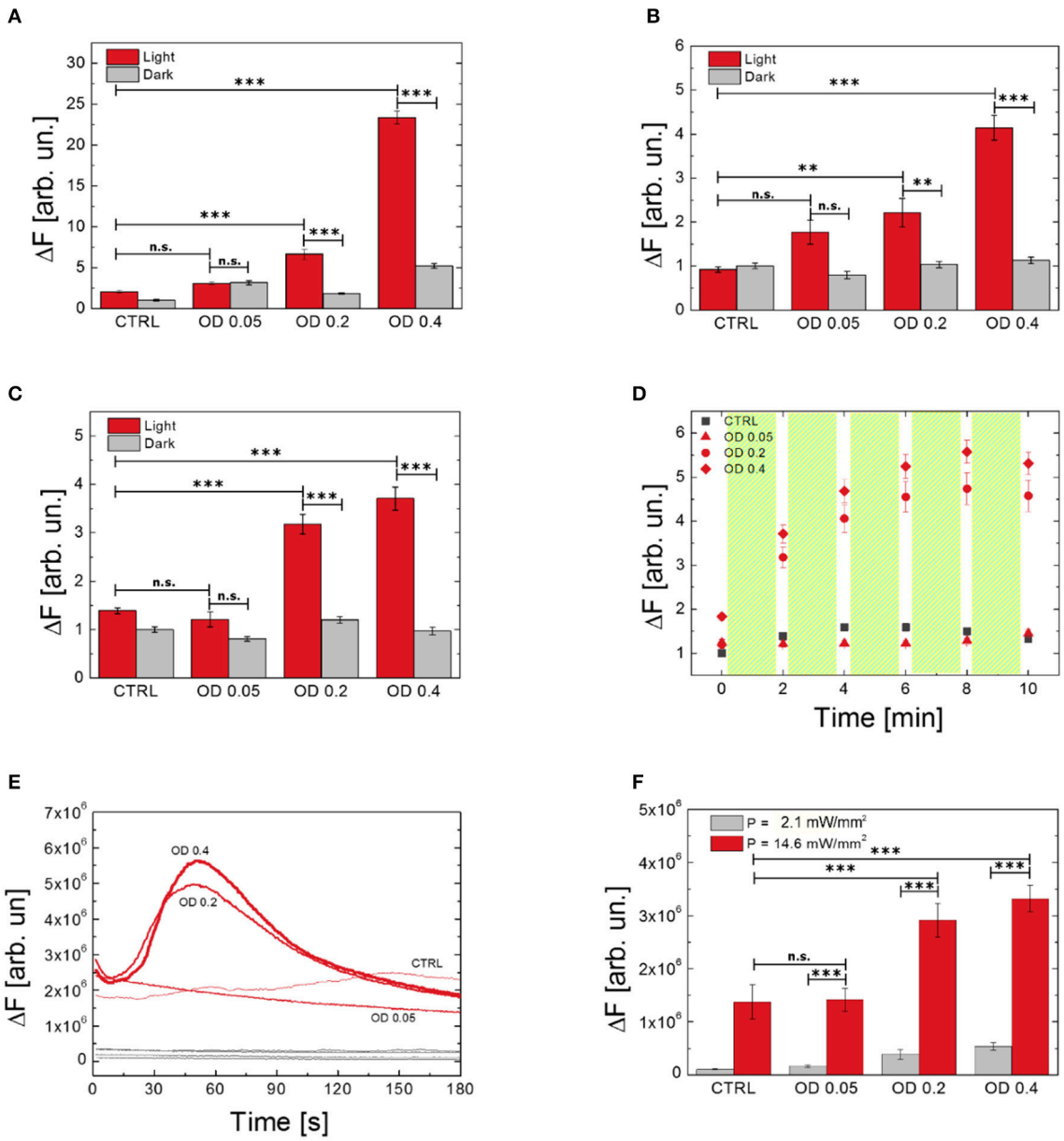

FIGURE 5 | Effect of P3HT NPs dispersion concentration on ROS generation by using different probes (**A**, H_2DCF-DA; **B**, HPF; **C,D**, APF) and Ca^{2+} modulation **(E,F)**. Data report the mean values over populations, three experiments for each condition, of $N_{H2DCF-DA\_Light\_OD0.4} = 66$, $N_{H2DCF-DA\_Dark\_OD0.4} = 40$, $N_{H2DCF-DA\_Light\_OD0.2} = 46$, $N_{H2DCF-DA\_Dark\_OD0.2} = 40$, $N_{H2DCF-DA\_Light\_OD0.05} = 48$, $N_{H2DCF-DA\_Dark\_OD0.05} = 30$, $N_{H2DCF-DA\_Light\_untreated} = 42$, $N_{H2DCF-DA\_Dark\_untreated} = 30$, $N_{HPF\_Light\_OD0.4} = 48$, $N_{HPF\_Dark\_OD0.4} = 46$, $N_{HPF\_Light\_OD0.2} = 48$, $N_{HPF\_Dark\_OD0.2} = 43$, $N_{HPF\_Light\_OD0.05} = 54$, $N_{HPF\_Dark\_OD0.05} = 52$, $N_{HPF\_Light\_untreated} = 47$, $N_{HPF\_Dark\_untreated} = 39$, $N_{APF\_Light\_OD0.4} = 56$, $N_{APF\_Dark\_OD0.4} = 56$, $N_{APF\_Light\_OD0.2} = 69$, $N_{APF\_Dark\_OD0.2} = 69$, $N_{APF\_Light\_OD0.05} = 48$, $N_{APF\_Dark\_OD0.05} = 48$, $N_{APF\_Light\_untreated} = 42$, $N_{APF\_Dark\_untreated} = 42$, $N_{FLUO-4\_OD0.4} = 43$, $N_{FLUO-4\_OD0.2} = 51$, $N_{FLUO-4\_OD0.05} = 60$, $N_{FLUO-4\_untreated} = 56$. **(D)** Shows the effect on ROS production of repeated light stimulation events, each one of 2 min overall duration, as evidenced by using the APF probe. Statistical analysis has been carried out by one-way ANOVA, followed by *post-hoc* Tukey test. *P*-values of the test are assigned as follows: ***for $p < 0.001$, **for $p < 0.005$. Statistically non-significant results are marked as n.s. in the figures. See SI section for all details of statistical analysis.

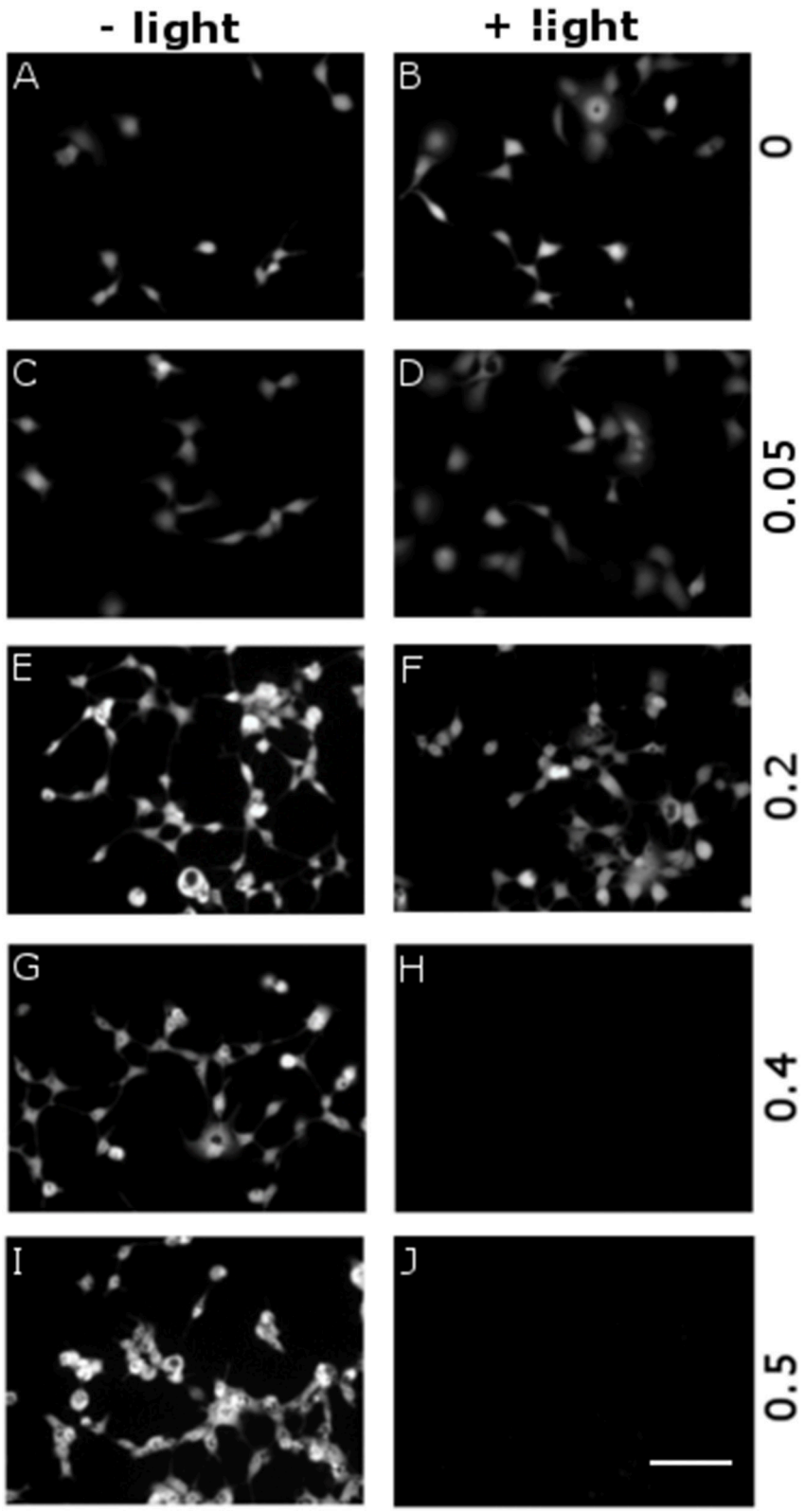

FIGURE 6 | Dependence of cytotoxicity on P3HT NPs dose and optical excitation. P3HT NPs at different concentrations, corresponding to OD in the range 0–0.5 (from top to bottom panels), have been administered to HEK-293 cells at the plating step. A sub-set of samples has been treated with the same illumination protocol

(Continued)

FIGURE 6 | used for ROS production (CW LED light illumination, peak emission wavelength $\lambda = 540$ nm, closely matching the polymer absorption spectrum; photoexcitation density $P = 95$ mW/mm^2; overall duration of the photoexcitation protocol, 2 min), 24 h after NPs administration and upon careful rinsing of the cell growth medium **(B, D, F, H, J)**. All other samples have been subjected exactly to the same preparation protocol, but they did not undergo photoexcitation **(A, C, E, G, I)**. Viable cells are finally detected by FDA staining. Representative images have been acquired at 2 DIV. Scale bar, 100 μm.

dependence on NPs concentration with respect to H_2DCF-DA, probably due to their higher selectivity. Interestingly, **Figure 5D** shows the temporal dynamics of ROS evolution upon a photostimulation pattern (2 min photoexcitation followed by 10 s in dark, repeated five times), as detected by the APF probe. After three photoexcitation events, the ROS production reaches a saturation concentration. We conclude that the main effect is achieved within the first minutes of photostimulation. We carried out the same experiment using H_2DCF-DA and HPF probes, but unfortunately, these probes undergo photo-oxidation and bleaching phenomena upon prolonged illumination, which makes them unreliable for this kind of study.

Ca^{2+} dynamics as well are heavily affected, upon visible light excitation, by the concentration of P3HT NPs**.** Intracellular Ca^{2+} dynamics and averaged maximum fluorescence variation at different NPs concentrations and two photoexcitation densities (2.1 and 14.6 mW/mm^2) are shown in **Figures 5E,F,** respectively. In line with results obtained for ROS production, the lowest employed NPs concentration, corresponding to an initial optical density of the dispersion of 0.05, does not lead to sizable effects. The Ca^{2+} response upon photostimulation density of 2.1 mW/mm^2 is fully comparable to the physiological Ca^{2+} concentration, as obtained in control samples. Conversely, effective NPs excitation, with a photoexcitation density of 14.6 mW/mm^2, leads to a pronounced modulation of Ca^{2+} dynamics. Overall, these data show that both ROS and Ca^{2+} increase strongly depends on the concentration of P3HT NPs, and further demonstrate the key-role of polymer charge generation upon visible light.

Photo-Toxicity Assays

We evaluated the cytophototoxicity effects eventually determined by optical excitation of polymer NPs, as compared with samples treated with NPs but not subjected to the illumination protocol, i.e., in which no ROS generation was optically activated. We considered five NPs doses, corresponding to OD in the range 0–0.5 (0, 0.05, 0.2, 0.4, and 0.5 OD values). Photoexcitation was carried out 24 h after cell plating/NPs administration, by using the same protocol employed for inducing ROS generation (see **Figure 5** and related methods). In all cases (i.e., for both illuminated and non-illuminated samples) cell viability was evaluated 48 h after plating and NPs administration. **Figure 6** displays representative images obtained by fluorescein diacetate (FDA) assay. FDA is a non-fluorescent molecule, which is hydrolyzed to fluorescent fluorescein in live cells only. We notice that cells not subjected to the illumination protocol show good viability at all considered NPs doses (**Figures 6A,C,E,G,I**). In the case of illuminated samples (**Figures 6B,D,F,H,J**), photoexcitation of P3HT NPs leads to substantial toxicity effects at the two highest NPs concentrations considered here (**Figures 5H,J**). Conversely, at P3HT NPs doses corresponding to 0–0.2 OD values no remarkable toxicity effect is detected. By combining these results with data reported in **Figure 5**, we identify the intermediate NPs concentration, corresponding to OD 0.2, as the most suitable one, leading to effective ROS production and reliable Ca^{2+} ions modulation, but with no detrimental effects on cell viability, as evaluated 24 h after photoexcitation.

However, it is known that ROS can also lead to delayed toxicity effects, visible only after few days after production. Thus, we carried out viability tests at different time points, up to 72 h after NPs photoexcitation (at 4 DIV) and related ROS generation. **Figure 7** shows representative images of viable cells stained by FDA. The comparison among 4 different sample cohorts (NPs treated/untreated and illuminated/non-illuminated) does not show significant differences in the staining of viable cells. Most importantly, no remarkable signs of delayed photocytotoxicity effects are evidenced.

DISCUSSION

In this work, we study the coupling mechanism at the abiotic/biotic interface between polymer NPs and living cells upon photoexcitation with visible light. Our NPs are good candidates for light-driven cell actuation. Indeed, functional effects on HEK-293 cells electrophysiology and in *Hydra Vulgaris* have been recently demonstrated (Tortiglione et al., 2017; Zangoli et al., 2017). Here, experimental data demonstrate that optical excitation of polymer NPs enhances the physiological ROS production and elicits intracellular Ca^{2+} dynamics. We propose that this is occurring to a suitable extent to cause physiological effects and yet it is below the phototoxic regime.

First, we observe that upon photoexcitation with visible light P3HT NPs suspended into an aqueous electrolyte generate a photocurrent signal. We assign this to redox processes, accordingly to what occurs in P3HT films when used as the light-sensitive working electrode in photo-electrochemical cells. The same process is invoked to explain the observed generation of ROS in the cytosol compartment within living cells.

Several inorganic NPs, including metallic NPs (Wang et al., 2017), inorganic nanocrystals (Ipe et al., 2005; Wang et al., 2015) and magnetic NPs, have been reported to have sizable effects on the ROS population, thus representing an interesting strategy for photothermal therapies (Ye and Chen, 2016; Dayem et al., 2017). Among carbon-based materials, carbon nanotubes, graphene and polymer nano-bioconjugates can also sustain photo-thermal stimulation (Miyako et al., 2014; Chechetka et al., 2016; Lyu et al., 2016; Li et al., 2017). Yet, there is a fundamental difference to be taken into account when comparing those

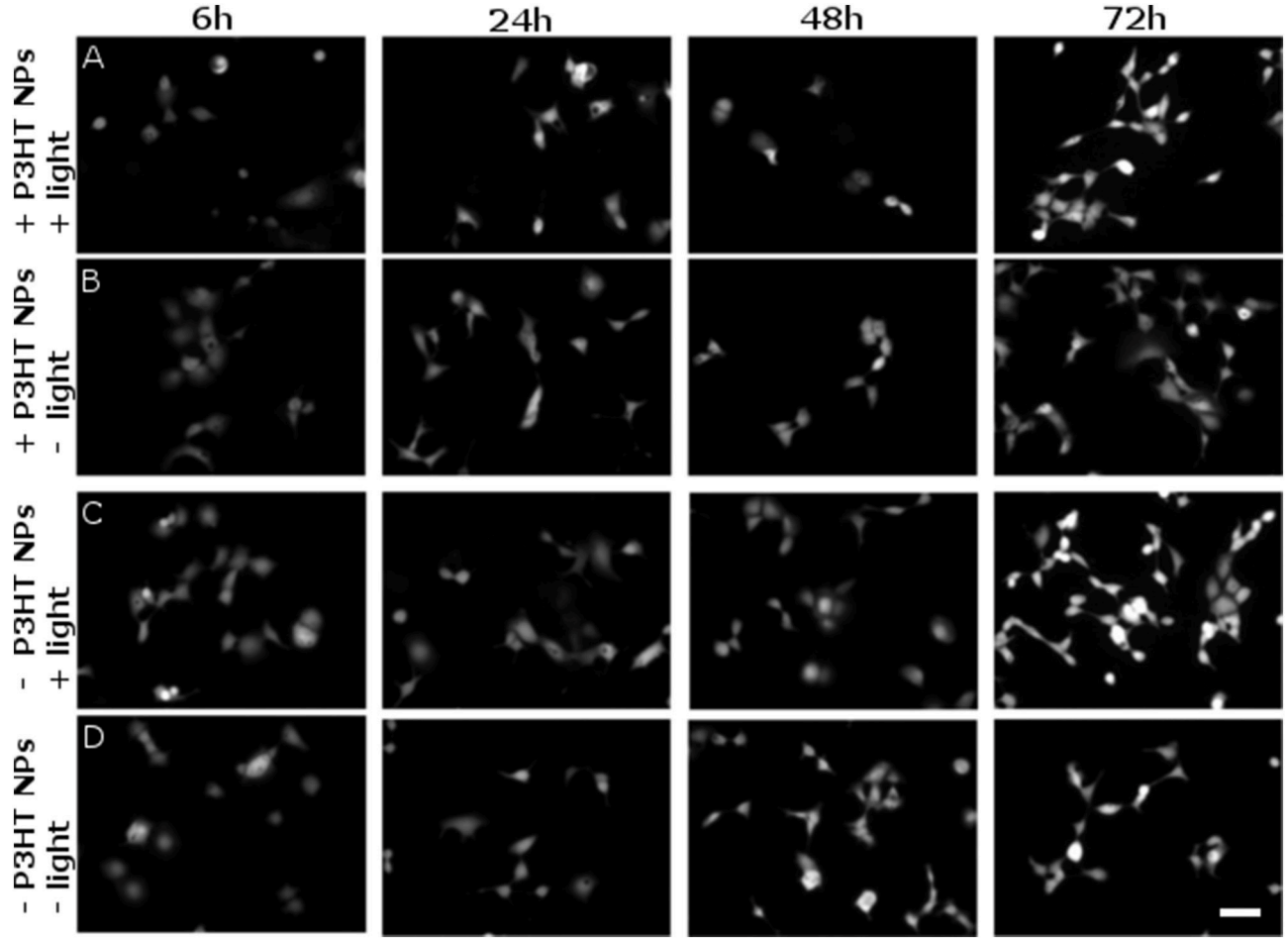

FIGURE 7 | Evaluation of delayed cytotoxicity effects. Cell viability has been tested by FDA staining assay, in presence and absence of P3HT NPs (± P3HT NPs, 0.2 OD, panel lines **A–D** respectively), and in presence or absence of polymer photoexcitation (± light, panel lines **A–D**, respectively), at fixed time points after plating and NPs administration. At 1 DIV, the same illumination protocol used for ROS generation was applied to samples treated by light (CW LED light illumination, peak emission wavelength $\lambda = 540$ nm, closely matching the polymer absorption spectrum; photoexcitation density $P = 95$ mW/mm^2; overall duration of the photoexcitation protocol, 2 min). Viable cells were then stained at fixed time points, namely 6, 24, 48, 72 h after the illumination protocol, corresponding to a maximum of 4 DIV (from left to right panels, respectively). Scale bar, 100 μm.

systems with our P3HT NPs: for both inorganic- and organic-based systems reported so far, NIR-mediated photo-thermal heating is the main phenomenon, *indirectly* leading to ROS enhancement. Conversely, in our case, significant thermal effects can be ruled out. In fact, for a single NP upon light excitation density of $I_0 = 100$ mW/mm^2 the expected temperature increase is $\Delta T = I_0 \pi R_{NP}^2 / (4 \pi K r)$, where $R_{NP} = 240$ nm is the average NP radius, $K = 0.6$ W/ mK is the thermal conductivity of water and r is the distance from the NP center. At the particle surface ($r = R_{NP}$), the expected ΔT is in the order of 10 mK, a value considered too low for provoking sizable effects. In order to directly test the effect of NPs-mediated thermal increase also on an experimental ground, we carried out electrophysiology experiments (whole cell patch clamp configuration) in HEK-293 cells stably transfected with temperature-sensitive channels (TRPV1), a system which intrinsically bears enhanced sensibility to temperature variations. Upon photoexcitation of P3HT NPs internalized within the cell cytosol we could not observe any significant effect (**Figure S9**) mediated by TRPV1 channel response. This confirms the numerical evaluation and rules out the thermal effect as a primary result of photoexcitation.

We conclude that the observed changes in ROS concentration and Ca^{2+} dynamics are most plausibly caused by a direct photocatalytic effect. The dependence of the cell response on internalized NPs concentration and light excitation protocol further supports this hypothesis (**Figure 5**).

It is important to notice again that as soon as the delicate balance of ROS production is altered, or the intracellular levels of antioxidants is lowered, ROS can become highly harmful, causing oxidative stress which, in some cases, leads to irreversible cell damage (Martindale and Holbrook, 2002). Based on a detailed dose-response analysis and cell viability tests, we identify a suitable NPs concentration, corresponding

to 0.2 OD value of the colloidal dispersion as an optimal compromise between reliable functional photomodulation of ROS generation and intracellular Ca^{2+} ions increase, on one side, and occurrence of cytophototoxicity effects on the other side (**Figure 6**). In these conditions, and within the temporal window considered in the present work, up to 4 DIV (compatibly with the use of *in vitro* HEK-293 cell model), we do not observe sizable toxicity effects within treated cells, as documented by fluorescence imaging before and immediately after the photoexcitation protocol (Figure S10), as well as at different time points after photoexcitation, up to 72 h (**Figure 7**).

The proposed interaction mechanisms leading to ROS enhancement are depicted in **Figure 8**, based on the well-known P3HT photo-physical scenario. P3HT belongs to the class of polymeric organic semiconductors. It has a carbon conjugated backbone that supports π-electron delocalization. In solution, as isolated chains, such polymers behave like large organic molecules. The main photo-excited species are singlet and triplet states, the latter mostly produced by intersystem crossing from the initial singlet. Due to the extended conjugation, a fraction of the initial singlet states may dissociate into charge pairs. Those are very short-lived (<1 ps) in isolated chains, but in a solid, where inter-chain coupling may be non-negligible, they can separate on different chains and survive up to the milliseconds' timescale. In presence of oxygen (or any other dopants) this scenario dramatically changes. The singlet state quenches at the dopant, by energy or charge transfer. In the latter case, this generates fairly mobile holes and trapped electrons, a behavior often referred to as p-type. P3HT has a remarkably small triplet photogeneration yield (below 0.1%) (Jiang et al., 2002). This has important implications for biophotonics, since it substantially reduces the photo-toxicity of the material, cutting down singlet oxygen generation, the major killing path in photodynamic therapy. Accordingly, we think that optical excitation of the polymer NPs leads to singlet and polaron (charged) states. Singlets or negative polarons react with the oxygen dissolved in the aqueous dispersion (**Figure 2**) or in the cytosol environment, first reducing oxygen. The superoxide further evolves leading to a generation of different ROS (**Figure 3**). Because we use CW light, the steady state population of the singlet state is small (the lifetime is in the order of 1 ns). For this reason, the polaron-mediated path seems the most plausible one.

Polymer-mediated production of ROS deterministically triggers an increase in the intracellular Ca^{2+} concentration, as demonstrated by the fact that upon ROS inhibition by a selective pharmacological agent (NAC), variations in Ca^{2+} dynamics are completely suppressed (**Figure 4**). Moreover, we evidence that the main source of intracellular Ca^{2+} increase resides within the cytosol, thus indicating a crucial role in the Ca^{2+} release by mitochondria and/or the endoplasmic reticulum, being these organelles mostly involved in Ca^{2+} dynamics. Further studies would be needed, however, to exactly identify the organelle involved in the photo-transduction effect triggered by illuminated P3HT NPs, and also to assess if the Ca^{2+} pathway on the cell membrane is eventually changed.

Both Ca^{2+} ions and ROS represent prominent signaling pathways able to finely tune several cell functions (Chakraborti et al., 1999). Importantly, dysfunctions of the delicate equilibrium in Ca^{2+}/ROS balance have been reported to have serious

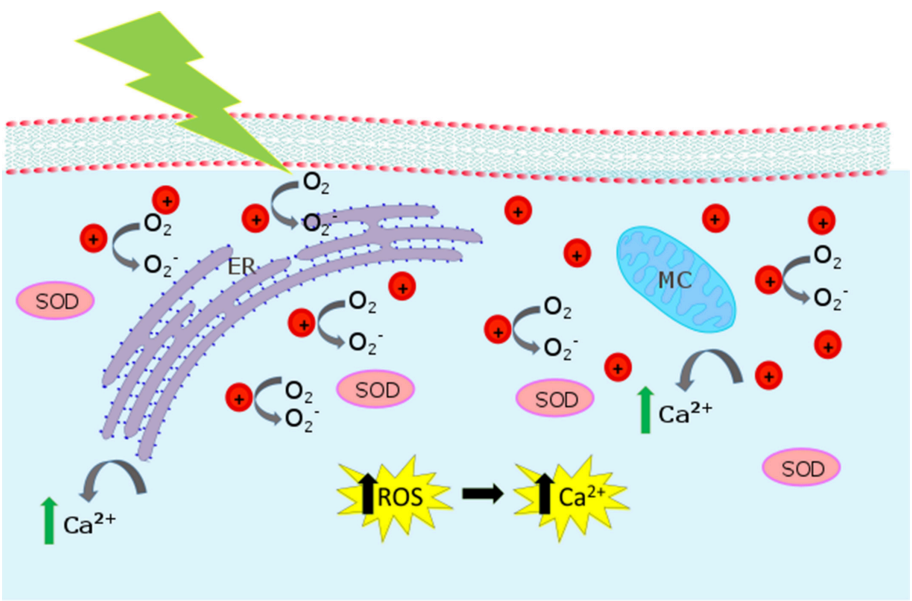

FIGURE 8 | Biological pathways activated by P3HT-NP photostimulation. The cartoon represents the intracellular compartment, showing mitochondria (MC) and endoplasmic reticulum (ER). When P3HT NPs are irradiated, O_2^- is produced. O_2^- is expected to act as an intermediate toward the formation of other ROS and to increase the SOD (superoxide dismutase) concentration. Increased Ca^{2+} release from intracellular sources is also observed.

implications in various disorders, including, among others, neurodegenerative diseases such as Parkinson's and Alzheimer's disease, inflammatory diseases, metabolic diseases, and ischemic events (Chinopoulos and Adam-Vizi, 2006; Chaudhari et al., 2014; Sharma and Nehru, 2015; Zucchetti et al., 2016). In perspective, our results represent a novel, minimally invasive and locally confined tool for efficient modulation of ROS and intracellular Ca^{2+} concentration.

AUTHOR CONTRIBUTIONS

CB carried out all the experimental measurements, with help from IA (electrochemical characterization, ROS measurements, Ca^{2+} Dynamics), GT (electrochemical characterization). EZ fabricated P3HT NPs, DD carried out TEM experiments. MZ and FD synthesized P3HT for the NPs. MA and GL planned and supervised the research. All authors contributed to manuscript drafting and approved the final version of the manuscript.

FUNDING

The work was supported by a national grant from Fondazione Cariplo (project ON-IRIS 2013–0738).

ACKNOWLEDGMENTS

The authors are grateful to Dr. F. Lodola for help in patch clamp electrophysiology measurements on HEK-293 cells transfected with TRPV1 channel, and to Dr. G. Barbarella from Mediteknology SRL for useful discussions and manuscript reading.

SUPPLEMENTARY MATERIAL

The Supplementary Material for this article can be found online at: https://www.frontiersin.org/articles/10.3389/fbioe.2018.00114/full#supplementary-material

REFERENCES

Antognazza, M. R., Martino, N., Ghezzi, D., Feyen, P., Colombo, E., Endeman, D., et al. (2015). Shedding light on living cells. *Adv. Mater.* 27, 7662–7669. doi: 10.1002/adma.201403513

Bar-Shir, A., Avram, L., Yariv-Shoushan, S., and Anaby, D. (2014). Alginate-coated magnetic nanoparticles for noninvasive MRI of extracellular calcium. *NMR Biomed.* 27, 774–783. doi: 10.1002/nbm.3117

Bellani, S., Ghadirzadeh, A., Meda, L., Savoini, A., Tacca, A., Marra, G., et al. (2015). Hybrid organic / inorganic nanostructures for highly sensitive photoelectrochemical detection of dissolved oxygen in aqueous media. *Adv. Funct. Mater.* 25, 4531–4538. doi: 10.1002/adfm.201500701

Bergamini, C., Gambetti, S., Dondi, A., and Cervellati, C. (2004). Oxygen, reactive oxygen species and tissue damage. *Curr. Pharm. Des.* 10, 1611–1626. doi: 10.2174/1381612043384664

Brookes, P. S., Yoon, Y., Robotham, J. L., Anders, M. W., and Sheu, S. (2004). Calcium, ATP and ROS: a mitochondrial love-hate triangle. *Cell Physiol.* 287, C817–C833. doi: 10.1152/ajpcell.00139.2004

Bruni, F., Pedrini, J., Bossio, C., Santiago-Gonzalez, B., Meinardi, F., Bae, W. K., et al. (2017). Two-color emitting colloidal nanocrystals as single-particle ratiometric probes of intracellular pH. *Adv. Funct. Mater.* 27, 1–9. doi: 10.1002/adfm.201605533

Chakraborti, T., Das, S., Mondal, M., Roychoudhury, S., and Chakraborti, S. (1999). Oxidant, mitochondria and calcium: an overview. *Cell. Signal* 11, 77–85. doi: 10.1016/S0898-6568(98)00025-4

Chaudhari, N., Talwar, P., Parimisetty, A., and Lefebvre, C. (2014). A molecular web: endoplasmic reticulum stress, inflammation and oxidative stress. *Front. Cell. Neurosci.* 8:213. doi: 10.3389/fncel.2014.00213

Chechetka, S. A., Doi, M., Pichon, B. P., Begin-Colin, S., and Miyaco, E. (2016). Photothermal and mechanical stimulation of cells via dualfunctional nanohybrids. *Nanotechnology* 27, 475101–475112. doi: 10.1088/0957-4484/27/47/475102

Chen, R., Romero, G., Christiansen, M. G., Mohr, A., and Anikeeva, P. (2015). Wireless magnetothermal deep brain stimulation. *Neurotechniques* 347, 1477–1480. doi: 10.1126/science.1261821

Chinopoulos, C., and Adam-Vizi, V. (2006). Calcium, mitochondria and oxidative stress in neuronal pathology Novel aspects of an enduring theme. *FEBS J.* 273, 433–450. doi: 10.1111/j.1742-4658.2005.05103.x

Colombo, E., Feyen, P., Antognazza, M. R., Lanzani, G., and Benfenati, F. (2016). Nanoparticles: a challenging vehicle for neural stimulation. *Front. Neurosci.* 10:105. doi: 10.3389/fnins.2016.00105

Dayem, A. A., Hossain, M. K., Lee, S. B., Kim, K., Saha, S. K., Yang, G., et al. (2017). The role of reactive oxygen species (ROS) in the Biological activities of metallic nanoparticles. *Int. J. Mol. Sci.* 18:120. doi: 10.3390/ijms18010120

Deisseroth, K. (2011). Optogenetics. *Nat. Methods* 8, 26–29. doi: 10.1038/nmeth.f.324

Di Maria, F., Zanelli, A., Liscio, A., Kovtun, A., Salatelli, E., Mazzaro, R., et al. (2017). Poly(3-hexylthiophene) nanoparticles containing thiophene-s,s-dioxide: tuning of dimensions, optical and redox properties, and charge separation under illumination. *ACS Nano* 11, 1991–1999. doi: 10.1021/acsnano.6b08176

Dröge, W. (2002). Free radicals in the physiological control of cell function. *Physiol. Rev.* 82, 47–95. doi: 10.1152/physrev.00018.2001

Farah, N., Zoubi, A., Matar, S., Golan, L., Marom, A., Butson, C. R., et al. (2013). Holographically patterned activation using photo-absorber induced neural–thermal stimulation. *J. Neural Eng.* 10, 056004–056015. doi: 10.1088/1741-2560/10/5/056004

Feng, L., Zhu, C., Yuan, H., Liu, L., Lv, F., and Wang, S. (2013). Conjugated polymer nanoparticles: preparation, properties, functionalization and biological applications. *Chem. Soc. Rev.* 42, 6620–6633. doi: 10.1039/c3cs60036j

Feng, X., Lv, F., Liu, L., Tang, H., Xing, C., Yang, Q., et al. (2010). Conjugated polymer nanoparticles for drug delivery and imaging. *Appl. Mater. Interface* 2, 2429–2435. doi: 10.1021/am100435k

Feyen, P., Colombo, E., Endeman, D., Nova, M., Laudato, L., Martino, N., et al. (2016). Light-evoked hyperpolarization and silencing of neurons by conjugated polymers. *Sci. Rep.* 6:22718. doi: 10.1038/srep22718

Finkel, T., and Holbrook, N. J. (2000). Oxidants, oxidative stress and the biology of ageing. *Nature* 408, 239–247. doi: 10.1038/35041687

Fu, P. P., Xia, Q., Hwang, H.-M., Ray, P. C., and Yu, H. (2014). Mechanisms of nanotoxicity: generation of reactive oxygen species. *J.Food Drug Anal.* 22, 64–75. doi: 10.1016/j.jfda.2014.01.005

Giron, R. M., Martinez, J. M., Bellani, S., Insuasty, A., Comas Rojas, H., Tullii, G., et al. (2016). Synthesis of modified fullerenes for oxygen reduction reactions. *J. Mater. Chem. A* 4, 14284–14290. doi: 10.1039/C6TA06573B

Glassman, S. J. (2011). Vitiligo, reactive oxygen species and T-cells. *Clin. Sci.* 120, 99–120. doi: 10.1042/CS20090603

Goda, Y., and Colicos, M. A. (2006). Photoconductive stimulation of neurons cultured on silicon wafers. *Nat. Protoc.* 1, 461–467. doi: 10.1038/nprot.2006.67

Gomes, A., Fernandes, E., and Lima, J. L. F. C. (2005). Fluorescence probes used for detection of reactive oxygen species. *J. Biochem. Biophys. Methods* 65, 45–80. doi: 10.1016/j.jbbm.2005.10.003

Görlach, A., Bertram, K., Hudecova, S., and Krizanova, O. (2015). Calcium and ROS: a mutual interplay. *Redox Biol.* 6, 260–271. doi: 10.1016/j.redox.2015.08.010

Halliwell, B. (2015). *Free Radicals in Biology and Medicine*. Oxford, UK: Oxford University Press, 351–550.

Howes, P. D., Chandrawati, R., and Stevens, M. M. (2014). Colloidal nanoparticles as advanced biological sensors. *Science* 346, 53–65. doi: 10.1126/science.1247390

Huang, H., Delikanli, S., Zeng, H., Ferkey, D. M., and Pralle, A. (2010). Remote control of ion channels and neurons through magnetic-field heating of nanoparticles. *Nat. Nanotechnol*. 5, 602–606. doi: 10.1038/nnano.2010.125

Hühn, D., Kantner, K., Geidel, C., Brandholt, S., De Cock, I., Soenen, S. J. H., et al. (2013). Polymer-coated nanoparticles interacting with proteins and cells: focusing on the sign of the net charge. *ACS Nano* 7, 3253–3263. doi: 10.1021/nn3059295

Ipe, B. I., Lehnig, M., and Niemeyer, C. M. (2005). Free radicals On the generation of free radical species from quantum dots. *Small* 1, 706–709. doi: 10.1002/smll.200500105

Jiang, B. X., Österbacka, R., Korovyanko, O., An, C. P., Horovitz, B., Janssen, R. A. J., et al. (2002). Spectroscopic studies of photoexcitations in regioregular and regiorandom polythiophene films. *Adv. Funct. Mater.* 9, 587–597. doi: 10.1002/1616-3028(20020916)12:9<587::AID-ADFM587>3.0.CO;2-T

Kamata, H., and Hirata, H. (1999). Redox regulation of cellular signalling. *Cell. Signal* 11, 1–14. doi: 10.1016/S0898-6568(98)00037-0

Lanzarini, E., Antognazza, M. R., Biso, M., Ansaldo, A., Laudato, L., Bruno, P., et al. (2012). Polymer-based photocatalytic hydrogen generation. *J. Phys. Chem. C* 116, 10944–10949. doi: 10.1021/jp212107f

Lee, J. H., Kim, J. W., Levy, M., Kao, A., Noh, S. H., Cheon, J., et al. (2014). Magnetic nanoparticles for ultrafast mechanical control of inner ear hair cells. *ACS Nano* 8, 6590–6598. doi: 10.1021/nn5020616

Lee, M. Y., and Griendling, K. K. (2008). Redox signaling, vascular function, and hypertension. *Antioxid. Redox Signal*. 10, 1045–1059. doi: 10.1089/ars.2007.1986

Li, Q., Hong, L., Li, H., and Liu, C. (2017). Biosensors and bioelectronics graphene oxide-fullerene C 60 (GO-C 60) hybrid for photodynamic and photothermal therapy triggered by near-infrared light. *Biosens. Bioelectron*. 89, 477–482. doi: 10.1016/j.bios.2016.03.072

Lyu, Y., Xie, C., Chechetka, S. A., Miyako, E., and Pu, K. (2016). Semiconducting polymer nanobioconjugates for targeted photothermal activation of neurons. *J. Am. Chem. Soc*. 138, 9049–9052. doi: 10.1021/jacs.6b05192

Marotta, R., Falqui, A., Curcio, A., Quarta, A., and Pellegrino, T. (2013). Immunocytochemistry, electron tomography, and energy dispersive X-ray spectroscopy (EDXS) on cryosections of human cancer cells doped with stimuli responsive polymeric nanogels loaded with iron oxide nanoparticles.*Methods Mol. Biol*. 1025, 179–198. doi: 10.1007/978-1-62703-462-3_14

Martindale, J. L., and Holbrook, N. J. (2002). Cellular response to oxidative stress: signaling for suicide and survival. *J. Cell. Physiol*. 192, 1–15. doi: 10.1002/jcp.10119

Martino, N., Feyen, P., Porro, M., Bossio, C., Zucchetti, E., Ghezzi, D., et al. (2015). Photothermal cellular stimulation in functional bio-polymer interfaces. *Sci.Rep*. 5:8911. doi: 10.1038/srep08911

Maya-Vetencourt, J. F., Ghezzi, D., Antognazza, M. R., Colombo, E., Mete, M., Feyen, P., et al. (2017). A fully organic retinal prosthesis restores vision in a rat model of degenerative blindness. *Nat. Mater*. 16, 681–689. doi: 10.1038/nmat4874

Medintz, I. L., Uyeda, H. T., Goldman, E. R., and Mattoussi, H. (2005). Quantum dot bioconjugates for imaging, labelling and sensing. *Nat. Mater*. 4, 435–446. doi: 10.1038/nmat1390

Miyako, E., Russier, J., Mauro, M., Cebrian, C., Yawo, H., Menard-Moyon, C., et al. (2014). Photofunctional nanomodulators for bioexcitation. *Angew. Chem. Int. Ed*. 53, 13121–13125. doi: 10.1002/anie.201407169

Morshedian, A., and Fain, G. L. (2017). The evolution of rod photoreceptors. *Philos. Trans. R. Soc. B Biol. Sci*. 372:20160074. doi: 10.1098/rstb.2016.0074

Nakatsuji, H., Numata, T., Morone, N., Kaneko, S., Mori, Y., Imahori, H., et al. (2015). Thermosensitive ion channel activation in single neuronal cells by using surface-engineered plasmonic nanoparticles angewandte. *Angew. Chem. Int. Ed*. 8501, 11725–11729. doi: 10.1002/anie.201505534

Newsholme, P., Homem De Bittencourt, P. I., O.' Hagan, C., De Vito, G., Murphy, C., and Krause, M.S. (2010). Exercise and possible molecular mechanisms of protection from vascular disease and diabetes: the central role of ROS and nitric oxide. *Clin. Sci*. 118, 341–349. doi: 10.1042/CS20090433

Saravanakumar, G., Kim, J., and Kim, W. J. (2017). Reactive-oxygen-species-responsive drug delivery systems: promises and challenges. *Adv. Sci*. 4:1600124. doi: 10.1002/advs.201600124

Shapiro, M. G., Homma, K., Villarreal, S., Richter, C. P., and Bezanilla, F. (2012). Infrared light excites cells by changing their electrical capacitance. *Nat. Commun*. 3:736. doi: 10.1038/ncomms1742

Sharma, N., and Nehru, B. (2015). Neurochemistry International Characterization of the lipopolysaccharide induced model of Parkinson's disease: role of oxidative stress and neuroinflammation. *Neurochem. Int*. 87, 92–105. doi: 10.1016/j.neuint.2015.06.004

Stanley, S. A., Gagner, J. E., Damanpour, S., Yoshida, M., Dordick, J. S., and Friedman, J. M. (2012). Radio-wave heating of iron oxide nanoparticles can regulate plasma glucose in mice. *Science* 336, 604–609. doi: 10.1126/science.1216753

Stein, M., Breit, A., Fehrentz, T., Gudermann, T., and Trauner, D. (2013). Optical control of TRPV1 channels. *Angew. Chem. Int. Ed*. 52, 9845–9848. doi: 10.1002/anie.201302530

Takano, Y., Numata, T., Fujishima, K., Miyake, K., Nakao, K., Grove, W. D., et al. (2016). Optical control of neuronal firing via photoinduced electron transfer in donor–acceptor conjugates. *Chem. Sci*. 7, 3331–3337. doi: 10.1039/C5SC04135J

Tortiglione, C., Antognazza, M. R., Tino, A., Bossio, C., Marchesano, V., Bauduin, A., et al. (2017). Semiconducting polymers are light nanotransducers in eyeless animals. *Sci. Adv*. 3:e1601699. doi: 10.1126/sciadv.1601699

Trachootham, D., Alexandre, J., and Huang, P. (2009). Targeting cancer cells by ROS-mediated mechanisms: a radical therapeutic approach. *Nat. Publ. Group* 8, 579–591. doi: 10.1038/nrd2803

Tullii, G., Desii, A., Bossio, C., Bellani, S., Colombo, M., Martino, N., et al. (2017). Bimodal functioning of a mesoporous, light sensitive polymer/electrolyte interface. *Org. Electron*. 46, 88–98. doi: 10.1016/j.orgel.2017.04.007

Tuncel, D., and Demir, H. V. (2010). Conjugated polymer nanoparticles. *Nanoscale* 2, 484–494. doi: 10.1039/b9nr00374f

Waiskopf, N., Ben-Shahar, Y., Galchenko, M., Carmel, I., Moshitzky, G., and Soreq, H. B. (2016). Photocatalytic reactive oxygen species formation by semiconductor – metal hybrid nanoparticles, toward light-induced modulation of biological processes. *Nano Lett*. 16, 4266–4273. doi: 10.1021/acs.nanolett.6b01298

Wang, B., Yuan, H., Zhu, C., Yang, Q., Lv, F., Liu, L., et al. (2012). Polymer-drug conjugates for intracellar molecule-targeted photoinduced inactivation of protein and growth inhibition of cancer cells. *Sci. Rep*. 2:766. doi: 10.1038/srep00766

Wang, H., and Joseph, J. A. (1999). Cellular oxidative stress by dichlorofluorescein assay using microplate reader. *Free Radic. Biol. Med*. 27, 612–616. doi: 10.1016/S0891-5849(99)00107-0

Wang, L., Chen, Y., Lin, H. Y., Hou, Y., Yang, L., Sun, A. Y., et al. (2017). Near-IR-absorbing gold nanoframes with enhanced physiological stability and improved biocompatibility for *in vivo* biomedical applications. *Appl. Mater. Interfaces* 9, 3873–3884. doi: 10.1021/acsami.6b12591

Wang, L., Liu, D., Zhou, R., Wang, Z., and Cuschieri, A. (2015). Tumour cell membrane poration and ablation by pulsed low-intensity electric field with carbon nanotubes. *Int. J. Mol. Sci*. 16, 6890–6901. doi: 10.3390/ijms16046890

Wheeler, M. A., Smith, C. J., Ottolini, M., Barker, B. S., Purohit, A. M., Grippo, R. M., et al. (2016). Genetically targeted magnetic control of the nervous system. *Nat. Neurosci*. 7, 1–9. doi: 10.1038/nn.4265

Yang, D., Yang, G., Yang, P., Lv, R., Gai, S., Li, C., et al. (2017). Assembly of Au plasmonic photothermal agent and iron oxide nanoparticles on ultrathin black phosphorus for targeted photothermal and photodynamic cancer therapy. *Adv. Funct. Mater*. 27:1700371. doi: 10.1002/adfm.201700371

Ye, D., and Chen, H. (2016). Two-photon excitation nanoparticles for photodynamic therapy. *Chem. Soc. Rev.* 45, 6725–6741. doi: 10.1039/C6CS00442C

Zangoli, M., Di Maria, F., Zucchetti, E., Bossio, C., Antognazza, M. R., Lanzani, G., et al. (2017). Engineering thiophene-based nanoparticles to induce photodransduction in live cells under illumination. *Nanoscale* 26, 9202–9209. doi: 10.1039/C7NR01793F

Zucchetti, E., Zangoli, M., Bargigia, I., Bossio, C., Di Maria, F., Barbarella, G., et al. (2016). Poly(3-hexylthiophene) nanoparticles for biophotonics: study of the mutual interaction with living cells. *J. Mater. Chem. B* 5, 565–574. doi: 10.1039/C6TB02047J

Conflict of Interest Statement: The authors declare that the research was conducted in the absence of any commercial or financial relationships that could be construed as a potential conflict of interest.

frontiers in Bioengineering and Biotechnology

MINI REVIEW
published: 09 November 2018
doi: 10.3389/fbioe.2018.00167

Photogenerated Electrical Fields for Biomedical Applications

*Giuseppina Polino†, Claudia Lubrano†, Giuseppe Ciccone† and Francesca Santoro**

Center for Advanced Biomaterials for Healthcare, Istituto Italiano di Tecnologia, Naples, Italy

The application of electrical engineering principles to biology represents the main issue of bioelectronics, focusing on interfacing of electronics with biological systems. In particular, it includes many applications that take advantage of the peculiar optoelectronic and mechanical properties of organic or inorganic semiconductors, from sensing of biomolecules to functional substrates for cellular growth. Among these, technologies for interacting with bioelectrical signals in living systems exploiting the electrical field of biomedical devices have attracted considerable attention. In this review, we present an overview of principal applications of phototransduction for the stimulation of electrogenic and non-electrogenic cells focusing on photovoltaic-based platforms.

Keywords: bioelectronics, photovoltaics, tissue engineering, biointerfaces, electrical stimulation

OPEN ACCESS

Edited by:
Gianni Ciofani,
Politecnico di Torino, Italy

Reviewed by:
Ilaria Elena Palamà,
Istituto di Nanotecnologia (NANOTEC), Italy
Erhan Zor,
Necmettin Erbakan University, Turkey

****Correspondence:***
Francesca Santoro
francesca.santoro@iit.it

†These authors have contributed equally to this work

Specialty section:
This article was submitted to Nanobiotechnology, a section of the journal Frontiers in Bioengineering and Biotechnology

Received: *23 September 2018*
Accepted: *23 October 2018*
Published: *09 November 2018*

Citation:
Polino G, Lubrano C, Ciccone G and Santoro F (2018) Photogenerated Electrical Fields for Biomedical Applications. Front. Bioeng. Biotechnol. 6:167. doi: 10.3389/fbioe.2018.00167

INTRODUCTION

Bioelectronics devices are meant to probe and stimulate biological entities through electricity by adopting smart biocompatible materials which are also conductive (Liao et al., 2015). In particular, traditional inorganic conductors, semiconductors and, more recently introduced, conjugated polymers had find major application in the development of bioelectronic platforms (Zhang and Lieber, 2016).

Electrical fields can be generated either intrinsically or upon transduction as, for instance, in photovoltaic materials, where light can induce the generation of relevant currents through the bulk of a photoconductive material.The materials in which this phenomenon happens can be inorganic, fully organic, or hybrid mixtures.

In particular, electrical fields can be exploited to locally stimulate cells and tissue inducing responses of different nature, for instance, altering the electrophysiological activity of electrogenic cells or modulate certain cellular processes and functionalities, i.e., polarity, proliferation, differentiation, in non-electrogenic cells (Blau, 2013; Pennacchio et al., 2018).

For example, silicon-based devices are widely employed for electrical interfaces both at the micro and nanometer scale with neural tissues (Thukral et al., 2018) and, furthermore, have gained major interest in the niche of photovoltaic-based platforms for retinal implants (Di Maria et al., 2018). However, these materials exhibit some limitations in terms of flexibility and stiffness in general, which make the cell-device coupling still not optimal.

In the last decade, new generation of hybrid or fully organic, highly biocompatible and functionally self-powered prostheses have been developed to treat, among various applications, blindness proposing a cutting-edge paradigm to interface phototransductive materials with biological cells (Khraiche et al., 2013; Maya-Vetencourt et al., 2017; Benfenati and Lanzani, 2018; Ferlauto et al., 2018). In addition, photovoltaic platforms have been recently proposed to directly interface non-electrogenic cells, such as fibroblasts, to trigger their proliferation and open up the possibility to use such materials as optimal candidate for wound healing purposes (Jin et al., 2013).

Here, we present an overview of the main applications photovoltaic-based platforms have found in the recent years to mimic biological component with similar basic functionalities, i.e., retina, and in addition we aim to highlight the important potential of those materials have for cell stimulation in general.

ELECTRICAL PHOTOTRANSDUCTION IN DEVICES FOR BIOMEDICAL APPLICATIONS

Electrical phototransduction is the process through which photons are converted into electrical signals. For instance, inorganic semiconductors are exploited for their capacity to convert light into electrons flow by means of their P-N junction (Richter et al., 2018). However, their rigid nature, together with their poor biocompatibility has generated a major attention toward their organic counterparts for biomedical applications. Organic photovoltaic devices are able to deliver photocurrents thanks to the generation of electrical fields when light is absorbed in their photoactive layers, composed of a donor, and an acceptor semiconducting material. The donor material donates electrons transporting holes while the acceptor material withdraws electrons and further transports them (Polino et al., 2015).

In both inorganic and organic cases, charges are finally transported to an electrode, which can be in contact with a biological cell or a tissue. Starting from the carrier transport at the electrode, an electrical field is generated between the device and the biological matter and this bioelectronic coupling can modulate biological processes at different matter of scale and cellular architectures (Pennacchio et al., 2018).

The effects of this interface on cells can be investigated by observing capacitive, chemical and thermal mechanisms involving the cell membrane (Di Maria et al., 2018). In particular, platforms based on electrical photo-transduction have aroused the interest of many research groups with the purposes of recording and stimulating single cells, cell networks or tissues (Sim et al., 2014; Chenais et al., 2017; Jeong et al., 2017).

For example, in the work of Ghezzi et al. (2011), first attempts have successfully shown that stimulation of primary neurons *via* light absorption in a P3HT-based biointerface is possible. In particular, the bioelectronic interface consisted in a very thin film (≈150 nm) of a P3HT:PCBM blend deposited on an ITO-coated glass substrate. One step further was accomplished by the same group using a platform for neuronal stimulation which consisted of an active layer only in the n-type conjugated polymer P3HT (Ghezzi et al., 2013). This is just an example of how photo-transduction can take place in 2D materials and how this phenomenon can be exploited for generating electrical fields to trigger certain processes at the membrane of cells. However, it is interesting to note that even bioelectronic platforms are moving fast toward more biomimetic approaches inspired by those of tissue engineering (Pennacchio et al., 2018).

In this context, first attempts to create 3D photovoltaic platforms for skin regeneration have been carried and the local photo-transduction mechanism of 3D meshes is still under discussion (Jin et al., 2014). Here, we explore the use of light photo-trasduction effect on single cells particularly focusing on tuning cellular behavior and act as cell-instructive platforms for various applications such as platforms for immunorecognition, or as activation/inhibition of the activity of electrogenic and non-electrogenic cells.

ELECTROGENIC CELLS

Platforms based on transduction of photons in to current/voltage generation have found major applications in the modulation of the electrical activity in electrogenic cells. In fact, these cells, such as cardiomyocytes or neuronal cells, are capable of changing their membrane potential upon stimuli generating fast-changing events (action potentials). Thus, using certain electrical fields can be a suitable approach to trigger action potential inhibition or activation (Love et al., 2018).

Moreover, photovoltaic platforms has found a niche in the design of implantable devices for restoring lost functionalities in the retina (Benfenati and Lanzani, 2018; Di Maria et al., 2018).

Numata and co-workers reported the first example of photoinhibition of ion transport in PC-12 cells by using charge-separation molecules ferrocene (Fc)–porphyrin (P)–C60 linked triads. This compound was delivered close to the plasma membrane using drug carriers and, after light stimulation a depolarization of the membrane potential and an inhibition of potassium channels was observed. This result suggests thatmore sophisticated molecules can lead to the control of firingneuronal cells (Numata et al., 2012).

Abdullaeva and co-workers, with the intent to create organic-based artificial photoreceptors, developed a photoactive layer consisting of an anilino-squaraine donor blended with a fullerene acceptor as support for N2A cells (neuronal model cell line) growth. They supposed that during the pulse stimulation there is an accumulation of negative charge carriers at the photoconductor–electrolyte interface (**Figure 1A**), which results into cell depolarization. When the light is turned off instead, a rapid hyperpolarization of the cell membrane was detected (Abdullaeva et al., 2016). Similarly, induced photocapacitance can be exploited for modulation of the membrane potential in cells.

In fact, Martino and co-workers observed a similar effect on human embryonic kidney (HEK-293) cells growth on a conjugated polymer poly(3-hexylthiophene) (P3HT). The local heating of the material produced an increase in the ion transport through membrane channels, causing a decrease of the membrane resistance (Martino et al., 2015). Recently, Glowacki and co-workers have proposed an approach for neural photostimulation employing an electrolytic photocapacitor (**Figure 1B**) built with a trilayer of metal and p–n semiconducting organic nanocrystals (Rand et al., 2018).

Moving toward the coupling of photovoltaic platforms with tissues, retina implants have found major interest in the last years (Benfenati and Lanzani, 2018). Photovoltaic devices which are foldable and flexible have been developed for wide-field epiretinal

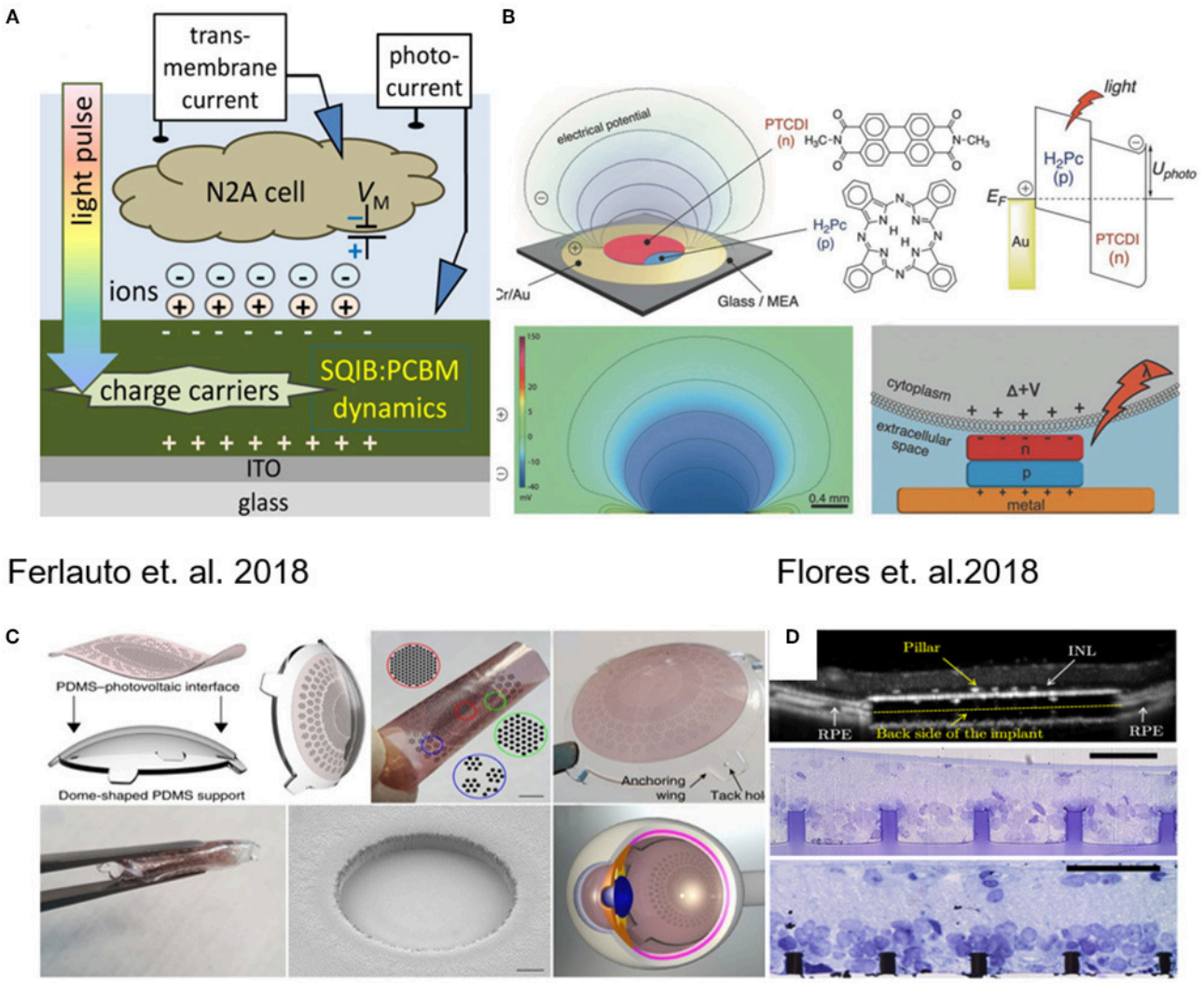

FIGURE 1 | (A) Schematic of experimental setup for transient photocurrent generation through a fullerene film. Reprinted with permission from Abdullaeva et al. (2016). **(B)** Layout of the photocapacitor, molecular structures of the pigment semiconductors and energy band illustration of a metal–p–n device. Reprinted with permission from Rand et al. (2018). **(C)** 3D photovoltaic wide-field retinal prosthetics realized on a PDMS support (POLYRETINA) Reprinted with permission from Ferlauto et al. (2018). **(D)** Pillar-based subretinal implant. Reprinted with permission from Flores et al. (2018).

prosthesis. These devices are capable of stimulating wireless retinal ganglion cells. The material stack included poly(3,4-ethylenedioxythiophene) polystyrene sulfonate (PEDOT:PSS) as anode and Poly(3-hexylthiophene) (P3HT) blend based as photo-active layer (**Figure 1C**) (Maya-Vetencourt et al., 2017; Ferlauto et al., 2018).

Retinal and subretinal inorganic prostheses were developed to restore sight in patients blinded by retinal degeneration by stimulating the inner retinal neurons using 3D pillar electrodes (**Figure 1D**) which enhance the cell-chip coupling and the integration the implant in the target tissue (Mathieson et al., 2012; Flores et al., 2018). In a recent work done by Ho et al. (2018a) a photodiode array made of boron-doped silicon-on-insulator (SOI) wafers was used to perform *in vivo* and *in vitro* measurements, in which the retina is placed between the recording array (ganglion cell side) and the photodiode array (photoreceptor side). In a recent work, transparent extracellular microelectrode arrays (MEA) were used to characterize the spatial and temporal response properties of retinal ganglion cells (RGCs) to photovoltaic stimulation in the healthy and degenerate rat retina (Ho et al., 2018b). It was demonstrated that using silicon photodiodes to build photovoltaic pixels arrays and it is possible to convert signals into patterns of current to stimulate the inner retinal neurons for wireless

neural stimulation in translucent tissues (Boinagrov et al., 2016).

NON-ELECTROGENIC CELLS

Beside electrogenic cells and tissues, photoelectrical devices can be used also for promoting cellular proliferation, for instance, in tissue regeneration applications.

One successful approach in tissue engineering is the use of photovoltaic platforms as novel treatments for angiogenesis. In this approach, a solar cell generates an electrical field promoting the formation of capillaries and arterioles at the ischemic region, attenuating muscle necrosis and fibrosis and promoting the secretion of angiogenic growth factors and the migration of mesenchymal stem cells (MSCs), myoblasts, endothelial progenitor cells, and endothelial cells in *in vitro* experiments (**Figure 2A**) (Jeong et al., 2017).

Many efforts are carried out on different types of cells like adipose-derived stem cells (ASC) and endothelial cells, evaluating the influence of pulsed LED light of three different wavelengths using continuous LLLT stimulation (Rohringer et al., 2017). In Couto et al., it was shown that a treatment of skin lesions with coherent and incoherent light sources (laser and LED, respectively) enables the wound healing process in elderly rats, with good results in terms of collagen deposition, fibroblasts proliferation and inflammatory cellular response (Couto et al., 2017). In fact, other studies have been developed on fibroblasts treatment using laser or led therapy to inhibit keloid fibroblasts after irradiation (Couto et al., 2017; Lee et al., 2017). In the end, different studies demonstrated the importance of therapy with coherent light in the visible spectrum to optimize the process of tissue repair, and some studies suggests that comparable effectiveness could be reached with the lower costs non-coherent light in the same spectral region.

Another interesting approach involved the fabrication of nanoweb substrates made of poly(3-hexylthiophene) (P3HT) to enhance the neurogenesis of human fetal neural stem cells (hfNSCs) and control their behavior *via* optoelectrical stimulation (**Figure 2B**) (Yang et al., 2017). Low-level laser therapy (LLLT) based on low-level laser or light-emitting diodes (LEDs) was used for tissue regeneration in mouse neural stem cell on 3D printed scaffolds (Zhu et al., 2017).

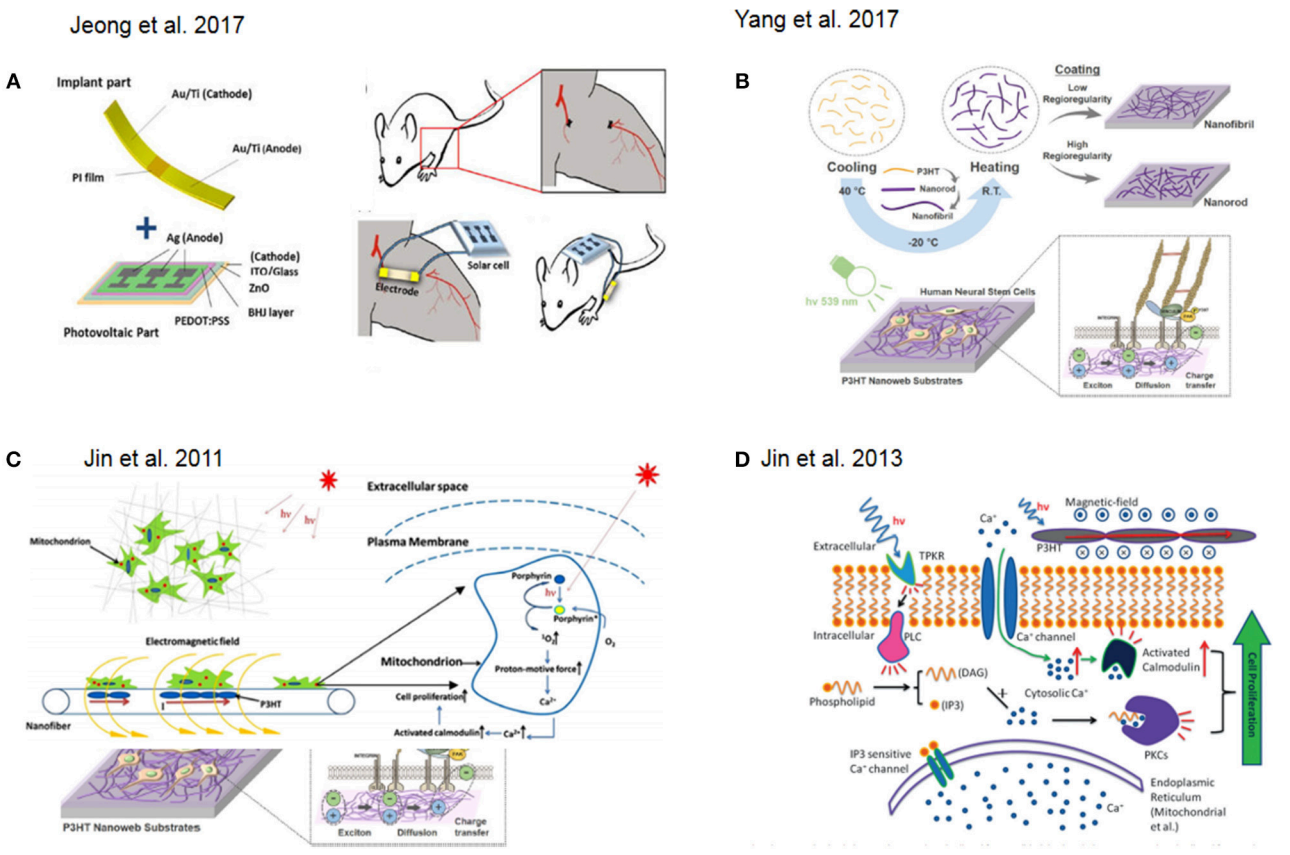

FIGURE 2 | (A) Schematic representation of a of solar cell device for in vivo experiment. Reprinted with permission from Jeong et al. (2017). **(B)** Fabrication flow and application of photoelectrical poly(3-hexylthiophene) (P3HT) nanoweb substrates for neuronal differentiation Reprinted with permission from Yang et al. (2017). **(C)** Schematic illustration of photocurrent stimulation for regenerative medicine. Reprinted with permission from Jin et al. (2011). **(D)** Signal pathway involved in light stimulation inducing cell proliferation. Reprinted with permission from Jin et al. (2013).

An interesting novelty regards the possibility to treat diseases delivering cellsto an injured or diseased organ/tissue. Usually this is accomplished by collecting cells through a digestion process with enzymes which can lead to Undesired enzymatic residuces. In orer to overcome this, cells have been cultured onsilicon based photovoltaic surfaces have been released through light stimulation as presented in the work of Bhuyan et al. (2016).

In a recent work done by Diring et al. (2017), photoactive zirconium-based metal organic framework (MOF) particles embedded in a polymer matrix were employed as growth substrate for HeLa cells. The substrate was able to release CO upon light irradiation, and its subsequent cellular uptake was monitored using a fluorescent probe.

In this context, one example, which also attempted to recapitulate 3D tissue-like environment with particular focus on regenerative medicine, was presented by Jin and co-workers. They reported on the photocurrent stimulation effect on cells with particular focus on understanding the combined effect of direct light interaction together with the responseto the induced electromagnetic field. In fact, porphyrins are activated by photons interactions while calcium ions translocate through the voltage-gated channels at the membrane due to the electromagnetic field. Overall, this results in an increase of cytosolic Ca^{2+} which might trigger protein pathways responsible for cell proliferation (Jin et al., 2011) (**Figure 2C**). Furthermore, they showed how to combine 3D structures with photoactive materials in order to achieve skin regeneration. In particular, they used human dermal fibroblasts (HDFs) and prepared a photosensitive nanofibrous scaffolds by electrospinning using Poly(3-hexylthiophene) (P3HT) and Polycaprolactone (PCL) as base materials to fabricate the nanofibers. Here, they further discussed how the cytosolic Ca2+ increase would led to the activation of the low molecular weight protein calmodulin, which causes the activation of several key intracellular processes leading to cell division (Tomlinson et al., 1984) in combination with direct light activation of protein kinase C. As a result, these two effects led to an increase in cell proliferation (Jin et al., 2013, 2014) (**Figure 2D**). Furthermore, Jin and co-workers designed a new photosensitive semiconductive polymer, PDBTT (poly (N,N-bis (2-octyldodecyl)-3,6-di(thiophen-2-yl)-2,5-dihydropyrrolo[3,4-c]pyrrole- 1,4-dione-alt-thieno[3,2-b]thiophene), with maximum absorbance at 600 nm. This polymer with nanofibers of PCL incorporated, was electrospun and tested to study the proliferative effect of PCL/PDBTT nanofibers on HDFs under red LED illumination (Jin et al., 2017). Another interesting study showed how a scaffold made of electrospun fiber of P3HT in combination with a typical polymer used for tissue engineering, poly(L-lactic acid)-co-poly-(e-caprolactone) could be successfully used as photosensitive platforms for enhancing fibroblast proliferation and thus as good precursor of a wound dressing solution (Jin et al., 2014).

CONCLUSION

In this review, we reported the last advances in electrical phototransduction applied to biomedical applications. In particular, we focused the attention on the possible effects of photoelectrical stimulation driven on cells and tissues. The aim was to report the behavior of the biological system at the biotic-abiotic interface considering various approaches for enhancement/inhibition of electrogenic and non-electrogenic cells functionalities. In particular, we highlighted how the use of photovoltaic platforms had found major application in designing retinal prosthetics. Moreover, organic photovoltaic materials are used for building new bio-compliant platforms and, in perspective, represent the foremost class of material for cell-chip coupling. We foresee an increasing application of these materials also for tissue engineering purposes as preliminarily proposed for wound healing. Furthermore, the few examples of photovoltaic-based scaffolds paved the way to advanced platforms which need to be developed toward more biomimetic 3D environments.

AUTHOR CONTRIBUTIONS

All authors listed have made a substantial, direct and intellectual contribution to the work, and approved it for publication.

REFERENCES

Abdullaeva, O. S., Schulz, M., Balzer, F., Parisi, J., Lützen, A., Dedek, K., et al. (2016). Photoelectrical stimulation of neuronal cells by an organic semiconductor–electrolyte interface. *Langmuir* 32, 8533–8542. doi: 10.1021/acs.langmuir.6b02085

Benfenati, F., and Lanzani, G. (2018). New technologies for developing second generation retinal prostheses. *Lab Anim.* 47, 71–75. doi: 10.1038/s41684-018-0003-1

Bhuyan, M. K., Rodriguez-Devora, J., Tseng, T.-L. B., and Boland, T. (2016). Photovoltaic surfaces enable clonal myoblastic cell release using visible light as external stimulation. *Biotechnol. J.* 11, 393–398. doi: 10.1002/biot.201500126

Blau, A. (2013). Cell adhesion promotion strategies for signal transduction enhancement in microelectrode array *in vitro* electrophysiology: an introductory overview and critical discussion. *Curr. Opin. Colloid Interface Sci.* 18, 481–492. doi: 10.1016/j.cocis.2013.07.005

Boinagrov, D., Lei, X., Goetz, G., Kamins, T. I., Mathieson, K., Galambos, L., et al. (2016). Photovoltaic pixels for neural stimulation: circuit models and performance. *IEEE Trans. Biomed. Circuits Syst.* 10, 85–97. doi: 10.1109/TBCAS.2014.2376528

Chenais, N., Leccardi, A., Ildelfonsa, M. J., Ferlauto, L., Sivula, K., and Ghezzi, D. (2017). *Photovoltaic Stimulation of Retinal Ganglion Cells with Wide-Field Epiretinal Prosthesis.* Available online at: https://infoscience.epfl.ch/record/231326 (Accessed August 30, 2018).

Couto, J. P. A., do, Nicolau, R. A., Munin, E., Castillo, M. A. S., Fadin, -Priscila Silva, L., et al. (2017). Skin tissue healing induced by coherent (laser) or non-coherent (led) light therapy on aged rats. *Int. Phys. Med. Rehabil. J.* 1, 1–6. doi: 10.15406/ipmrj.2017.1.00029

Di Maria, F., Lodola, F., Zucchetti, E., Benfenati, F., and Lanzani, G. (2018). The evolution of artificial light actuators in living systems: from planar to nanostructured interfaces. *Chem. Soc. Rev.* 47, 4757–4780. doi: 10.1039/C7CS00860K

Diring, S., Carné-Sánchez, A., Zhang, J., Ikemura, S., Kim, C., Inaba, H., et al. (2017). Light responsive metal-organic frameworks as controllable CO-releasing cell culture substrates. *Chem. Sci.* 8, 2381–2386. doi: 10.1039/c6sc04824b

Ferlauto, L., Leccardi, M. J. I. A., Chenais, N. A. L., Gilliéron, S. C. A., Vagni, P., Bevilacqua, M., et al. (2018). Design and validation of a foldable and photovoltaic wide-field epiretinal prosthesis. *Nat. Commun.* 9:992. doi: 10.1038/s41467-018-03386-7

Flores, T., Lei, X., Huang, T., Lorach, H., Dalal, R., Galambos, L., et al. (2018). Optimization of pillar electrodes in subretinal prosthesis for enhanced proximity to target neurons. *J. Neural Eng.* 15:036011. doi: 10.1088/1741-2552/aaac39

Ghezzi, D., Antognazza, M. R., Maccarone, R., Bellani, S., Lanzarini, E., Martino, N., et al. (2013). A polymer optoelectronic interface restores light sensitivity in blind rat retinas. *Nat. Photonics* 7, 400–406. doi: 10.1038/nphoton.2013.34

Ghezzi, D., Antognazza, M. R., Maschio, M. D., Lanzarini, E., Benfenati, F., and Lanzani, G. (2011). A hybrid bioorganic interface for neuronal photoactivation. *Nat. Commun.* 2:166. doi: 10.1038/ncomms1164

Ho, E., Lorach, H., Goetz, G., Laszlo, F., Lei, X., Kamins, T., et al. (2018a). Temporal structure in spiking patterns of ganglion cells defines perceptual thresholds in rodents with subretinal prosthesis. *Sci. Rep.* 8:3145. doi: 10.1038/s41598-018-21447-1

Ho, E., Smith, R., Goetz, G., Lei, X., Galambos, L., Kamins, T. I., et al. (2018b). Spatiotemporal characteristics of retinal response to network-mediated photovoltaic stimulation. *J. Neurophysiol.* 119, 389–400. doi: 10.1152/jn.00872.2016

Jeong, G.-J., Oh, J. Y., Kim, Y.-J., Bhang, S. H., Jang, H.-K., Han, J., et al. (2017). Therapeutic Angiogenesis via Solar Cell-Facilitated Electrical Stimulation. *ACS Appl. Mater. Interfaces* 9, 38344–38355. doi: 10.1021/acsami.7b13322

Jin, G., Li, J., and Li, K. (2017). Photosensitive semiconducting polymer-incorporated nanofibers for promoting the regeneration of skin wound. *Mater. Sci. Eng. C* 70, 1176–1181. doi: 10.1016/j.msec.2016.04.107

Jin, G., Prabhakaran, M. P., Kai, D., Kotaki, M., and Ramakrishna, S. (2013). Electrospun photosensitive nanofibers: potential for photocurrent therapy in skin regeneration. *Photochem. Photobiol. Sci.* 12, 124–134. doi: 10.1039/c2pp25070e

Jin, G., Prabhakaran, M. P., Liao, S., and Ramakrishna, S. (2011). Photosensitive materials and potential of photocurrent mediated tissue regeneration. *J. Photochem. Photobiol. B* 102, 93–101. doi: 10.1016/j.jphotobiol.2010.09.010

Jin, G., Prabhakaran, M. P., and Ramakrishna, S. (2014). Photosensitive and biomimetic core–shell nanofibrous scaffolds as wound dressing. *Photochem. Photobiol.* 90, 673–681. doi: 10.1111/php.12238

Khraiche, M. L., El Emam, S., Akinin, A., Cauwenberghs, G., Freeman, W., and Silva, G. A. (2013). Visual evoked potential characterization of rabbit animal model for retinal prosthesis research. *Conf. Proc. IEEE Eng. Med. Biol. Soc.* 2013, 3539–3542. doi: 10.1109/EMBC.2013.6610306

Lee, H. S., Jung, S.-E., Kim, S. K., Kim, Y.-S., Sohn, S., and Kim, Y. C. (2017). Low-level light therapy with 410 nm light emitting diode suppresses collagen synthesis in human keloid fibroblasts: an *in vitro* study. *Ann. Dermatol.* 29, 149–155. doi: 10.5021/ad.2017.29.2.149

Liao, C., Zhang, M., Yao, M. Y., Hua, T., Li, L., and Yan, F. (2015). Flexible organic electronics in biology: materials and devices. *Adv. Mater.* 27, 7493–7527. doi: 10.1002/adma.201402625

Love, M. R., Palee, S., Chattipakorn, S. C., and Chattipakorn, N. (2018). Effects of electrical stimulation on cell proliferation and apoptosis. *J. Cell. Physiol.* 233, 1860–1876. doi: 10.1002/jcp.25975

Martino, N., Feyen, P., Porro, M., Bossio, C., Zucchetti, E., Ghezzi, D., et al. (2015). Photothermal cellular stimulation in functional bio-polymer interfaces. *Sci. Rep.* 5:8911. doi: 10.1038/srep08911

Mathieson, K., Loudin, J., Goetz, G., Huie, P., Wang, L., Kamins, T. I., et al. (2012). Photovoltaic retinal prosthesis with high pixel density. *Nat. Photonics* 6, 391–397. doi: 10.1038/nphoton.2012.104

Maya-Vetencourt, J. F., Ghezzi, D., Antognazza, M. R., Colombo, E., Mete, M., Feyen, P., et al. (2017). A fully organic retinal prosthesis restores vision in a rat model of degenerative blindness. *Nat. Mater.* 16, 681–689. doi: 10.1038/nmat4874

Numata, T., Murakami, T., Kawashima, F., Morone, N., Heuser, J. E., Takano, Y., et al. (2012). Utilization of photoinduced charge-separated state of donor–acceptor-linked molecules for regulation of cell membrane potential and ion transport. *J. Am. Chem. Soc.* 134, 6092–6095. doi: 10.1021/ja3007275

Pennacchio, F. A., Garma, L. D., Matino, L., and Santoro, F. (2018). Bioelectronics goes 3D: new trends in cell–chip interface engineering. *J. Mater. Chem. B*. doi: 10.1039/C8TB01737A. [Epub ahead of print].

Polino, G., Casaluci, S., Dianetti, M., Dell'Elce, S., Liscio, A., Mirruzzo, V., et al. (2015). Inverted bulk-heterojunction solar cells using polyethylenimine-ethoxylated processed from a fully aqueous dispersion as electron-transport layer. *Energy Technol.* 3, 1152–1158. doi: 10.1002/ente.201500154

Rand, D., Jakešová, M., Lubin, G., Vebraite, I., David-Pur, M., Đerek, V., et al. (2018). Direct electrical neurostimulation with organic pigment photocapacitors. *Adv. Mater.* 30:1707292. doi: 10.1002/adma.201707292

Richter, A., Benick, J., Fell, A., Hermle, M., and Glunz, S. W. (2018). Impact of bulk impurity contamination on the performance of high-efficiency n-type silicon solar cells. *Prog. Photovolt. Res. Appl.* 26, 342–350. doi: 10.1002/pip.2990

Rohringer, S., Holnthoner, W., Chaudary, S., Slezak, P., Priglinger, E., Strassl, M., et al. (2017). The impact of wavelengths of LED light-therapy on endothelial cells. *Sci. Rep.* 7:10700. doi: 10.1038/s41598-017-11061-y

Sim, S. L., Szalewski, R. J., Johnson, L. J., Akah, L. E., Shoemaker, L. E., Thoreson, W. B., et al. (2014). Simultaneous recording of mouse retinal ganglion cells during epiretinal or subretinal stimulation. *Vision Res.* 101, 41–50. doi: 10.1016/j.visres.2014.05.005

Thukral, A., Ershad, F., Enan, N., Rao, Z., and Yu, C. (2018). Soft ultrathin silicon electronics for soft neural interfaces: a review of recent advances of soft neural interfaces based on ultrathin silicon. *IEEE Nanotechnol. Mag.* 12, 21–34. doi: 10.1109/MNANO.2017.2781290

Tomlinson, S., MacNeil, S., Walker, S. W., Ollis, C. A., Merritt, J. E., and Brown, B. L. (1984). Calmodulin and cell function. *Clin. Sci. Lond. Engl.* 66, 497–507.

Yang, K., Oh, J. Y., Lee, J. S., Jin, Y., Chang, G.-E., Chae, S. S., et al. (2017). Photoactive poly(3-hexylthiophene) nanoweb for optoelectrical stimulation to enhance neurogenesis of human stem cells. *Theranostics* 7, 4591–4604. doi: 10.7150/thno.20169

Zhang, A., and Lieber, C. M. (2016). Nano-Bioelectronics. *Chem. Rev.* 116, 215–257. doi: 10.1021/acs.chemrev.5b00608

Zhu, W., George, J. K., Sorger, V. J., and Zhang, L. G. (2017). 3D printing scaffold coupled with low level light therapy for neural tissue regeneration. *Biofabrication* 9:025002. doi: 10.1088/1758-5090/aa6999

Conflict of Interest Statement: The authors declare that the research was conducted in the absence of any commercial or financial relationships that could be construed as a potential conflict of interest.

frontiers in Bioengineering and Biotechnology

MINI REVIEW
published: 27 November 2018
doi: 10.3389/fbioe.2018.00177

Targeting Inflammation With Nanosized Drug Delivery Platforms in Cardiovascular Diseases: Immune Cell Modulation in Atherosclerosis

*Antonio Cervadoro[1], Roberto Palomba[2], Giuseppe Vergaro[3,4], Roberta Cecchi[1,5], Luca Menichetti[6], Paolo Decuzzi[2], Michele Emdin[3,4] and Stefano Luin[1,7]**

[1] NEST Laboratory, Scuola Normale Superiore, Pisa, Italy, [2] Laboratory of Nanotechnology for Precision Medicine, Fondazione Istituto Italiano di Tecnologia, Genova, Italy, [3] Division of Cardiology and Cardiovascular Medicine, Fondazione Toscana Gabriele Monasterio, Pisa, Italy, [4] Institute of Life Sciences, Scuola Superiore Sant'Anna, Pisa, Italy, [5] Center for Nanotechnology Innovation (CNI@NEST), Istituto Italiano di Tecnologia, Pisa, Italy, [6] CNR Institute of Clinical Physiology (IFC), Pisa, Italy, [7] NEST Laboratory, Istituto Nanoscienze, CNR, Pisa, Italy

OPEN ACCESS

Edited by:
Gianni Ciofani,
Politecnico di Torino, Italy

Reviewed by:
Ciro Chiappini,
King's College London,
United Kingdom
Vincenzo Calcagno,
Universität Leipzig, Germany
Stefano Leporatti,
Istituto di
Nanotecnologia (NANOTEC), Italy

***Correspondence:**
Stefano Luin
s.luin@sns.it

Specialty section:
This article was submitted to Nanobiotechnology, a section of the journal Frontiers in Bioengineering and Biotechnology

Received: 14 October 2018
Accepted: 06 November 2018
Published: 27 November 2018

Citation:
Cervadoro A, Palomba R, Vergaro G, Cecchi R, Menichetti L, Decuzzi P, Emdin M and Luin S (2018) Targeting Inflammation With Nanosized Drug Delivery Platforms in Cardiovascular Diseases: Immune Cell Modulation in Atherosclerosis. Front. Bioeng. Biotechnol. 6:177. doi: 10.3389/fbioe.2018.00177

Atherosclerosis (AS) is a disorder of large and medium-sized arteries; it consists in the formation of lipid-rich plaques in the intima and inner media, whose pathophysiology is mostly driven by inflammation. Currently available interventions and therapies for treating atherosclerosis are not always completely effective; side effects associated with treatments, mainly caused by immunodepression for anti-inflammatory molecules, limit the systemic administration of these and other drugs. Given the high degree of freedom in the design of nanoconstructs, in the last decades researchers have put high effort in the development of nanoparticles (NPs) formulations specifically designed for either drug delivery, visualization of atherosclerotic plaques, or possibly the combination of both these and other functionalities. Here we will present the state of the art of these subjects, the knowledge of which is necessary to rationally address the use of NPs for prevention, diagnosis, and/or treatment of AS. We will analyse the work that has been done on: (a) understanding the role of the immune system and inflammation in cardiovascular diseases, (b) the pathological and biochemical principles in atherosclerotic plaque formation, (c) the latest advances in the use of NPs for the recognition and treatment of cardiovascular diseases, (d) the cellular and animal models useful to study the interactions of NPs with the immune system cells.

Keywords: atherosclerosis, inflammatory diseases, smart nanomaterials, drug delivery, nanomedicine, imaging and theranostics, immune cells, cardiovascular diseases

ATHEROSCLEROSIS AND INFLAMMATION

Atherosclerotic disease, or simply atherosclerosis (AS), is initially characterized by the formation of fatty streaks, with the accumulation of lipids [primarily cholesterol, but also triglycerides (Goldberg, 2018)] in the intima and inner media of arterial wall, especially in regions with abnormal flow patterns (Chistiakov et al., 2017). Fatty streaks may then evolve into soft, lipid-rich plaques, and eventually into thick cap-calcified lesions and/or unstable plaques characterized by inflammatory infiltration and sustained oxidative processes. Stable fibrocalcific atheroma is characterized by

calcium deposits, small lipid deposits, slight lumen reduction, and, often, by poor functional relevance. Vulnerable atheroma, which is more prone to rupture, is characterized by a large lipid-rich necrotic core, thin fibrous cap (<65 μm), neovascularization, spotty calcifications, inflammatory cells, and positive remodeling (Moore and Tabas, 2011; Hansson et al., 2015). The possibility of plaque regression has been reviewed in Chistiakov et al. (2017) focusing on animal models, and in Fisher (2016) also considering the dynamic changes in lipid and immune cells distributions.

AS is currently considered an inflammatory disorder, characterized by the infiltration into sub-endothelial space of various immune cells (ICs), especially circulating monocytes (MCs) that subsequently differentiate into macrophages (MΦs) and then into foam cells (FCs), going along with plaque formation and evolution (Moore et al., 2013; Zhang et al., 2017). Such simplified picture is complicated by the heterogeneity of the cells within and close to lesions during evolution [MCs, MΦs, and FCs, but also neutrophils, dendritic cells (Butcher and Galkina, 2012), T cells (Taleb, 2016), and possibly others]. In the cited reviews particular attention is given to the markers of the various IC phenotypes, although cells can present more than one function and can express a continuum of markers of different subtypes (Butcher and Galkina, 2012).

A key example regards MΦs, the characterizing cells in AS: their different subtypes can have antithetic roles. Initially classified only as classically activated M1 (pro-inflammatory) or alternatively activated M2 (anti-inflammatory), evidences have brought to the definitions of additional subtypes (e.g., Mox, M4, Mhem) and even "sub-subtypes" (e.g., M2a, M2b, M2c); there could actually be a continuum of specializations, and MΦs could even convert into each other (Butcher and Galkina, 2012; Leitinger and Schulman, 2013). It must be noted that also smooth muscle cells (SMCs) can assume some of the functions usually assigned to MΦs (efferocytosis, internalization of lipids or cholesterols), and may transform in foam cells (Chistiakov et al., 2017).

In any case, cells with phenotypes closer to Mox or M1 cells are the most active in internalizing lipids (particularly cholesterol), especially if agglomerated within oxidized low density lipoprotein (oxLDL). Upon this process, efferocytosis efficiency of cells is reduced, they transform into foam cells, and are easily subjected to imbalances in cholesterol influx/efflux process and hypoxia. The final outcome is most often apoptosis or necrosis, which resolve in local accumulation of the lipid content, the major constituent of the inner (possibly necrotic) core of the atherosclerotic plaque (Moore and Tabas, 2011). At the same time, the cell's residual components promote further inflammation signals and generation of oxidative species, in a persistent cycle of recruitment of intimal macrophages and their polarization toward pro-inflammatory subsets (Libby et al., 2014). Moreover, both monocytes and macrophages have been shown to contribute to the increase of the gamma-glutamyl transferase enzyme (γGT) in AS lesions, increasing the oxidative character of these zones (Pucci et al., 2014; Belcastro et al., 2015).

This self-sustained state of inflammation (similar to what happens in chronic wound environments) is characteristic of the vulnerable plaque. The presence of activated macrophages leads to the secretion of matrix-components degrading enzymes (such as matrix metalloproteinases-MMPs), inhibits the production of collagen by the SMCs, and finally contributes to vascular wall reshaping. These mechanisms are useful in early lesions, supporting resolution of disrupted endothelial layers and avoiding accumulation of toxic species, as well as for the reduction of atherosclerotic plaques; but, at the same time, they induce fragility in late plaques, with the possible final consequence of plaque rupture (Libby et al., 2014; Hansson et al., 2015; Martinez and White, 2018). Inflammation also modulates the clinical consequences of the thrombotic complications of AS, while its inhibition could attenuate progression, mitigate the risk of plaque rupture, and even promote regression of AS (Awan and Genest, 2015; Bäck and Hansson, 2015; Bäck et al., 2015; Kamaly et al., 2016).

ATHEROSCLEROSIS TREATMENTS

Current therapeutic approaches to AS aim at reducing promoting factors, including hypertension, smoke, and dyslipidemias; considered drugs (e.g., inhibitors of cholesterol hepatic synthesis like statins) particularly affect production and transport of cholesterol (or other lipids) to the arterial walls (Coomes et al., 2011; Duivenvoorden et al., 2014; Tsujita et al., 2015). Different approaches have been investigated, such as blocking absorption of cholesterol in the intestine (e.g., by ezetamibe) or controlling its reverse transport in ICs, e.g., by using an agonist for the liver X receptor (LXR) like GW3965, or administering artificial forms of high density lipoproteins (HDL; Duivenvoorden et al., 2014; Tsujita et al., 2015; Pulakazhi Venu et al., 2017; Goldberg, 2018; Mueller et al., 2018).

Controlling inflammation is another promising strategy; in particular, the interleukin-1 pathway has been identified as a possible therapeutic target. Canakinumab, a monoclonal antibody targeting interleukin-1β, was tested in the CANTOS (Canakinumab ANti-inflammatory Thrombosis Outcomes Study) trial (Ridker et al., 2011, 2017). Moreover, the chemotherapeutic drug methotrexate (MTX), largely used as an immunomodulatory and anti-inflammatory (AI) drug, was described to lower the risk for total cardiovascular diseases in patients with chronic inflammation (Popkova et al., 2015; Gomes et al., 2018), and has been observed to inhibit atherogenesis and macrophage migration to the intima in animal models (Bulgarelli et al., 2012). Although its mechanisms of action are not fully clear, this molecule is capable of reducing the secretion of pro-inflammatory cytokines and the expression of adhesion molecules on both immune and endothelial cells (Coomes et al., 2011).

While promising, systemic administration of AI drugs is often limited by a narrow therapeutic index and by severe adverse effects, including bone marrow suppression, neutropenia and immunodepression. Blockade and stimulation of the mechanisms involved in inflammation can hold positive, null, or even detrimental results depending on the phase of the atherogenic process (Aluganti Narasimhulu et al., 2016). Based

on these premises, it is authors' belief that a rational modulation of the functions of ICs is promising for an efficient treatment and hopefully comes with fewer adverse effects.

Ideally, it would be desirable to identify an effective strategy for all of the AS phases; e.g., in (Libby et al., 2014) Resolvin E1 is indicated as a mediator that reverses all the advanced lesions associated processes, while contributing to the resolution of the plaque also in earlier phases. Another promising possibility is controlling release or activation of compounds used to alleviate or cure AS symptoms/consequences. Possible approaches include: the use of drugs modified with a glutamyl in order to exploit the increased concentration of γGT in AS lesions (Belcastro et al., 2015); developing methods exploiting high cholesterol concentrations; tackling pathways leading the transformation process from monocyte to pro-inflammatory MΦs and finally to foam cells (Rousselle et al., 2013).

Due to their ambivalent role of inducing inflammation and regulating tissue regeneration, macrophages have been the first candidates addressed in order to control AS. Vannella and Wynn presented an interesting review describing macrophages behavior in different tissues, the mediators of the various mechanisms involved, and finally several possible ways to modulate them (Vannella and Wynn, 2017). It would be ideal to force their egress from AS lesions as transformation into foam cells is occurring; to this end, a suggestive idea could be activating or releasing a "macrophage migration-enhancement factor" (Weisbart et al., 1974; Ueno et al., 1997; Nunami et al., 1998), or interfering with cell surface adhesion molecule only in over-abundancy of cholesterol or other AS markers, e.g. by stopping the phosphorylation of CD44 (Qin, 2012).

TOWARD TARGETED THERANOSTICS NPs

As hinted above, spatial and temporal control of drug activity can reduce collateral short and long term effects; moreover, it can result in more convenient administration methods. These premises strongly call for the development of efficient, targeted delivery strategies for AI molecules, just like the ones based on their encapsulation into NPs (Costa Lima and Reis, 2015). Several kinds of NP have been considered for drug delivery; characteristics and production protocols for some of these are reviewed in Allen et al. (2016), Ulbrich et al. (2016), Cheraghi et al. (2017), and Matoba et al. (2017). There are still limitations and drawbacks for the clinical use of many NPs; these could arise from a not-yet perfect control of the final fate of many formulations, since they often accumulate also in the organs of the reticuloendothelial system (RES), from polydispersion and/or poor reproducibility in their preparation, or from the often difficult scale-up and high cost for their production, especially when multifunctional capabilities are added (Cheng et al., 2012; Ulbrich et al., 2016). However, NP physicochemical properties can be finely tailored during their synthesis and this allows optimizing drug loading and NP target specificity (Allen et al., 2016; Pentecost et al., 2016).

In the clinical setting of atherosclerotic disease, NPs loaded with anti-inflammatory drugs can be a powerful tool to hit inflammatory targets at the plaque level, preventing systemic side effects (Jokerst and Gambhir, 2011; Di Mascolo et al., 2013). Drug-loaded NPs targeting macrophages and other immune cells could control their pro-inflammatory activities and thus prevent, attenuate, and possibly reverse related disorders (i.e., increased atherosclerosis, but also altered adipocyte function and insulin resistance). At the same time, NPs could also be loaded with imaging agents allowing the detection of vulnerable atherosclerotic plaques; similar theranostic strategies already showed potential for detection and treatment of other diseases (including cancer and neurodegenerative disorders), exploiting a number of imaging modalities, among which optical imaging (OI), magnetic resonance imaging (MRI), ultrasound and photoacoustic (US-PA), computed tomography (CT), and nuclear imaging based on single photon and positron emission tomography (SPECT, PET; Xie et al., 2010; Kim et al., 2014; Weissleder et al., 2014; Atukorale et al., 2017; Stigliano et al., 2017; Zhang et al., 2017).

There is evidence that NPs can segregate into the plaque in preclinical models of AS via a "passive" targeting mechanism (Weissleder et al., 2014); while such a relative selectivity has not been completely understood, some hypotheses have been proposed. First, the abnormal hemodynamic forces where plaques develop may favor NPs deposition (Hossain et al., 2015); second, the endothelium appears discontinuous with openings for sufficiently small objects (Kim et al., 2014); third, there can be an active role of immune cells in vehiculating or accumulating the nanoparticles in inflamed districts (Moore et al., 2017).

Other strategies focused on specific targeting, e.g., toward inflammatory factors, dysfunctional endothelial cells, or specific macrophage receptors involved in cholesterol transport. Examples are drug carriers functionalization with selectin ligands or antibodies directed to CAMs (sialyl-Lewis X, PSFL-1, ICAM and VICAM ligands, anti-ICAM, anti-VCAM; Robbins et al., 2010) or anti-oxLDL receptor (Li et al., 2010). Li et al. used liposomes decorated with LOX-1 antibodies, Indium (^{111}In) or Gadolinium (Gd), and DiI fluorescence markers to image atherosclerotic plaques in ApoE$^{-/-}$ mice. Alternatively, it has been proposed to target collagen IV, which is present on the vascular basement and exposed when vascular permeability increases (Chan et al., 2011; Chen et al., 2013; Kamaly et al., 2016; Meyers et al., 2017). Also common strategies to target macrophages are based on functionalizing nanoparticles with dextran sulfate coating or peptides mimicking low-density lipoproteins (LDL) such as apolipoprotein A1 (ApoA-1), whose receptors (Class A Scavenger Receptor 1 MSR-1, and class B Scavenge Receptor CD36) are expressed on macrophages cell membrane (Canton et al., 2013). Further works focusing on visualization of macrophages distribution using nanoparticles are well reviewed in Weissleder et al. (2014).

Active targeting was achieved also using a "biomimetic" approach: NPs can derive from, or have properties similar to, aggregates like LDL or HDL, naturally accumulating in AS plaques (Allijn et al., 2013; Duivenvoorden et al., 2014; Gomes et al., 2018). More specific tissue or cell targeting can be found testing nanoparticle libraries *in-vitro* or *in-vivo* (Kamaly et al., 2016; Tang et al., 2016), but the mechanisms of the found

specificity should be understood, also in order to ensure it is preserved downhill of modifications of nanoconstructs or in different biological environments. Libraries are often tested preliminarily in cell cultures, but *in-vivo* tests are necessary at least to evaluate the impact of the different biological media.

Indeed, upon entry in an organism, NPs are usually coated by a protein corona (PC), changing their biological identity. PC formation (or "opsonisation") is often the first step toward the sequestration of NPs by the RES. Various approaches have been considered to avoid such phenomenon. Recent strategies are based on controlling nanoconstruct stiffness, since it was found that deformable particles are less subject to uptake by macrophages in RES in off-target tissues (Key et al., 2015; Palomba et al., 2018). Other methods exploit different coatings and functionalization developed for controlling the PC, e.g., by using polymers like PEG. This is thought to be an antifouling agent, but it actually seems to modulate the PC (Schöttler et al., 2016); moreover, it has been shown to be immunogenic, requiring the use of additional functionalizing moieties (Mima et al., 2017). Other possible coating molecules are based on peptides: examples comprise zwitterionic ones, for limiting serum-protein adsorption (Ranalli et al., 2017), or aptamer-likes, for enriching the PC with specific molecules present in biological fluids, which act as targeting moieties when properly oriented (Santi et al., 2017). All these approaches easily grant nanoconstructs with extended circulation half-life.

An advantage that will play important role consists in NPs potential multimodality: not only they can contain more than one drug and/or imaging agent, but it could also be possible to implement a trigger for drug release/activation. This could either be intrinsic (provided by the pathological environment) or exogenous (ultrasound, light, oscillating magnetic fields).

Especially under this view, an interesting development can arise from a synergy between nanotechnology and personalized medicine (Mendes et al., 2018). Early screening of the most suited bioactives (Tang et al., 2016; Risum et al., 2017), real time monitoring of local accumulations (Zavaleta et al., 2018), observing early feedbacks to the treatment (Qiao et al., 2017), and predicting patient responses (Sykes et al., 2016) are all possible aspects of personalized medicine. We believe that the rational application of nanotools in all these steps will embody a fundamental role in the upcoming clinical and pre-clinical research (Mura and Couvreur, 2012; Polyak and Ross, 2017; Yordanova et al., 2017).

NPs FOR AS TREATMENT AND DIAGNOSIS

The use of NPs for treatment of AS and visualization of plaques up to 2015 has been elegantly reviewed in Zhang et al. (2017); we further selected more recent works not reported there (**Table 1**). In this session, we describe some of these and other relevant works.

Often, intrinsic properties of NPs lead to the exploitation of drug delivery strategies together with photothermal- and radiofrequency-mediated triggering effects; e.g., Johnston proposed the possibility to use photothermal destruction of macrophages using iron oxide NPs with thin gold and dextran coating, excited by a laser pulse at 755 nm. In this manuscript the particles were used for MRI and *in vitro* photothermolysis (Ma et al., 2009). A similar approach has been tested in the NANOM-FIM trial (Kharlamov et al., 2015); here, NPs composed by silica shells containing gold and eventually magnetic nanoparticles were delivered on AS plaques by a bioengineered on-artery patch or using a magnetic navigation system; detonation of NPs using a NIR laser caused a significant final reduction of the total atheroma volume.

A different, interesting strategy consists on preventively acting on the selective recruitment of monocytes from the precursors of pro-inflammatory macrophages M1 (Nakashiro et al., 2016; Matoba et al., 2017). The authors proposed polymeric NPs loaded with Pioglitazone, an agonist of the receptor PPARγ shown to be able to influence macrophage polarization. The formulation was tested in $ApoE^{-/-}$ mice fed a high fat diet (HFD) and infused with angiotensin II, promoting inflammation driven by monocytes/macrophages. 2 days post injection the ratio between peripheral pro- and non-inflammatory monocytes subsets decreased substantially, and tissue macrophage polarity was regulated toward the non-inflammatory phenotype M2, with consequent suppression of EMMPRIN/MMP pathway and reduction of plaque destabilization risk.

In a similar approach, Stigliano et al. (2017) confirmed the potentiality of MTX in preventive-oriented treatments by loading it into NPs. The authors demonstrated specific accumulation of NPs into macrophages residing within lipid-rich plaques along the arterial tree. In the aortic arch of $ApoE^{-/-}$ mice on HFD treated with MTX-NPs, 50% less coverage of plaques was found in comparison to the control group. Importantly, this result was obtained by injecting a dose four times lower than reported in literature (Leite et al., 2015; Gomes et al., 2018).

MTX has also been investigated in synergy with different bioactive compounds. The group of Serrano Jr. (Gomes et al., 2018) tested the combined effect of injecting Paclitaxel (PTX)-loaded LDL-mimicking NPs and MTX-loaded NPs. In New Zealand white rabbits on atherogenic diet treated with both the NPs formulations, the regression of the lesion area and the intimal width reduction corresponded to 17 and 63%, respectively, compared to the group treated with PTX-NPs alone. The authors speculate that this athero-regression is mostly due to the macrophage reduction effect and not to an inhibition of SMCs migration into the intima.

Other possible applications of nanomedicine in the treatment of AS are based on gene regulation. Majmudar et al injected siRNA-containing polymeric NPs to silence the expression of C–C chemokine receptor type 2 (CCR-2), a key player in recruiting inflamed monocytes to atherosclerotic plaques; they observed reduced PET signals from ^{89}Zr-labeled dextran nanoparticles in aortic root when compared to mice treated with an irrelevant siRNA (Majmudar et al., 2013). Another example is the downregulation of the tissue inhibitor of metalloproteinase 3 by the use of miR-712, delivered by cationic lipid NPs targeting VCAM1. The treatment was performed in $ApoE^{-/-}$

TABLE 1 | Selected recent original works on detection and treatment of atherosclerosis using nanoparticles.

Molecular/functional target	Nanoparticles	Imaging platforms	Animal model/patients, dose, and administration route	Results	References
Macrophages; TNF-α, MMP9.	LDE: Lipid core NPs resembling the lipid structure of low-density lipoprotein, carrying PTX and/or MTX.	*Ex-vivo* optical imaging.	*Model:* 38 New Zealand white rabbit, 1% cholesterol diet for 8 weeks. - *Treatment:* I.V. injections 4 mg/kg 1/w.	Increased regression of plaque areas (−59%) and of intima area (−57%) by LDE-PTX + LDE-MTX. Macrophage presence in aortic lesions reduced (−48% by LDE-PTX, −43% by LDE-PTX + LDE-MTX). Reduced expression of MMP-9 (−74% LDE-PTX, −78% LDE-PTX + LDE-MTX) and TNF-α (-65% by LDE-PTX, −79% by LDE-PTX + LDE-MTX).	Gomes et al., 2018
Macrophages, foam cells.	Lipid coated polymeric NPs loaded with MTX.	Fluorescence imaging, PET/CT.	*Model:* ApoE$^{-/-}$ male mice on HFD. - *Treatment:* retro-orbital NPs injection, with 20 μg equivalent of MTX, 2/w, 30 days.	Fifty percent less plaque coverage (athero-protective effect) in the aortic arch as compared to the control groups of saline and free MTX injection ($p < 0.05$).	Stigliano et al., 2017
Monocytes and macrophages, reverse cholesterol efflux.	Library of high-density lipoprotein-mimicking NPs loaded with liver X receptor agonist GW3965.	Fluorescence imaging, PET, NIRF.	*Model:* ApoE$^{-/-}$ male mice. - *Treatment:* 10 mg/kg equivalent of GW3965, I.V. 2/w, 6 weeks.	Rational library screening strategy for identifying NPs with favorable immune cell specificity and biodistribution in an AS mouse model. 28% reduction of total lipids in aortic macrophages, 43% reduction in monocytes, 40% reduction in all CD45^{-} non-immune cells. Abolished GW3965 liver toxicity.	Tang et al., 2016
Collagen IV.	Col-IV IL-10 NP22: polymeric NPs containing anti-inflammatory IL-10 and decorated with the targeting peptide *Col IV*.	Confocal fluorescence microscopy.	*Model:* Ldlr$^{-/-}$ mice fed a Western-type high-fat/high-cholesterol diet for 12 weeks. - *Treatment:* Col IV II-10 NPs (5 μg /mouse equivalent of IL-10) I.V. 1/w for 4 weeks.	In lesions: oxidative stress significantly decreased compared with control NPs; no effects on macrophage or smooth muscle cell content. Stabilized and remodeled pre-existing advanced atherosclerotic plaques, via improved fibrous cap thickness and decreased necrotic core.	Kamaly et al., 2016
Monocytes, macrophages.	Polymer based spherical NPs loaded with pioglitazone and/or fluorescein isothiocyanate.	Flow cytometry, *ex-vivo* optical microscopy.	*Model:* ApoE$^{-/-}$ mice under HFD. 1.9 mg/kg/day angiotensin II administered intraperitoneally. - *Treatment:* Weekly treated with injection of pioglitazone-NP (7 or 0.7 mg/kg/week)	Altered inflammatory polarity of peripheral monocytes; tissue macrophage polarity regulated toward less inflammatory phenotypes (M2) by suppressing the EMMPRIN/MMP pathway; atherosclerotic plaque destabilization and rupture more effectively inhibited than with oral pioglitazone. NPs found in circulating monocytes and aortic macrophages.	Nakashiro et al., 2016
Macrophages, atherosclerotic plaque.	Hyaluronan NPs (HA-NPs).	Super Resolution Microscopy (dSTORM), PET/MRI.	*Models:* ApoE$^{-/-}$ mice with early (6 weeks HFD) or advanced (12 weeks HFD) AS; New Zealand white male rabbits with angioplastical endothelial denudation of the aorta. - *Treatment:* 25 mg/kg (for biodistribution) or 50 mg/kg/week (therapeutic study) of HA equivalent.	HA-NPs uptake by macrophages in early aortic lesions is five-fold higher than in advanced lesions. Lesions were significantly smaller than in control groups, with 30% fewer macrophages, and 30–40% higher collagen content, an important factor for plaque stability. No relevant relative differences between the organs bio-distributions between mice and rabbits, underlining the translational aspect of the study.	Beldman et al., 2017
Collagen IV, arterial injury.	Gold NPs coated with a collagen-binding peptide labeled with Alexa Fluor 546.	Fluorescence microscopy.	*Model:* adult male Sprague–Dawley rats after carotid artery balloon injury. - *Treatment:* NPs I.V. injection (2 mg/kg).	Fluorescence was detected at the site of left carotid arterial injury; no fluorescence was detected for controls conditions. Fluorescence can be detected from 20 min up to 96 h post injection, and the fluorescence pattern shifts from binding within the arterial media toward adventitial binding.	Meyers et al., 2017
EMMPRIN.	NAP9: Paramagnetic-fluorescent micellar NPs conjugated with the EMMPRIN binding peptide AP-9.	Echocardiography, MRI, confocal fluorescence microscopy.	*Model:* Wild type C57BL/6 mice with ischemia induced by coronary artery ligation. - *Treatment:* Single injection 50 mg/kg, I.V.	The research focused on acute myocardial infarction, but EMMPRIN has an active role also in AS. Treatment resulted in improved heart contractility, reduced cardiac necrosis, and reduction of levels of MMP-2 and MMP-9 almost to those in healthy animals.	Cuadrado et al., 2016

AS, atherosclerosis; PET, positron emission tomography; CT, computed tomography; PTX, Paclitaxel; MTX, Methotrexate; I.V., intravenous; NP, nanoparticle; MMP, matrix metalloproteinase; TNF, tumor necrosis factor; HFD, high fat diet; ApoE, apolipoprotein E; w, week(s); NIRF, near infrared fluorescence; IL, interleukin; EMMPRIN, extracellular matrix metalloproteinase inducer; Ldlr, low density lipoprotein receptor.

TABLE 2 | Selected reviews.

Review focus	Covered topics	Covered period	Study models treated	Remarks	References
Nanoparticle mediated detection and treatment of AS; prevention of plaque progression.	Atherogenesis, NPs for structural/functional imaging and therapy, preclinical stages, anti-inflammation and lipid lowering strategies, targeting routes.	Mainly 2000–2015, back to 1993.	*In vitro*, *in vivo*, pre-clinical stage.	NPs efficiency in the field is plenty documented *in vitro* and *in vivo* only, preclinical and clinical studies still fall behind. Useful tables summarizing researches done on detection and treatment of atherosclerosis using nanoparticles.	Zhang et al., 2017
Immune cells in healthy and AS-prone aorta.	(Sub)phenotypes classification of dendritic cells and MΦs possibly present in aortic walls, their roles in AS; mixed phenotypes	Mainly 2004–2011, back to 1913.	*In vitro*, *in vivo*.	Useful table of ICs classification, markers, secreted factors, functions, impact on plaque stability.	Butcher and Galkina, 2012
Lipids in cardiovascular systems	Metabolism and blood transport of cholesterols, triglycerides and other lipids.	1973–2017, one from 1954.	*In vitro, in vivo, clinical.*	Focus on the role of triglycerides, but contains a short and efficient discussion on cholesterol metabolism and transport, interaction with MΦs and role in AS.	
NPs as drug delivery systems for cardiovascular disorder.	NPs performances on drug kinetics and toxicity, various nanoconstructs design/synthesis and their physiological behavior, AS, most fundamental MCs and MΦs types in humans and mice.	Mainly 2005–2016, back to 1994.	*In vitro*, *in vivo*, pre-clinical stage.	Short review.	Matoba et al., 2017
Vascular targeting of NPs for molecular imaging of diseased endothelium.	Rational design of physicochemical NPs properties, AS, cancer, disease-impaired blood flows. Imaging modalities (nuclear, optical, computed, tomography, magnetic resonance, ultrasound, multimodal) for NPs.	Mainly 2006–2016, back to 1981.	*In vitro*, *in vivo*, pre-clinical stage.	Imaging should be pondered to achieve complex information, not just images. No significant discrepancies in clinical translation of results from animal models of the disease. Authors feel a lack in clear clinical relevance or of a well-defined endpoint; this leads to poorly designed preclinical studies. However, also early-stage researches in the field are starting to consider clinical deployments.	Atukorale et al., 2017
Rational design of NPs for AS.	Early and late stage of the disease, NPs/cell interaction, biodistribution, drug delivery, multi-modal imaging, AS-oriented gene therapies.	Mainly 2008–2016, back to 1958.	*In vitro*, *in vivo*, pre-clinical stage.	Useful table with a summary of nanomaterials designed to image or modulate atherosclerotic lesions.	Allen et al., 2016
Taking advance of the immune system cells for therapeutic purposes.	NPs fate upon injection, physicochemical properties for rational design, cellular uptake mechanism, passive and active targeting. MΦs subtypes, markers, produced cytokines, polarization control; imaging of inflammation.	Mainly 2003–2015, back to 1977.	*In vitro*, *in vivo*, clinical.	NPs targeting MΦs and controlling their polarization are just beginning to be elaborated by the community and probably their potential are not yet grasped. Authors suggest the implementation of MΦs specificity in theranostic nano-constructs constitutes a strategic step to expedite transition into clinical phase.	Pentecost et al., 2016
Nanoliposomes and NPs toward cardiovascular related disorders.	Principles of action, drug release and interaction, infarcted heart, lesions imaging modalities.	Mainly 2005–2016, back to 1998.	*In vitro*, *in vivo*, clinical.	Nanoliposomal formulations are promising vectors for cardiovascular disorders diagnosis and treatment, but side effects should be reduced bioactives controlled release optimized, also for fastening clinical translation.	Cheraghi et al., 2017

(Continued)

TABLE 2 | Continued

Review focus	Covered topics	Covered period	Study models treated	Remarks	References
Mouse models for AS.	Disease development and plaque rupture, pro and cons of most common mouse models, endoplasmic reticulum stress, mitochondrial dysfunction.	Mainly 2004–2016, back to 1977.	*In vivo*, clinical.	The complexity of the topic does not allow for a single, good-for-all animal model. Importantly, a correct study design must go through the identification and comprehension of the molecular events involved.	Lee et al., 2017
Animal models for AS.	Mice models for AS and for plaque rupture, rabbit models, pigs, non-human primates.	Mainly 2000–2016, back to 1980.	*In vivo*.	One discriminant among different animal models for AS plaques is the topography of the generated lesions, compared to humans. In this scenario mice became the predominant species for models related to inflammatory cardiovascular diseases. Rabbits fall just behind and are mainly exploited due to their plasma metabolism similarity with humans. $ApoE^{-/-}Fbn1^{C1039G+/-}$ mice hold high promises for the future, being the very first animal model presenting spontaneous plaque rupture with end-points similar to humans.	Emini Veseli et al., 2017

AS, atherosclerosis; IC, immune cell; MC, monocyte; MΦ, macrophage; NP, nanoparticle; ApoE, apolipoprotein E.

mice and was able to significantly attenuate the development of atherosclerotic plaques (Kheirolomoom et al., 2015).

TOOLS AND IDEAS FOR ADDITIONAL RESEARCH

As reviewed above, fundamental and pre-clinical researches on AI-drugs-loaded NPs against AS are beginning to bloom, and there are also clinical trials for the (separated) use of NPs and AI drugs for regression or consolidation of AS plaques. More fundamental and translational research on the mechanisms underlying their action could inspire and motivate future more efficient clinical trials using AI-drug loaded NPs against AS.

Important future steps for the development of new NP-based theranostics strategies can arise from the study of interaction mechanisms between NPs and immune cells, with particular regard to what fate NPs and their components will face upon site deposition and cellular uptake. Investigations on these directions will remarkably improve the development of NPs rational designs aimed at specific accumulation and cargo smart activation.

Indeed, where, how and in which proportion NPs are internalized in the various subtypes of ICs is still not clear, also due to the different internalization routes observed even in close phenotypes (Lunov et al., 2011), nor it is clear how or if they are exocytosed (Oh and Park, 2014). In particular, are NPs mostly internalized by circulating monocytes that enter the lesions, or by resident macrophages in lesions, where NPs enter because of the enhanced permeability of inflamed endothelium?

Immortalized cell lines can be used for preliminary experiments. The most used are murine macrophage-like RAW 264.7 and J774, and human monocyte-like THP-1 and U937 (Luster et al., 1995; Qin, 2012; Andreu et al., 2017) reviews in particular the use of THP-1, unchanged or differentiated toward a MΦ phenotype (especially M1), but also cites other human monocyte/macrophage models. Following these models, even though there are evident parallelisms, care must be taken for intrinsic differences: between cells originating from different organisms (Ingersoll et al., 2010; Matoba et al., 2017; Zhang et al., 2017); between immortalized cell lines and primary cells (Andreu et al., 2017); even between possible different differentiations ICs may undergo during regular cultures. Primary cells should be used in final tests, but in this case the last type of unwanted differentiations are even more critical [e.g., monocytes are extremely sensible and may be activated just by sole adhering on surfaces (Belcastro et al., 2015)]. For these reasons, a thoughtful characterization of their phenotypes (by visual inspection or, better, by markers analysis) should be carried out before every experiment.

Together with the internalization pathway, also the bio-distribution of NPs deserves attention; a nice review for both these issues, which considers MC and MΦs, can be found in Pentecost et al. (2016), with interesting discussions about dependencies on NP geometry and surface chemistry, targeting, control on MΦ phenotype, and imaging. In addition, medium and long-term fates of nano-construct components (in particular its bioactive cargo) should be addressed; these details can indeed

impact the efficacy of the researched treatment, but also the long-term effects on the patients' health.

Finally, various animal models have been developed for the different phases of AS, as reviewed in Emini Veseli et al. (2017) and Lee et al. (2017). A recently developed model of controllable and reversible hypercholesterolemia is based on transient knockdown of the hepatic LDL receptor (LDLR) by antisense oligonucleotides in wild type C57BL/6 mice, followed by its rapid restoration (Basu et al., 2018).

CONCLUSION

Cardiovascular events, such as acute myocardial infarction and stroke, are often associated with erosion/rupture of arterial atherosclerotic plaques and superimposed thrombosis. These can cause arterial-vessel occlusion, downstream ischemia and necrosis, with subsequent heart failure and the whole clinical spectrum of vascular encephalopathies. Being AS an important source of morbidity and mortality, intense research efforts toward precision and personalized medicine in this field are motivated.

There are several reviews for selected aspects of the highly complicated issue of AS and its theranostics with NPs (**Table 2**). Here, we shortly presented the broad background necessary to understand the use of NPs for smart delivery and activation of anti-inflammatory drugs. We tried to focus on how basic science, together with the translational and clinical aspects, can address different portions of this, aiming at providing a better answer for the underlying mechanisms of NPs intra-plaque internalization, as well as for the molecular and cellular processes at the bases of different treatments. We stressed that a more thorough understanding of these would help foresee possible side effects, even long term ones, and also the opportunity to employ similar techniques and (nano)tools to other pathologies.

While single studies can be carried out in specialized groups, a deeper understanding of concepts, mechanisms and applicability of the developed (nano)tools needs a highly interdisciplinary environment, involving e.g. cardiologists, biologists, physicists, chemists, engineers; professionals able to talk with each other, and fostering the formation of multi-faceted scientists.

AUTHOR CONTRIBUTIONS

SL conceived the idea. SL and AC wrote the manuscript, with major contributions from RP, RC, and GV, starting from texts written in collaboration with LM, ME, and PD. All authors discussed, edited, and contributed to the manuscript.

FUNDING

SL acknowledges funding from Scuola Normale Superiore (university coordinated project Visualization and theranostic of atherosclerotic PLAQUEs VIA compound NANOparticles, PLAQUEviaNANO, in collaboration with Scuola Superiore Sant'Anna) and Fondazione Pisa (project Nanotechnology for tumor molecular fingerprinting and early diagnosis, RST 148/16).

REFERENCES

Allen, S., Liu, Y. G., and Scott, E. (2016). Engineering nanomaterials to address cell-mediated inflammation in atherosclerosis. *Regen. Eng. Transl. Med.* 2, 37–50. doi: 10.1007/s40883-016-0012-9

Allijn, I. E., Leong, W., Tang, J., Gianella, A., Mieszawska, A. J., Fay, F., et al. (2013). Gold nanocrystal labeling allows low-density lipoprotein imaging from the subcellular to macroscopic level. *ACS Nano* 7, 9761–9770. doi: 10.1021/nn403258w

Aluganti Narasimhulu, C., Fernandez-Ruiz, I., Selvarajan, K., Jiang, X., Sengupta, B., Riad, A., et al. (2016). Atherosclerosis — do we know enough already to prevent it? *Curr. Opin. Pharmacol.* 27, 92–102. doi: 10.1016/j.coph.2016.02.006

Andreu, N., Phelan, J., De Sessions, P. F., Cliff, J. M., Clark, T. G., and Hibberd, M. L. (2017). Primary macrophages and J774 cells respond differently to infection with *Mycobacterium tuberculosis*. *Sci. Rep.* 7:42225. doi: 10.1038/srep42225

Atukorale, P. U., Covarrubias, G., Bauer, L., and Karathanasis, E. (2017). Vascular targeting of nanoparticles for molecular imaging of diseased endothelium. *Adv. Drug Deliv. Rev.* 113, 141–156. doi: 10.1016/j.addr.2016.09.006

Awan, Z., and Genest, J. (2015). Inflammation modulation and cardiovascular disease prevention. *Eur. J. Prev. Cardiol.* 22, 719–733. doi: 10.1177/2047487314529350

Bäck, M., and Hansson, G. K. (2015). Anti-inflammatory therapies for atherosclerosis. *Nat. Rev. Cardiol.* 12:199. doi: 10.1038/nrcardio.2015.5

Bäck, M., Weber, C., and Lutgens, E. (2015). Regulation of atherosclerotic plaque inflammation. *J. Intern. Med.* 278, 462–482. doi: 10.1111/joim.12367

Basu, D., Hu, Y., Huggins, L.-A., Mullick, A. E., Graham, M. J., Wietecha, T., et al. (2018). Novel reversible model of atherosclerosis and regression using oligonucleotide regulation of the LDL receptor. *Circ. Res.* 122, 560–567. doi: 10.1161/CIRCRESAHA.117.311361

Belcastro, E., Franzini, M., Cianchetti, S., Lorenzini, E., Masotti, S., Fierabracci, V., et al. (2015). Monocytes/macrophages activation contributes to b-gamma-glutamyltransferase accumulation inside atherosclerotic plaques. *J. Transl. Med.* 13:325. doi: 10.1186/s12967-015-0687-6

Beldman, T. J., Senders, M. L., Alaarg, A., PéRez-Medina, C., Tang, J., Zhao, Y., et al. (2017). Hyaluronan nanoparticles selectively target plaque-associated macrophages and improve plaque stability in atherosclerosis. *ACS Nano* 11, 5785–5799. doi: 10.1021/acsnano.7b01385

Bulgarelli, A., Dias, A. A. M., Caramelli, B., and Maranhão, R. C. (2012). Treatment with methotrexate inhibits atherogenesis in cholesterol-fed rabbits. *J. Cardiovasc. Pharmacol.* 59, 308–314. doi: 10.1097/FJC.0b013e318241c385

Butcher, M. J., and Galkina, E. V. (2012). Phenotypic and functional heterogeneity of macrophages and dendritic cell subsets in the healthy and atherosclerosis-prone aorta. *Front. Physiol.* 3:44. doi: 10.3389/fphys.2012.00044

Canton, J., Neculai, D., and Grinstein, S. (2013). Scavenger receptors in homeostasis and immunity. *Nat. Rev. Immunol.* 13, 621–634. doi: 10.1038/nri3515

Chan, J. M., Rhee, J.-W., Drum, C. L., Bronson, R. T., Golomb, G., Langer, R., et al. (2011). *In vivo* prevention of arterial restenosis with paclitaxel-encapsulated targeted lipid–polymeric nanoparticles. *Proc. Natl. Acad. Sci.* 108, 19347–19352. doi: 10.1073/pnas.1115945108

Chen, W., Cormode, D. P., Vengrenyuk, Y., Herranz, B., Feig, J. E., Klink, A., et al. (2013). Collagen-specific peptide conjugated HDL nanoparticles as MRI contrast agent to evaluate compositional changes in atherosclerotic plaque regression. *JACC Cardiovasc. Imaging* 6, 373–384. doi: 10.1016/j.jcmg.2012.06.016

Cheng, Z., Al Zaki, A., Hui, J. Z., Muzykantov, V. R., and Tsourkas, A. (2012). Multifunctional nanoparticles: cost versus benefit of adding targeting and imaging capabilities. *Science* 338, 903–910. doi: 10.1126/science.1226338

Cheraghi, M., Negahdari, B., Daraee, H., and Eatemadi, A. (2017). Heart targeted nanoliposomal/nanoparticles drug delivery: an updated review. *Biomed. Pharmacother.* 86, 316–323. doi: 10.1016/j.biopha.2016.12.009

Chistiakov, D. A., Myasoedova, V. A., Revin, V. V., Orekhov, A. N., and Bobryshev, Y. V. (2017). The phenomenon of atherosclerosis reversal and regression: Lessons from animal models. *Exp. Mol. Pathol.* 102, 138–145. doi: 10.1016/j.yexmp.2017.01.013

Coomes, E., Chan, E. S., and Reiss, A. B. (2011). Methotrexate in atherogenesis and cholesterol metabolism. *Cholesterol* 2011:503028. doi: 10.1155/2011/503028

Costa Lima, S. A., and Reis, S. (2015). Temperature-responsive polymeric nanospheres containing methotrexate and gold nanoparticles: a multi-drug system for theranostic in rheumatoid arthritis. *Colloids Surfaces B* 133, 378–387. doi: 10.1016/j.colsurfb.2015.04.048

Cuadrado, I., Piedras, M. J. G. M., Herruzo, I., Del Carmen Turpin, M., Castejón, B., Reventun, P., et al. (2016). EMMPRIN-targeted magnetic nanoparticles for *in vivo* visualization and regression of acute myocardial infarction. *Theranostics* 6:545. doi: 10.7150/thno.13352

Di Mascolo, D., Lyon, C. J., Aryal, S., Ramirez, M. R., Wang, J., Candeloro, P., et al. (2013). Rosiglitazone-loaded nanospheres for modulating macrophage-specific inflammation in obesity. *J. Controll. Release* 170, 460–468. doi: 10.1016/j.jconrel.2013.06.012

Duivenvoorden, R., Tang, J., Cormode, D. P., Mieszawska, A. J., Izquierdo-Garcia, D., Ozcan, C., et al. (2014). A statin-loaded reconstituted high-density lipoprotein nanoparticle inhibits atherosclerotic plaque inflammation. *Nat. Commun.* 5:3065. doi: 10.1038/ncomms4065

Emini Veseli, B., Perrotta, P., De Meyer, G. R. A., Roth, L., Van Der Donckt, C., Martinet, W., et al. (2017). Animal models of atherosclerosis. *Eur. J. Pharmacol.* 816, 3–13. doi: 10.1016/j.ejphar.2017.05.010

Fisher, E. A. (2016). The regression of atherosclerosis-the journey from the liver to the plaque and back. *Arterioscler. Thromb. Vasc. Biol.* 36:226. doi: 10.1161/ATVBAHA.115.301926

Goldberg, I. J. (2018). Fat in the blood, fat in the artery, fat in the heart: triglyceride in physiology and disease. *Arterioscler. Thrombosis Vasc. Biol.* 38, 700–706. doi: 10.1161/ATVBAHA.117.309666

Gomes, F. L., Maranhão, R. C., Tavares, E. R., Carvalho, P. O., Higuchi, M. L., Mattos, F. R., et al. (2018). Regression of atherosclerotic plaques of cholesterol-fed rabbits by combined chemotherapy with paclitaxel and methotrexate carried in lipid core nanoparticles. *J. Cardiovasc. Pharmacol. Ther.* 2018:8836. doi: 10.1177/1074248418778836

Hansson, G. K., Libby, P., and Tabas, I. (2015). Inflammation and plaque vulnerability. *J. Intern. Med.* 278, 483–493. doi: 10.1111/joim.12406

Hossain, S. S., Zhang, Y., Fu, X., Brunner, G., Singh, J., Hughes, T. J., et al. (2015). Magnetic resonance imaging-based computational modelling of blood flow and nanomedicine deposition in patients with peripheral arterial disease. *J. R. Soc. Interface* 12:20150001. doi: 10.1098/rsif.2015.0001

Ingersoll, M. A., Spanbroek, R., Lottaz, C., Gautier, E. L., Frankenberger, M., Hoffmann, R., et al. (2010). Comparison of gene expression profiles between human and mouse monocyte subsets. *Blood* 115, e10–e19. doi: 10.1182/blood-2009-07-235028

Jokerst, J. V., and Gambhir, S. S. (2011). Molecular imaging with theranostic nanoparticles. *Acc. Chem. Res.* 44, 1050–1060. doi: 10.1021/ar200106e

Kamaly, N., Fredman, G., Fojas, J. J., Subramanian, M., Choi, W. I., Zepeda, K., et al. (2016). Targeted interleukin-10 nanotherapeutics developed with a microfluidic chip enhance resolution of inflammation in advanced atherosclerosis. *ACS Nano* 10, 5280–5292. doi: 10.1021/acsnano.6b01114

Key, J., Palange, A. L., Gentile, F., Aryal, S., Stigliano, C., Di Mascolo, D., et al. (2015). Soft discoidal polymeric nanoconstructs resist macrophage uptake and enhance vascular targeting in tumors. *ACS Nano* 9, 11628–11641. doi: 10.1021/acsnano.5b04866

Kharlamov, A. N., Tyurnina, A. E., Veselova, V. S., Kovtun, O. P., Shur, V. Y., and Gabinsky, J. L. (2015). Silica–gold nanoparticles for atheroprotective management of plaques: results of the NANOM-FIM trial. *Nanoscale* 7, 8003–8015. doi: 10.1039/C5NR01050K

Kheirolomoom, A., Kim, C. W., Seo, J. W., Kumar, S., Son, D. J., Gagnon, M. K. J., et al. (2015). Multifunctional nanoparticles facilitate molecular targeting and miRNA delivery to inhibit atherosclerosis in ApoE−/−mice. *ACS Nano* 9, 8885–8897. doi: 10.1021/acsnano.5b02611

Kim, Y., Lobatto, M. E., Kawahara, T., Chung, B. L., Mieszawska, A. J., Sanchez-Gaytan, B. L., et al. (2014). Probing nanoparticle translocation across the permeable endothelium in experimental atherosclerosis. *Proc. Natl. Acad. Sci.* 111, 1078–1083. doi: 10.1073/pnas.1322725111

Lee, Y. T., Lin, H. Y., Chan, Y. W. F., Li, K. H. C., To, O. T. L., Yan, B. P., et al. (2017). Mouse models of atherosclerosis: a historical perspective and recent advances. *Lipids Health Dis.* 16:12. doi: 10.1186/s12944-016-0402-5

Leite, A. C., Solano, T. V., Tavares, E. R., and Maranhão, R. C. (2015). Use of combined chemotherapy with etoposide and methotrexate, both associated to lipid nanoemulsions for atherosclerosis treatment in cholesterol-fed rabbits. *Cardiovasc. Drugs Ther.* 29, 15–22. doi: 10.1007/s10557-014-6566-1

Leitinger, N., and Schulman, I. G. (2013). Phenotypic polarization of macrophages in atherosclerosis. *Arterioscler. Thromb. Vasc. Biol.* 33, 1120–1126. doi: 10.1161/ATVBAHA.112.300173

Li, D., Patel, A. R., Klibanov, A. L., Kramer, C. M., Ruiz, M., Kang, B.-Y., et al. (2010). Molecular imaging of atherosclerotic plaques targeted to oxidized LDL receptor LOX-1 by SPECT/CT and magnetic resonance. *Circulation* 3, 464–472. doi: 10.1161/CIRCIMAGING.109.896654

Libby, P., Tabas, I., Fredman, G., and Fisher, E. A. (2014). Inflammation and its resolution as determinants of acute coronary syndromes. *Circ. Res.* 114, 1867–1879. doi: 10.1161/CIRCRESAHA.114.302699

Lunov, O., Syrovets, T., Loos, C., Beil, J., Delacher, M., Tron, K., et al. (2011). Differential uptake of functionalized polystyrene nanoparticles by human macrophages and a monocytic cell line. *ACS Nano* 5, 1657–1669. doi: 10.1021/nn2000756

Luster, A. D., Greenberg, S. M., and Leder, P. (1995). The IP-10 chemokine binds to a specific cell surface heparan sulfate site shared with platelet factor 4 and inhibits endothelial cell proliferation. *J. Exp. Med.* 182, 219–231. doi: 10.1084/jem.182.1.219

Ma, L. L., Feldman, M. D., Tam, J. M., Paranjape, A. S., Cheruku, K. K., Larson, T. A., et al. (2009). Small multifunctional nanoclusters (nanoroses) for targeted cellular imaging and therapy. *ACS Nano* 3, 2686–2696. doi: 10.1021/nn900440e

Majmudar, M. D., Yoo, J., Keliher, E. J., Truelove, J. J., Iwamoto, Y., Sena, B., et al. (2013). Polymeric nanoparticle PET/MR imaging allows macrophage detection in atherosclerotic plaques. *Circ. Res.* 112, 755–761. doi: 10.1161/CIRCRESAHA.111.300576

Martinez, B. K., and White, C. M. (2018). The emerging role of inflammation in cardiovascular disease. *Ann. Pharmacother.* 52, 801–809. doi: 10.1177/1060028018765939

Matoba, T., Koga, J.-I., Nakano, K., Egashira, K., and Tsutsui, H. (2017). Nanoparticle-mediated drug delivery system for atherosclerotic cardiovascular disease. *J. Cardiol.* 70, 206–211. doi: 10.1016/j.jjcc.2017.03.005

Mendes, M., Sousa, J., Pais, A., and Vitorino, C. (2018). "Clinical applications of nanostructured drug delivery systems: From basic research to translational medicine," in *Core-Shell Nanostructures for Drug Delivery and Theranostics: Challenges, Strategies and Prospects for Novel Carrier Systems, In Woodhead Publishing Series in Biomaterials*, eds M. L. Focarete and A. Tampieri (Cambridge, UK: Woodhead Publishing, Elsevier), 43–116. doi: 10.1016/B978-0-08-102198-9.00004-1

Meyers, M. W., Rink, J. S., Jiang, Q., Kelly, M. E., Vercammen, J. M., Thaxton, C. S., et al. (2017). Systemically administered collagen-targeted gold nanoparticles bind to arterial injury following vascular interventions. *Physiol. Rep.* 5:13128. doi: 10.14814/phy2.13128

Mima, Y., Abu Lila, A. S., Shimizu, T., Ukawa, M., Ando, H., Kurata, Y., et al. (2017). Ganglioside inserted into PEGylated liposome attenuates anti-PEG immunity. *J. Controll. Release* 250, 20–26. doi: 10.1016/j.jconrel.2017.01.040

Moore, K. J., Sheedy, F. J., and Fisher, E. A. (2013). Macrophages in atherosclerosis: a dynamic balance. *Nat. Rev. Immunol.* 13, 709–721. doi: 10.1038/nri3520

Moore, K. J., and Tabas, I. (2011). Macrophages in the pathogenesis of atherosclerosis. *Cell* 145, 341–355. doi: 10.1016/j.cell.2011.04.005

Moore, T. L., Hauser, D., Gruber, T., Rothen-Rutishauser, B., Lattuada, M., Petri-Fink, A., et al. (2017). Cellular shuttles: monocytes/macrophages exhibit transendothelial transport of nanoparticles under physiological flow. *ACS Appl. Mater. Interfaces* 9, 18501–18511. doi: 10.1021/acsami.7b03479

Mueller, P. A., Zhu, L., Tavori, H., Huynh, K., Giunzioni, I., Stafford, J. M., et al. (2018). Deletion of macrophage low-density lipoprotein receptor-related protein 1 (LRP1) accelerates atherosclerosis regression and increases CCR7 expression in plaque macrophages. *Circulation* 117:031702. doi: 10.1161/CIRCULATIONAHA.117.031702

Mura, S., and Couvreur, P. (2012). Nanotheranostics for personalized medicine. *Adv. Drug Deliv. Rev.* 64, 1394–1416. doi: 10.1016/j.addr.2012.06.006

Nakashiro, S., Matoba, T., Umezu, R., Koga, J.-I., Tokutome, M., Katsuki, S., et al. (2016). Pioglitazone-incorporated nanoparticles prevent plaque destabilization and rupture by regulating monocyte/macrophage differentiation in ApoE–/– mice. *Arterioscler. Thromb. Vasc. Biol.* 36, 491–500. doi: 10.1161/ATVBAHA.115.307057

Nunami, K.-I., Yamada, M., and Shimizu, R. (1998). Design of novel tripeptides with macrophage migration-enhancing activity. *Bioorg. Med. Chem. Lett.* 8, 2517–2520. doi: 10.1016/S0960-894X(98)00410-7

Oh, N., and Park, J.-H. (2014). Endocytosis and exocytosis of nanoparticles in mammalian cells. *Int. J. Nanomedicine* 9, 51–63. doi: 10.2147/IJN.S26592

Palomba, R., Palange, A. L., Rizzuti, I. F., Ferreira, M., Cervadoro, A., Barbato, M. G., et al. (2018). Modulating phagocytic cell sequestration by tailoring nanoconstruct softness. *ACS Nano* 12, 1433–1444. doi: 10.1021/acsnano.7b07797

Pentecost, A. E., Lurier, E. B., and Spiller, K. L. (2016). "Nanoparticulate systems for controlling monocyte/macrophage behavior," in *Microscale Technologies for Cell Engineering,* eds A. Singh and A. Gaharwar (Cham: Springer), 291–304.

Polyak, A., and Ross, T. L. (2017). Nanoparticles for SPECT and PET imaging: towards personalized medicine and theranostics. *Curr. Med. Chem*. 24, 1–26. doi: 10.2174/0929867324666170830095553

Popkova, T. V., Novikova, D. S., Gasparyan, A. Y., and Nasonov, E. L. (2015). Cardiovascular effects of methotrexate in rheumatoid arthritis revisited. *Curr. Med. Chem.* 22, 1903–1910. doi: 10.2174/0929867322666150415122039

Pucci, A., Franzini, M., Matteucci, M., Ceragioli, S., Marconi, M., Ferrari, M., et al. (2014). b-Gamma-glutamyltransferase activity in human vulnerable carotid plaques. *Atherosclerosis* 237, 307–313. doi: 10.1016/j.atherosclerosis.2014.09.028

Pulakazhi Venu, V. K., Adijiang, A., Seibert, T., Chen, Y.-X., Shi, C., Batulan, Z., et al. (2017). Heat shock protein 27–derived atheroprotection involves reverse cholesterol transport that is dependent on GM-CSF to maintain ABCA1 and ABCG1 expression in ApoE–/– mice. *FASEB J.* 31, 2364–2379. doi: 10.1096/fj.201601188R

Qiao, R., Qiao, H., Zhang, Y., Wang, Y., Chi, C., Tian, J., et al. (2017). Molecular imaging of vulnerable atherosclerotic plaques *in vivo* with osteopontin-specific upconversion nanoprobes. *ACS Nano* 11, 1816–1825. doi: 10.1021/acsnano.6b07842

Qin, Z. (2012). The use of THP-1 cells as a model for mimicking the function and regulation of monocytes and macrophages in the vasculature. *Atherosclerosis* 221, 2–11. doi: 10.1016/j.atherosclerosis.2011.09.003

Ranalli, A., Santi, M., Capriotti, L., Voliani, V., Porciani, D., Beltram, F., et al. (2017). Peptide-based stealth nanoparticles for targeted and pH-triggered delivery. *Bioconjug. Chem.* 28, 627–635. doi: 10.1021/acs.bioconjchem.6b00701

Ridker, P. M., Everett, B. M., Thuren, T., Macfadyen, J. G., Chang, W. H., Ballantyne, C., et al. (2017). Antiinflammatory therapy with canakinumab for atherosclerotic disease. *N. Engl. J. Med.* 377, 1119–1131. doi: 10.1056/NEJMoa1707914

Ridker, P. M., Thuren, T., Zalewski, A., and Libby, P. (2011). Interleukin-1β inhibition and the prevention of recurrent cardiovascular events: rationale and design of the Canakinumab Anti-inflammatory Thrombosis Outcomes Study (CANTOS). *Am. Heart J.* 162, 597–605. doi: 10.1016/j.ahj.2011.06.012

Risum, S., Knigge, U., and Langer, S. W. (2017). Hitherto unseen survival in an ALK-positive-patient with advanced stage adult ganglioneuroblastoma treated with personalized medicine. *Clin. Case Rep.* 5, 2085–2087. doi: 10.1002/ccr3.1262

Robbins, G. P., Saunders, R. L., Haun, J. B., Rawson, J., Therien, M. J., and Hammer, D. A. (2010). Tunable leuko-polymersomes that adhere specifically to inflammatory markers. *Langmuir* 26, 14089–14096. doi: 10.1021/la1017032

Rousselle, A., Qadri, F., Leukel, L., Yilmaz, R., Fontaine, J.-F., Sihn, G., et al. (2013). CXCL5 limits macrophage foam cell formation in atherosclerosis. *J. Clin. Invest.* 123, 1343–1347. doi: 10.1172/JCI66580

Santi, M., Maccari, G., Mereghetti, P., Voliani, V., Rocchiccioli, S., Ucciferri, N., et al. (2017). Rational design of a transferrin-binding peptide sequence tailored to targeted nanoparticle internalization. *Bioconjug. Chem.* 28, 471–480. doi: 10.1021/acs.bioconjchem.6b00611

Schöttler, S., Becker, G., Winzen, S., Steinbach, T., Mohr, K., Landfester, K., et al. (2016). Protein adsorption is required for stealth effect of poly (ethylene glycol)- and poly (phosphoester)-coated nanocarriers. *Nat. Nanotechnol.* 11:372. doi: 10.1038/nnano.2015.330

Stigliano, C., Ramirez, M. R., Singh, J. V., Aryal, S., Key, J., Blanco, E., et al. (2017). Methotraxate-loaded hybrid nanoconstructs target vascular lesions and inhibit atherosclerosis progression in ApoE(-/-) mice. *Adv. Healthc. Mater.* 6:201601286. doi: 10.1002/adhm.201601286

Sykes, E. A., Dai, Q., Sarsons, C. D., Chen, J., Rocheleau, J. V., Hwang, D. M., et al. (2016). Tailoring nanoparticle designs to target cancer based on tumor pathophysiology. *Proc. Natl. Acad. Sci.* 2016:201521265. doi: 10.1073/pnas.1521265113

Taleb, S. (2016). Inflammation in atherosclerosis. *Arch. Cardiovasc. Dis.* 109, 708–715. doi: 10.1016/j.acvd.2016.04.002

Tang, J., Baxter, S., Menon, A., Alaarg, A., Sanchez-Gaytan, B. L., Fay, F., et al. (2016). Immune cell screening of a nanoparticle library improves atherosclerosis therapy. *Proc. Natl. Acad. Sci. U.S.A.* 113, E6731–E6740. doi: 10.1073/pnas.1609629113

Tsujita, K., Sugiyama, S., Sumida, H., Shimomura, H., Yamashita, T., Yamanaga, K., et al. (2015). Impact of dual lipid-lowering strategy with ezetimibe and atorvastatin on coronary plaque regression in patients with percutaneous coronary intervention: the multicenter randomized controlled PRECISE-IVUS trial. *J. Am. Coll. Cardiol.* 66, 495–507. doi: 10.1016/j.jacc.2015.05.065

Ueno, M., Sugita, T., Murakami, T., and Takata, I. (1997). The novel anti-rheumatic drug TA-383 has a macrophage migration enhancing activity. *Jap. J. Pharmacol.* 74, 221–224. doi: 10.1254/jjp.74.221

Ulbrich, K., Holá, K., Šubr, V., Bakandritsos, A., Tuček, J., and Zboril, R. (2016). Targeted drug delivery with polymers and magnetic nanoparticles: covalent and noncovalent approaches, release control, and clinical studies. *Chem. Rev.* 116, 5338–5431. doi: 10.1021/acs.chemrev.5b00589

Vannella, K. M., and Wynn, T. A. (2017). Mechanisms of organ injury and repair by macrophages. *Annu. Rev. Physiol.* 79, 593–617. doi: 10.1146/annurev-physiol-022516-034356

Weisbart, R. H., Bluestone, R., Goldberg, L. S., and Pearson, C. M. (1974). Migration enhancement factor: a new lymphokine. *Proc. Natl. Acad. Sci.* 71, 875–879. doi: 10.1073/pnas.71.3.875

Weissleder, R., Nahrendorf, M., and Pittet, M. J. (2014). Imaging macrophages with nanoparticles. *Nat. Mater.* 13, 125–138. doi: 10.1038/nmat3780

Xie, J., Lee, S., and Chen, X. (2010). Nanoparticle-based theranostic agents. *Adv. Drug Deliv. Rev.* 62, 1064–1079. doi: 10.1016/j.addr.2010.07.009

Yordanova, A., Eppard, E., Kürpig, S., Bundschuh, R. A., Schönberger, S., Gonzalez-Carmona, M., et al. (2017). Theranostics in nuclear medicine practice. *Onco. Targets. Ther.* 10:4821. doi: 10.2147/OTT.S140671

Zavaleta, C., Ho, D., and Chung, E. J. (2018). Theranostic nanoparticles for tracking and monitoring disease state. *SLAS Technol.* 2018:2472630317738699. doi: 10.1177/2472630317738699

Zhang, J., Zu, Y., Dhanasekara, C. S., Li, J., Wu, D., Fan, Z., et al. (2017). Detection and treatment of atherosclerosis using nanoparticles. *Wiley Interdiscip. Rev. Nanomed. Nanobiotechnol.* 9:1412. doi: 10.1002/wnan.1412

Conflict of Interest Statement: The authors declare that the research was conducted in the absence of any commercial or financial relationships that could be construed as a potential conflict of interest.

frontiers in Bioengineering and Biotechnology

REVIEW
published: 14 November 2018
doi: 10.3389/fbioe.2018.00170

Frontiers of Medical Micro/Nanorobotics: *in vivo* Applications and Commercialization Perspectives Toward Clinical Uses

Fernando Soto[1]* *and Robert Chrostowski*[2]

[1] Department of Nanoengineering, University of California, San Diego, La Jolla, CA, United States, [2] Texas Materials Institute, The University of Texas at Austin, Austin, TX, United States

The field of medical micro/nanorobotics holds considerable promise for advancing medical diagnosis and treatment due to their unique ability to move and perform complex task at small scales. Nevertheless, the grand challenge of the field remains in its successful translation towards widespread patient use. We critically address the frontiers of the current methodologies for *in vivo* applications and discuss the current and foreseeable perspectives of their commercialization. Although no "killer application" that would catalyze rapid commercialization has yet emerged, recent engineering breakthroughs have led to the successful *in vivo* operation of medical micro/nanorobots. We also highlight how standardizing report summaries of micro/nanorobotics is essential not only for increasing the quality of research but also for minimizing investment risk in their potential commercialization. We review current patents and commercialization efforts based on emerging proof-of-concept applications. We expect to inspire future research efforts in the field of micro/nanorobotics toward future medical diagnosis and treatment.

Keywords: nanomedicine, medical translational research, *in vivo*, commercialization, microrobot, nanorobot

OPEN ACCESS

Edited by:
Gianni Ciofani, Politecnico di Torino, Italy

Reviewed by:
Arianna Menciassi, Scuola Sant'Anna di Studi Avanzati, Italy
Edoardo Sinibaldi, Fondazione Istituto Italiano di Technologia, Italy

***Correspondence:**
Fernando Soto
f1soto@ucsd.edu

Specialty section:
This article was submitted to Nanobiotechnology, a section of the journal Frontiers in Bioengineering and Biotechnology

Received: *29 August 2018*
Accepted: *25 October 2018*
Published: *14 November 2018*

Citation:
Soto F and Chrostowski R (2018) Frontiers of Medical Micro/Nanorobotics: in vivo Applications and Commercialization Perspectives Toward Clinical Uses. Front. Bioeng. Biotechnol. 6:170. doi: 10.3389/fbioe.2018.00170

INTRODUCTION

Imagine a world where robots the size of cells operate inside our body. This might sound like a science fiction story written by Isaac Asimov, or a visionary speech from Richard Feynman; however, it is conceivable that micro/nanorobotics will soon play a prominent role in medicine. (Wang, 2013; Wang et al., 2013; Li et al., 2017b) We use the term medical micro/nanorobots to refer to all nano- to micron-size structures (300 nm−300 μm) capable of converting power sources into kinetic energy.Three groups of powered micro/nanorobots are mainly described. Biohybrid systems integrate synthetic nanostructures with motile microorganisms as the engine of the micro/nanorobot. (Kim and Tung, 2015; Ricotti et al., 2017; Bente et al., 2018; Palagi and Fischer, 2018). Chemically powered micro/nanorobots use asymmetric catalytic engines to selectively convert chemical fuels into locomotion (Chen et al., 2016; Nourhani et al., 2017; Schattling et al., 2017). Physically powered nanorobots convert external energy inputs (e.g., magnetic, ultrasound, or light fields) into translational motion based on engine geometry and material designs (Garcia-Gradilla et al., 2013; Dai et al., 2016; Bi et al., 2018; Pal et al., 2018).

The ability of micro/nanorobots to perform different task has been demonstrated at the laboratory scale, reporting their use for diverse proof of concept applications, including targeted

cargo delivery (Solovev et al., 2010; Srivastava et al., 2018), fluid mixing (Orozco et al., 2013; Singh et al., 2015) and physical manipulation of micro objects (Cappelleri et al., 2014; Schuerle et al., 2017). The clinical aspirations of medical micro/nanorobots are still beyond the current capabilities of nanotechnology and bioengineering. Nevertheless, recent engineering breakthroughs have led to the successful *in vivo* operation of medical micro/nanorobots, illustrating initial proofs of concept for biopsy, delivery, healing and retention, as represented by the scheme in **Figure 1A.** While promising, these technological innovations are still challenging to translate into actual clinical therapies due to the safety concerns and the complexity of operating inside the human body.

This review focuses on the recent progress in the *in vivo* usage of micro/nanorobotics and on the efforts to commercialize and translate laboratory results into clinical applications. While there are several micro/nanorobot reviews addressing power and actuation principles (Sánchez et al., 2014; Teo and Pumera, 2016; Tu et al., 2017; Ren et al., 2018), fabrication procedures (Lin et al., 2015; Wang and Pumera, 2015; Jurado-Sánchez et al., 2017), and applications (Guix et al., 2014; Peng et al., 2017; Kim et al., 2018; Luo et al., 2018; Safdar et al., 2018), none of these reviews have addressed the crucial emerging clinical translations and potential commercial uses. We envision medical micro/nanorobotics as the frontier in treatment and diagnosis, potentially entailing benefits to human health by opening new therapies that are otherwise impossible to achieve.

In vivo MICRO/NANOROBOTIC APPLICATIONS

The applications of micro/nanorobots for medical purposes in animal models are still limited compared to the large number of *in vitro* proofs of concept. However, the increase in the number of cumulative *in vivo* micro/nanorobotic publications (**Figure 1B**) and the high impact factor of the journals in which they are published (**Figure 1C**), both attest to the advancement in medical applications for micro/nanorobots, and to the encouraging level of interest within the scientific community (based on reviewed articles summarized in **Table 1**). Although there are multiple methodologies to power micro/nanorobots, we identify that only biohybrid (20%), chemical (30%), and physical systems (50%) have been used within inside living animals. The *in vivo* studies are detailed in the following sections based on their clinical aspiration or area of study.

Delivery of Therapeutic and Imaging Agents for Cancer Therapy

Medical micro/nanorobotics hold great potential to deliver drugs with a higher degree of precision and speed when compared to passive diffusion methods. In general, this direction has been the motivation for *in vivo* applications (Erkoc et al., 2018). Thus, targeted delivery has benefited by recent *in vitro* developments in micro/nanorobotic chemotaxis (Peng et al., 2015; Shao et al., 2017) and material research using stimuli triggered drug release (Genchi et al., 2017; Rao et al., 2018). For example, magnetically guided nanorobots were used toward the delivery of fluorouracil medication for reducing tumor growth in a mice model. The released drug was externally triggered, allowing the nanorobotic platform to distribute a high amount of the therapeutic agent in a localized area of the tumor (Hoop et al., 2018).

Biohybrid nanorobots have also been used for targeted delivery of payloads inside living animals. *Listeria monocytogenes* has been used to deliver attached nanoparticles containing a payload of genes and proteins within a mouse. These payloads were used to monitor gene expression through differences in the luminescence produced within the different mouse organs (Akin et al., 2007). Magnetotactic bacterias, which naturally produce magnetic iron oxide nanoparticles, have been coupled with liposomes loaded with therapeutic payloads *in vitro*, as shown in **Figure 2A** (Taherkhani et al., 2014). More recently, these modified bacteria were guided using an external magnetic field to deliver the drug-loaded liposomes *in vivo* to a mouse tumor site (**Figure 2B**) (Felfoul et al., 2016).

The use of fully bio-engineered biohybrid micro/nanorobots without any inorganic/artificial components for carrying and transporting the therapeutic cargo has become possible through recent advances in synthetic biology. The use of genetically engineered bacteria, *S. Typhimurium*, have been reported to locally produce a therapeutic payload (α-emolysin E, a pore-forming toxin) and to trigger the payload's release upon bacterial lysis. A small number of bacteria survive the lysis event, which allows for a continuous and cyclical delivery process controlled by an activator/repressor, synchronized lysis circuit (Din et al., 2016).

Transport and Release of Cells

Micro/nanorobots have also been used toward delivering stem cells to a damaged location for tissue restoration. Magnetically guided microrobots have been reported toward carrying and delivering live cells to targeted areas in the body. *In vivo* transport and proliferation of *HeLa* cells in a nude mouse model demonstrated that the carried cells could be spontaneously released from the microrobot to the surrounding tissues and proliferate as shown in **Figure 3** (Li et al., 2018). These applications demonstrate that micro/nanorobots could serve as platforms for regenerative medicine and cell-based therapy, potentially proving to be especially useful in the later stages of life, when organs and systems start to fail. Moreover, there are still plenty of other promising *in vitro* applications to be developed for biohybrid microrobots, such as using a helical structure to guide a sperm toward an egg, for assisted fertilization (Magdanz et al., 2017).

Retention of Payloads in the Gastrointestinal Tract

The aim of medical micro/nanorobotics is not only to deliver therapeutic payloads to a specific site but also, to retain the payloads within site as long as possible. In this direction, Wang's group has proposed the use of biodegradable zinc and magnesium powered microrobots that utilize gastric and intestinal fluids as fuels to promote cargo retention in the

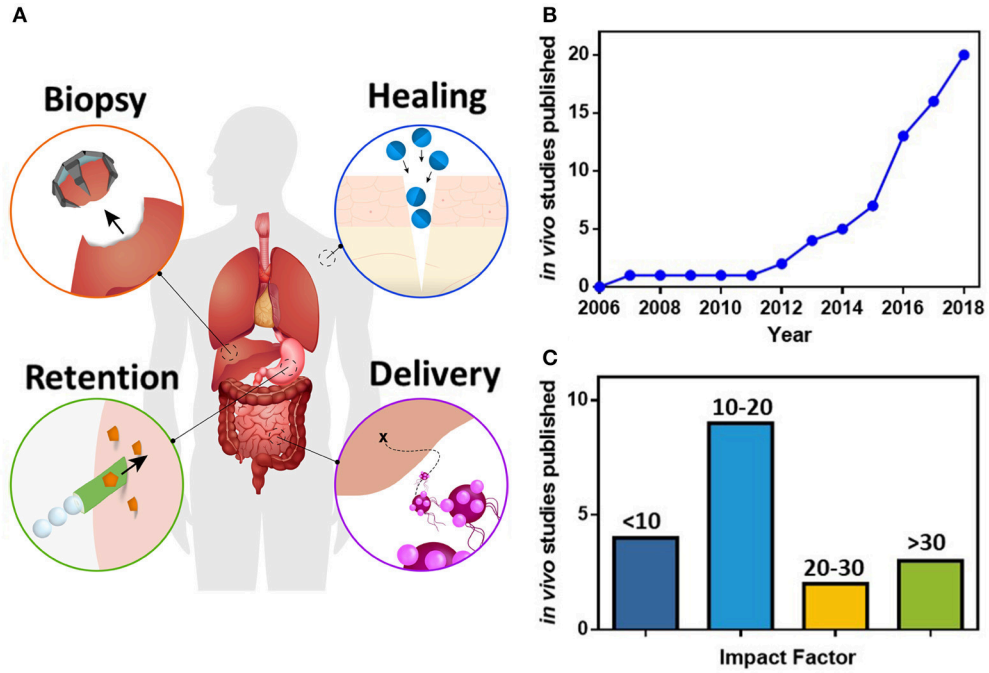

FIGURE 1 | (A) Scheme of medical perspectives in micro/nanorobotics for *in vivo* human applications, including machines capable of performing biopsy (Gultepe et al., 2012), healing wounds (He et al., 2016), enhanced retention in tissues (Gao et al., 2015), and deliver their cargoes to specific destinations (Felfoul et al., 2016). Analysis of the published articles (see **Table 1**), including micro/nanorobots for *in vivo* applications, showing **(B)** the cumulative number of published articles, and **(C)** the impact factor of those publications.

stomach and intestinal tissues (Gao et al., 2015; Esteban-Fernández de Ávila et al., 2017a). This retention platforms have been applied toward pH neutralization of the gastric fluid (Li et al., 2017a) and for the treatment of a bacterial infection (*Helicobacter pylori*) in the stomach (Esteban-Fernández de Ávila et al., 2017b). This retention of the microrobot could be explained by direct piercing the surrounding tissue, or by an improvement in mass transport and nucleation due to the gas bubbles generated as means of locomotion for the microrobot, in an effect similar to effervescence.

Magnesium-based microrobots have also been designed with built-in delay activation, by using polymeric enteric coatings that activate the microrobot motion based on their thickness or environmental pH conditions. The polymeric coating only dissolves at neutral pH conditions found in the intestinal fluids resulting in localized ignition of the microrobot. The thickness of the coating allows to selectively localize the retention of the microrobots in different target sections of the gastrointestinal tract (the duodenum, jejunum, and ileum) (**Figure 4**) (Li et al., 2016). More recently, microrobots were integrated/loaded inside a pill matrix toward streamlining their administration with existing pharmaceutical protocols (Karshalev et al., 2018). In general, the use of magnesium-based microrobots could benefit medical applications where autonomy and simplicity are desired. However, these chemically-propelled microrobots might be limited to operate in large-scale areas, such as the digestive system, as their depletion of propellant through bubble generation results in a short lifetime that could create unexpected complications in smaller capillaries.

Wound Healing

The human body has diverse mechanisms and biological triggers for identifying wounds and repairing them. Nevertheless, these biological mechanisms can fall short when the wound is bleeding profusely, or there are not enough localized coagulant agents in the target region (Das and Baker, 2016). In this direction, medical micro/nanorobotics aim to simulate such systems by using active delivery toward fast and effective wound healing. Chemically-propelled calcium carbonate-based microrobots have been reported for delivering thrombin to halt the bleeding of wounds in the vasculature of mouse and pig models. The distribution mechanism relied on a combination of lateral propulsion, buoyant rise and convection (Baylis et al., 2015). Another reported approach consisted in the use of locomotive microrobots toward laser-based wound sealing. The high temperature generated by the laser-microrobot interaction produced localized collagen denaturation and melting, whereby a subsequent temperature decrease allowed condensation and wound closure (He et al., 2016).

Biopsy

Other *in vivo* applications with potential implications in medicine are the ones targeting biopsy/surgery. Diverse *in vitro* platforms have been proposed toward precision micro/nanoscale surgery but still have not been translated to *in vivo* models

TABLE 1 | *In-vivo* applications of micro/nanorobots divided into the power source, robotic design, animal model, and function.

Power source	Robotic design (dimension)	*In vivo* animal model (location)	Function	References
Biohybrid	*L. monocytogenes* streptavidin-polystyreneNP (1 μm)	Mouse (intra-peritoneal cavity)	Targeted payload delivery for monitoring gene expression using fluorescence imaging	Akin et al., 2007
	S. typhimurium funtionalzied μ-particle (3 μm)	Mouse (circulatory system, thigh, tail vein).	Imaging of tumor site using fluorescence imaging	Park et al., 2013
	S. Typhimurium Engineered bacteria (1.2 μm)	Mouse(colon)	Controlled delivery and localized production of α-emolysin E (pore-forming toxin) against tumor	Din et al., 2016
	Magnetococcus marinu/MC-1 receptor (2 μm)	Mouse (peritumoral region)	Targeting hypoxic tumor regions	Felfoul et al., 2016
Chemical	Zn microrocket (15 μm)	Mouse (stomach)	Retention of cargo in the stomach	Gao et al., 2015
	$CaCO_3$ Janus NP (10 μm)	Mouse (tail, liver) Pig (femoral artery)	Stop bleeding	Baylis et al., 2015
	Mg microrocket/enteric coating (15 μm)	Mouse (gastrointestinal tract)	Targeted retention of cargo in different parts of the gastrointestinal tract	Li et al., 2016
	Mg /Au /enteric coating Janus (20 μm)	Mouse (stomach)	Temporal neutralization of gastric acid and triggered payload release	Li et al., 2017b
	Mg TiO_2 Janus NP (20 μm)	Mouse (stomach)	Pill to deliver large amount of microrobots	Karshalev et al., 2018
	Mg/TiO_2/Chitosan Janus NP (20 μm)	Mouse (stomach)	*H. pylori* infection targeted therapy	Esteban-Fernández de Ávila et al., 2017b
Physical	Polymeric griper (300 μm)	Pig (biliary tree, bile duct)	Tissue biopsy	Gultepe et al., 2012
	Magnetic microrod (300 μm diameter)	Rabbit (eye)	Intraocular navigation	Ullrich et al., 2013; Pokki et al., 2016
	Ni Magnetic rod (300 nm x 2 μm)	Mouse (femoral vessels, brain)	Acceleration of thrombolysis	Cheng et al., 2014 Hu et al., 2018
	Helical structures (20 μm)	Mouse (intra-peritoneal cavity)	Controlled navigation and localization using optical imaging	Servant et al., 2015
	PEM–magnetite–gold Janus NP 5 μm	Mouse (skin)	Infrared laser-assisted tissue welding	He et al., 2016
	Spirulina microalgae magnetized 100 nm Fe_3O_4	Mouse (subcutaneous tissue, intraperitoneal cavity, stomach)	Controlled navigation and localization using optical and magnetic imaging	Yan et al., 2017
	FePd nanorod (300 nm x 4 μm)	Mouse (subcutaneous tissue)	Targeted delivery and triggered activation of fluorouracil	Hoop et al., 2018
	Burr-like porous sphere (50 μm)	Mouse (left dorsum)	Transport and delivery of cell cultures	Li et al., 2018

(Nelson et al., 2010; Xi et al., 2013; Kwan et al., 2015; Soto et al., 2015). Nonetheless, micro/nanorobotics could serve as a complement to current minimally surgical procedures, allowing unprecedented access into diseased tissues for biopsy analysis or therapeutic applications.

Microrobots with star-shaped grippers, which can reach narrow conduits in the body, have been used to excise tissue samples from a pig bile duct (Gultepe et al., 2012). Additionally, an initial proof of concept based on magnetic microrobots has demonstrated controlled navigation inside the eye of a living rabbit. Although this method has not been demonstrated directly for a surgical procedure, a magnetic coil system enabled the precise navigation of the untethered magnetic microrobots in the posterior eye section (Ullrich et al., 2013; Pokki et al., 2016). Ultimately, biopsy applications are fertile ground for further micro/nanorobotics research as the success of these applications depends on the ability of the robot to physically manipulate its environment and on the ability of the robot's controller to retrieve the robot. Both these problems have been studied much less extensively than propulsion.

Local Mixing for Enhanced Thrombolysis

The potential modes through which a micro/nanorobot can physically manipulate its environment are not limited to merely excising tissue. Another recent trend in *in vivo* micro/nanorobots applications is the use of mixing effects to promote blood clot dissolution. In this case, magnetically actuated nanorobots loaded with tissue plasminogen activator were intravenously injected.

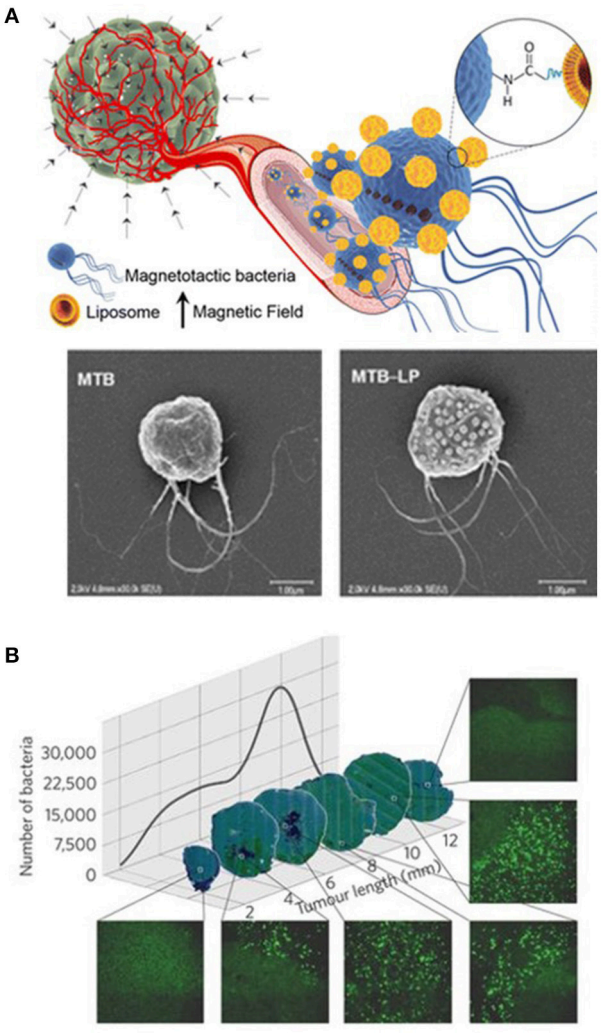

FIGURE 2 | Nanorobots for delivery usage. **(A)** Schematic illustration and SEM of biohybrid nanorobot including a magnetotactic bacteria loaded with liposomes. Reprinted with permission from Taherkhani et al. (2014). Copyright 2014 American Chemical Society. **(B)** Fluorescent images of transverse tumor sections illustrating the biohybrid robot distribution and population inside the tumor. Reprinted with permission from Felfoul et al. (2016). Copyright 2016 Springer Nature.

The vasculature flow drove the nanorobots to the blood clot. Once at their destination, the nanorobots were rotated by an external magnetic field. Their rotation generated local flow mixing which induces an increased interaction of the tissue plasminogen activator molecule with the blood clot interface, resulting in acceleration of thrombolysis (Cheng et al., 2014). More recently, it was demonstrated that nanorobots can target blood clots in mice's brains (Hu et al., 2018).

Real-Time Imaging

From the reviewed articles, none of the chemically propelled micro/nanorobots are supported with real-time imaging, which introduces a severe limitation for understanding their therapeutic effect. 75% of biohybrid robots are supported with real-time imaging, but fluorescence is the only technique used (Akin et al., 2007; Park et al., 2013; Din et al., 2016). Physical robots are supported with the most diverse type of imaging techniques, but only 60% of articles are supported with real-time imaging. Represented techniques include the use of endoscopy and X-rays to detect microgrippers inside the gastrointestinal tract (Gultepe et al., 2012), use of optical camera to visualize movement inside the eye (Ullrich et al., 2013; Pokki et al., 2016), and fluorescence imaging techniques to track the position of magnetically actuated helical microrobots inside the peritoneal cavity of a mouse (Servant et al., 2015) or subcutaneously (Li et al., 2018). Moreover, a dual imaging approach was used to detect biodegradable magnetic microhelix nanorobots in mice. Fluorescence imaging was used to detect the nanorobot's position inside the subcutaneous tissue, and the intraperitoneal cavity of a mouse and magnetic resonance-based imaging was used to detect the nanorobot's position inside the mouse's stomach, as shown in **Figure 5** (Yan et al., 2017). Future research such address this important parameter, a key aspect for medical micro/nanorobotic use in clinical uses will rely on individual or population tracking, with consideration of tissue background signal (Medina-Sánchez and Schmidt, 2017; Vilela et al., 2018; Wang et al., 2018a).

Toxicity

Most of the review micro/nanorobot studies used in animal models, provide only qualitative analyses of safety and toxicology based on histological assays. Achieving accurate targeted delivery requires an understanding of how foreign materials accumulate throughout the body and how to minimize the distribution of the administered micro/nanorobots to non-target tissue, establishing their specific effect on health. Each micro/nanorobot design has different safety concerns. Biohybrids could infiltrate and proliferate in undesired ways. Chemically propelled micro/nanorobots might change the local chemical environment which could have a significant effect on the microbiome of the gastrointestinal tract. For physical micro/nanorobots, most of the materials themselves pose a danger, as they are rigid and non-degradable. Despite these differences, researchers could report more relevant parameters to address the toxicity even at this early stage. Potential parameters to be considered include: the number of motors used for treatment (number or grams) indicated the escalation of units/dosage (limit for toxicity and inefficacy), but most importantly the distribution and toxicity of the nanorobot's constitutive materials within the living system.

Administration and Retrieval

The administration and retrieval strategy of nanorobots is not discussed in length in the reviewed articles, which present as the most common administration method injection (60%), followed by oral administration (30%), catheter (5%), and topical administration (5%). Regarding the retrieval strategy for micro/nanorobots, both biohybrid and chemical systems were considered to be biodegradable by the authors. Although, in some cases, the fate of their synthetic components was not explicitly stated or demonstrated. For physically powered robots, in most cases, the fate of the nanorobot structure was not clearly stated,

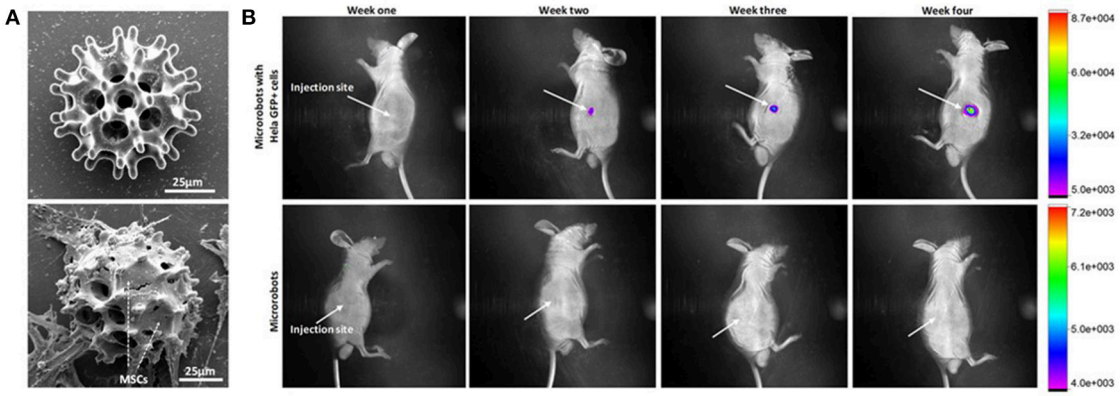

FIGURE 3 | Use of microrobots for cell transport and proliferation of cells. **(A)** SEM images of magnetically actuated nanorobot before and after cell seeding. **(B)** *In vivo* fluorescence imaging of HeLa GFP with cells loaded nanorobots illustrating the migration of cells after injection into the right dorsum of the nude mice (Li et al., 2018). Copyright 2018 The American Association for the Advancement of Science.

only three articles provide a retrieval mechanism and one other is biodegradable. One plausible solution for retrieval consists of the use of a magnetic catheter to enable both the deployment and retrieval of microrobots in clinical practice (Iacovacci et al., 2018). We note that recent *in vitro* research efforts have described micro/nanorobot systems that are fully biodegradable (Peters et al., 2015; Chen et al., 2016; Yan et al., 2017; Bozuyuk et al., 2018; Wang et al., 2018c).

MICRO/NANOROBOTS: STEPS TOWARD CLINICAL TRANSLATION

Basic science research is fundamental for creating both breakthrough medical advances and economic growth. Nevertheless, most basic science research will not achieve clinical translation. This challenge arises, in part, from the prolonged time required to go from basic research to clinical trials. Moreover, the conclusion of most trials indicates that most of the new technologies are less effective or more harmful than the current standards of care. This is a lesson to be learned in the micro/nanorobotic community. It is essential to identify strengths/weaknesses and remain objective about their relevance for later development.

The potential of the current generation of micro/nanorobotics is based on their translational motion and mixing capabilities. The idea of "smart" nanorobots that explore their surroundings and respond to environmental stimuli, commonly described in the field, is still beyond the current capabilities of micro/nanorobotics. Crucial questions of environmental manipulation, micro/nanorobot retrieval, and toxicology still need to be addressed. Indeed, we are far away from a killer app, but this should not be considered uncommon or discouraging to current researchers in the field. As previously mentioned, medical technologies have a significant time delay from lab to the clinic/commercialization, in many cases, taking several decades.

Nevertheless, considerable progress has been achieved in the field. It took less than a decade to go from the initial proof of concept using chemically propelled nanowires in peroxide (Paxton et al., 2004) to the recent explosion of *in vivo* studies over the past 3 years. In order to reach the inflection point toward clinical translation, it is necessary first to standardize the methodologies and reproducibility of micro/nanorobotics research and to actively consider their commercialization outlook. Scientists without clear monetary value proposition rarely see their discoveries materialize.

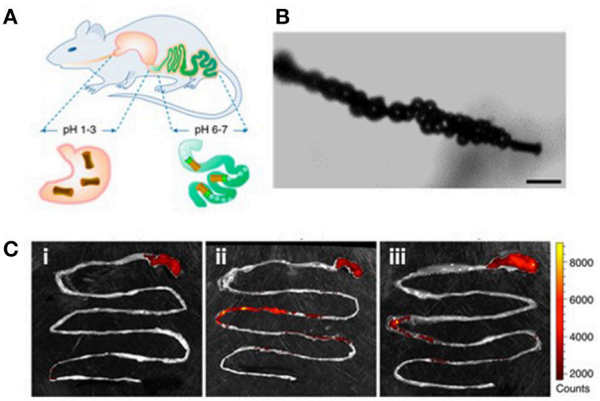

FIGURE 4 | Use of microrobots for enhanced retention of payloads in the gastrointestinal tract. **(A)** Schematic illustration of *in vivo* operation of microrobots in mouse model. **(B)** Micrograph illustrating the bubble generation at the end of the microorobot responsible for locomotion. Scale bar: 20 μm. **(C)** Fluorescent images illustrating the gastrointestinal track retention of the dye Rhodamine 6G delivered by the chemically propelled microrobot (i: control, ii: after 6 h, and iii: after 12 h of administration. Reprinted with permission from Li et al. (2016). Copyright 2016 American Chemical Society.

Reproducibility and Standardization

Commonly, the performance of micro/nanorobotic medical technology *in vitro* is reported by measurements of movement, such as their velocity and directionality, or on indirect methods such as measuring the mean squared displacement of tracer

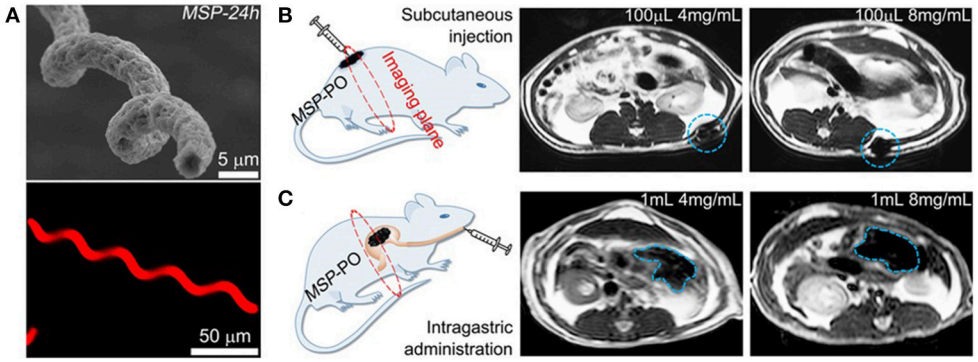

FIGURE 5 | *In vivo* imaging of magnetically propelled microrobot. **(A)** Scanning electron microscopy (SEM) (**top**) and fluorescence images (**bottom**) of the helical structured microrobot. Schematic of the target *in vivo* area and magnetic resonance imaging of microrobots inside rats. Illustrating different microrobot concentrations at the **(B)** subcutaneous tissues and **(C)** inside the mouse stomach. Reprinted with permission from Yan et al. (2017). Copyright 2017 The American Association for the Advancement of Science.

particles or comparing a clinical outcome (e.g., the percentage of dead cancer cells) vs. passive diffusion. Although these methods serve to validate early proof-of-concept studies, they are not good predictors for successful clinical translation.

The variability between currently used *in vivo* micro/nanorobotic platforms makes it almost impossible to provide a comparative or quantifiable analysis of their efficiency vs. current standards of care. Moreover, there cannot be a clear definition of clinical efficiency when there is no minimum standardized information for reporting micro/nanorobotic research. Therefore, we need clear information standards in reporting experimental methodology, characterization, and results, which will be key for the successful translation of multidisciplinary research into improved health outcomes.

Some journals have implemented reporting summaries as a requisite for submission (Faria et al., 2018), which has shown to increase the quality of reporting for preclinical biomedical research (Han et al., 2017). In general, an experimental finding can be considered to have a stronger case for translation when the experiments supporting it have been carried out using blinding and randomization, and when, most importantly, those findings have been replicated in other laboratories apart from the inventors' group. Currently, no study presented in this review covers these standards. In this direction, here we suggest guidelines (measures that should be reported in parenthesis) for reporting micro/nanorobotic research that should allow better comparisons, both qualitative and quantitative, of micro/nanorobot performance in addition to already established checklists for safety and toxicology. The goal of the checklist is not to propose research trends or criticize current research, as new technologies start without clear standards. Instead, the homogeneity of experimental reporting can facilitate comparison, improve experimental design, and increase reproducibility between various micro/nanorobotic platforms.

The justification of the power source used to provide energy/movement to the micro/nanorobot could help to establish the unique advantage of each method. Material characterization of the micro/nanorobot, including their size distribution (length units), average lifetime of propulsion (time unit), surface charge (zeta potential), and storage lifetime (days), can help to plan into eventual fabrication and transport in medical uses. Moreover, is important to quantify the performance of the nanorobotic platform by evaluating the therapeutic effect based on experiment dependent parameters. For drug delivery applications, an important parameter is the administered and delivered dose (% by mass). For retention studies the number of nanomotors localized in the target region (% of administered population). For biopsy applications, the micro/nanorobot force applied to a specific area of tissue (Pascal). Moreover, the micro/nanorobot therapeutic effect should be compared against the state-of-the-art treatment, not only passive diffusion. Finally, parameters covered through the review includes, imaging (real time localization), toxicity (folllowing establish guidelines), Administration route (Target Area and method of insertion), and retrival region (% of administered population) could streamline their tranlatio into exisitng therapies.

Intellectual Property and Commercialization

Clinical efficacy alone is not enough to warrant translation to market. The transition of new technologies from lab to market requires extensive research and development costs, overcoming regulatory barriers, and most importantly, having the right commercialization potential. The potential customer for micro/nanorobotics' technology is not the general population or the physicians, but rather pharmaceutical companies and insurance providers. Therefore, micro/nanorobotics research should consider their commercialization opportunities from the research stages, in order to provide tangible therapies that reduce cost, increase throughput efficiency and productivity.

Minimizing the investment risk can be achieved by protecting the intellectual property of the new technological developments (which is one of the most valuable assets for high-tech companies) and establishing a clear business model with identifiable revenue streams. New technological developments

are commonly initiated using patents filed by research groups through their university system, which are later licensed to emerging start-up companies or larger corporations. The prohibitive cost of prototyping and clinical trials is initially financed by non-dilute financing, which includes government research and industry grants, and at later stages by investment from venture capital and industry partnerships.

Tracking the filing of relevant patents, and the formation of relevant startups, provides useful insight into the progress made in identifying potential markets, competitors and consumer needs. **Figure 6** traces the accumulated United States applied and granted patents in nanorobotics, while also separating them into the categories of fabrication, actuation, imaging, and application. The patent filing data were collected manually, as keyword searches do not accurately capture the state of nanorobotic technology due to the multiple names used to refer to nanorobots in the literature (micro/nanobot, micro/nanorobot, micro/nanorocket, micro/nanoengines, micro/nanomotor, micro/nano-swimmer, active colloid). Instead, the search was conducted by reviewing the output of the most prolific nanomotor research groups in the field that have published results in animal models and by reviewing relevant Google patents.

The first patents published consisted of the fabrication methods commonly used for parallel mass fabrication using template platforms, consisting of nanorod structures (Stonas et al., 2005; Natan et al., 2007; Fan et al., 2017b; Odell et al., 2018), microcoils (Schmidt et al., 2010; Jeong et al., 2018), tubular structures (Yao et al., 2015; Wang et al., 2016a), emulsions (Percec et al., 2017), biohybrids (Schmidt and Leibniz-Institut Fuer Festkoerper-Und Werkstofffor Schung, 2017), and colloid chains (Duan et al., 2017).

The next wave of patents consists of tracking/imaging nanorobots using magnetic (Martel et al., 2015; Muntwyler et al., 2017; Odell et al., 2017), optical (Benaron et al., 2008), and ultrasound methods (Mattrey et al., 2017). Followed by methods to power micro/nanorobots using magnetic (Solomon and Solomon Res LLC, 2011; Vollmers et al., 2013; Abbott et al., 2014; Fischer et al., 2014; Mahoney et al., 2014; Odell et al., 2016; Sitti et al., 2016; Tasci et al., 2016; Wang, 2017; Weinberg et al., 2017), ultrasound (Wang and Zhang, 2017; Wang et al., 2017), chemical (Paxton et al., 2009; Sen et al., 2017; Tang et al., 2017), and biohybrid propulsion mechanisms (Magdanz et al., 2018; Martel et al., 2018).

The final, most recent wave, has focused on applications for these micro/nanorobots, including for intracellular delivery by nanospearing (Cai et al., 2011) exploration of subterranean geophysical formations and oil retrieval (Kamal et al., 2015), nanomotor-based patterning of surface microstructures (Wang et al., 2016b), transporting, positioning and assembling nanorobots using electric twisers (Chien et al., 2017; Fan et al., 2017a), capturing and isolating of target biomolecules and living organisms using microrobots (Wang et al., 2018b).

There are only a few active companies working toward the commercialization of nanorobots for use in medical applications. Most notably, Nelson's group has spun off two companies. The first was Aeon Scientific, based on the electromagnetic manipulations systems developed to guide magnetic motors. However, they have recently shifted their focus to developing new manipulation systems for catheters. Indeed, it is not surprising that the technology developed around micro/nanorobots could have applications that were never envisioned at the beginning.

The second, Swiss Magnetibox formed in 2014 is based on wireless tools for actuating and imaging micro/nanomachines using magnetic fields. They primarily sell microscopy equipment coupled with magnetic actuation systems and rod shape microrobots toward expanding basic science in micro/nano robotics research. Although these systems are not specifically designed for *in vivo* use, they provide the necessary tools to test proof of concept applications (Schuerle et al., 2017).

Finally, Weingberg medical physics has developed an image-guided therapy for targeted delivery of magnetic micro/nanorobots that uses ultra-fast MRI to generate magnetic fields for imaging and manipulation of the magnetic nanorobots. They have demonstrated diverse *in vitro* applications using the mechanical force of the nanorobots to dislodge bacteria biofilm using rotating nanorobots (Mair et al., 2017) and drilling into mice's brain post-mortem (Jafari et al., 2019).

The mass fabrication of nanorobotics is one of the first challenges to be addressed toward tangible translation to market.

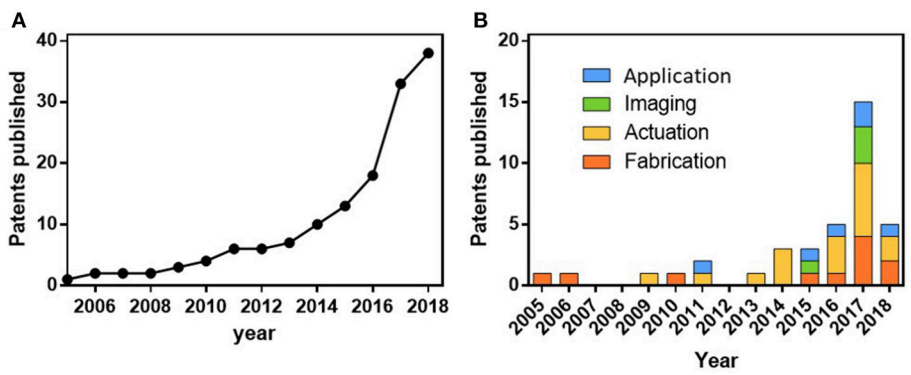

FIGURE 6 | Overview of micro/nanorobotics intellectual property, as described in section Intellectual Property and Commercialization. **(A)** Accumulative published patents in the last years. **(B)** Graph illustrating patents considering the application per year.

Reproducibility and availability of templates will be significant hurdles that must be solved with traditional micro/nanorobotic fabrication techniques. New methods based on 3D printing and two-photon lithography could allow for complex designs such as microhelices or cell carriers. Although, the cost and slow production throughput of these methods may limit the use of such intricate designs. Moreover, new methods of characterization and manipulation of individual nanorobots are necessary to ensure the quality of each batch. In this regard, nano-manipulation systems are ideal for transporting, inspecting and testing nanorobotic designs (Wang et al., 2015; Lu et al., 2017; Meng et al., 2017; Zhang et al., 2018). Once these technical capabilities are well established, the reduction in the cost to reach the market will allow new companies to spring up and provide innovative medical value propositions.

A possible path toward early adoption of micro/nanorobots in the clinic could be achieved by offering micro/nanorobotic technology as a complementary tool to existing medical procedures. For example, their integration with current oral delivery platforms such as pills, allow for dose escalation by increased retention of therapeutic payloads at the mucosae wall. Although special consideration should be placed in therapies where the primary therapeutic effect is based on systemic distribution, as in this case, the dose escalation proposed by micro/nanorobotic platforms is not desired. Moreover, micro/nanorobots used for tissue biopsy and suturing veins could be integrated with a catheter and mili surgical robotics, allowing the larger robots to reach scale ranges where their size normally does not permit them to operate. The possibilities discussed here are driven by the need to improve patients' outcomes after surgical procedures including reduced hospital stay, lower chances of infection, and minimum scarring. We should note that it is not likely that micro/nanorobots will be used for preventive care or as a chronic treatment since the sustained introduction of synthetic objects into the human body might produce unknown repercussion due to possible accumulation.

FUTURE OUTLOOK

The field of medical nanorobotics has achieved considerable advances. However, several issues and challenges must be addressed before micro/nanorobots could have real-world clinical applications. The goal of the *in vivo* model is not only to evaluate the therapeutic efficiency of the platforms, but to identify the clinical risk, as evaluating off-target effects of nanorobots is as essential as evaluating efficacy. Indeed, there is a discrepancy between the aspirations of medical nanorobotics and reality, as the legacy of science fiction has set the conceptual boundaries of what to expect long before scientists could. The manufacturing of the micro/nanostructure engines must be optimized, with special consideration for material biocompatibility and degradation, to address *in vivo* safety concerns.

Furthermore, proper standards should be established to clarify the advantages of micro/nanorobot therapies over traditional methods which already fulfill FDA standards. Nonetheless, micro/nanorobotics might potentially improve medical diagnosis and treatment. We should also consider that the designs and aspirations of a small group of scientist and engineers could soon affect the lives of millions of people directly and profoundly, therefore it is essential to consider the economic, social, and ethical implications of the use of medical nanorobotics. These implications are likely to be on par with those of the most significant technological revolutions.

AUTHOR CONTRIBUTIONS

FS and RC wrote and revised the manuscript and approved it for publication.

ACKNOWLEDGMENTS

FS acknowledges the funding from the UC MEXUS-CONACYT program. RC acknowledges his funding from the Cockrell School of Engineering at The University of Texas at Austin.

REFERENCES

Abbott, J. J., Kratochvil, B., Kummer, M. P., and Nelson, B., Eidgenoessische Technische Hochschule Zurich (2014). *Magnetic Manipulation and Navigation System for a Magnetic Element*. U.S. Patent 8, 830,648.

Akin, D., Sturgis, J., Ragheb, K., Sherman, D., Burkholder, K., Robinson, J. P., et al. (2007). Bacteria-mediated delivery of nanoparticles and cargo into cells. *Nat. Nanotech*. 2, 441–449. doi: 10.1038/nnano.2007.149

Baylis, J. R., Yeon, J. H., Thomson, M. H., Kazerooni, A., Wang, X., John, A. E. S., et al. (2015). Self-propelled particles that transport cargo through flowing blood and halt hemorrhage. *Sci. Adv.* 1:e1500379. doi: 10.1126/sciadv.1500379

Benaron, D. A., and Parachikov, I. H., Spectros Corp (2008). *Systems and Methods for the Detection and Analysis of in vivo Circulating Cells, Entities, and Nanobots*. U.S. Patent Application 11/729,395.

Bente, K., Codutti, A., Bachmann, F., and Faivre, D. (2018). Biohybrid and bioinspired magnetic microswimmers. *Small* 31:e1704374. doi: 10.1002/smll.201704374

Bi, C., Guix, M., Johnson, B., Jing, W., and Cappelleri, D. (2018). Design of microscale magnetic tumbling robots for locomotion in multiple environments and complex terrains. *Micromachines* 9:68. doi: 10.3390/mi9020068

Bozuyuk, U., Yasa, O., Yasa, I. C., Ceylan, H., Kizilel, S., and Sitti, M. (2018). Light-triggered drug release from 3D-printed magnetic chitosan microswimmers. *ACS Nano* 12, 9617–9625. doi: 10.1021/acsnano.8b05997

Cai, D., Carnahan, D. L., and NanoLab Inc (2011). *Nanospearing for Molecular Transportation Into Cells*. U. S. Patent 7, 935, 517.

Cappelleri, D., Efthymiou, D., Goswami, A., Vitoroulis, N., and Zavlanos, M. (2014). Towards mobile microrobot swarms for additive micromanufacturing. *Int. J. Adv. Robot Syst.* 11:150. doi: 10.5772/58985

Chen, C., Karshalev, E., Li, J., Soto, F., Castillo, R., Campos, I., et al. (2016). Transient micromotors that disappear when no longer needed. *ACS Nano* 10, 10389–10396. doi: 10.1021/acsnano.6b06256

Cheng, R., Huang, W., Huang, L., Yang, B., Mao, L., Jin, K., et al. (2014). Acceleration of tissue plasminogen activator-mediated thrombolysis by magnetically powered nanomotors. *ACS Nano* 8, 7746–7754. doi: 10.1021/nn5029955

Chien, C. L., Fan, D., Cammarata, R., and Johns Hopkins University (2017). *System and Method for Precision Transport, Positioning, and Assembling of Longitudinal Nano-Structures*. U.S. Patent 9,718,683.

Dai, B., Wang, J., Xiong, Z., Zhan, X., Dai, W., Li, C.-C., et al. (2016). Programmable artificial phototactic microswimmer. *Nat. Nanotech.* 11, 1087–1092. doi: 10.1038/nnano.2016.187

Das, S., and Baker, A. B. (2016). Biomaterials and Nanotherapeutics for Enhancing Skin Wound Healing. *Front. Bioeng. Biotechnol.* 4. doi: 10.3389/fbioe.2016.00082

Din, M. O., Danino, T., Prindle, A., Skalak, M., Selimkhanov, J., Allen, K., et al. (2016). Synchronized cycles of bacterial lysis for *in vivo* delivery. *Nature* 536, 81–85. doi: 10.1038/nature18930

Duan, H., Zhou, J., Lam, Y. C., Lim, C. Y., Xiong, Q., and Nanyang Technological University of Singapore (2017). *Method for Preparing a Magnetic Chain Structure*. U.S. Patent Application 15/529,748 Application.

Erkoc, P., Yasa, I. C., Ceylan, H., Yasa, O., Alapan, Y., and Sitti, M. (2018). Mobile microrobots for active therapeutic delivery. *Adv. Ther.* 1800064. doi: 10.1002/adtp.201800064

Esteban-Fernández de Ávila, B., Angsantikul, P., Li, J., Gao, W., Zhang, L., and Wang, J. (2017a). Micromotors go *in vivo*: from test tubes to live animals. *Adv. Funct. Mater.* 28:1705640. doi: 10.1002/adfm.201705640

Esteban-Fernández de Ávila, B., Angsantikul, P., Li, J., Lopez-Ramirez, M. A., Ramírez-Herrera, D. E., Thamphiwatana, S., et al. (2017b). Micromotor-enabled active drug delivery for *in vivo* treatment of stomach infection. *Nat. Commun.* 8:272. doi: 10.1038/s41467-017-00309-w

Fan, D., Kim, K., Guo, J., and University of Texas System (2017b). *Electrode Design and Low-cost Fabrication Method for Assembling and Actuation of Miniature Motors With Ultrahigh and Uniform Speed*. U.S. Patent Application 15/509,782.

Fan, D., Xiaobin, X. U., and University of Texas System (2017a). *Plasmonic-Magnetic Bifunctional Nanotubes for Biological Applications*. U.S. Patent 9,638,639.

Faria, M., Björnmalm, M., Thurecht, K. J., Kent, S. J., Parton, R. G., Kavallaris, M., et al. (2018). Minimum information reporting in bio–nano experimental literature. *Nat. Nanotech.* 13, 777–785. doi: 10.1038/s41565-018-0246-4

Felfoul, O., Mohammadi, M., Taherkhani, S., Lanauze, D. D., Xu, Y. Z., Loghin, D., et al. (2016). Magneto-aerotactic bacteria deliver drug-containing nanoliposomes to tumour hypoxic regions. *Nat. Nanotech.* 11, 941–947. doi: 10.1038/nnano.2016.137

Fischer, P., Ghosh, A., and Max-Planck-Gesellschaft zur Forderung der Wissenschaften (2014). *Magnetic Nanostructured Propellers*. U.S. Patent 8,768,501.

Gao, W., Dong, R., Thamphiwatana, S., Li, J., Gao, W., Zhang, L., et al. (2015). Artificial micromotors in the mouse's stomach: a step toward *in vivo* use of synthetic motors. *ACS Nano* 9, 117–123. doi: 10.1021/nn507097k

Garcia-Gradilla, V., Orozco, J., Sattayasamitsathit, S., Soto, F., Kuralay, F., Pourazary, A., et al. (2013). Functionalized ultrasound-propelled magnetically guided nanomotors: toward practical biomedical applications. *ACS Nano* 7, 9232–9240. doi: 10.1021/nn403851v

Genchi, G. G., Marino, A., Tapeinos, C., and Ciofani, G. (2017). Smart materials meet multifunctional biomedical devices: current and prospective implications for nanomedicine. *Front. Bioeng.Biotechnol.* 5:80. doi: 10.3389/fbioe.2017.00080

Guix, M., Mayorga-Martinez, C. C., and Merkoçi, A. (2014). Nano/micromotors in (bio)chemical science applications. *Chem. Rev.* 114, 6285–6322. doi: 10.1021/cr400273r

Gultepe, E., Randhawa, J. S., Kadam, S., Yamanaka, S., Selaru, F. M., Shin, E. J., et al. (2012). Biopsy with thermally-responsive untethered microtools. *Adv. Mat.* 25, 514–519. doi: 10.1002/adma.201203348

Han, S., Olonisakin, T. F., Pribis, J. P., Zupetic, J., Yoon, J. H., Holleran, K. M., et al. (2017). A checklist is associated with increased quality of reporting preclinical biomedical research: a systematic review. *PLoS ONE* 12:e0183591. doi: 10.1371/journal.pone.0183591

He, W., Frueh, J., Hu, N., Liu, L., Gai, M., and He, Q. (2016). Guidable thermophoretic janus micromotors containing gold nanocolorifiers for infrared laser assisted tissue welding. *Adv. Sci.* 3:1600206. doi: 10.1002/advs.201600206

Hoop, M., Ribeiro, A. S., Rösch, D., Weinand, P., Mendes, N., Mushtaq, F., et al. (2018). Mobile magnetic nanocatalysts for bioorthogonal targeted cancer therapy. *Adv. Funct. Mater.* 28:1705920. doi: 10.1002/adfm.201705920

Hu, J., Huang, S., Zhu, L., Huang, W., Zhao, Y., Jin, K., et al. (2018). Tissue plasminogen activator-porous magnetic microrods for targeted thrombolytic therapy after ischemic stroke. *ACS Appl. Mater. Interfaces* 10, 32988–32997. doi: 10.1021/acsami.8b09423

Iacovacci, V., Ricotti, L., Sinibaldi, E., Signore, G., Vistoli, F., and Menciassi, A. (2018). An intravascular magnetic catheter enables the retrieval of nanoagents from the bloodstream. *Adv. Sci.* 5:1800807. doi: 10.1002/advs.201800807

Jafari, S., Mair, L. O., Weinberg, I. N., Baker-Mckee, J., Hale, O., Watson-Daniels, J., et al. (2019). Magnetic drilling enhances intra-nasal transport of particles into rodent brain. *J. Magn. Magn. Mater.* 469, 302–305. doi: 10.1016/j.jmmm.2018.08.048

Jeong, H. H., Lee, T. C., and Fischer, P., Max-Planck-Gesellschaft zur Forderung der Wissenschaften (2018). *Method for Encapsulating a Nanostructure, Coated Nanostructure and use of a Coated Nanostructure*. U.S. Patent Application 15/562,221.

Jurado-Sánchez, B., Pacheco, M., Maria-Hormigos, R., and Escarpa, A. (2017). Perspectives on Janus Micromotors: Materials and Applications. *Appl. Mater. Today* 9, 407–418. doi: 10.1016/j.apmt.2017.09.005

Kamal, R. A., Sanni, M. L., Kanj, M. Y., and Saudi Arabian Oil Co (2015). *System, Method, and Nanorobot to Explore Subterranean Geophysical Formations*. U.S. Patent 9,063,252.

Karshalev, E., Ávila, B. E.-F. D., Beltrán-Gastélum, M., Angsantikul, P., Tang, S., Mundaca-Uribe, R., et al. (2018). Micromotor pills as a dynamic oral delivery platform. *ACS Nano* 12:8397–8405. doi: 10.1021/acsnano.8b03760

Kim, J.-W., and Tung, S. (2015). Bio-hybrid micro/nanodevices powered by flagellar motor: challenges and strategies. *Front. Bioeng. Biotechnol.* 3:100. doi: 10.3389/fbioe.2015.00100

Kim, K., Guo, J., Liang, Z., and Fan, D. (2018). Artificial micro/nanomachines for bioapplications: biochemical delivery and diagnostic sensing. *Adv. Funct. Mater.* 28:1705867. doi: 10.1002/adfm.201705867

Kwan, J. J., Myers, R., Coviello, C. M., Graham, S. M., Shah, A. R., Stride, E., et al. (2015). Ultrasound-propelled nanocups for drug delivery. *Small* 11, 5305–5314. doi: 10.1002/smll.201501322

Li, J., Angsantikul, P., Liu, W., Esteban-Fernández de Ávila, B., Thamphiwatana, S., Xu, M., et al. (2017a). Micromotors spontaneously neutralize gastric acid for pH-responsive payload release. *Angew. Chem.* 56, 2156–2161. doi: 10.1002/anie.201611774

Li, J., Esteban-Fernández de Ávila, B., Gao, W., Zhang, L., and Wang, J. (2017b). Micro/nanorobots for biomedicine: delivery, surgery, sensing, and detoxification. *Sci. Robot.* 2:eaam6431. doi: 10.1126/scirobotics.aam6431

Li, J., Li, X., Luo, T., Wang, R., Liu, C., Chen, S., et al. (2018). Development of a magnetic microrobot for carrying and delivering targeted cells. *Sci. Robot.* 3:eaat8829. doi: 10.1126/scirobotics.aat8829

Li, J., Thamphiwatana, S., Liu, W., Ávila, B. E.-F. D., Angsantikul, P., Sandraz, E., et al. (2016). Enteric micromotor can selectively position and spontaneously propel in the gastrointestinal tract. *ACS Nano* 10, 9536–9542. doi: 10.1021/acsnano.6b04795

Lin, X., Wu, Z., Wu, Y., Xuan, M., and He, Q. (2015). Self-propelled micro-/nanomotors based on controlled assembled architectures. *Adv. Mater.* 28, 1060–1072. doi: 10.1002/adma.201502583

Lu, X., Soto, F., Li, J., Li, T., Liang, Y., and Wang, J. (2017). Topographical manipulation of microparticles and cells with acoustic microstreaming. *ACS Appl. Mater. Interfaces* 9, 38870–38876. doi: 10.1021/acsami.7b15237

Luo, M., Feng, Y., Wang, T., and Guan, J. (2018). Micro-/nanorobots at work in active drug delivery. *Adv. Funct. Mater.* 28:1706100. doi: 10.1002/adfm.201706100

Magdanz, V., Medina-Sánchez, M., Schwarz, L., Xu, H., Elgeti, J., and Schmidt, O. G. (2017). Spermatozoa as functional components of robotic microswimmers. *Adv. Mat.* 29:1606301. doi: 10.1002/adma.201606301

Magdanz, V., Samuel Sanchez, S., Oliver, G., and Schmidt, O. G.,(2018). *Method for the Controlled Movement of Motile Cells in Liquid or Gaseous Media*. U.S. Patent 9,883,889.

Mahoney, A. W., and Abbott, J. J., and University of Utah Research Foundation UURF (2014). *Control of Magnetically Actuated Tools in Any Position Using a Rotating Magnetic Source*. U. S. Patent 8, 803, 643.

Mair, L. O., Nacev, A., Hilaman, R., Stepanov, P. Y., Chowdhury, S., Jafari, S., et al. (2017). Biofilm disruption with rotating microrods enhances antimicrobial efficacy. *J. Magn. Mater* 427, 81–84. doi: 10.1016/j.jmmm.2016.10.100

Martel, S., Felfoul, O., and Polyvalor LP (2018). *Aggregation and Control of Magneto-Responsive Entities*. U. S. Patent 9,905,347.

Martel, S., Mathieu, J. B., Felfoul, O., Beaudoin, G., Val.-Chum Limited Partnership, and Polyvalor LP (2015) *MR-Tracking Based on Magnetic Signature Selective Excitation*. U.S. Patent 8,948,841.

Mattrey, R., Wu, Z., Olson, E., Wang, J., Gao, W., and Malone, C. D. (2017). *Method and System for in vivo Hydrogen Peroxide Detection With Ultrasound*. U.S. Patent 9,713,459.

Medina-Sánchez, M., and Schmidt, O. G. (2017). Medical microbots need better imaging and control. *Nature* 545, 406–408. doi: 10.1038/545406a

Meng, X., Zhang, H., Song, J., Fan, X., Sun, L., and Xie, H. (2017). Broad modulus range nanomechanical mapping by magnetic-drive soft probes. *Nat. Commun.* 8:1944. doi: 10.1038/s41467-017-02032-y

Muntwyler, S., Kratochvil, B., Nelson, B., Frutiger, D., Bell, D., and Baumann, J., et al. (2017). *Magnetic Navigation System with Soft Magnetic Core Electromagnets for Operation in the Non-Linear Regime*. U. S. Patent 9,681,859.

Natan, M. J., Mallouk, T. E., and Oxonica, I. N. C. (2007). *Colloidal rod Particles as Nanobar Codes*. U. S. Patent 7225082.

Nelson, B. J., Kaliakatsos, I. K., and Abbott, J. J. (2010). Microrobots for minimally invasive medicine. *Annu. Rev. Biomed. Eng.* 12, 55–85. doi: 10.1146/annurev-bioeng-010510-103409

Nourhani, A., Brown, D., Pletzer, N., and Gibbs, J. G. (2017). Engineering contactless particle-particle interactions in active microswimmers. *Adv. Mat.* 29:1703910. doi: 10.1002/adma.201703910

Odell, L., Nacev, A. N., Weinberg, I. N., and Weinberg Medical Physics Inc (2017). *Imaging of Intelligent Magnetic Particles*. U. S. Patent 9,833,170.

Odell, L., Nacev, A. N., Weinberg, I. N., and Weinberg Medical Physics, L. L. C. (2016). *Method and Apparatus for Non-Contact Axial Particle Rotation and Decoupled Particle Propulsion*. U. S. Patent Application 14/930,126.

Odell, L., Weinberg, I. N., and Weinberg Medical Physics Inc (2018). *Scalable, Massively Parallel Process for Making Micro-Scale Particles*. U. S. Patent 9, 865, 887.

Orozco, J., Cheng, G., Vilela, D., Sattayasamitsathit, S., Vazquez-Duhalt, R., Valdés-Ramírez, G., et al. (2013). Micromotor-based high-yielding fast oxidative detoxification of chemical threats. *Angew. Chem. Int. Ed.* 52, 13276–13279. doi: 10.1002/anie.201308072

Pal, M., Somalwar, N., Singh, A., Bhat, R., Eswarappa, S. M., Saini, D. K., et al. (2018). Maneuverability of magnetic nanomotors inside living cells. *Adv. Mat.* 30:1800429. doi: 10.1002/adma.201800429

Palagi, S., and Fischer, P. (2018). Bioinspired microrobots. *Nat. Rev. Mater.* 3, 113–124. doi: 10.1038/s41578-018-0016-9

Park, S. J., Park, S.-H., Cho, S., Kim, D.-M., Lee, Y., Ko, S. Y., et al. (2013). New paradigm for tumor theranostic methodology using bacteria-based microrobot. *Sci. Rep.* 3:3394. doi: 10.1038/srep03394

Paxton, W., Sen, A., Mallouk, T. E., Catchmark, J. M., and Penn State Research Foundation (2009). *Autonomous Moving Microstructures*. U. S. Patent 7, 516, 759.

Paxton, W. F., Kistler, K. C., Olmeda, C. C., Sen, A., Angelo, S. K. S., Cao, Y., et al. (2004). Catalytic nanomotors: autonomous movement of striped nanorods. *J. Amer. Chem. Soc.* 126, 13424–13431. doi: 10.1021/ja047697z

Peng, F., Tu, Y., Van Hest, J. C. M., and Wilson, D. A. (2015). Self-guided supramolecular cargo-loaded nanomotors with chemotactic behavior towards cells. *Angew. Chem. Int. Ed.* 54, 11662–11665. doi: 10.1002/anie.201504186

Peng, F., Tu, Y., and Wilson, D. A. (2017). Micro/nanomotors towards *in vivo* application: cell, tissue and biofluid. *Chem. Soc. Rev.* 46, 5289–5310. doi: 10.1039/C6CS00885B

Percec, V., Hughes, A. D., Leowanawat, P., Wilson, D. A., Wilson, C. J., and University of Pennsylvania (2017). *Amphiphilic Janus-Dendrimers*. U. S. Patent 9, 623, 046.

Peters, C., Hoop, M., Pané, S., Nelson, B. J., and Hierold, C. (2015). Degradable magnetic composites for minimally invasive interventions: device fabrication, targeted drug delivery, and cytotoxicity tests. *Adv. Mat.* 28, 533–538. doi: 10.1002/adma.201503112

Pokki, J., Ergeneman, O., Chatzipirpiridis, G., Lühmann, T., Sort, J., Pellicer, E., et al. (2016). Protective coatings for intraocular wirelessly controlled microrobots for implantation: corrosion, cell culture, and *in vivo* animal tests. *J. Biomed. Mater. Res. B Appl. Biomaterials* 105, 836–845. doi: 10.1002/jbm.b.33618

Rao, N. V., Ko, H., Lee, J., and Park, J. H. (2018). Recent progress and advances in stimuli-responsive polymers for cancer therapy. *Front. Bioeng. Biotechnol.* 6:110. doi: 10.3389/fbioe.2018.00110

Ren, L., Wang, W., and Mallouk, T. E. (2018). Two forces are better than one: combining chemical and acoustic propulsion for enhanced micromotor functionality. *Acc. Chem. Res.* 51, 1948–1956. doi: 10.1021/acs.accounts.8b00248

Ricotti, L., Trimmer, B., Feinberg, A. W., Raman, R., Parker, K. K., Bashir, R., et al. (2017). Biohybrid actuators for robotics: a review of devices actuated by living cells. *Sci. Robot.* 2:eaaq0495. doi: 10.1126/scirobotics.aaq0495

Safdar, M., Khan, S. U., and Jänis, J. (2018). Progress toward catalytic micro- and nanomotors for biomedical and environmental applications. *Adv. Mat.* 30:1703660. doi: 10.1002/adma.201703660

Sánchez, S., Soler, L., and Katuri, J. (2014). Chemically powered micro- and nanomotors. *Angew. Chem. Int. Ed.* 54, 1414–1444. doi: 10.1002/anie.201406096

Schattling, P. S., Ramos-Docampo, M. A., Salgueiriño, V., and Städler, B. (2017). Double-fueled janus swimmers with magnetotactic behavior. *ACS Nano* 11, 3973–3983. doi: 10.1021/acsnano.7b00441

Schmidt, O. G., Deneke, C., and Max-Planck-Gesellschaft zur Forderung der Wissenschaften (2010). *Method for Producing a Microcoil*. U. S. Patent 7, 707, 714.

Schmidt, O. G., Leibniz-Institut Fuer Festkoerper-Und Werkstofffor Schung, and Dresden, E. V. (2017). *Method for Mobilizing Immobilized Cells*. U. S. Patent Application 15/115, 380.

Schuerle, S., Vizcarra, I. A., Moeller, J., Sakar, M. S., Özkale, B., Lindo, A. M., et al. (2017). Robotically controlled microprey to resolve initial attack modes preceding phagocytosis. *Sci. Robot.* 2:eaah6094. doi: 10.1126/scirobotics.aah6094

Sen, A., Sengupta, S., Patra, D., Ortiz-Rivera, I., and Penn State Research Foundation (2017). *Self-Powered Enzyme Micropumps*. U. S. Patent Application 15/123,348.

Servant, A., Qiu, F., Mazza, M., Kostarelos, K., and Nelson, B. J. (2015). Controlled *in vivo* swimming of a swarm of bacteria-like microrobotic flagella. *Adv. Mat.* 27, 2981–2988. doi: 10.1002/adma.201404444

Shao, J., Xuan, M., Zhang, H., Lin, X., Wu, Z., and He, Q. (2017). Chemotaxis-guided hybrid neutrophil micromotors for targeted drug transport. *Angew. Chem. Int. Ed.* 56, 12935–12939. doi: 10.1002/anie.201706570

Singh, V. V., Soto, F., Kaufmann, K., and Wang, J. (2015). Micromotor-based energy generation. *Angew. Chem. Int. Ed.* 127, 7000–7003. doi: 10.1002/ange.201501971

Sitti, M., Diller, E., Miyashita, S., and Carnegie-Mellon University (2016). *Remotely Addressable Magnetic Composite Micro-Actuators*. U. S. Patent 9, 281, 112.

Solomon, N., and Solomon Res LLC (2011). *System, Methods and Apparatuses for Integrated Circuits for Nanorobotics*. U. S. Patent 7, 921, 384.

Solovev, A. A., Sanchez, S., Pumera, M., Mei, Y. F., and Schmidt, O. G. (2010). Nanomotors: magnetic control of tubular catalytic microbots for the transport, assembly, and delivery of micro-objects. *Adv. Funct. Mater.* 20. 2430–2435. doi: 10.1002/adfm.200902376

Soto, F., Martin, A., Ibsen, S., Vaidyanathan, M., Garcia-Gradilla, V., Levin, Y., et al. (2015). Acoustic microcannons: toward advanced microballistics. *ACS Nano* 10, 1522–1528. doi: 10.1021/acsnano.5b07080

Srivastava, S. K., Clergeaud, G., Andresen, T. L., and Boisen, A. (2018). Micromotors for drug delivery *in vivo*: the road ahead. *Adv. Drug Deliv. Rev.* doi: 10.1016/j.addr.2018.09.005. [Epub ahead of print].

Stonas, W., Dietz, L. J., Walton, I. D., Natan, M. J., Winkler, J. L., and Nanoplex Technologies Inc (2005). *Method of Manufacture of Colloidal Rod Particles as Nanobarcodes*. U. S. Patent 6,919,009.

Taherkhani, S., Mohammadi, M., Daoud, J., Martel, S., and Tabrizian, M. (2014). Covalent binding of nanoliposomes to the surface of magnetotactic bacteria for the synthesis of self-propelled therapeutic agents. *ACS Nano* 8, 5049–5060. doi: 10.1021/nn5011304

Tang, J., Dai, B., Wang, J., and University of Hong Kong HKU (2017). *Nanomotor Propulsion*. U.S. Patent Application 15/370,783.

Tasci, T. O., Neeves, K. B., Marr, D. W., and Colorado School of Mines Foundation. Inc. (2016). *Magnetic-Field Driven Colloidal Microbots, Methods for Forming and Using the Same*. U.S. Patent Application 15/069,681.

Teo, W. Z., and Pumera, M. (2016). Motion control of micro-/nanomotors. *Chem. Eur. J.* 22, 14796–14804. doi: 10.1002/chem.201602241

Tu, Y., Peng, F., and Wilson, D. A. (2017). Motion manipulation of micro- and nanomotors. *Adv. Mat.* 29:1701970. doi: 10.1002/adma.201701970

Ullrich, F., Bergeles, C., Pokki, J., Ergeneman, O., Erni, S., Chatzipirpiridis, G., et al. (2013). Mobility experiments with microrobots for minimally invasive intraocular surgery. *Invest. Ophthalmol. Vis. Sci.* 54:2853. doi: 10.1167/iovs.13-11825

Vilela, D., Cossío, U., Parmar, J., Martínez-Villacorta, A. M., Gómez-Vallejo, V., Llop, J., et al. (2018). Medical imaging for the tracking of micromotors. *ACS Nano* 12, 1220–1227. doi: 10.1021/acsnano.7b07220

Vollmers, K., Nelson, B., Kratochvil, B., Frutiger, D., and Eidgenoessische Technische Hochschule Zurich (ETHZ) (2013). Wireless resonant magnetic acutation for untethered microrobots. U. S. Patent 8,405,256.

Wang, B., Zhang, Y., and Zhang, L. (2018a). Recent progress on micro- and nano-robots: towards *in vivo* tracking and localization. *Quant Imaging Med Surg.* 8, 461–479. doi: 10.21037/qims.2018.06.07

Wang, H., Huang, Q., Shi, Q., Yue, T., Chen, S., Nakajima, M., et al. (2015). Automated assembly of vascular-like microtube with repetitive single-step contact manipulation. *IEEE Trans. Biomed. Eng.* 62, 2620–2628. doi: 10.1109/TBME.2015.2437952

Wang, H., and Pumera, M. (2015). Fabrication of micro/nanoscale motors. *Chem. Rev.* 115, 8704–8735. doi: 10.1021/acs.chemrev.5b00047

Wang, J. (2013). *Nanomachines: Fundamentals and Applications*. Weinheim: Wiley-VCH. doi: 10.1002/9783527651450

Wang, J. (2017). *Fuel-Free Nanowire Motors*. U. S. Patent 9, 698, 708.

Wang, J., Balasubramanian, S., Kagan, D., and Campuzano-Ruiz, S. (2018b). *Nano/Microscale Vehicles for Capture and Isolation of Target Biomolecules and Living Organisms*. U. S. Patent 9,879,310.

Wang, J., Esener, S. C., Kagan, D., Benchimol, M., and Claussen, J. (2017). *Acoustically Triggered Nano/Micro-Scale Propulsion Devices*. U. S. Patent 9,726,114.

Wang, J., Gao, W., and Sattayasamitsathit, S. (2016a). *Membrane Template Synthesis of Microtube Engines*. U. S. Patent 9,347,143.

Wang, J., Manesh, K. M., and Balasubramanian, S. (2016b). *Nanomotor-Based Patterning of Surface Microstructures*. U. S. Patent 9,352,963.

Wang, J., and Zhang, L. (2017). *Cellular Micromotors and Uses Thereof*. U. S. Patent Application 15/356,977.

Wang, W., Duan, W., Ahmed, S., Mallouk, T. E., and Sen, A. (2013). Small power: autonomous nano- and micromotors propelled by self-generated gradients. *Nano Today* 8, 531–554. doi: 10.1016/j.nantod.2013.08.009

Wang, X., Qin, X.-H., Hu, C., Terzopoulou, A., Chen, X.-Z., Huang, T.-Y., et al. (2018c). 3D printed enzymatically biodegradable soft helical microswimmers. *Adv. Funct. Mat.* 28:1804107. doi: 10.1002/adfm.201804107

Weinberg, I. N., Nacev, A. N., Stepanov, P., and Weinberg Medical Physics Inc (2017). *System, Method and Equipment for Implementing Temporary Diamagnetic Propulsive Focusing Effect With Transient Applied Magnetic Field Pulses*. U. S. Patent 9,694,196.

Xi, W., Solovev, A. A., Ananth, A. N., Gracias, D. H., Sanchez, S., and Schmidt, O. G. (2013). Rolled-up magnetic microdrillers: towards remotely controlled minimally invasive surgery. *Nanoscale* 5, 1294–1297. doi: 10.1039/C2NR32798H

Yan, X., Zhou, Q., Vincent, M., Deng, Y., Yu, J., Xu, J., et al. (2017). Multifunctional biohybrid magnetite microrobots for imaging-guided therapy. *Sci. Robot.* 2:eaaq1155. doi: 10.1126/scirobotics.aaq1155

Yao, K., Manjare, M., Barrett, C. A., Salguero, T. T., Zhao, Y., and University of Georgia Research Foundation Inc (2015). *Functional Nanostructured "Jelly Rolls" With Nanosheet Components*. U. S. Patent 9,202,606.

Zhang, Z., Dai, C., Huang, J. Y., Wang, X., Liu, J., Ru, C., et al. (2018). Robotic immobilization of motile sperm for clinical intracytoplasmic sperm injection. *IEEE Trans. Biomed. Eng.* 62, 2620–2628. doi: 10.1109/TBME.2018.2848972

Conflict of Interest Statement: The authors declare that the research was conducted in the absence of any commercial or financial relationships that could be construed as a potential conflict of interest.

frontiers in Bioengineering and Biotechnology

ORIGINAL RESEARCH
published: 21 November 2018
doi: 10.3389/fbioe.2018.00173

Transdifferentiating Astrocytes Into Neurons Using ASCL1 Functionalized With a Novel Intracellular Protein Delivery Technology

Meghan Robinson[1], *Ian Fraser*[1,2], *Emily McKee*[2], *Kali Scheck*[3], *Lillian Chang*[4] *and Stephanie M. Willerth*[1,2,5,6,7]*

[1] Division of Medical Sciences, University of Victoria, Victoria, BC, Canada, [2] Biomedical Engineering Program, University of Victoria, Victoria, BC, Canada, [3] Biology Program, University of Victoria, Victoria, BC, Canada, [4] Biochemistry Program, Bates College, Lewiston, ME, United States, [5] Mechanical Engineering, Faculty of Engineering, University of Victoria, Victoria, BC, Canada, [6] Center for Biomedical Research, Faculty of Engineering, University of Victoria, Victoria, BC, Canada, [7] International Collaboration for Repair Discovery, University of British Columbia, Vancouver, BC, Canada

Cellular transdifferentiation changes mature cells from one phenotype into another by altering their gene expression patterns. Manipulating expression of transcription factors, proteins that bind to DNA promoter regions, regulates the levels of key developmental genes. Viral delivery of transcription factors can efficiently reprogram somatic cells, but this method possesses undesirable side effects, including mutations leading to oncogenesis. Using protein transduction domains (PTDs) fused to transcription factors to deliver exogenous transcription factors serves as an alternative strategy that avoids the issues associated with DNA integration into the host genome. However, lysosomal degradation and inefficient nuclear localization pose significant barriers when performing PTD-mediated reprogramming. Here, we investigate a novel PTD by placing a secretion signal sequence next to a cleavage inhibition sequence at the end of the target transcription factor–achaete scute homolog 1 (ASCL1), a powerful regulator of neurogenesis, resulting in superior stability and nuclear localization. A fusion protein consisting of the amino acid sequence of ASCL1 transcription factor with this novel PTD added can transdifferentiate cerebral cortex astrocytes into neurons. Additionally, we show that the synergistic action of certain small molecules improves the efficiency of the transdifferentiation process. This study serves as the first step toward developing a clinically relevant *in vivo* transdifferentiation strategy for converting astrocytes into neurons.

Keywords: reprogramming, transcription factors, neuroscience, small molecules, drug delivery

OPEN ACCESS

Edited by:
Gianni Ciofani,
Politecnico di Torino, Italy

Reviewed by:
Stefania Moscato,
Università degli Studi di Pisa, Italy
Madoka Suzuki,
Osaka University, Japan

***Correspondence:**
Stephanie M. Willerth
willerth@uvic.ca

Specialty section:
This article was submitted to Nanobiotechnology, a section of the journal Frontiers in Bioengineering and Biotechnology

Received: *12 September 2018*
Accepted: *31 October 2018*
Published: *21 November 2018*

Citation:
Robinson M, Fraser I, McKee E, Scheck K, Chang L and Willerth SM (2018) Transdifferentiating Astrocytes Into Neurons Using ASCL1 Functionalized With a Novel Intracellular Protein Delivery Technology. Front. Bioeng. Biotechnol. 6:173. doi: 10.3389/fbioe.2018.00173

INTRODUCTION

Transdifferentiation converts mature cells from one specialized cell type into another by varying gene expression patterns (Tanabe et al. 2015). These expression patterns are controlled by transcription factors, regulatory proteins which bind to DNA promoter regions to activate transcription of key developmental genes. Ectopic expression of these transcription factors in somatic cells can change cell fates without the need for inducing a pluripotent

state (Tanabe et al., 2015). This process avoids the risk of tumorigenesis associated with transplanting pluripotent stem cell-derived therapies *in vivo*, where incomplete differentiation leads to uncontrolled proliferation (Gordeeva and Khaydukov, 2017). The final genetic signatures of these transdifferentiated cells are stable and not restricted to the lineage of the original cell type, allowing cells to be sourced directly from endogenous tissue local to the site of injury (Tanabe et al., 2015). Performing *in vivo* transdifferentiation would eliminate the need for cell transplantation and immunosuppression depending on the target application.

Ectopic transcription factor expression can be efficiently accomplished through insertion into the genome by viral vectors encoding the amino acid sequence of the desired transcription factor. However, this method is not safe for *in vivo* use in clinical trials due to the risk of activating oncogenes by random DNA insertion into the host genome (Li et al., 2002; Modlich et al., 2006; Medvedev et al., 2010). Non-integrating vectors have been developed capable of transdifferentiation, but at lower efficiencies. Some well-known examples of non-integrating methods include vectors composed of single-stranded RNA, such as the Sendai virus, circular DNA, such as plasmid vectors and minicircles, and mRNA vectors, which reside in the cytoplasm where they are translated into proteins. Despite these improvements in non-viral delivery, vector-based transdifferentiation strategies still face challenges such as transgene silencing, inflammation due to the presence of residual bacterial DNA, and poor nuclear uptake due to their physical size (Hardee et al., 2017).

The search for non-integrating, non-viral reprogramming methods has led to the discovery of transdifferentiation using microRNAs and small molecules (Ma et al., 2017). In 2011, it was determined that the microRNAs miR-124 and miR-9/9* were sufficient to induce neurons from fibroblasts (Ambasudhan et al., 2011; Yoo et al., 2011;). Later in 2014 Zhu et al. discovered that viral-mediated expression of octamer binding transcription factor 4 (OCT4) was sufficient to transdifferentiate somatic cells into neural stem cells when combined with small molecules that promote lineage-specific signaling (Zhu et al., 2014). Morphogens and bioactive small molecules can potentially enhance the action of transcription factors by improving chromatin accessibility, targeting key signaling pathways, and regulating metabolism (Lin and Wu, 2015). These results led several groups to identify combinations of small molecules capable of transdifferentiating somatic cells such as fibroblasts, astrocytes and even glioblastoma cells into neurons (Cheng et al., 2014; Hu et al., 2015; Li et al., 2015; Zhang et al., 2015, 2016; Gao et al., 2017; Lee et al., 2018). Although the transdifferentiation methods differ, these small molecule and microRNA protocols share a common thread in that they produce mainly one neuronal subtype–medium spiny neurons in the case of microRNAs, or interneurons in the small molecules methods with the exception of the glioblastoma-transdifferentiated neurons which resulted in immature post-mitotic neurons. The inability to produce the neuronal subtypes which are lost in neurodegenerative disorders like Parkinson's Disease, Alzheimer's Disease, amyotrophic lateral sclerosis (ALS), Huntingdon's Disease, spinal cord injury and blindness, represents a major limitation in current small molecule and microRNA reprogramming protocols.

Researchers have begun to explore protein transduction domains (PTDs), also known as cell penetrating peptides (CPPs), as tools for transdifferentiation to address these limitations (Zahid and Robbins, 2012). These CPPs are small peptides that penetrate the cell membrane to deliver bioactive macromolecules. The first PTD was derived from the transactivator of transcription (TAT) protein sequence of the human immunodeficiency virus (HIV), which binds to a phospholipid component of the inner surface of the cell membrane through a cationic poly-arginine sequence to enable cellular internalization (Yang et al., 2012b; Gordeeva and Khaydukov, 2017). Other examples of PTDs include Penetratin, a cationic arginine-rich sequence taken from the Drosophila protein antennapedia homeotic transcription factor (Antp), and CADY, a sequence combining arginine residues with aromatic tryptophan, whose helical conformation within the cellular membrane favors cellular uptake (Crombez et al., 2009; van den Berg and Dowdy, 2011). PTDs have the potential to be fitted with binding domains to target specific cell populations, making them ideal tools for *in vivo* reprogramming of endogenous cells (van den Berg and Dowdy, 2011; Zahid and Robbins, 2015). For example, C-end rule (CendR) is an amino acid sequence containing a carboxy (C)-terminal motif which binds to neuropilin-1, a cell surface receptor expressed in epithelial, neuronal, and cancer cells (Teesalu et al., 2009; Pang et al., 2014). In 2014, Hu et al. successfully transdifferentiated neuropilin-1 expressing retinal pigmented epithelial cells into neurons using a C-end rule PTD fused to the transcription factor self-determining region Y-box2 (SOX2) (Hu et al., 2014).

Little work has been done to develop such protocols to date despite the promise of PTDs as a tool for *in vivo* transdifferentiation. A search using the Pubmed database revealed only one further publication using PTD delivery where Islas et al. transdifferentiated human dermal fibroblasts into immature contractile cardiomyocytes (Islas et al., 2012). They fused TAT-PTDs to two cardiac transcription factors, erythroblastosis virus E26 oncogene homolog 2 (ETS2) and mesoderm posterior 1 (MESP1). Treatment with these TAT-PTDs followed by treatment with cardiac gene-inducing morphogens activin A and BMP2 resulted in successful transdifferentiation of fibroblasts into functional cardiomyocytes. Morphogen treatment significantly improved induction of key cardiac genes, whereas addition of the morphogens alone had no effect, further illustrating the transdifferentiation potential of combining morphogens or bioactive small molecules with transcription factors.

In this work, we developed a protocol using a novel PTD to transdifferentiate somatic cells into interneurons. We hypothesized that the delivery of the neural transcription factor achaete scute homolog 1 (ASCL1) by this novel PTD design in combination with the action of bioactive small molecules would promote neuronal transdifferentiation of astrocytes, the most abundant cell type in the central nervous system. ASCL1 is a transcription factor and master regulator of neurogenesis

(Vasconcelos and Castro, 2014). Its ability to bind readily to closed chromatin and promote the appearance of new regions of open chromatin allows coordinated activation of previously silenced genes (Iwafuchi-Doi and Zaret, 2014; Raposo et al., 2015). In 2015, Liu et al. showed that *in vivo* viral delivery of ASCL1 to mouse dorsal midbrain astrocytes was sufficient for neural transdifferentiation, with 76.8% of astrocytes adopting a neural fate by day 10 (Liu et al., 2015). ASCL1 was also chosen for its versatility. While the action of ASCL1 alone leads to an interneuron fate, it is known to induce dopaminergic, cholinergic or serotonergic neuronal subtypes when combined with dopaminergic factors LMX1B/NURR1 (Addis et al., 2011; Theka et al., 2013), cholinergic factors MYT1L/BYRN2/LHX3/HB9/ISL1/NGN2 (Son et al., 2011), or serotonergic factors FOXA2/LMX1B/FEV (Xu et al., 2016). The PTD employed for these experiments was designed by iProgen Biotech Inc. to take advantage of the cell's innate retrograde transport pathway by integrating a secretion signal peptide and a cleavage inhibition peptide to a cargo protein (Lee et al., 2013). Initially the PTD integrates itself into the cell surface membrane due to its amphipathic nature. Once internalized, the secretion signal peptide preferentially binds to its native binding partner, translocon, a complex of proteins tasked with translocating polypeptides with a targeting signal sequence into the interior space of the endoplasmic reticulum (ER). As the translocon retrogrades back through the ER into the cytoplasm, so does the cargo. This combination of secretion signal peptide and cleavage inhibition peptide, termed IPTD, shows greatly improved delivery of proteins into the cytoplasmic space over conventional PTDs such as TAT and poly-arginine. In 2016, we showed that ASCL1-IPTD could efficiently generate neurons from human induced pluripotent stem cells (hiPSCs) (Robinson et al., 2016). We show here that ASCL1-IPTD in combination with the small molecules LDN193189, SB431542, DAPT and valproic acid can rapidly reprogram astrocytes into mature GABAergic and glutamatergic interneurons with high efficiency, and that this process is unique to the transcription factor ASCL1. We also show that in the absence of these small molecules ASCL1-IPTD cannot transdifferentiate into a neuronal fate, but does generate a divergent cell fate of myoblasts. Because of its inherent versatility in generating other neuronal subtypes, this ASCL1-IPTD protocol serves as a starting point for further development through the functionalization of subtype-specific factors with IPTD to generate subtypes of neurons. Additionally, the use of IPTD allows for future adaption with specific tissue-targeting motifs. This method can be applied as novel treatment for neurodegenerative diseases or spinal cord injury by transdifferentiating astrocytes into specific neuronal populations as a way to restore function.

MATERIALS AND METHODS

Cell Culture

Human fetal astrocytes (ScienCell cat#1800) were cultured on poly-L-lysine coated plates in Astrocyte Media (ScienCell). Media was changed every 2 days and cells were passaged 1:6 when 90% confluent using trypsin-EDTA (ScienCell). 10% fetal bovine serum (FBS, Gibco) was added to media for 6 passages (6 weeks) as previously described to purify astrocyte cultures of neural progenitors (Zhang et al., 2015). Astrocytes were incubated for 24 h on an orbital shaker plate at 200 rpm as previously described to purify low passage (P2) astrocytes of neural progenitors (Lian et al., 2016). Mouse embryonic fibroblasts (MEFs) were purchased from MTI GlobalStem and thawed onto poly-L-ornithine (PLO)/laminin (Sigma Aldrich) substrates in high glucose DMEM (Gibco) supplemented with 10% FBS.

Astrocyte Reprogramming

Astrocytes were grown to confluence before reprogramming. Cells were cultured on poly-L-lysine (PLO)/laminin substrates and media was changed to high glucose Dulbecco's Modified Eagle Medium (DMEM) with 2 mM Glutamax (Gibco), 1% N2/B27 (ThermoFisher Scientific), 1% Human Serum Replacement 3 (Sigma Aldrich), and 1% penicillin/streptomycin (ThermoFisher Scientific) for cellular reprogramming experiments. 15 μg/mL ASCL-IPTD (iProgen Biotech) was supplemented for all 12 days, with 50% media changes every 2 days. For days 1-2, 5μM SB431542 (Stemcell Technologies) and 0.25 μM LDN193189 (Stemcell Technologies) were added to cultures. For days 3–12 the following small molecules were added: forskolin (F, 10 μM, Medchem Express), CHIR99021 (C, 1.5 μM, Medchem Express), ISX9 (I, 20 μM, Medchem Express), DAPT (D, 5 μM, Medchem Express). The combinations tested were C, F, D, I, CF, CI, CD, FI, FD, ID, FCI, FCD, CID, FID, CFID. For days 3–6, 0.5 μM valproic acid (Stemcell Technologies) was also added to improve chromatin accessibility.

Fibroblast Reprogramming

MEFs were seeded 40,000 cells/cm^2 on PLO/laminin and cultured for 24 h in high glucose DMEM + 10% FBS to adhere. Media was then switched to high glucose DMEM, 1% N2/B27, 1% Human Serum Replacement 3, 2 mM GlutaMAX, 1% penicillin/streptomycin, 15 μg/mL ASCL1-IPTD and 20 mM forskolin for 14 days, with media changes of 50% every 2nd day.

Immunocytochemistry

Immunocytochemistry was performed as described previously (Agbay et al., 2018). Cells were fixed with 3.7% formaldehyde/phosphate buffered saline (PBS) solution for 1 h, then permeabilized in 0.1% Triton X-100 (Sigma Aldrich) in PBS for 45 min at 4°C, then blocked with 5% normal goat serum (NGS, Sigma Aldrich) in PBS for 2 h at 4°C. Cells were then incubated with the primary antibodies mouse anti-TUJ1 (Millipore), rabbit anti-MYH3 (Abcam), rabbit anti-ASCL1 (Abcam), rabbit anti-DCX (Abcam), rabbit anti-SOX2 (Abcam), rabbit anti-MAP2 (Abcam), rabbit anti-GLUT1 (Abcam), rabbit anti-GAD65/67 (Abcam), mouse anti-NEUN (Novus Biologicals), mouse anti-TH (Stemcell Technologies), or goat anti-CHAT (Millipore), diluted 1:500 in PBS, and incubated overnight at 4°C in the dark. The next day cells were washed with PBS three times for 15 min each, and incubated with secondary antibodies goat anti-mouse IgG AlexaFluor488 (ThermoFisher

Scientific), goat anti-rabbit IgG AlexaFluor568 (ThermoFisher Scientific), or donkey anti-goat AlexaFluor405 (Abcam) diluted 1:200 in PBS for 4 h at 4°C. Cells were washed again three times as previously described. For cells counterstained with DAPI nucleic acid stain, a 300 nM DAPI solution (Invitrogen) in PBS was added to the cultures after the final wash and incubated for 3 min, followed by rinsing with PBS. Cells were visualized and imaged with a Cytation5 (Biotek) Imaging platform at 20 × magnification. Fluorescently labeled cells were visualized with Biotek Dapi (377/477), GFP (469/525), and Texas Red (586/647) filter cubes, using dichroic mirror-based wavelength selection.

Flow Cytometry

Flow cytometry was performed as previously described (Montgomery et al., 2015). The cells were stained for SOX2-PE Mouse IgG2A (R&D Systems) with IgG2A-PE isotype control (R&D Systems), TUJ1-PerCP Mouse IgG2A (R&D Systems) with IgG2A-PerCP isotype control (R&D Systems), MAP2-PE Mouse IgG1 (Clone AP20, Milli-Mark) with Mouse IgG1 PE isotype control (R&D Systems), and NEUN-PE Mouse IgG1 (Clone A60) with Mouse IgG1 PE isotype control (R&D Systems). Cells were collected rinsed with PBS 3 times, followed by incubation in fixation/permeabilization buffer (R&D Systems) for 10 min, and 3 more washes with PBS. Next cells were resuspended in permeabalization/wash buffer (R&D Systems) with each antibody, diluted as per manufacturer's instructions, for 45 min at 4°C in the dark. Cells were then washed in permeabilization/wash buffer 3 times. Data was collected using the Millipore Guava EasyCyte HT flow cytometer. Cells were gated to exclude small debris and clustered cells, and a maximum of 5,000 gated events were collected for each sample. All analysis was completed using GuavaSoft EasyCyte software.

Quantification of Transdifferentiated Neurons

Cells were first immunostained with the neuronal cytoskeletal marker TUJ1 to quantify transdifferentiated neurons in each group of the small molecule screen. Next, a grid of 5 × 5 images was taken in each of 3 wells for each group (25 images per well, $n = 3$ biological replicates). Cells were visualized with a Leica DMI 3000B microscope equipped with an XCite Series 120Q fluorescent light source and QImaging RETIGA 2000R camera at 100 × magnification, and images were captured using QCapture Software 2.9.12 with a GFP filter (blue/470, Leica Systems) and a DAPI filter (400, Leica Systems) and dichroic mirrors (500, Leica Systems). Cells were counted manually if they were positive for TUJ1 and possessed a small rounded soma, with at least 2 neuritic processes. Total cells were counted by DAPI stain using ImageJ: images were made binary and a watershed was applied to separate nuclei that were touching by a single pixel width, and each cell was counted as a particle under the Analyze-Particles Menu.

Statistical Analysis

Statistical analysis was performed by a one-way ANOVA followed by a one-tailed Student's *t*-test with a 95% confidence level ($\alpha = 0.05$). Results are presented as the mean ± standard deviation. All experiments were carried out with a biological $n = 3$.

RESULTS

Transdifferentiation Protocol Developmental

We sought to characterize the transdifferentiation strength of ASCL1-IPTD before designing our protocol. We executed a well-known protocol where ectopic expression of ASCL1 alone converts mouse embryonic fibroblasts (MEFs) into neurons, and at lower expression levels, into skeletal myoblasts (Treutlein et al., 2016). The addition of the small molecule forskolin, an activator of cyclic adenosine monophosphate (cAMP) signaling, dramatically improves the efficiency of this protocol and so it was tested in parallel to determine if conversion efficiency could be similarly improved with ASCL1-IPTD (Shi et al., 2016). After 14 days of treatment, skeletal myoblasts were generated instead of neurons as indicated by myosin heavy chain 3 (MYH3) expression, with or without the addition of forskolin (**Figure 1**). Increasing the concentration of ASCL1-IPTD 5-fold also had no effect in generating neurons (**Supplemental Figure 1**).

We concluded that the strength of ASCL1-IPTD was not meeting the threshold expression level necessary for neuronal transdifferentiation. Accordingly, we adopted the strategy to first lower this threshold by repressing astrocytic gene expression using small molecules to inhibit transforming growth factor β1 (TGF-β1)/SMAD and bone morphogenic protein (BMP)/SMAD signaling pathways, which are jointly responsible for astrocyte commitment and maintenance (Stipursky and Gomes, 2007; Chambers et al., 2009; Yang et al., 2013; Zhang et al., 2015). Human cerebral cortex astrocytes were primed for 2 days followed by screening of a set of small molecules known to have neuronal transdifferentiation potential: CHIR99021, an inhibitor of glycogen synthase kinase 3 (GSK3) signaling; DAPT, an inhibitor of Notch signaling; forskolin, an activator of cAMP signaling; and isoxazole 9 (ISX9), an activator of calcium-mediated signaling (Zhang et al., 2015; Gascón et al., 2016, 2017; Gao et al., 2017). For days 3–6, valproic acid, a histone deacetylase inhibitor, was added to enhance chromatin accessibility (Huangfu et al., 2008). ISX9 induced a significant degree of toxicity in cultures, and the combination of CHIR99021 and ISX9 caused all the cells to detach from the plate (data not shown). All remaining combinations produced some degree of transdifferentiation from astrocytes into neurons within 10 days, with DAPT alone being the most effective enhancer of this process (**Figure 2**).

The Action of DAPT Does Not Translate to NGN2-Mediated Transdifferentiation

We exchanged ASCL1-IPTD with another functionalized neurogenic transcription factor, NGN2-IPTD to determine if ASCL1 could be replaced with NGN2. NGN2 also serves

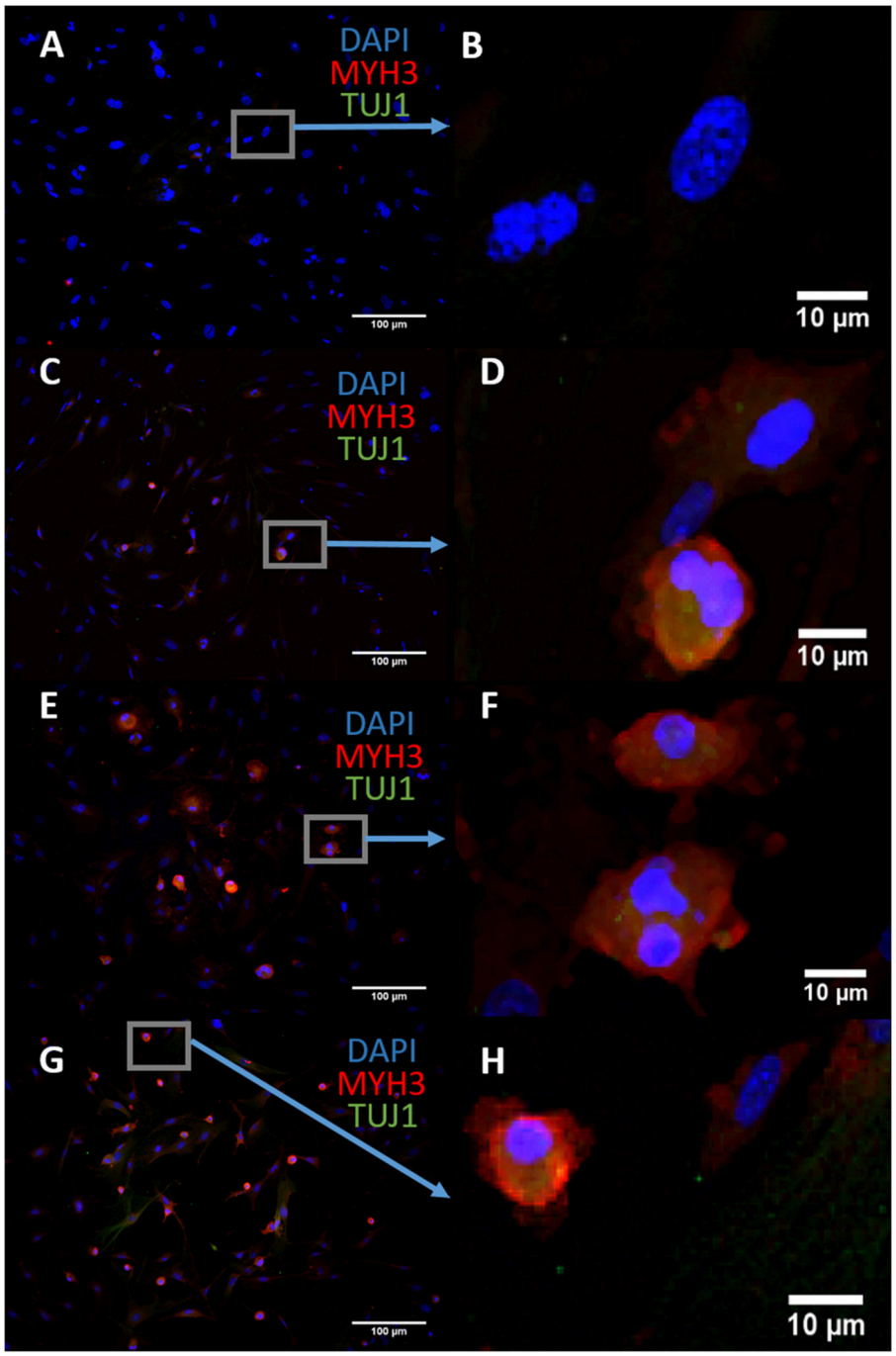

FIGURE 1 | Mouse embryonic fibroblasts (MEFs) express the skeletal myoblast gene myosin heavy chain 3 (MYH3) and lack the neuronal gene beta tubulin (TUJ1) after 14 days of exposure to ASCL1-IPTD and the cAMP activator forskolin, indicating that they have adopted a myogenic cell fate rather than a neuronal cell fate. **(A)** Control. Scale bar is 100 μm. **(B)** High magnification of **(A)**. Scale bar is 10 μm. **(C)** Forskolin only. Scale bar is 100 μm. **(D)** High magnification of **(C)**. Scale bar is 10 μm. **(E)** ASCL1-IPTD only. Scale bar is 100 μm. **(F)** High magnification of **(E)**. Scale bar is 10 μm. **(G)** ASCL1-IPTD with forskolin. Scale bar is 100 μm. **(H)** High magnification of **(H)**. Scale bar is 10 μm.

as a master regulator of neural fate, and when delivered virally is sufficient to transdifferentiate astrocytes into neurons with high efficiency (71%) (Parras et al., 2002; Berninger et al., 2007). However, replacing ASCL1-IPTD with NGN2-IPTD in combination with DAPT did not generate neurons, but was seen by immunocytochemistry to generate a population of cells expressing the neuroblast gene doublecortin (DCX), suggesting that ASCL1 and NGN2 are not interchangeable in our protocol **(Figure 3).**

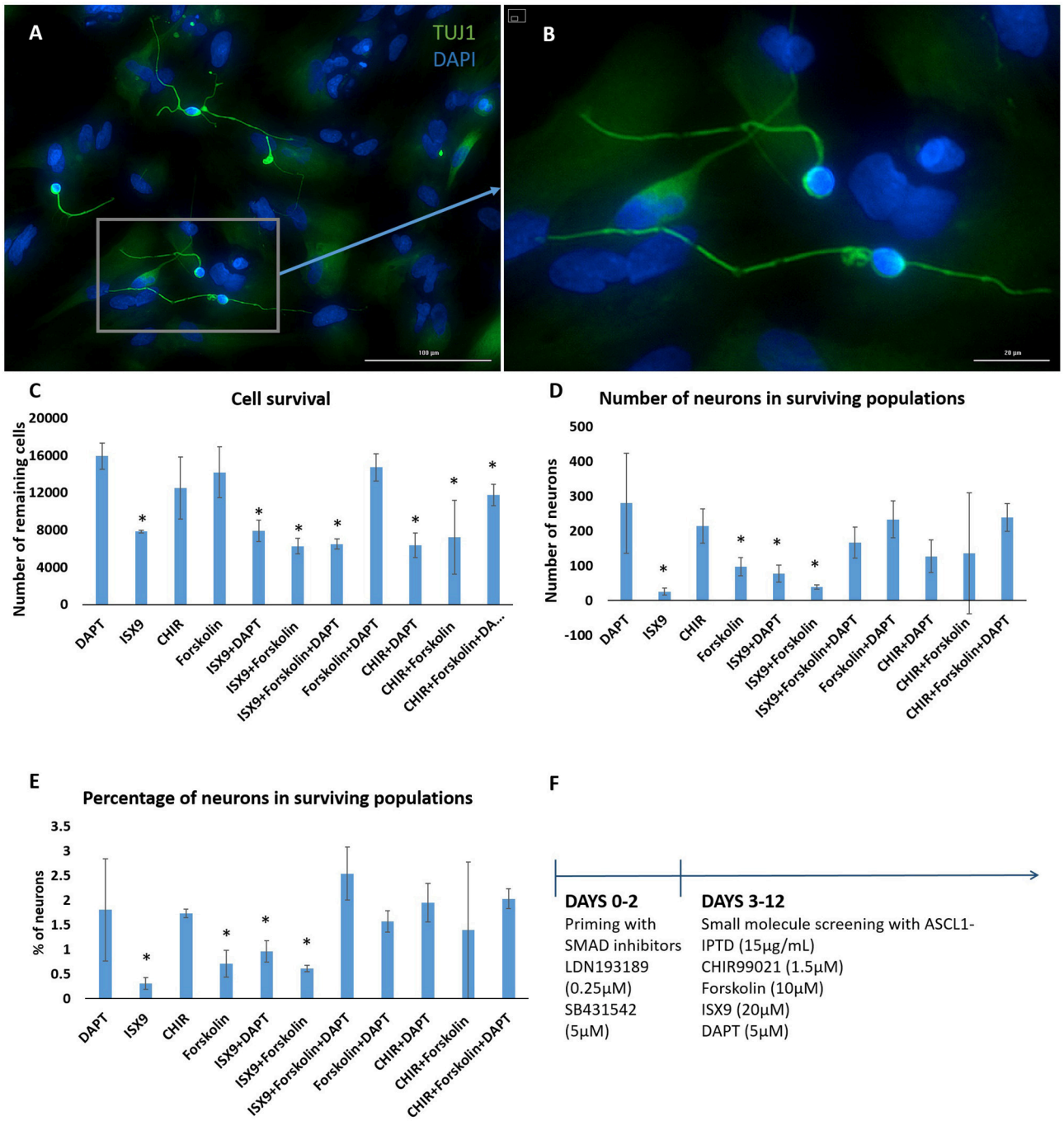

FIGURE 2 | Small molecule screening of combinations of forskolin, ISX9, DAPT and CHIR99021 with ASCL1-IPTD show that DAPT is the most potent inducer of neural transdifferentiation. **(A)** Cells express beta tubulin (TUJ1), an early neuronal marker, and ASCL1 after 2 days of priming with LDN193189 and SB431542 and ASCL1-IPTD followed by 10 days of treatment with ASCL1-IPTD and DAPT. Scale bar is 100 μm. **(B)** High magnification of **(A)**. Scale bar is 20 μm. **(C)** Cell survival varied in each condition, with the DAPT alone condition being the least toxic by far ($n = 3$). **(D)** Neurons counted from each small molecule combination on day 12 ($n = 3$). **(E)** Neuronal conversion percentages. **(F)** Protocol timeline: 2 days of priming with SMAD inhibitors LDN193189 and SB431542 followed by 10 days of small molecule combinations. All 12 days included the addition of ASCL1-IPTD. Statistical analysis was performed by a one-way ANOVA followed by a one-tailed Student's *t*-test with a 95% confidence level ($\alpha = 0.05$). Results are presented as the mean ± standard deviation, with a * representing a statistically significant difference between that condition and the DAPT alone condition.

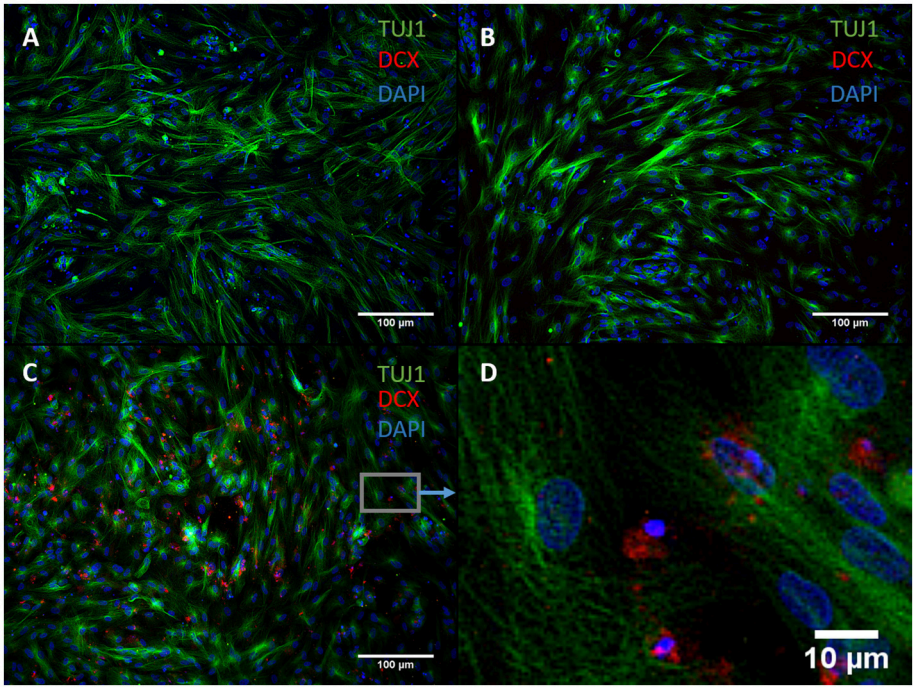

FIGURE 3 | NGN2-IPTD in place of ASCL1-IPTD does not generate neurons, but does produce cells expressing doublecortin (DCX), a marker for neuroblasts. **(A)** Control. Scale bar is 100 µm. **(B)** Small molecules only. Scale bar is 100 µm. **(C)** NGN2-IPTD plus small molecules. Scale bar is 100 µm. **(D)** High magnification image of **(C)**. Scale bar is 10 µm. Note that TUJ1 is weakly expressed in astrocytes in addition to neurons and can be regarded as background stain in these images.

Astrocytic Plasticity Dramatically Improves Transdifferentiation of Neurons

Both early astrocytes and astrocytes found at the site of injury possess the ability to form multi-potent neurospheres, making them highly plastic (Yang et al., 2012a; Götz et al., 2015; Sirko et al., 2015; Wang et al., 2015; Michelucci et al., 2016). We investigated the extent to which our protocol might transdifferentiate plastic astrocytes by applying it to early passage (P3) astrocytes. Indeed, analysis by flow cytometry showed that efficiency was dramatically improved to 73.09 ± 5.83% (from 1.81 ± 1.04%) by priming and DAPT exposure alone (**Figures 2G**,**4**,**6**), while the further addition of ASCL-IPTD resulted in abundant neurosphere formation, giving rise to cells expressing the mature neuronal markers MAP2 (8.48 ± 2.29%, vs. 2.56 ± 0.47% without) and NEUN (2.20 ± 1.01% with ASCL1-IPTD vs. 0.47 ± 0.05% without) by day 12 (**Figures 5**, **6**). These neurons were seen by immunocytochemistry to express both glutamatergic and GABAergic neurotransmitter genes, suggesting a mix of excitatory and inhibitory interneurons, while treatment with small molecules alone were negative for neurotransmitter markers (**Figure 5**).

DISCUSSION

In this work, we show that ASCL1-IPTD combined with the complementary action of SMAD and Notch signaling inhibition serves an efficient inducer of neurons from astrocytes, particularly those which exhibit plasticity. This effect is important since astrocytes become reactive at the site of injury *in vivo* and acquire enhanced plasticity, enabling them to proliferate and de-differentiate to generate multipotent neurospheres with the potential to self-renew and give rise to astrocytes, neurons or oligodendrocytes (Yang et al., 2012a; Götz et al., 2015; Sirko et al., 2015; Wang et al., 2015; Michelucci et al., 2016). SMAD signaling regulates genes involved in astrocyte commitment and maintenance (Stipursky and Gomes, 2007; Chambers et al., 2009; Yang et al., 2013; Zhang et al., 2015), therefore we treated cells with SMAD inhibitors from days 1 to 2 to disrupt astrocyte commitment. Our screening process identified DAPT to be the most potent enhancer of ASCL1-IPTD in transdifferentiating neurons from astrocytes. Notch signaling maintains neural progenitors in a state of proliferation by repressing genes responsible for cell cycle arrest and neural differentiation such as ASCL1 and NGN2 (Dhanesh et al., 2016), thus inhibition of Notch signaling is a necessary action for the generation of mature neurons.

A unique aspect of our transdifferentiation protocol is the presence of a progenitor stage characterized by neurosphere formation. Neurospheres are 3-D clusters of neural stem cells possessing the characteristics of self-renewal and multipotency (Bez et al., 2003). Since neurospheres were absent from cultures treated with small molecules alone we attribute the progenitor stage in our protocol to the action of ASCL1-IPTD. Furthermore, only neurons arising from neurospheres expressed mature neuronal markers MAP2 and NEUN by day 12. Passing through

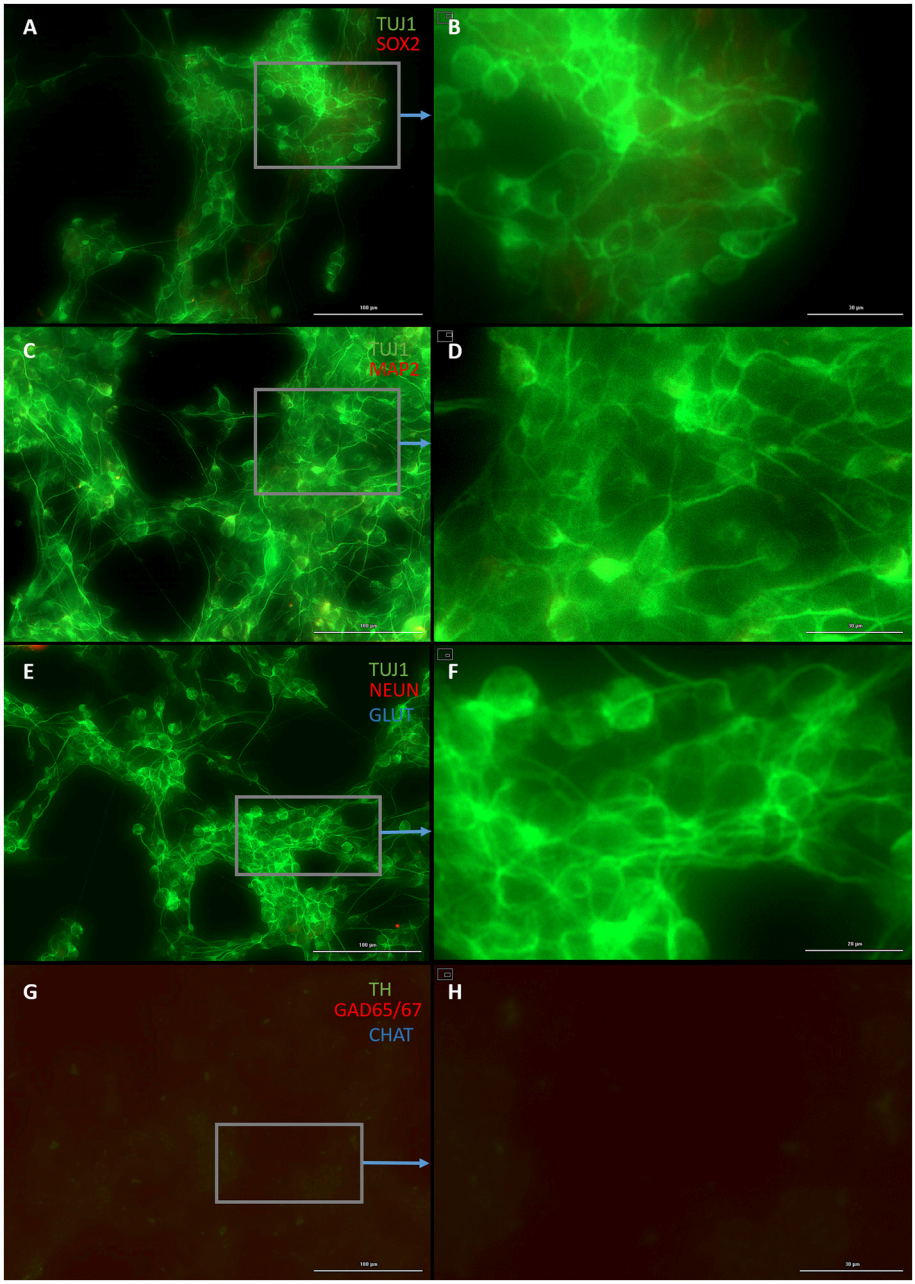

FIGURE 4 | Small molecule only group after 2 days of priming by LDN193189 and SB431542 followed by 10 days of treatment with DAPT. **(A)** Cells express the early neural marker TUJ1 and weakly express the neural stem cell marker SOX2. Scale bar is 100 μm. **(B)** High magnification of **(A)**. Scale bar is 30 μm. **(C)** Cells are negative for the mature neural marker MAP2. Scale bar is 100 μm. **(D)** High magnification of **(C)**. Scale bar is 10 μm **(E)** Cells are negative for the mature neural marker NEUN and the neurotransmitter glutamate expressed by excitatory interneurons GLUT. Scale bar is 100 μm. **(F)** High magnification of **(E)**. Scale bar is 20 μm. **(G)** Cells are negative for the neurotransmitter tyrosine hydroxylase expressed by dopaminergic neurons TH, the neurotransmitter glutamic acid decarboxylase expressed by inhibitory interneurons GAD65/67, and the neurotransmitter choline acetyltransferase expressed by motor neurons CHAT. Scale bar is 100 μm. **(H)** High magnification of **(G)**. Scale bar is 30 μm. Note that some fluorescence is picked up by all the cells producing background fluorescence which can be ignored.

a progenitor stage has two advantages. First, the rapid metabolic transition that takes place during the fate switch from somatic cell to neuron puts enormous stress on the cell, leading to the formation of reactive oxygen species (ROS), known to induce toxicity and affect cell fate regulation, posing a major barrier to transdifferentiation. It stands to reason that an intermediate stage would reduce this oxidative stress, promoting a safer transition between cell fates and improving efficiency (Gascón et al., 2016). Second, the generation of neural stem cells improves the efficiency of the protocol since each neural stem cell can produce

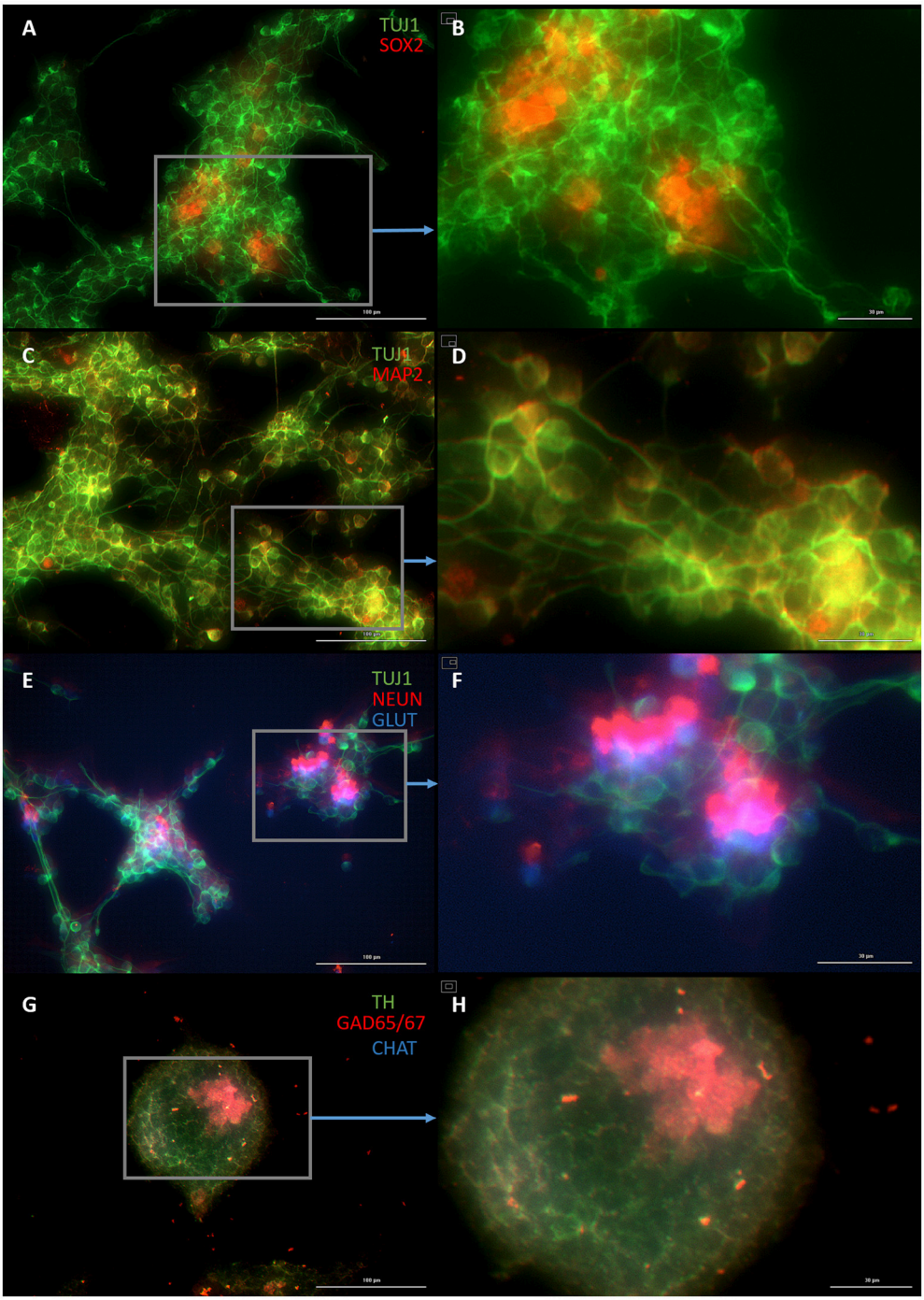

FIGURE 5 | Plastic astrocytes generate neurospheres and mature neurons after 12 days of exposure to ASCL1-IPTD, including 2 days of priming by LDN193189 and SB431542 followed by 10 days of DAPT. **(A)** Cells express the early neural marker TUJ1 and the neural stem cell marker SOX2. Scale bar is 100 μm. **(B)** High magnification of **(A)**. Scale bar is 30 μm. **(C)** Cells express the mature neural marker MAP2. Scale bar is 100 μm. **(D)** High magnification of **(C)**. Scale bar is 30 μm **(E)** Cells express the mature neural marker NEUN and the neurotransmitter glutamate expressed by excitatory interneurons GLUT. Scale bar is 100 μm. **(F)** High magnification of **(E)**. Scale bar is 30 μm. **(G)** Cells are negative for the neurotransmitter tyrosine hydroxylase expressed by dopaminergic neurons TH, and negative for the neurotransmitter choline acetyltransferase expressed by motor neurons CHAT, but do express the neurotransmitter glutamic acid decarboxylase expressed by inhibitory interneurons GAD65/67. Scale bar is 100 μm. **(H)** High magnification of **(G)**. Scale bar is 30μm. Note that some fluorescence is picked up by all the cells producing background fluorescence which can be ignored.

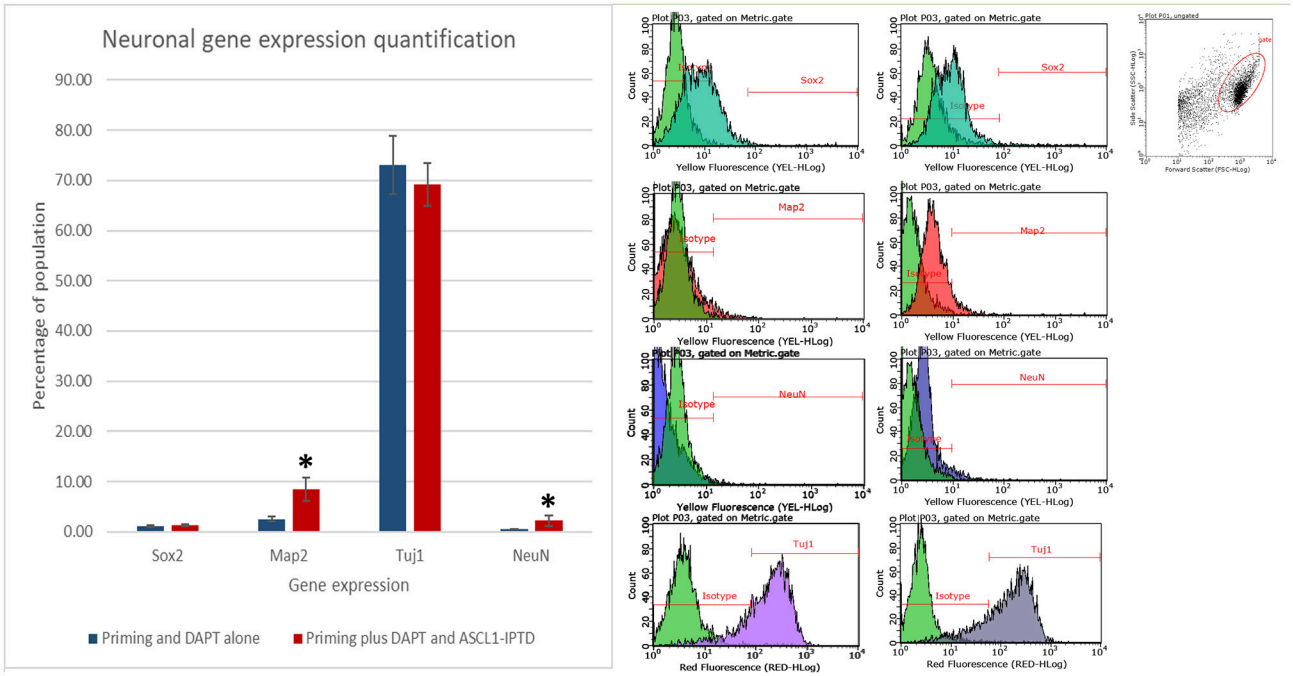

FIGURE 6 | Quantification of neural gene expression for the immature neural marker TUJ1 and the mature neuronal markers MAP2 and NEUN by flow cytometry. Plastic astrocytes were exposed to 2 days of priming by LDN193189 and SB431542 followed by 10 days of exposure to DAPT, with or without ASCL1-IPTD. Results show that TUJ1 expression is similar in both groups, whereas MAP2 and NEUN expression are significantly upregulated in the ASCL1-IPTD group. Statistical analysis was performed by a one-way ANOVA followed by a one-tailed Student's t-test with a 95% confidence level ($\alpha = 0.05$). Results are presented as the mean ± standard deviation, with a * representing a statistically significant difference between the ASCL1-IPTD group with the DAPT Alone group.

several neurons. *In vivo,* the effect of neural stem cells may also be to prolong the activity of neural regeneration, providing neurotrophic support and newly formed neurons for a sustained period of time (Abe, 2000; Lu et al., 2003; Chen et al., 2017).

Our transdifferentiation process was highly efficient in comparison with protocols using viral ASCL1 for similar applications. For instance, viral delivery of 3 transcription factors, ASCL1, BYRN2, and MYT1L, is reported to transdifferentiate MEFs into neurons after 22 days with an efficiency of 15–19% (Vierbuchen et al., 2010), while viral ASCL1 alone is reported to also transdifferentiate human fibroblasts into neurons by day 22, but at lower efficiencies (Chanda et al., 2014). Astrocytes have proven easier to transdifferentiate into neurons, and viral ASCL1 delivered to postnatal mouse astrocytes is reported to convert 77% into neurons by day 21 (Liu et al., 2015), and when delivered to human astrocytes (Sciencell #1800) in combination with the pluripotency transcription factor Nanog homeobox (NANOG) is reported to produce 41% neurons by day 15 (Corti et al., 2012). By comparison, our protocol generated 69% neurons from human astrocytes (Sciencell #1800) by day 12.

Small molecule protocols are reported to generate neurons from astrocytes with similarly high efficiencies, but with considerable cell death in the process, ultimately reducing total efficiency. For instance, Gao et al. used a combination of 6 small molecules (valproic acid, CHIR99021, repsox, forskolin, i-Bet151, and ISX9) to transdifferentiate human adult astrocytes into neurons in 12 days, reporting an efficiency of 70% of surviving cells, or 8% of the initial cell population (Gao et al., 2017). In contrast, Zhang et al. showed that by adding fewer small molecules in a sequential manner, cell death can be avoided in small molecule protocols. In their protocol they used a combination of 9 small molecules (LDN193189, SB431542, TTNPB, Thiazovivin, CHIR99021, DAPT, valproic acid, SAG and purmorphamine) in a step-wise manner to transdifferentiate human astrocytes (ScienCell #1800) into neurons after 14 days, with an efficiency of 67% (Zhang et al., 2015). They used the priming small molecules LDN193189 and SB431542 for days 1-2 similar to our protocol. They found by removing small molecules one at a time that the Notch signal inhibitor DAPT was the most significant enhancer of transdifferentiation, followed closely by the GSK3 signal inhibitor CHIR99021. GSK3 signaling represses canonical Wnt signaling and NGN2 expression, both key regulators of neurogenesis (Hirabayashi et al., 2004; Li et al., 2012; Valvezan and Klein, 2012), thus GSK3 inhibition can be used to promote neurogenesis. Surprisingly, our screening data showed that while either CHIR99021 or DAPT were necessary to enhance transdifferentiation with ASCL1-IPTD, when used together actually decreased transdifferentiation by ∼50%. This suggests that although efficiencies are similar, the signaling pathways involved in our protocol differ substantially from the small molecule protocol.

Cooperation between ASCL1 and Notch signal inhibition can occur naturally in astrocytes *in vivo* after injury (Magnusson

et al., 2014). Magnusson *et al.* identified Notch inhibition shortly after injury as a trigger for a latent neural transdifferentiaton program in resident astrocytes. The similarities between this latent program and the protocol we developed are striking. In their study, they observed a downregulation of Notch receptors and ligands in astrocytes followed by the appearance of ASCL1 expression after a stroke. These ASCL1-positive astrocytes clustered around the lesion and multiplied, giving rise to small, round DCX-positive neural stem cells by week 2, and eventually to mature NEUN-positive neurons by week 7, some of which expressed nitric oxide synthase (nNOS), a marker for GABAergic striatal interneurons. Based on these similarities, it is possible that our protocol takes advantage of this latent program in astrocytes by first recapitulating the plastic aspects of astrocytes at the site of an injury using SMAD inhibition, followed by the concerted action of ASCL1 upregulation by IPTD and Notch signal inhibition by DAPT. By this reasoning, it can be hypothesized that *in vivo* application of ASCL1-IPTD may be sufficient to trigger transdifferentiation of astrocytes at a site of injury into functional neurons. Although further work will be required to verify such a strategy, it would lend itself well to *in vivo* translation using a version of IPTD fitted with a domain to specifically target reactive astrocytes.

CONCLUSION

Here we have shown a novel and non-viral protocol for efficient transdifferentiation of astrocytes into neurons. This protocol requires the delivery of only one transcription factor, ASCL1, by a novel PTD, and 4 small molecules, the SMAD inhibitors LDN193189 and SB431542, the Notch inhibitor DAPT, and the histone deacetylase inhibitor valproic acid. The efficiency of this protocol is enhanced significantly by the natural plasticity of astrocytes, suggesting its suitability for application *in vivo* where injuries lead to increased plasticity in reactive astrocytes. Future work will determine if the small molecules are necessary *in vivo*, and incorporate an astrocyte-targeting motif in the IPTD design. Further work will also adapt this protocol for producing specific neuronal subtypes through cooperation of ASCL1-IPTD with other IPTD-functionalized transcription factors.

AUTHOR CONTRIBUTIONS

MR designed the experiments, analyzed results, and wrote the manuscript. IF assisted in background research, guidance on experimental design and analysis of the small molecule screening experiment. KS assisted in executing the ASCL-IPTD experiments on astrocytes. EM assisted in executing and analysing the NGN2-IPTD experiments on astrocytes. LC assisted in executing the ASCL1-IPTD experiments on MEFs and providing background research. SW provided experimental guidance, provided help writing and editing the final manuscript.

FUNDING

Funding for this project was provided by a Collaborative Research and Development grant (CRD) and a Discovery Grant (DG) by the Natural Sciences and Engineering Research Council (NSERC), along with the Canada Research Chair (CRC) program.

ACKNOWLEDGMENTS

We would like to acknowledge NSERC and the CRC for funding this project, and iProgen Biotech for their support by providing the functionalized transcription factors.

SUPPLEMENTARY MATERIAL

The Supplementary Material for this article can be found online at: https://www.frontiersin.org/articles/10.3389/fbioe.2018.00173/full#supplementary-material

Supplemental Figure 1 | Mouse embryonic fibroblasts (MEFs) express the skeletal myoblast gene myosin heavy chain 3 (MYH3) and lack the neuronal gene beta tubulin (TUJ1) after 14 days of exposure to ASCL1-IPTD and the cAMP activator forskolin, indicating that they have adopted a myogenic cell fate rather than a neuronal cell fate. **(A)** Exposure to 3 μg/mL ASCL1-IPTD is insufficient for transdifferentiation. Scale bar is 100μm. **(B)** Addition of forskolin results in transdifferentiation into myoblasts rather than neurons. Scale bar is 100μm. **(C)** Increasing the concentration of ASCL1-IPTD 5-fold still generates myoblasts rather than neurons. Scale bar is 100μm. **(D)** Increasing the concentration of ASCL1-IPTD 5-fold and adding forskolin still generates myoblasts rather than neurons. Scale bar is 100 μm **(E)** Control. Scale bar is 100 μm **(F)** Forskolin only control. Scale bar is 100 μm.

REFERENCES

Abe, K. (2000). Therapeutic potential of neurotrophic factors and neural stem cells against ischemic brain injury. *J. Cereb. Blood Flow Metab.* 20, 1393–1408. doi: 10.1097/00004647-200010000-00001

Addis, R. C., Hsu, F.-C., Wright, R. L., Dichter, M. A., Coulter, D. A., and Gearhart, J. D. (2011). Efficient conversion of astrocytes to functional midbrain dopaminergic neurons using a single polycistronic vector. *PLoS ONE* 6:e28719. doi: 10.1371/journal.pone.0028719

Agbay, A., De La Vega, L., Nixon, G., and Willerth, S. (2018). Guggulsterone-releasing microspheres direct the differentiation of human induced pluripotent stem cells into neural phenotypes. *Biomed. Mater.* 13:034104. doi: 10.1088/1748-605X/aaaa77

Ambasudhan, R., Talantova, M., Coleman, R., Yuan, X., Zhu, S., Lipton S. A., et al. (2011). Direct reprogramming of adult human fibroblasts to functional neurons under defined conditions. *Cell Stem Cell* 9, 113–118. doi: 10.1016/j.stem.2011.07.002

Berninger, B., Costa, M. R., Koch, U., Schroeder, T., Sutor, B., Grothe,B., et al. (2007). Functional properties of neurons derived from *in vitro* reprogrammed postnatal astroglia. *J. Neurosci.* 27, 8654–8664. doi: 10.1523/JNEUROSCI.1615-07.2007

Bez, A., Corsini, E., Curti, D., Biggiogera, M., Colombo, A., Nicosia, R. F., et al. Parati (2003). Neurosphere and neurosphere-forming cells: morphological and ultrastructural characterization. *Brain Res.* 993, 18–29. doi: 10.1016/j.brainres.2003.08.061

Chambers, S. M., Fasano, C. A., Papapetrou, E. P., Tomishima, M., Sadelain, M., and Studer, L. (2009). Highly efficient neural conversion of human ES and iPS cells by dual inhibition of SMAD signaling. *Nat. Biotechnol.* 27, 275–280. doi: 10.1038/nbt.1529

Chanda, S., Ang, C. E., Davila, J., Pak, C., Mall, M., Lee, Q. Y., et al. (2014). Generation of induced neuronal cells by the single reprogramming factor ASCL1. *Stem cell Reports* 3, 282–296. doi: 10.1016/j.stemcr.2014.05.020

Chen, T., Yu, Y., Tang, L. J., Kong, L., Zhang, C. H., Chu, H. Y., et al. (2017). Neural stem cells over-expressing brain-derived neurotrophic factor promote neuronal survival and cytoskeletal protein expression in traumatic brain injury sites. *Neural Regen. Res.* 12, 433–439. doi: 10.4103/1673-5374.202947

Cheng, L. W., Hu, B., Qiu, J., Zhao, Y., Yu, W., Guan W., et al., (2014). Generation of neural progenitor cells by chemical cocktails and hypoxia. *Cell Res.* 24:665–679. doi: 10.1038/cr.2014.32

Corti, S., Nizzardo, M., Simone, C., Falcone, M., Donadoni, C., Salani, S., et al. (2012). Direct reprogramming of human astrocytes into neural stem cells and neurons. *Exp. Cell Res.* 318, 1528–1541. doi: 10.1016/j.yexcr.2012.02.040

Crombez, L., Aldrian-Herrada, G., Konate, K., Nguyen, Q. N., McMaster, G. K., Brasseur, R., et al. (2009). A new potent secondary amphipathic cell–penetrating peptide for siRNA delivery into mammalian cells. *Mol. Ther.* 17, 95–103. doi: 10.1038/mt.2008.215

Dhanesh, S. B., Subashini, C., and James, J. (2016). Hes1: the maestro in neurogenesis. *Cell. Mol. Life Sci.* 73, 4019–4042. doi: 10.1007/s00018-016-2277-z

Gao, L., Guan, W., Wang, M., Wang, H., Yu, J., Liu, Q., et al. (2017). Direct generation of human neuronal cells from adult astrocytes by small molecules. *Stem Cell Rep.* 8, 538–547. doi: 10.1016/j.stemcr.2017.01.014

Gascón, S., Murenu, E., Masserdotti, G., Ortega, F., Russo, G. L., Petrik, D., et al. (2016). Identification and successful negotiation of a metabolic checkpoint in direct neuronal reprogramming. *Cell Stem Cell* 18, 396–409. doi: 10.1016/j.stem.2015.12.003

Gascón, S., Ortega, F., and Götz, M. (2017). Transient CREB-mediated transcription is key in direct neuronal reprogramming. *Neurogenesis* 4:e1285383. doi: 10.1080/23262133.2017.1285383

Gordeeva, O., and Khaydukov, S. (2017). Tumorigenic and differentiation potentials of embryonic stem cells depend on TGFβ family signaling: lessons from teratocarcinoma cells stimulated to differentiate with retinoic acid. *Stem Cells Int.* 2017:7284872. doi: 10.1155/2017/7284872

Götz, M., Sirko, S., Beckers, J., and Irmler, M. (2015). Reactive astrocytes as neural stem or progenitor cells: *in vivo* lineage, *in vitro* potential, and Genome-wide expression analysis. *Glia* 63, 1452–1468. doi: 10.1002/glia.22850

Hardee, C. L., Arévalo-Soliz, L. M., Hornstein, B. D., and Zechiedrich, L. (2017). Advances in non-viral DNA vectors for gene therapy. *Genes* 8:65. doi: 10.3390/genes8020065

Hirabayashi, Y., Itoh, Y., Tabata, H., Nakajima, K., Akiyama, T., Masuyama, N., et al. (2004). The Wnt/β-catenin pathway directs neuronal differentiation of cortical neural precursor cells. *Development* 131, 2791–2801. doi: 10.1242/dev.01165

Hu, Q., Chen, R., Teesalu, T., Ruoslahti, E., and Clegg, D. O. (2014). Reprogramming human retinal pigmented epithelial cells to neurons using recombinant proteins. *Stem Cells Transl. Med.* 3, 1526–1534. doi: 10.5966/sctm.2014-0038

Hu, W., Qiu, B., Guan, W., Wang, Q., Wang, M., Li, W., et al. (2015). Direct conversion of normal and Alzheimer's disease human fibroblasts into neuronal cells by small molecules. *Cell Stem Cell* 17, 204–212. doi: 10.1016/j.stem.2015.07.006

Huangfu, D., Maehr, R., Guo, W., Eijkelenboom, A., Snitow, M., Chen, A. E., et al. (2008). Induction of pluripotent stem cells by defined factors is greatly improved by small-molecule compounds. *Nat. Biotechnol.* 26, 795–797. doi: 10.1038/nbt1418

Islas, J. F., Liu, Y., Weng, K. C., Robertson, M. J., Zhang, S., Prejusa, A., et al. (2012).Transcription factors ETS2 and MESP1 transdifferentiate human dermal fibroblasts into cardiac progenitors. *Proc. Natl. Acad. Sci. U.S.A.* 109, 13016–13021. doi: 10.1073/pnas.1120299109

Iwafuchi-Doi, M., and Zaret, K. S. (2014). Pioneer transcription factors in cell reprogramming. *Genes Dev.* 28, 2679–2692. doi: 10.1101/gad.253443.114

Lee, C., Robinson, M., and Willerth, S. M. (2018). Direct reprogramming of glioblastoma cells into neurons using small molecules. *ACS Chem. Neurosci.* doi: 10.1021/acschemneuro.8b00365. [Epub ahead of print].

Lee, K. H., Lin, L. Y.-C., and Wang, A. (2013). *Intracellular Protzein Delivery*. U.S. Patent 9,994,829, issued July 2, 2013.

Li, S., Mattar, P., Zinyk, D., Singh, K., Chaturvedi, C. P., Kovach, C., et al. (2012). GSK3 temporally regulates neurogenin 2 proneural activity in the neocortex. *Journal of Neuroscience* 32, 7791–7805. doi: 10.1523/JNEUROSCI.1309-12.2012

Li, X., Zuo, X., Jing, J., Ma, Y., Wang, J., Liu, D., et al. (2015). Small-molecule-driven direct reprogramming of mouse fibroblasts into functional neurons. *Cell Stem Cell* 17, 195–203. doi: 10.1016/j.stem.2015.06.003

Li, Z., Düllmann, J., Schiedlmeier, B., Schmidt, M., von Kalle, C., Meyer, J., et al. (2002). Murine leukemia induced by retroviral gene marking. *Science* 296, 497–497. doi: 10.1126/science.1068893

Lian, H., Litvinchuk, A., Chiang, A. C., Aithmitti, N., Jankowsky, J. L., and Zheng, H. (2016). Astrocyte-microglia cross talk through complement activation modulates amyloid pathology in mouse models of Alzheimer's disease. *J. Neurosci.* 36, 577–589. doi: 10.1523/JNEUROSCI.2117-15.2016

Lin, T., and Wu, S. (2015).Reprogramming with small molecules instead of exogenous transcription factors. *Stem Cells Int.* 2015: 794632. doi: 10.1155/2015/794632

Liu, Y., Miao, Q., Yuan, J., Han, S., Zhang, P., Li, S., et al. (2015). Ascl1 converts dorsal midbrain astrocytes into functional neurons *in vivo*. *J. Neurosci.* 35, 9336–9355. doi: 10.1523/JNEUROSCI.3975-14.2015

Lu, P., Jones, L. L., Snyder, E. Y., and Tuszynski, M. H. (2003). Neural stem cells constitutively secrete neurotrophic factors and promote extensive host axonal growth after spinal cord injury. *Exp. Neurol.* 181, 115–129. doi: 10.1016/S0014-4886(03)00037-2

Ma, X., Kong, L., and Zhu, S. (2017). Reprogramming cell fates by small molecules. *Protein Cell* 8, 328–348. doi: 10.1007/s13238-016-0362-6

Magnusson, J. P., Göritz, C., Tatarishvili, J., Dias, D. O., Smith, E. M., Lindvall, O., et al. (2014). A latent neurogenic program in astrocytes regulated by Notch signaling in the mouse. *Science* 346, 237–241. doi: 10.1126/science.346.6206.237

Medvedev, S. P., Shevchenko, A. I., and Zakian, S. M. (2010). Induced pluripotent stem cells: problems and advantages when applying them in regenerative medicine. *Acta Naturae* 2, 18–28. Available online at: http://actanaturae.ru/catalog/225.aspx

Michelucci, A., Bithell, A., Burney, M. J., Johnston, C. E., Wong, K. Y., Teng, S. W., et al. (2016). The neurogenic potential of astrocytes is regulated by inflammatory signals. *Mol. Neurobiol.* 53, 3724–3739. doi: 10.1007/s12035-015-9296-x

Modlich, U., Bohne, J., Schmidt, M., von Kalle, C., Knöss, S., Schambach, A., et al. (2006). Cell-culture assays reveal the importance of retroviral vector design for insertional genotoxicity. *Blood* 108, 2545–2553. doi: 10.1182/blood-2005-08-024976

Montgomery, A., Wong, A., Gabers, N., and Willerth, S. M. (2015). Engineering personalized neural tissue by combining induced pluripotent stem cells with fibrin scaffolds. *Biomater. Sci.* 3, 401–413. doi: 10.1039/C4BM00299G

Pang, H. B., Braun, G. B., Friman, T., Aza-Blanc, P., Ruidiaz, M. E., Sugahara, K. N., et al. (2014). An endocytosis pathway initiated through neuropilin-1 and regulated by nutrient availability. *Nat. Commun.* 5:4904. doi: 10.1038/ncomms5904

Parras, C. M., Schuurmans, C., Scardigli, R., Kim, J., Anderson, D. J., and Guillemot, F. (2002). Divergent functions of the proneural genes Mash1 and Ngn2 in the specification of neuronal subtype identity. *Genes Dev.* 16, 324–338. doi: 10.1101/gad.940902

Raposo, A. A., Vasconcelos, F. F., Drechsel, D., Marie, C., Johnston, C., Dolle, D., et al. (2015). Ascl1 coordinately regulates gene expression and the chromatin landscape during neurogenesis. *Cell Rep.* 10, 1544–1556. doi: 10.1016/j.celrep.2015.02.025

Robinson, M., Chapani, P., Styan, T., Vaidyanathan, R., and Willerth, S. M. (2016). Functionalizing Ascl1 with novel intracellular protein delivery technology for promoting neuronal differentiation of human induced pluripotent stem cells. *Stem Cell Rev. Rep.* 12, 476–483. doi: 10.1007/s12015-016-9655-7

Shi, Z., Zhang, J., Chen, S., Li, Y., Lei, X., Qiao, H., et al. (2016). Conversion of fibroblasts to parvalbumin neurons by one transcription factor, Ascl1, and the chemical compound forskolin. *J. Biol. Chem* 291, 13560-70. doi: 10.1074/jbc.M115.709808

Sirko, S., Irmler, M., Gascón, S., Bek, S., Schneider, S., Dimou, L., et al. (2015). Astrocyte reactivity after brain injury—: the role of galectins 1 and 3. *Glia* 63, 2340–2361. doi: 10.1002/glia.22898

Son, E. Y., Ichida, J. K., Wainger, B. J., Toma, J. S., Rafuse, V. F., Woolf, C. J., et al. (2011). Conversion of mouse and human fibroblasts into functional spinal motor neurons. *Cell Stem Cell* 9, 205–218. doi: 10.1016/j.stem.2011.07.014

Stipursky, J., and Gomes, F. C. (2007). TGF-β1/SMAD signaling induces astrocyte fate commitment *in vitro*: implications for radial glia development. *Glia* 55, 1023–1033. doi: 10.1002/glia.20522

Tanabe, K., Haag, D., and Wernig, M. (2015). Direct somatic lineage conversion. *Phil. Trans. R. Soc. B* 370:20140368. doi: 10.1098/rstb.2014.0368

Teesalu, T., Sugahara, K. N., Kotamraju, V. R., and Ruoslahti, E. (2009). C-end rule peptides mediate neuropilin-1-dependent cell, vascular, and tissue penetration. *Proc. Natl Acad. Sci. U.S.A.* 106, 16157–16162. doi: 10.1073/pnas.0908201106

Theka, I., Caiazzo, M., Dvoretskova, E., Leo, D., Ungaro, F., Curreli, S., et al. (2013). Rapid generation of functional dopaminergic neurons from human induced pluripotent stem cells through a single-step procedure using cell lineage transcription factors. *Stem Cells Transl. Med.* 2, 473–479. doi: 10.5966/sctm.2012-0133

Treutlein, B., Lee, Q. Y., Camp, J. G., Mall, M., Koh, W., Shariati, S. A., et al. (2016). Dissecting direct reprogramming from fibroblast to neuron using single-cell RNA-seq. *Nature* 534:391–395. doi: 10.1038/nature18323

Valvezan, A. J., and Klein, P. S. (2012). GSK-3 and Wnt signaling in neurogenesis and bipolar disorder. *Front. Mol. Neurosci.* 5:1. doi: 10.3389/fnmol.2012.00001

van den Berg, A., and Dowdy, S. F. (2011). Protein transduction domain delivery of therapeutic macromolecules. *Curr. Opin. Biotechnol.* 22, 888–893. doi: 10.1016/j.copbio.2011.03.008

Vasconcelos, F. F., and Castro, D. S. (2014). Transcriptional control of vertebrate neurogenesis by the proneural factor Ascl1. *Front. Cell. Neurosci.* 8:412. doi: 10.3389/fncel.2014.00412

Vierbuchen, T., Ostermeier, A., Pang, Z. P., Kokubu, Y., Südhof, T. C., and Wernig, M. (2010). Direct conversion of fibroblasts to functional neurons by defined factors. *Nature* 463:1035. doi: 10.1038/nature08797

Wang, C., Fong, H., and Huang, Y. (2015). Direct reprogramming of RESTing astrocytes. *Cell Stem Cell* 17, 1–3. doi: 10.1016/j.stem.2015.06.011

Xu, Z., Jiang, H., Zhong, P., Yan, Z., Chen, S., and Feng, J. (2016). Direct conversion of human fibroblasts to induced serotonergic neurons. *Mol. Psychiatry* 21, 62. doi: 10.1038/mp.2015.101

Yang, H., Feng, G.-D., Olivera, C., Jiao, X.-Y., Vitale, A., Gong, J., et al. (2012a). Sonic hedgehog released from scratch-injured astrocytes is a key signal necessary but not sufficient for the astrocyte de-differentiation. *Stem Cell Res.* 9, 156–166. doi: 10.1016/j.scr.2012.06.002

Yang, Y., Higashimori, H., and Morel, L. (2013). Developmental maturation of astrocytes and pathogenesis of neurodevelopmental disorders. *J. Neurodev. Disord.* 5:22. doi: 10.1186/1866-1955-5-22

Yang, Y., Liu, B., Dong, J., Zhang, L., Pang, M., and Rong, L. (2012b). Proteins reprogramming: present and future. *Sci. World J.* 2012:453185. doi: 10.1100/2012/453185

Yoo, A. S., Sun, A. X., Li, L., Shcheglovitov, A., Portmann, T., Li, Y., et al. (2011). MicroRNA-mediated conversion of human fibroblasts to neurons. *Nature* 476, 228–231. doi: 10.1038/nature10323

Zahid, M., and Robbins, P. D. (2012). Protein transduction domains: applications for molecular medicine. *Curr. Gene Ther.* 12, 374–380. doi: 10.2174/156652312802762527

Zahid, M., and Robbins, P. D. (2015). Cell-type specific penetrating peptides: therapeutic promises and challenges. *Molecules* 20, 13055–13070. doi: 10.3390/molecules200713055

Zhang, L., Yin, J. C., Yeh, H., Ma, N. X., Lee, G., Chen, X. A., et al. (2015). Small molecules efficiently reprogram human astroglial cells into functional neurons. *Cell Stem Cell* 17, 735–747. doi: 10.1016/j.stem.2015.09.012

Zhang, M., Lin, Y. H., Sun, Y. J., Zhu, S., Zheng, J., Liu, K., et al. (2016). Pharmacological reprogramming of fibroblasts into neural stem cells by signaling-directed transcriptional activation. *Cell Stem Cell* 18, 653–667. doi: 10.1016/j.stem.2016.03.020

Zhu, S., Ambasudhan, R., Sun, W., Kim, H. J., Talantova, M., Wang, X., et al. (2014). Small molecules enable OCT4-mediated direct reprogramming into expandable human neural stem cells. *Cell Res.* 24, 126–129. doi: 10.1038/cr.2013.156

Conflict of Interest Statement: This research was in part funded by an NSERC-CRD grant which we hold with iProgen Biotech who owns the PTD technology. This work was conducted in collaboration with iProgen Biotech who provided the functionalized transcription factors used in this work.

Advantages of publishing in Frontiers

OPEN ACCESS
Articles are free to read for greatest visibility and readership

FAST PUBLICATION
Around 90 days from submission to decision

HIGH QUALITY PEER-REVIEW
Rigorous, collaborative, and constructive peer-review

TRANSPARENT PEER-REVIEW
Editors and reviewers acknowledged by name on published articles

Frontiers
Avenue du Tribunal-Fédéral 34
1005 Lausanne | Switzerland

Visit us: www.frontiersin.org
Contact us: info@frontiersin.org | +41 21 510 17 00

REPRODUCIBILITY OF RESEARCH
Support open data and methods to enhance research reproducibility

DIGITAL PUBLISHING
Articles designed for optimal readership across devices

FOLLOW US
@frontiersin

IMPACT METRICS
Advanced article metrics track visibility across digital media

EXTENSIVE PROMOTION
Marketing and promotion of impactful research

LOOP RESEARCH NETWORK
Our network increases your article's readership